NATO ASI Series

Advanced Science Institutes Series

A series presenting the results of activities sponsored by the NATO Science Committee, which aims at the dissemination of advanced scientific and technological knowledge, with a view to strengthening links between scientific communities.

The Series is published by an international board of publishers in conjunction with the NATO Scientific Affairs Division

A Life Sciences B Physics	Plenum Publishing Corporation London and New York
C Mathematical and Physical Sciences D Behavioural and Social Sciences E Applied Sciences	Kluwer Academic Publishers Dordrecht, Boston and London
F Computer and Systems Sciences G Ecological Sciences H Cell Biology I Global Environmental Change	Springer-Verlag Berlin Heidelberg New York London Paris Tokyo Hong Kong Barcelona Budapest

NATO-PCO DATABASE

The electronic index to the NATO ASI Series provides full bibliographical references (with keywords and/or abstracts) to more than 30000 contributions from international scientists published in all sections of the NATO ASI Series. Access to the NATO-PCO DATABASE compiled by the NATO Publication Coordination Office is possible in two ways:

- via online FILE 128 (NATO-PCO DATABASE) hosted by ESRIN, Via Galileo Galilei, I-00044 Frascati, Italy.
- via CD-ROM „NATO Science & Technology Disk" with user-friendly retrieval software in English, French and German (© WTV GmbH and DATAWARE Technologies Inc. 1989).

The CD-ROM can be ordered through any member of the Board of Publishers or through NATO-PCO, Overijse, Belgium.

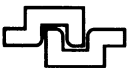

Series I: Global Environmental Change, Vol. 7

The ASI Series Books Published as a Result of Activities of the Special Programme on Global Environmental Change

---

This book contains the proceedings of a NATO Advanced Research Workshop held within the activities of the NATO Special Programme on Global Environmental Change, which started in 1991 under the auspices of the NATO Science Committee.

The volumes published as a result of the activities of the Special Programme are:

Vol. 1: **Global Environmental Change.** Edited by R. W. Corell and P. A. Anderson. 1991.
Vol. 2: **The Last Deglaciation: Absolute and Radiocarbon Chronologies.** Edited by E. Bard and W. S. Broecker. 1992.
Vol. 3: **Start of a Glacial.** Edited by G. J. Kukla and E. Went. 1992.
Vol. 4: **Interactions of C, N, P and S Biogeochemical Cycles and Global Change.** Edited by R. Wollast, F. T. Mackenzie and L. Chou. 1993.
Vol. 5: **Energy and Water Cycles in the Climate System.** Edited by E. Raschke and D. Jacob. 1993.
Vol. 6: **Prediction of Interannual Climate Variations.** Edited by J. Shukla. 1993.
Vol. 7: **The Tropospheric Chemistry of Ozone in the Polar Regions.** Edited by H. Niki and K. H. Becker. 1993.

The Tropospheric Chemistry of Ozone in the Polar Regions

Edited by

H. Niki

York University
Center for Atmospheric Chemistry
and Chemistry Department
4700 Keele Street
North York, Ontario, M3J 1P3, Canada

K. H. Becker

Bergische Universität
Physikalische Chemie – FB9
Gaußstraße 20
W-5600 Wuppertal, FRG

Springer-Verlag
Berlin Heidelberg New York London Paris Tokyo
Hong Kong Barcelona Budapest
Published in cooperation with NATO Scientific Affairs Division

Proceedings of the NATO Advanced Research Workshop on The Tropospheric Chemistry of Ozone in the Polar Regions held at Wolfville, Nova Scotia, Canada, August 23–28, 1992

ISBN-13:978-3-642-78213-8 e-ISBN-13:978-3-642-78211-4
DOI: 10.1007/978-3-642-78211-4

Library of Congress Cataloging-in-Publication Data

Typesetting: Camera ready by authors
31/3145 - 5 4 3 2 1 0 - Printed on acid-free paper

TABLE OF CONTENTS

NATO/ARW
"The Tropospheric Chemistry of Ozone in the Polar Regions"
August 23 - 28, 1992
Wolfville, Nova Scotia, Canada

Front Row - Left to Right: 1. Len Barrie, 2. Stu Penket, 3. Hiromi Niki, 4. Tony Cox, 5. Karl Becker, 6. Brian Thrush, 7. Dieter Ehhalt, 8. Harold Schiff, 9. Robert Moore

Middle Row - Left to Right: 1. Hiram Levy II, 2. Bernard Bonsang, 3. Constantine Andronarche, 4. Ian Barnes, 5. Shao Meng Li, 6. Dan Jaffe, 7. Jan Bottenheim, 8. Albrecht Neftel, 9. Michel Legrand, 10. Cornelius Zetzsch, 11. Mario Molina, 12. David Simpson

Back Row - Left to Right: 1. Tom Jobson, 2. Michael Jenkin, 3. Jack McConnell, 4. David Parrish, 5. A.R. Ravishankara, 6. Paul Wine, 7. George Le Bras, 8. Geert Moortgat, 9. Trond Iversen, 10. Stanley Sander, 11. Sam Oltmans, 12. Allen Lavigne

INTRODUCTION

The Arctic troposphere (0 to ca. 8 km) plays an important role in environmental concerns for global change. It is a unique chemical reactor influenced by human activity and the Arctic ocean. It is surrounded by industrialized continents that in winter contribute gaseous and particulate pollution (Arctic haze). It is underlain by the flat Arctic ocean from which it is separated by a crack-ridden ice membrane 3 to 4 m thick. Ocean to atmosphere exchange of heat, water vapor and marine biogenic gases influence the composition of the reactor. From September 21 to December 21 to March 21, the region north of the Arctic circle goes from a completely sunlit situation to a completely dark one and then back to light. At the same time the lower troposphere is stably stratified. This hinders vertical mixing. During this light period, surface temperature reaches as low as -40 °C.

In this environment, chemical reactions involving sunlight are generally much slower than further south. Thus, the abundance of photochemically reactive compounds in the atmosphere can be high prior to polar sunrise. Between complete dark in February and complete light in April, a number of chemical changes in the lower troposphere take place. Perhaps, the most striking is the occasional decrease of ozone concentrations to quite low levels, which was first observed in 1985 by Canadian researchers at Alert (82.5° N, 62.3° W), Northwest Territories. Subsequent studies have shown that the destruction of lower tropospheric ozone is accompanied by production of filterable bromine and iodine, and concurrent decrease in hydrocarbons such as acetylene and ethylene. Although the significance of this observation is as yet not fully understood, it is widely speculated that the ozone is chemically depleted by a catalytic cycle involving Br-containing radicals. A source of the Br atoms required to support this proposed mechanism has not been positively identified. Also, the ozone concentrations at the ground based station in Alert appear to be closely related to the wind direction at the site. Thus, it has been hypothesized that a Br-atom source exists somewhere over the ice sheet, and that the ozone depletion mechanism operates on a sufficiently fast enough time scale that the arctic boundary layer inversion is strong enough to prevent ozone replenishment by vertical mixing with free tropospheric air. Other significant chemical changes include a shift in the fraction of total sulfur in its final oxidation state (VI) from 50% to 90% and a rise in methane sulfonic acid of marine biogenic origin.

There remain many outstanding questions concerning the above observations in terms of the relevant sources and sinks, temporal and spatial distributions, and physical and chemical processes. A coordinated field study on Arctic air chemistry (Polar Sunrise Experiment 92) took place at Alert during January 15 - May 15, 1992, under the auspices of the International Global Atmospheric Chemistry (IGAC) program. The timing for this ARW, i.e., end of August 1992, was chosen to make preliminary results from this study available for

presentation at the workshop. In combination with the earlier observations including those from the Arctic troposphere, these new field data provided an excellent framework for theoretical modelling and laboratory kinetic studies to be carried out in the future. Emphasis was also placed on understanding to be gained from contrasting behavior of tropospheric ozone between the Arctic and Antarctic. This ARW was intended to facilitate interactions among prominent researchers representing several key disciplinary areas of field measurements, laboratory studies and modelling with experience of air chemistry in the continental lower troposphere, the stratosphere and the polar regions of the stratosphere.

The NATO/ARW on the "Tropospheric Chemistry of Ozone in the Polar Regions" was held at the Old Orchard Inn, Wolfville, Nova Scotia, August 23 to 28, 1992 with 34 participants from 7 countries. H.G. McAdie, Executive Director of the Canadian Institute for Research in Atmospheric Chemistry (CIRAC), was instrumental in assisting us to select the location in Wolfville, situated ~100 km. northwest of Halifax, overlooking the Bay of Fundy; a rather secluded site which turned out to be highly appropriate for this NATO/ARW.

We are particularly grateful to Brian Thrush for participating in this workshop as a representative of the NATO Board. We very much appreciated Lorretta Buchanan, Manager of the Old Orchard Inn for her attention and industry which enabled our week to be especially enjoyable and productive. Also, we thank Carol V. Francis, York University, Centre for Atmospheric Chemistry for the workshop organization and preparation and for her efforts as technical editor of this book. Her suburb professional abilities and enthusiasm were essential for the successful outcome of the meeting and completion of this proceeding.

Organizing Committee

Hiromi Niki, York University, Canada (Director)
Karl H. Becker, Bergische Universität - GH, Germany (Co-Director)
Len A. Barrie, Atmospheric Environment Service, Canada
Richard A. Cox, Marine and Atmospheric Sciences, U.K.
Stu A. Penkett, University of East Anglia, U.K.

FEATURES OF POLAR REGIONS RELEVANT TO TROPOSPHERIC OZONE CHEMISTRY

Len A. Barrie
Atmospheric Environment Service
4905 Dufferin St. Downsview Ontario
M3H 5T4 Canada

INTRODUCTION

It is becoming increasingly apparent that the polar regions play an important role in the atmospheric cycle of ozone. What is perhaps less well recognized is that this is true not only in the stratosphere (above 8 to 10 km) but also in the troposphere (0 to 8 km). The aim of this paper is to "set the scene" for the following discussions by describing characteristics of geography, climate and chemical environment in the Arctic and Antarctic that help us to understand polar tropospheric ozone. The use of "polar" here refers to those areas poleward of 40° latitude. This represents approximately 36% of the total surface area of the globe. 40° is chosen to include areas of the northern hemisphere that are frequented by arctic air masses during winter as indicated by the mean position of the arctic front in January (Figure 1).

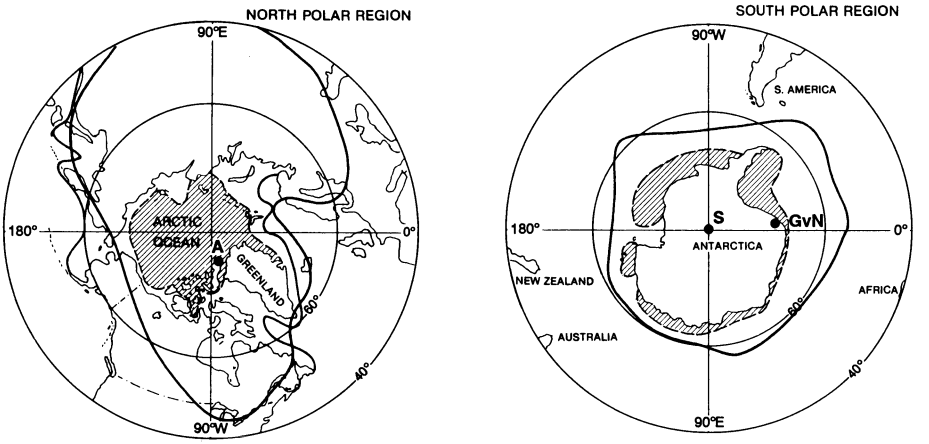

Fig. 1. A comparison of the geography of the northern and southern polar regions. The minimum and maximum limits of sea ice coverage at both poles are shown by dashed and solid lines, respectively. The average position of the arctic front is shown by the heavy-solid line.

NATO ASI Series, Vol. I 7
The Tropospheric Chemistry of Ozone in the Polar Regions
Edited by H. Niki and K. H. Becker

It is convenient to differentiate between three classes of ozone sources and sinks to the polar troposphere: i) horizontal transport to or from mid-latitudes, ii) vertical exchange with the ozone-rich stratosphere, and iii) chemical destruction/production within the domain. Although this proceeding deals with the last topic, it is important to be aware of processes associated with transport and physical/chemical environment.

PHYSICAL ENVIRONMENT

One of the most remarkable features of polar geography is the tremendous contrast between the Arctic and Antarctica in the land-ocean-ice configuration (Figure 1). The Arctic troposphere is underlain by an active ocean surrounded by pollutant-emitting, industrialized continents while the Antarctic troposphere lies over a massive, 4 km thick, ice sheet surrounded by the pollution-free southern ocean region. Sea-ice coverage fluctuates seasonally, affecting the climate and atmosphere-ocean exchange (Figure 1). The ice - generally 1 to 6 metres thick - forms a cracked membrane, through which the ocean and troposphere interact. Microalgae that grow at the ice water interface and within the ice are players in ocean-atmosphere chemical interactions. Their nature and influence are only now beginning to be studied [cf. Moore and Sturges, in this volume].

Topography plays a key role in shaping atmospheric circulation in the polar regions. In the north, the Greenland continent covered by a 3 km thick ice sheet and the mountains of western North America and Alaska are major obstructions to lower tropospheric winds. The mountains of Norway, the Urals and of eastern Siberia play a secondary role. In the south, the ice sheet covering Antarctica having the configuration shown in Figure 2 is the dominant feature.

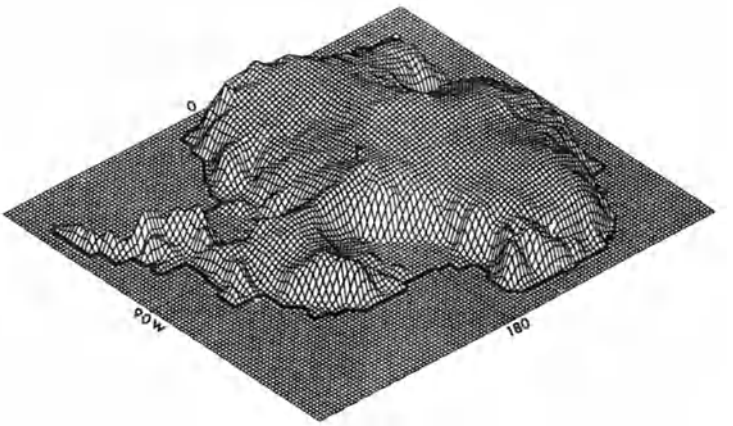

Fig. 2. A schematic of the topography of the Antarctic ice sheet reaching a maximum altitude of approximately 4 km.

Radiative cooling at elevated locations on the large ice sheets of Greenland and Antarctic causes air to drain toward sea level, setting up a complex katabatic wind regime that often dominates winds driven by high and low air pressure systems - so-called synoptic systems.

The mean circulation of air in the polar regions driven by synoptic systems is illustrated in Figures 3 to 5, showing the mean atmospheric pressure distribution for January and July at sea level in the north and the mean height of the 700 hPa (~3 km) pressure surface in the north and south. Because the plateau of Antarctica is very high (3 to 4 km), sea level pressure maps are not useful for showing circulation at lower levels which tends to be dominated by katabatic winds. In the northern hemisphere, air flows parallel to isobars (or, for the 700 hPa height fields parallel to contours of pressure field heights) in a clockwise direction around lows and counter clockwise around highs. The opposite holds in the southern hemisphere.

The lower tropospheric circulation of the northern polar region (Figure 3) is dominated in winter (January) by high pressures over the continents and low pressures over the northern Pacific and Atlantic Oceans. In particular, the intense Siberian high pressure cell tends to force air on its western side northward into the Arctic. In the next section, it will be shown that this leads to elevated pollution in the north. The high pressure ridge over North America tends to drive air out of the Arctic southward. In short, the mean flow in winter is out of Eurasia into the Arctic and out of the Arctic into North America. Of course, some air is also exchanged with the south, when low pressure vortices along the Arctic front (Figure 1) mix warm southern air with cold northern air in a large scale turbulent eddy. In summer (July), the continental high pressure cells disappear and the oceanic low pressure cells weaken, particularly in the north Pacific. Northward transport from mid-latitudes decreases accordingly. At 700 hPa (3 km), the circulation is considerably different (Figure 4). A clockwise flow prompted by polar low pressures is prominent in both summer and winter. The winter Siberian high pressure cell at the lower level has disappeared.

Although possessing some similarities, the Antarctic circulation (Figure 5) is driven by much deeper lows at the pole and is more circular around the pole than its northern counterpart (Figure 4). In the latitude band, 40° to 60° around the periphery of the ice covered continent, winds are strongly from the west, hence the term "roaring forties". They are more intense in winter than in summer and stronger than their northern hemispheric counterparts. This upper level wind pattern tends to steer intense low pressure storm cells around the southern ocean at the surface. This makes for a stormy, wet, lower troposphere, through which soluble substances from the polluted north cannot readily pass, and for strong exchange of gases and particles between the ocean and atmosphere.

The mean pressure maps illustrate an over-simplified picture of the circulation. Exchange of mass or heat between polar regions and extrapolar regions are effected by three types of flow regimes: i) mean meridional circulation (MMC), ii) standing eddies (SE) and iii) transient eddies (TE). To illustrate that these can all contribute substantially to north-south mass exchange, consider the seasonal distribution of energy exchange for each flow regime calculated by

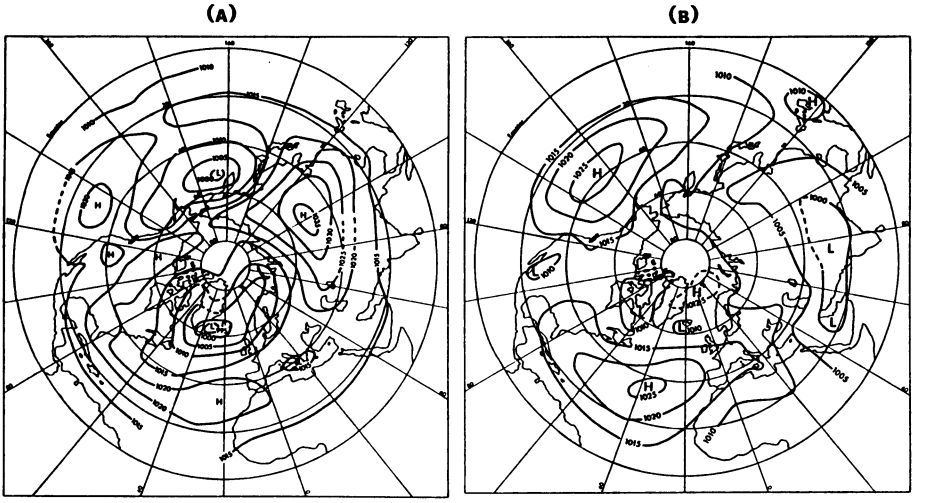

Fig. 3. The mean sea-level pressure distribution in hPa in (A) January and (B) July for the northern hemisphere 1950-1959 [Barry and Chorley, 1987].

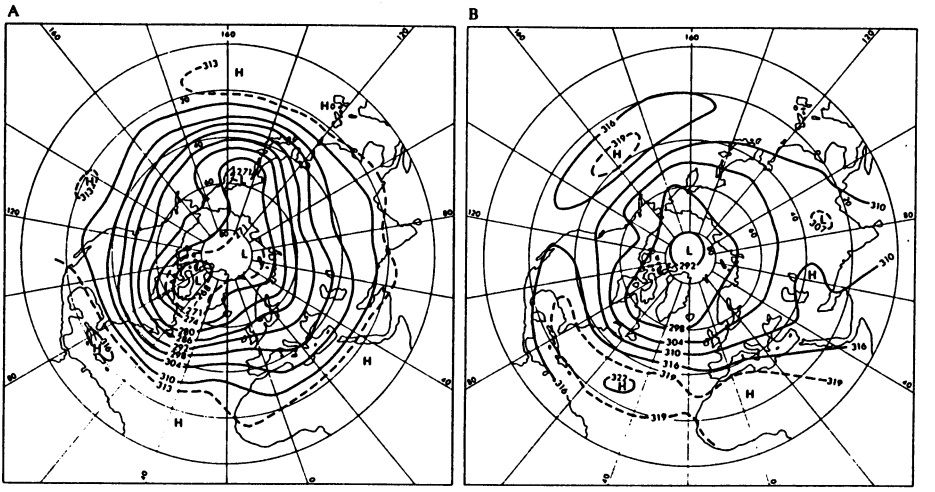

Fig. 4. The mean contours (in deci-km) of the 700 hPa pressure surface in (A) January and (B) July for the northern hemisphere 1950-59 [Barry and Chorley, 1987].

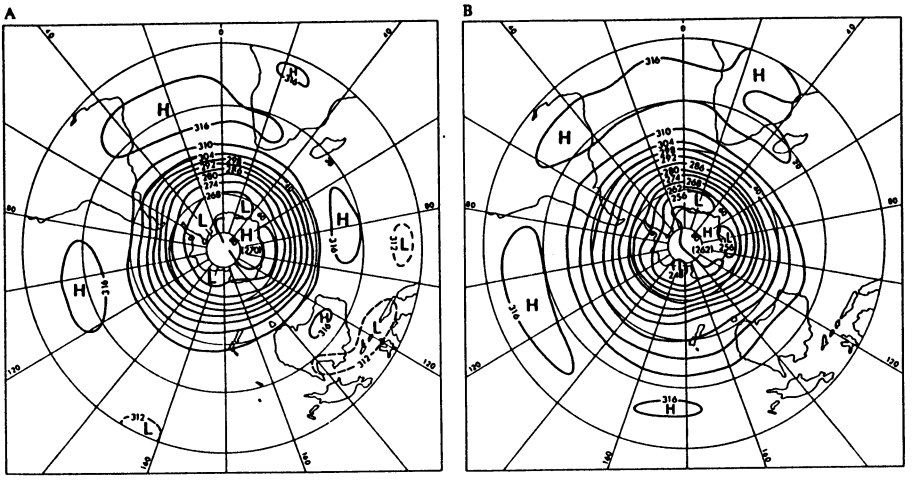

Fig. 5. The mean contours (in deci-km) of the 700 hPa pressure surface in (A) January and (B) July for the southern hemisphere 1949-60 [Barry and Chorley, 1987].

Nakamura and Oort [1988] for the Arctic and Antarctic (Figure 6). Exchange of heat is least in summer and greatest in winter. Furthermore, standing eddies such as the Siberian high pressure cell (Figure 3) tend to play a more prominent role in the northern hemispheric winter than in summer or than in the Antarctic at any time of year. Furthermore, total eddy exchange (SE+TE) is stronger than MMC at all times in the northern hemisphere but not during winter in the southern hemisphere when MMC dominates. The reader should be cautioned that to draw quantitative parallels between heat exchange and mass exchange can lead to erroneous deductions, since it depends on the lifetime and spatial temporal distribution of sources of an atmospheric constituent. But, qualitatively this analogy is valid and hence instructive.

The spatial distributions of mean surface temperature in January and July are shown in Figures 7 and 8 for the south and north polar region, respectively. In Antarctica, they are very circular and centred on the pole, while those in the Arctic are more irregular and a minimum at the elevated surface of Greenland. The minimum surface Antarctic temperature is about - 30° and - 70° C in summer and winter, respectively, while that in the Arctic on Greenland is -10° and -50° and over the Arctic ocean 0° and -34° C. Because of heat transfer from ocean to

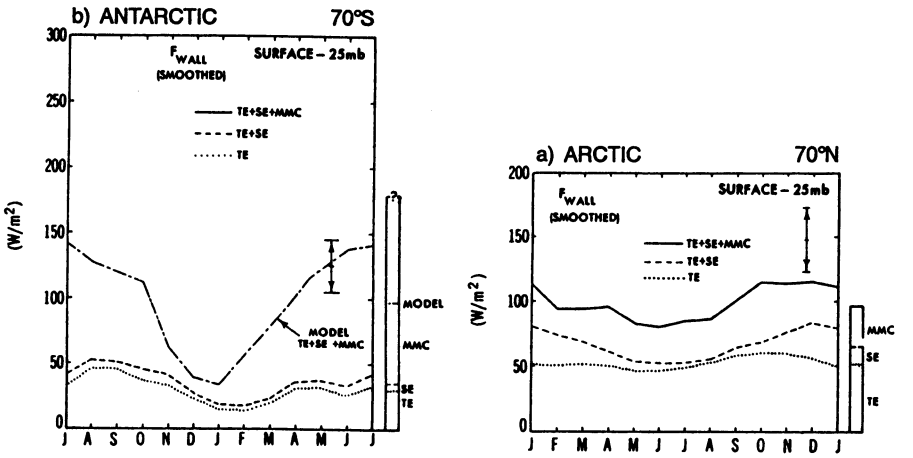

Fig. 6. Annual variation in poleward energy flux as effected by transient eddies (TE), standing eddies (SE) and mean meridional circulation (MMC) for the atmosphere from surface to 25 hPa for a) the Arctic and b) the Antarctic [Nakamura and Oort, 1988].

atmosphere through the Arctic ice, winter surface temperatures are never as low as they are over the surrounding continental land masses in Canada and Russia.

The vertical distribution of temperature in the polar troposphere is governed largely by the net radiative heat balance at the Earth's surface. It is typically like that shown in Figure 9a for Antarctic which features a stably stratified region at the bottom of the atmosphere up to 1 km thick, in which temperature increases with increasing height. The thermally stable surface-based inversion (SBI) layer is poorly mixed. Hence, exchange of air with the free troposphere is weak. The effects of an addition or removal of chemicals by exchange with the surface or of a chemical or physical reaction in the air is, therefore, more clearly manifested in the SBI than it would be in a well-mixed layer that freely exchanges air with the troposphere above. This property makes the SBI an attractive natural chemical reactor. The temperature difference across it is a measure of the SBI's strength. The spatial distribution of its strength in winter in Antarctica (Figure 9b) is a maximum in the centre of the ice sheet (-25 °C) and a minimum on the edge (-10 °C). SBIs also occur in the Arctic where they host the destruction of surface level ozone at polar sunrise [Barrie

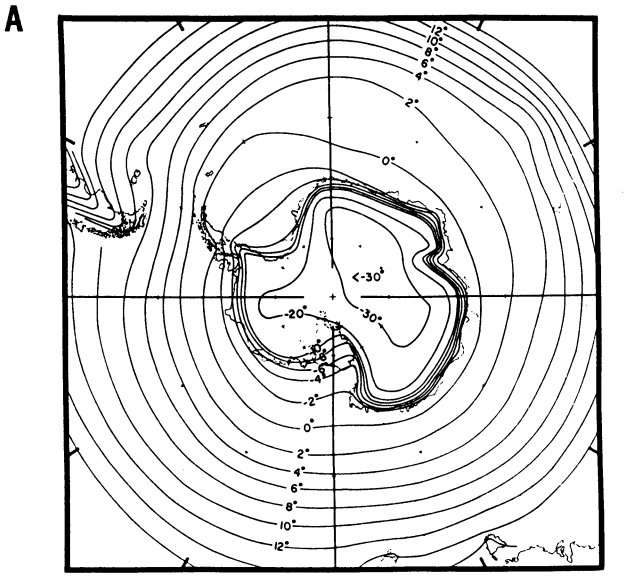

Fig. 7. Distribution of mean surface temperature in the Antarctic region for (A) January (summer) and (B) July (winter) from Orvig [1970].

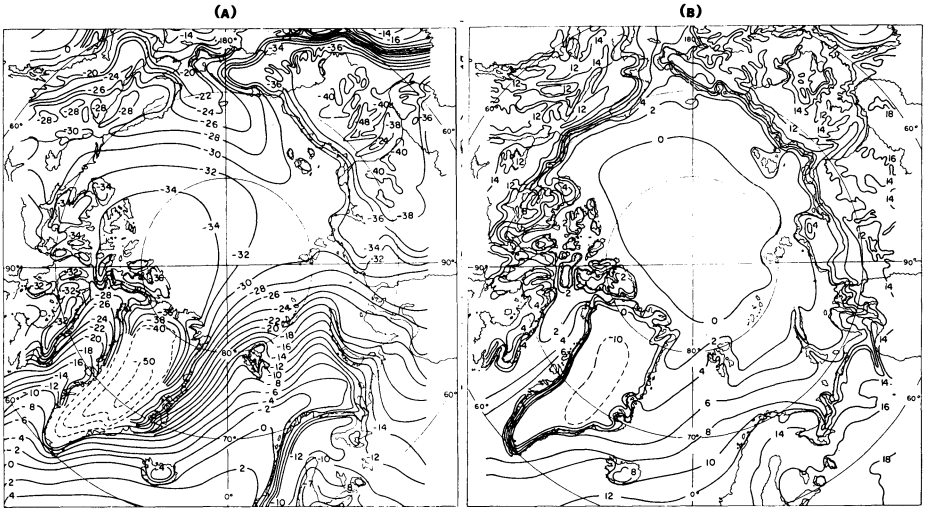

Fig. 8. Distribution of mean surface temperature in the Arctic region for (A) January (winter) and (B) July (summer) from Orvig [1970].

et al., 1988]. A thorough investigation of SBI climatology has been done in the North American Arctic [Kahl et al., 1992; Bradley et al., 1992] They form most frequently in the dark period between the end and beginning of 24 hour sunlight (mean 60 to 90% depending on location) and less frequently in summer (10 to 60%). For a variety of locations investigated, Bradley et al. [1992] showed that the inversion depth (H) was well correlated with surface air temperature (T) taking the form:

$$H = -aT + b \quad (1)$$

where "a" varies between 8.4 and 13.0 m C^{-1} (mean 10.7) and "b" between 267 and 386 m (mean 317 m). The depth is typically 700-1000 m in the winter and 200 to 400 m in the summer. An elevated inversion, not based at the ground but still in the boundary layer, occurs in summer but not often in winter.

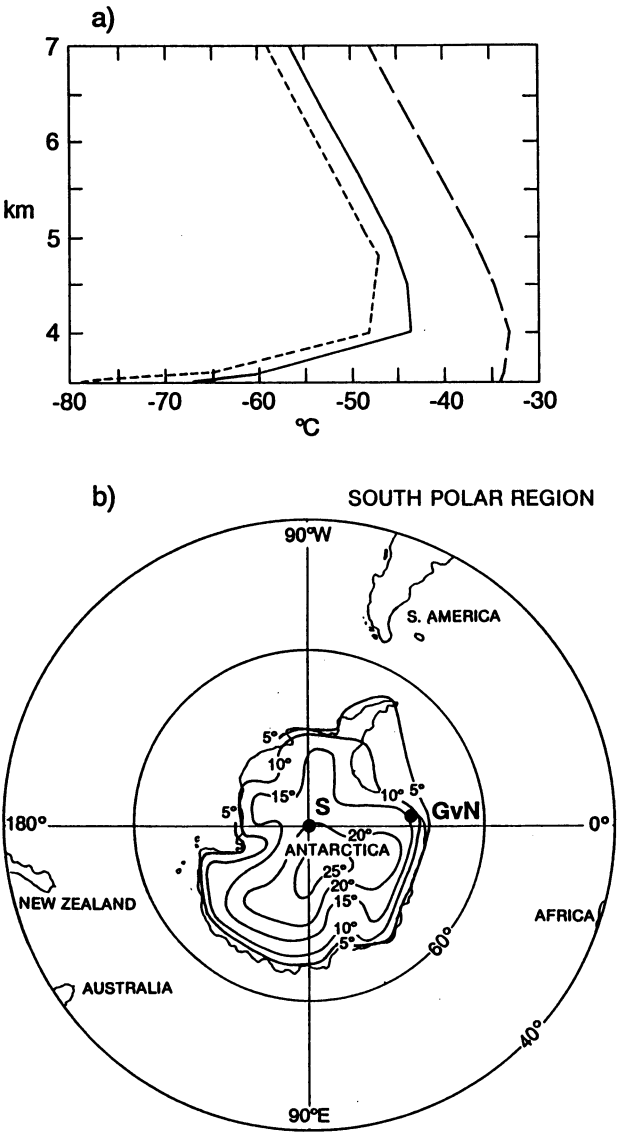

Fig. 9. a) Vertical distribution of average temperature between surface and 4 km in the summer (December, January) and winter (April-September) in Antarctica. The surface-based region of increasing temperature with height is the surface-based inversion layer (SBI). b) The spatial distribution of temperature difference across the SBI in Antarctica in winter (June-August). [From Orvig, 1970]. S - South Pole Station. GvN - Georg von Neumayer Station.

Precipitation in the polar regions is generally lower than at mid-latitudes due to the inability of air to hold water vapour at cold temperatures. Not surprisingly, there is a strong seasonal variation in precipitation paralleling that of temperature. For instance, in the Canadian high Arctic precipitation peaks in July to September at about 20 mm H_2O-equivalents per month, whereas between December and April it averages about 4 mm per month [Barrie, 1986]. In the Arctic region, annual precipitation has a large spatial variability ranging from 150 mm H_2O-equivalents near the pole to 500 mm on the periphery near major oceans [Barry, 1989]. Precipitation is higher on the route between Eurasia and the pole which is the predominant pathway of lower tropospheric air into the Arctic. Most of this precipitation falls in summer, forming a seasonal block to northward movement of pollution. In Antarctica, annual precipitation shows a spatial pattern similar to the Arctic [Schwerdtfeger, 1984], but it is much lower at the south pole (~30 mm) than at the north pole (150 mm). At sea level on the continental periphery, it is in the range 300 to 1000 mm which is similar to that over the northern oceans.

Another unique feature of the Antarctic and Arctic is the one-day, one-night per year light regime which differs markedly from that on the rest of the globe. This is illustrated in Figure 10 for Alert, Canada (82.5° N, 62.3° W). There is total darkness from 30 October to 13 February and 24 hours direct sunshine from early April to early September. At Alert, the transition between

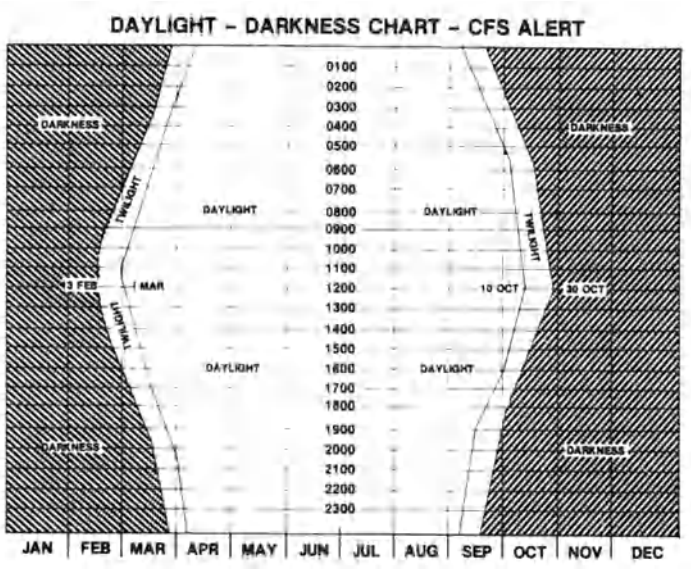

Fig. 10. A schematic showing the light regime at ground level at Alert Canada (82.5° N, 62.3 °W).

these two regimes is about 7 weeks. Meteorological changes lag behind changes in sunlight. Thus, at polar sunrise near the poles, the light regime changes rapidly from complete dark to complete light with little attendant change in meteorology. This offers a unique opportunity to study changes in the atmosphere involving photochemical reactions. As one proceeds from the pole to the periphery of the Arctic or Antarctic to the polar circle, the light regime changes to one of complete dark for only a day at winter solstice but with prolonged dark and twilight periods in winter and very long days in summer peaking at 24 hours of sunshine near summer solstice.

CHEMICAL ENVIRONMENT

The chemical environment of the northern polar region is markedly different than that of the south in many respects. First, it is much more polluted by anthropogenic emissions from surrounding continents. The emissions of sulphur dioxide in the northern hemisphere are indicators of this pollution (Figure 11). Elevated concentrations of sulphate aerosols - oxidation products of sulphur dioxide - are found throughout the polar region, particularly in winter when

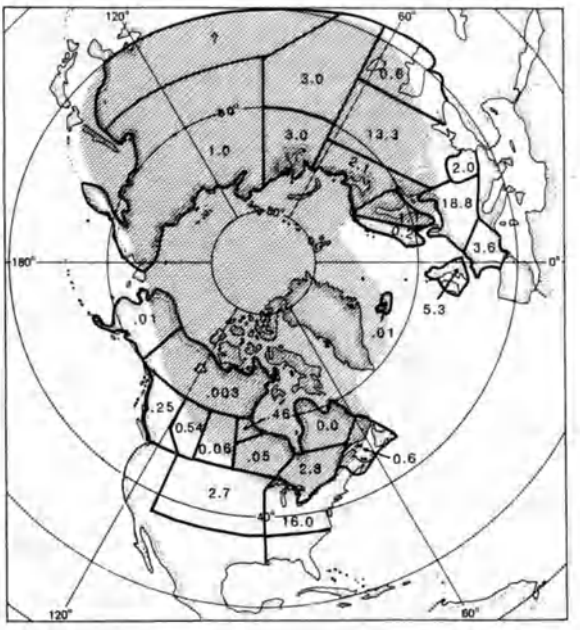

Fig. 11. Annual emissions of sulphur dioxide (megatonnes) in the northern hemisphere that influence the Arctic region [Barrie, 1986]. Representative of the early 1980s. The shaded area is the mean position of the Arctic air mass in winter.

transport out of Eurasia is strongest. Second, it tends to have more wind blown dust compounds such as clay minerals in the air arriving from surrounding continents. Third, the concentration of sea salt is higher and its seasonal variation different in the lower troposphere at the North Pole than at the South Pole.

Seasonal variations

The seasonal variations of $SO_4^=$, the sea salt tracer Na^+ and the wind blown dust tracer Al are shown in Figure 12 for Alert, Canada near the North Pole. These can be compared with a year of observations at the South Pole (Figure 13). In the Arctic, $SO_4^=$ and Na^+ are a maximum in winter and a minimum in summer. This is because north to south transport of air is stronger in winter than in summer, the removal of aerosols from the atmosphere by precipitation is strongest in summer and, in the case of sea salt, the northern oceans are stormier in winter [Erickson et al, 1986]. Soil Al peaks in the spring around April and May because of long range transport of Asian desert dust generated most intensely by dust storms at this time of year [Merrill et al., 1989]. Most of the $SO_4^=$ aerosol in winter is anthropogenic in origin [Barrie, 1986; Barrie and Barrie, 1990] while in summer, it is approximately 10% sea salt, 60% anthropogenic and 30% marine biogenic in origin [Li and Barrie, 1993]. In contrast to the Arctic, south polar aerosol S which is mainly $SO_4^=$ (Figure 13) is mainly of marine biogenic and sea salt origin [Bodhaine et al., 1987]. It peaks in summer rather than in

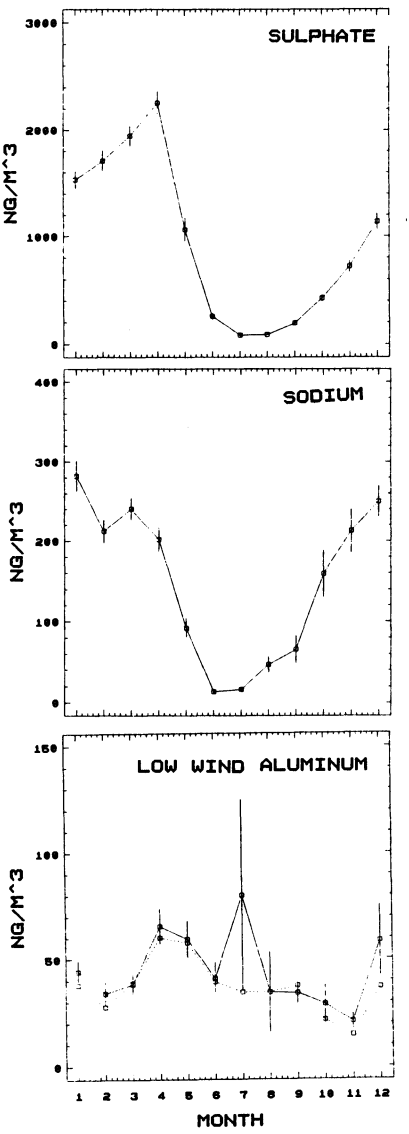

Fig. 12. Seasonal variations of aerosol $SO_4^=$, sea salt Na^+, and soil Al for winds < 20 km h^{-1} at Alert Canada (82.5° N) from 1980 to 1990. Error bars represent standard error of the monthly mean concentration. Dashed line in Al series joins monthly median values. July (month 7) is affected by local road dust.

winter. Marine biogenic emissions of the gaseous sulphur precursors are at a maximum in that season. Sea salt Na aerosols are a maximum in late winter and spring reflecting more frequent transport of air from the periphery of the Antarctic continent to the pole in that season and possibly to stronger oceanic sources of sea spray associated with more intense cold season winds.

The flux of anthropogenic sulphur into the Arctic from mid-latitudinal sources has been modelled by Barrie et al. [1989b], using observed wind fields and SO_2 emissions inventories for July 1979 to June 1980 and using observed air concentrations in northern Scandinavia to check the model. Annually, 96% of total anthropogenic sulphur inputs were from Eurasia and only 4% from North America. There is a strong seasonality of input peaking from October to April, consistent with seasonality in atmospheric circulation patterns described above and with observed $SO_4^=$ levels (Figure 12). Most of the S pollution was calculated to be entering between 0 and 2 km altitude. This latter fact is consistent with observed vertical profiles of anthropogenic pollution in the Arctic air mass that show highest concentrations in the first two kilometers of the atmosphere [Barrie, 1986]. This scenario of sulphur inputs to the Arctic has been confirmed by other model calculations [Iversen, this volume].

The seasonality of inputs of pollution to the Arctic related to transport is also reflected in the concentrations of many relatively inert gaseous tracers of pollution such as anthropogenic halocarbons, CO and CH_3Cl [Khalil and Rasmussen, 1983] which peak in the winter months of

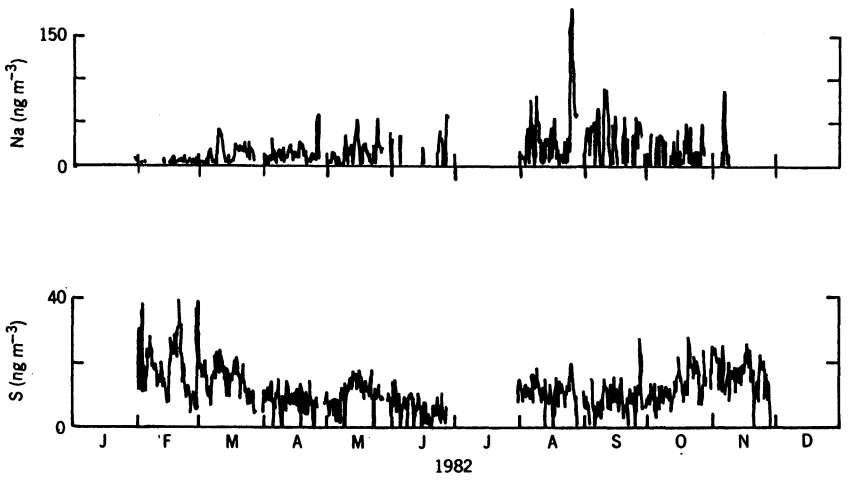

Fig. 13. Seasonal variations of the concentration of aerosol sulphur and sea salt Na at the South Pole during 1982 [Bodhaine et al, 1987]. Multiply S by 3 to get sulphate for comparison with Figure 12.

the year. Other chapters in this volume show that reactive non-methane hydrocarbons whose cycle is governed by seasonally varying destruction by OH and other radicals peak in concentration in the polar regions in the winter half of the year.

Nitrogen oxides are important reagents in the oxidant chemistry of the troposphere. It has been asserted [Bottenheim et al., 1993] that peroxyacetylnitrate (PAN) is a major component of total oxides (NO_y) in the Arctic troposphere. PAN concentrations peak in the winter half of the year at 100 to 500 ppt v and are a minimum in summer at < 10 ppt v [Barrie and Bottenheim, 1991]. A prominent peak in spring (April - May) may be related to enhanced production in the mid-latitude source regions, since a peak in transport at this time is not indicated by seasonal variations of inert tracers of anthropogenic pollution [Khalil and Rasmussen, 1983].

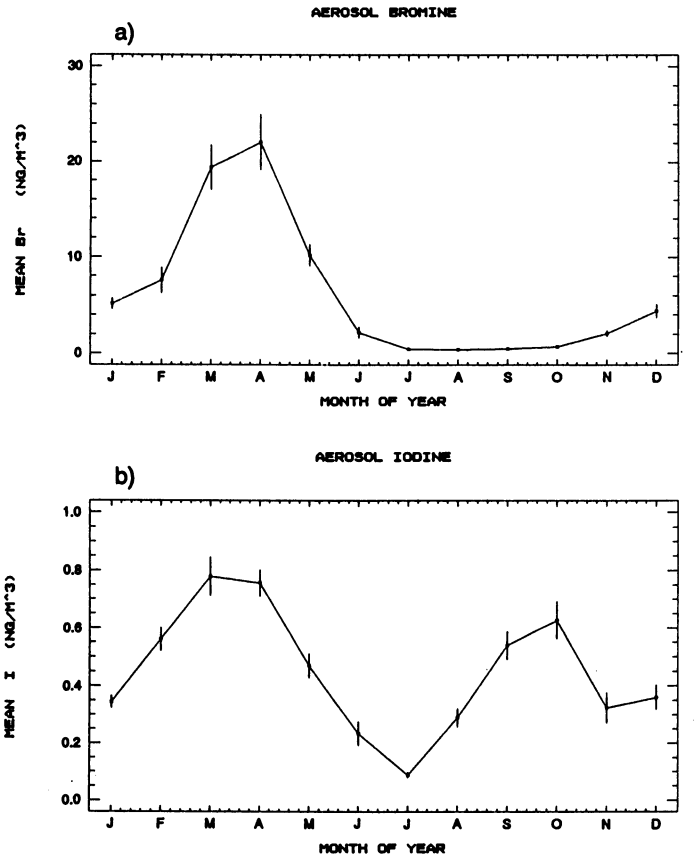

Fig. 14. The seasonal variation of (a) filterable bromine and (b) iodine concentrations at Alert in the 1980s.

Filterable Br (f-Br) and I (f-I) collected on cellulose acetate filters undergo a consistent seasonal variation throughout the Arctic [Sturges and Barrie, 1988]. The average variation at Alert for the 1980's (Figure 14) shows a polar sunrise maximum for both halogens and an additional maximum for I but not for Br in late September and early October. The spring peak occurs progressively earlier in the year as one proceeds from Alert at 82.5° N to Igloolik at 69° N as polar sunrise occurs earlier.

Arctic Polar Sunrise

There is growing evidence for considerable change in the state of the lower tropospheric Arctic at polar sunrise associated with chemical reactions induced by sunlight. These include the destruction of ozone and attendant production of f-Br and f-I [Barrie et al., 1989a] as well as an apparently unrelated increase in the fraction of total sulphur in the troposphere that exists as $SO_4^=$ as one proceeds into spring, and a decrease in free tropospheric non-methane hydrocarbon concentrations from a mid-winter peak.

Consider ground level ozone at Alert from the depth of winter into spring (Figure 15), it is relatively constant at 40 ± 5 ppb v in the dark, but as the sun rises it shows depletions departing from this level which are a maximum in April. At the same time as ozone is depleted, f-Br and bromoform gas ($CHBr_3$) peak [Barrie et al., 1988; Bottenheim et al., 1990]. The explanation for this observation at Alert is that after polar sunrise chemical reactions are induced in air in the SBI over the Arctic Ocean that lead to ozone depletion in a few days. The signal at Alert is a meteorologically modulated one alternating between undepleted free tropospheric air when winds blow off the rough terrain of Ellesmere Island, and depleted air when winds blow from the northwest to east off the Arctic ocean. A discussion of the chemistry of ozone depletion at polar sunrise is found elsewhere in this volume.

A glimpse of the conditions that prevail in the SBI over the Arctic Ocean is provided by measurement made on aircraft flights north of Alert in April 1986 [Leaitch et al., 1989]. Average vertical profiles of temperature, ozone and number concentration of particles of diameter > 0.15 μm (Figure 16) from 21 aircraft flights show that the SBI was about 900 m thick and approximately 15 °C strong. Ozone was depleted progressively to a low value at the surface. Particles change little in the vertical with concentrations of 250 cm^{-3}.

Another feature of the SBI over the Arctic ocean that may be relevant to chemistry in that layer is the type and amount of surface area available for heterogeneous reactions. Sulphuric acid particles may host chemical reactions that regenerate Br from HBr and HOBr [McConnell, this volume]. In April 1986 at Alert, particle surface area was observed to peak in the 0.3 to 0.6 μm range [Den Hartog, 1992] in which sulphate aerosols dominate. Total aerosol surface area in these particles ranged from 22 to 62 μm^2 cm^{-3}. At 40 μm^2 cm^{-3}, the surface area of aerosol in a column 1 m^2 by 900 m deep (SBI depth Figure 16) is 0.036 m^2 or 3.6% of the snow surface area

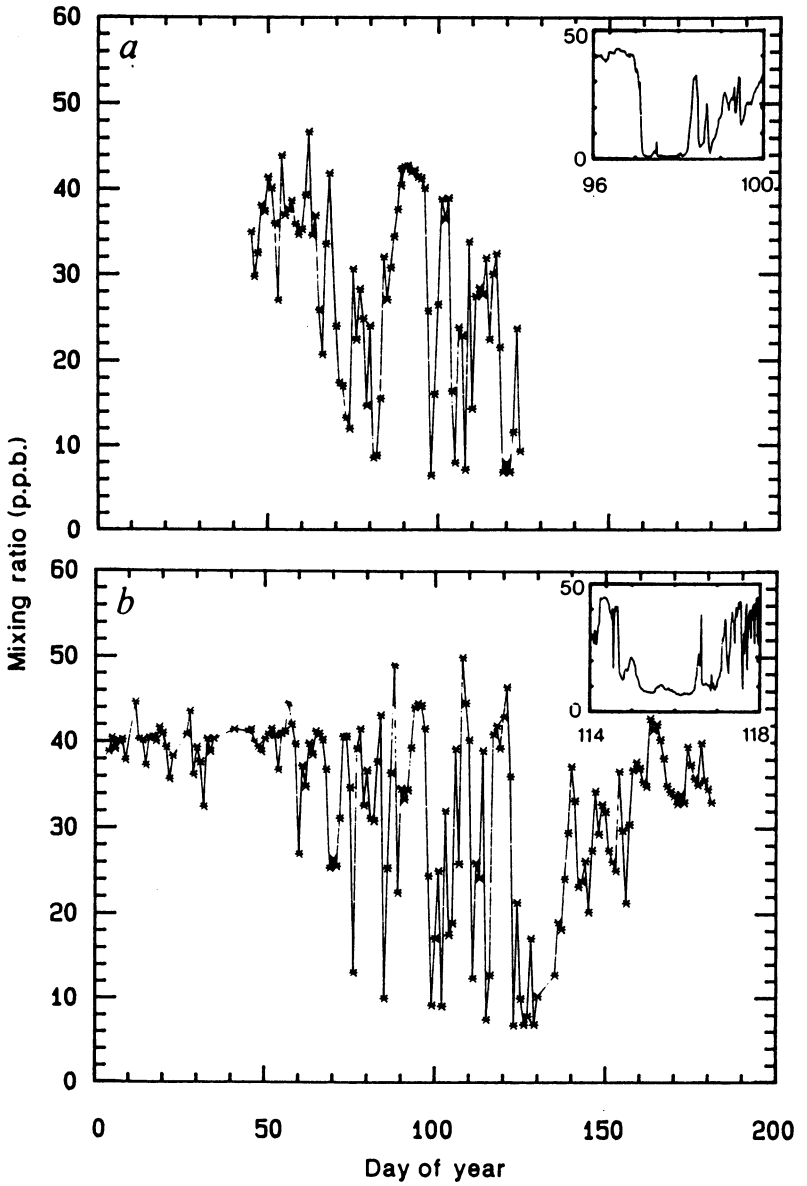

Fig. 15. Daily average concentrations of ozone observed at ground level at Alert in the Canadian high Arctic during the first half of (a) 1986 and (b) 1987 [from Barrie et al, 1988]. Insert in (a) is an expanded view of continuous ozone in a selected window from day 96 to 100.

at the bottom. In addition to sulphate aerosols and snow at the surface, ice surfaces in the form of suspended ice crystals are common.

On the basis of lidar and meteorological observations from November 1985 to April 1986 at Alert [Hoff and Leaitch, 1989], it was concluded that 2/3 of the time either blowing surface snow or ice crystals were present in the air obscuring lidar aerosol observations. During 30% of the time suitable for lidar observations, ice crystals caused greater visibility reduction than Arctic haze sulphate aerosols. Ice crystals can range in size from 1 to 1000 μm as observed by laser optical probes [Hoff and Leaitch, 1989] and in cascade impactor deposits by the author. To date, their size distributions have not been thoroughly investigated in the Arctic troposphere. If one assumes the number density of ice crystals to be 10 L^{-1} for 20 μm crystals and 1 L^{-1} for 200 μm [Trivett et al., 1988] and columnar crystals of length to width ratio 1.4, the available surface area in suspended ice is 0.011 or 0.11 m^2, respectively. This is 1 to 11% of the surface snow area available. On occasion, ice crystal concentrations can reach as high as 30 L^{-1} for particles of diameter 200 μm [Hoff and Leaitch, 1989]. The associated surface area in a 900 m by 1 m^2 column is 3.4 m^2. Thus, ice crystal surface area is highly variable and cannot be neglected relative to surface snow in calculations of ozone depletion in the SBI involving heterogeneous reactions on ice [Molina and by Ravishankara, this volume].

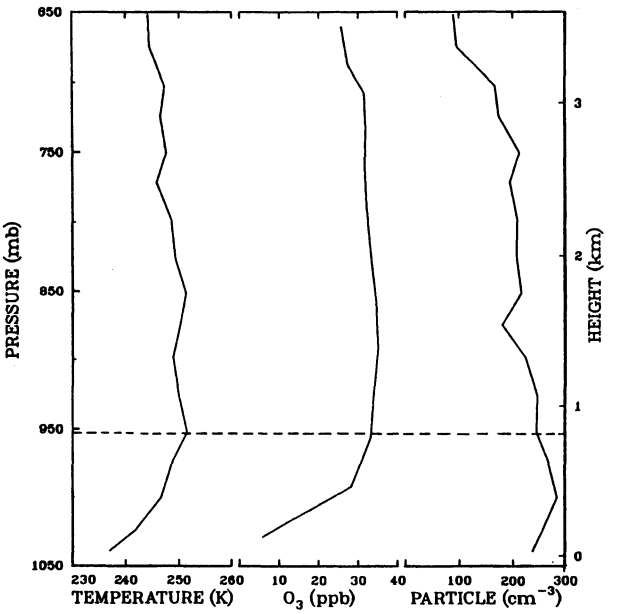

Fig. 16. Mean vertical profiles of air temperature, ozone and particle number concentration (diameter >0.15μm) above the frozen Arctic ocean north of Alert [adapted from Leaitch et al.,1989].

As mentioned above, sulphuric acid aerosols have been implicated in heterogeneous chemistry of ozone depletion at polar sunrise. Six years of observations of aerosol acidity and major ion composition at Alert have been analyzed statistically [Barrie and Barrie, 1990] to reveal two types of anthropogenic sulphate aerosols (Figure 17a). One type associated with remote anthropogenic sources comprised of $NH_4HSO_4^=$ and a second photochemical component of H_2SO_4 that originates from anthropogenic SO_2 oxidation within the Arctic. The latter increases in importance as one proceeds from winter into spring, paralleling the increase in fraction of total airborne sulphur oxide that is oxidized (Figure 17b). Thus, at polar sunrise, the anthropogenic sulphate aerosol present in the SBI over the Arctic ocean is more acidic than in the dark. It is present at sulphate concentrations of 1 to 4 $\mu g\ m^{-3}$.

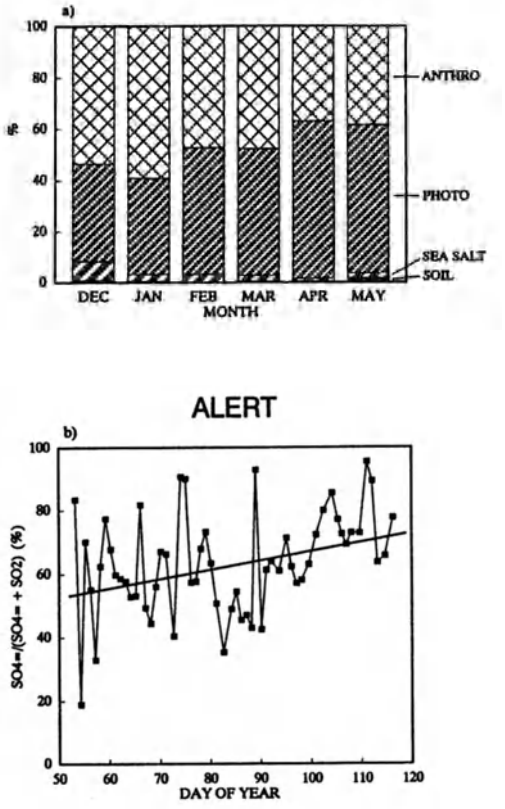

Fig. 17. a) Components of aerosol sulphate at Alert as deduced by Barrie and Barrie [1990]. b) Trends in fractional amount of total atmospheric sulphur oxides that are oxidized to sulphate at Alert in 1988.

Evidence of Stratospheric Influence on Ground Level Arctic Air Composition

Beryllium 10 and 7 isotopes are produced cosmogenically in the atmosphere at a molar ratio Be-10/Be-7 of approximately 0.6 [McHarque and Damon, 1991]. In the polar regions, maximum production occurs at about 15 km altitude well into the stratosphere. Further south, the production maximum falls partly in the stratosphere and partly in the troposphere. Be-10 is a long lived isotope (1.5 million years) while Be-7 has a half life of only 53.2 days. An indication of how much stratospheric air is influencing ground level ozone concentrations can be obtained from observations of these isotopes in ground level air at Alert (Figure18) over a period of one year. With the exception of a few deviations down to 1 and up to 4, the ground level ratio of Be-10 to Be-7 is close to 2.2 corresponding to a transit time from the point of formation of 300 days. This is much longer than northern tropospheric mixing times and suggests a stratospheric source. The absolute concentrations of both isotopes peaked in the period March to May, suggesting stronger stratospheric-tropospheric exchange at that time of year. Calculations of the fraction of surface level air that is stratospheric (X) made using a simple two source (stratospheric and tropospheric) mixing model with this data [Dibb et al., 1992] indicate that depending on the level of stratospheric air, X is between 0.1 and 3.5% peaking in the spring when the surface Be peaks. The results suggest substantial contributions of stratospheric ozone sources to tropospheric ozone, but do not preclude the possibility that some ozone is produced by high nitrogen oxide photochemistry in the troposphere. The constancy of ozone concentrations during dark winter at ground level (Figure 15) implys that whatever the source, ozone is produced, mixed well and not destroyed rapidly in such a way that relatively constant concentrations at the ground are maintained. After polar sunrise, however, the picture changes. The breakup of the polar stratospheric vortex and photochemical destruction at the surface within the Arctic increases the variance in observed ground level ozone concentrations. In the Antarctic region at the South Pole and at Georg von Neumayer Station (Figure 18), Be-7 at ground level has a weak seasonal cycle with a maximum in local summer [Wagenbach et al., 1988].

CONCLUSION

The arctic and antarctic tropospheres are very different geographical, climatic and chemical environments. The north surrounded by industrialized continents is much more impacted by pollutants that affect ozone chemistry than is the south. Furthermore, it is underlain by a biologically active ocean while the south is ringed by ocean. The north contains a relatively small contiguous area of glaciation while the southern continent is mostly glacier.

Free tropospheric ozone in the north is changing differently than that in the south, but is this change due to natural or anthropogenic factors? There is widespread destruction of ozone in the atmosphere at or near the surface of the Arctic ocean at polar sunrise that has not been

observed in Antarctica. Is this due to differences in natural environment or is pollution playing a role? Is the ozone depletion observed in the SBI at polar sunrise occurring in the free troposphere but masked by vertical mixing? To what degree do chemical reactions effecting ozone destruction in the stratosphere apply to this lower tropospheric ozone destruction and vice versa? What is the magnitude of the ozone surface sink relative to other sources/sinks in the northern troposphere? These are all questions that need to be addressed by a multi-disciplinary group such as that gathered here.

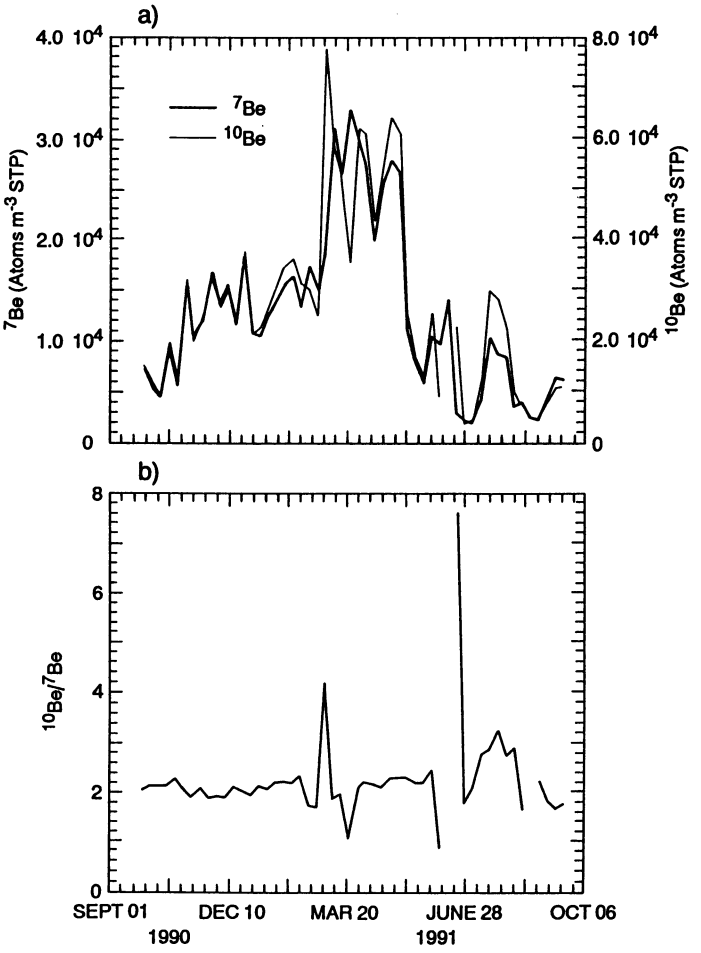

Fig. 18. Observed ground level concentrations (a) and ratio (b) of Be-10 and Be-7 in aerosols at Alert September 1990 to September 1991 [Dibb et al, 1992].

REFERENCES

Barrie, L.A. and J.W. Bottenheim, Sulphur and nitrogen pollution in the Arctic atmosphere, in Ed. W. Sturges, *Pollution of the Arctic Atmosphere*, Elsevier Press, 334 pp., 1991.

Barrie, L.A. and M.L. Barrie, Chemical components of lower tropospheric aerosols in the high Arctic: Six years of observations, *J. Atmos. Chem., 11*, 211-266, 1990.

Barrie, L.A., G. den Hartog, J.W. Bottenheim and S. Landsberger, Anthropogenic aerosols and gases in the lower troposphere at Alert, Canada in April 1986, *J. Atmos. Chem., 9*, 101-127, 1989a.

Barrie, L.A., M.P. Olson and K.K. Oikawa, The flux of anthropogenic sulphur into the Arctic from mid-latitudes, *Atmos. Environ., 23*, 2502-2512, 1989b.

Barrie, L.A., J.W. Bottenheim, R.C. Schnell, P.J. Crutzen and R.A. Rasmussen, Ozone destruction and photochemical reactions at polar sunrise in the lower Arctic atmosphere, *Nature, 334*, 138-141, 1988.

Barrie, L.A., Arctic air pollution: an overview of current knowledge, *Atmos. Environ., 20*, 643-663,1986.

Barry, R.G., The present climate of the Arctic Ocean and possible past and future states, *in The Arctic Seas, (Ed. Y. Herman)*, Van Nostrand Reinhold Company, New York, 888 pp., 1989.

Barry, R.G. and R.J. Chorley, Atmosphere, weather and climate, *5th Ed., Methuen Press*, London, 460 pp., 1987.

Bodhaine, B.A., J.J. Deluisi, J.M. Harris, P. Houmere and S. Bauman, PIXE analysis of south pole aerosol, *Nuclear Instruments And Methods in Physics Research, B22*, 241-247, North Holland Amsterdam, 1987.

Bottenheim, J.W., L.A. Barrie, E. Atlas, L.E. Heidt, H. Niki, R.A. Rasmussen and P.B. Shepson, Depletion of lower tropospheric ozone during Arctic Spring: The polar sunrise experiment 1988, *J. Geophys. Res., 9*, 101-127, 1990.

Bottenheim, J.W., L.A. Barrie and E. Atlas, The partitioning of nitrogen oxides in the lower arctic troposphere during spring 1988, *J. Atmos. Chem.*, in press, 1993.

Bradley, R.S., F.T. Keimig and H.F. Diaz, Climatology of surface-based inversions in the North American Arctic, *J. Geophys. Res., 97*, 15699-15712, 1992.

Den Hartog, G, personal communication, recalculated from PMS probe data reported in Barrie et al., 1989a, 1992.

Dibb, J.E., R.C. Finkel, J. Southon, M. Caffee, and L.A. Barrie, Stratospheric influence on surface air at Alert: evidence from Be^7, Be^{10} and O_3, Proc. Fall AGU Meeting, *EOS, 73 (43)*, 93, 1992.

Erickson, D.J. J.T. Merrill and R. Duce, Seasonal estimates of global atmospheric sea salt distributions, *J. Geophys. Res., 91D*, 1067-1072, 1986.

Hoff, R.M. and W.R. Leaitch, 1989, Ground-based cirrus clouds in the Arctic, *in Symp. on the Role of Clouds in Atmospheric Chemistry and Global Climate, 324-327, Anaheim California, Amer. Met Soc. Boston Mass*, 1989.

Kahl, J.D., M.C. Serreze and R.C. Schnell, Tropospheric low-level temperature inversions in the Canadian Arctic, *Atmosphere-Ocean, 30 (4)*, in press, 1992.

Khalil, M.A.K. and R.A. Rasmussen, Gaseous tracers of arctic haze, *Envir. Sci. Technol., 17*, 157-164, 1983.

Leaitch, W.R., R.M. Hoff and J.I. MacPherson, Airborne and lidar measurements of aerosol and cloud particles in the troposphere over Alert, Canada in April 1986, *J. Atmos. Chem., 9*, 187-212, 1989.

Li, S.M. and L.A. Barrie, Biogenic sulphur aerosols in the arctic troposphere I: contribution to total sulphate, *J. Geophys. Res., 98D*, submitted, 1993.

McHarque, L.R. and P.E. Damon, The global beryllium 10 cycle, *Reviews of Geophysics*, 29, 141-158, 1991.

Merrill, J.T., M. Uematsu and R. Bleck, Meteorological analysis of long range transport of mineral aerosols over the North Pacific, *J. Geophys. Res., 94D*, 8584-8598, 1989.

Nakamura, N. and A.H. Oort, Atmospheric heat budgets of the polar regions, *J. Geophys. Res., 93D*, 9510-9524, 1988.

Orvig, S., Climates of the polar regions, *World Survey of Climatology Series, Vol.14, Elsevier, Amsterdam, 367 pp.*, 1970.

Sturges, W.T. and L.A. Barrie, Chlorine, bromine and iodine in Arctic aerosols, *Atmos. Envir., 22*, 1179-1194, 1988.

Trivett, N.B.A., L.A. Barrie, J.W. Bottenheim, J.-P. Blanchet, G. den Hartog, R.M. Hoff and R.E. Mickle, An experimental investigation of Arctic haze at Alert, N.W.T., March 1985, *Atmos. Ocean. 26 (3)*, 341-376, 1988.

Wagenbach, D., U. Görlach, K. Moser and K.O. Münnich, Coastal Antarctic aerosol: The seasonal pattern of its chemical composition and radionuclide content, *Tellus, 40B*, 426-436, 1988.

CLIMATOLOGY OF ARCTIC AND ANTARCTIC TROPOSPHERIC OZONE

Samuel J. Oltmans
Climate Monitoring and Diagnostics Laboratory
National Oceanic and Atmospheric Administration
325 Broadway
Boulder, Colorado 80303
U.S.A.

INTRODUCTION

Ozone in the troposphere, though it represents only a relatively small fraction of the total column amount, is now recognized for its important role in the chemical and radiative balance of the atmosphere. Because of the lower tropopauses found in the polar regions, the contribution of the tropospheric component to the total column ranges from about 3-15%. In the north polar region the contribution falls in a narrower range of about 5-8%. Over Antarctica, during the spring when stratospheric ozone depletion is severe, the troposphere can comprise up to 15% of the total, otherwise it is about 3-5%. In the polar regions, there are several unique characteristics that play an important role in determining the distribution of ozone in the troposphere [Oltmans, 1992]. These include the extremely cold winter temperatures, long periods of darkness and sunlight, and transport regimes that may incorporate ozone precursors into polar latitudes or mix ozone from the stratosphere into the troposphere. Sources of anthropogenic ozone precursors are significant primarily in the northern hemisphere (NH).

In the NH, there are several high latitude locations where regular ozone vertical profile measurements have been made. At two sites in Canada--Churchill (60° N), near the southern edge of the polar region, and Resolute (75° N), at a higher polar latitude--longer term records are available that provide an opportunity to assess possible ozone trends in the arctic troposphere. In addition, shorter records at Barrow, AK (71° N) and Alert, NWT (82° N) give a picture of the seasonal variation over a wide range of polar latitudes.

At Barrow the 20-year surface ozone record is examined for seasonal and long-term variability. This high resolution (hourly) time series is compared to the surface observations from the ozonesonde stations where observations are made about once a week.

In the Antarctic, ozonesonde data from South Pole (90° S) and Syowa (69° S) give a representative picture of conditions from the coast to the interior of the continent. At South Pole, the 17-year surface ozone record is examined for long-term changes.

NATO ASI Series, Vol. I 7
The Tropospheric Chemistry of Ozone in the Polar Regions
Edited by H. Niki and K. H. Becker

SEASONAL VARIATIONS

In the lower troposphere at the more southerly arctic location of Churchill, there is a definite spring (MAR-APR-MAY) maximum (Figure 1a), while in the upper troposphere the maximum occurs during the summer (JUN-JUL-AUG) but with relatively high values in the spring as well. The upper troposphere summer maximum is probably related to the persistent stratosphere/troposphere exchange observed by Browell et al. [1992]. Summer is also the season of the steepest gradient between the upper troposphere and surface, while during the winter this gradient is a minimum.

At Resolute [Figure 1b], the picture in the lower troposphere is quite different with MAR-APR-MAY having the lowest amounts near the surface and with summer and spring values nearly identical through the troposphere. Autumn and winter patterns are similar to those at Churchill. Figure 2 shows the seasonal values for Churchill, Barrow, Resolute, and Alert for spring (2a) and autumn (2b) and brings out the marked difference in the lowest level of the spring troposphere between Churchill and the higher latitude sites. At mid-tropospheric levels, Churchill and Barrow have more ozone than Resolute and Alert, which means there is a much sharper boundary layer gradient at Barrow. During the autumn, all four sites have nearly identical tropospheric ozone amounts.

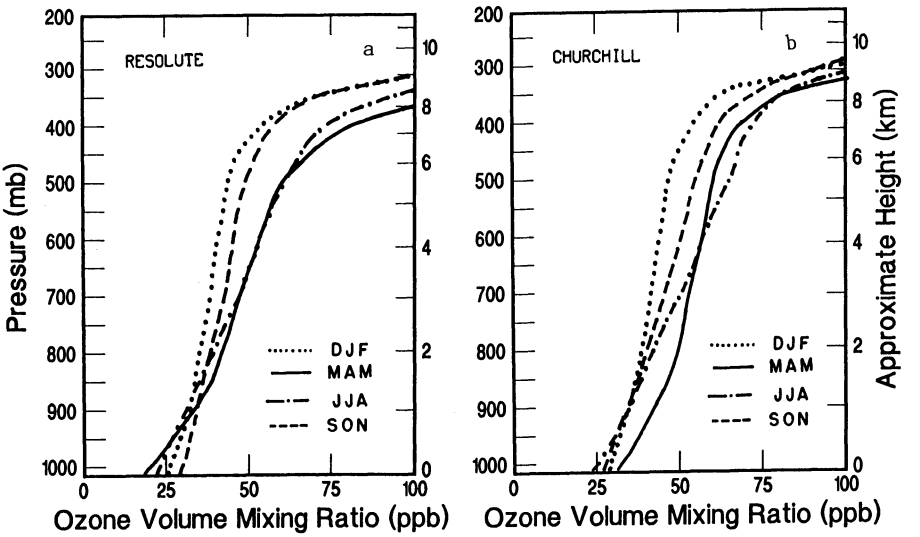

Fig. 1: Seasonally averaged ozone mixing ratio profiles in the troposphere for a) Churchill and b) Resolute.

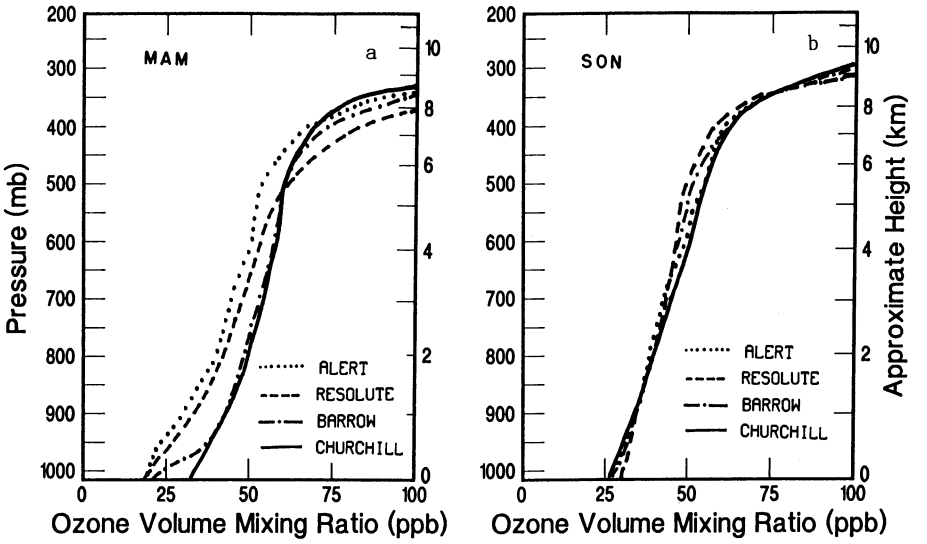

Fig. 2: Spring (a) and autumn (b) ozone mixing ratio profiles for Churchill (-----), Barrow (-·-·-), Resolute (- - -), and Alert (·····).

The more detailed seasonal pattern can be seen in Figure 3 where the smoothed (.25, .50, .25) monthly means are shown for several tropospheric levels and one lower stratospheric level 125 mb (~5 km). At the surface, the dramatically lower values during MAR-JUN at the Arctic Ocean sites compared to Churchill is very apparent. By 850 mb (~1.5 km) the spring minimum at Barrow has disappeared and ozone amounts are similar to those at Churchill. At 700mb (~3 km), all sites show a spring maximum while at 500 mb (~6 km) at Churchill, the maximum is not reached until summer. By 300 mb (~9 km), the differing average height of the tropopause becomes the controlling mechanism for ozone variations at each site. In the lower stratosphere (125 mb), the seasonal maximum occurs in the winter at Churchill but in March at the other locations. At a site in northern Finland (67° N) there is little evidence of a spring decline in the boundary layer [Taalas and Kyrö, 1992], and in fact in the lowest 3 km there is a spring maximum. This is further evidence that the spring depletion is associated with ice covered areas of the Arctic Ocean.

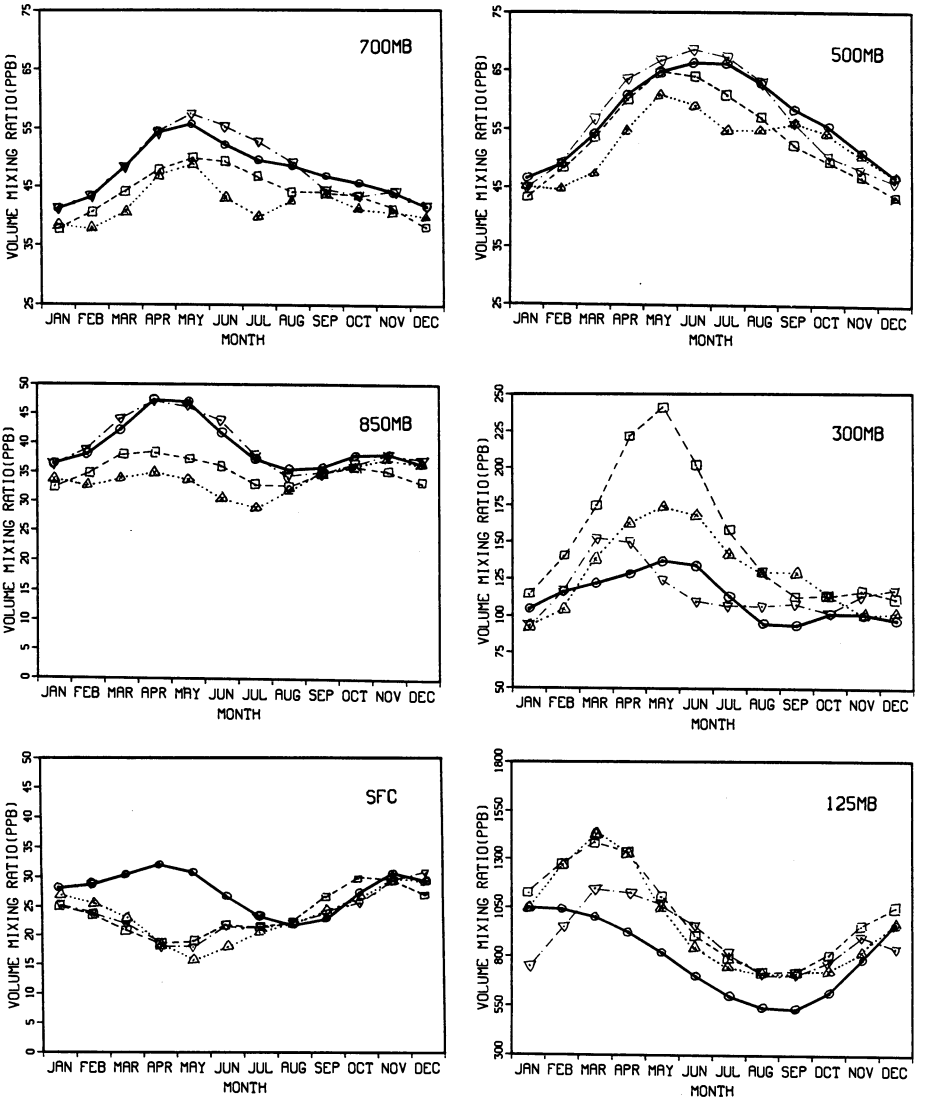

Fig. 3: Smoothed monthly average ozone mixing ratios at the surface, 850mb (~1.5 km), 700 mb (~3 km), 500 mb (~6 km), 300 mb (~9 km), and 125 mb (~15 km) at Churchill (-----), Barrow (-·-·-), Resolute (- - -), and Alert (·····).

LONG-TERM VARIATIONS IN THE ARCTIC

The locations making long-term tropospheric ozone measurements in the arctic are limited to the surface record at Barrow and the ozonesonde profiles from Resolute and Churchill. At Resolute ozonesonde measurements began in 1966 and continue to the present. Beginning in December 1979, the type of ozonesonde was switched from the Brewer-Mast sonde to the electrochemical concentration cell (ECC) sonde. Because of differences in the operation of these sondes, the two data sets are considered separately, although others have attempted to combine them [London and Liu, 1992; Bojkov and Reinsel, 1985] and have obtained quite different results. At Churchill, the ozone profiles began in 1973 and the switch of instrument types took place in September 1979. Data through 1990 are used at each site. The surface record at Barrow spans the 20-year period 1973-1992.

Figure 4 shows the trend of annual mean values at Resolute for three layers encompassing the troposphere. For all three layers, SFC-700 mb, 700-500 mb, and 500-300 mb (corresponding to approximately 3 km intervals from the surface to 9 km), there is a clear difference in the trend between the earlier period (1966-1979) and the more recent data (1980-1990). In the earlier period there is a statistically significant increase in the lower two layers based on a linear fit (Table 1). For the later period the decrease is significant for all three layers. At least in the lowest two layers, there is some suggestion that a discontinuity exists between the two periods with different instrument types. At Churchill, the disparity between the two periods is pronounced (Figure 5). The pattern is similar to that at Resolute, however, with increasing values during the period when the Brewer-Mast sonde was in use and decreasing amounts during the time the ECC sonde has been used. The trend pattern at Resolute for the two periods also differs in that the seasonal trends during the later period show uniform decreases during all seasons at all levels (Table 1), while during the period prior to 1979 the increases are primarily a spring and summer phenomena (Figure 6). At Churchill the 1980-1990 period shows declines during all seasons. The short record at Churchill in the earlier period makes any conclusions about the seasonal trends unreliable. This may indicate that the mechanism for the trends is different in the two periods, and that the declines since 1980 are not necessarily a result of an abatement in the causes for the increases prior to that time.

During each of the periods studied there was a decline in the stratospheric ozone amounts, particularly during the earlier period when tropospheric ozone was increasing. Thus, long-term tropospheric changes do not appear to be a reflection of stratospheric changes.

At Edmonton and Goose Bay, two Canadian stations at 54° N, there are also long records of ozonesonde measurements. The pattern of trends at these sites is different than that seen at the more northerly Canadian locations (Figure 7). Though both sites show the

Table 1. Seasonal trends in percent per year with the 95% confidence interval based on Student's t-test

	Dec-Jan-Feb	Mar-Apr-May	Jun-Jul-Aug	Sep-Oct-Nov	Annual
Resolute (1966-79)					
sfc-700 mb	0.57±1.80	1.49±1.61	1.92±1.86	0.72±2.30	1.17±1.41
700-500 mb	-0.08±1.52	1.56±0.86	1.64±1.25	1.12±2.03	1.12±1.07
500-300 mb	-1.47±2.05	1.86±3.53	-1.31±2.19	1.10±1.83	0.19±1.53
Resolute (1980-90)					
sfc-700 mb	-1.91±2.41	-1.95±2.32	-2.02±1.90	-1.86±1.32	-1.95±1.09
700-500 mb	-2.66±2.12	-1.29±1.45	-1.24±1.90	-1.49±1.82	-1.56±0.62
500-300 mb	-2.38±4.48	-3.63±4.44	-0.43±1.73	-0.77±1.66	-1.67±1.79
Churchill (1974-79)					
sfc-700 mb	4.34±11.3	2.14±4.49	-1.76±4.94	-1.55±4.71	1.43±3.60
700-500 mb	1.83±8.12	2.92±7.49	-2.76±4.25	-1.52±6.06	0.61±3.98
500-300 mb	2.68±10.5	-0.46±8.86	-0.66±12.2	3.05±7.31	1.25±5.80
Churchill (1980-90)					
sfc-700 mb	0.14±1.65	-0.74±1.96	-1.14±1.54	-1.88±1.58	-0.99±1.00
700-500 mb	-0.68±1.35	-0.19±1.57	-0.97±1.40	-2.78±1.45	-1.20±0.73
500-300 mb	-2.10±2.87	-0.40±2.22	-2.27±2.38	-2.42±2.43	-1.78±1.38
Edmonton (1971-79)					
sfc-700 mb	-0.90±2.13	-0.91±2.62	-1.20±4.59	-2.17±3.18	-0.83±2.05
700-500 mb	-0.68±2.70	-0.18±1.15	0.01±2.88	-1.92±2.40	-0.30±1.54
500-300 mb	-1.08±4.49	0.30±1.36	0.23±4.66	-2.05±3.88	-0.24±2.41
Edmonton (1980-90)					
sfc-700 mb	0.82±2.26	1.08±2.15	1.60±2.46	1.49±1.90	1.35±1.83
700-500 mb	-0.37±1.80	0.04±1.32	0.43±1.67	0.63±1.36	0.23±0.95
500-300 mb	0.01±2.12	-0.25±2.49	-0.56±2.37	0.33±1.40	-0.13±1.24
Goose Bay (1969-80)					
sfc-700 mb	-0.70±2.48	-0.01±2.22	-1.09±2.72	-0.74±3.81	-0.51±1.70
700-500 mb	-0.75±2.46	0.23±2.28	0.14±2.72	-0.16±3.08	-0.06±1.50
500-300 mb	-1.58±2.82	-4.23±2.25	-0.76±2.82	-1.91±3.81	-1.78±1.43
Goose Bay (1981-90)					
sfc-700 mb	-0.78±1.56	-0.58±2.52	-0.43±2.21	-0.67±1.42	-0.63±1.56
700-500 mb	-1.43±1.06	-0.61±1.68	-0.72±1.62	0.00±1.36	-0.64±1.21
500-300 mb	1.12±2.51	1.10±2.63	-0.66±5.01	-0.14±2.16	0.53±2.01

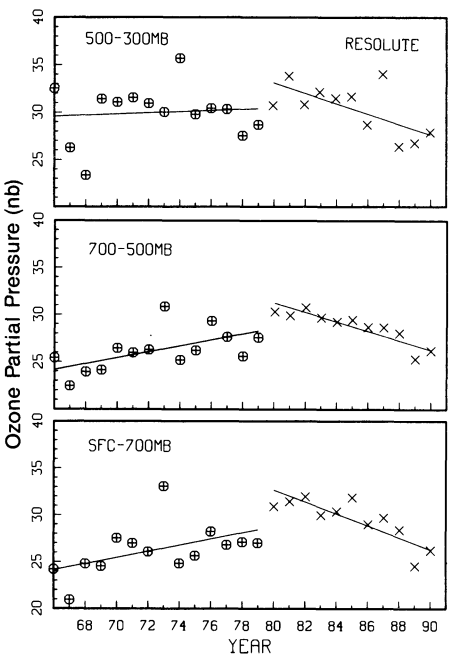

Fig. 4: Annual average ozone mixing ratios at Resolute (0 for values prior to 1980 and X for 1980 and later). The line is a linear least squares fit to the data.

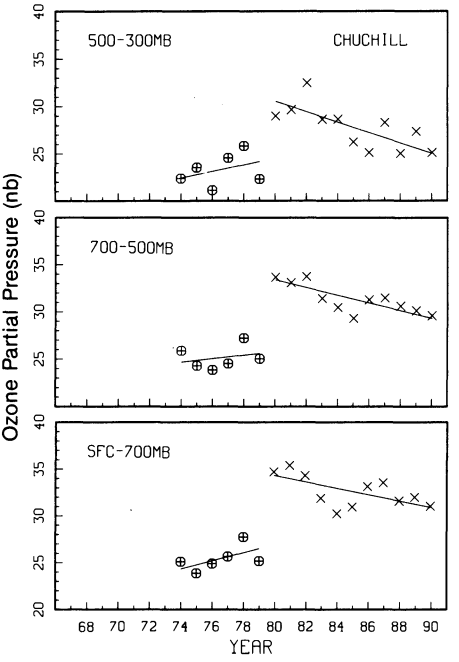

Fig. 5: As in Fig. 4 but for Churchill.

strong discontinuity at the time of change in the type of ozonesonde used, the tendency for increasing values during the period prior to 1980 is not evident. Also, during the period after 1980 there are not the nearly uniform decreases seen at Resolute and Churchill. In fact, there is no evidence for increasing ozone amounts at either Goose Bay or Edmonton except in the lowest layer at Edmonton after 1980. This increase is primarily a summer and autumn phenomena (JUN-NOV). Edmonton is the only one of the Canadian stations located near an urban area and the increases may reflect photochemical ozone production in a location with ample emissions of ozone precursors. The different trend pattern seen at Edmonton and Goose Bay from that at Resolute and Churchill strongly suggests that the trends are not an artifact of the procedures used for making the measurements since uniform procedures have been used throughout the Canadian network. It is also clear that at all of the sites there is a shift to higher values at the time of the switch in ozonesonde types, and it is highly questionable whether an overall trend should be determined that combines the records from the two instrument types.

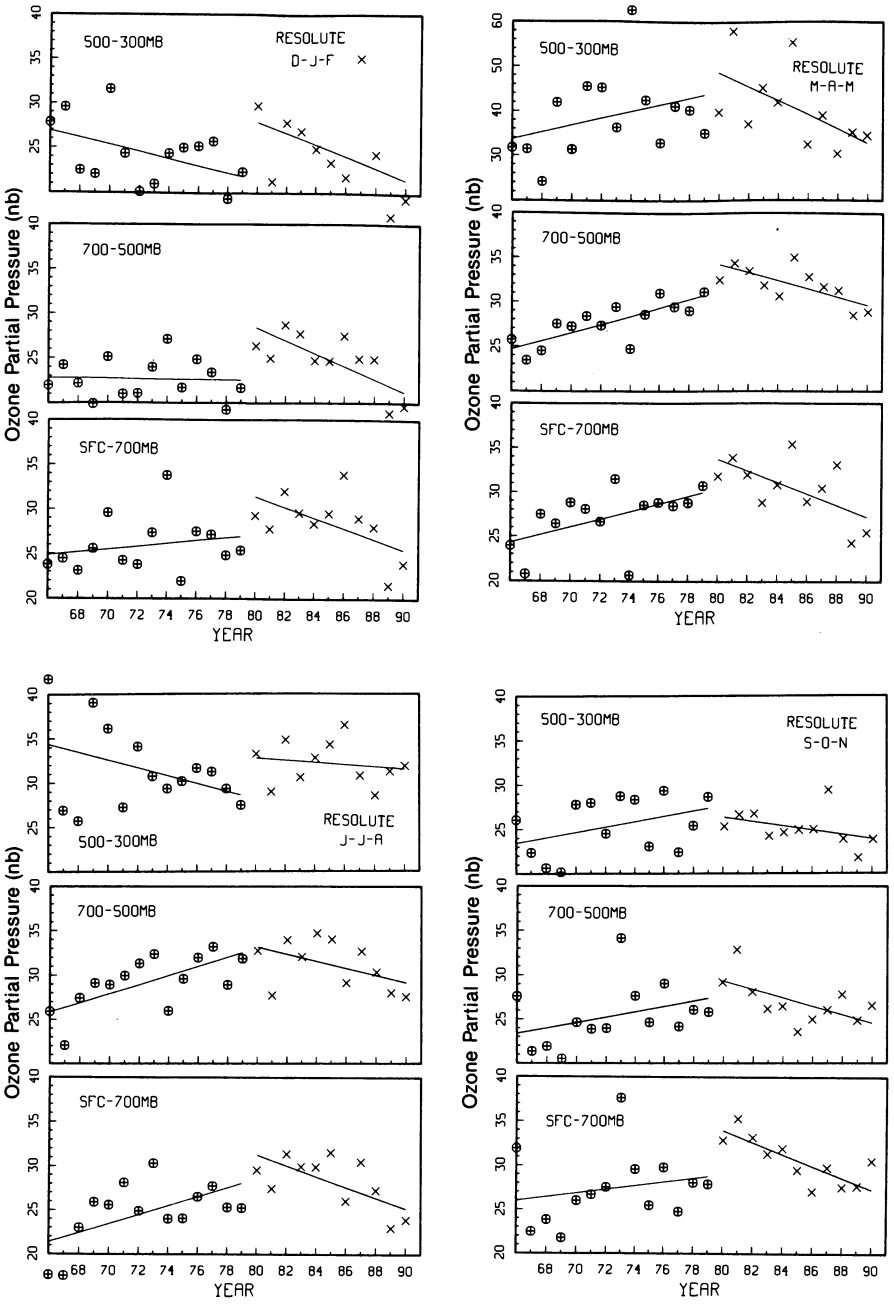

Fig. 6: As in Figure 4 but seasonal values (DEC-JAN-FEB and JUN-JUL-AUG)

From the essentially continuous record of surface ozone observations at Barrow (Figure 8), it is apparent that there has been an overall increase in concentration. The linear trend is 0.70%/yr with a 95% confidence limit based on the Student's t-test of 0.30%/yr. This trend is highly seasonally dependent (Figure 9) with large increases (~1%/yr or more) in every month from May through September. This amounts to more than a 25% increase over the 20 years of observations. Since the season of strong increase also is the one of maximum solar isolation, the possibility of photochemical production of ozone exists. Jaffe [1991] has suggested the increase at Barrow may be related to petroleum extraction activities on the North Slope of Alaska that began in the mid-1970's and evidently produces significant amounts of NO_x. That the source of the enhanced ozone concentrations is the result of relatively nearby emission of ozone precursors (Prudhoe Bay is approximately 300 km from Barrow) is suggested by the fact that ozone levels have decreased over the same period at Resolute.

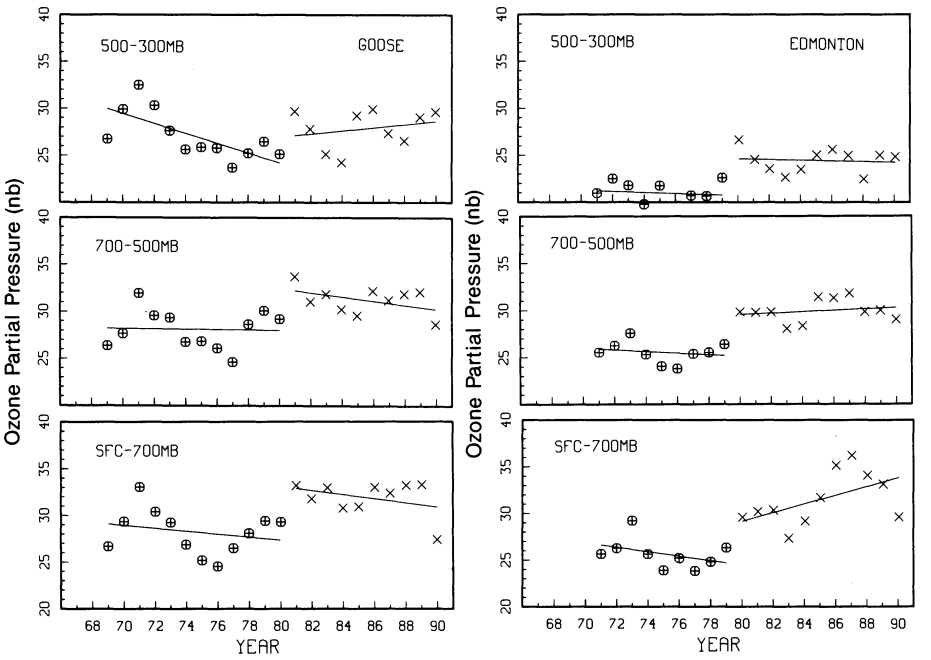

Fig. 7: As in Figure 4 but for Edmonton and Goose Bay. JUL-AUG) at Resolute.

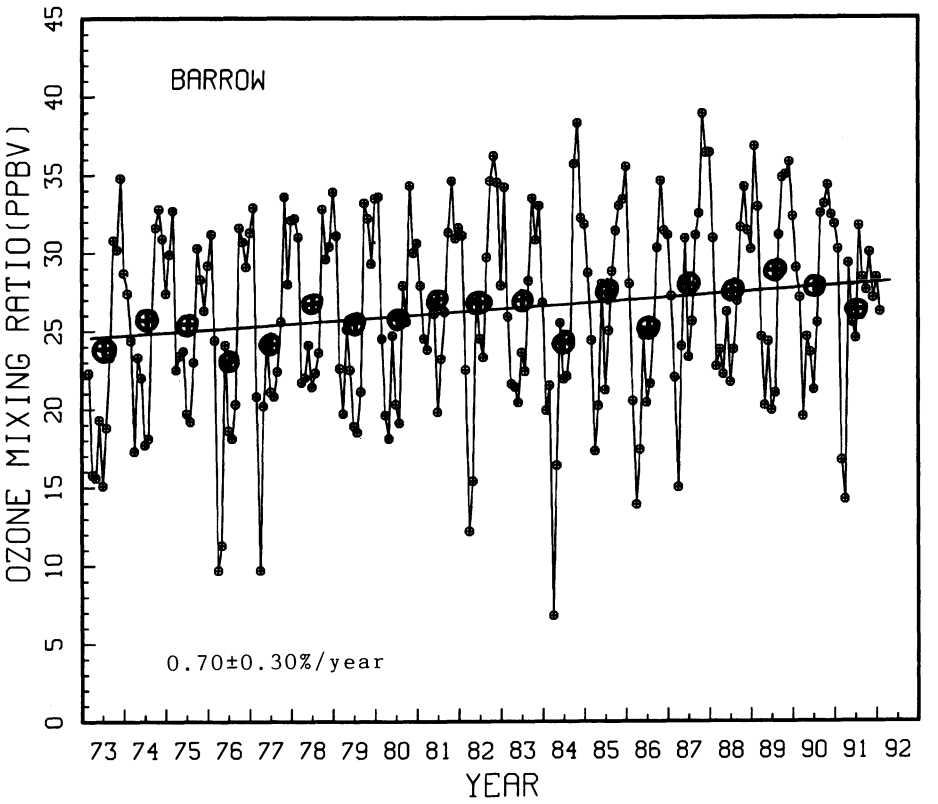

Fig. 8: Monthly surface ozone mixing ratios at Barrow. The line through the data is a linear fit to the monthly anomalies.

SEASONAL VARIATIONS IN THE ANTARCTIC

There are two sites on the Antarctic continent with relatively lengthy records of year-round profile measurements. At Syowa (69° S) on the coast of Antarctica, measurements were begun in 1966, but most years do not have a complete record of observations. Although this prevents using the record for long-term trend determination, there are sufficient data to determine averaged patterns. At South Pole (90° S) regular soundings were begun in 1986. Figure 10 shows the seasonal variation with altitude for Syowa. Throughout the entire troposphere except in the region near the tropopause (above 8 km), the seasonal maximum is during the winter (DEC-JAN-FEB) while the minimum is during the summer. Figure 11 shows the seasonal values (DEC-JAN-FEB, JUN-JUL-AUG) for South

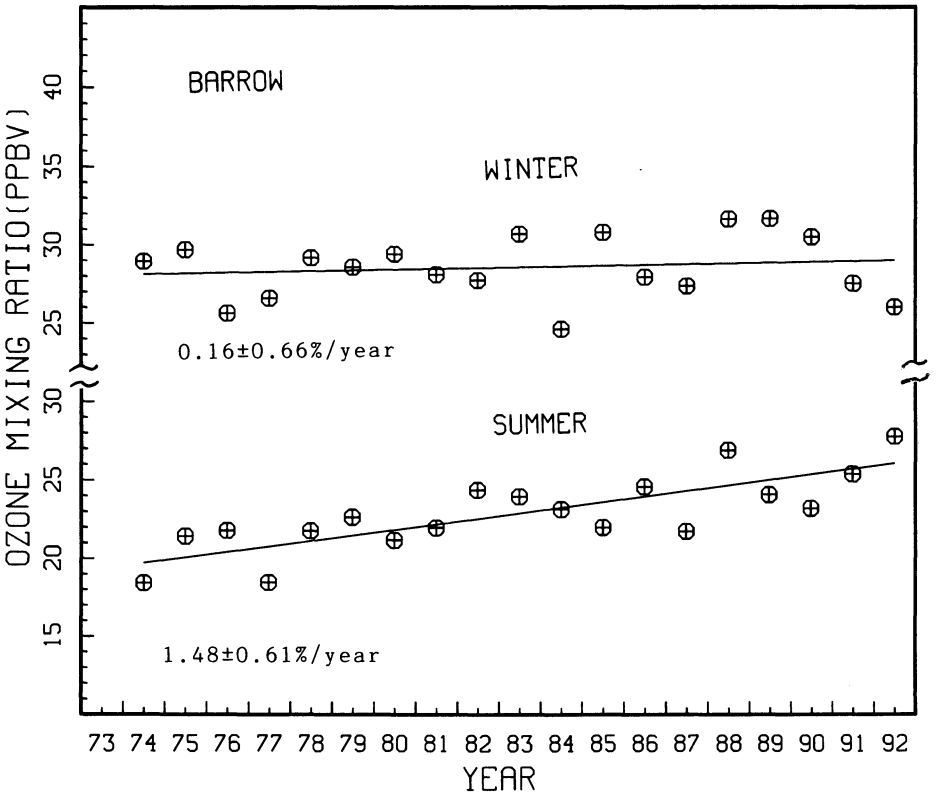

Fig. 9: Seasonal ozone mixing ratios at Barrow for summer (MAY-SEP) and winter (OCT-APR) with the linear fit to the data.

Pole with those from Syowa. Below the tropopause region (<8 km), they are essentially the same. This implies that processes operating on a continent-wide scale are responsible for this seasonal variation. In the upper troposphere near the tropopause, the seasonal cycle reverses with a maximum in the summer (South Pole) or autumn (Syowa). There is also a change in the spatial gradient at these altitudes (300 mb) with South Pole having more ozone during the summer but less during the remainder of the year.

LONG-TERM VARIATIONS IN THE ANTARCTIC

Based on the widespread uniformity of the seasonal variation as well as the coherence of the seasonal cycle with altitude, it is reasonable to expect that a single surface location may be able to provide information on long-term changes over Antarctica. At South Pole, there is

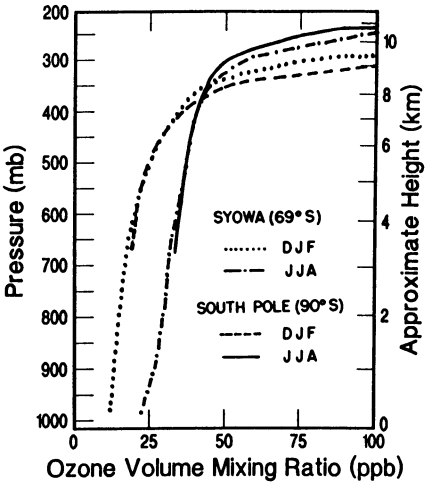

Fig. 10: Seasonally averaged ozone mixing ratio profiles in the troposphere for Syowa.

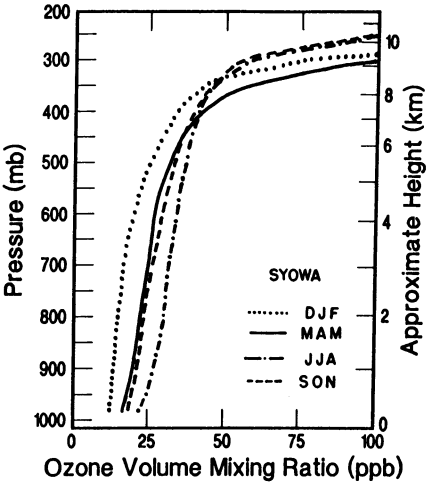

Fig. 11: Austral summer (DEC - JAN-FEB) ozone mixing ratio profiles at Syowa (·····) and South Pole (- - -) and for the winter (JUN-JUL-AUG) at Syowa (-·-·-) and South Pole (-----).

a 17-year (1975-1991) series of essentially continuous hourly observations of surface ozone. There has been a significant decrease in ozone near the surface at South Pole (Figure 12) that is dominated by decreases during the austral summer when ozone has decreased by nearly 25% since the start of measurements. A likely cause of this decrease is an indirect effect of declining ozone levels in the stratosphere [Schnell et al., 1991].

Summer is the seasonal minimum in tropospheric ozone at South Pole. Unlike other times of the year, there are significant day-to-day variations in ozone which are marked by influxes of air relatively low in ozone from the coast of Antarctica to South Pole [Schnell et al., 1991]. Two effects of sharply reduced stratospheric ozone concentrations that have occurred over the past decade may be responsible for the summer decline in surface ozone. With reduced levels of ozone in the stratosphere, enhanced amounts of ultraviolet radiation penetrate the troposphere. With very low nitrogen oxide concentrations in this region and increased ozone photolysis, there is a net reduction in tropospheric ozone especially near the surface [Schnell et al., 1991]. In addition, there is evidence for enhanced transport from the

coastal area to the interior of Antarctica [Dutton et al., 1991 and Schnell et al, 1991]. A possible cause of such increased transport has also been attributed to the decline in stratospheric ozone during the spring and summer [Neff, 1992] through the weakening of the stability aloft due to weaker radiative heating of the stratosphere.

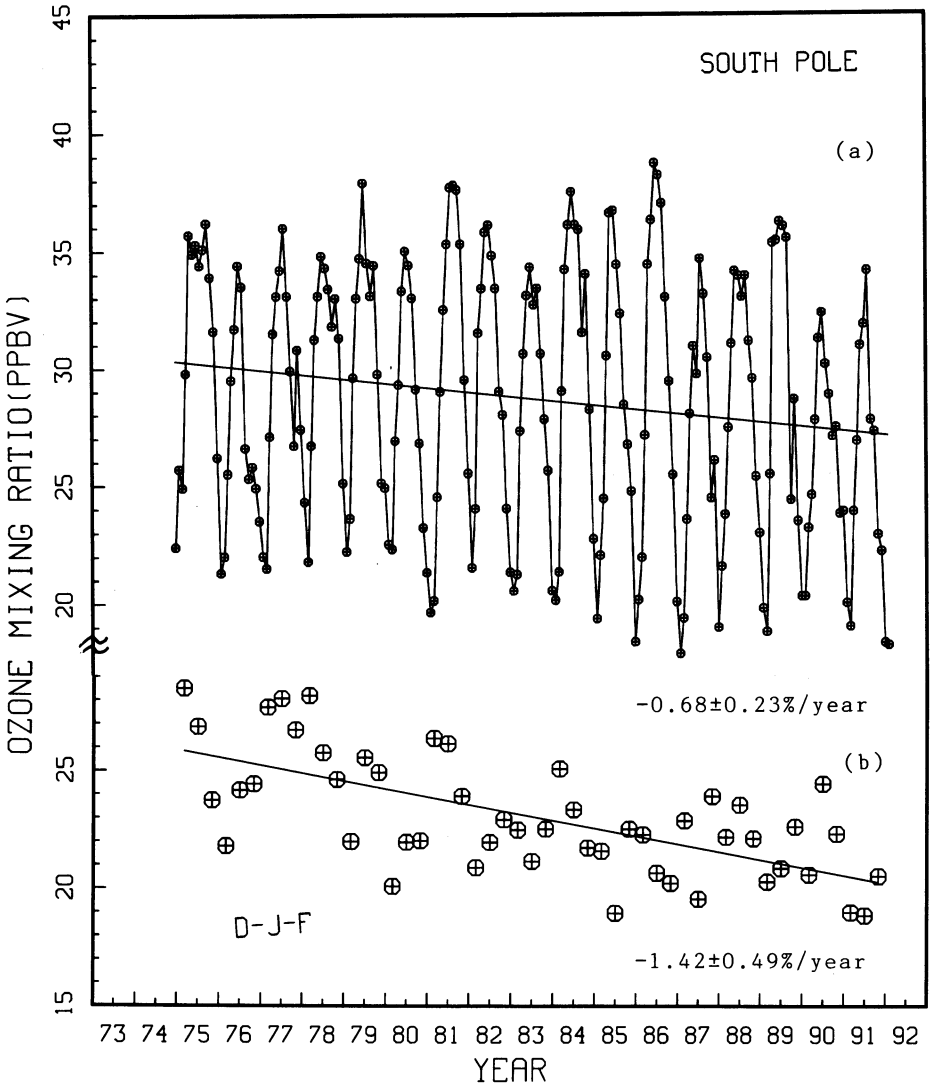

Fig. 12: Monthly (a) and summer seasonal (b) surface ozone mixing ratios at South Pole. The line through the data is a linear fit.

COMPARISON OF THE NORTH AND SOUTH POLAR REGIONS

Comparison of the profiles for the maximum and minimum seasons (JUN-JUL-APR, DEC-JAN-FEB) for Resolute and Syowa (Figure 13) shows that through most of the troposphere (the exception being at Resolute below about 1.5 km) both polar regions have seasonal variations that are approximately in phase with each other. During all seasons and at all altitudes (with the exception of spring surface values at Resolute), the ozone mixing rate is approximately twice as high in the north polar region compared to the south polar. This is consistent with non-polar latitudes where at most locations there is more ozone in the NH than at the corresponding latitude in the southern hemisphere (SH) [Fishman et al., 1978, Oltmans et al., 1989, and Oltmans and Levy, 1992a].

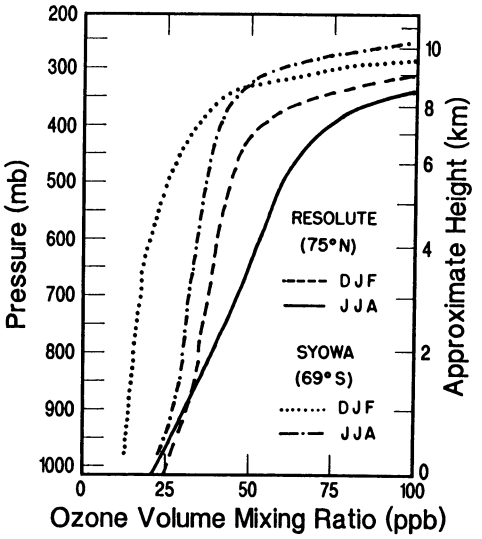

Fig. 13: Resolute DEC-JAN-FEB (- - -) and JUN-JUL-AUG (-----) average profiles compared with those from Syowa for DEC-JAN-FEB (·····) and JUN-JUL-AUG (-·-·-).

The vertical gradient during DEC-JAN-FEB at the two polar locations is very similar except near the surface where the boundary layer at Resolute shows a more rapid increase with altitude. During JUN-JUL-AUG the gradient is much stronger in the Arctic than over Antarctica. This probably reflects both greater surface losses and more efficient stratosphere/ troposphere exchange bringing more ozone into the upper troposphere [Browell et al., 1992].

CONCLUSIONS

In the Arctic, the seasonal variation above the boundary layer is dominated by the spring and summer exchange of ozone from the stratosphere into the troposphere [Oltmans et al., 1989 and Browell et al., 1992]. The gradients are relatively steep and the seasonal maximum occurs during one of these seasons at all tropospheric altitudes above the boundary layer. At all of the Arctic Ocean basin locations (Barrow, Resolute, Alert), there is a prominent spring seasonal minimum in the boundary layer which is not present at the lower latitude site at Churchill. This prominent low level minimum has been associated with the dramatic increase in atmospheric bromine compounds during the spring at these sites [Barrie et al., 1988 and Oltmans et al., 1989].

Over Antarctica, both the coastal and continental interior sites show nearly identical seasonal variations. This seasonal pattern dominates much of the SH troposphere with winter maxima and summer minima [Oltmans and Levy, 1992a and Oltmans et al., 1989]. This seasonal pattern appears to be related to both the summer loss of ozone in the low NO_x regime that seems to prevail in much of the SH [Oltmans and Levy, 1992b] and enhanced transport from the stratosphere during the winter [Levy et al., 1985].

The pattern of long-term ozone changes in the Arctic is somewhat unclear. At Barrow near the surface, there has been a significant 20-year increase of 25% in summer ozone amounts that may be associated with oil and gas exploration and extraction activities on the North Slope of Alaska. At Resolute, on the other hand, there have been significant decreases in ozone throughout the troposphere during the past decade after similar sized increases during the previous 15 years. Churchill in the sub-arctic shows a very similar pattern to Resolute. At both sites the determination of the overall trend during the past 25 years is complicated by the change of ozonesonde used to make the profile measurements.

At the South Pole, there has been a dramatic decrease in summertime ozone that is probably indirectly related to the development of strong spring and summer stratospheric ozone depletion over the past decade. The diminished stratospheric ozone layer over Antarctica and the surrounding region allows greater penetration of ultraviolet radiation to the surface giving rise to stronger summer ozone loss in the low NO_x regime [Schnell et al., 1991] and, through changes in the stability of the atmosphere, to enhanced transport from the coast to the interior of Antarctica [Neff, 1992].

REFERENCES

Barrie, L.A., J.W. Bottenheim, R.C. Schnell, P.J. Crutzen, and R.A. Rasmussen, Ozone destruction and photochemical reactions at polar sunrise in the low arctic atmosphere, *Nature, 334*, 138-41, 1988.

Bojkov, R.D., and G.C. Reinsel, Trends in tropospheric ozone concentration in *Atmospheric*

Ozone, C.S. Zerefos and A. Ghazi (Eds.), Reidel, Dordrecht, 775-781, 1985.

Browell, E.V., C.F. Butler, M.A. Fenn, S.A. Kooi, and W.B. Grant, Tropospheric ozone and aerosol variability observed at high northern latitudes with an airborne lidar, *Proceedings of the 1992 Quadrennial Ozone Symposium*, Charlottesville, VA, 4-13 June 1992 (in press).

Dutton, E.G., R.S. Stone, D.W. Nelson, and B.G. Mendonca, Recent interannual variations in solar radiation, cloudiness, and surface temperature at the South Pole, *J. Climate, 4*, 848-858, 1991.

Fishman, J., S. Solomon, and P.J. Crutzen, Observational and theoretical evidence in support of a significant in-situ photochemical source of tropospheric ozone, *Tellus, 31*, 432-446, 1979.

Jaffe, D.A., Local sources of pollution in the Arctic: From Prudhoe Bay to the Taz Peninsula in *Pollution of the Arctic Atmosphere*, W.T. Sturges (Ed.), Elsevier, New York, 255-287, 1991.

Levy II, H., J.D. Mahlman, W.J. Moxim, and S.C. Liu, Tropospheric ozone: The role of transport, *J. Geophys. Res., 90*, 3753-3772, 1985.

London, J. and S.C. Liu, Long-term tropospheric and lower stratospheric ozone variations from ozonesonde observations, *J. Atmos. and Terr. Phys., 54*, 599-625, 1992.

Neff, W.D., On the influence of stratospheric stability on lower tropospheric circulations over the South Pole. *Proceedings of the Conference on Polar Meteorology*, Portland, OR, October 1992 (preprint).

Oltmans, S.J., W.D. Komhyr, P.R. Franchois, and W.A. Matthews, Tropospheric ozone: Variations from surface and ECC ozonesonde observations in *Ozone in the Atmosphere*, Proceedings of the Quadrennial Ozone Symposium 1988 and Tropospheric Ozone Workshop, R.D. Bojkov and P. Fabian (Eds.), A. Deepak, Hampton, VA, 539-543, 1989a.

Oltmans, S.J., W.E. Raatz, and W.D. Komhyr, On the transfer of stratospheric ozone into the troposphere near the North Pole, *J. Atmos. Chem., 9*, 245-253, 1989b.

Oltmans, S.J., R.C. Schnell, P.J. Sheridan, R.E. Peterson, S.M. Li, J.W. Winchester, P.P. Tans, W.T. Sturges, J.D. Kahl, and L.A. Barrie, Seasonal surface ozone and filterable bromine relationship in the high Arctic, *Atmos. Environ., 23*, 2431-2441, 1989c.

Oltmans, S.J., Arctic ozone chemistry in *Pollution of the Arctic Atmosphere*, W.T. Sturges (Ed.), Elsevier, New York, 185-215, 1991.

Oltmans, S.J. and H. Levy II, Ozone measurements from a global network of surface sites, *Proceedings of the 1992 Quadrennial Ozone Symposium*, Charlottesville, VA, 4-13 June 1992 (in press).

Oltmans, S.J. and H. Levy II, Seasonal cycle of surface ozone over the western North Atlantic, *Nature, 358*, 392-394, 1992.

Schnell, R.C., S.C. Liu, S.J. Oltmans, R.S. Stone, D.J. Hofmann, E.G. Dutton, T. Deshler, W.T. Sturges, J.W. Harder, S.D. Sewell, M. Trainer, and J.M. Harris, Decrease of summer tropospheric ozone concentrations in Antarctica, *Nature, 351*, 726-729, 1991.

Taalas, P. and E. Kyrö, Two years of regular ozone soundings in the European Arctic, Sodankylä, *J. Geophys. Res., 91*, 8093-8098, 1992.

POLAR SUNRISE STUDIES

Jan Bottenheim
Atmospheric Environment Service
4905 Dufferin St.
Downsview, Ontario, Canada M3H 5T4

INTRODUCTION

The polar night is long and cold. Locations such as Alert at the northern edge of Ellesmere Island (82° N) do not receive any sunlight from late September until the beginning of March, and the average ambient temperature is normally below -30 °C during that time. This fact has interesting consequences for the chemistry that can occur in the ambient air at this part of the world. Most notably, the absence of sunlight effectively prevents the primary photochemical production of atomic and free radical compounds that initiate many of the important atmospheric chemical processes. Furthermore, the comparatively low temperatures generally lead to slower bimolecular reactions. This also leads to a drastically reduced water content of the air. All these factors combined imply that whenever airborne contaminants are somehow transported to the Arctic, their lifetime is considerably longer than at climatically more moderate mid-latitude regions. Combined with the absence of efficient transport routes out of the Arctic basin, it has the effect that the arctic atmosphere serves as a holding reservoir: a buildup of contaminants is expected - and observed. This picture changes at the time when the sun reappears. More active chemistry once again becomes possible through the photochemical production of reactive atomic and free radical compounds. Polar sunrise studies are specifically concerned with attempts to catch the chemical changes that take place during this transition from dark-phase to sunlight-irradiated chemistry.

The study of arctic tropospheric chemistry in recent years was initially driven by the desire to understand the phenomenon of "Arctic haze". It is now well established that this is due largely to sulphate aerosols [Barrie and Bottenheim, 1991]. Their presence reflects the transport of sulphur oxides from predominantly Eurasian anthropogenic sources to the Arctic, where they tend to accumulate in the air during the dark winter. In context with these studies much attention was also devoted to the determination of the levels of trace metal ions, in particular since it was expected that this would allow a more precise determination of the specific origin of the observed atmospheric pollution. Much less attention was devoted to the study of oxidant chemistry. Inorganic nitrates were determined using the same methods as employed for the sulphur oxides, viz. filter techniques and ion chromatographic analysis. The

NATO ASI Series, Vol. I 7
The Tropospheric Chemistry of Ozone in the Polar Regions
Edited by H. Niki and K. H. Becker

levels were at least an order of magnitude lower (on a molecular basis) than the sulphates, and hence nitrate chemistry was considered of lesser interest. Similarly, tropospheric ozone was only monitored in the context of NOAA's GMCC program at Barrow, Alaska. Nevertheless, intensive field studies were organized in late winter, early spring, and it was only a matter of time for the peculiar oxidant chemistry occurring at that time in the Arctic to be discovered.

The first indication of oxidant chemistry having an impact on the lower tropospheric air in the Arctic came from an analysis of the seasonal cycle of the $SO_2/SO_4^=$ ratio by Barrie and Hoff [1984], who observed that this ratio appeared to decrease noticeably in the spring, before the time that the total loading of sulphur oxides was observed to decrease. It was proposed that this was due to the emergence of OH radicals that could oxidize SO_2 to $SO_4^=$ particles. Similarly, Shaw [1984] reported that sulphate particles observed in the spring in Northern Alaska showed a trimodal size distribution; the presence of a measurable nucleation mode was interpreted as due to local production of sulphate particles, possibly due to the OH + SO_2 reaction. The NO_y chemistry became more focussed by the airborne studies of Dickerson in the European Arctic [1985], and the surface measurements of PAN and other nitrogen oxides at Alert [Bottenheim et al., 1986]. The latter study also reported the first O_3 measurements at Alert which showed occasionally large decreases in mixing ratio over a three week period, quite similar to what had been observed for several years at Barrow [Oltmans and Kohmyr, 1986]. The Alert experiments were repeated over a longer period in 1986 as part of the AGASP-II experiments, and the results confirmed and reinforced the 1985 data. The most interesting result, however, came from a combination of the O_3 with Br data obtained from 24 hour integrated filter samples. The exceptionally strong anti-correlation (Figure 1) suggested more than a coincidental relation, and it is this relationship that has become the focus of the so-called Polar Sunrise studies in the last few years. In the following sections the results from field studies over the period 1986-1990 will be reviewed in this light, followed by a summary on what is and what is not known.

1986: AGASP-II

AGASP-II in the spring of 1986 was primarily organized to study the details of arctic haze formation. Included were intensive surface measurements at Barrow, AK and Alert, NWT, as well as several aircraft surveys originating in Anchorage, AK (NOAA), Alert (AES), and Thule, Greenland (UW). Most results from this study were published in a special issue of the Journal of Atmospheric Chemistry [volume 9, 1989]. The key experiments for what follows were performed at Alert: for the first time at that location daily samples were obtained using both high-volume and low-volume filter methods, while concurrently

continuous ozone data were collected. Severe ozone depletion episodes were again observed, but it was now possible to search the extensive additional database and discover the striking negative correlation with filterable bromine (F-Br) as shown in Figure 1 [Barrie et al., 1989]. This discovery immediately raised several questions, the most prominent being:

- Were there any other major compounds that might be related to the $-O_3$ /Br correlation?
- Was this observation specific for Alert, or did it have wider implications?
- What could be the reason for this observation?

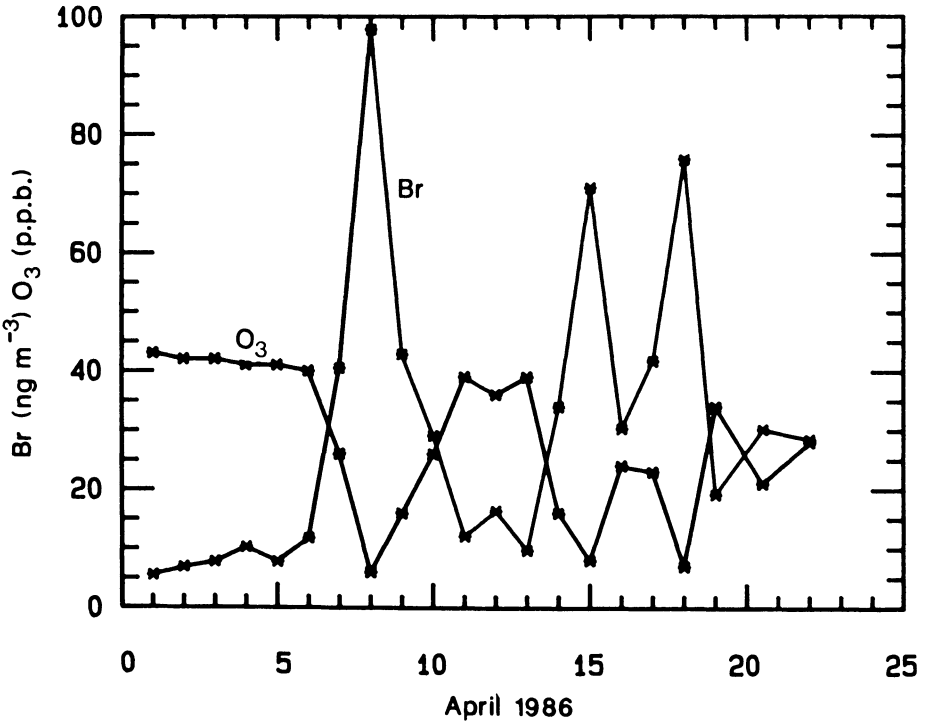

Fig. 1: A comparison of daily mean ground level O_3 and filterable bromine at Alert, Canada, in April 1986. [From Barrie et al., 1989]

A check on other chemical data collected was largely negative. In particular it appeared that the main haze parameters (both SO_x and NO_y, or metal ions) showed no correlation. Similarly, other halogens showed only marginal covariance.

Analysis of aircraft datasets from AGASP-II showed that very low ozone mixing ratios were not limited to Alert and Barrow, but were often observed elsewhere in the Arctic,

albeit only in the lower boundary layer, i.e., in the commonly quite shallow surface inversion layer [Barrie et al., 1988, Leaitch et al., 1989]. The latter fact is particularly clear from ozone profiles obtained at Alert using a tethersonde (Figure 2) [Mickle et al., 1989]. It was mentioned earlier that low ozone episodes had also been observed regularly at Barrow. Analysis of the bromine datasets was rather ambivalent. In particular, reanalysis of the bromine data from Barrow indicated the occasional presence of low-ozone and high bromine days, but the data were much less convincing [e.g.,. Oltmans et al., 1989; Li et al., 1990].

A first attempt was made to explain the Alert data, based on the assumption that the ozone destruction was due to the catalytic cycle: $Br + O_3 \rightarrow BrO + O_2$; $BrO + BrO \rightarrow 2\ Br + O_2$ [Barrie et al., 1988]. Termination of this cycle was predicted to be in the form of HBr, which would lead to the Br- ion that was observed in the filter analysis. The source of the Br atoms was postulated to be the photolysis of bromoform. There were several arguments for this thesis:

- Several years of arctic F-Br observations showed a strong peak during March-April that could not be explained as originating from identifiable sources (anthropogenic, crustal, or sea salt) [Sturges and Barrie, 1988]. An organic bromine source, probably of marine origin was speculated to be involved.
- A comparison of the mixing ratios of organic bromine compounds (CH_xBr_y) between the Arctic and the Antarctic suggested a relatively larger abundance of bromoform in the Arctic [Khalil et al., 1986].
- Inspection of the ozone record at Alert over a longer period than the AGASP-II study suggested that the ozone depletion episodes were somehow related to the reappearance of the sun in the spring. Although not published, it was suggested by Penkett [1987] that the spectral properties of bromoform were such that it could be photolyzed by sunlight, eventually yielding three Br atoms.

In terms of the physical processes that led to the strong negative correlation between O_3 and F-Br, it was postulated that this was due to the difference between lower boundary layer air and free tropospheric air that reached the observation site at Alert (Figure 3). Boundary layer air, uncoupled from the large free tropospheric reservoir of O_3 due to the normally strong surface temperature inversion in the Arctic (see Figure 2) would be rich in bromoform from marine sources, which would have led to the destruction of O_3 and buildup of F-Br, in contrast with O_3 rich, $CHBr_3$ poor free tropospheric air. The specific geography of the measurement location at Alert should make it possible to clearly see this distinction as a sort of natural modulation effect. At Barrow this should be much less the case; furthermore local and regional pollution sources as well as influx of warmer air from the Pacific would impede the clear observation of the O_3/-Br signal.

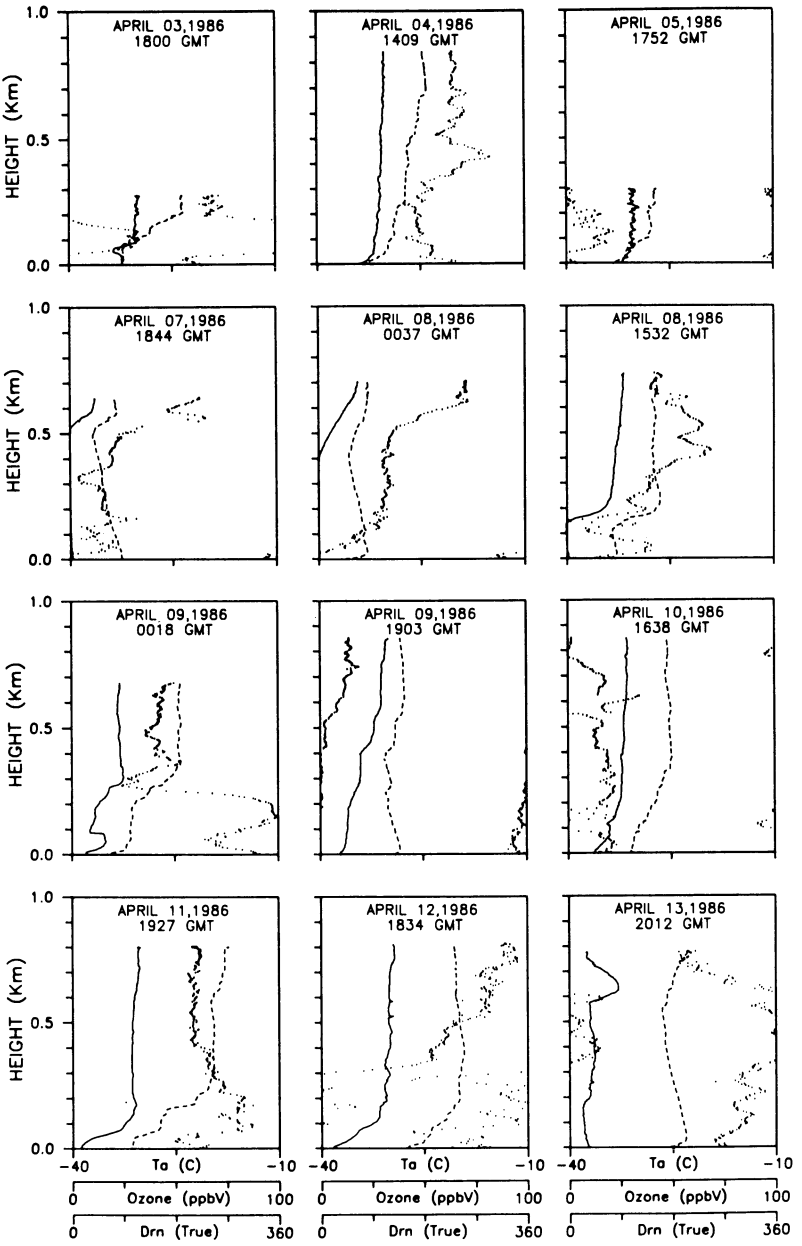

Fig. 2: Detailed tethersonde profiles during 4-13 April 1986 at Alert, Canada. Ozone mixing ratio in ppbv (___), ambient temperature (-----), and wind direction (·····) are shown. [From Mickle et al., 1989]

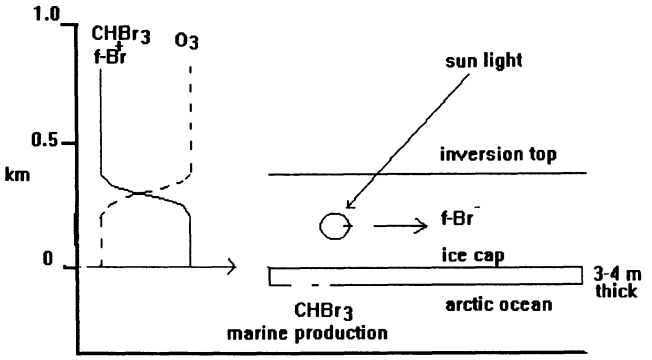

Fig. 3: Schematic description of the mechanism of ozone destruction in the arctic atmospheric boundary layer.

1988: POLAR SUNRISE EXPERIMENT

The 1988 Polar Sunrise Experiment [Bottenheim et al., 1990] was organized to confirm the observations made at Alert in 1986, and to test the mechanism proposed by Barrie et al. [1988] that might explain the observed O_3/Br negative correlation. While successful in supplying supporting evidence, some new features were observed that complicated the overall picture. This study ran from late February to the end of April, so that a much larger fraction of the important period between dark and light could be covered.

Foremost was the confirmation of the O_3/Br negative correlation. Correlation of O_3 with meteorological parameters at the observation site, furthermore, showed a strong dependence on wind direction and temperature. This was exactly as expected, if modulation between free tropospheric and surface boundary layer air masses was responsible for the observed variations in O_3 levels. Thus, only the colder air coming direct from the polar ice-cap showed depleted O_3 levels.

More puzzling was the observation that analysis of the filter data (using a Teflon/nylon combination) suggested that it was the fraction of Br^- on the front Teflon filter that seemed to correlate best with O_3 depletion. Not only was there proportionally much more Br found on the nylon filter, but moreover if the product of the chemistry was HBr, then this was expected to be in the gas phase which was not expected to be trapped on the Teflon filter (which should collect mainly particles) but on the nylon filter (HBr being an

acid). This problem has not been resolved to date, and there is a need to unambiguously identify how the different filter media interact with the different bromine compounds.

During this study a concerted effort was made to determine the presence and trend in organic bromine compounds (CH_xBr_y). The results showed that the bromoform mixing ratio was between 1 and 5 pptv; it was negatively correlated somewhat more weakly with O_3 than Br^- (Figure 4). CH_3Br was present at levels comparable with $CHBr_3$; however, it did not correlate with O_3. Some other methylhalides were also identified; but their mixing ratio was generally lower than that of $CHBr_3$. While some methylhalides correlated with -O_3 (e.g., $CHBr_2Cl$, CH_2Br_2), others did not (e.g., $C_2H_4Br_2$).

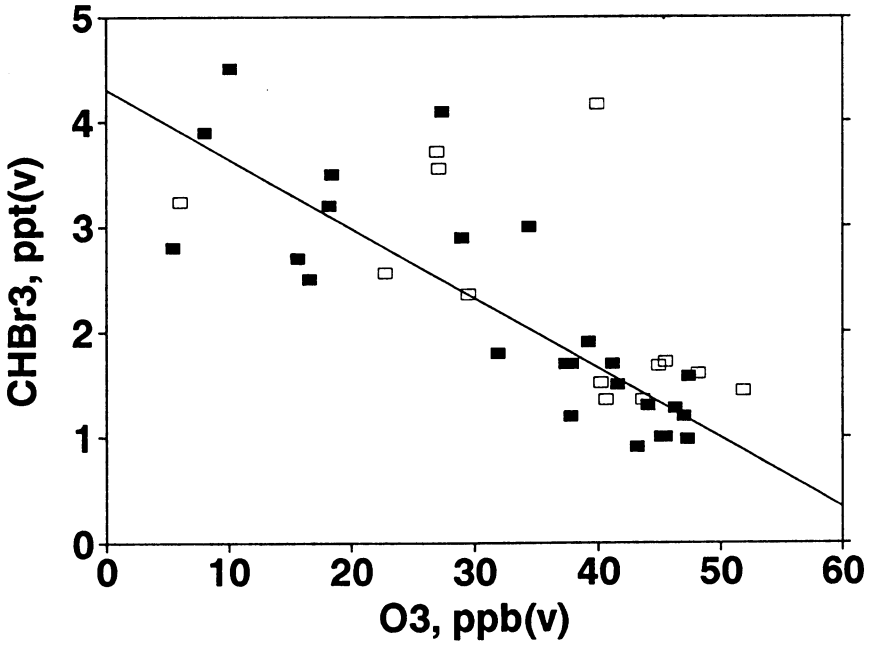

Fig. 4: Negative correlation between ozone and bromoform at Alert, Canada in February-April 1988. [From Bottenheim et al., 1990]

As far as hydrocarbons were concerned, it was observed that acetylene and possibly ethylene correlated positively with O_3. New chemical kinetic data that appeared in 1989 [Barnes et al., 1989] led to the suggestion that acetylene and ethylene could have been depleted by Br atom chemistry as well, contrary to the paraffins. Indeed, the variation in paraffin mixing ratios (CH_4 and up) was so small that no trend with O_3 was apparent.

The presence of carbonyl compounds and NO_2 was also investigated. CH_2O was proposed by Barrie et al. [1988] as the likely source for HBr formation, although its level was predicted to be low. Using DNPH coated cartridges, an upper limit to its mixing ratio at less than 50 pptv was derived, but in addition it was observed that CH_3CHO was present at least comparable levels. Since its rate of reaction with Br is reported to be faster than the CH_2O + Br reaction [Niki et al., 1985], this added yet another dimension to the chemistry.

NO_2 measurements were performed using the luminol chemiluminescence technique, which yielded levels of the order of 100 pptv. Careful screening of the data gave hints that its mixing ratio would decrease concurrently with O_3, but that this effect was masked by local as well as long range pollution effects. It also appeared entirely possible that the measured amount of NO_2 would actually represent the sum of NO_2 + N_2O_5. This was relevant in view of the proposal by Finlayson-Pitts et al. [1990] that an alternate source of Br atoms might be the reaction sequence

$$N_2O_5 + NaBr \rightarrow NO_2Br + NaNO_3$$
$$NO_2Br + h\nu \rightarrow NO_2 + Br$$

Finally, it is noteworthy that a principal component analysis of all data once more confirmed that the O_3/Br negative correlation was not related to the presence of arctic haze (no covariance with $SO_4^{=}$). As far as other halogens were concerned, only a weak correlation with I^- seemed to exist, but not with Cl^-.

1989: AGASP-III

Following the results obtained at Alert, a concerted effort was made at Barrow to expand the scope of the Br/O_3 phenomenon (the results of this study have not appeared in press at this time, and what follows is therefore probably incomplete). Pertinent data have been reported in a manuscript by Sturges et al. [1991*a*]. As before, it was observed that O_3 depletion episodes were generally correlated with a marked increase in F-Br, although the correlation was again less clear than at Alert. Of special note is the fact that the authors are quite specific in mentioning that this pertains only to *particle* Br^-. Both the use of a second filter (in this case KOH impregnated Whatman-41) and MgO coated denuder tubes showed that gas-phase Br^- was much less abundant than particle Br^-. It also revealed no significant relation with O_3.

During this study, total organic bromine was collected with specially prepared charcoal traps as well as on Tenax traps. Significant from these data is the observation that organic bromine compounds, in particular $CHBr_3$ and $CHClBr_2$ were also negatively

correlated with the O_3 depletion episodes. An attempt to derive a total Br balance suggested that often the organic bromine compounds were more abundant than the inorganic bromines at that time.

This study also addressed the question of the origin of the organic bromine compounds. It had been speculated that this might be related to ice algae that would be able to release bromocarbons in the spring via the many open leads in the arctic ice cap. Sturges et al. used trajectory calculations and satellite imagery to show that air masses containing high levels of $CHBr_3$ in general had passed within the last 24 hour over open leads in the ice. This was interpreted as suggesting that if $CHBr_3$ was somehow connected with the O_3 destruction, then this had to be a very fast process.

In a related experiment, nighttime ambient air was irradiated in a flowchamber with sun lamps. These experiments showed a marked increase in F-Br in the irradiated air, as compared with air that was not irradiated. Only a few minutes of exposure was necessary to obtain this result, and it was concluded that very efficient, photochemically induced reactions could take place in the ambient air leading to the build-up of F-Br.

Aircraft observations during AGASP III reinforced the surface measurements [Sheridan et al., 1991]. Sturges et al. actually attempted to sample during day and night periods independently, and obtained indications (confirmed in 1990, see below) that while organic bromine seemed to maximize at night, inorganic Br would be at a minimum. The aircraft data showed again the strong negative correlation between O_3 and F-Br. Furthermore, samples collected at roughly the same location two days apart showed that in relative terms substantial O_3 depletion might have occurred in the interim period; concurrently there was an obvious increase in particle Br, and decrease in organic bromine.

The aircraft measurements yielded in a set of conditions, all of which appeared to have been satisfied for O_3 depletion to be apparent: 1) sample collection over pack ice with relatively little open water nearby, 2) a strong surface temperature inversion, 3) a stable layer capping the O_3 depleted layer, 4) light winds, and 5) winds transporting Arctic rather than marine air masses to the research area.

1989: AERIAL SURVEY OUT OF ALERT

Another attempt to gain insight into the extent of the O_3 depletion over the Arctic was made by aircraft flying out of Alert in 1989 [Kieser et al., 1991]. This study involved extensive traverses over the ice-cap at an altitude of *ca.* 300 m, and provided further evidence for the large spatial extent of the O_3 depletion. However, the O_3 levels were not invariably close to zero; in fact quite a variability was observed during individual transects. This could be interpreted as an indication that O_3 depletion occurs in highly specific, localized areas, although a variation in the depth of the surface boundary layer might also be responsible.

As far as the timing of O_3 depletion was concerned, it was observed that after a major storm episode (which should have mixed free tropospheric air down to the surface) it took approximately one day before O_3 depleted air was again encountered. Hence it was postulated that the O_3 depletion process is effective in a period of less than one day, qualitatively in agreement with the irradiation experiments of Sturges et al. [1991*a*].

Results from hydrocarbon observations added a new twist to the picture. The good (positive) correlation between O_3 and acetylene was again noted, but in addition it appeared that paraffins were also following the trend (Figure 5). This was a surprising result since these compounds are not known to be reactive towards Br. It opens the possibility that Cl atoms are involved in the active chemistry, even though no direct experimental data have so far been obtained to substantiate this. Unfortunately, due to experimental problems no reliable ethylene data were obtained. However, propylene did not show good correlation with O_3. Its rate of reaction with Br is not expected to be substantially different from that of ethylene. Since the ocean is a known source of olefins but not acetylene [Rudolph et al., 1991], this could be construed as an argument that the ocean is the likely origin of whatever compound is the source of Br atoms.

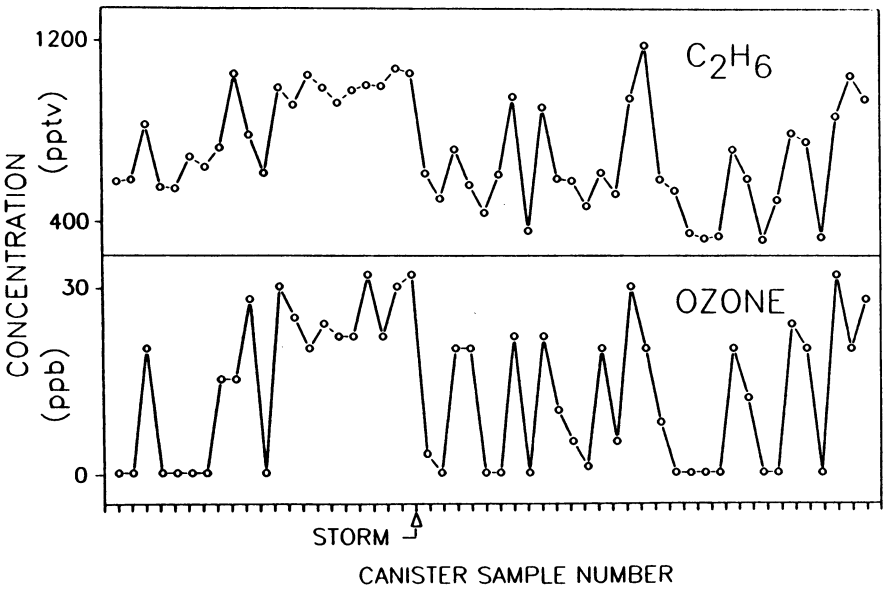

Fig. 5: A comparison of ethane and ozone observations during aircraft survey flights north of Alert, Canada, in May 1989. [From Kieser et al., 1991]

1990: SPRING EXPERIMENTS AT BARROW

Additional experiments were performed at Barrow in 1990 [Sturges et al., 1991*b*]. No O_3 depletion episodes were encountered during the period of the study, but some notable results on the bromine chemistry were obtained.

As was the case in 1989, sampling was roughly divided between day and night intervals. A clear inverse relationship between organic Br gas and inorganic particulate Br was observed with the organic fraction maximizing at night, in contrast with the inorganic fraction which tended to maximize during the day. In a qualitative sense, this is precisely what would be expected if photochemical reactions transform organic Br compounds into inorganic Br^- via the formation of Br atoms. Furthermore, during this study a Teflon/nylon filter combination was used to distinguish between gaseous and particle inorganic bromine. Hence, the experimental procedures more resembled those employed at Alert. Nevertheless, as in 1989, it appeared that the gaseous fraction of inorganic Br was negligibly small.

Further evidence for a photochemical component in the chemical mechanism was obtained from renewed experiments with irradiation of night time ambient air. It was shown that *ca.* 30 minutes exposure of the air in the illuminated chamber was sufficient to destroy all the O_3. However, this result has to be considered with caution, since presently little else has been reported on the composition of the ambient air at that time.

Finally, although organic Br and Cl were well correlated, suggesting similar sources (presumably from arctic marine biological activity), their ratio appeared to show some diurnal variation, with the Br/Cl ratio being lower during the day than during the night. This could at least qualitatively be interpreted as an argument for photochemical reactions, since the organic Cl compounds are much less, if at all, expected to be photolyzed by sunlight in the lower troposphere.

1988-1990: NO/NO_y MEASUREMENTS AT BARROW

Although not directly related to O_3 depletion, the observations of Honrath and Jaffe at Barrow should be mentioned here. During a three year period NO/NO_y measurements were made, mostly during spring and summer [Honrath, 1991]. As far as O_3 depletion in the spring is concerned, the data of 1990 were carefully analyzed to search indications that the Finlayson-Pitts et al. mechanism of Br formation was feasible. The results were mixed: using NO as an indicator for possible levels of N_2O_5, it appeared that at one period of depleted O_3 levels, indeed sufficient N_2O_5 could have been present, but decidedly not at another time. Direct correlation between O_3 depletion and NO_y was not reported, nor should it be expected: the observations at Alert in 1988 hinted at correlation with NO_2, but not with PAN (which is believed to be the main component of NO_y).

1992 POLAR SUNRISE EXPERIMENT II

From January 13 to April 20, 1992, a second Polar Sunrise Experiment was undertaken at Alert. Principal investigators came from Canada, Japan, Germany, and Sweden. The major objectives of this study were to further broaden insight into the mechanism of ozone destruction, as well as obtain more detailed information on nitrogen oxides, VOCs (volatile organic carbons), inorganic and organic halogen containing compounds, and sulphur species of both natural and anthropogenic origin. Analysis of the data is currently in progress, but some preliminary highlights can be reported at this time:

- The occurrence of episodes of essentially zero ozone were observed not only at Alert but also on an ice floe 200 km north of Alert. Aircraft survey flights further confirmed the widespread occurrence of such low ozone episodes. The rate of ozone deposition to the ice floe was estimated using eddy correlation flux measurements; this will set limits on the rate of ozone destruction.

- Bromine chemistry was extensively detailed. Sufficiently comprehensive observations of different bromine compounds (gaseous and particulate inorganic bromine, as well as most organic bromine) and total bromine will allow the construction of an overall bromine budget in the atmosphere. Highly significant anti-correlation between ozone and bromoform was observed. Furthermore, BrO was positively identified and quantified in April, permitting an evaluation of its possible role in ozone depletion.

- Selective destruction of hydrocarbons and alkylnitrates, and the production of formaldehyde and acetone was observed, which is interpreted as clear (albeit indirect) evidence for the implication of chlorine in polar sunrise chemistry.

- The total sum of nitrogen oxides (NO_y) and many individual compounds were measured with confidence, confirming that peroxyacetylnitrate (PAN) is the dominant constituent of NO_y. Peak nitrogen dioxide mixing ratios were 200 pptv in the dark, and 100 pptv in the light, but on average substantially lower than these levels. Gaseous nitrite, possibly nitrous acid, was observed in the dark winter at ca. 20 pptv, and approximately 8 pptv in the light period in April. Experimental evidence was obtained that may shed light on its possible formation via heterogeneous chemical reactions involving ice crystals.

SUMMARY AND CONCLUSIONS: WHERE DO WE STAND?

In the previous sections, pertinent experimental results from recent field studies in the Arctic have been reviewed. It has been shown that:

- frequent periods of drastic reduction in boundary layer O_3 are observed in the Arctic starting roughly at the same time as polar sunrise; these periods of very low O_3 last well into the spring (at Alert frequently until mid May), but are not observed during other periods of the year,
- from observations at Barrow, Alert and from aircraft studies elsewhere, it appears to be a very widespread phenomenon,
- both the timing of the onset of O_3 depletion, and the irradiation experiments at Barrow make a case for a photochemical component to the mechanism responsible for the O_3 depletion,
- the irradiation experiments, and aircraft observations of 1989 both argue for a relatively fast process, possibly occurring in a period of less than a day,
- the occurrence of O_3 depletion appears to be coincident with a noticeable increase in Br compounds, both organic and inorganic,
- particulate Br (Br collected on Teflon filters, and analyzed by ion chromatography as Br^-, or instrumental neutron activation analysis as Br) increases during O_3 depletion episodes; the negative correlation is particularly strong in the Alert database, as a result of favorable geographic features at the observation site,
- there is conflicting evidence concerning the relative amounts of particle and gas-phase Br that makes up the F-Br fraction. The Alert measurements indicate the presence of a substantial gaseous fraction of Br that can be analyzed as the Br^- ion (therefore strongly suggesting that this is not organic Br), but at Barrow only very limited amounts of gaseous inorganic Br are observed,
- a substantial fraction of the organic Br fraction is identified as $CHBr_3$,
- to date there is no experimental evidence for a possible contribution of Cl atom initiated chemistry; similarly, evidence for I atom chemistry is weak at best,
- all hydrocarbon observations are in agreement that O_3 depletion is positively correlated with a marked decrease in acetylene; data on other hydrocarbons are conflicting from different studies,
- concurrent measurements of NO_2 and CH_2O at Alert to date have mainly yielded qualitative information on order of magnitude mixing ratios (< 50 pptv and ca.100 pptv respectively),
- although the much better characterized phenomenon of arctic haze occurs roughly during the same time of the year, no correlation between haze components, *viz.* $SO_4^=$ particles or PAN gas, and O_3 depletion has been found.

Efforts to rationalize these observations with a coherent chemical mechanism have been made, and will be discussed elsewhere in more detail. Central to all mechanisms is the assumption that the Br to BrO catalytic cycle is responsible for the actual O_3 destruction. Although to date no direct evidence for this cycle has been reported, known kinetics does not contradict this hypothesis, but major questions remain to be resolved before it can be accepted. This is reflected in the difference between the overall mechanisms. Two main questions arise:

- What is the primary source of Br, if indeed this atom is the key to the O_3 destruction process?
- How can other products of Br chemistry, notably HBr and other brominated organic compounds be recycled into chemically more reactive bromine?

As far as the first question is concerned, all experimental evidence has been interpreted as suggesting a marine origin. Barrie et al. [1988] suggested photolysis of $CHBr_3$. Although not unambiguously shown to be impossible, it appears that this process is probably not able to generate enough Br atoms (Moortgat and this Proceeding). The suggestion by Finlayson-Pitts et al. [1990] of the formation of photochemically labile $BrNO_2$ from the reaction of N_2O_5 with NaBr as a source of Br atoms is problematic, since it requires a longer residence time for arctic air than is usually observed in order to generate sufficient Br atoms. The most recent proposal by McConnell et al. [1992] invokes heterogeneous photochemical conversion of Br^- ions into Br_2 on ice crystals, where the Br^- ions would originate from sea-spray. This mechanism, therefore, does not need organic Br compounds to activate the O_3 destruction process. Although thermodynamically feasible, there is no experimental evidence to support this mechanism.

Recycling of inactive Br (HBr and organic Br) is another issue of contention. Barrie et al. [1988] deduced from their mechanism that this could be due to OH chemistry. In contrast, McConnell et al. [1992] speculated that the recycling could again be due to adsorption of inactive Br on ice particles, followed by photochemical conversion into Br_2.

In summary then, the yearly springtime phenomenon of arctic boundary layer O_3 depletion appears to be related to a photochemical process involving Br compounds. Although there is an increasing wealth of data outlining the chemical composition of the air in which this process takes place, important information is yet to be obtained. Some pertinent observations are conflicting between studies at different locations and times. As a result, a satisfactory explanation is still outstanding.

REFERENCES

Barnes, I., V. Bastian, K.H. Becker, R. Overath, and Z. Tong, Rate constants for the reactions of Br atoms with a series of alkanes, alkenes, and alkynes in the presence of O_2, *Int. J. Chem. Kinet., 21,* 499-517, 1989.

Barrie, L.A., and R.M. Hoff, The oxidation rate and residence time of SO_2 in the Arctic atmosphere, *Atmos. Environ., 18,* 2711-2722, 1984.

Barrie, L.A., J.W. Bottenheim, R.C. Schnell, P.J. Crutzen, and R.A. Rasmussen, Ozone destruction and photochemical reactions at polar sunrise in the lower arctic atmosphere, *Nature, 334,*, 138-141, 1988.

Barrie, L.A., G. den Hartog, J.W. Bottenheim, and S.J. Landsberger, Anthropogenic aerosols and gases in the lower troposphere at Alert, Canada in April 1986, *J. Atmos. Chem., 9,* 101-127, 1989.

Barrie, L.A. and J.W. Bottenheim, Sulphur and nitrogen pollution in the arctic atmosphere, in: *Pollution of the arctic atmosphere*, W.T. Sturges, Editor, p.155-183, Elsevier Science Publishers, London, 1991.

Bottenheim, J.W., A.J. Gallant, and K.A. Brice, Measurements of NO_y species and O_3 at 82° N latitude, *Geophys. Res. Lett., 13,* 113-116, 1986.

Bottenheim, J.W., L.A. Barrie, E. Atlas, L.E. Heidt, H. Niki, R.A. Rasmussen, and P.B. Shepson, Depletion of lower tropospheric ozone during arctic spring: the polar sunrise experiment 1988, *J. Geophys. Res., 95D,* 18555-18568, 1990.

Bottenheim, J.W., L.A. Barrie, and E. Atlas, The partitioning of NO_y in the lower arctic troposphere during spring 1988, *J. Atmos. Chem.*, accepted, 1993.

Dickerson, R.R., Reactive nitrogen compounds in the Arctic, *J. Geophys. Res., 90C,* 10739-10743, 1985.

Finlayson-Pitts, B.J., F.E. Livingstone, and H.N. Berko, Ozone destruction and bromine photochemistry in the arctic spring, *Nature, 343,* 622-625, 1990.

Honrath R.E., Nitrogen oxides in the arctic troposphere, Ph. D. Thesis, University of Alaska, 1991.

Khalil, M.A.K., R.A. Rasmussen, and R. Gunawardena, Atmospheric bromine in polar regions, *NOAA/GMCC Ann. Rep., 15,* 123-125, 1986.

Kieser, B.N., T. Sideris, H. Niki, J.W. Bottenheim, and W.R. Leaitch, Spring 1989 observations of tropospheric chemistry in the Canadian Arctic, *Atmos. Environ.*, submitted, 1991.

Leaitch, W.R., R.M. Hoff, and J.I. MacPherson, Airborne and lidar measurements of aerosol and cloud particles in the troposphere over Alert, Canada, in April 1986, *J. Atmos. Chem., 9,* 187-212, 1989.

Li, S.M., J.W. Winchester, J.D. Kahl, S.J. Oltmans, R.C. Schnell, and P.J. Sheridan, Arctic boundary layer ozone variations associated with nitrate, bromine, and meteorology: a case study, *J. Geophys. Res., 95D,* 22433-22440, 1990.

McConnell, J.C., G.S. Henderson, L. Barrie, J. Bottenheim, H. Niki, C.H. Langford, and E.M.J. Templeton, Photochemical bromine production implicated in arctic boundary-layer ozone depletion, *Nature, 355,* 150-152, 1992.

Mickle, R.E., J.W. Bottenheim, W.R. Leaitch, and W. Evans, Boundary layer ozone depletion during AGASP-II, *Atmos. Environ., 23,* 2443-2449, 1989.

Niki, H., P.D. Maker, L.M. Savage, and L.P. Breitenbach, An FTIR spectroscopic study of the reactions Br + CH_3CHO → HBr + CH_3CO and $CH_3C(O)OO$ + NO_2 → $H_3C(O)OONO_2$ (PAN), *Int. J. Chem. Kinet., 17,* 525-534, 1985.

Oltmans, S.J., and W.D. Komhyr, Surface ozone distributions and variations from 1973-1984 measurements at the NOAA Geophysical Monitoring for Climate Change Baseline observatories, *J. Geophys. Res., 91D,* 5229-5236, 1986.

Oltmans, S.J., R.C. Schnell, P.J. Sheridan, R.E. Peterson, S.M. Li, J.W. Winchester, P.P. Tans, W.T. Sturges, J.D. Kahl, and L.A. Barrie, Seasonal surface ozone and filterable bromine relationship in the high Arctic, *Atmos. Environ., 23,* 2431-2441, 1989.

Penkett, S.A., discussions at the 4th International symposium on arctic chemistry, Norway, 1987.

Rudolph, J., and F.J. Johnen, Measurements of light atmospheric hydrocarbons over the Atlantic in regions of low biological activity, *J. Geophys. Res., 95D,* 20583-20591, 1990.

Shaw, G., Discussions at the 3rd International symposium on arctic chemistry, Toronto, Canada, 1984.

Sheridan, P.J., R.C. Schnell, and J.M. Harris, Boundary layer ozone fluctuations related to organobromine photochemistry in the springtime Arctic, *NOAA/CMDL Annual, Report, 19,* 74-80, 1991.

Sturges, W.T. and L.A. Barrie, Chlorine, bromine and iodine in arctic aerosols, *Atmos. Environ., 22,* 1179-1194, 1988.

Sturges, W.T., R.C. Schnell, S. Landsberger, S.J. Oltmans, J.M. Harris, and S.M. Li, Chemical and meteorological influences on surface ozone destruction at Barrow, Alaska, during spring 1989, *Atmos. Environ.* , submitted, 1991a.

Sturges, W.T., R.C. Schnell, G.S. Dutton, S.R. Garcia, and J.A. Lind, Atmospheric bromine measurements at Barrow, Alaska, using a sequential filter pack and carbon tube sampler, *NOAA/CMDL Annual Report, 19,* 117-119, 1991b.

METEOROLOGY AND TRANSPORT OF AIR MASSES IN ARCTIC REGIONS

Trond Iversen
Institute of Geophysics
University of Oslo
P. O. Box 1022 - Blindern
N-0315 Oslo, Norway

ATMOSPHERIC DISPERSION

Airborne dispersion of a gravitationally neutral tracer is determined by the macroscopic atmospheric motions. These atmospheric motions generally take shapes as wavelike meanders and closed circulations, in short generally referred to as eddies. The nature of the transport of air parcels is determined by the kinetic energy of these eddies as a function of their size and fluctuation period. According to Taylor's statistical theory of plume-diffusion (particles continuously released over an infinitely long time in a fixed point [e.g., Pasquill and Smith, 1983], the energy-containing eddies with periods longer than the elapsed time (T) since the particle release determine the further plume shape. In reality, emissions take place over a finite time interval, or one is interested in the shape averaged over a finite time interval T_S. Taylor's theory can be applied as long as $T \ll T_S$, otherwise puff-diffusion theory, which takes into account the diffusion of particles relative to each other, is applicable. Puff diffusion was first addressed by Richardson in the 1920s and elaborated further by Batchelor in the 1950s by using similarity theory [Pasquill and Smith, 1983]. Eddies of the same size as a puff are the most efficient contributors to the increase of the puff-size by causing a complete shape distortion, whilst those that are significantly smaller only cause a gradual entrainment of clean air by mixing through the boundaries. Eddies much larger than a puff will cause a general displacement of the puff without dilution, viz. advection.

The fate of a continuous plume, or a puff of a given size, will depend on the distribution of energy between eddy-components of different periods and sizes. In plume-diffusion it is the spectral density of the eddy kinetic energy as experienced by individual air particles (Lagrangian spectral density), which is essential. For puff-diffusion a combination of the Lagrangian and Eulerian spectral densities are influencing the development. In the incipient stage of plume dispersion the diffusion coefficient (K) increases linearly with time since the point release, but it approaches a constant value when the time is longer than the longest energy-containing periods of the eddies. In between these extremes K varies with a decreasing derivative with respect to T as the amount of kinetic energy causing diffusion decreases. Since the efficiency of puff-diffusion is crucially depending on the eddies in a

NATO ASI Series, Vol. I 7
The Tropospheric Chemistry of Ozone in the Polar Regions
Edited by H. Niki and K. H. Becker

narrow size-range selected by the spatial dimensions of the puff, the development is even more dependent on the actual spectral density distribution than plume-diffusion. Quite frequently a puff-size lies in a range where the eddy kinetic energy increases with size, in which case the puff grows much faster with T than a corresponding plume. Batchelor's similarity theory also predicts an initial linear increase of K with T, but at intermediate time-levels puff-diffusion enters into a phase when K increases with T^2 (the accelerating phase). At very large T-values K approaches a constant value as for plume-diffusion.

These results are all based on the assumption of homogeneous and stationary turbulence, i.e., all statistical properties are uniformly distributed in space and time. This limits the practical validity of the theory, e.g., there is an abrupt vertical gradient in the eddy kinetic energy across the top of the atmospheric boundary layer, as well as between middle and high latitudes. In order to understand atmospheric dispersion processes, it is necessary to know the distribution of eddies in space and time, as well as their structure and transport capacities.

THE ATMOSPHERIC SYSTEMS OF MOTION

The atmospheric motions possess all spatial scales from millimeters to a few ten-thousands of kilometres. The only source of energy for these motions is the sun's radiation, and the loss of energy is through frictional dissipation transferring kinetic to internal energy which, in turn, is lost by radiation to the universe. The distribution of received solar energy is far from being homogeneous and steady. As a consequence, the temperature of the air is a complex function of space and time, a feature responsible for the onset of an equally complex picture of air motions. Averaged over several years, the atmosphere-ocean-earth system is net heated between the two latitude circles 39° N and 37° S, while the system is net cooled outside [Lorenz, 1967]. For the atmosphere alone the radiative balance is negative at all latitudes, however, the atmosphere receives a major part of the net energy in the tropics through sensible heating, and more importantly, through latent heating by evaporation of water from the ground. Most of this latent heating is quickly turned into sensible heating by release of precipitation in the tropics, and the heating is distributed throughout the troposphere. In conclusion, the atmosphere is net heated where its temperature is high and cooled where it is low. The whole global system is driven as a heat engine where macroscopic work is produced through maintenance of air and ocean currents transporting internal energy from the warm to the cold reservoir. A major part of this transport (75%) is taking place in the atmosphere.

The air currents created by the global scale differential heating are responsible for the well known cells of zonally averaged motions in the meridional-height direction. A zonal

average for the mass transport (viz. Lagrangian zonal averages) will mostly show up with one cell on each hemisphere in the troposphere, which transport air polewards in upper levels. In the stratosphere there is one cell transporting air from the summer hemisphere to the winter hemisphere at the solstices [Kida, 1983; Plumb and Mahlman, 1987]. Due to the rotation of the earth and the budget law for angular momentum, air parcels following the poleward currents at upper tropospheric levels turns eastwards creating the westerly jet-stream systems at middle latitudes. Since the time-scale of these global scale motions are much larger than the period of the earth's rotation, the wind-vectors of the westerlies are nearly parallel to isobars in constant height surfaces, in fulfillment of the geostrophic assumption. These quasi-geostrophic conditions are also applicable for even smaller scales, and the atmosphere thus has an ability through non-linear processes (frontogenetic advection) to create sharp gradients and build up reservoirs of available potential energy (APE). The classical example is a front; a sloping thin layer of air separating air masses of different temperature being kept in equilibrium by a corresponding difference in the coriolis force caused by a cyclonic wind-shear across the front.

The APE and kinetic energy of the westerly basic current is converted into eddy kinetic energy by growing and travelling waves, causing the slope to decrease so that cold and heavy air sinks below warm and the cross-frontal wind-shear to decrease accordingly. This hydrodynamic instability is released when the frontal zone is sufficiently sharp, and causes frontal cyclones with wavelength about 2000 km to evolve in the lower portion of the troposphere. A similar process on a larger scale involving the whole depth of the troposphere may also take place, causing growing and travelling baroclinic waves of length 3000 to 6000 km on the westerly jet (low-frequency transient waves). These instabilities constitute sources of kinetic energy with eddy periods ranging from about 1 to 10 days and even longer for ultralong waves which may become stationary or move westwards relative to the ground in approximate accordance with the Rossby formula. The major part of the eddy kinetic energy in the troposphere is found in this range of periods. Due to non-linear effects, eddies of different sizes interacts to produce eddies of smaller sizes, and the kinetic energy is cascading down the scales eventually reaching the scale of molecular motion and is thus turned into internal energy. The size-range of eddies between those where the kinetic energy is produced and those where frictional dissipation takes place, is called the inertial subrange. The shape of the kinetic energy density spectrum in this range can be determined by the well-known Kolmogorov similarity theory which predicts the energy density to be proportional to the wavenumber to the power -5/3 for three-dimensional and -3 for two-dimensional turbulence [Pasquill and Smith, 1983].

Although the above-mentioned instability phenomena are responsible for most of the eddy kinetic energy production in the troposphere, they are not the only processes creating eddies. Thus, a measured energy spectrum will show several deviations from the theoretical

spectrum of the inertial subrange. These are signatures of different ranges of energy-input caused by other instability phenomena or circulations forced by differential heating on all scales. On the mesoscale there are inertio-gravity waves induced by topography and time-dependent phenomena causing an imbalance between wind and pressure, tropical cyclones, polar lows and similar vortices normally created in a shallow layer of cold air over open sea, sea-land breeze and mountain-valley wind circulations, lee vortices, katabatic flows, etc. An even more important input of energy is normally observed to take place on the microscale, causing eddies of periods shorter than 15 minutes with a maximum around 100 s [e.g., Fiedler and Panofsky, 1970]. This energy-input range is less evident in the free troposphere than in the atmospheric boundary layer (ABL). It is caused by instabilities of the Rayleigh-Fjørtoft type (barotropic instability), depending on buoyancy and wind-shear. In a static unstable ABL relatively low-frequency convection currents are created, in a near neutrally stratified ABL with wind, a high-frequency turbulence is created; by shear-instability and surface roughness; and in the static stable ABL with the Richardson's number $Ri > 1/4$, a wide range of frequencies with relatively little energy are created through surface induced gravity-waves and weak circulations forced by local differential heating. In the free troposphere, microscale eddy input is regularly caused by penetrative cumulus convection, clear air turbulence in the vicinity of jet-streams, and gravity-waves which may break under supercritical conditions. Frequently, the conditions inside large-scale precipitation areas are unstable and dominated by convective currents (e.g., frontal rain-bands).

It is quite clear that the eddy kinetic density spectrum will vary in time and space, contradicting the assumption of homogeneous and stationary turbulence in the classical theory of diffusion. Thus, a spectrum for a typical situation in Arctic areas will be considerably different from spectra in middle latitudes, and spectra in the free troposphere are different from spectra in the ABL [Vinichenko, 1970; Atkinson, 1981]. The schematic Figure 1 shows two energy maxima corresponding to the macro- and micro-scale input ranges. The frequencies in between these maxima ("the meso-scale spectral gap") and on the high-frequency side of the micro-scale input range, the shape of the spectrum approximately follows the law of inertial subrange. It is a clear difference between the free troposphere and the ABL in the amount of energy carried by macro- and meso-scale eddies. In the ABL the energy amount at low frequencies are similar to that for high frequencies, and in between the energy virtually falls off to zero at periods close to 15 minutes separating the micro- from the meso- scale. The vortices of the macro- and large meso-scales are well reproduced in numerical weather prediction models which assimilate measurements taken in the international network operated through WMO, with such a quality that they can be forecasted deterministically with skill up to about 5-7 days. Analysed windfields from such models, therefore, fully resolves the low-frequency energy-rich eddies. The high-frequency eddies are, however, necessary to parameterize as turbulent diffusion. If one wishes to

calculate concentrations of a pollutant averaged over a few hours, this would seem to be done accurately enough by resolved winds from a NWP model with a constant horizontal diffusion coefficient for the microscale. If a model is designed for longer time-averages, the diffusion coefficient must also include macroscale eddies and thus increase with travel-time, and for averages of one month or longer another constant but much larger coefficient is applicable.

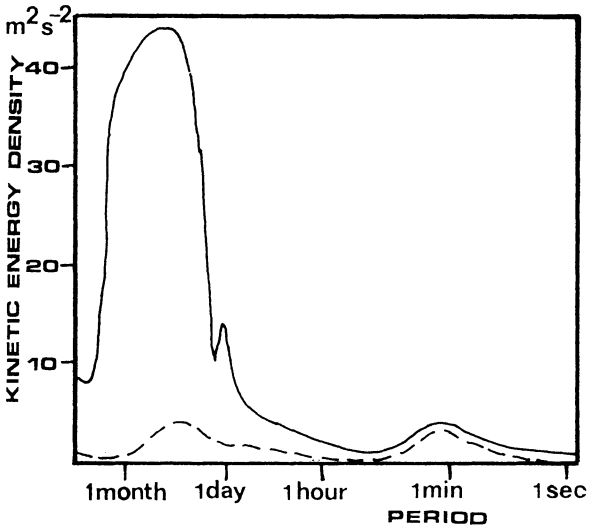

Fig. 1: A composite of kinetic energy spectra of the zonal wind in the free troposphere (continuous curve) and in the ABL (dashed curve) [After Vinichenko, 1970].

PROCESSES CAUSING TRANSPORT TO THE ARCTIC

Air transport to and from the Arctic is generally an exchange of air between areas characterized by different regimes of eddy kinetic energy. In middle latitudes, travelling cyclones and anticyclones embedded in the jet-streams dominate the kinetic energy spectrum at medium low frequencies. In the Arctic, such eddies are much less frequent (Figure 4b). A typical spectrum of kinetic energy inside the Arctic is, therefore, expected to show considerably less low-frequency energy. This heterogeneous distribution of eddies tends to prevent a systematic transport over considerable meridional distances. In the southern hemisphere this is also seen to be the case; transport from middle latitudes into the Antarctic region is very slow. In the Northern hemisphere, however, quasi-stationary waves with large

amplitudes frequently occur at high latitudes, and that is mainly why the pollution situation in the Arctic is different from that in the Antarctic.

In the northern hemisphere, oceans and continents which constitute large temperature contrasts lie in more or less well defined sectors, and there are a few extensive ranges of mountains, in particular Rocky Mountains and the Himalayas. These geographically determined lower boundary conditions for the atmosphere act as sources and sinks for vorticity which cause the middle-latitude jet streams at different longitudes to deviate systematically from the zonally averaged westerly flow. Figure 2 taken from Blackmon [1976] shows, in addition to a seasonal difference in wind-speed and average latitudinal position of the jet streams, clear stationary waves with ridges over extensive mountain ranges and (especially in winter) deep troughs downstream. In winter, the oceans are relatively warmer than the continents, and a similar but weaker ridge-trough pattern can be recognised with ridges over oceans. In summer, the oceans are cooler than the continents and the pattern is opposite.

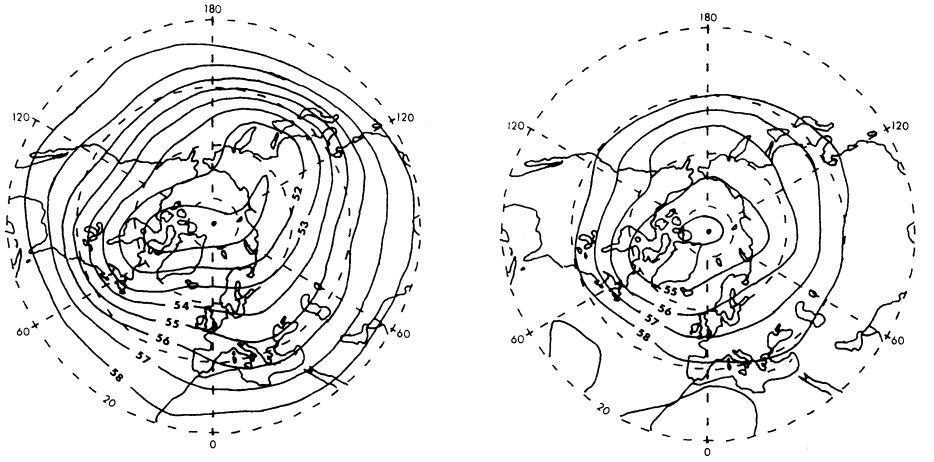

a) 9 winter seasons **b)** 10 summer seasons

Fig. 2: Average geopotential height of the 500 hPa surface. Unit and equidistance 100 m. [After Blackmon, 1976].

On a given day the 500 hPa surface will deviate considerably from Figure 2, and show waves of very different amplitudes, wave-lengths and phase-speeds. The jet-stream system as a whole may, from time to time, be dominated by slowly travelling (quasi-stationary) waves

with high amplitudes and long wavelengths. Such a quasi-stationary wave hampers the eastward movement of cyclones, and is, therefore, called a blocking. It can be regarded as resulting from interference between the stationary waves and low-frequency transient waves released by deep baroclinic instability. The situation is characterized in synoptic meteorology by a split in the jet-stream with one branch turning equatorwards and another turning poleward, and may cause transport from middle latitudes into the Arctic. A more modern description is not to regard the split as a specific phenomenon, but as a result of an occasional co-positioning of the polar and sub-tropical jets caused by differences in phases and amplitudes of the long waves associated with the respective currents. About 15-20 degrees to the east of the split, a dipole structure with a warm anticyclone centered around 60° N and a cold cyclone around 40° N is seen in many cases (Figure 3). Often, the blocking centre is more of a monopole-type dominated either by a warm anticyclone ("omega circulation") or a cold cyclone. Blockings dominated by cold cyclones are believed to be the least efficient in provoking transport into the Arctic. Blocking action may also be provoked by stationary Rossby wave-trains radiating from tropical heat anomalies [Hoskins and Karoly, 1981]. These resemble the teleconnection patterns diagnosed from observations, such as the Pacific-North-American pattern, the West and East Atlantic pattern, the Eurasian pattern and the West Pacific pattern [Wallace and Gutzler, 1981].

Rex [1950] established a set of criteria in order to subjectively select blocking cases, and thus obtained a 19-year statistics for their occurrence. His criteria pointed out the north-east Atlantic Ocean and north-east Pacific Ocean as preferred regions, the Atlantic cases being 2.5 times as frequent as the Pacific. Both areas experienced a clear seasonal trend with maximum occurrence from January to May and a minimum in autumn. The Atlantic blocking cases were particularly frequent in May with more than 40% of the days signified as blocked days. Later studies applying more objective methods have largely confirmed the results of Rex [1950]. Lejenäs and Økland [1983] selected dipole-type blocking cases by requiring the 500 hPa geopotential height at 60° N to be larger than that at 40° N, yielding a statistical distribution of blocking very similar to Rex [1950], though with the maximum frequency of Pacific blocking occurrence shifted from spring to winter with maximum in January. Both these investigations fail to select blocking cases over the central Eurasian continent (Ural area), which have been discovered by other studies [Blackmon, 1976; Shukla and Mo, 1983; Kanestrøm et al., 1985]. The Eurasian blockings were shown by Kanestrøm et al. [1985] to mainly occur as anticyclonic monopoles, and are efficient in transporting polluted air from Europe to the Arctic.

The relevance of blocking anticyclones in relation to Arctic air pollution has been suggested by Raatz [1983], and the relevance of long planetary waves by Reiter [1981]. Iversen [1989a] defined a meridional index brought about by the zonal wavenumbers 1, 2, 3 and 4 to select blocking cases with a potential of causing transport of air from middle

latitudes to the Arctic, and compared with the statistics obtained with the method of Lejenäs and Økland [1983]. The emphasis on these very long waves is partly theoretically based on the calculations of Hoskins and Karoly [1981], contradicting the possibility of stationary waves on middle and high latitudes for higher wavenumbers than 4. It is also partly inspired by data studies in which the low-frequency variability is mostly seen to have the major part of its energy on very long waves [e.g., Blackmon, 1976; Wallace and Blackmon, 1983]. Figure 4 shows how the long periodic waves contribute to blocking action over well-defined areas in the Atlantic, Eurasian and Pacific sectors in high latitudes during winter. The variance caused by periods of medium length emphasizes cyclonic storm tracks which are seen to be found at middle latitudes over wide longitudinal bands in the Pacific and the Atlantic extending into Eurasia.

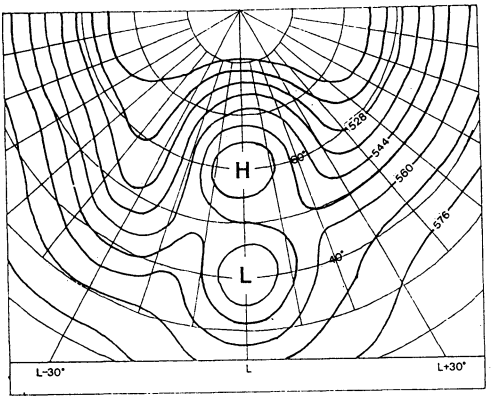

Fig. 3: A prototype dipole blocking centered at longitude L as seen in the geopotential height field of 500 hPa in spring. Unit 10 m. [Taken from Iversen, 1989a].

The results of Iversen [1989a] are given in Figure 5. They are valid only for the rather limited period of 2 years and 3 months. Nevertheless, the statistics are very much in agreement with the climatological investigations mentioned above. The full definition of an event of high meridional index is defined in detail in the original paper, but can be thought of as incidents when the 4 longest zonal waves composes a poleward transport larger than 10 degrees of latitude per 36 hours between 60° N and 70° N. This index focuses on the part of a blocking, which is directly relevant for transport to the Arctic and is independent of the mono- or di- pole structure. The Pacific, Atlantic and Eurasian maxima are recognized from Figure 5, and there is a very clear seasonal cycle. By correlating the meridional index with ground level measurements of particulate SO_4^{-2} taken at Norwegian Arctic sites, the

relevance of these features in explaining the occurrence of Arctic haze was documented by Iversen [1989a]. They were seen to account for the observed seasonal variation as well as the short-term episodic variations of the Arctic haze. The most frequent intrusions of air into Arctic seems to take place over the North Atlantic Ocean, while transport over Northern Eurasia and North Pacific Ocean seems to occur less frequently. Transport over certain sectors in North America has very low frequency.

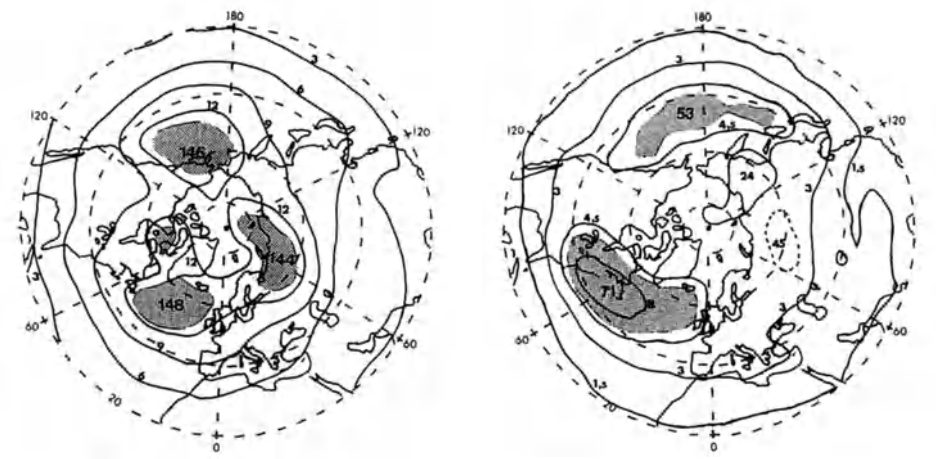

a) Low-pass filtered data emphasizing periods longer than 10 days. Equidistance 10m.

b) Band-pass filtered data emphasizing periods between 2.5 and 6 days. Equidistance 5m.

Fig. 4: Variance of 500 hPa geopotential height for 18 winter seasons after the removal of the climatological mean annual cycle. Unit 10 m. [After Wallace and Blackmon, 1983].

TRANSPORT LEVELS

It is evident that there would not be any significant atmospheric motions without the joint action of differential heating and viscous dissipation, both processes causing a change of an air parcel's entropy. The time-scale of these processes is, however, generally longer than the time-scale of displacement and growth of cyclone-waves, and the instability processes causing the waves are fully described with an adiabatic and frictionless model of the atmosphere. Of course, heating and friction will modify any development, in particular the release of latent heat in precipitation areas, but assuming the entropy of an air parcel to be conserved, can be justified as a first approximation over a few days. A measure of the

entropy of dry air is the potential temperature θ defined as the temperature an air parcel will obtain by changing its pressure adiabatically to 1000 hPa. Outside precipitation areas, θ is thus a very good tracer. The average time taken for an air parcel to hit precipitation starting from an arbitrary time, has been estimated by measurements in middle latitudes by Rodhe and Grandell [1972] to be 90 hours in summer and 35 hours in winter. Thus, air parcels tend to stick to surfaces of constant potential temperature. Cooling of a particle causes subsidence of air through these surfaces towards lower values of θ, while heating causes ascending towards higher θ. Figure 6 shows a climatological meridional distribution of θ in summer and winter [Iversen, 1989b].

In winter the surfaces are more tightly packed than in summer. Particularly in the Arctic, the very stable boundary layer is clearly recognized. In winter, there is a pronounced separation of possible ground level sources of Arctic pollution; 1) areas inside the Arctic ABL may contribute efficiently to ground level pollution; 2) areas south of the Arctic ABL but north of the polar front system may contribute to pollution somewhat higher, though with a larger possibility to be washed out on its way; 3) sources south of the polar front may contribute to pollution high up in the troposphere, however, for water-soluble species there is a large probability of washout *en route*, and turbulent diffusion in the polar frontal zone causes considerable dilution. In summer, the separation between sources is less clear and there is also less frequent transport into the Arctic (Figure 7). Furthermore, the probability of wet removal processes inside Arctic is higher in the summer. The situation even in summer is a stable ABL, but with a smaller lateral extension the ABL is often saturated. Open water and polynyas in the ice-cover cause a high frequency of deep fog and stratus clouds [e.g., Steffensen, 1982]. Thus, heterogeneous chemistry in the arctic ABL should be expected during summer.

As an example, results from a numerical model aimed at estimating the sources of Arctic haze is presented in Figure 7 [Iversen, 1989b; Tarrason and Iversen, 1992]. Particulate sulphate averaged over the area north of 70° N latitude circle for March and July, 1983 are shown. The general concentration level reflects the seasonal difference in transport into the Arctic. The vertical segregation of contributing sources as a function of their distance from the Arctic is particularly evident in March, but less evident in July. This is in accordance with the seasonal variation of the distribution of θ-surfaces, but also reflects the more efficient removal of particles due to ABL fog and stratus in July.

Not all atmospheric constituents of anthropogenic origins found in the Arctic are injected directly from emissions at lower latitudes, but are either chemically produced as secondary compounds in the atmosphere, or are long-lived components which may be transported far away from their sources before being caught by a current injecting air into the Arctic atmosphere. For such components the middle-latitude origin may be in the middle troposphere, and the arguments about the vertical distribution in the Arctic and the distance

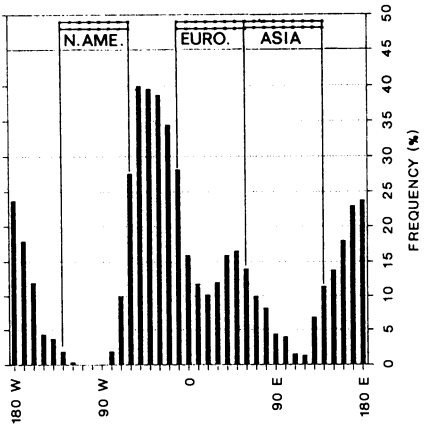

a) Winter (Dec., Jan., Feb.)

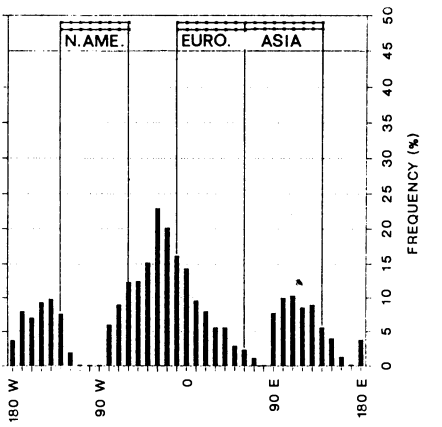

b) Spring (Mar., Apr., May)

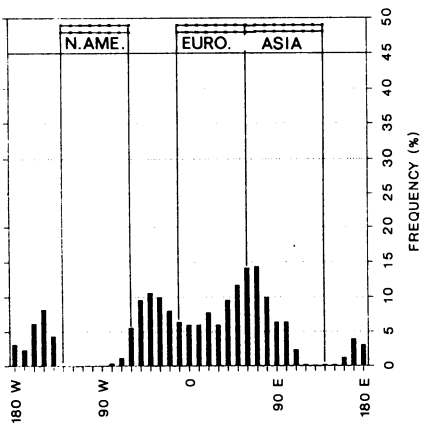

c) Summer (Jun., Jul., Aug.)

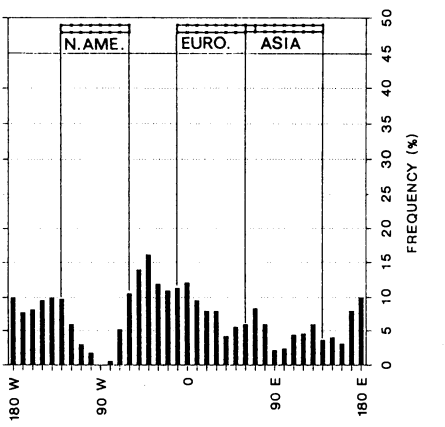

d) Autumn (Sep., Oct., Nov.)

Fig. 5: Relative frequency of high meridional index (%) for every 10 degree longitude over a period of 2 years and 3 months. [Based on Iversen, 1989a]

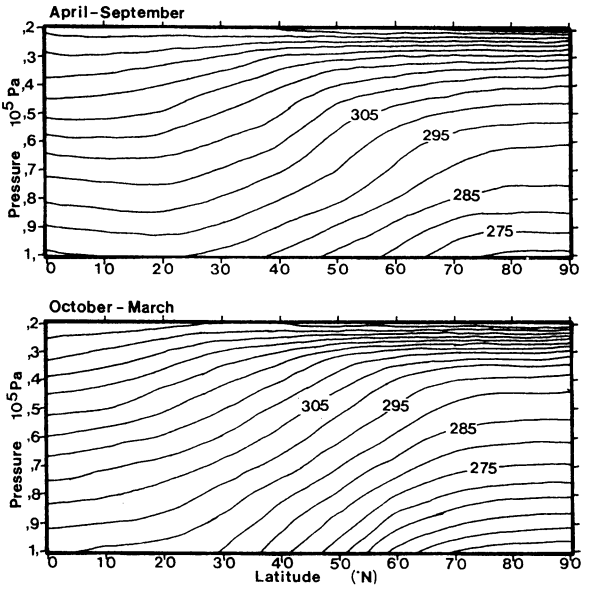

Fig. 6. Potential temperature calculated from seasonally averaged temperature [Lorenz, 1967] in a pressure/latitude section. [Taken from Iversen, 1989b]

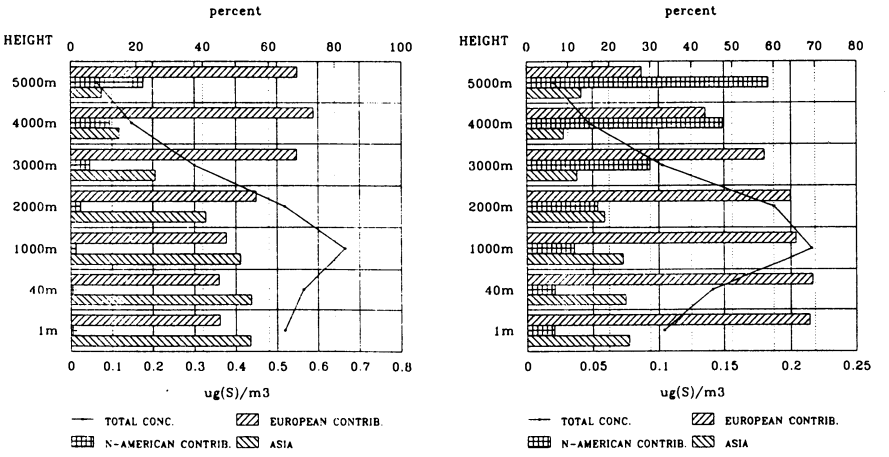

a) MARCH 1983 **b)** JULY 1983

Fig. 7: Monthly averaged concentrations north of 70° N calculated by a model. [Calculations made by L. Tarrason; see Tarrason and Iversen, 1992]

to the source is not as relevant. In particular, ozone is occasionally injected into the troposphere at middle latitudes from the stratosphere. These intrusions are probably more important for the Arctic ozone budget than that for the whole globe, since the processes take place close to its boundaries. A full quantitative understanding of the injection processes is not obtained yet, but in the condensed review by Vaughan [1988] the transport during episodes of tropospheric foldings is presented as the most probable contributor. Strong folding events occur when an upper-level jet streak is moving into a cold low causing a rapid cyclogenesis on the ground. The ageostrophic thermally direct, transversial circulation forced by the upper level geostrophic frontogenesis in the foremost part of the jet-streak, causes subsidence in the lower stratosphere and a downward advection of stratospheric air along isentropic surfaces. Parts of this air may be transported back to the stratosphere as the jet-streak passes, but a significant portion will remain in the troposphere. The stratospheric air is characterized by high ozone mixing ratios, low relative humidity and high potential vorticity. The mixing of these stratospheric characteristics into the troposphere takes place through small scale turbulence which is pronounced in the vicinity of the jet. Early studies of the folding of the troposphere were made by Reed [1955] and Reed and Danielsen [1959], but the phenomenon has been further studied by several investigators [e.g., Danielsen, 1968; Danielsen and Mohnen, 1977; Shapiro, 1980; Keyser and Shapiro, 1986; Danielsen et al, 1987]. Estimates of the flux of stratospheric ozone through the tropopause have been made by regression against potential vorticity and stratospheric radioactive isotopes in the 60s. Estimates made by general circulation models, which involve a parameterization of the actual folding process, leads to an estimate of 7×10^{10} molec. cm^{-2} s^{-1} in the northern hemisphere [e.g., Levy et al., 1985]. According to the seasonal variation of rapid cyclogenesis, it is to be expected that the flux is larger in the cold seasons.

SIMPLIFIED PLUME ESTIMATES

As a final example of the effects of atmospheric dispersion processes relevant for Arctic pollution, the fate of continuous ground level emissions at different latitudes are estimated by a simplified model of the "Rodhe-Venkatram"-type. A southerly wind U is assumed and the concentration of the emitted compound is c. The height and width of the plume is H and D, respectively. H and D and c are all dependent on the Lagrangian time t = x/U since the emission release, where x is the distance downwind from the source. The flux F = cDHU is conserved. If there is no flux from the ambient air, no deposition and no production. In general:

$$\frac{\partial F}{\partial t} = -\lambda F + \bar{F} \qquad (1)$$

where λ is a decay coefficient encompassing dry and wet scavenging and chemical destruction, and $\bar{F}$ is a production term including emission, influx from ambient air and chemical production. If λ is assumed constant, and $F(0) = Q$ is the initial condition, the solution to equation (1) is:

$$F(t) = \frac{\bar{F}}{\lambda} + [Q - \frac{\bar{F}}{\lambda}] \exp(-\lambda t) \qquad (2)$$

where Q is the emission strength of the point source. We now want to calculate the concentration at 80° N resulting from plumes originating from point sources at different latitudes; B_a south of the polar front, B_b between the polar front and the arctic front, and B_c north of the arctic front. We assume a typical winter/spring event with an established quasi-stationary northward flow of U = 10 degrees per 36 h $\approx$ 8.6 m s^{-1}, which is the minimum for classification as high meridional index. A plume which intersects a front at ground level is assumed to be detached from the ground as it rises along an isentropic surface, and the plumes a and b will, therefore, undergo three phases (Figure 8). We neglect the production term F since we only are addressing the fate of the emission Q, and the depletion coefficient is assumed to be written as:

$$\lambda = \frac{1}{T_d} + \frac{1}{T_w} + \frac{1}{T_c} \qquad (3)$$

where T_d, T_w and T_c are time-scales for dry and wet scavenging and chemical depletion, respectively. The values for the time-scales will depend on the component and take different values in the different phases. We intend to estimate concentrations of airborne oxidised sulphur (SO_x), nitrogen oxides (NO_x), PAN, a typical non-methane alkane (HCa) and an alkene (HCe), and Table 1 gives chosen values for the time-scales. The values for dry deposition are achieved by assuming a value for the dry deposition speed v_d and for the mixing height H, so that $T_d = H/v_d$. The values for T_w is based on the work by Rodhe and Grandell [1972] with values of parameters taken from Hamrud et al. [1981], except that T_w is halved in the polar front zone and doubled inside the stable Arctic air mass. The T_c for NO_x is includes reactions in darkness initiated by O_3, day-time reactions initiated by OH, as well as loss to PAN [Iversen et al., 1991]. The T_c-value for PAN is the thermal decomposition to NO_x. For the hydrocarbons T_c is determined by an initial OH reaction [Simpson and Hov, 1990 and Simpson, 1992]. In order to calculate PAN, a coupled set of equation must be solved, involving the NO_x-equation:

$$\frac{dN}{dt} = -\kappa N + \lambda_{P\to N} P \qquad and \qquad \frac{dP}{dt} = -\alpha P + \lambda_{N\to P} N \tag{4}$$

where N and P are fluxes of NO_x and PAN respectively, and κ and α are their total depletion coefficients. Rate coefficients for transformation from NO_x to PAN and vice versa are $\lambda_{N\to P}$ and $\lambda_{P\to N}$. If the term $\lambda_{P\to N} P$ in the equation for N can be removed compared with the other terms, the solution is:

$$N = Q_{NOX} \exp[-\kappa t]$$

$$P = \frac{\lambda_{N\to P}\, Q_{NOX}}{\kappa - \alpha} [1 - \exp[-(\kappa - \alpha) t]] \exp[-\alpha t] \tag{5}$$

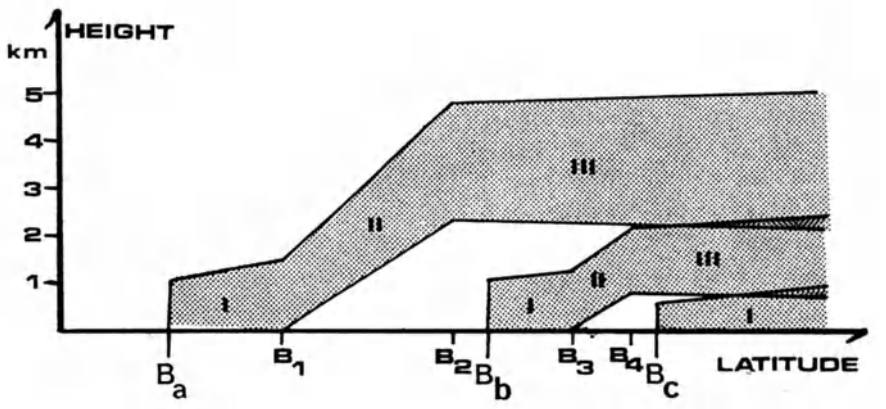

Fig. 8: The assumed shapes of plumes originating at latitudes B_a, B_b, and B_c. The position of the polar front is defined by B_1 and B_2, and the arctic front by B_3 and B_4.

The time-scale for transformation from NO_x to PAN is estimated at $T_{c,N\text{-}P} = \lambda_{N\text{-}P}^{-1} = 30 \times 10^4$ s. In Table 2, the result of the calculations are given as the fraction between the concentration at 80° N and the emission. The growth of D and H with t is assumed to follow an approximate shape according to plume-diffusion. The dilution is assumed most efficient as

Table 1: Time-scales used in the different phases (I, II and III) of transport to 80° N

Emission Latitude	Species	T_d (10^4s)			T_w (10^4s)			T_c (10^4s)		
		I	II	III	I	II	III	I	II	III
B_a = 40° N	SO_x	25	∞	∞	18	9	36	∞	∞	∞
	NO_x	50	∞	∞	∞	∞	∞	8	10	12
	PAN	50	∞	∞	∞	∞	∞	20	100	700
	HCa (n-but.)	∞	∞	∞	∞	∞	∞	50	200	∞
	HCe (ethene)	∞	∞	∞	∞	∞	∞	10	20	∞
B_b = 55° N	SO_x	25	∞	∞	18	18	36	∞	∞	∞
	NO_x	50	∞	∞	∞	∞	∞	8	10	12
	PAN	50	∞	∞	∞	∞	∞	100	700	700
	HCa (n-but.)	∞	∞	∞	∞	∞	∞	200	∞	∞
	HCe (ethene)	∞	∞	∞	∞	∞	∞	20	∞	∞
B_c = 77° N	SO_x	25	-	-	36	-	-	∞	-	-
	NO_x	100	-	-	∞	-	-	12	-	-
	PAN	100	-	-	∞	-	-	100	-	-
	HCa (n-but.)	∞	-	-	∞	-	-	∞	-	-
	HCe (ethene)	∞	-	-	∞	-	-	∞	-	-

long as the size is moderate and at middle latitudes. The plume growth is particularly fast when passing the polar front, and particularly slow inside the Arctic. Table 1 also includes estimates of concentrations at 80° N due to emissions in Europe at different latitudes. The plumes are spread out much more widely in these estimates, reflecting the actual size of the emission domains and larger spread due to relative diffusion (puff). The estimated vertical and horizontal extensions of the plumes in this case are given in this table. In order to arrive at a seasonal average, the average frequency of high meridional index over the European sector is used. Comparing the results for sulphur with the much more complete calculations presented in Figure 7, it is seen that the agreement is fair for the European contribution. If the simple calculations have equally as fair quality for the other components, one may conclude that the major part of oxidised nitrogen in Arctic air consists of PAN. Exceptions might be contributions from emission sources inside the Arctic boundary layer which potentially contribute more NO_x at levels close to the ground. At least in the European sector, however, these emissions are not significant (as they are for sulphur). Similarly, alkanes may seem to accumulate in larger quantities in the wintertime Arctic than alkenes, partly due to their lower reactivity and partly to higher emission rates.

Finally, it should be remarked that these calculations are made only as a crude illustration of features which influence Arctic air quality. Full model-calculations including all seasons and all emissions, actual meteorological data must be used for a complete calculation of concentrations which can be compared with measurements. Using only European emission in this example does not reflect any opinion about the relative importance of Europe as a contributor to Arctic pollution. A full survey of emissions must be included to estimate this. In particular pollutants which are slowly dissolved in water and thus not scavenged by precipitation (e.g., persistent organic compounds) may be efficiently transported to the Arctic from any source. In the Russian part of Asia, there are also very large sources of SO_x and heavy metals inside the winter Arctic boundary layer (Norilsk).

Table 2. Results of estimated typical winter-spring air quality in the Arctic (80° N) for single plumes and for averaged concentrations due to emissions in Europe

Species	Emission latitude	Single plume conc./emis.	European plume characteristics					
			emis.	Transp.	plume extension			average conc.
				freq.	vertical low	bounds high	hor. width	
	(deg. N.)	(pptv/kt a^{-1})	(kt/a)	(%)	(m)	(m)	(km)	(pptv)
SO_x (as S)	40	0.164	9000	20	2000	5000	3400	19.444
	55	1.017	11000	20	500	2500	2600	109.35
	70	9.985	4000	15	0	800	600	107.83
NO_x (as N)	40	0.0468	1920	20	2000	5000	3400	1.1825
	55	0.654	4130	20	500	2500	2600	26.405
	70	15.53	25	15	0	800	600	10.483
PAN (as N)	40	1.661	1920	20	2000	5000	3400	41.963
	55	4.495	4130	20	500	2500	2600	181.42
	70	12.27	25	15	0	800	600	8.2796
HCa (n-but.)	40	29.06	2550	20	2000	5000	3400	974.48
	55	77.92	5140	20	500	2500	2600	3912.8
	70	263.9	17	15	0	800	600	118.11
HCe (ethe.)	40	3.922	225	20	2000	5000	3400	11.557
	55	19.05	450	20	500	2500	2600	84.045
	70	125.7	2	15	0	800	600	4.9420

REFERENCES

Atkinson, B. W., *Meso-scale Atmospheric Circulations*, Academic Press, 495 pp., 1981.

Blackmon, M. L., A climatological spectral study of the 500 mb geopotential height of the northern hemisphere, *J. Atmos. Sci., 33*, 1607-1623, 1976.

Danielsen, E. F., Stratospheric-tropospheric exchange based on radioactivity, ozone and potential vorticity, *J. Atmos. Sci., 25*, 502-518, 1968.

Danielsen, E. F. and V. A. Mohnen, Project duststorm report: Ozone transport, in situ measurements and meteorological analyses of tropopause folding, *J. Geophys. Res., 82*, 5867-5977, 1977.

Danielsen, E. F., R. S. Hipskind, S. E. Gaines, G. W. Sachse, G. L. Gregory, and G. F. Hill, Three-dimensional analysis of potential vorticity associated with tropopause folds and observed variations of ozone and carbon monoxide, *J. Geophys. Res., 92*, 2103-2111, 1987.

Fiedler, F. and H. A. Panofsky, Atmospheric scales and spectral gaps, *Bull. Am. Met. Soc., 51*, 1114-1119, 1970.

Hamrud, M., H. Rodhe, and J. Grandell, A numerical comparison between Lagrangian and Eulerian rainfall statistics, *Tellus, 33*, 235-241, 1981.

Hoskins, B. J. and D. J. Karoly, The steady linear response of a spherical atmosphere to thermal and orographic forcing, *J. Atmos. Sci., 38*, 1179-1196, 1981.

Iversen, T., Some statistical properties of ground level air pollution at Norwegian Arctic stations and their relation to large scale atmospheric flow systems, *Atmos. Environ., 23*, 2451-2462, 1989a.

Iversen, T., Numerical modelling of the long range atmospheric transport of sulphur dioxide and particulate sulphate to the Arctic, *Atmos. Environ., 23*, 2571-2595, 1989b.

Iversen, T., N. E. Halvorsen, S. Mylona, S. and H. Sandnes, Calculated budgets for airborne acidifying components in Europe, 1985, 1987, 1988, 1989 and 1990. EMEP/MSC-W Report 1/91, The Norwegian Meteorological Institute, Oslo, Norway, 1991.

Kanestrøm, I., K. Pedersen, and H. Skaåtun, Major stationary ridges and troughs at 500 mb, *Geophysica Norvegica, 33*, 1-40, 1985.

Keyser, D. and M. A. Shapiro, A review of the structure and dynamics of upper level frontal zones, *Mon. Wea. Rev., 114*, 452-499, 1986.

Kida, H., General circulation of air parcels and transport characteristics derived from a hemispheric GCM. Part 2. Very long-term motions of air parcels in the troposphere and stratosphere, *J. Met. Soc. Japan, 61*, 510-523, 1983.

Levy, H. B., J. D. Mahlman, W. J. Moxim, and S. Liu, Tropospheric ozone: the role of transport. *J. Geophys. Res., 90*, 3753-3771, 1985.

Lejenäs, H. and H. Økland, Characteristics of northern hemispheric blocking as determined from long time-series of observational data,. *Tellus, 35A*, 350-362, 1983.

Lorenz, E. N., *The nature and theory of the general circulation of the atmosphere,* World Meteorological Organization, Geneva. 161 pp, 1967.

Pasquill, F. and F. B. Smith, *Atmospheric diffusion*, 3rd edition, John Wiley & Sons, 437 pp., 1983.

Plumb, R. A. and J. D. Mahlman, The zonally averaged transport characteristics of the GFDL circulation/transport model, *J. Atmos. Sci., 44*, 298-327, 1987.

Raatz, W. E., Arctic Haze: Meteorological aspects of long-range transport, Ph.D.-thesis, Univ. of Alaska, Fairbanks, 1983.

Reed, R. J., A study of a characteristic type of upper level frontogenesis, *J. Meteorol. 12*, 226-237, 1955.

Reed, R. J. and E. F. Danielsen, Fronts in the vicinity of the tropopause, *Arch. Met. Geophys. Bioklim., 11*, 1-17, 1959.

Reiter E. R., Planetary wave behaviour and Arctic air pollution. *Atmos. Environ., 15*, 1465-1471, 1981.

Rex D. F., Blocking action in the middle troposphere and its effects upon regional climate - II. The climatology of blocking action, *Tellus, 2*, 275-301, 1950.

Rodhe, H. and Grandell, J. (1972) On the removal time of aerosol particles from the atmosphere by precipitation scavenging. *Tellus, 24*, 442-454, 1972.

Shapiro, M. A., Turbulent mixing within tropopause folds as a mechanism for the exchange of chemical constituents between the stratosphere and the troposphere,. *J. Atmos. Sci., 37*, 994-1004, 1980.

Shukla, J. and K. C. Mo, Seasonal and geographical variation of blocking, *Mon. Wea. Rev., 111*, 388-402, 1983.

Simpson, D., Long period modelling of photochemical oxidants in Europe: A) Hydrocarbon reactivity and ozone formation in Europe, B) On the linearity of country-to-country ozone calculations in Europe, EMEP/MSC-W Note 1/92, The Norwegian Meteorological Institute, Oslo, Norway, 1992.

Simpson, D. and Ø. Hov, Long period modelling of photochemical oxidants in Europe. Calculations for July 1985. EMEP/MSC-W Note 2/90, The Norwegian Meteorological Institute, Oslo, Norway, 1990.

Steffensen, E. L., The climate at Norwegian Arctic stations, *Klima, 5*. The Norwegian Meteorological Institute, Oslo, 1982.

Tarrason, L. and T. Iversen, The influence of north American anthropogenic sulphur emissions over western Europe, *Tellus, 44B*, 114-132, 1992.

Vaughan, G., Stratosphere-troposphere exchange of ozone. In *Tropospheric Ozone, I. S. A. Isaksen (ed.)*, 125-135, D. Reidel Publishing Company, 1988.

Vinnichenko, N. K., The kinetic energy spectrum in the free atmosphere - 1 second to 5 years. *Tellus, 22*, 158-166, 1970.

Wallace, J. M. and M. L. Blackmon, Observation of low-frequency atmospheric variability, In *Large-scale Dynamical Processes in the Atmosphere* (eds. by B. J. Hoskins and R. P. Pearce), 55-94, 1983.

Wallace, J. M. and D. S. Gutzler, Teleconnections in the geopotential height field during the northern hemispheric winter. *Mon. Wea. Rev., 109*, 785-812, 1981.

IMPACT OF GLOBAL NO_x SOURCES ON THE NORTHERN LATITUDES

Hiram Levy II, Walter J. Moxim and Prasad S. Kasibhatla[1]
Geophysical Fluid Dynamics Laboratory/NOAA
Princeton University
Post Box 308
Princeton, NJ 08542
U.S.A.

INTRODUCTION

Nitrogen oxides (NO_x), through their control of tropospheric ozone production, play a major role in determining the global reactivity of the atmosphere. The concentration of these oxides varies by as much as a factor of 1000 between continental source regions and remote locations and fluctuates significantly with season at high latitudes. While NO_x levels appear to be rather low (<50 pptv) away from local sources, high levels of PAN, an important reservoir for NO_x, have been measured at the surface in the winter polar regions [Barrie and Bottenheim, 1991] and in the free troposphere north of 30^o N [Singh, Salas and Viezee, 1986]. Furthermore, our recent global chemical transport model (GCTM) study finds PAN to be the major reactive nitrogen species in the northern latitudes [Kasibhatla et al., 1992].

Based on a limited set of chemical measurements, primarily from the surface, it has been argued that the thermal decomposition of this sequestered PAN supplies much of the NO_x in the northern latitudes, and that emissions from fossil fuel combustion are the dominant source [e.g. Barrie and Bottenheim, 1991; Honrath and Jaffe, 1992]. After checking model predictions against the available observations, we examine the hemispheric fields of NO_x and PAN generated by our GCTM and quantify the contribution from fossil fuel combustion. We then determine the amount of NO_x stored as PAN in the northern latitudes and compare it to direct emission from surface fossil fuel combustion and from jet aircraft.

DESCRIPTION OF THE MODEL

We explicitly separate reactive nitrogen [NO_y] into three classes of transported species; NO_x, HNO_3, and peroxyacetyl nitrate [PAN]. The conservation equations for their

---

1. School of Earth and Atmospheric Sciences, Georgia Institute of Technology, Atlanta, GA, 30332, USA

NATO ASI Series, Vol. I 7
The Tropospheric Chemistry of Ozone in the Polar Regions
Edited by H. Niki and K. H. Becker

mixing ratios [R],

$$\frac{\partial}{\partial t}(R) = Advection + Diffusion + Filling - Sink_{dry} - Sink_{wet} \quad (1)$$
$$+ Sources + Chemistry,$$

are expressed in flux convergence form and integrated globally using a medium resolution (~265 km horizontal grid, 11 vertical levels) 3-D global chemical transport model (GCTM). By using the flux convergence form of (1), the global mass integral for each transported species is conserved exactly. The GCTM is driven by 6-hour time-averaged winds and a consistent total-precipitation field from the parent general circulation model (GCM) (see section 2. of Mahlman and Moxim [1978] for a summary, and Manabe et al. [1974] and Manabe and Holloway [1975] for details).

Advection represents tracer transport by the GCM's resolved winds. It is integrated in flux convergence form, using a centered leap-frog numerical scheme which is 2nd order in the horizontal and 4th order in the vertical. A detailed derivation of the 6-hour time-averaged form of *Advection* and a discussion of the numerical integration technique are given in section 3. of Mahlman and Moxim [1978].

The principal difficulty in simulating atmospheric transport lies in the numerical treatment of those atmospheric processes that are not resolved by, in our case, a 265 km grid: details of cyclones, fronts, squall lines, convection, and turbulence on a wide range of scales. All these subgrid-scale processes must be represented by parameterizations based on the resolved grid-scale variables. In all cases, including this study, the parameterizations are very crude physical representations of the actual physical process. This is particularly true of our treatment of vertical subgrid-scale transport by convective clouds. Using a diffusive closure, which is a product of the local tracer gradient and a diffusion coefficient, we attempt to capture the ensemble average of such processes, if not the individual detail, with a subgrid-scale tracer transport that is down-gradient. However, our diffusion coefficients are much more than simple constants and depend on properties of the local winds and local gradients of the tracer field.

Horizontal *Diffusion* employs a highly scale-selective diffusion coefficient, K_H, that follows from the formulation first introduced by Smagorinsky [1963]. K_H is constructed so that, at the limit of very low horizontal-variability in the tracer field, the coefficient is 1/2 of the value used by the parent GCM, while in the limit of very high horizontal-variability, it is 10 times that value. This formulation was first developed and tested for a study of nuclear test debris, a high variability case, and for a study of tropospheric N_2O, a very low variability case. A detailed derivation and discussion of K_H is given in section 3. of Mahlman and

Moxim [1978] and in appendix A.2 of Levy et al. [1982].

There are two coefficients for vertical *Diffusion*, both of which are proportional to the square of a mixing length and to the vertical wind shear. The first coefficient, K_{vcon}, acts throughout the vertical column, has a constant mixing length of 30 m, and represents subgrid-scale vertical transport by moist and dry convective processes. It is activated only when the moist bulk Richardson number, as defined in equation A5 of Levy et al. [1982], is less than a specified critical value, which is meant to represent the onset of turbulence. A small additional term that depends on the tracer's vertical gradient is also included to reduce $2\Delta z$ fluctuations. The derivation and a detailed discussion of K_{vcon} are given in appendix A.3 of Levy et al. [1982].

Finding that the transport model underestimates vertical mixing in the boundary layer, under conditions of large-scale stability when K_{vcon} is shut off, we have included an additional vertical shear-dependent coefficient, K_{vbl}, in the lowest three levels. Its form is

$$K_{vbl} = A \cdot L(z)^2 \left| \frac{\partial \vec{V}}{\partial z} \right| \qquad (2)$$

where $L(z)$ are the same height-dependent mixing lengths used by the parent GCM, $\frac{\partial \vec{V}}{\partial z}$ is the vertical wind shear, and A is a scaling parameter that was 1.0 for the GCM and, based on observed tracer profiles, has been set to 0.5 for these transport studies. Further details are provided in section 2.1 of Levy and Moxim [1989] and section 2. of Kasibhatla et al., [1992].

Filling explicitly corrects negative mixing ratios, which are generally produced upstream of sharp gradients by numerical advection error. This model utilizes an essentially diffusive downstream borrowing approach, as explained in Mahlman and Moxim [1978].

$Sink_{dry}$, the deposition of gas molecules and aerosols on soil, water, ice, snow and vegetation at the earth's surface, is represented by

$$Sink_{dry} = \frac{w_d(i)}{\Delta z} \cdot R_{11}(i) \left[\frac{1}{\left[1 + w_d(i) / (C_d \left| \vec{V}_{eff} \right|) \right]} \right]. \qquad (3)$$

The term in the large brackets, which assumes a balance between surface deposition and the turbulent flux of the trace species in the bottom half of the lowest model level, reduces the mixing ratio in the lowest model level to its value at the earth's surface. $w_d(i)$ is the measured deposition velocity for the i^{th} species, $R_{11}(i)$ is its mixing ratio in the lowest model level, Δz is the thickness of that bottom level, C_d is the GCM's globally averaged surface drag coefficient [0.002], and $\left| \vec{V}_{eff} \right|$ is the model's effective surface wind speed [for details, see section 2.4 in Levy and Moxim, 1989]. Over the ocean, w_d is 0.3 cm/s for HNO_3 and 0.0 for PAN and NO_x. It is 0.5 cm/s for HNO_3 and 0.0 for the other two over ice and snow. Over land, when the temperature in the lowest level, T_{11}, is $>10^{\circ}$ C, w_d is 1.5 cm/s for HNO_3 and

0.25 cm/s for PAN and NO_x. $T_{11} < -10^o$ C over land is treated the same as ice and snow. For temperatures between 10^o C and -10^o C over land, the w_d values are linearly interpolated between the two land values mentioned above.

$Sink_{wet}$ is the deposition of soluble gases and aerosols in precipitation. We need only consider the highly soluble tracer HNO_3 for this study. The wet removal scheme we use distinguishes between stable or shallow convective and deep convective precipitation. The fraction of HNO_3 removed from the grid box is a function of the local precipitation rate, and the wet removal tendency is proportional to the local tracer mixing ratio (see section 2. in Kasibhatla et al. [1991] for details].

Sources consist of anthropogenic emissions of NO_x from fossil fuel combustion (21.3 tgN/yr) and biomass burning (8.5 tgN/yr) and natural or primarily natural sources, biogenic emissions from soil (7.5 tgN/yr), injection of stratospheric NO_x (0.6 tgN/yr) and lightning discharge (3-5 tg/yr).

The construction of the gridded fossil-fuel *Source* data base for NO_x is described in section 2.2 and the global distribution is given in Figure 1 of Levy and Moxim (1989). Detailed emission inventories from the U.S., Canada (7.5 tgN/yr) and Western Europe (5.9 tgN/yr) are supplemented with global estimates by Hameed and Dignon [1988] that are based on UN fuel use statistics. In the GCTM, the emissions, which are assumed to be constant throughout the year, are partitioned into a surface flux and volume sources in the bottom two model levels. We have added 0.015 tgN/yr of NO_x emissions from Prudhoe Bay [Jaffe et al., 1991] for this study. However, commercial aircraft, which emit ~0.5 tgN/yr of NO_x to the free troposphere of the northern latitudes [Beck et al., 1992], are not included. While much smaller than the other anthropogenic sources, this direct emission into the free troposphere may have a significant impact, as is discussed by Ehhalt et al. in this proceeding

The global biomass burning *Source* of 8.5 tgN/yr, (see Figure 43.1 in Levy et al. [1991]), is emitted as a surface flux. It is constructed from a gridded [1^o latitude x 1^o longitude] CO biomass burning source developed by Logan [private communication, 1990] and measured (field and laboratory) emission ratios for NO_x/CO_2 and CO/CO_2 [Andrea et al., 1988; Hao et al., 1989]. The burning period for each gridbox in the model between 35^o N and 35^o S, primarily the tropical rainforests and subtropical savannas of Africa and South America, is based on the precipitation data from the parent GCM. The driest three contiguous months are designated as the main burning period and 25% of the emissions is released in each month. The balance is emitted equally in the month preceding and the month following the burning period. Emissions only occur when precipitation is less than 0.01 inch/day. Poleward of 35^o, the emissions from agricultural burning and forest fires are released during the summer months.

The Soil biogenic emissions *Source* (7.5 tgN/yr), which is sensitive to both soil temperature and nitrate level, is predominately from the subtropical savannas (3.2 tgN/yr) and the intensive agriculture regions of the mid-latitudes (2.8 tgN/yr) and should be considered both natural and anthropogenic. Net NO_x emissions above the forest canopy are relatively low and NO_x emissions from the tundra and taiga woodland of the North are extremely low, even during the summer [Bakwin et al., 1992]. Further details of the source are under preparation.

We use zonally and monthly averaged O_3 and N_2O fields to calculate the production of NO in the stratosphere from the oxidation of N_2O by O(1D) (see Kasibhatla et al. [1991] for details), and find a maximum rate of 200-240 molecule/cm^3/s. The zonal distribution of the annual-average *Source* is shown in Figure 2 of Kasibhatla et al. [1991]. While NO_x is produced continuously in the stratosphere, it is only injected episodically into the troposphere, particularly during the winter and spring at mid- and high latitudes. While this small source has a significant impact on NO_y levels in the mid- and upper troposphere, it is predominately HNO_3 and has very little impact on NO_x and PAN levels.

Lightning, which has been observed primarily over land in the tropics and subtropics [Orville and Spencer, 1979; Turman and Edgar, 1982], is an important *Source* of NO_x in the free troposphere, particularly away from regions with strong surface sources. While estimates of the global source have ranged from 1-100 tgN/yr (see Logan [1983] and Liaw, et al. [1990] for detailed discussions), 20 tgN/yr is the upper limit permitted by known rates of nitrate deposition in remote regions [Logan, 1983]. However, due to lower OH and weaker deposition, the effective atmospheric lifetime for NO_x emitted by lightning in the free troposphere is much longer than that for NO_x emitted at the surface. Therefore, a few tgN/yr of lightning will have a major impact on the level of NO_x and NO_y in much of the free troposphere. Our lightning source is based on the incidence of deep moist convection in the parent GCM, with convection over the ocean weighted by 0.1 because lightning is much less frequent in maritime deep convection [Price and Rind, 1992]. The latitudinal distribution of our lightning source compares well with the observed yearly averaged lightning flash distributions of Turman and Edgar [1982] and Orville and Spencer [1979]. The vertical distribution of the source is based on the distribution of the height of flash origin and the ratio of cloud-cloud to cloud-ground lightning strokes from the study by Proctor [1991]. We assume that cloud-ground flashes produce 10 times as much NO_x and use upper tropospheric observations of NO_x near Dakar, Senegal [Drummond et al., 1988], NO_y over the eastern Pacific during the NASA/CITE mission [Ridley, 1991], and NO_y near Darwin, Australia [Murphy et al., 1992] to bracket the lightning source between 3-5 tgN/yr. We use 3 tgN/yr in this study.

Chemistry, involves the chemical interconversion of NO_x, HNO_3, and PAN. The gas phase scheme described in section 3 and the appendix in Kasibhatla et al. (1991) is used for all sources, excepting fossil fuel combustion. In that case we use a standard O_3-CO-CH_4-NO_x-H_xO_y chemical scheme [e.g. Chameides and Tans, 1981]. Hemispheric-average 1-D profiles of CO and NO_x and 2-D fields of CH_4, O_3, H_2O, T, p and total column ozone are specified from either available observations or GCM data (see the appendix in Kasibhatla et al. [1991] for details). The chemical production and loss terms for the 3 transported species are then calculated off-line and carried in the model as monthly 2-D tables. The following modifications have been made since Kasibhatla et al. [1991]: The night-time conversion of NO_x to HNO_3, by the reaction of NO_2 with O_3, followed by the reaction of NO_3 with NO_2, is included in the bottom two model levels; The ethane and propane fields needed for PAC (the PAN precursor) formation are now taken from the 2-D simulation of Kanakidou et al. [1991]; HO_2 and RO_2 reactions are included in the calculation of NO/NO_2; The new OH + CH_4 reaction rate has been used [Vaghjiani and Ravishankara, 1991]. The resulting 2-D OH fields give a global CH_3CCl_3 lifetime of ~6.2 years and are in reasonable agreement with more detailed calculations [e.g. Spivakovsky et al., 1990].

RESULTS

The January average PAN distribution at the lowest model level [990 mb or ~80 m] is given in Figure 1. With mixing ratios of ~300 pptv, this NO_x reservoir specie is the major reactive nitrogen compound, both at the surface and in the free troposphere. PAN accumulates throughout the winter in the North, because it is extremely stable and unreactive in cold air and is not removed by surface deposition to ice, snow and frozen vegetation. Its mixing ratio remains relatively uniform from the ground to the upper troposphere and grows to a maximum of ~500 pptv in the spring. As the atmosphere and surface warm up in the summer months, PAN levels, away from local sources, drop to ~50 pptv at the surface and to 100-200 pptv in the free troposphere. While its mixing ratio is significantly lower in the summer, PAN remains relatively uniform and the dominant reactive nitrogen specie in the free troposphere. The January NO_x mixing ratios shown in Figure 2 are much more variable than those of PAN. Near source regions, NO_x levels exceed 1ppbv, while in the remote far north they drop to less than 100 pptv. In the free troposphere they range from 100 - 300 pptv and are comparable to PAN. However, unlike PAN, NO_x levels, away from local sources, reach a maximum in January and decrease steadily until the next fall when the rate of chemical conversion of NO_x to PAN and HNO_3 again starts to decrease. In the summer, NO_x levels drop to less than 50 pptv throughout much of the northern troposphere. The one exception is in the boundary

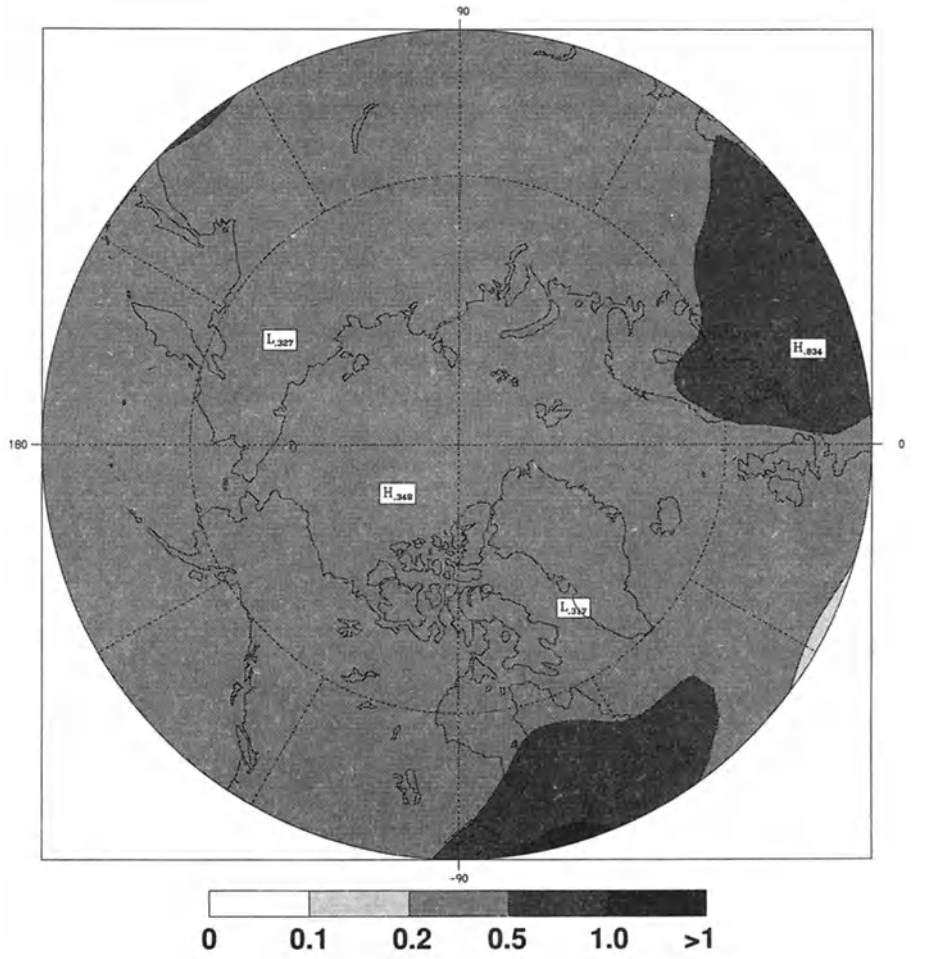

Figure 1. January monthly-average PAN mixing ratios [ppbv] in the lowest model level

layer near local sources such as biomass burning, soil biogenic activity and fossil fuel combustion. In this case, NO_x levels easily exceed 200 pptv and even reach 1 -10 ppbv in some polluted areas.

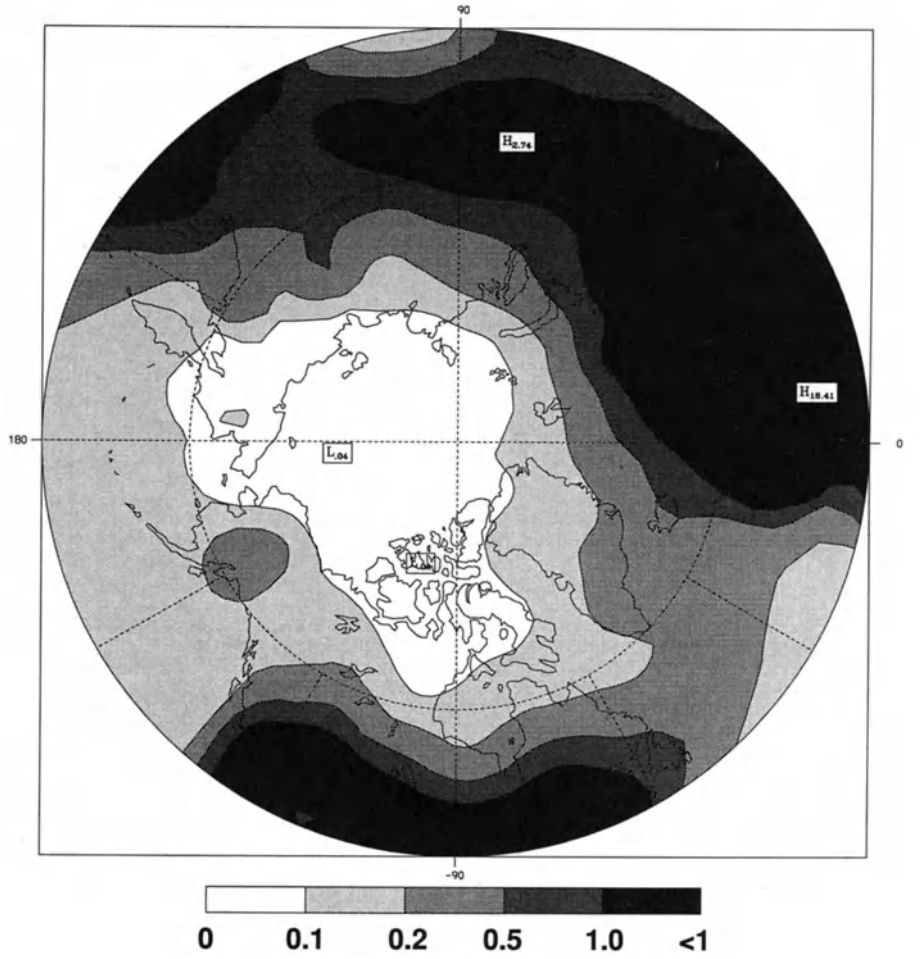

Figure 2. January monthly-average NO_x mixing ratios [ppbv] in the lowest model level

Before continuing with further analysis of the numerical simulation, it is instructive to compare the model simulations with available observations. It is difficult to compare short-term observations for a particular meteorological event with the simulations from a GCTM, which creates climatic statistics. Time-average values, particularly from multiple-year time-series, are best. In Table 1, we compare data from the lowest model level with two relatively

lengthy sets of surface observations: 1) A multiple year record of PAN (pptv) at Alert in Arctic Canada (82^{o} N, 62^{o} W) [Barrie and Bottenheim, 1991]; and 2) A 10 month record of NO_y (pptv) at Barrow, Alaska (71^{o} N, 157^{o} W) [Honrath and Jaffe, 1992]. It would appear from the comparison in Table 1 that the model captures both the magnitude and the seasonal cycle of NO_y and its major specie, PAN, in the Arctic boundary layer. At this time,

Table 1: Surface Mixing Ratio (pptv) Measurements and Model Results in the Arctic

	Winter	Spring	Summer	Fall
	obs. model	obs. model	obs. model	obs. model
Alert PAN	150-250 350	250-500 490	<50 35	75-100 130
Barrow NO_y		500-700 530	50-100 50-75	100-200 130
NO_x			15-50* 15-30	

* Only NO was measured. NOx was calculated.

while the expected long lifetime of PAN and a few spot measurements support the model's prediction that PAN is the principal reactive nitrogen specie throughout the free troposphere, conclusive confirmation is not yet available.

Given the fact that NO_x emissions from lightning, biogenic emissions and biomass burning primarily occur in the summer, it should come as no surprise that fossil fuel emissions are the overwhelming source of NO_x and PAN throughout the winter and spring in the northern latitudes. From our GCTM simulations, we find that 85 to 90% of the winter and spring storage comes from fossil fuel emissions. In the summer, other sources become important, and the contribution from fossil fuel combustion drops to ~50%. For the final study, which considers the potential impact of the stored PAN and NO_x on springtime NO_x levels in the northern latitudes, we will focus on fossil fuel combustion only.

While the GCTM predicts, as previous observations have suggested, that high levels of PAN and NO_x are stored throughout the winter in the northern latitudes, the relative importance of such storage, when compared with ongoing NO_x emissions, has never been quantified. Integrating the NO_x and PAN fields from 40^{o} N to the Pole and from the ~900 mb

to ~240 mb, which excludes the boundary layer emission region, we find that 0.07 tgN of each are stored in January. The integral of stored PAN in the region increases to ~0.11 tgN by March, while NO_x drops to 0.025 tgN. The total amount of NO_x and PAN, itself a potential indirect source of NO_x, stored in the northern latitudes during the winter and early spring is ~0.14 tgN, and it can be compared to the monthly midlatitude emissions from fossil fuel combustion in the boundary layer (~1.5 tgN) and from commercial aircraft in the free troposphere (~0.05 tgN). While the PAN and NO_x stored at high latitudes are potentially important sources of NO_x at midlatitude during the springtime onset of ozone photochemistry, the levels are of the same order as direct emissions into the free troposphere by aircraft and only 0.1 of the surface emissions from fossil fuel combustion. A quantitative examination of the impact of stored PAN and NO_x on springtime NO_x levels and of the relative roles of PAN chemistry and atmospheric transport is now in progress and will be discussed in a later paper.

REFERENCES

Andrea, M.O., et al., Biomass-burning emissions and associated haze layers over Amazonia, *J. Geophys. Res., 93*, 1509 - 1527, 1988.

Bakwin, P. S., et al., Reactive nitrogen oxides and ozone above a taiga woodland, submitted to *J. Geophy. Res.*, 1992.

Barrie, L. A. and J. W. Bottenheim, Sulfur and nitrogen pollution in the Arctic atmosphere, in: *Pollution of the arctic atmosphere,* W.T. Sturges, Editor, p.155-183, Elsevier Science Publishers, London, 1991.

Beck, J. P., C. E. Reeves, F. A. A. M. de Leeuw, and S. A. Penkett, The effect of aircraft emissions on tropospheric ozone in the northern hemisphere, *Atmos. Environ., 26A,* 17 - 29, 1992.

Chameides, W. L. and A. Tans, The two-dimensional diagnostic model for tropospheric OH: An uncertainty analysis, *J. Geophys. Res., 86*, 5209-5223, 1981.

Drummond, J. W., D. H. Ehhalt, and A. Volz, Measurements of nitric oxide between 0-12 km altitude and 67° N to 60° S latitude obtained during STRATOZ III, *J. Geophys. Res., 93,* 15831-15849, 1988.

Hao, W. M., M. H. Liu, and P. J. Crutzen, Estimates of annual and regional releases of CO_2 and other trace gases to the atmosphere from fires in the tropics, based on FAO statistics from the period 1975 - 1980, *Presented at Third International Symposium on Fire Ecology,* Frieburg University, Federal Republic of Germany, 1989.

Hameed, S. and J. Dignon, Changes in the geographical distributions of global emissions of NO_x and SO_x from fossil fuel combustion between 1966 and 1980, *Atmos. Environ., 22,* 441-449, 1988.

Honrath, R. E. and D. A. Jaffe, The seasonal cycle of nitrogen oxides in the Arctic troposphere at Barrow, Alaska, *J. Geophys. Res., in press*, 1992.

Jaffe, D. A., R. E. Honrath, J. A. Herring, S.-M. Li, and J. D. Kahl, Measurements of nitrogen oxides at Barrow, Alaska during spring: Evidence for regional and Northern Hemisphere sources of pollution, *J. Geophys. Res., 96,* 7395-7405, 1991.

Kanakidou, M., H. B. Singh, K. M. Valentin and P. J. Crutzen, A two-dimensional study of ethane and propane oxidation in the troposphere, *J. Geophys. Res., 96*, 15395-15425, 1991.

Kasibhatla, P. S., H. Levy II, W. J. Moxim, and W. L. Chameides, The relative impact of stratospheric photochemical production on tropospheric NO_y levels: A model study, *J. Geophys. Res., 96*, 18631 - 18646, 1991.

Kasibhatla, P. S., H. Levy II, and W. J. Moxim, Global NOx, HNO3, PAN and NOy distributions from fossil-fuel combustion emissions: A model study, *J. Geophys. Res., submitted*, 1992.

Liaw, Y., D. L. Sisterson and N. L. Miller, Comparison of field, laboratory, and theoretical estimates of global nitrogen fixation by lightning, *J. Geophys. Res., 95*, 22489-22494, 1990.

Levy II, H., J. D. Mahlman, and W. J. Moxim, Tropospheric N_2O variability, *J. Geophys. Res., 87,* 3061 - 3080, 1982.

Levy II, H., and W. J. Moxim, Simulated global distribution and deposition of reactive nitrogen emitted by fossil fuel combustion, *Tellus, 41,* 256 - 271, 1989.

Levy II, H., W. J. Moxim, P. S. Kasibhatla, and J. A. Logan, The global impact of biomass burning on tropospheric reactive nitrogen, in: *Global biomass burning: Atmospheric, climatic, and biospheric implications,* J.S. Levine, Editor, p. 363-369, MIT Press, Cambridge, Mass., 1991.

Logan, J. A., Nitrogen oxides in the troposphere: Global and regional budgets, *J. Geophys. Res., 88,* 10785 - 10807, 1983.

Mahlman, J. D., and W. J. Moxim, Tracer simulation using a global general circulation model: Results from a midlatitude instantaneous source experiment, *J. Atmos. Sci., 35,* 1340 - 1374, 1978.

Manabe, S., D. G. Hahn, and J. L. Holloway, Jr., The seasonal variation of the tropical circulation as simulated by a global model of the atmosphere, *J. Atmos. Sci., 31,* 43 - 83, 1974.

Manabe, S., and J. L. Holloway, Jr., The seasonal variation of the hydrologic cycle as simulated by a global model of the atmosphere, *J. Geophys. Res., 80,* 1617 - 1649, 1975.

Murphy, D. M., D. W. Fahey, S. C. Liu, M. H. Proffitt, and C. S. Eubank, Measurements of reactive odd nitrogen and ozone in the upper troposphere and lower stratosphere, *J. Geophys. Res., in press,* 1992.

Orville, R. E. and Spencer D. W., Global lightning flash frequency, *Mon. Weather Rev., 107,* 934, 1979.

Price, C. and D. Rind, A simple lightning parameterization for calculating global lightning distributions, *J.Geophys. Res.*, 97, 9919-9934, 1992.

Proctor, D. E., Regions where lightning flashes began, *J. Geophys. Res., 96,* 5099 - 5112, 1991.

Ridley, B. A., Recent measurements of oxidized nitrogen compounds in the troposphere, *Atmos. Environ., 25A*, 1905 - 1926, 1991.

Singh, H. B., L. J. Salas and W. Viezee, Global distribution of peroxyacetyl nitrate, *Nature, 321*, 588-591, 1986.

Smagorinsky, J., General circulation experiments with the primitive equations. I. The basic experiment, *Mon. Wea. Rev., 91,* 99-164, 1963.

Spivakovsky, C. M., S. C. Wofsy, and M. J. Prather, A numerical method for parameterization of atmospheric chemistry: Computation of tropospheric OH, *J. Geophys. Res., 95*, 18433-18440, 1990.

Turman, B. N. and Edgar, B. C., Global lightning distribution at dawn and dusk, *J. Geophys. Res., 87*, 1191-1206, 1982.

Vaghjiani, G. L. and A. R. Ravishankara, New measurements of the rate coefficient for the reaction of OH with methane, *Nature, 350,* 406-409, 1991.

OZONE DEPLETION DURING POLAR SUNRISE

John C. McConnell[1] and Grant S. Henderson[2]
Department of Earth and Atmospheric Science
York University, North York

INTRODUCTION

In 1988 Barrie et al. [1988] drew attention to the startling drop in O_3 at polar sunrise at Alert and the concomitant increase in filterable Bromine (f-Br). As shown in the paper of Bottenheim in this workshop, the measurements indicated sharp periodic drops in the mixing ratio of O_3 with a time scale of several hours or less. On occasions the O_3 levels would be below the detection limit of the instruments used. Simultaneously, they confirmed dramatic *increase* in the levels of f-Br (more than 100 times the levels anticipated from sea salt aerosols) that had been measured earlier by Berg et al. [1983]. (Although one should point out that different filters had been used. In addition, one uses the term "simultaneously" loosely since the time of a single measurement is substantially longer for the f-Br measurements than for the O_3 measurements.) Many measurements since that time have confirmed the negative-correlation between the O_3 and the f-Br [e.g., Bottenheim et al., 1990; Oltman et al., 1989 etc.] and the effect has been observed at Barrow as well as Alert. Seasonal measurements of O_3 at Barrow indicate values well below the yearly average during polar sunrise. The sharp depletion seems to be correlated with stable conditions in the boundary layer with the depletion of O_3 occurring only within the first kilometer.

From the early measurements it was not clear if the phenomenon of low O_3 values was due to temporal or spatial effects or both. Aircraft-borne measurements of O_3 [Kieser et al., 1992] have indicated that there was a strong spatial variation in O_3 mixing ratios. Kieser et al. [1992] noted that the ozone had decayed to undetectable amounts within a day or two after a storm had passed through mixing the lower boundary. This is perhaps the strongest piece of evidence that points to the decay of the ozone being due to a chemical effect on a short time scale.

CHEMICAL MECHANISMS

The first attempt to explain this phenomenon was by Barrie et al. [1988] who suggested that gas-phase Br chemistry might be adequate to account for the depletion.

[1]Also affiliated with Centre for Atmospheric Chemistry, York University
[2]Geology Department, University of Toronto, Ontario, Canada

NATO ASI Series, Vol. I 7
The Tropospheric Chemistry of Ozone in the Polar Regions
Edited by H. Niki and K. H. Becker

They suggested the reaction scheme:

$$BrO + BrO \rightarrow Br_2 + O_2$$

$$Br_2 + h\nu \rightarrow 2Br$$

$$2 \times (Br + O_3 \rightarrow BrO + O_2)$$

$$\text{net effect :} \quad 2O_3 \rightarrow 3O_2$$

However, the catalytic efficiency of this scheme is reduced by the presence of NO_x; NO can short circuit O_3 destruction via

$$BrO + NO \rightarrow Br + NO_2$$

which results in the production of odd oxygen. Also, NO_2 can form $BrNO_3$ and slow down the reaction scheme by tying up reactive Br. Further the Br atoms can react with aldehydes, HO_2, and non-methane hydrocarbons (NMHC) forming HBr (for example) which at these low sun angles is not readily oxidized to Br by OH + HBr. Thus, the catalytic cycle shuts down very rapidly. This was confirmed by McConnell et al. [1992].

Another serious problem that was partially addressed by Barrie et al. [1988] is the source of the f-Br. Barrie et al. [1988] had suggested that oxidation of organic bromines such as $CHBr_3$ produced biologically in the sea or on sea ice could supply the necessary Br atoms. The measurements of Cicerone et al. [1988] of brominated organics at Barrow, Alaska, had indicated that the $CHBr_3$ decreased from January. However, it is not clear if sufficient bromine is present in the organics and nor that it can be released sufficiently rapidly. At this meeting we have seen that Moortgat et al. have measured the cross sections for $CHBr_3$: their calculations of the $J(CHBr_3)$ clearly indicate that gas phase photolysis would not release Br rapidly enough to destroy ozone within the time scale that we have inferred above.

McConnell et al. [1992] tried to address the problem of the bromine source. They suggested that there was an accumulation of sea salt during the winter, and that it was released from the snow pack surface during polar sunrise by photocatalysed heterogeneous reactions. They were unable to specify a precise mechanism. Figure 1 is a cartoon showing the various processes envisaged to be occurring.

Although McConnell et al. [1992] did not discuss Cl chemistry, (this was addressed in an oral presentation [McConnell and Henderson, 1991]). It is possible that Cl may be released by a similar, but much less efficient process than for bromine. If so, then a substantial increase in free Cl atoms or HCl might not be noticed in the background Cl^- on the ubiquitous tropospheric aerosol and so not violate any of the observational constraints. We will return to this point later.

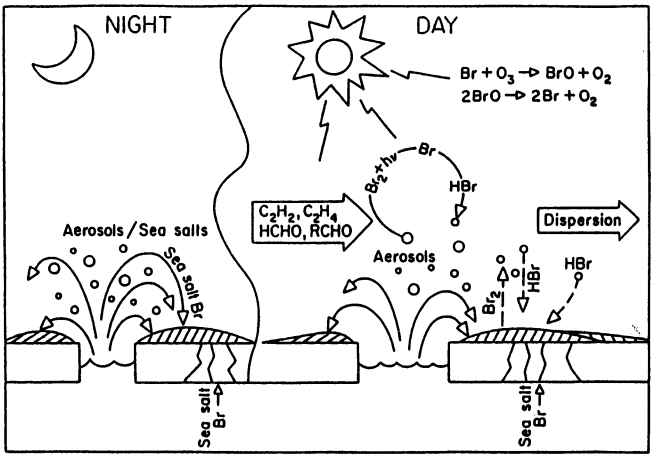

Fig. 1. During the night there is a build up of aerosols and sea salts around open leads and near the open ocean. At polar sunrise the sunlight releases Br_2 from the surface and possibly from aerosols and ice crystals. The Br_2 is rapidly photolysed to Br atoms which are converted to HBr. It is surmised that the HBr is scavenged by the aerosols, ice crystals and surface thereby recycling HBr back to Br_2.

Finlayson-Pitts et al. [1991] suggested that heterogeneous reactions might play a role. In particular, they suggested that the reaction of N_2O_5 with NaBr would release BrONO

$$N_2O_5 + NaBr(s) \rightarrow BrONO + NaNO_3(s)$$

which would photolyse rapidly at polar sunrise releasing BrO that would self-associate forming Br. They confirmed in the laboratory that this reaction proceeded at least using laboratory salt crystals. They also estimated that sufficient Br could be produced during a polar winter. However, the effect of such a process would not accumulate during the winter since the residence time of polar air is only one to two weeks. However, what is possible is that these species might build up over the polar night on the Arctic snow pack forming a reactive mix waiting to be primed by sunlight.

One of the interesting pieces of information that came to light during the 1988 campaign was the result that there was substantial amounts of aldehydes, $\sim$ 30 ppt of HCHO and $\sim$ 60 ppt of CH_3CHO. These species are important, as noted above, by virtue of their capacity to react with Br and form HBr thus shutting off the catalytic cycle. In addition, extensive NMHC measurements made which hinted that ethane and acetylene decreased during incidents of low O_3. It was, however, not clear if this modulation of the NMHC was due to a chemical or transport signature. It is important to note that Br does not react rapidly with the alkanes but Cl does. (The decrease in NMHC during periods of ozone depletion in other years has subsequently been confirmed [Niki, 1992, private communication].)

The status of NO_x measurements to us at the time of writing is not clear. Early measurements indicated that NO_2 levels could be 50-100 ppt, but there was a suspicion that these measurements could actually be a signal of N_2O_5 that thermally decomposed in the inlet tube [cf. Bottenheim et al., 1990]. One certainly expects N_2O_5 formation within the airparcel on the journey from Northern Asia. At the levels quoted above, it appeared that $BrNO_3$ formation could also shut down the catalytic O_3 destruction cycle. However, more recent work suggests that this is not necessarily true [McConnell et al., 1992; Fan and Jacobs, 1992]. In fact the gas-phase modelling done so far, with or without heterogeneous chemistry, suggests that NO_x will rapidly get tied up with other species such as PAN or PAN-like species or get oxidized to HNO_3. Interestingly, Jaffe in his presentation at this workshop indicated that NO reaches $\sim$ 30 ppt during low ozone events. This strongly suggests that NO_x is $\sim$ 30 ppt since the ozone is sufficiently low during these events that little NO_x resides in NO_2.

Heterogeneous chemistry plays an important role in modifying gas-phase chemistry in the stratosphere and is probably equally important in the troposphere. McConnell et al. [1992] noted that many of the NMHC that had been reported by Bottenheim et al. [1990] such as C_2H_2, C_2H_4, etc [see also Hov et al., 1984, 1989; Rasmussen, 1983] react with bromine atoms and this would imply even more rapid transformation of "active" Br into HBr and brominated organic compounds (BOC), some possibly PAN like (see Table 1). Thus they suggested that perhaps any HBr formed, or the BOC such as HCBrO would be scavenged by aerosols and by photocatalytic processes be released as Br_2 or some such photolytic reactive species. This would give a catalytic cycle as shown in Figure 1 whereby the Br_2 is photolysed to Br which is rapidly converted to HBr. The latter is then scavenged by aerosols, ice crystals, or the surface to Br^- ready to be recycled again.

Some of the diagnostic features of this scheme are the high levels of BrO that form during the day. Further during the relatively brief period when a diurnal cycle is present the BrO will be converted to Br_2 during the night. It is also anticipated that HBr would largely disappear during the night, since it would be scavenged by the aerosol and not released. In addition, as the O_3 disappear there is a switching of the active Br from BrO to Br. If these high levels persisted for about a day then alkenes would disappear (Figure 2), and even C_2H_2 would be consumed if they persisted for several days. To some extent this is consistent with the NMHC measurements. However, C_2H_2 always appears to be present at above the 200 ppt level even when O_3 disappears. Furthermore, even the alkanes appear to decrease during the low O_3 episodes.

Figure 2 show some details of the calculations presented by McConnell et al. [1992]. The standard conditions assumed were 100 ppt of Br_x (which now appears to be too high), 800 ppt of C_2H_2, 200 ppt of C_2H_4, 40 ppt HCHO, 60 ppt CH_3CHO and 50 ppt NO_2. Solar irradiance conditions are assumed to be typical of Alert (82.5 N) at the

Table 1: Bromine reactions with C_2H_2 and C_2H_4 included [†]

Chemical Reactions			
	Reaction	Rate constant[†]	Notes
$Br + O_3$	$\rightarrow BrO + O_2$	6.9×10^{-13}	a
$BrO + BrO$	$\rightarrow 2Br + O_2$	2.6×10^{-12}	a
$BrO + BrO$	$\rightarrow Br_2 + O_2$	6.6×10^{-13}	a
$Br + HO_2$	$\rightarrow HBr + O_2$	1.4×10^{-12}	a
$BrO + h\nu$	$\rightarrow Br + O$	6.7×10^{-3}	a
$BrO + HO_2$	$\rightarrow HOBr + O_2$	5.0×10^{-12}	a
$BrO + NO$	$\rightarrow Br + NO_2$	2.5×10^{-11}	a
$BrO + NO_2$	$\rightarrow BrNO_3$	4.7×10^{-12}	a
$BrNO_3 + h\nu$	$\rightarrow Br + NO_3$	1.9×10^{-4}	a
$HOBr + h\nu$	$\rightarrow OH + Br$	1.0×10^{-3}	b
$Br + CH_3CHO$	$\xrightarrow{O_2} CH_3CO.O_2 + HBr$	3.7×10^{-12}	a
$Br_2 + h\nu$	$\rightarrow 2Br$	1.2×10^{-2}	c
$HBr + OH$	$\rightarrow Br + H_2O$	1.1×10^{-11}	a
$Br + HCHO$	$\rightarrow HBr + HCO$	6.9×10^{-13}	a
$Br + BrCHO$	$\rightarrow HBr + Br + CO$	1.0×10^{-13}	b
$CHBr_3 + OH$	$\rightarrow CO + 3Br + H_2O$	7.5×10^{-15}	a
$Br + C_2H_2$	$\xrightarrow{O_2} HBr + 2CO + HO_2$	6.0×10^{-14}	d
	$\rightarrow BrCHO + CO + HO_2$	6.0×10^{-14}	d
	$\rightarrow Br + (CHO)_2$	6.0×10^{-14}	d
$BrCHO + h\nu$	$\rightarrow Br + CO\ HO_2$	$1.0\times10^{-4}\ s^{-1}$	b
$Br + (CHO)_2$	$\rightarrow HBr + HO_2 + 2CO$	1.0×10^{-12}	e
$(CHO)_2 + h\nu$	$\xrightarrow{2O_2} 2HO_2 + 2CO$	2.0×10^{-5}	f

Table 1 (continued)

Chemical Reactions			
	Reaction	Rate constant†	Notes
$Br + C_2H_4$	$\xrightarrow{O_2}$ $BrC_2H_4O_2$	1.0×10^{-12}	c
$BrC_2H_4O_2 + NO_2$	$\rightarrow$ $BrC_2H_4O_2NO_2$	1.0×10^{-12}	b
$BrC_2H_4O_2NO_2$	$\rightarrow$ $BrC_2H_4O_2 + NO_2$	1.0×10^{-4}	b
$BrC_2H_4O_2 + HO_2$	$\rightarrow$ $BrC_2H_4OOH + O_2$	5.0×10^{-12}	b
$2BrC_2H_4O_2$	$\rightarrow$ $BrCH_2CHO + BrCH_2CH_2OH + O_2$	2.4×10^{-12}	g
	$\xrightarrow{O_2}$ $2BrCH_2CHO + 2HO_2$	5.6×10^{-12}	g
$Br + BrCH_2CHO$	$\rightarrow$ $Br + CH_2CO + HBr$	6.0×10^{-14}	h
	$\xrightarrow{O_2}$ $HBr + BrCH_2CO.O_2$	1.4×10^{-13}	h
$BrCH_2CO.O_2 + HO_2$	$\rightarrow$ $BrCH_2CO.OOH + O_2$	1.0×10^{-13}	b
	$\rightarrow$ $BrCH_2COOH + + O_3$	1.0×10^{-13}	b
$2BrCH_2CO.O_2$	$\xrightarrow{2O_2}$ $O_2 + 2CO_2 + 2BrCH_2O_2$	1.0×10^{-12}	b
$BrCH_2O_2 + HO_2$	$\rightarrow$ $BrCH_2OOH + O_2$	1.0×10^{-12}	g
$2BrCH_2O_2$	$\xrightarrow{O_2}$ $2BrCHO + 2HO_2$	1.0×10^{-13}	b
	$\rightarrow$ $2HCHO + 2Br + O_2$	1.0×10^{-12}	h
$Br + BrCH_2CH_2OH$	$\rightarrow$ $Br + HBr +$ products	3.0×10^{-11}	g
HBr	$\rightarrow$ $Br_{aerosol}$	3.0×10^{-4} s^{-1}	i
$BrCH_2CHO$	$\rightarrow$ $Br_{aerosol}$	3.0×10^{-4} s^{-1}	i
$BrCH_2CH_2OOH$	$\rightarrow$ $Br_{aerosol}$	3.0×10^{-4} s^{-1}	i
$Br_{aerosol}$	$\rightarrow$ $0.5Br_2$	3.0×10^{-4} s^{-1}	i
$BrCHO$	$\rightarrow$ Br_2	3.0×10^{-4} s^{-1}	i

† Units are cm^3 s^{-1} for 2 body or psuedo 2 body rate constants at a temperature of 240 K and s^{-1} for photolysis rates.

a) JPL [1990]. b) Estimate but the results are not sensitive to this value. c) Calculated. d) From data in Barnes et al. [1989]. e) From Niki et al. [1985a]. f) Plum et al. [1983]. g) Wallington et al. [1990]. h) Niki et al. [1985b]. i) Estimate based on data in Rancher and Kritz [1980].

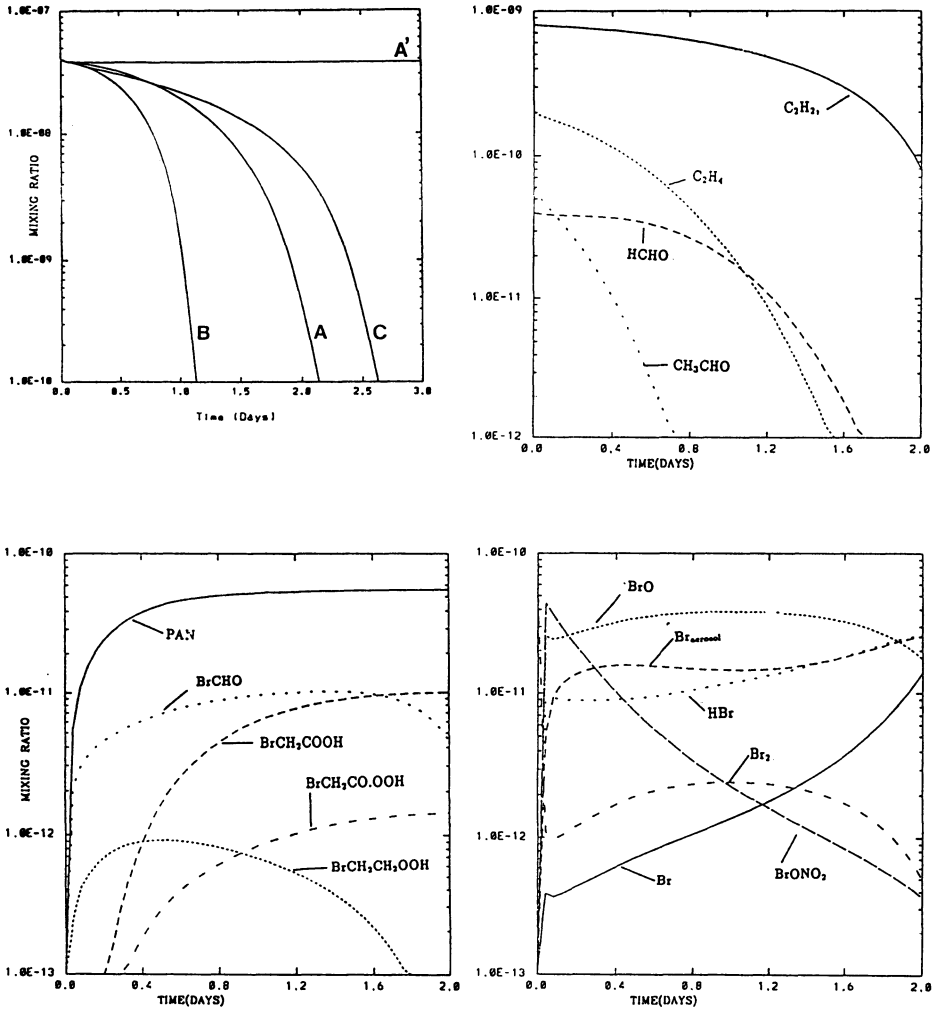

Fig. 2(a) Boundary-layer O_3 concentrations against time. Curve A is for standard initial conditions described in the text. Curve B is for the C_2H_2, C_2H_4 initial densities reduced by a factor of 4. Curve C shows the O_3 loss when the initial HCHO and CH_3CHO densities are set to zero. Curves A-C include simulation of heterogeneous chemistry. Curve A' is for the same conditions as A but with no heterogeneous mechanism operating. Concentration against time (b) C_2H_2, C_2H_4 HCHO and CH_3CHO. (c) $BrCH_2COOH$, PAN, $BrCH_2CO.OOH$,$BrCH_2CH_2OOH$,BrCHO and (d) Br,BrO,HBr, $Br_{aerosol}$ and $BrONO_2$ for the standard conditions described in the text. [after McConnell et al., 1992]

beginning of April.

Fan and Jacobs [1992] have investigated possible mechanisms for the release of active Br from aerosols. They suggest that gas-phase HOBr will dissolve into the aqueous phase and then react with Br^- in the aerosol. The steps suggested are:

$$HBr(g) \rightarrow H^+ + Br^-(aq)$$

$$HOBr(g) \rightarrow HOBr(aq)$$

$$HOBr + H^+ + Br^- \rightarrow H_2O(aq) + Br_2$$

In addition, any $BrNO_3$ formed in the gas phase, by analogy with $ClNO_3$, might be expected to react with H_2O on the aerosols

$$BrNO_3(aq) + H_2O \rightarrow HNO_3 + HOBr(aq)$$

They find that the rates of these reactions are sufficiently rapid that the general picture of McConnell et al. [1992] can be supported. However, interestingly, their scheme results in the rapid conversion of gas-phase NO_x into aqueous phase HNO_3.

As we found out from Hausmann during this meeting, high levels of BrO $\sim$ 10 ppt have indeed measured [Hausmann and Platt, 1992] . For the few periods where there were measurements of both BrO and O_3 there does not appear to be a correlation between low O_3 and BrO. This later point may not be inconsistent with the Br catalysed destruction, since as can be seen from Figure 2 there is an induction period where there are both high levels of BrO and O_3. If the BrO measurements have been taken during this period there would be no negative-correlation. One point to note is that if the 10 ppt mixing ratios of BrO are indeed indicative of maximum BrO, then these are too small to account for the decrease of ozone on a time scale of a few days or less. The BrO mechanism requires BrO mixing ratios of $\sim$ 30 ppt in order to rapidly destroy ozone, since we require

$$\int_{1\ day} k[BrO]^2 dt \approx 10^{12}\ \ cm^{-3}$$

where 10^{12} is approximately the initial amount of ozone present. Because of the quadratic dependence of the destruction 30 ppt would destroy ozone 9 times faster than the observations would allow. *If the observations are assumed to be representative of maximum BrO mixing ratios, then BrO cannot be the major species destroying ozone.* It may be that the high levels of BrO are a signature of aerosol chemistry, but that other processes such as heterogeneous reactions are the cause of the O_3 destruction. However, given the sparse nature of this difficult measurement it is too soon to totally preclude Br as playing a role.

The model results indicate some dependance on the initial conditions. Figure 3 shows the results of O_3 depletion with the amounts of NMHC reduced. McConnell

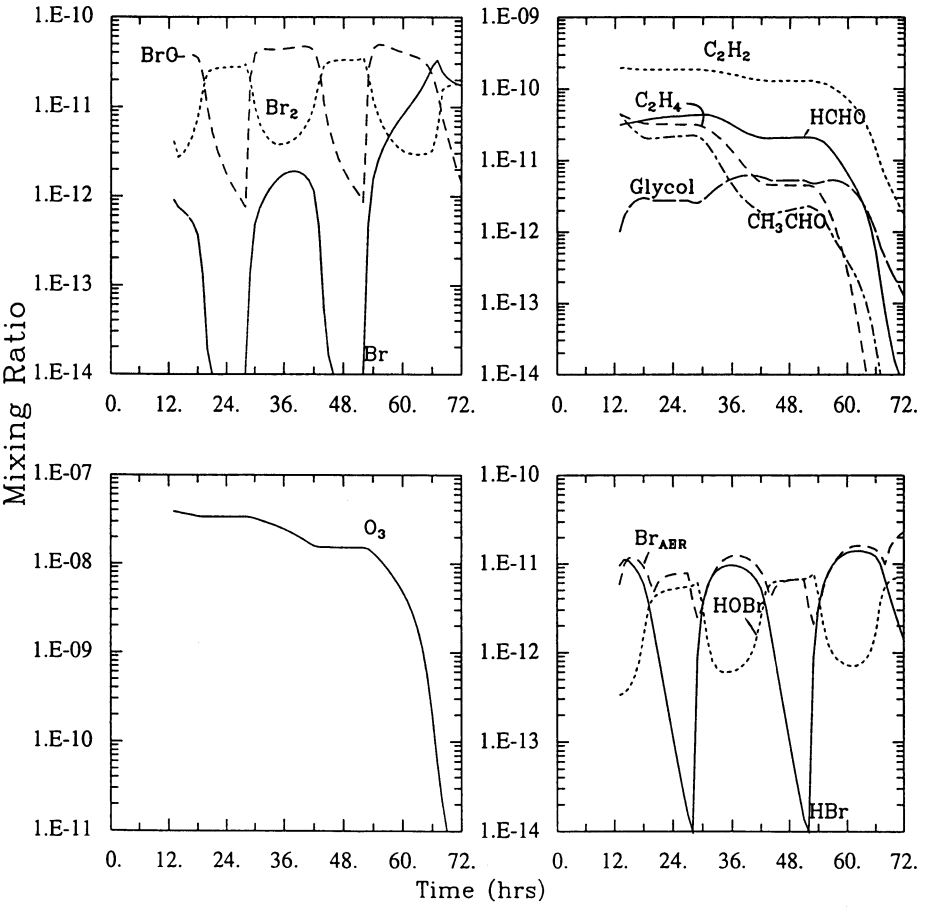

Fig. 3. The Bromine chemistry used in Figure 2 and given in Table 1 has been used to simulate the depletion of ozone during a period with a rising and setting sun. The initial C_2H_2 mixing ratios were reduced by a factor of 4 from those in Figure 2. Note the diurnal behaviour of BrO and Br_2 and the rapid depletion of HCHO and CH_3CHO although they are produced as a result of the destruction of the alkenes and acetylene.

et al. [1992] results indicate that the presence or absence aldehydes can affect the induction period.

An analysis of night time chemistry by Peng et al. [1992] has indicated that given typical lifetimes of air parcels in Arctic air of 5-7 days and typical levels of NMHCs and NO_x from northern Asia, quite a lot of O_3 induced processing of the air can take place and quite a lot of N_2O_5 can be formed. This will have to considered in future analyses.

As noted above, decreases in the alkanes appear to be correlated with decreases in O_3. This may be simply due to transport effects with the concomitant implication that low levels of NMHCs are required for destruction of O_3. However, this latter effect is contrary to most of the catalytic models that require the NMHCs to produce HBr for rapid recycling of the Br_x.

An alternative hypothesis is that Cl_x may be involved in the destruction of O_3. McConnell and Henderson [1991] have carried out preliminary calculations which consider the feasibility of such processes from a mechanistic perspective, but they did not include the physical chemical details. Their work was stimulated by the measurements of Zetzsch and his co-workers [Behnke and Zetzsch, 1989; Zetzsch et al., 1988] who found that there was heterogeneous destruction of O_3 concurrent with the loss of HCl to aerosol or wall surface and evolution of Cl_2 into the gas phase. This process occurred in the dark but more rapidly in the light. The reaction sequence that lead to this observed behaviour has not been defined, and because of the particular surface involved it may have no relevance to the atmosphere. However, it is intriguing to look at possible atmospheric effects. These are shown in Figure 4. We see strong O_3 depletion, which is affected by the heterogeneous reactions in the aerosol which have (over) simply been represented by

$$HCl(g) \rightarrow HCl(s)$$

$$HCl(s) + O_3 \rightarrow 0.5Cl_2$$

This latter reaction must *not* be taken as representing the very slow reaction which has been studied in the laboratory! Rather it is meant to indicate the possible rate limiting nature of the conversion. The atomic Cl levels calculated are such that results in little gas phase destruction of O_3 by

$$Cl + O_3 \rightarrow ClO + O_2$$

the opposite of what occurs in the stratosphere. Most of the destruction of O_3 occurs on the aerosol surface. Still, the Cl levels in these particular runs are sufficiently high that the alkanes are decreased in addition to the alkenes as shown in the Figure 4.

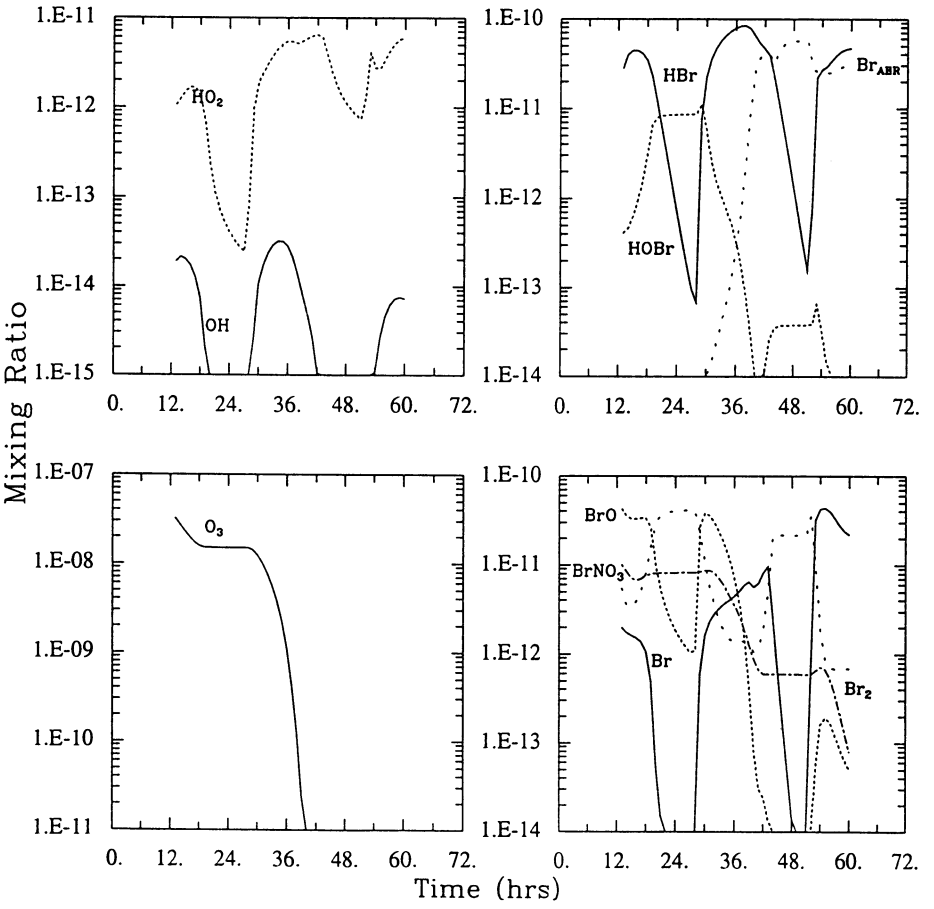

Fig. 4(a) The same chemistry and initial conditions have been used as in Figure 3 except that the reaction HCl + O_3 → 0.5 Cl_2 (as noted in the text) has been added to simulate the rate limited evolution of Cl_2. Note the rapid depletion of O_3 which is due mainly to heterogeneous loss of O_3. There is a rapid loss of $BrNO_3$ as the NO_x ends up as PAN. 1ppb of Cl_x was used for these calculations.

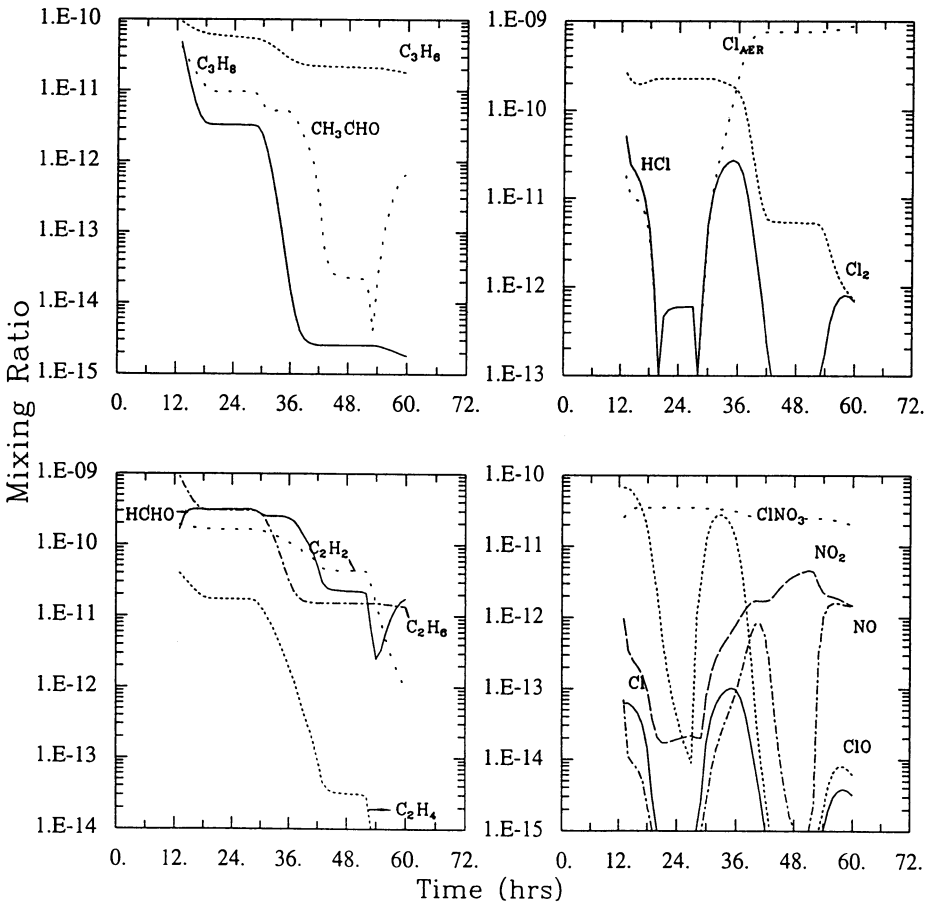

Fig. 4(b) For this scenario and HCl + O_3 rate the Cl densities are too high. Even at the end of the incident there is about 5 ppt of NO_2. Several NMHCs are shown as well as HCHO and CH_3CHO. The destruction of propane is shown to be rapid (too rapid perhaps) while for ethane the destruction is likewise rapid. Inadvertently, Cl destruction of the alkenes and acetylene was omitted in the model calculations!

DISCUSSION

Given that we assume that the lifetime of ozone against chemical depletion is $\sim$ 1 day, there are some extremely interesting conclusions that can be derived. Furthermore, if the destruction is due to gas-phase destruction by Br atoms, then we must have, $\tau_{O_3}^{Br} \sim 1$ day which, given the rate coefficient for ozone destruction by Br, gives a mean Br mixing ratio $\sim$ 1-2 ppt. This, in turn, implies a limit on the lifetime of some measured NMHCs, $\tau_{C_2H_2}^{Br} \leq 1.3$ days, $\tau_{C_2H_4}^{Br} \sim 9$ hours, $\tau_{CH_3CHO}^{Br} \leq 2.5$ hours and $\tau_{HCHO}^{Br} \leq 11$ hours. The aldehydes have been measured at mixing ratios $\sim$ 50, ppt so it is difficult to understand these measurements given the model calculations (cf., Figure 3), even though the calculations of McConnell et al. [1992] do allow for generation of RHCOs. More importantly, C_2H_2 and C_2H_4 should not persist at the measured levels given the inferred high levels of Br, (this is seen in Figure 2.) Additionally, the ozone time constant requires BrO mixing ratios $\sim$ 30 pptv, and if the mechanism of Fan and Jacob were playing a role there would be an almost complete depletion of NO_x. Again, this does not agree with the measurements reported at this workshop by Jaffe.

Let us assume that the reduction in the mixing ratios of the alkanes is due to chemical attack and not transport, then the most likely candidate as mentioned earlier is Cl atoms. If we assume that the lifetime of the alkanes is about 3 days, (i.e. $\tau_{alkane}^{Cl} \sim 3$), then since the rate coefficient is almost gas kinetic this implies a mean Cl density, of 4×10^4 cm^{-3}. Even though this represents an elevated Cl density, it yields $\tau_{O_3}^{Cl} \geq 12$ days. Thus Cl atoms cannot be playing a major role in the gas-phase destruction of ozone. (We note that the $\tau_{CH_4}^{Cl} \sim 20$ years, so that we do not expect to see an effect on CH_4.) So if neither Br nor Cl gas-phase destruction of ozone is adequate to duplicate the measurements, then heterogeneous destruction of ozone on snow pack, aerosol, or ice crystal surfaces be playing a major role. In addition, the mechanism must be stimulated by light, since during the long winter the ozone mixing ratios in the stable boundary layer remain relatively constant.

In summary, the observations that we must understand are the low ozone amounts and the quasi-correlation with f-Br, the behaviour of the NMHCs, the presence of aldehydes and other organics. What are the real levels of NO and NO_2 and how do they compare with gas phase modelling? What are the sources of the Br? Is it organic or inorganic? Not discussed above but of critical importance may be the diurnal behaviour of the inorganic Br measurements, and then it becomes essential to understand the behaviour of the filters used in the various experiments.

Acknowledgements The authors wishes to thank the Atmospheric Environment Service of Environment Canada and the Natural Sciences and Engineering Research Council of Canada for continuing support. We would also like to thanks Ms. E. Templeton for doing the model runs. It is a particular pleasure to thank Barrie, Bot-

tenheim, Niki and Shepson for illuminating conversations and Jacob and Zetzsch for preprints for their work. Lastly, I would like to thank the organizers for an extremely interesting and stimulating workshop.

REFERENCES

Barnes, I., Bastian, V., Becker, K.H., Overath, R. and Tong Zhu, Rate constants for the reactions of Br atoms with a series of alkanes, alkenes and alkynes in the presence of O_2. *Int. J. Chem. Kinetics., 21* 499-517, 1989.

Barrie, L. A., J. W. Bottenheim, R. C. Schnell, P. J. Crutzen, and R. A. Rasmussen, Ozone destruction and photochemical reactions at polar sunrise in the lower Arctic atmosphere, *Nature, 334,* 138–141, 1988.

Behnke, W., and C. Zetzsch, Smog chamber investigations of the influence of NaCl aerosol on the concentration of O_3 in a photosmog system, in "Ozone in the atmosphere", Eds R. M. Bojkov and P. Fabian, pp 519–523, Deepak,. Hampton, 1989.

Berg, W. W. P. D. Sperry, K. A. Rahn and E. S. Gladney, Atmospheric Bromine in the Arctic, *J. Geophys. Res., 88,* 6719–6736, 1983.

Bottenheim, J. W., L.A. Barrie, E. Atlas, L.E. Heidt, H. Niki, R.A. Rasmussen and P.B. Shepson, Depletion of lower troposphere ozone during Arctic spring: The polar sunrise experiment 1988, *J. Geophys. Res., 95,* 18555–18568, 1990.

DeMore, W.B., S.P. Sander, D.M. Golden, M.J. Molina, R.F. Hampson, M.J. Kurylo, C.J. Howard and A.R. Ravishankara, Chemical kinetics and photochemical data for use in stratospheric modelling, Evaluation number 9, JPL/NASA Publication Number 90-1, Jet Propulsion Laboratory, Pasadena California, 1990.

Doskey, P. V. and J. S. Gaffney, Non-methane hydrocarbons in the Arctic atmosphere at Barrow, Alaska, *Geophys. Res. Lett., 19,* 381–384, 1992.

Fan, S.-M. and D. J. Jacob, Surface ozone depletion in Arctic spring sustained by bromine reactions on aerosols, *Nature, 359,* 522–524, 1992.

Finlayson-Pitts, B. J., F. E. Livingston and H. N. Berko, Ozone destruction and bromine photochemistry at ground level in the Arctic Spring, *Nature, 343,* 622–624, 1990.

Hov, Ø, S. A. Penkett, I. S. A. Issaken and A. Semb, Organic gases in the Norwegian Arctic, *Geophys. Res. Lett., 11,* 425–428, 1984.

Hov, Ø. N. Schmidbauer and M. Oehme, Light hydrocarbons in the Norwegian Arctic, *Atmos. Environ., 23,* 2471–2482, 1989.

Kieser, B. N., T. Sideris, H. Niki, J. W. Bottenheim, and W. R. Leaitch, Spring 1989 observations of tropospheric chemistry in the Canadian high Arctic, submitted to Atmos. Environ, 1992.

Livingstone, F. E. and B. J. Finlayson-Pitts, The reaction of gaseous N_2O_5 with solid NaCl at 298 K: estimated lower limit to the reaction probability and its potential role in tropospheric and stratospheric chemistry, *Geophys. Res. Lett., 18,* 17–20, 1991.

McConnell, J. C., G. S. Henderson, L. A. Barrie, J. W. Bottenheim, H. Niki, C. H. Langford, and E, M. J. Templeton, Photochemical bromine production implicated in Arctic boundary-layer ozone destruction, *Nature, 355,* 150–152.

McConnell, J.C. and G. S. Henderson, IUGG, Vienna, August, 1991.

Mickle, R. E., J. W. Bottenheim, W. R. Leaitch, and W. F. J. Evans, Boundary layer ozone depletion during AGASP-II, *Atmos. Environ., 23,* 2443–249, 1989.

Niki, H., P.D. Makar, C.M. Savage, and L.P. Breitenbach, An FTIR spectroscopic study of the reactions Br + $CH_3CHO \rightarrow$ HBr + CHO_3CO and $CH_3C(O)OO + NO_2 \rightleftharpoons CH_3C(O)OONO_2$(PAN), *Int. J. Chem. Kinetics, 17,* 525-534, 1985a.

Niki, H., Makar, P.D., Savage, C.M. & Breitenbach, L.P., An FTIR study of the Cl-atom-initiated reaction of glyoxal, *Int. J. Chem. Kinetics, 17,* 547-558, 1985b.

Oltmans, S. J., R.C. Schnell, P.J. Sheridan, R.E. Peterson, S.-M. Li, J.W. Winchester, P.P. Tans, W.T. Sturges, J.D. Kahl and L.A. Barrie, Seasonal surface ozone and filterable bromine relationship in the high Arctic, *Atmos. Environ., 23,* 2431–2441, 1989.

Peng, N., J. C. McConnell and H. Niki, Arctic nighttime chemistry: A box model study of the gas phase reactions of O_3 and NO_3 with selected alkenes and DMS, in preparation, 1992.

Plum, C.N., E. Sanhueza, R. Atkinson, W.P.L. Carter and J.N. Pitts Jr. OH radical rate constrants and photolysis rates of α-dicarbonyls, *Envir. Sci. Technol., 17,* 479-484, 1983.

Rancher, J and Kritz, M.A., Diurnal Fluctuations of Br and I in the Tropical Marine Atmosphere, *J. Geophys. Res., 85,* 5581-5587, 1980.

Rasmussen, R. A., M.A.K. Khalil, and R.J. Fox, Altitudinal and temporal variation of hydrocarbons and other gaseous tracers of arctic haze, *Geophys. Res. Lett., 10,* 144-147, 1983.

Rudolph, J., Light hydrocarbons in the Norwegian Arctic, *Atmos environ, 24A,* 2889-2890, 1990.

Sturges, W. T. and L. A. Barrie, Chlorine, bromine and iodine in Arctic aerosols, *Atmos. Environ., 22,* 1179–1194, 1988.

Wallington, T.J., Andino, J.M. and S.M. Japar, FTIR product study of the self-reaction of $CH_2ClCH_2O_2$ radicals in air at 29SK, *Chem. Phys. Lett., 165,* 189-194, 1990.

Zetzsch, C., G. Pfahler, and W. Behnke, Heterogeneous formation of chlorine atoms for NaCl in a photosmog system, *J. Aerosol Sci., 19,* 1203-1206, 1988.

THE RELATIONSHIP BETWEEN ANTHROPOGENIC NITROGEN OXIDES AND OZONE TRENDS IN THE ARCTIC TROPOSPHERE

Dan Jaffe
University of Alaska Fairbanks
Geophysical Institute and Department of Chemistry

INTRODUCTION

Low solar insolation and low precipitation rates dramatically slow down the oxidation and removal of many anthropogenic pollutants in the Arctic, including hydrocarbons and nitrogen oxides. These processes give rise to a seasonal pollutant accumulation in the Arctic often referred to as "Arctic Haze", with a maximum in the winter-spring period. There is some evidence that the wintertime accumulation of these constituents occurs not only in the Arctic but also in other remote Northern Hemispheric locations as well. Penkett and Brice [1986] suggest that a hemispheric buildup of nitrogen oxides and hydrocarbons contributes to the observed springtime maximum in ozone which is usually attributed to stratospheric exchange. Based on modeling studies, Isaksen et al. [1985] have found that the arctic reservoir of nitrogen oxides can play a significant role in ozone production in the spring.

Similar to other Northern Hemispheric locations, tropospheric ozone concentrations at Barrow, Alaska have shown a statistically significant increase of 1-2 %/year over the past two decades at the surface. As a working hypothesis we start with the idea that the tropospheric ozone trend is being driven by anthropogenic emissions. Given this assumption, then, there are at least three different possible causes for this temporal ozone increase:

1. Ozone is photochemically produced in the arctic troposphere from local NO_X emissions;
2. Ozone is photochemically produced in the arctic troposphere from non-local NO_X emissions; and
3. Ozone is generated at lower latitudes and transported to the Arctic via wet or dry pathways.

The goal of this work is to understand this long term increase in tropospheric ozone in the Arctic and its relationship to nitrogen oxide concentrations.

TROPOSPHERIC OZONE TRENDS IN THE ARCTIC

Two arctic stations have been monitoring tropospheric ozone for a sufficient period of time so as to permit an evaluation of long-term trends. At Barrow, Alaska surface

NATO ASI Series, Vol. I 7
The Tropospheric Chemistry of Ozone in the Polar Regions
Edited by H. Niki and K. H. Becker

observations using in-situ UV absorption have been made since 1973. At Resolute, N.W.T. ozonesonde data has been collected since 1966, although a change in the ozonesonde type took place in 1979 raising the possibility of a systematic difference between the earlier and later records. This data has been reported by Logan [1985], Oltmans [1991; and this volume]. Table 1 summarizes the observed tropospheric trends at Barrow and Resolute (through the 1979 data) by different seasons and heights for which statistically significant increases are present.

Table 1 Barrow data from 1973-1988; Resolute data from 1966-1979

STATION	HEIGHT	SEASON	TREND (%/yr)	95% CONF. INT.
Barrow	Surface	June-Sept.*	1-2%	
Resolute	700 mb	spring	1.8	± 0.8
Resolute	700 mb	summer	2.3	± 1.1
Resolute	500 mb	spring	1.6	± 0.9
Resolute	500 mb	spring	1.7	± 1.2

*At Barrow, each individual month from June-Sept. shows a statistically significant positive trend. April, May, October and November also show a positive trend but it is not statistically significant.

In general, the Barrow and 1966-1979 Resolute data are in agreement, with two notable exceptions:

1) the lack of a clear trend at Barrow during spring;
2) the lack of any trend at the surface at Resolute.

There is some evidence for a surface O_3 trend at Barrow during spring (April and May), although it is not statistically significant [S. Oltmans personal communication 1992]. The lack of a statistical significance during spring is most likely due to the high variability in the surface ozone concentrations at this time, which is believed to be due to natural Br emissions [Barrie, et al., 1988; Oltmans, 1991].

The fact that Resolute does not show a trend in ozone at the surface whereas Barrow does has two possible causes. First, the Resolute surface data may be being impacted from a localized or regional increase in boundary layer SO_2 concentrations over this period. This would offset an in-situ ozone trend since SO_2 causes a negative interference in the ozonesonde measurements on a 1:1 basis [Logan 1985]. An alternative explanation is that the Barrow surface increase is a localized effect, not observed at Resolute. This will be discussed in more detail below.

The more recent Resolute ozonesonde data have been analyzed by Oltmans [this

volume] and found to differ significantly from the earlier data. There appears to be an offset which results from the two different types of ozonesondes used and, for much of the Resolute data, a significant negative trend in the ozone concentrations. The negative trends are approximately similar throughout the troposphere, a result which is inconsistent with changes in the stratospheric source term. Regarding the apparent discrepancy between the earlier and later Resolute ozonesonde data sets, one can only conclude that 12 years of measurements once per week is not sufficient to deduce a long term trend in a species as variable as ozone.

Additional information on high latitude tropospheric ozone can be garnered from the satellite derived tropospheric residuals calculated by Fishman et al. [1990] and Fishman [1991]. Although the observations do not extend above 50° N and do not consider trends, there is one important point that can be made from this data which relate to the high latitude tropospheric trends. The summer residuals clearly show regions of maximum ozone extending from about 25° N to greater than 50° N which originate in the populated regions, especially Europe and Asia. This suggests that at lower latitude, photochemically produced tropospheric ozone from anthropogenic emissions is being transported to the high latitudes and contributes to the tropospheric trends there. If so, this ozone rich air would be most predominant in the mid-troposphere, as the air traveled along lines of constant potential temperature. Once in the free troposphere, vertical mixing would bring this air to the surface. This scenario is consistent with the observation that surface concentrations of easily scrubbed species like SO_4^{2-} [Barrie and Bottenheim, 1991] are low and free-tropospheric concentrations of PAN remain elevated during summer [Singh et al., 1992].

NITROGEN OXIDE OBSERVATIONS IN THE ARCTIC

Ground-based measurements of NO and NO_y have been conducted at Barrow, Alaska during three separate campaigns [Honrath and Jaffe, 1990; Jaffe et al., 1991; Honrath and Jaffe, 1992]. The 8 month record collected during 1990 constitute the most complete record of surface NO_y concentrations in the Arctic. The seasonal distribution of NO_y at Barrow is shown in Figure 1.

In the 1990 observations during spring, we found that when 10 day isobaric back trajectories originated in the Arctic, concentrations were about a factor of 2 higher compared to when the trajectories originated from lower latitudes (e.g., the North Pacific). (However, it must be pointed out that this pattern was less clear during the 1991 measurements.) Even when the trajectories came from lower latitudes, NO_y concentrations were still about a factor of 3 higher than the summertime concentrations [Jaffe et al., 1991]. This is consistent with the notion of a springtime hemispheric build-up of PAN in the Northern Hemisphere, as suggested by Penkett and Brice [1986]. Examples of these back trajectories and the resulting NO_y distributions are shown in Figures 2 and 3.

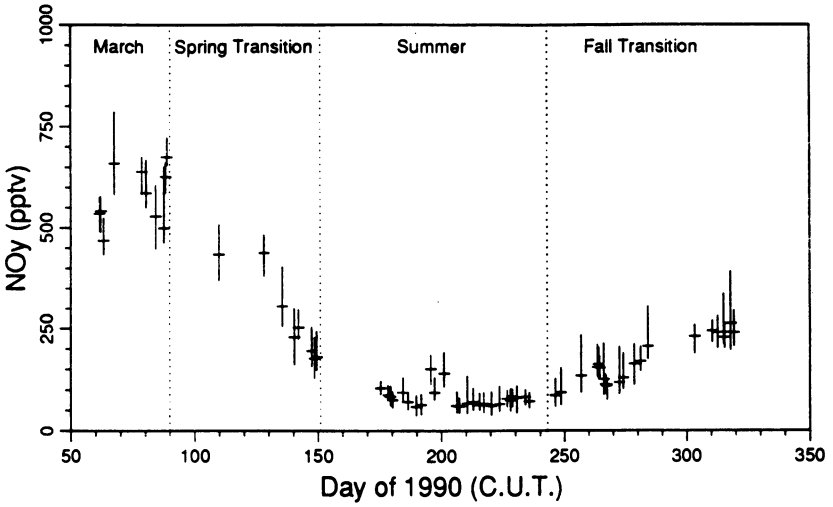

Fig. 1: Seasonal distribution of NO_y measured at Barrow, Alaska. The boxes show the median concentration during background periods and the vertical bars give the range.

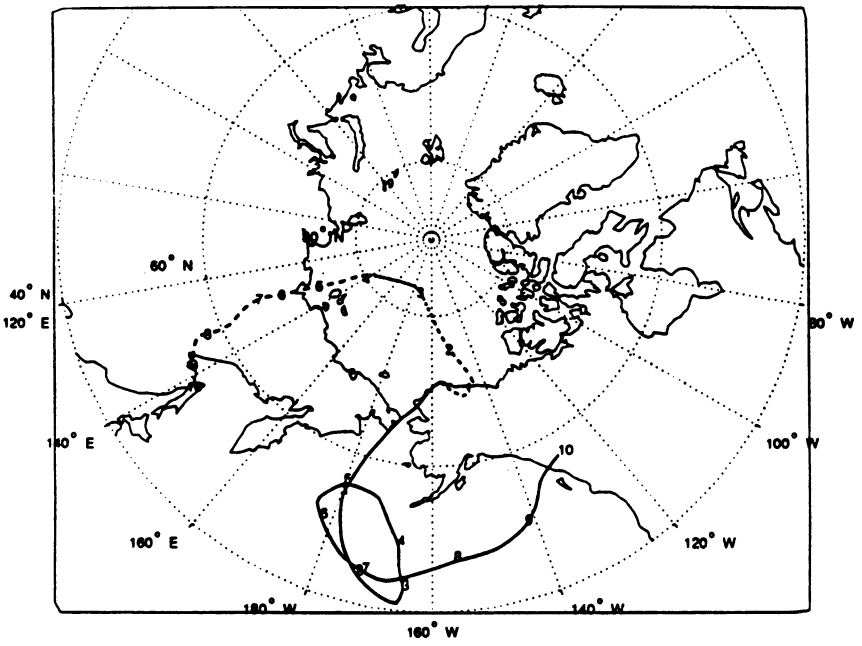

Fig. 2: Isobaric back-trajectories arriving at Barrow, Alaska during spring showing typical "Arctic" and Southerly/Pacific flow patterns. The "Arctic" trajectory is for March 25, 1989 1900 GMT and the Southerly trajectory is for March 10, 1989 1900 GMT.

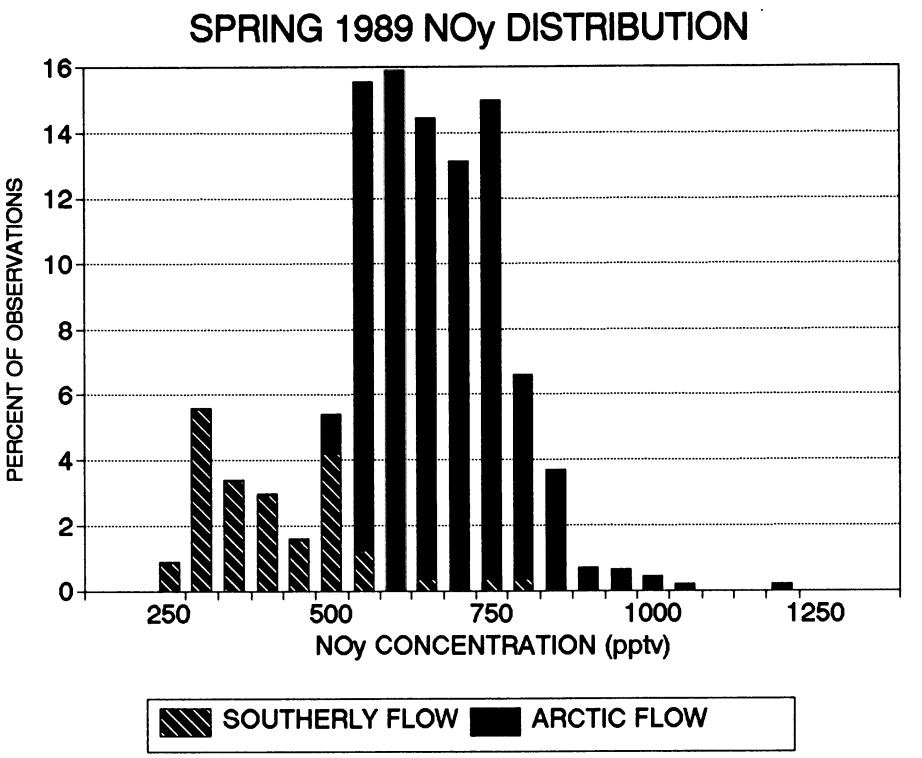

Fig. 3: Distributions of NO_y observed during periods defined by Arctic and Southerly flow

Figure, 4a and 4b show the day-and-night averaged NO concentrations measured during 1991 at Barrow. At night, NO concentrations are expected to rapidly go to zero due to reaction with ambient O_3, and this is in fact what is observed. Concentrations were observed to be below detection limit (3 pptv) except during during late spring and occasionally during summer. The summertime periods of elevated NO were associated with flow from the interior and are believed to be due to biomass/tundra fires. During late spring, corresponding to the extended period of relatively enhanced NO and a period of decreasing, NO_y concentrations are believed to be due to the thermal decomposition of PAN. An example of one period with relatively elevated NO concentrations is shown in Figure 5, along with the solar elevation angle [Honrath and Jaffe, 1992].

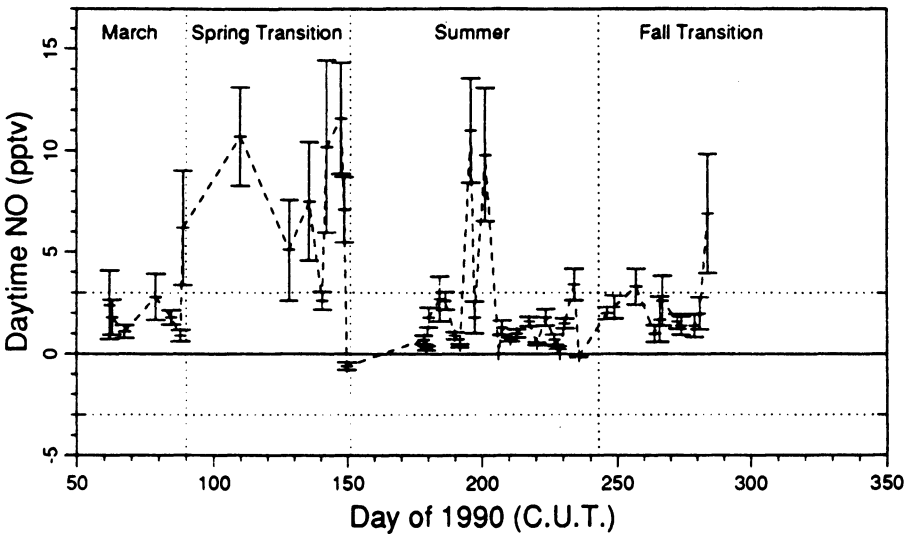

Fig. 4a: Daytime NO concentrations during 1991 background periods

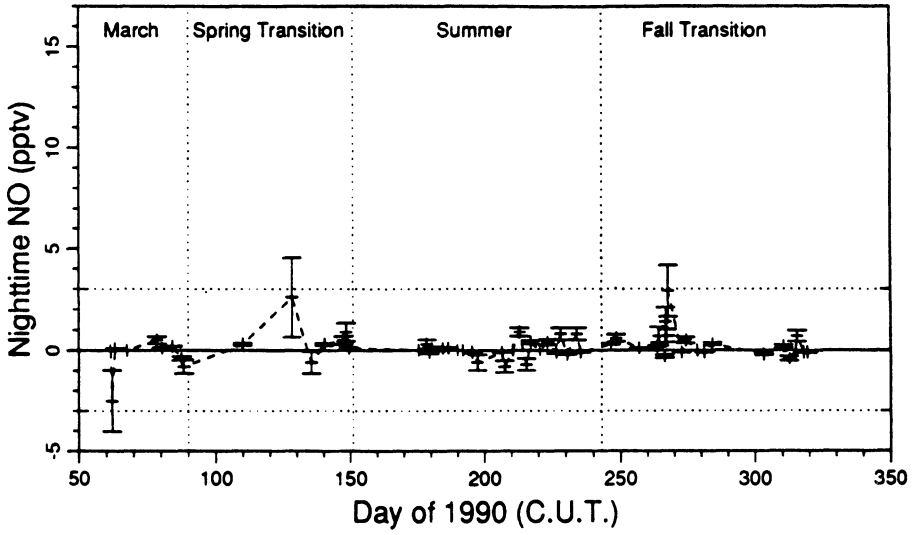

Fig. 4b: Nighttime NO concentrations during 1991 background periods

There appear to be interactions between depleted boundary layer ozone and the observed NO concentrations. During the period mentioned above, when NO reached a maximum hourly average concentration of 34 pptv, surface O_3 showed concentrations in the range of 0 -1 ppbv. The relatively high NO concentrations can be explained, at least in part, by the photostationary state relationship for the $[NO]/[NO_2]$ ratio. Ignoring the role of peroxy radicals, the $[NO]/[NO_2]$ ratio is given by:

$$[NO]/[NO_2] = J_1 / k_1 [O_3]$$

where J_1 is the NO_2 photolysis frequency and k_1 the rate constant for the NO + N_3 reaction.

At an ozone concentration of 1 ppbv, we would expect the $[NO]/[NO_2]$ ratio to be perturbed by about a factor of 30 compared to a "normal" ozone concentration of 30 ppbv. However, even in the total absence of O_3, peroxy radicals would prevent the complete disappearance of NO_2. Thus, we can conclude that under conditions of low ozone, NO_x concentrations are of order 30-50 pptv, mostly NO during the day and NO_2 at night. At sunset, the NO concentration returns to zero, indicating that O_3 still exceeds the NO concentration. Even at these low NO_x concentrations, an input of NO_x will increase the O_3 concentration by decreasing the net ozone destruction rate.

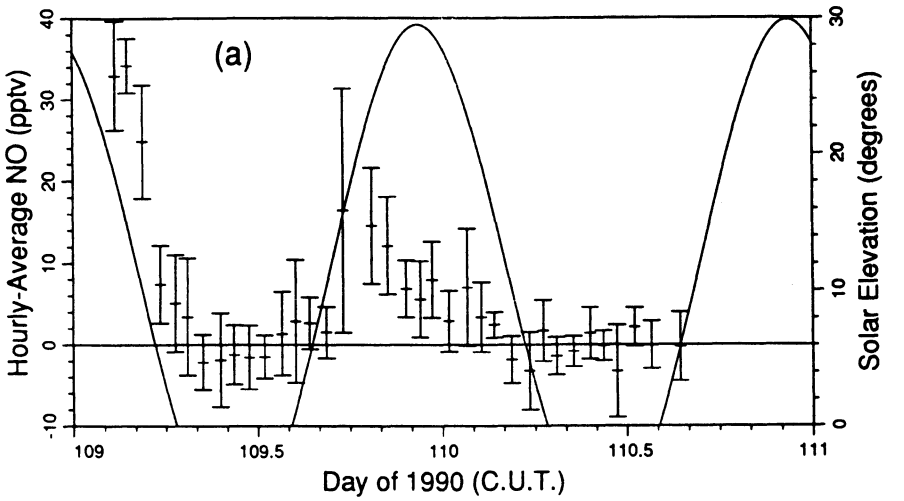

Fig. 5: Hourly averaged NO concentrations at Barrow during background period #11, April 19-20, 1991. Time is given in Coordinated Universal Time. The crosses show the mean; the vertical bars show 2 s.d. of the mean. The solid lines show the solar elevation angle.

In addition to the regional/hemispheric scale pollution sources which affect any measurement site, local pollution sources can impact it as well. At Barrow, two local sources of pollution are important, the town of Barrow and the Prudhoe Bay oil fields approximately 300 km to the east. The Prudhoe Bay industrial area is a significant source of NO_x, CO_2, CH_4 and other pollutants [Jaffe et al., 1992]. Approximately 15-20 x 10^3 tons/year of NO_x are released. At Barrow, we occasionally observe elevated concentrations of NO_y when surface winds are from the direction of Prudhoe Bay. These "Prudhoe Bay events" result in NO_y concentrations in the range of 2-17 ppbv [Jaffe et al., 1991]. Conceivably, these emissions, which began in 1977 and have increased steadily, could result in enhanced surface ozone at Barrow [Jaffe, 1991].

Ground-based measurements of peroxyacetyl nitrate (PAN) have been conducted at several Arctic locations, including Spitsbergen and Alert. Based on the work of Barrie and Bottenheim [1991, and references therein], PAN is believed to be the predominant NO_y compound in the Arctic during spring. The ground based measurements of PAN in the Canadian arctic are roughly 50-90% of our measured NO_y concentrations, consistent with the notion of PAN as a major NO_y species in the Arctic.

Vertical distributions of NO_y in the spring have been measured once in the region of Spitsbergen [Dickerson, 1985]. The NO_y concentrations were typically in the range of 0.6-1.4 ppbv with generally decreasing concentrations with altitude. Layers of enhanced NO_y were observed in the 1-4 km range.

The most extensive arctic tropospheric campaign was conducted during the summer of 1988 as part of the ABLE 3A mission [Singh et al., 1992]. Several important conclusions were reached from this campaign. NO_y concentrations observed in the boundary layer were very low (0.1 - 0.2 ppbv) and were consistent with the surface observations [Honrath and Jaffe, 1990]. However, NO_y increased rapidly in the free troposphere reaching a median concentrations of around 1 ppbv at 4-5 km. The NO_y reservoir in the free troposphere (4-6 km) consisted of about 33% PAN, with other measured NO_y species (NO_x, HNO_3) accounting for only an additional 12%. On one flight, a layer of anthropogenic pollutants in the 4-6 km region was attributed to sources in Eastern Asia. Based on the similarity to other anthropogenic tracers, Singh et al. [1992] argues that the arctic summer NO_y is largely of anthropogenic in origin.

PHOTOCHEMICAL SIGNIFICANCE

When NO_x concentrations and photolysis rates are sufficiently large and in the presence of CO, CH_4 and non-methane hydrocarbons (NMHC's), ozone production will occur. Within the arctic troposphere, this could possibly occur during late spring through early fall, depending most importantly on the NO_x concentrations. Summertime

measurements during the ABLE-3A mission [Singh et al., 1992] and during the summer of 1990 [Honrath and Jaffe, 1991] have found that NO_x concentrations in the arctic troposphere are generally too low to give rise to net photochemical ozone production during summer. However, changes in the NO_x concentrations, even at these low levels, can still give rise to changes in ozone concentrations [Jacobs et al., 1992].

Our measurements of NO during late spring (April-May) suggest that sufficient NO_x may be present to yield net photochemical production of ozone. During this period, hourly average NO concentrations reach as high as 34 pptv. Based on measured UV radiation in central Alaska [Ambach et al., 1991] and an empirical relationship between UV radiation and photolysis rates [Madronich, 1987], we estimate that the photolysis rate [$J(NO_2)$] for May 1 at Barrow (minimum solar zenith angle is around 55°) may be as high as 8×10^{-3} sec^{-1}, largely due to the influence of surface albedo [Ambach et al., 1991; Madronich, 1987]. Thus, during a period when PAN decomposition appears to be supplying NO_x and sufficient solar UV is available, in-situ ozone production may be possible at Barrow. The critical unknown, then, is the NO_2 concentration.

EVALUATION OF HYPOTHESES

From the available data we can proceed to evaluate the three hypotheses mentioned earlier.

1. Ozone is photochemically produced in the arctic troposphere from local NO_x emissions: The idea that local emissions from the Prudhoe Bay industrial facility could impact the ozone record at Barrow was proposed by Jaffe [1991]. Using a simple box model it was shown that the NO_x emissions could cause the observed 1-2%/year summertime surface ozone increase. However, despite frequent occurrence of Prudhoe Bay emissions arriving at Barrow, we have seen no evidence for ozone production in the plume which reaches Barrow [Honrath and Jaffe, 1992]. One possible explanation is that because the ozone production rate in the Arctic is reduced by the zenith angle compared to lower latitudes, the transport time for emissions from Prudhoe Bay to Barrow is too short to observe significant ozone enhancements. Nonetheless, these emissions would still be effective in increasing ozone concentrations over some area of the arctic. A realistic simulation for these emissions might answer this question. However, emissions from Prudhoe Bay probably do not explain the trends observed at Resolute, N.W.T.

2. Ozone is photochemically produced in the arctic troposphere from non-local NO_x emissions: The NO data from our 1991 campaign suggests that ozone production may be possible during late spring. Once this ozone is produced, it could impact both spring and

summer distributions. In this scenario, NOx is provided by the thermal decomposition of the substantial PAN reservoir from lower latitude NO_x emissions. High surface albedo offsets the low zenith angle to yield significant NO_2 photolysis rates. High organics and CO concentrations are also present at this time. During the spring of 1993 we will conduct a campaign which will provide a rigorous test of this hypothesis.

3. Ozone is generated at lower latitudes and transported to the Arctic via wet or dry pathways: The similarity of the tropospheric ozone trend in the Arctic with the mid-latitudes trends can not be overlooked. Certainly ozone can be produced and transported into the Arctic along with primary emissions. The satellite-derived tropospheric "residuals" calculated by Fishman [1991] suggest that ozone can be transported into the Arctic during summer and one such event was observed during ABLE 3A [Singh et al., 1992]. This runs counter to the ground based observations which show very low SO_4^{2-} and other pollutant concentrations during summer [Barrie and Bottenheim, 1991]. However, longer lived species which are not efficiently removed by precipitation, such as ozone and PAN (at cold temperatures) can be transported to the Arctic during summer via a number of pathways.

SUMMARY

Tropospheric ozone concentrations in the Arctic show significant trends at two stations, Barrow and Resolute. The two stations give a similar picture of the trends which are present at the surface during summer (at Barrow) and in the free troposphere during spring and summer (at Resolute). In this paper we have proposed three mechanisms by which anthropogenic emissions can drive the tropospheric ozone increase. The available data provide some support for these mechanisms but are not totally convincing. The arctic tropospheric NO_y cycle is quite complex with significant seasonality to it, strong vertical gradients and substantial seasonal changes in the chemical speciation. One of the most important questions to answer is; how does the springtime NO_y reservoir change with increasing temperature and light and consequently, how does the springtime reservoir impact upon summer NO_y and O_3 concentrations?

Acknowledgements: Much of the Alaskan data was collected in collaboration with Dr. Richard Honrath. The author also acknowledges many helpful discussions with Dr. Glenn Shaw and assistance with the experimental work at Barrow from the North Slope Borough Department of Wildlife Management and NOAA, Climate Monitoring and Diagnostics Laboratory. Funding for this work was provided by the National Science Foundation, Division of Atmospheric Chemistry.

REFERENCES

Ambach, W., M. Blumthaler and Wendle G. A Comparison of Ultraviolet Radiation Measured at an Arctic and an Alpine Site, *Solar Energy, 47*, 121-126, 1991.

Barrie, L.A. and J. W. Bottenheim, Sulphur and Nitrogen Pollution in the Arctic Atmosphere. In, W.T.Sturges Ed. *Pollution of the Arctic Atmosphere*, Elsevier Applied Science, N.Y., 1991.

Barrie, L.A., J.W. Bottenheim, R.C. Schnell, P.J. Crutzen, and R.A. Rasmussen, Ozone Destruction and Photochemical Reactions at Polar Sunrise in the Lower Arctic Atmosphere, Nature, 334, 138-141, 1988.

Dickerson, R.R, Reactive Nitrogen Compounds in the Arctic, *J. Geophys. Res., 90*, 10,739-10,743, 1985.

Fishman, J., C.E. Watson, J. C. Larsen, and J.A. Logan, Distribution of Tropospheric Ozone Determined from Satellite Data, *J. Geophys. Res., 95*, 3599-3617, 1990.

Fishman, J., Probing Planetary Pollution from Space, *Env. Sci.Tech., 25*, 612-621, 1991.

Honrath, R.E. and D.A. Jaffe, Measurements of Nitrogen Oxides in the Arctic, *Geophys. Res. Letts., 17*, 611-614, 1990.

Honrath, R.E. and D.A. Jaffe, The Seasonal Cycle of Nitrogen Oxides in the Arctic Troposphere at Barrow, Alaska. *J. Geophys. Res.*, In Press, 1992.

Isaksen, I.S.A., O. Hov, S.A. Penkett, A. Semb, Model Analysis of the Measured Concentrations of Organic Gases in the Norwegian Arctic, *J. Atm. Chem., 3*, 3-27, 1985.

Jacobs, D.J., S.C. Wofsy, P.S. Bakwin, S.M. Fan, R.C. Harriss, R.W. Talbot, J.D. Bradshaw. S.T. Sandholm, H.B. Singh, G.L. Gregory, G.W. Sachse, M.Shipham, D.R. Blake, and D.R. Fitzjarrald, Summertime Photochemistry of the Arctic Troposphere. *J. Geophys. Res.*, In Press, 1992.

Jaffe, D.A., R.E. Honrath D. Furness, T.J. Conway, E. Dlugokencky, and L.P. Steele, An Estimate of the CH_4, NO_x, and CO_2 Emissions from the Prudhoe Bay, Alaska Oil Development, manuscript in preparation, 1992.

Jaffe, D.A., Local Sources of Pollution in the Arctic: From Prudhoe Bay to the Taz Peninsula, In, W.T.Sturges Ed. *Pollution of the Arctic Atmosphere* Elsevier Applied Science, N.Y., 1991.

Jaffe, D.A., R.E. Honrath, J.A. Herring, S.M. Li, and J.D. Kahl, Measurements of Nitrogen Oxides at Barrow, Alaska During Spring: Evidence for Regional and Hemispheric Sources of Pollution. *J. Geophys. Res., 96*, 7395-7405, 1991.

Logan, J.A., Tropospheric Ozone: Seasonal Behavior, Trends, and Anthropogenic Influences. *J. Geophys. Res., 90*, 10,463-10,482, 1985.

Madronich, S., Intercomparison of NO_2 Photodissociation and U.V. Radiometer Measurements, *Atmos. Environ., 21*, 569-578, 1987.

Oltmans, S.J., Arctic Ozone Chemistry. In, W.T. Sturges, Ed., *Pollution of the Arctic Atmosphere,* Elsevier Applied Science, N.Y., 1991.

Penkett, S.A., and K.A. Brice, The Spring Maximum in Photo-Oxidants in the Northern Hemisphere Troposphere, Nature, 319, 655-657, 1986.

Singh, H.B., D. Herlth, D. O'Hara, K. Zahnle, J.D. Bradshaw, S.T. Sandholm, R. Talbot, P.J. Crutzen and M.A. Kanakidou, Relationship of PAN to Active and Total Odd Nitrogen at Northern High Latitudes: Influence of Reservoir Species on NO_x and O_3, *J. Geophys. Res.*, In Press, 1992.

HALOCARBONS IN THE ARCTIC AND ANTARCTIC ATMOSPHERE

William T. Sturges
Cooperative Institute for Research in Environmental Sciences, University of Colorado &
National Oceanic and Atmospheric Administration, US Department of Commerce
325 Broadway
Boulder, Colorado 80303, USA

INTRODUCTION

A wide range of halocarbon gases (those containing one or more of the halogens chlorine, fluorine, bromine and iodine) have been identified in the polar atmosphere. Their origins are various, from both anthropogenic and natural sources. Although much is known about the transformations of halocarbons in the stratosphere, and their apparent involvement in Antarctic stratospheric ozone depletion in particular, much less is know about their potential impact on tropospheric ozone chemistry. Nevertheless, the Arctic spring bromine "pulse" and negative correlation between particulate bromine and ozone is compelling evidence for halogen-ozone reactions in the polar troposphere. In the Antarctic, the progressive decline in free tropospheric ozone in austral summer has been attributed to greater UV penetration through the ozone-depleted stratosphere; a possible example of an indirect effect of halocarbons on tropospheric ozone.

CLASSES OF HALOCARBONS IN THE POLAR ATMOSPHERE

Table 1 lists some of the more important halocarbon gases that have been identified in the polar atmosphere. The chlorofluorocarbons (CFCs) are of anthropogenic origin (e.g., refrigerants, foam blowing agents, industrial solvents). They are long-lived in the atmosphere, and have essentially no reactivity in the troposphere [WMO, 1991]. They do, however, photolyze in the stratosphere, and have been implicated as a major cause of the Antarctic ozone "hole" [Solomon, 1990]. Schnell et al. [1991] noted that surface ozone at South Pole has declined in the past decade. They attributed this to enhanced UV penetration to the troposphere as a result of stratospheric ozone depletion, leading to accelerated photochemical loss of tropospheric ozone. In addition, changes in atmospheric circulation patterns over the Antarctic continent were evident from more frequent transport of ozone-depleted marine air to the Pole. Both the enhanced UV flux to the surface, and changes in circulation patterns [Neff, 1992], may be considered to be the indirect results of CFC breakdown and ozone removal in the stratosphere. Concentrations of the CFCs have been

NATO ASI Series, Vol. I 7
The Tropospheric Chemistry of Ozone in the Polar Regions
Edited by H. Niki and K. H. Becker

Table 1: Classes of volatile halocarbons and some representative species in the polar atmosphere.

Class	Common Name	Formula	Source*
CFCs:	F11	CCl_3F	A
	F12	CCl_2F_2	A
	F113	$C_2Cl_3F_3$	A
HCFCs/HFCs:	HCFC-22	$CHClF_2$	A
	HCFC-141b	$C_2H_3Cl_2F$	A
	HFC-134a	$C_2H_2F_4$	A
Halons:	H1211	$CClF_2Br$	A
	H1301	CF_3Br	A
Bromoalkanes:	Methyl bromide	CH_3Br	A, N
	Bromoform	$CHBr_3$	N (A)
	Dibromomethane	CH_2Br_2	N
	1,2-dibromoethane	CH_2BrCH_2Br	A
	Dibromochloromethane	$CHBr_2Cl$	N
	Bromodichloromethane	$CHBrCl_2$	N
Chloroalkanes:	Methyl chloroform	CH_3CCl_3	A
	Carbon tetrachloride	CCl_4	A
	Methyl chloride	CH_3Cl	A, N
	Chloroform	$CHCl_3$	N (A)
Iodoalkanes:	Methyl iodide	CH_3I	N (A)
	Chloroiodomethane	CH_2ClI	N
	Ethyl iodide	CH_3CH_2I	N

*Source: A=anthropogenic, N=natural, ()=minor component.

increasing in the atmosphere for the past several decades. Recent evidence, however, indicates that their growth rates are declining [Elkins et al., 1992] as a result of voluntary and mandatory reductions in their use.

Halons are brominated CFC-type compounds used in fire extinguishers. They too have long atmospheric lifetimes and no tropospheric sinks. Although halon concentrations are lower than the CFCs, bromine is more reactive in the stratosphere than chlorine [Salawitch et al., 1988]. Anderson et al. [1991] estimate that reactions involving BrO can account for 21%, on average, of ozone loss in the Antarctic "ozone hole". The growth rate of global halon concentrations have, like the CFCs, recently begun to decline [Butler et al., 1992].

The HCFCs and HFCs are proposed replacement compounds for the CFCs. At least one hydrochlorofluorocarbon [HCFC-22] is already in use and has been measured in the atmosphere [Montzka et al., 1992]. Unlike CFCs, HCFCs and HFCs can be attacked by OH

in the troposphere. HFCs contain no chlorine and should have no impact on stratospheric ozone. The tropospheric breakdown compounds include halohydroperoxide, peroxynitrate, and carbonyl compounds [WMO, 1991]. Although there is no evidence at present to suggest that these compounds might have any significant effect on tropospheric chemistry, some decomposition pathways involve the generation of Cl atoms, which would react with ozone. This issue has yet to be fully investigated.

Bromoalkanes may be of most importance in terms of direct effects on polar tropospheric ozone chemistry. Methyl bromide has a relatively long lifetime [1.5 yr: WMO, 1991], but other bromoalkanes have shorter lifetimes, and might participate in troposphere chemistry. Because of their believed importance to polar surface ozone chemistry, bromoalkanes will be discussed in detail in the remaining sections of this paper.

The chloroalkane group includes long-lived man-made species such as methyl chloroform and carbon tetrachloride, which are also important carriers of chlorine to the stratosphere. In general, the chloroalkanes have slower tropospheric photolysis rates than analogous bromine species [Molina et al., 1982], and are thus unlikely to be involved in polar tropospheric ozone chemistry. Iodoalkanes, on the other hand, have a significant, but not well established, role in tropospheric chemistry. Iodoalkanes will be discussed elsewhere in this volume.

BROMOALKANES IN THE POLAR TROPOSPHERE

A review of bromoalkane measurements in the Arctic and Antarctic troposphere is presented in Tables 2 and 3, respectively. In general, methyl bromide is the most abundant bromoalkane in the polar troposphere. Its concentration is also the least variable, reflecting its relatively long lifetime. Bromoform is the next most abundant, followed by dibromo methane, then the mixed bromochloroalkanes. There are, however, many inconsistencies in the reported observations.

Cicerone et al. [1988], have reported the only semi-continuous long term measurements of bromoform and methyl bromide in the Arctic (Barrow, AK) to date. The plots in their paper are of three and twelve month running averages. In Figure 1 the monthly mean values have been plotted instead, using tabulated CH_3Br concentrations from the Cicerone et al. paper, and the original bromoform data from W. Pollock [personal communication). A pronounced seasonal variation in bromoform is evident with low summer values and high winter values. Methyl bromide showed much less seasonal variation, but appeared to follow a similar pattern (this was not apparent in the 12 month running averages).

Table 2: Bromo- and bromochloroalkane measurements from the Arctic troposphere (pptv). Arithmetic mean concentrations shown except where indicated.

Ref	Location	CH_3Br	$CHBr_2$	CH_2BrCl	$CHBr_3$	$CHBr_2Cl$	$CHBCl_2$	$C_2H_4Br_2$
1	Arctic flights:[a]							
	<200 m	11.1	14.5		16.5			11.6
	200-8400 m	11.7	14.9		13.6			10.1
	Tropo folding[b]	14.7	33.7		30.3			17.7
2	Spitsbergen							
	Mar 83	14.4						
3	Barrow							
	spr 83	10.7	5.4	2.9				1.2
	sum 83	12.9	4.8	2.4				1.2
	Flights in haze[a]	10.5	4.2	2.3				1.2
	Flights out of haze	10.8	2.5	2.0				0.4
4	Barrow							
	spr 85-87	12.3			6.6			
	sum 85-87	9.7			3.1			
5	Alert							
	spr 86-87				3.6			
	sum 86-87				5.5			
	Arctic flights[c]							
	<200 m				4.9[d]			
	200-8400 m				0.5[d]			
6	Alert, Feb-Apr 88							
	RAR[e]				19.9			
	YU[f]				1.2			
	LEH[g]		1.2		5.6			0.4
	EA[h]	10.6	0.7		2.1	0.3		0.2
7	Barrow							
	Mar-Apr 89				5.3	0.2	0.7	
8	Barrow							
	Mar-Apr 90		1.9	0.5	2.3	0.3	0.6	0.1
9	Resolute							
	May 91				2.6			
10	Resolute							
	May 92				1.4			

Spr = spring months (March, April, May); sum = summer months (June, July, August)
(a) March-April, 1983; (b) tropopause folding event at 8.4-8.8 km (O_3 49-260 ppb); (c) April, 1986; (d) median value; (e) Rasmussen flasks analyzed at Oregon Graduate Center; (f) Rasmussen flasks analyzed at York University (Canada); (g) flasks analyzed by Heidt at National Center for Atmospheric Research (NCAR); (h) carbon tubes, solvent extracted, analyzed by Atlas at NCAR.
References: (1) Berg et al., [1984]; (2) Høv et al., [1984]; (3) Rasmussen and Khalil [1984]; (4) Cicerone et al., [1988]; (5) Barrie et al., [1988]; (6) Bottenheim et al., [1990]; (7) Sturges et al. [1992c]; (8) Sturges, [unpublished data]; (9) Sturges et al., [1992]); (10) Sturges, Cota and Buckley, [unpublished data].

Table 3: Bromo- and bromochloroalkane measurements from the Antarctic troposphere (pptv).

Ref	Location	CH_3Br	CH_2Br_2	CH_2BrCl	$CHBr_3$	$CHBr_2Cl$	$CHBrCl_2$	$C_2H_4Br_2$
1	S Pole	7.5		2.5	1.0	0.7		1.0
2	Antarctic Peninsula[a]		3.7		6.3		3.8	
3	McMurdo Sound							
	Ice edge	9.5			1.2			
	Annual ice	9.0			1.5			
	Lake Bonney[b]	7.5			0.3			

(a) Shipboard samples; (b) ca. 50 km inland, with air flow from polar ice cap.
References: (1) Khalil and Rasmussen [1985]; (2) Reifenhäuser and Heumann [1992]; (3) Sturges et al. [1992d].

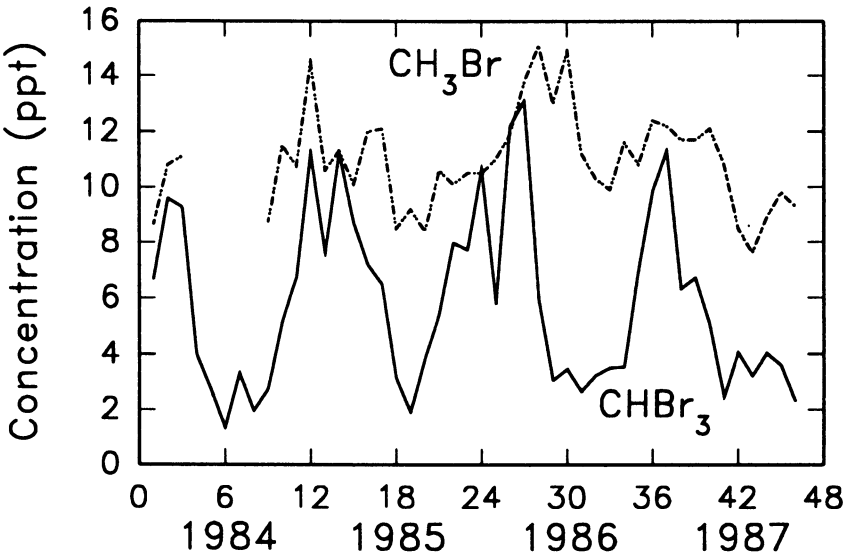

Fig. 1: Monthly mean concentrations of methyl bromide and bromoform at Barrow, AK (after Cicerone et al., [1988]).

The same trends were not, however, indicated in other studies. Rasmussen et al. [1984] reported a reverse seasonal trend to that of Cicerone et al. for methyl bromide at the same location (Table 2). Bottenheim et al. [1990] reported an intercomparison study of bromoform measurements at Alert, NWT. Their results are shown in Figure 2 (from data

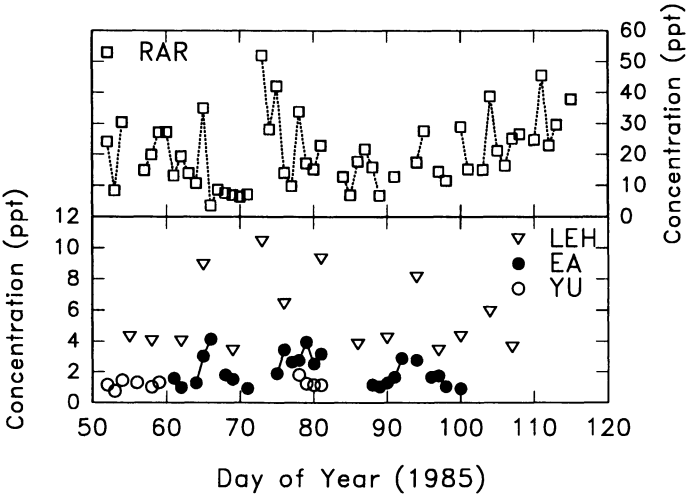

Fig. 2: Bromoform concentrations at Alert, NWT, measured by four groups of investigators (after Bottenheim et al., [1990]: see Table 2 for explanation of legend).

tabulated in the paper). Firstly, there were wide discrepancies in the measurements by different groups. Note the different scaling, and much higher values, reported by RAR. The same investigator reported much lower values for the same site and season in the preceding two years [Barrie et al., 1988; Table 2]. Secondly, none of the sets of measurements in Bottenheim et al. showed any consistent trend over the three month period for which Cicerone et al. reported a strong decline in bromoform at Barrow. One of the data sets (LEH) was produced by the same investigators as in Cicerone et al., and thus should be consistent between both studies. This suggests that there may be some genuine differences in bromoform distributions between the two sites.

A comparison of standards in the Bottenheim et al. study indicated that there was a factor of 2.0-2.5 difference between the LEH and EA data. Applying this to the LEH data brought them more into line with the EA and YU results. This implies that the bromoform data of Cicerone et al. (Figure 1) should also be reduced by the same factor.

There are further discrepancies in reported altitudinal profiles (Table 2). Berg et al. [1984] showed only a small altitudinal gradient in bromoform, whilst Barrie et al. [1988]

reported a sharp decline in concentration above about 200 m. The Berg et al. data are in some doubt because of the high concentrations of 1,2-dibromoethane and dibromomethane observed. They also reported values for all species, including methyl bromide, that were higher in the lower stratosphere (troposphere folding event) than at the surface. No explanation has been advanced for these findings.

It is of considerable importance to resolve these differences. For instance, a sharp gradient of bromoform across the surface inversion layer would be consistent with a local surface source of the gas and rapid processing (order of days). A lack of altitudinal variation would be more in keeping with a long atmospheric lifetime and transport from more distant sources. Similarly, a strong seasonal variation in bromoform indicates pronounced annual variations in either source strengths and/or atmospheric removal processes. Conversely, a lack of seasonal variation might also imply a relatively long atmospheric lifetime. If the observations of Berg et al. [1984] of elevated bromoalkane concentrations in the lower stratosphere can be confirmed, then effects on polar stratospheric ozone may need to be considered.

Relationship Between Bromoalkanes and Surface Ozone Chemistry

The reasoning for a relationship between bromoalkanes and surface ozone loss in the Arctic is largely based on the observation that particulate bromine and surface ozone during the spring are often strongly negatively correlated (e.g., r = -0.94 by Barrie et al., [1988]). It is speculated that bromine atoms react with ozone to produce O_2 and BrO. Although BrO is a gas, it is further assumed that the BrO is in some way converted to, or adsorbed on to, particulate matter. The question, then, is what is the source of the bromine atoms? Inorganic sources have been suggested [Sturges, 1989; Finlayson-Pitts et al., 1990; McConnell et al., 1991, and this volume), as have organic sources [Barrie et al., 1988]. Oltmans et al. [1989] suggested that bromoform might be the source, based on the measurements of Cicerone et al. [1988], which showed rapidly declining levels of bromoform in the spring (Figure 1) at the time of maximum surface ozone destruction. Perhaps more convincing is the observation by Bottenheim et al. [1990] of a strong negative correlation between ozone and bromoform at Alert (r = -0.69). This, however, like the negative correlation of particulate bromine with ozone, may be emphasized by meteorological modulation, i.e., an alternation between upper tropospheric air flowing down from the mountains, and ozone-depleted marine air rich in marine-derived bromoalkanes and particulate bromine.

Sturges et al. [1992c] noted a similar relationship at Barrow, AK. Bromoform and particulate bromine tended to be elevated during major ozone depletion events, although the three were not as closely interrelated as at Alert, perhaps due to a lesser meteorological

modulation. In the same study, Sturges et al. examined the air trajectories associated with high and low ozone events, and attempted to relate these to satellite observations of areas of open water in the Arctic Ocean. They concluded that high surface ozone concentrations, typical of free tropospheric air, occurred with either downslope transport from the Brooks Range or rapid transport of well mixed air from the Pacific. Moderate ozone depletion of 10-20 ppb occurred with transport across the central Arctic Ocean where leads were visible a few days upwind. Major ozone depletion (O_3 < 25 ppb) occurred with air transport from leads located within a few 100 km of Barrow. This suggests that there is an intimate relationship between ozone loss and some substance released from leads (perhaps organic bromine) and, further, that the processing time for ozone removal is less than 1-2 days.

Total organic gaseous bromine has been measured in the Arctic by collection on carbon tubes followed by total elemental analysis by neutron activation. This was pioneered by Berg et al. [1983] at Barrow, although only five measurements were reported, and more recently extended at the same location by Sturges et al. [1992b]. Both authors found that organic gaseous Br dominated the bromine budget, followed by particulate Br collected on filters. Sturges et al. found that particulate Br tended to be higher during the day, whereas organic Br was lower (Figure 3), giving a diurnal variation in the ratio of particulate to organic Br. This suggests that rapid photolysis of organic Br can occur leading to particulate Br formation. There was an increase in particulate to organic ratios during an ozone depletion event (Figure 3d). Ozone, however, did not show a diurnal variation, although such an effect might be negated by diurnal variations in surface mixing and inversion height [Sturges et al., 1992c].

The above field observations are not in accord with laboratory measurements of the gas phase photolysis of bromoform [Barrie et al., 1988, and this volume], which yield lifetimes at arctic latitudes in spring on the order of weeks. Either bromoform is not involved in surface ozone and particulate bromine chemistry, or some heterogeneous process can speed its decomposition. Sturges et al. [1992b] showed that total elemental Br measurements were invariably higher than measurements of water soluble Br^- ions in particulate matter at Barrow, and that there was an apparent diurnal variation in the ratio between the two, suggesting conversion of non-ionic Br to ionic Br during the day. Although circumstantial, this might be taken as evidence for photochemically labile organic Br contained in suspended particles. More work is needed to examine the photochemistry of bromoalkanes on suspended particles and on snow and ice surfaces.

SOURCES OF BROMOALKANES IN THE POLAR TROPOSPHERE

Methyl bromide is believed to have both natural (oceanic) and anthropogenic (fumigants, leaded gasoline combustion) sources. The division between the natural and man-

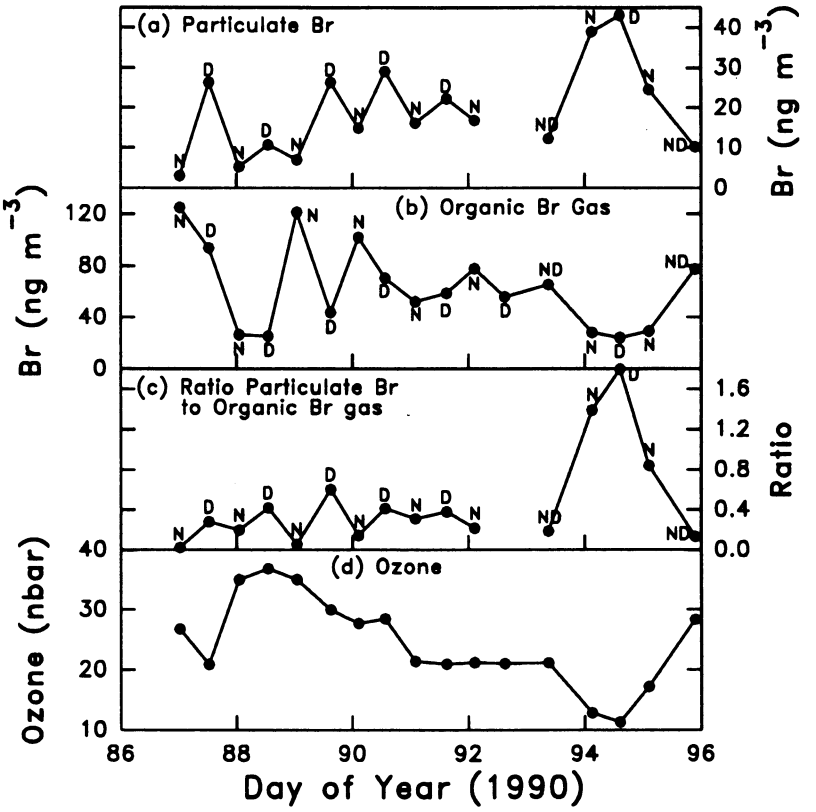

Fig. 3: Measurements of particulate Br, total organic gaseous Br, and ozone at Barrow, AK (from Sturges et al., 1992b]. N=night sample; D=day sample.

made sources has been a matter of debate [Methyl Bromide Global Coalition, 1992], and is of some importance since it has been proposed that the compound should be regulated along with the other ozone-depleting gases. There is some evidence for natural sources within the polar regions. Sturges et al. [1992d] reported higher concentrations over McMurdo Sound, Antarctica, than at an inland site (Table 3). They also found evidence for release of methyl bromide by ice algae retrieved from the underside of annual ice in McMurdo Sound. Rasmussen and Khalil [1984] found no difference in methyl bromide concentrations on aircraft flights in and out of "Arctic haze" layers of polluted air originating predominantly

from Eurasia (Table 2), thus a large Eurasian anthropogenic source is not indicated. Penkett et al. [1981], in contrast, reported higher CH_3Br concentrations in the North Atlantic than the South Atlantic, although it has not been firmly established whether this was due to Northern Hemisphere anthropogenic production, variations in marine biogenic production, or a greater oceanic sink in the Southern Hemisphere.

1,2-dibromoethane is used as a fumigant, and is a constituent of leaded gasoline. It is not known to have any natural sources. In contrast, the other bromoalkanes have few anthropogenic sources; mostly minor release from chlorination of seawater [Gschwend et al., 1985], although Rasmussen and Khalil [1984] did find higher levels of dibromomethane in haze layers (Table 2). Bottenheim et al. [1990] noted strong intercorrelations between $CHBr_3$, $CHBr_2Cl$ and CH_2Br_2. Correlations with $C_2H_4Br_2$ were much weaker. Sturges et al. [1992c] also noted strong correlations between $CHBr_3$, $CHBr_2Cl$, and $CHBrCl_2$. This suggests a common origin of these compounds to the polar atmosphere.

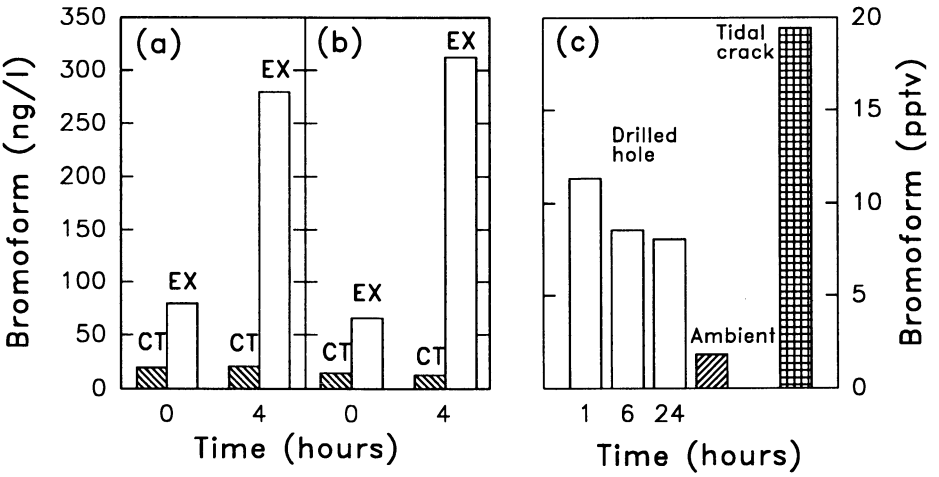

Fig.: 4 (a,b) Examples of bromoform release to seawater in ice algae incubations at under-ice temperature and light flux. The controls (CT) were deep seawater, the experiments (EX) were ice algae cells suspended in deep seawater. Concentrations are ng $CHBr_3$ per litre of seawater. The high initial experiment value was due to an initial release of intracellular or intersticial ice $CHBr_3$. (c) Atmospheric $CHBr_3$ concentrations (pptv) in a flux chamber placed over a hole drilled through sea ice, in ambient air over sea ice, and over a tidal crack. All experiments were conducted at Resolute Bay, NWT [Sturges et al., 1992a].

Marine macrophytes have for decades been known to produce numerous halogenated compounds, including seaweeds found in arctic and subarctic regions [Wever, 1991, and this volume]. Seaweeds are light-limited to water shallower than 10-15 m, and require a rocky substrate on which to anchor. In the Arctic they are most prolific on coastlines that remain ice free, since ice-scouring disrupts colonization. Open ocean phytoplankton blooms are known in both Arctic and Antarctic waters [Smith et al.,1991] but these occur in the summer, not during the season of high bromine and low ozone levels. Sturges et al. [1992a and 1992d], have identified the release of several bromoalkanes, notably bromoform, from polar ice microalgae in both the Arctic and Antarctic (Figures 4a,b). These microalgae colonize the underside of sea ice, are highly photoadapted to low light levels, and undergo an intense bloom during the spring. Unlike the macrophytes, they are not restricted to shallow water and narrow coastal margins, but are believed to inhabit the underside of all annual and pack ice in the polar seas: an area of $7x10^6$ km^2 in the Arctic and $16x10^6$ km^2 in the Antarctic (6% of the world ocean area). In Lancaster Sound, NWT, Welch et al. [1992] determined a total annual average carbon production of 60 g C m^{-2} y^{-1}, of which approximately 90% was contributed by phytoplankton, 10% by ice microalgae, and less than 1% by macrophytes. In the open Arctic Ocean it is expected that the relative carbon production by macrophytes will be much less. The Antarctic has less coastal perimeter than the Arctic, and all of it is ice locked for at least part of the year, thus macrophytes are likely to have a lower abundance in the Antarctic.

Based on their measurements of bromoform release to seawater by ice microalgae in Resolute Bay, NWT, Sturges et al. [1992a] calculated that to sustain the observed levels of atmospheric bromoform at that location (Table 2) would require 2-19% of the bromoform released to seawater by the microalgae to reach the atmosphere. They demonstrated that bromoform escaped through natural cracks and holes drilled through the ice (Figure 4c). The overall porosity and permeability of annual ice is not known, and thus the actual flux rate of bromoform released under the ice to the atmosphere cannot be calculated at present. On an annual basis, assuming that all of the bromoform released to seawater eventually migrated to the atmosphere, they estimated that ice microalgae emission of organobromine to the atmosphere was of the same order as that from both global macroalgae and anthropogenic sources. The ice algae are evidently a potentially large source of bromoform to the polar atmosphere.

Most recently Sturges, Cota and Buckley [unpublished data] have measured bromoform profiles from the snow surface to the sea floor at Resolute Bay. As well as an expected bromoform-rich layer at the base of the sea ice, corresponding to the ice microalgal layer, they also found a layer with equal or higher bromoform concentrations at the top of the sea ice, under the snow-pack. It is speculated that this layer forms during the initial fall freeze by scavenging of cells and organics from the water column by ice crystals rising

through the supercooled surface water layer. Flux rates to the atmosphere from the surface bromoform-rich layer have not yet been measured. If indeed this layer is present throughout the winter, then even a slow release of bromoform may lead to elevated atmospheric levels, due to the absence of photochemical-mediated removal mechanisms, scant precipitation, low deposition velocities to snow and ice surfaces, and the isolation and slow mixing of the arctic winter air mass.

Winter bromoform levels might also be explained in whole or in part by macrophyte production [see this volume]. Dunton [1982] determined that certain arctic kelps produced new tissue almost exclusively during the winter and spring. Transport from dense macrophyte populations outside of the High Arctic, such as the Norwegian coast, is also a possibility. In this context it is noted that intrusions of lower latitude air into the arctic vortex in winter is principally from Eurasia. The distribution and bromoalkane production rates of arctic macro-and microalgae or not sufficiently well known at present to judge their relative contributions of bromoalkanes to the polar atmosphere.

CONCLUSIONS

Halocarbons may exert an influence on tropospheric ozone either via indirect effects on stratospheric ozone, and thus tropospheric photochemistry, or directly by photolysis near the surface, and reaction of halogen (notably bromine atom) radicals with ozone. Bromoform is considered a likely candidate because of the elevated concentrations observed in the Arctic boundary layer, and because its UV absorption cross-section extends to wavelengths that can reach ground level. There are, unfortunately, many inconsistencies in reported bromoform distributions in the atmosphere, and evidence for its involvement in surface ozone destruction is largely circumstantial. It is recommended that more emphasis be placed on obtaining reliable measurements of brominated species in the polar atmosphere, and on studies to directly examine the possibility of gas phase and heterogenous reactions between bromoalkanes and ozone.

Acknowledgements I wish to acknowledge the support of the Atmospheric Chemistry Project of the National Oceanic and Atmospheric Administration's Global Climate Change Program, and the Division of Polar Programs of the National Science Foundation. I also thank G. Cota, University of Tennessee, for useful discussions.

REFERENCES

Anderson, J.G., W.H, Brune, S.A. Lloyd, D.W. Toohey, S.P. Sander, W.L. Starr, M. Loewenstein, J.R. Podolske, Kinetics of O_3 destruction by ClO and BrO within the Antarctic vortex: an analysis based on in situ ER-2 data. *J. Geophys. Res. 94(D)*: 11,480, 1989.

Barrie, L.A., J.W. Bottenheim, R.C. Schnell, P.J. Crutzen, R.A. Rasmussen, Ozone destruction and photochemical reactions at polar sunrise in the lower arctic atmosphere, *Nature, 334*: 138-141, 1988.

Berg, W.W., L.E. Heidt, W. Pollock, P.D. Sperry, R.J. Cicerone, Brominated organic species in the Arctic atmosphere, *Geophys. Res. Lett.*, 11: 429-432, 1984.

Berg, W.W., P.D. Sperry, K.A. Rahn, E.S. Gladney, Atmospheric bromine in the Arctic, *J. Geophys. Res., 88(C)*: 6719-6736, 1983.

Bottenheim, J.W., L.A. Barrie, E. Atlas, L.E. Heidt, H. Niki, R.A. Rasmussen, P.B. Shepson Depletion of lower tropospheric ozone during Arctic Spring: the polar sunrise experiment 1988, *J. Geophys. Res., 95(D)*: 18,555-18,568, 1990.

Butler, J.H., J.W. Elkins, B.D. Hall, S.O. Cummings, S.A. Montzka, A decline in the growth rates of atmospheric halons, *Nature, 359*: 403-405, 1992.

Cicerone, R.J., L.E. Heidt, W.H. Pollock, Measurements of atmospheric methyl bromide and bromoform, *J. Geophys. Res., 93(D4)*: 3745-3749, 1988.

Dunton, K.H., E. Reimnitz, S. Schonberg, An arctic kelp community in the Alaskan Beaufort Sea. *Arctic, 35*: 465-484, 1982.

Elkins J.W., T.M. Thompson, T.H. Swanson, J.H. Butler, B.D. Hall, S.O. Cummings, D.A. Fisher, A.G. Raffo, Slowdown in the growth rates of atmospheric chlorofluorocarbons 11 and 12, *Nature*: submitted, 1992.

Finlayson-Pitts, B.J., F.E. Livingstone, H.N. Berko, Ozone destruction and bromine photochemistry at ground level in the Arctic spring, *Nature, 343*: 622-625, 1990.

Hov. Ø., S.A. Penkett, I.S.A. Isaksen, A. Semb, Organic gases in the Norwegian Arctic, *Geophys. Res. Lett., 11*: 425-428, 1984.

Gschwend, P.M., J.K. McFarlane, K.A. Newman, Volatile halogenated organic compounds released to seawater from temperate marine macroalgae, *Science, 227*: 1033-1035, 1985.

Khalil, M.A.K., R.A. Rasmussen, The trend of bromochlorodifluoromethane and the concentrations of other bromine-containing gases at the South Pole, *Antarctic J. US*: 206-207, 1985.

McConnell, J.C., G.S. Henderson, L. Barrie, J. Bottenheim, H. Niki, C.H. Langford, E.M.J. Templeton, A new mechanism for Arctic O_3 depletion at polar sunrise: heterogeneous photochemical bromine production, *Nature, 355*:150-152, 1992.

Methyl Bromide Global Coalition, *Proceedings of The Methyl Bromide Science Workshop Arlington VA June 2-3 1992,* Atmospheric and Environmental Research Inc. Cambridge MA, 1992.

Molina, L.T., M.J. Molina, F.S. Rowland, Ultraviolet absorption cross-sections of several brominated methanes and ethanes of atmospheric interest, *J. Phys. Chem., 86:* 2672-2676, 1982.

Montzka S.A., R.C. Myers, J.H. Butler, S.O. Cummings, J.W. Elkins, Global measurements of HCFC-22, *Am. Geophys. Union Fall Meeting, Dec. 7-11 1992 San Francisco*, AGU Washington, 1992.

Neff ,W.D., On the influence of stratospheric stability on lower tropospheric circulation over the South Pole, Preprints: *Third Conference on Polar Meteorology and Oceanography,*

29 Sept.-2 Oct. 1992, Amer. Met. Soc., Portland OR, 1992.

Oltmans, S.J., R.C. Schnell, P.J. Sheridan, R.E. Peterson, J.W. Winchester, S.M. Li, P.P. Tans, W.T. Sturges, J. Kahl, L.A. Barrie, Seasonal surface ozone and filterable bromine relationship in the High Arctic, *Atmos Environ., 23*: 2431-2441, 1989.

Penkett, S.A., B.M.R. Jones, M.J. Rycroft, D.A. Simmons, An interhemispheric comparison of the concentrations of bromine compounds in the atmosphere, *Nature, 318*: 550-553, 1985.

Rasmussen, R.A., M.A.K. Khalil, Rare trace gases at the South Pole, *Antarctic J. US*: 250-251, 1983.

Rasmussen, R.A., M.A.K. Khalil, Gaseous bromine in the Arctic and Arctic haze, *Geophys. Res. Lett., 11*: 433-436, 1984

Reifenhäuser, W., K.G Heumann, Bromo- and bromochloromethanes in the Antarctic atmosphere and the south polar sea, *Chemosphere, 24*: 1293-1300, 1992.

Salawitch, R.J., S.C. Wofsy, M.B. McElroy, Chemistry of OClO in the Antarctic stratosphere: Implications for bromine, *Planet. Space Sci. 36*: 213, 1988.

Schnell , R.C., S.C. Liu, S.J. Oltmans, R.S. Stone, D.J. Hofmann, E.G. Dutton, T. Deshler, W.T. Sturges, J.W. Harder, S.D. Sewell, M. Trainer, J.M. Harris, Decrease of summer tropospheric ozone concentrations in Antarctica, *Nature, 351*: 726-729, 1991.

Smith, W.O. Jr, L.A. Codispoti, D.M. Nelson, T. Manley, E.J. Buskey, H.J. Niebauer, G.F. Cota, Importance of *Phaeocystis* blooms in the high-latitude ocean carbon cycle, *Nature, 352*: 514-516, 1991.

Solomon, S. Progress towards a quantitative understanding of Antarctic ozone depletion, *Nature, 347*: 347-354, 1990.

Sturges, W.T., Discussion: The reaction of NO_2 with NaBr: a possible source of BrNO in polluted marine atmospheres, *Atmos Environ, 23*: 1167-1168, 1989.

Sturges. W.T., G.F. Cota, P.T. Buckley, Bromoform emission from Arctic ice algae, *Nature, 358*: 660-662, 1992a.

Sturges, W.T., R.C. Schnell, G.S. Dutton, S.R. Garcia, J.A. Lind, Spring measurements of atmospheric bromine at Barrow, Alaska, *Geophys. Res. Lett.*: in press, 1992b.

Sturges, W.T., R.C. Schnell, S. Landsberger, S.J. Oltmans, J.M. Harris, S.M. Li, Chemical and meteorological influences on surface ozone destruction at Barrow, Alaska, during spring 1989, *Atmos. Environ.*: in press, 1992c.

Sturges, W.T., C.W. Sullivan, R.C. Schnell, L.E. Heidt, W.H. Pollock, Bromoalkane production by Antarctic ice algae, *Tellus*: in press, 1992d.

Welch, H.E., M.A. Bergmann, T.D. Siferd, K.A. Marten, M.F. Curtis, R.E. Crawford, R.J. Conover, H. Hop, Energy flow through the marine ecosystem of the Lancaster Sound region, *Arctic*: in press, 1992.

Wever, R., M.G.M. Tromp, B.E. Krenn, A .Marjani, M. Van Tol, Brominating activity of the seaweed *Ascophyllum nodosum*: impact on the biosphere, *Environ. Sci. Technol., 25*: 446-449, 1991.

World Meteorological Organization, Scientific Assessment of Ozone Depletion: 1991, WMO Geneva, 1991.

MEASUREMENTS OF HYDROCARBONS IN POLAR MARITIME AIR MASSES

S.A. Penkett
School of Environmental Sciences, University of East Anglia
Norwich, UK

INTRODUCTION

This paper is a shortened version of one to be published in the refereed literature [Penkett, et al., 1993]. Its relevance to the NATO Workshop held in Nova Scotia in 1992 is associated with the particular condition of meteorology and chemistry that pertain in the Arctic and allows large concentrations of relatively reactive molecules to build up in wintertime at high latitudes of the northern hemisphere. Also, the location of the densely populated continents of North America, Europe and parts of Asia with respect to the polar areas ensures that significant fractions of the pollutants emitted in these land areas are able to pollute the polar areas to a high degree. This phenomenon was first identified as the arctic haze [S.A. Penkett, 1981], however, the co-presence of many gases at high concentrations could be of considerably more consequence to the pollution of the northern hemisphere as a whole.

Various studies have been made of the non-methane hydrocarbon composition of air in the boundary layer over the ocean on individual ship cruises and using aircraft [Rudolph and Ehhalt, 1981; Blake and Rowland, 1986; Bonsang and Lambert, 1985; Rasmussen and Khalil, 1982; Singh and Salas, 1982]. These have tended to focus their efforts on the investigation of the vertical and latitudinal distribution of hydrocarbons over large regions of the unpolluted atmosphere. The studies have focused on the regular collection of data on the hydrocarbon composition of the free troposphere over the Atlantic Ocean throughout the year with the object of investigating the potential extent of the subhemispheric buildup of precursors to ozone. Investigations into the problem of ozone pollution in the lower atmosphere have led to the realization that it is not confined to areas like Los Angeles where it was first found nearly 50 years ago [Haagen-Smit, 1952]. Ozone pollution is now clearly recognized as a regional problem in the summer months [Penkett, 1991] and could be even more widespread, if precursors to ozone production can accumulate in the atmosphere in periods of low photochemical activity [Liu et al., 1987; Penkett, 1988].

Non-methane hydrocarbons are known to have a controlling influence on the production of ozone in the polluted boundary layer of the atmosphere. It is quite possible, however, that their influence is more widespread, particularly because in wintertime, photochemical degradation is much less efficient. In winter conditions, many non-methane hydrocarbons can

NATO ASI Series, Vol. I 7
The Tropospheric Chemistry of Ozone in the Polar Regions
Edited by H. Niki and K. H. Becker

escape from the boundary layer in source areas and disperse into the free troposphere over large parts of the northern hemisphere.

EXPERIMENTAL METHODS

The air samples were collected in stainless steel bottles using a Jetstream aircraft operated by Cranfield Institute of Technology. This has an operation ceiling of 3300 m when flown unpressurised, and a maximum endurance of 4 hours at 120 knots. It had the capability of reaching the normal sampling areas (north of Ireland, west of Scotland) without refueling. Nearly all the flights (approximately 18) were made in a polar air mass following the passage of a cold front.

Following on from preliminary studies of hydrocarbon concentrations in clean air [Lightman et al., 1990], at least 18 further flights were made to establish the detailed variation in concentration of over 20 hydrocarbons with season. For the first four flights shown here (J080, J087, J091, and J099), the hydrocarbons were analyzed using a packed column similar to that used for the previous studies [Lightman et al., 1990]. All subsequent data were produced with the capillary column referred to above. Nearly all these flights were made following the passage of a cold front, that is, in a polar or Arctic air mass. In January 1989, however, two consecutive flights were made with one (J124) in tropical maritime air and the next one (J125) four days later in maritime polar air. Isobaric wind back-trajectories are available for several of these flights and are referred to later when the data for flights J124 and J125 are contrasted. All flights sought to avoid very unstable showery conditions so as to minimize the possibility of sampling air recently convected up from the surface to the sampling altitude, which was typically in the region of 3 km, for the free tropospheric samples. The flights also sought to avoid circumstances in which the sampled air could have been recirculated around a low-pressure center. The location of the flights is shown in Table 1. Most of them took place over the Atlantic Ocean west of Scotland and north of Ireland. The exceptions were flight J080, which was made over the North Sea off Teesmouth, flights J094, J110, J129, and J167, that took place in the western approaches to the English Channel, flight J130 in the south of Lands End, and flight J167 made off eastern England. In the latter two cases, refueling of the aircraft was necessary in Cornwall.

The hydrocarbons were analyzed at the University of East Anglia using a Hewlett Packard 5890A gas chromatograph equipped with a flame ionization detector (FID), the output from which was fed to a Spectra Physics SP 4290 computing integrator.

Figure 1 shows a schematic diagram of the hydrocarbon preconcentrating system. Aliquots of between 700 and 1000 mL were dried by passage through a Nafion perm drier

TABLE 1: Background Jetstream Flights

Date	Code	Column Employed	Sampling Location	Comments
Jan. 28, 1987	J080	packed	Off Teesmouth	
March 25, 1987	J087	packed	W of Scotland	
Sep. 8, 1987	J091	packed	W of Scotland	
Oct. 13, 1987	J094	packed	W approaches to UK	
March 4, 1988	J099	capillary	W of Scotland	
May 18, 1988	J105	capillary	W of Scotland	
July 8, 1988	J110	capillary	W approaches to UK	
Aug. 23, 1988	J114	capillary	W of Scotland	
Oct. 28, 1988	J120	capillary	N of Ireland	
Nov. 18, 1988	J123	capillary	N of Ireland	
Jan. 6, 1989	J124	capillary	N of Ireland	Air temperature +5°C
Jan. 10, 1989	J125	capillary	N of Ireland	Air temperature -12°C
Feb. 20, 1989	J129	capillary	W approaches to UK	
March 13, 1989	J130	capillary	S of Lands End	
March 16, 1989	J131	capillary	W of Scotland	
May 3, 1989	J134	capillary	Hebrides	
April 4, 1990	J167	capillary	Flamborough Head	
April 19, 1990	J168	capillary	N of Ireland	

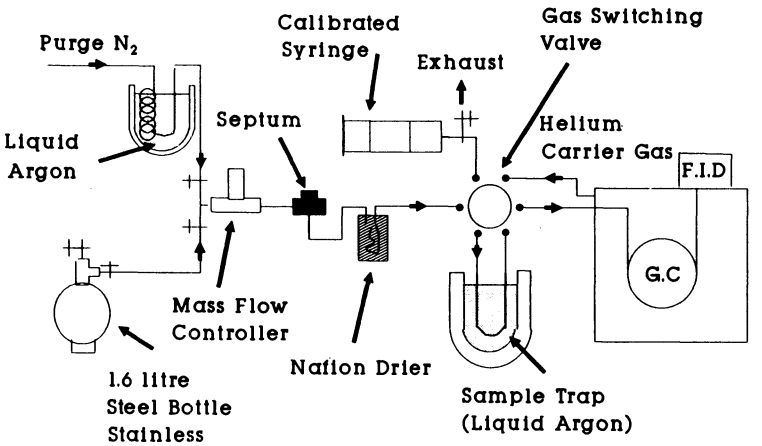

Fig. 1. Cryogenic concentration system for hydrocarbon analysis.

(International Science Consultants) at a flow rate of 30 cm^3 min^{-1}, and the non-methane hydrocarbons were trapped in a 20-cm-long 1/8" (0.32 cm) diameter stainless steel loop, packed with 60 mesh glass beads and immersed in liquid argon at -186°C. The hydrocarbons were introduced on to the chromatographic column via a six-port gas switching valve (Carle), after the cryogen had been quickly replaced with boiling water. The column used for most analyses was a fused-silica wide bore (50 m x 0.53 mm ID) Al_2O_3/KCl porous layer open tubular (PLOT) capillary column (Chrompack) and the carrier gas was helium at a flow rate of 12 cm^3 min^{-1}. The oven was programmed to remain at 30°C for 6 min, then increased in temperature from 30° to 70°C at a rate of 5°C min^{-1}, and from 70° to 220°C at 10°C min^{-1}. This final temperature exceeded the manufacturer's recommended maximum by 20°C, but it allowed measurements to be made of the C_8 aromatic molecules without difficulty. Some data were analyzed by a packed column system [Lightman et al., 1990].

Identification of the many species present in the polluted air samples was achieved by retention time, employing small quantities of pure gases or vapors. Unique identification of the peaks was assisted by the excellent resolution of the PLOT column and the good chromatographic reproducibility experienced. Blank chromatograms were obtained daily by treating nitrogen gas, cleaned by passage through a liquid argon trap, as a sample. With the exception of isobutene (2-methylpropene) the blank signals were very small for all species when compared to clean free tropospheric air samples. Tests made to consider possible contamination of air as a result of its storage in the sample bottles also indicated good sample integrity with no increase in concentration with time. This is also shown by lack of hydrocarbon concentration memory effects in bottles used for sampling clean air after previously being used for sampling polluted urban air.

Daily calibration was performed by injection through the septum, shown in Figure 1, of 1 cm^3 each of several commercial gas mixtures in the parts per million range (Alltech Associates). The accuracy of these standard mixtures was checked in the laboratory and adjusted where required by a calibration procedure involving dilution of known quantities of the pure gases, liquids, or vapors dispensed, by means of 1 mL or μL syringes or a vacuum line, respectively, into an aluminium static dilution chamber equipped with a small fan [Penkett et al., 1979].

As the project proceeded, it became clear that the integrity of the samples, including those species with carbon numbers above C_5, was very good in that consistent analyses were obtained from independent experiments without any obvious artefacts. It is probable that the use of a Nafion drier, rather than a more conventional drying agent such as potassium carbonate, plays an important part in allowing the quantitative passage, particularly of the aromatic species, through the concentrator system. A previous attempt to measure aromatic hydrocarbons, in which a solid adsorbent drier was used, gave rise to unreproducible data and

values for concentrations which were too low.

The detection limit for a 1000-mL sample was 2 (pptv) for the majority of species measured and less than 10 pptv for all quoted species. The overall accuracy of the analytical system was estimated to be 5%. The experimental conditions employed enabled the measurement of the concentration of 35 different C_2 to C_9 hydrocarbons in samples collected on the UK mainland, including the isomers of alkanes, alkenes, dienes including isoprene, and several aromatic species.

RESULTS

The contrast between the hydrocarbon content of air over the North Atlantic in winter and summer is shown clearly in the two chromatograms displayed in Figure 2. These represent analyses of equivalent quantities of air and the chromatograms are displayed at the same integrator attenuation. The winter concentrations are much larger than the equivalent summer values for all molecules, with the variations being more marked for some than for others. The individual seasonal variation for a number of prominent hydrocarbons is shown in Figures 3*a*, 3*b*, and 3*c*. The data are well spread throughout the year, although aircraft operational requirements meant that none of the data reported here was collected in the months of June, September, and December; most measurements were made in March.

A pronounced seasonal variation is observed for ethane, propane, acetylene, *n*- and *i*-butane, *n*- and *i*-pentane, *n*-hexane, *n*-heptane, benzene, and toluene, with a winter maximum and a summer minimum. Other saturated aliphatic and aromatic hydrocarbons also show the same type of seasonal variation, but the data are not displayed here. In the absence of any December data it is not possible to define the exact time of the maximum, but it is probable that it is after the solar solstice. The ethane and acetylene data appear to confirm this, with maximum values most likely being observed in February and in March, when all the data are taken into account. These two molecules have the largest atmospheric lifetimes and would therefore accentuate any such tendency.

The reproducibility of the amplitude of the seasonal cycle of hydrocarbon concentration in maritime polar air from year to year is good, as can be seen from Figure 4 for acetylene and propane for the years 1987, 1988, and 1989. Earlier data collected between 1982 and 1986 also show a similar amplitude reproducibility, which extends to the molecules ethane, acetylene, propane, *n*-butane and *i*-butane and most probably *n*-pentane and benzene [Lightman et al., 1990]. The winter/summer ethane ratio reported here (Table 2) is also very similar to that reported above the Jungfraujoch [Ehhalt et al., 1991]. The existing data do tend to confirm the previous suggestion that the seasonal cycle of the hydrocarbons extends

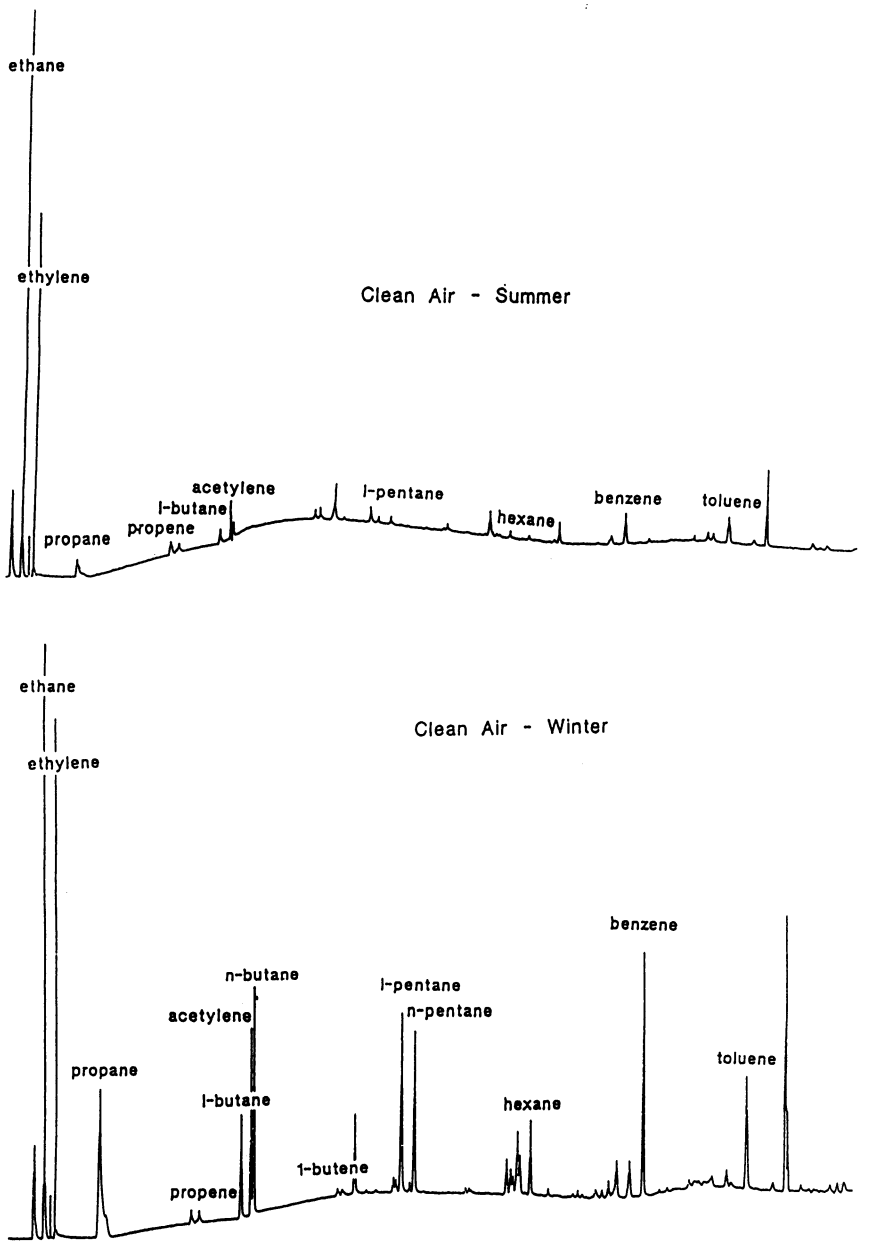

Fig. 2. Contrasting chromatograms (top, summer; bottom, winter) from the analysis of identical quantities of air samples collected over the North Atlantic Ocean.

TABLE 2: Relationship Between Winter and Summer Concentration Ratio and OH Rate Coefficient for Various Hydrocarbons

Hydrocarbon Species	Background Average Winter Maximum pptv	Background Average Summer Minimum pptv	Winter/ Summer Ratio	$k_{(OH)}$* T = 298 K 10^{-11} cm^3 molecule s^{-1}
Ethane	2220	1210	1.8	0.027
Propane	870	85	10.2	0.115
Acetylene	673	126	5.3	0.09
n-Butane	405	25	16.2	0.254
i-Butane	193	47	4.1	0.234
n-Pentane	147	8	18.4	0.394
n-Hexane	65	5	13.0	0.561
Benzene	230	25	9.2	0.123
Toluene	115	10	11.5	0.596

**Atkinson* [1990].

to large parts of the northern hemisphere, at least in the free troposphere north of the polar front. It is difficult to see otherwise how the cycle would be so reproducible.

The average maximum and minimum yearly concentrations obtained from fitting curves through the concentration data with respect to time are shown in Table 2, along with the values for the second order rate constants $k_{(OH)}$ for reaction of the individual hydrocarbons with hydroxyl radicals. There is a positive correlation between the winter/summer ratio and the $k_{(OH)}$ (Figure 5), which strongly suggests that hydroxyl chemistry is responsible for removing most of these hydrocarbons from the atmosphere. This point was made in the previous publication [Lightman et al., 1990] and will be examined in more detail subsequently.

The individual data points in Figures 3a, 3b, and 3c are separated into free tropospheric values and low altitude (~ 150 m above sea level) values. For most hydrocarbons there is only a small increase at lower altitudes, however the difference for *i*-butane is more pronounced, with the lower-level concentrations being up to a factor of 2 greater than those measured simultaneously in the free troposphere. This feature is emphasized when the maximum and minimum concentrations observed for *i*-butane and *n*-butane are examined in Table 2. The seasonal oscillation of i-butane is damped with a winter to summer average ratio of 4.1 compared to a value of 16.2 for n-butane, which has a similar rate for reaction with hydroxyl radicals. Both observations, an enriched boundary layer, and relatively high summer concentrations would be consistent with a significant oceanic source for *i*-butane. In

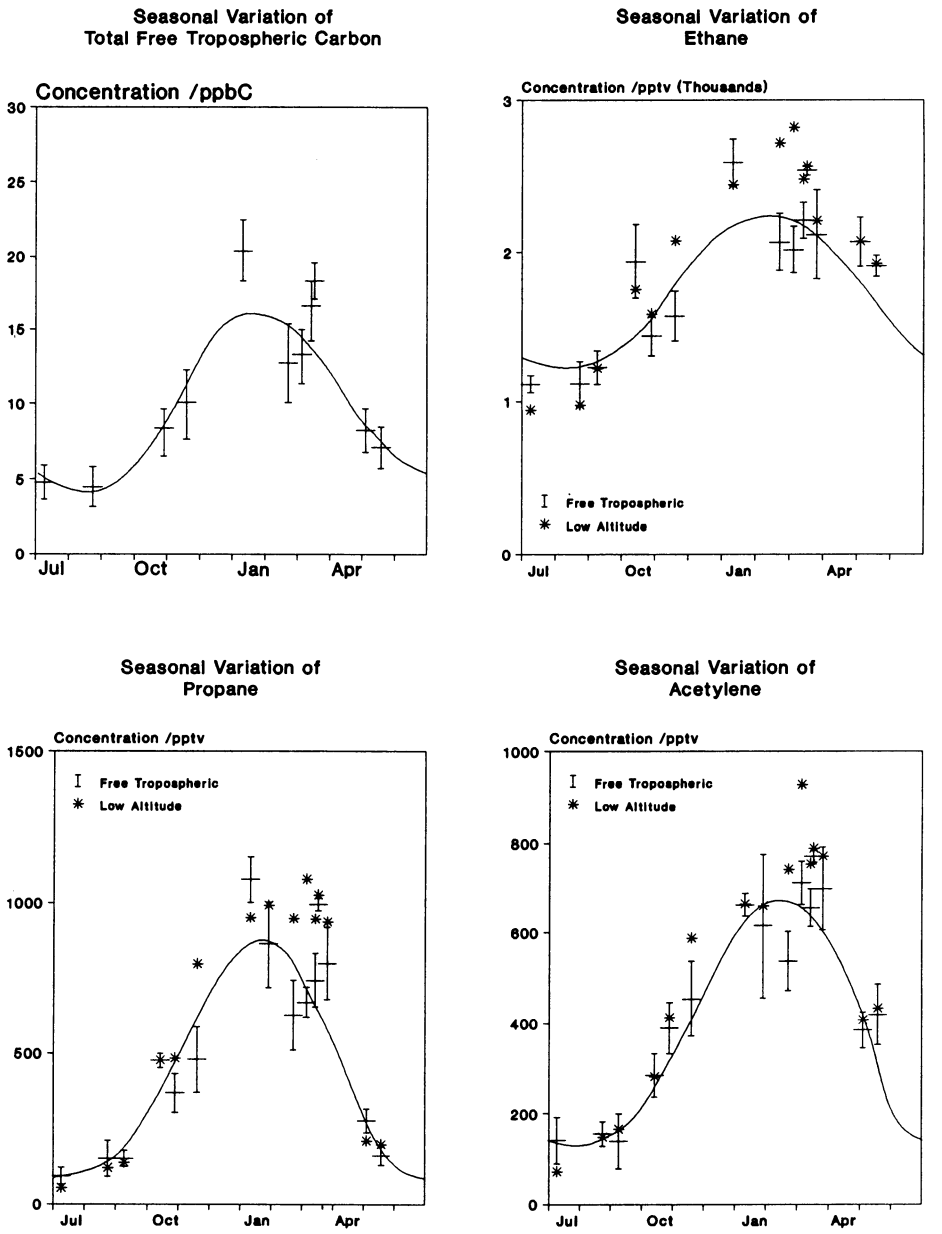

Fig. 3*a*. Seasonal variation of individual hydrocarbons in air collected over the North Atlantic Ocean in both the free troposphere and below 500 ft (152 m): Total free tropospheric carbon, ethane, propane and acetylene.

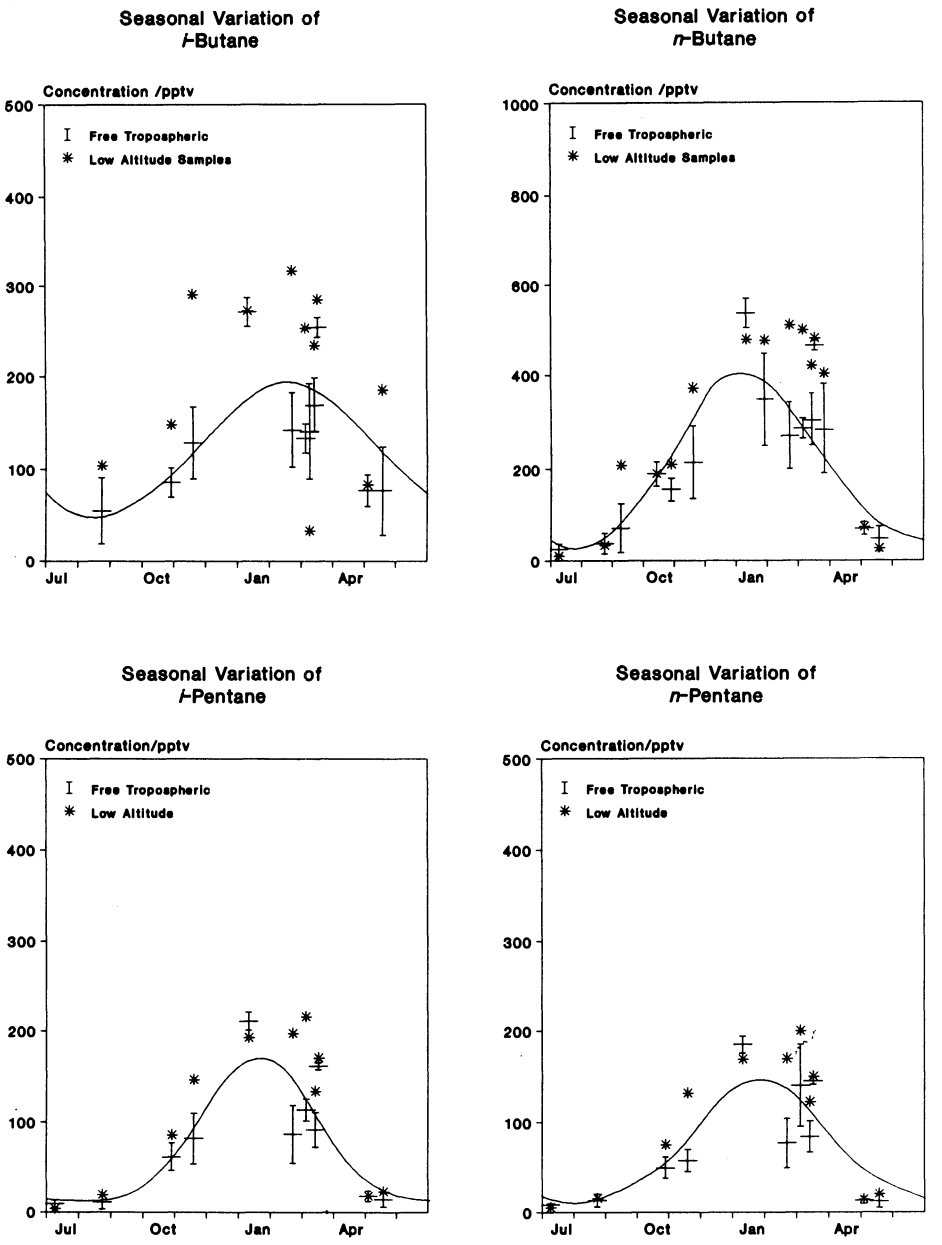

Fig. 3*b*. Seasonal variation of individual hydrocarbons in air collected over the North Atlantic Ocean in both the free troposphere and below 500 ft (152 m): *i*-butane, *n*-butane, *i*-pentane and *n*-pentane.

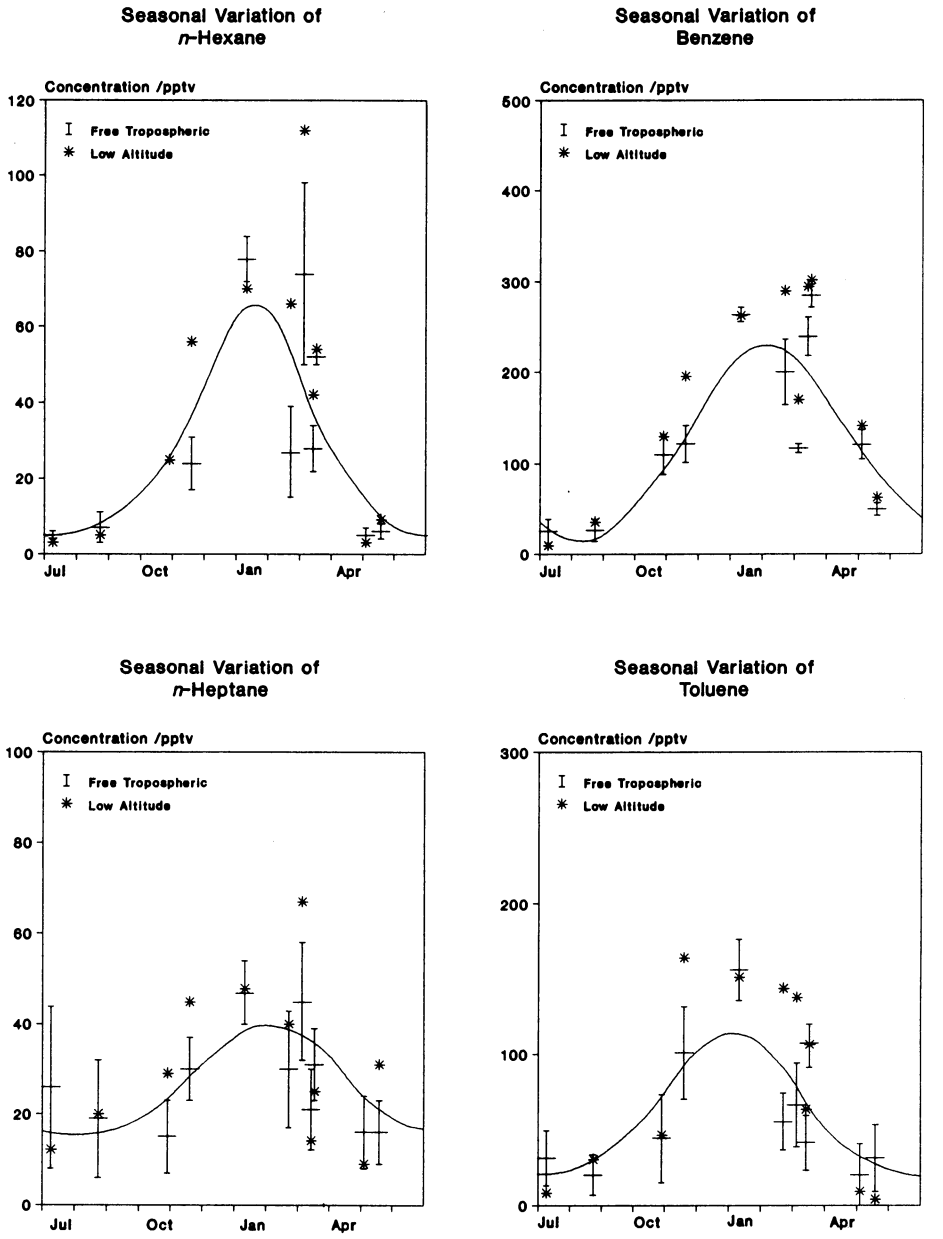

Fig. 3*c*. Seasonal variation of individual hydrocarbons in air collected over the North Atlantic Ocean in both the free troposphere and below 500 ft (152 m): *n*-hexane, benzene, *n*-heptane and toluene.

this respect, higher concentrations of *i*-butane than *n*-butane have been observed in outgassed seawater samples, in contrast to emissions from anthropogenic sources where the normal isomer predominates (see later).

The seasonal variability for the unsaturated aliphatic hydrocarbons is quite different from that observed for the saturated aliphatics and the aromatics. Accepting that the most recent ethylene data are unusable, Figure 6 shows the seasonal variation for propene and 1-pentene from January 1987 through to the winter of 1989. It is very noticeable that the concentrations decline with time and although the autumn values are higher, the seasonal oscillation is small by comparison with the less reactive molecules, propane and acetylene, shown in Figure 4. Part of the reason for these data may be that the sampling containers may act as a source of olefins and that this declines with aging; the data collected after April 1988 could be significant therefore. In this respect the later values shown in Figure 6 are not inconsistent with other published values in the free troposphere [Blake and Rowland, 1986]. Overall, it appears that the average concentrations of olefins in the free troposphere over the Atlantic Ocean are low, and there is very little seasonal variation. This presumably means that higher summer removal rates are compensated by higher emissions from the ocean.

The amplitude of the seasonal variation of the total free tropospheric carbon in the form of non-methane hydrocarbons, determined from the sum of carbon measured in winter and summer samples, is shown in Figure 7. It represents a change in reactive carbon, capable of being oxidized quickly to produce ozone in the free troposphere, of somewhere between 10 and 15 ppbv. This in itself is a substantial fraction of the 20 ppbv increase in ozone observed in measurements between January and May (Figure 8), and it is quite possible that the two observations are related, with oxidation of the non-methane hydrocarbons (and carbon monoxide) in the transition from winter to spring producing substantial amounts of ozone, provided sufficient nitrogen oxides are available. This is not known at present, although several observations have drawn attention to high PAN concentrations in the atmosphere at middle to high latitudes [Singh, 1989] and PAN may act as a source of NO_x [Crutzen, 1979].

The causes of the seasonal oscillation in concentration of hydrocarbons in the free troposphere over the Atlantic Ocean include changes in emission patterns, changes in the extent of chemical processing, and meteorological variability, which can influence the way in which contaminants are transported around the atmosphere. The arguments that follow are based on the assumption that chemical influences dominate, although it is acknowledged that meteorological influences are also relevant (see preceding section).

In a previous publication the seasonal oscillation of ethane and propane were shown to be consistent with removal from the atmosphere by hydroxyl chemistry at rates that were between 4 and 7 times faster in the summer than in the winter. This explanation will also

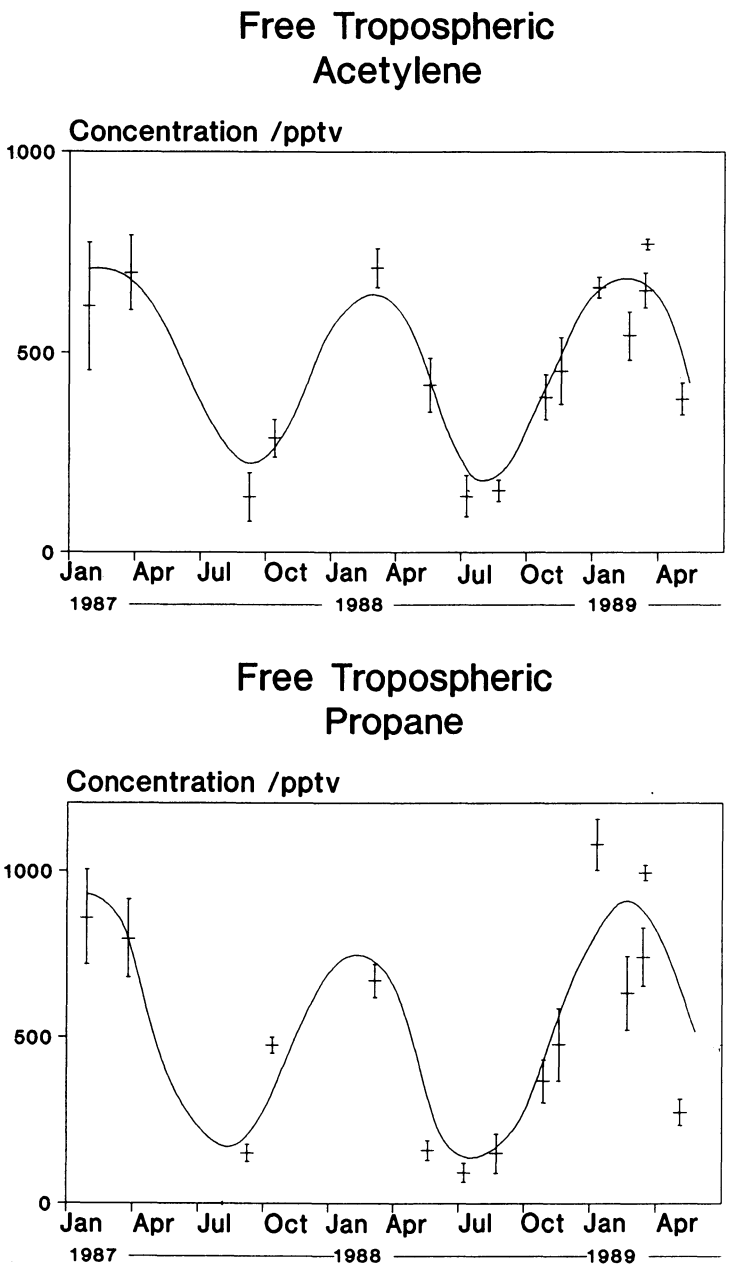

Fig. 4. Seasonal variation (1983, 1988, 1989) for acetylene (top) and propane (bottom) in the free troposphere over the North Atlantic Ocean.

largely account for the behavior of acetylene, *n*-butane, *n*-pentane, and benzene where a quantitative relationship is clearly visible from a plot (Figure 5) of the winter/summer concentration ratio and the $k_{(OH)}$ values from Table 2. This present data thus confirm the overriding importance of hydroxyl radical chemistry as a sink for atmospheric hydrocarbons. Considerable deviations begin to occur though from the universal hydroxyl radical interpretation when the data on the higher aliphatic hydrocarbons and the substituted aromatic hydrocarbons are examined closely.

It is less satisfactory to use the winter/summer ratios for the more reactive molecules because this will depend heavily on the summer values, which in many cases could be affected by contamination problems at the very low concentrations recorded. An alternative approach has therefore been used where ratios of hydrocarbon concentrations in winter over the Atlantic Ocean are compared to the same ratios in plumes spreading from cities such as London. This approach makes the assumption that the mid-latitude free troposphere in winter is in effect a very dilute, well-mixed continental plume which has a homogeneous source in populated areas throughout the northern hemisphere, as was suggested initially in an earlier paper [Lightman et al., 1990]. The assumption of a well-mixed free troposphere in middle to higher northern latitudes is supported by the reproducibility of the amplitude of seasonal variation for many molecules from year to year and by analysis of the hydrocarbon

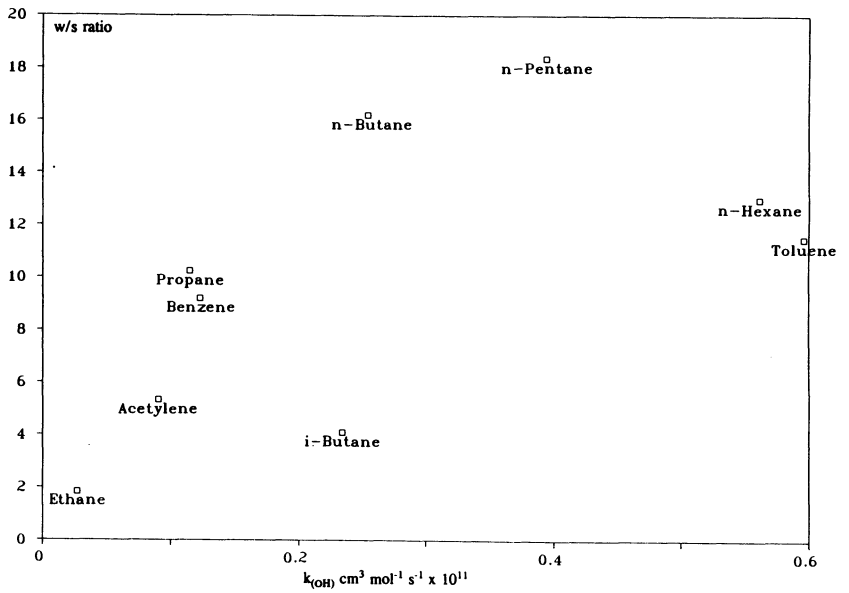

Fig. 5. Clean air winter-to-summer concentration ratios of some hydrocarbons versus their reaction rate coefficient with hydroxyl radicals.

TABLE 3: Hydrocarbon Composition From Various Source Areas

Hydrocarbons	European Cities (Mostly Germany) Range Low ppbv	High ppbv	Urban Background Sydney| ppbv	39 U.S. Cities‡ Median ppbv	London Street§ pptv	London Plume (J111) pptv	Winter Background (J125) pptv	OH Rate* T = 298 K 10^{11} cm^3 molecule s^{-1}
Acetylene	3	16.4	10.1	6.5	531	3131	663	0.09
n-Butane	1.5	12	7.5	10.1	147	2871	536	0.234
i-Butane	0.8	6.6	4.7	3.7	78	1506	271	0.254
Cyclopentane			0.7	0.4	4.5	80	14	0.516
i-Pentane	1.6	9	9	9.1	87	1593	211	0.39
n-Pentane	0.9	5.9	5	4.4	38	654	185	0.394
2,3-Dimethyl-butane			0.9	0.6	16	210	34	0.232
Cyclohexane				0.4	2.3	49	23	0.749
i-Hexane			4.2	4.3	55	784	110	0.565
n-Hexane+2-Ethylbutene			2.1	1.8	19	257	78	0.561
n-Heptane				0.7	8.3	140	47	0.715
i-Octane¶				0.9	14	178	9	0.368
n-Octane			0.4	0.3	4.1	67	19	0.868
n-Nonane			0.4	0.2	1.9	111	20	1.02
n-Decane			0.5	0.3	7.9	259	<10	1.16
Propyne					8.7	NA	10	0.59
Ethane	3	17.9	7.5	11.7	26	1761	2591	0.0268
Propane	2	10.7	5.9	7.8	15	737	1079	0.115
Ethene	3.2	15.2	12.5	10.7	217	3920		0.852
Propene	0.5	8	7.4	2.6	54	482	24	2.63
trans-2-Butene			1.1	0.6	9	58	10	6.4
1-Butene	0.6	2.1	1	0	10	113	10	3.14
iso+1-Butene			2.4	1.5	19	NA	<2	5.14
cis-2-Butene	0.1		1	0	7.1	47	1	5.64
1,3-Butadiene					12	68	<2	6.66
3-Methyl-butene					3.2	23	<2	3.51
1-Pentene			0.4		3.4	52	5	3.19
2-Methyl-butene			0.5	0.5	6	58	1	6.1
trans-2-Pentene			0.7	0.7	3.3	22	<2	6.5
Isoprene					5.1	55	1	10.1
1-Hexene					2	70	4	3.7
Benzene	1.1	28.7	2.6	2.1	64	558	263	0.123
Toluene	1.9	24.1	8.9	4.8	114	2476	156	0.596
Ethylbenzene	0.2	10.6	1.3	1	21	238	40	0.71
m+*p*-Xylene	0.4	20.7	3.9	2.3	68	615	46	1.95
o-Xylene			1.5	0.9	25	222	18	1.37
1,3,5-Trimethyl-benzene			0.5	0.3	6.1	32	<10	5.75
1,2,4-Trimethyl-benzene			1.3	1.2	12	145	<10	3.25

NA, not available.
**Atkinson* [1990].
†*Bouscaren et al.* [1987].
‡*Selia et al.* [1989].
§N.J. Blake, personal communication.
|*Nelson et al.* [1983].
¶2,2,4-Trimethylpentane.

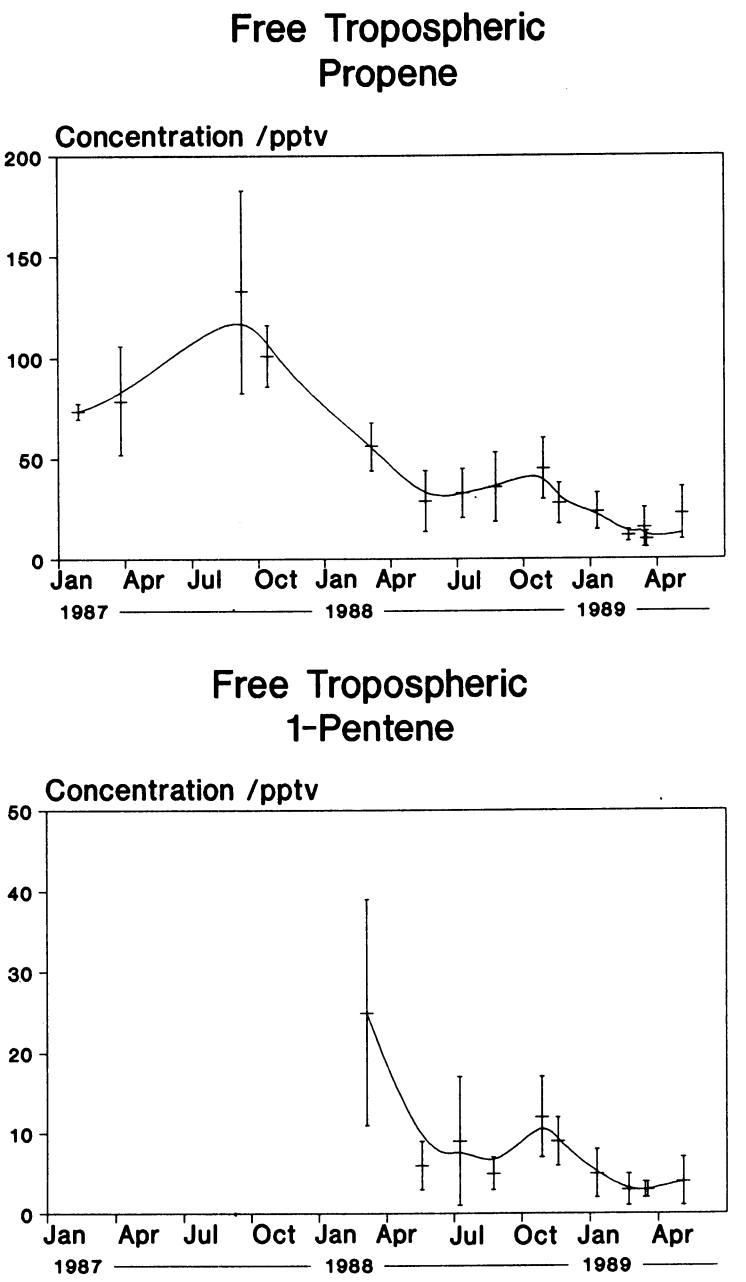

Fig. 6. Seasonal variation (1983, 1988, 1989) for propene (top) and 1-pentene (bottom) in the free troposphere over the North Atlantic Ocean.

composition of the free troposphere in combination with trajectory analyses for flights J124 and J125 made earlier in this paper. Also close examination of hydrocarbon emissions from different source areas does show some differences but these are outweighed by the similarities (see Table 3).

The use of hydrocarbon ratios to study chemical reactions in the atmosphere was applied in another aspect of studies of atmospheric hydrocarbons to a plume spreading from London in summer which was intercepted in two planes downwind (flights J111 and J112), separated by a travel time of several hours [Blake et al., 1993]. The ratio (R) of hydrocarbon concentration between the flights represented either dilution, in the case of the slower reacting molecules, or dilution plus reaction, in the case of the faster reacting molecules. The average ratio for acetylene, benzene, and many of the less reactive paraffins in the London plume was about 0.65, due mostly to dilution. With the exception of ethylene all the olefins had R values of less than 0.35 and for the aromatics (excepting benzene), R was less than 0.5, due to dilution and chemical removal.

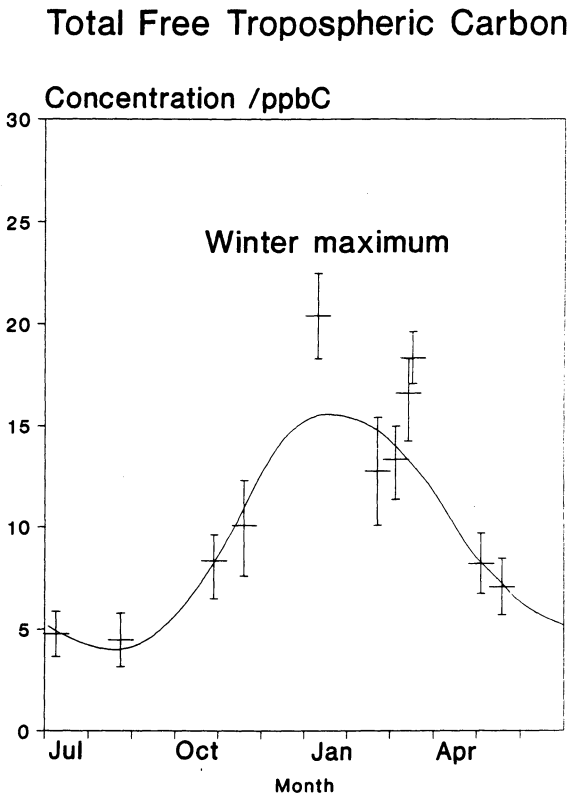

Fig. 7. Seasonal variation in the availability of reactive carbon in non-methane hydrocarbons over the North Atlantic Ocean.

In the present context, analytical data from flight J125, a background free tropospheric flight made in January 1989 (at the maximum of the seasonal cycle), was compared in a similar manner with the data from two flights which intercepted urban plumes close to London in July 1988 (J111) and in May 1989 (J137). R values were calculated and differences between indivi-dual molecules should reflect variations in chemical reactivity and/or source variability. In this respect, plume flights have been made throughout the year and little or no evidence for a change in hydrocarbon distribution was found. It is legitimate therefore to compare summer urban emission with winter background hydrocarbon distribution.

Table 4 shows the values of R for J125/J111. Most of the values are lower than for J112/J111 ($\sim$0.65) indicating that more extensive dilution and/or reaction had taken place. Even so, R for many molecules lay between 0.2 and 0.3, which must mean that the air over the Atlantic in midwinter is highly polluted. Of considerable interest in this respect is that the R values for ethane and propane are greater than unity, 1.47 and 1.40, respectively. Since it is most unlikely that these two molecules have large natural sources, especially in winter, the data are probably best explained in terms of the extensive nature and strength of sources of natural gas released around the northern hemisphere. This has consequences when considering the relative contribution of fossil sources to the growth of atmospheric methane.

The use of R values in this analysis of the winter background hydrocarbon concentration over the North Atlantic clearly has imperfections, for example, R for acetylene is smaller than R for the long-chain paraffins (*n*-pentane, etc.) even though it is much less reactive. The reason may be associated with the dominance of certain source areas which do not give rise to the homogeneous atmosphere assumed at the outset. However, this does not invalidate the analysis in most respects. Of particular interest the R values for the normal and iso isomers for the paraffins are not subject to dominance of source area (see later) but systematically R for the iso isomer is lower than that for the normal isomer. Thus for the pentanes, $R_i = 0.13$, $R_n = 0.28$; for the hexanes, $R_i = 0.14$, $R_n = 0.30$; and for the octanes, $R_i = 0.05$, $R_n = 0.28$. There are also indications of low R values for aromatic molecules, compared to aliphatic molecules with similar hydroxyl rate coefficient, that is, for toluene, R = 0.06, whereas for *n*-hexane, R = 0.30. The general picture obtained from a comparison of J125 with J111 is also shown from the comparison of J125 with J137. The ethane and propane concentrations are much higher over the Atlantic than could possibly be sustained from urban emissions of the composition shown in J111 or J137. The normal isomers are enriched with respect to the iso isomers, and toluene and ethyl benzene are preferentially removed with respect to the normal paraffins with similar hydroxyl rate coefficients.

TABLE 4: Comparison of Hydrocarbon Composition in Clean Air in Winter and in Urban Plumes

Hydrocarbon	Winter Background (J125) pptv	Urban Plume (J111) pptv	Urban Plume J137 pptv	R J125/ J111	R J125/ J137	OH rate* T = 298 K 10^{-11} cm^3 molecule s^{-1}
Acetylene	663	3131	5331	0.21	0.12	0.09
n-Butane	536	2871	7334	0.19	0.07	0.234
i-Butane	271	1506	4141	0.18	0.07	0.254
Neopentane	3	8		0.32		0.085
Cyclopentane	14	80	162	0.18	0.09	0.516
i-Pentane	211	1593	3792	0.13	0.06	0.39
n-Pentane	185	654	1307	0.28	0.14	0.394
Neohexane	34	210	436	0.16	0.08	0.232
Cyclohexane	23	49	62	0.47	0.38	0.749
iso-Hexane	110	784	1637	0.14	0.07	0.565
n-Hexane	78	257	502	0.30	0.16	0.561
n-Heptane	47	140	241	0.33	0.19	0.715
i-Octane	9	178	408	0.05	0.02	0.368
n-Octane	19	67	85	0.28	0.22	0.868
n-Nonane	20	111	116	0.18	0.17	1.02
Ethane	2591	1761	4172	1.47	0.62	0.0268
Propane	1079	737	1041	1.46	1.04	0.115
Benzene	263	558	2424	0.47	0.11	0.123
Toluene	156	2476	5003	0.06	0.03	0.596
Ethylbenzene	40	238	770	0.17	0.05	0.71
m+*p*-Xylene	46	615	2034	0.07	0.02	1.95
o-Xylene	18	222	888	0.08	0.02	1.37
Mesitylene	<10	32				5.75
1,2,4 Trimethyl-benzene	<10	145				3.25
Total Carbon, pbC	23	98				

**Atkinson* [1990]

One explanation of these differing R values for normal and iso isomers of the alkanes is that the source characteristics differ greatly from region to region and that the source of the hydrocarbons sampled over the Atlantic Ocean has a different distribution to that measured in London, UK. The data assembled in Table 3, however, for hydrocarbons measured in the United States, Germany, Australia, and the United Kingdom show remarkable similarities with regard to the distribution at point of emission of many hydrocarbons. The iso to normal ratio is certainly maintained, so this will not explain the different R values in Table 4. There are differences between the distinct source regions, the main one being the low abundance of acetylene and the possibly higher concentration of ethane and propane in the United States. The former may be associated with the greater use of catalytic converters in car exhausts in the United States.

Another explanation of the differing isomer ratios is that some hydrocarbons are removed more rapidly from the atmosphere than their rate of reaction with hydroxyl radicals would suggest. This would require the presence of other oxidants which specifically react faster with branched-chain hydrocarbons. This would seem to rule out chlorine atoms, which have been recently suggested by two groups [Singh and Kasting, 1988; Finlayson-Pitts et al., 1989] to play a role in tropospheric oxidation processes, since oxidation of the branched-chain paraffins is, if anything, slower than the equivalent straight-chain molecule [Atkinson and Aschmann, 1985; Wallington et al., 1988]. Oxidants which do show a significant difference in the oxidation rates of straight-chain and branched-chain alkanes are oxygen atoms and the nitrate radical (NO_3). It is most unlikely that oxygen atoms are present in sufficient abundance to oxidize even small amounts of the hydrocarbons, but it is not impossible that NO_3 radicals play a role in the wintertime removal of hydrocarbons from the atmosphere.

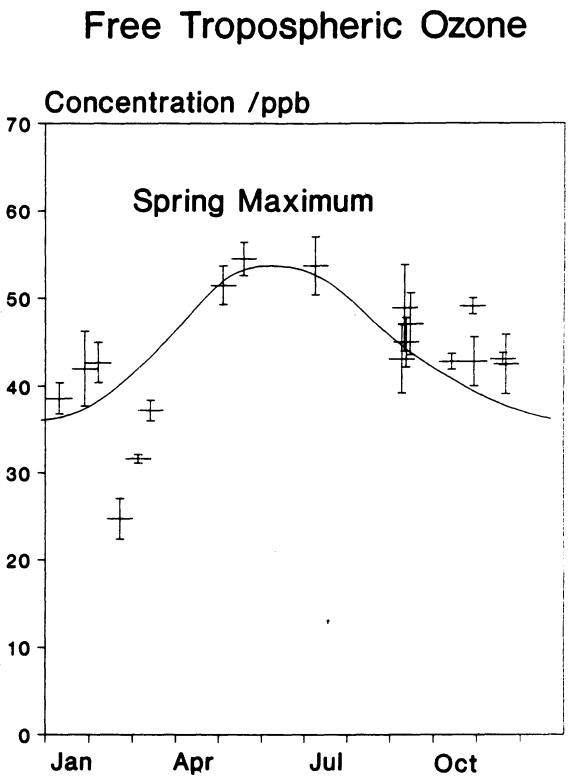

Fig. 8. Seasonal variation of free tropospheric ozone over the North Atlantic Ocean.

Rate constants for reactions of NO_3 radicals with many hydrocarbons and other molecules have recently been published [Wayne et al.,1991; Atkinson, 1991]. Table 5 shows a small summary of rate coefficients for NO_3 and OH with various hydrocarbons at 298 K. The data show that NO_3 does react preferentially with branched-chain alkanes and that the rate increases with increased branching. This is very much in line with the data in Table 4 where the isooctane (2,2,4-trimethyl pentane) is removed from the atmosphere much faster than normal octane, and the difference between the octanes is more marked than between the pentanes or the hexanes.

Removal by NO_3 radicals will not account for the aromatic data though in Table 3, since the ratio $k_{(OH)}/k_{(NO3)}$ for toluene is greater than $k_{(OH)}/k_{(NO3)}$ for *n*-hexane. Molecules which could be removed efficiently by NO_3 radicals are the alkenes, but since their concentrations are low and the concentration data is much less reliable than that for the alkanes and the aromatics, it is difficult to comment further.

The ratio $k_{(OH)}/k_{(NO3)}$ in Table 5 shows clearly the points made above with olefins being the most likely hydrocarbon to be removed efficiently by NO_3, followed by branched-chain alkanes and acetylene. Aromatics are least favored to be removed by NO_3. The ratio also indicates the increased molecular abundance of NO_3 over OH in the atmosphere needed

TABLE 5: Rate Coefficients for Reaction of Hydrocarbons with Hydroxyl and Nitrate Radicals

Hydrocarbon	$k_{(OH)}$ cm^3 $molecule^{-1}$ s^{-1}	$k_{(NO3)}$ cm^3 $molecule^{-1}$ s^{-1}	$k_{(OH)}/k_{(NO3)}$
n-Butane	2.54×10^{-12}	5.50×10^{-17}	4.60×10^{4}
i-Butane	2.34×10^{-12}	1.00×10^{-16}	2.34×10^{4}
n-Pentane	3.94×10^{-12}	8.00×10^{-17}	4.90×10^{4}
i-Pentane	3.90×10^{-12}	1.60×10^{-16}	2.40×10^{4}
n-Hexane	5.61×10^{-12}	1.05×10^{-16}	5.30×10^{4}
2,3-Dimethylbutane	6.20×10^{-12}	4.06×10^{-16}	1.52×10^{4}
Toluene	5.90×10^{-12}	6.90×10^{-17}	8.60×10^{4}
o-Xylene	1.37×10^{-11}	3.70×10^{-16}	3.70×10^{4}
Acetylene	8.20×10^{-13}	5.10×10^{-17}	1.60×10^{4}
Propene	2.56×10^{-11}	9.45×10^{-15}	2.70×10^{3}
1-Butene	3.14×10^{-11}	1.25×10^{-14}	2.50×10^{3}
cis-2-Butene	5.64×10^{-11}	3.60×10^{-13}	1.57×10^{2}

Source: *Wayne et al.* [1991]

for the NO_3 reaction to play a significant role in hydrocarbon removal. If the average winter OH concentration at higher latitudes is 1 x 10^5 molecules cm^{-3}, then an NO_3 concentration of about 4 x 10^9 molecules cm^{-3} is required for equal oxidation by both oxidants in the most favorable cases.

Measurements of NO_3 made in background air at the Jungfraujoch Observatory show maximum concentrations in the range 10^8 cm^{-3} [Wayne et al., 1991]. Measurements made at lower altitudes though show much higher values. For instance, 300 pptv ($\sim$ 8 x 10^9 cm^{-3}) was observed in a very polluted air mass in Riverside, California [Platt et al., 1980; Atkinson et al., 1986] and up to 2 x 10^9 cm^{-3} has been observed in Colorado at Fritz Peak Observatory in the presence of 0.7 ppbv NO_2 [Wayne et al., 1991]. An extensive survey [Atkinson, 1991] of NO_3 measurements has been made and he estimates a 12-hour average concentration of 5 x 10^8 molecules cm^{-3} (20 pptv) over continents.

It is not out of the question therefore that NO_3 chemistry can account for some of the deviation from that expected from a purely OH chemistry scenario indicated by Table 2 and Figure 5. The differences between iso and normal concentrations may be explained and possibly the low abundance of acetylene. Using Atkinson's average NO_3 concentration [Atkinson, 1991], the lifetime of dimethyl butane would be in the region of 114 days whereas that for *n*-hexane would be close to 500 days. A differential loss of the branched-chain molecule would therefore be expected to occur over the winter months, in agreement with the measurements. The NO_3 explanation will not account for the low abundance of aromatics relative to molecules such as hexane. However, rapid removal of aromatics (greater than would expected by OH) has also been observed in studies of plumes spreading from London [Blake et al., 1993]. No explanation is presented at this time but strongly suspect that it is not an experimental artefact.

REFERENCES

Atkinson, R., and S.M. Aschmann, Kinetics of the gas phase reactions of chlorine atoms with a series of organics at 296 ± 2 K and atmospheric pressure, *Int. J. Chem. Kinet., 17*, 33-41, 1985.

Atkinson, R., A.M. Winer, and J.N. Pitts, Jr., Estimation of night-time N_2O_5 concentrations from ambient NO_2 and NO_3 radical concentrations and the role of N_2O_5 in night-time chemistry, *Atmos. Environ., 20*, 331-339, 1986.

Atkinson, R., Gas-phase tropospheric chemistry of organic compounds: A review, *Atmos. Environ., 24*(A), 1-44, 1990.

Atkinson, R., Kinetics and mechanisms of the gas-phase reactions of the NO_3 radical with organic compounds, *Phys. Chem. Ref. Data, 20*, 459-507, 1991.

Blake, D.R., and F.S. Rowland, Global atmospheric concentrations and source strength of ethane, *Nature, 321*, 231-233, 1986.

Blake, N.J., S.A. Penkett, K.C. Clemitshaw, P. Anwyl, P. Lightman, A.R.W. Marsh, and G.

Butcher, Estimates of atmospheric hydroxyl radical concentrations from the observed decay of many reactive hydrocarbons in well-defined urban plumes, *J. Geophys. Res.*, in the press, 1993.

Bonsang, B., and G. Lambert, Non-methane hydrocarbons in an oceanic atmosphere, *J. Atmos. Chem.*, *2*, 257-271, 1985.

Bouscaren, R., R. Frank, and C. Veldt, Hydrocarbons: Identification of air quality problems in member states of the European communities, *Rep. EUR10646*, Commission of the European Communities, Luxembourg, 1987.

Crutzen, P.J., The Role of NO and NO_2 in the chemistry of the troposphere and the stratosphere, *Annu. Rev. Earth Planet. Sci.*, *7*, 443-372, 1979.

Ehhalt, D.H., U. Schmidt, R. Zander, P. Demoulin, and C.P. Rinsland, Seasonal cycle and secular trend of the total and tropospheric column abundance of ethane above the Jungfraujoch, *J. Geophys. Res.*, *96*, 4985-4994, 1991.

Finlayson-Pitts, B.J., M.J. Ezell, and J.N. Pitts, Jr., Formation of chemically active chlorine compounds by reactions of atmospheric NaCl particles with gaseous N_2O_5 and $ClONO_2$, *Nature*, *337*, 241-244, 1989.

Haagen-Smit, J.A., Chemistry and physiology of Los Angeles smog, *Ind. Eng. Chem.*, *44*, 1342-1346, 1952.

Lightman, P., A.S. Kallend, A.R.W. Marsh, B.M.R. Jones, and S.A. Penkett, Seasonal variation of hydrocarbons in the free troposphere at mid-latitudes, *Tellus 42*(B), 408-422, 1990.

Liu, S.C., M. Trainer, F.C. Fehsenfeld, D.D. Parish, E.J. Williams, D.W. Fahey, G. Hüber, and P.C. Murphy, Ozone production in the rural troposphere and the implications for regional and global ozone distributions, *J. Geophys. Res.*, *92*, 4191-4207, 1987.

Nelson, P.F., S.M. Quigley, and M.Y. Smith, Sources of atmospheric hydrocarbons in Sydney: A quantitative determination using a source reconciliation technique, *Atmos. Environ.*, *17*, 439-449, 1983.

Penkett, S.A., Implications of Arctic Air Pollution, *Nature (News and Views)*, **311**: (5984) 299 (1984).

Penkett, S.A., Indications and causes of ozone increase in the troposphere, in *The Changing Atmosphere*, edited by F.S. Rowland and I.S.A. Isaksen, pp. 91-103, John Wiley, New York, 1988.

Penkett, S.A., Changing Ozone: Evidence for a perturbed atmosphere, *Environ. Sci. Technol.*, *25*, 630-635, 1991.

Penkett, S.A., K.A. Brice, R.G. Derwent, and A.E.J. Eggleton, Measurement of CCl_3F and CCl_4 at Harwell over the period January 1975 - November 1977, *Atmos. Environ.*, *13*, 1011, 1979.

Penkett, S.A., N.J. Blake, P. Lightman, A.R.W. Marsh, P. Anwyl, and G. Butcher, The Seasonal Variation of Nonmethane Hydrocarbons in the Free Troposphere over the North Atlantic Ocean: Possible Evidence for Extensive Reaction of Hydrocarbons with the Nitrate Radical, J. Geophys. Res., in the press, 1993.

Platt, U., D. Perner, A.M. Winer, G.W. Harris, and J.N. Pitts, Jr., Detection of NO_3 in the polluted troposphere by differential optical absorption, *Geophys. Res. Lett.*, *7*, 89-92, 1980.

Rasmussen, R.A., and M.A.K. Khalil, Latitudinal distributions of trace gases in and above the boundary layer, *Chemosphere*, *11*, 227-235, 1982.

Rudolph, J., and D.H. Ehhalt, Measurements of C_2-C_5 hydrocarbons over the North Atlantic, *J. Geophys. Res.*, *86*, 11,959-11,964, 1981.

Seila, R., W. Lonneman, and S. Meeks, Determination of C_2 to C_{12} ambient air hydrocar-

bons in 39 U.S. cities from 1984 through 1986, *Off. Res. Dev. Rep./600/S3-89/058, U.S. Environ. Prot. Agency,* Research Triangle Park, North Carolina, 1989.

Singh H.B., PAN and precursor relationships in the free troposphere: Some results from the mid latitudes, tropics and the Arctic, paper presented at the International Conference on the Generation of Oxidants on Regional and Global Scales, University of East Anglia, Norwich, England, 1989.

Singh, H.B., and J.F. Kasting, Chlorine-hydrocarbon photochemistry in the marine troposphere and lower stratosphere, *J. Atmos. Chem., 7*, 261-285, 1988.

Singh, H.B., and J. Salas, Measurement of selected light hydrocarbons over the Pacific Ocean: Latitudinal and seasonal variations, *Geophys. Res. Lett., 9*, 842-845, 1982.

Wallington, T.J., L.N. Skewes, W.O Siegel, C.-H. Wu, and S.M. Japar, Gas phase reactions of Cl atoms with a series of oxygenated organic species at 295K, *Int. J. Chem. Kinet., 20*, 867-875, 1988.

Wayne R.P., et al., The nitrate radical: physics, chemistry and the atmosphere, *Atmos. Environ., 25*(A), 1-203, 1991.

CARBON MONOXIDE AND LIGHT ALKANES AS TROPOSPHERIC TRACERS OF ANTHROPOGENIC OZONE

David D. Parrish
NOAA Aeronomy Laboratory
325 Broadway
Boulder CO 80303

INTRODUCTION

Transport of pollutants from populated and industrialized continental areas affects the chemistry and radiation balance of the global troposphere [Duce et al., 1991]. A pollutant of particular interest is ozone (O_3), since its photolysis initiates the oxidizing processes in the atmosphere [Logan et al., 1981], and it is an important greenhouse gas, whose atmospheric trends are only poorly known [Watson et al., 1990]. Thus, the transport of ozone and its precursors from source regions affects the oxidizing capacity of the troposphere in the receptor areas and is important in climate change.

The anthropogenic source of tropospheric ozone is photochemical production from precursors - oxides of nitrogen and non-methane hydrocarbons (NMHCs) - that are emitted from a wide variety of anthropogenic sources [Logan et al., 1981]. These sources are predominately located in the continental boundary layer. The product ozone and unreacted precursors are transported from the continental boundary layer to the rest of the troposphere, where additional ozone is produced from the remaining precursors.

The predominant natural source of tropospheric ozone is injection from the stratosphere, where approximately 90% of the ozone in the atmosphere exists [Fehsenfeld and Liu, 1992]. This transport occurs throughout the globe. Therefore, an important question is whether the anthropogenic or the natural source dominates in regions well removed from the emission sources of the anthropogenic ozone precursors. One approach to answering this question is the identification and measurement of species that can act as tracers for the ozone produced from the anthropogenic sources.

For a species to be a suitable tracer it must be emitted from the same sources, or at least in the same region, as the ozone precursors, and it must be removed by processes at least roughly parallel to the removal processes for ozone, which are photochemically driven in the free troposphere and marine boundary layer. Generally, it also should have a lifetime in the troposphere of about the same order as ozone, approximately one month in summer in the free troposphere. Two example tracers that meet these criteria are carbon monoxide (CO) and the more slowly reacting NMHCs. CO has previously been used in this manner [Fishman

NATO ASI Series, Vol. I 7
The Tropospheric Chemistry of Ozone in the Polar Regions
Edited by H. Niki and K. H. Becker

and Seiler, 1983]. Described here are two studies; each demonstrates the use of one of these example tracers.

The heavily polluted eastern coast of North America is a particularly large source of ozone and ozone precursors that can be transported to the troposphere over the temperate North Atlantic Ocean [Pszenny et al., 1990]. Ozone and CO were measured during the summer of 1991 at three sites on the Atlantic coast of Canada. Measurements have continued for a full year at one of the sites. CO is an anthropogenic pollutant that is relatively unreactive (lifetime about one month in summer), and is utilized in this near-source region as an essentially inert tracer. The measured relationships between the concentrations of ozone and CO in the air advected over the North Atlantic, coupled with the inventoried emissions of CO in eastern North America, provide the basis to estimate the amount of ozone exported from North America in the summer, and give some indication of the processes that affect ozone in the winter.

The Asian continent is a potential source for similar transport to the North Pacific Ocean [Whepdale and Moody, 1990]. Measurements of ozone, peroxyacetyl nitrate (PAN), the C_2-C_4 alkanes, as well as other trace species, were made during a ten day period in April and May, 1985 at Point Arena on the Pacific Coast in northern California. Thus, this study was located across the Pacific Ocean from the source regions. The alkanes are also predominately from anthropogenic sources, but are more reactive than CO. They have variable lifetimes and the evolution of their ratios provides an effective "clock" for the photochemical removal processes that occur in the air masses as they are transported across the ocean. The correlation of the concentrations of ozone and PAN with the alkane ratios indicate that the observed ozone and PAN largely originated from continental sources, with removal processes dominating in the Pacific marine region. Some information regarding the effective lifetimes of ozone and PAN in this marine region is obtained.

MEASUREMENTS

Figure 1 shows the relationship of the land areas bounding the northern North Atlantic Ocean and the location of the three Canadian coastal sites. During the summertime the atmospheric circulation in this region is dominated by the Bermuda High, with northeasterly transport along the Atlantic seaboard. The sites thus are spaced at approximately 500 km intervals down-wind from the northeastern urban corridor of the U.S. and span approximately one-third of the distance from Boston to Ireland. Instruments to measure ozone and CO were placed in Canadian Coast Guard lighthouses on Seal Island, Nova Scotia (approximately 32 km east of Cape Sable - the southern tip of Nova Scotia) and at Cape Race, Newfoundland, and in a Canadian Atmospheric Environment Service weather

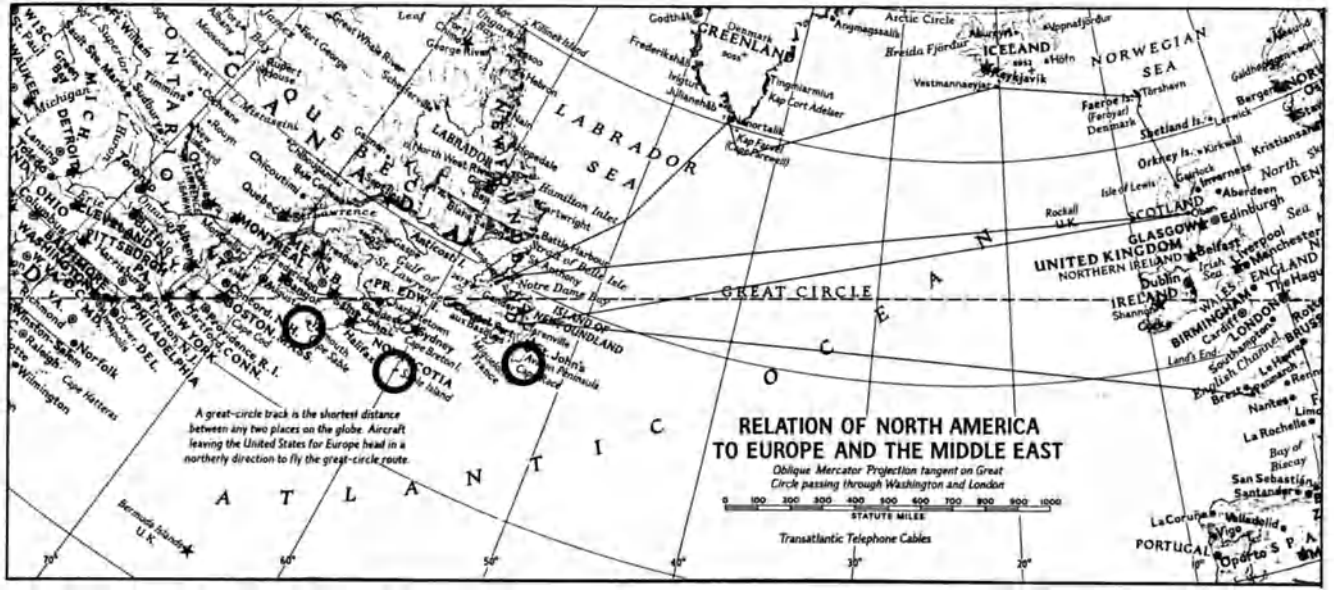

Fig. 1. Relation of the North Atlantic and surrounding continents shown on a map projected on the great circle passing through Washington D.C. and London. The three circles indicate the measurement sites: Seal Island, Sable Island and Cape Race at progressively eastward and further downwind from the Northeastern U.S. urban corridor. The map is a portion taken from a larger map [Grosvenor, 1963).

station on Sable Island, Nova Scotia. Measurements were made at all three sites from mid-July to mid-September, 1991, and continue to the present at Sable Island. Five minute average ozone and CO concentrations were calculated, and periods that evidenced contamination by local sources were discarded. The measurements and treatment of the data are described more fully by Parrish et al. [1992a].

Measurements in Pacific air masses were made on the Northern California coast, approximately 180 km northwest of San Francisco at Point Arena from April 24 to May 5, 1985. This season of the year is typically a period of onshore movement of maritime air masses. The C_2-C_4 alkanes were measured at the site by direct injection into a gas

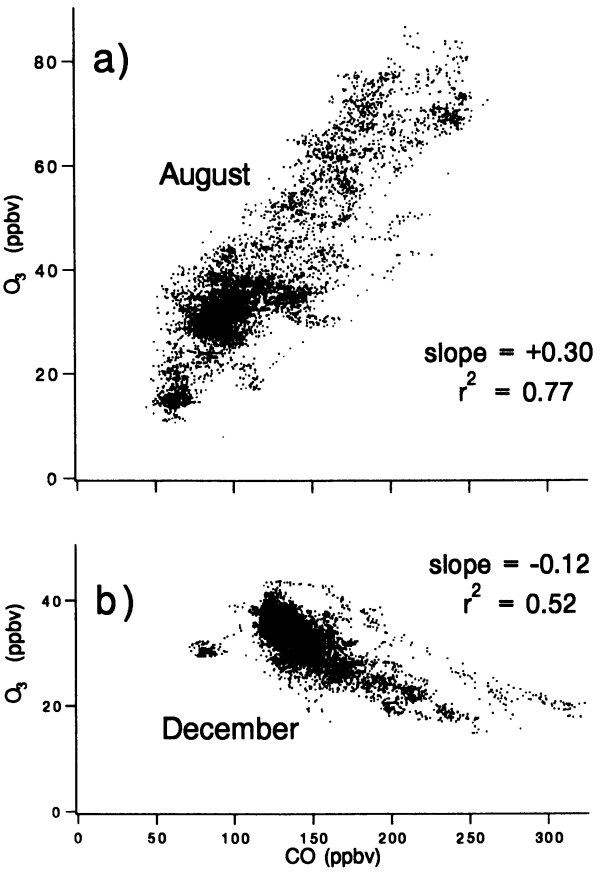

Fig. 2. Relation between ozone and CO at Sable Island in a) August and b) December. Each point indicates a five minute average. For each month, the slope from a linear, least-squares fit and the square of the linear correlation coefficient are given.

chromatograph [Singh et al., 1988]. The ozone and PAN measurement techniques and the selection of data characteristic of the Pacific marine environment are detailed by Parrish et al. [1992b].

RELATIONSHIPS OF OZONE AND CO IN THE NORTH ATLANTIC

At each of the three sites the summertime data were characterized by generally constant, low levels of ozone and CO interrupted frequently by episodes of correlated, elevated levels of both species. Figure 2a presents the resulting correlation between the five minute average ozone and CO levels for Sable Island in August. A strong, positive correlation is evident as demonstrated by the large linear correlation coefficient, which indicates that more than three-quarters of the variance in the measured ozone can be captured by a linear relationship between ozone and CO.

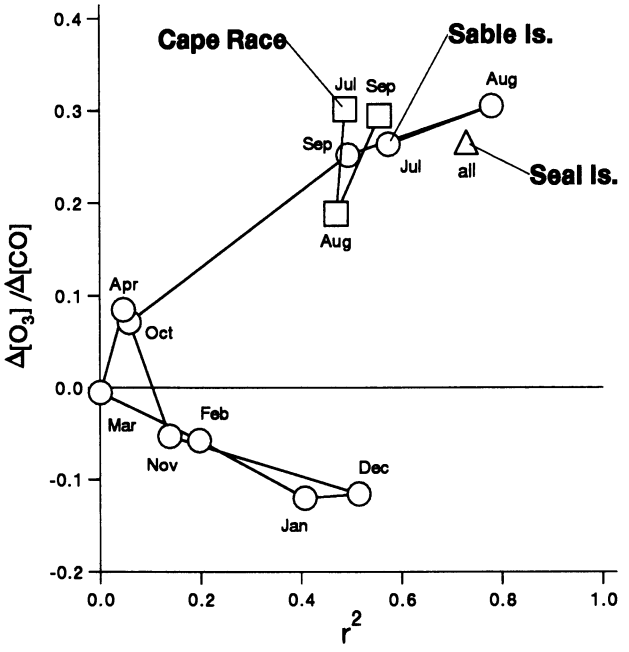

Fig. 3. Summary of the linear regression analyses of the monthly data sets. The abscissa gives the square of the linear correlation coefficient, and the ordinate gives the derived slope. The different symbols indicate the different sites, and the months are labeled. The data from the three months at Seal Island were combined in one analysis, since the time coverage was relatively poor at this site.

In the winter at Sable Island, the data again exhibited generally constant, low levels of ozone and CO interrupted by frequent episodes. However, these episodes were characterized by high CO levels and even lower ozone levels, which result in significant negative correlation between ozone and CO. Figure 2b presents the December data. For this month more than half of the variance in the measured ozone can be captured by a linear relationship.

Figure 3 summarizes the monthly linear correlations for the full data sets from the three sites. Strong positive correlations were found at all three sites for the summer months. At Sable Island the correlation disappeared as fall progressed, and a negative correlation developed in the winter. This negative correlation in turn disappeared as spring progressed, to be followed, presumably, by the reappearance of the positive correlation.

The variance in the data sets beyond that captured by the linear relationship seems to arise from several sources (in addition to experimental imprecision.) Examination of the details of the episodes of elevated summertime levels indicates that the ozone to CO ratio varied between episodes, probably due to differences in the intensity of the photochemical processes that occurred in the respective air masses. This variability is responsible for much of the spread and the apparent structure of the distribution of data points about the average slope in Figure 2a.

Several other factors also influenced the relation of ozone to CO. Injection of ozone from the stratosphere would be indicated by episodes of elevated ozone with low CO. Only one moderate episode was obvious. This was at Cape Race, when ozone varied between 40 and 60 ppbv (parts-per-billion by volume) with CO nearly constant at about 100 ppbv. However, this one example accounts for very little of the variance of that data set.

Another interesting event began on August 18, 1991. In advance of the passage of Hurricane Bob up the Atlantic coast, air with very low levels of both ozone and CO was transported into the region from the south. Such levels are characteristic of the tropical North Atlantic troposphere [Piotrowicz et al., 1990]. At Sable Island the ozone and CO remained below 25 and 75 ppbv, respectively, for 36 hours. The data from this episode correspond to the points in the lower left extreme of Figure 2a. To quantitatively investigate all of these features and thus account for all of the significant variance in the data sets will require computer modeling, which is presently underway.

SUMMER BUDGET FOR TRANSPORT OF OZONE FROM NORTH AMERICA TO THE NORTH ATLANTIC

Similar slopes were found from the regressions for the three sites in the summer. This indicates that the linear relationship is approximately constant over the 1000 km distance spanned by these sites. The common slope provides a quantitative relationship between the

amount of CO injected into the sampled air masses and the amount of ozone photochemically produced from the precursors that were emitted into the air masses with the CO. That is, in these transported air masses ozone to CO were at a molar ratio of about 30%. Since the amount of carbon monoxide emitted over North America is approximately known from emission inventories, and since the fraction of this CO that is transported to the North Atlantic can be estimated, it is possible to obtain an approximate budget for the amount of ozone exported to the lower troposphere over the North Atlantic Ocean from North America.

Emissions inventories have been compiled to facilitate the evaluation of air pollution control strategies. A recent comprehensive inventory has been complied for 1985 in North America by NAPAP (National Acid Precipitation Assessment Program) [Saeger et al., 1989]. The sources in the states and provinces lying east of the Mississippi River in this inventory emit 40.4 million tons of CO per year, which is about two-thirds of the U.S. and Canadian total. No significant seasonal cycle is present, so the CO emissions from eastern North America correspond to 330 billion moles per summer.

The fraction of this CO that is exported to the North Atlantic Ocean is simply approximated as unity. Atmospheric transport times across this region are a few days, much smaller than the one-month lifetime of CO. Thus, nearly all of the emitted CO flows from the continent before it is removed from the atmosphere. The prevailing wind direction is eastward, so nearly all of the CO emitted over Eastern North America is transported to the North Atlantic troposphere. Thus, the quantity of ozone photochemically produced from precursors emitted over North America and transported to the North Atlantic can be approximated by the product of the emissions of CO and the molar ratio of ozone to CO, which yields 100 billion moles of ozone per summer.

Such a simple budget estimate necessarily has significant uncertainties. The estimate of the eastern North American source of CO may be low for three reasons. First, some work has suggested that the emissions inventory for CO is underestimated by a factor of about three [Pierson et al., 1990], but other workers [Parrish et al., 1991; Buhr et al., 1992] have shown that any errors are likely to be much smaller. Second, CO is not only emitted directly, but also is produced as a photochemical intermediate in the atmospheric oxidation of hydrocarbons emitted from anthropogenic and natural sources. This production of CO over eastern North America is difficult to quantify, but is expected to be considerably smaller than the direct emissions [Logan et al., 1981]. Third, much of the CO emitted over western North America may also be transported over eastern North America and onto the North Atlantic. Correction for these potential underestimates would raise the calculated quantity of transported ozone. Additionally, some of the exported ozone may be removed by chemical processes or deposition before it is measured at the three sampling sites. If the removal of ozone is faster than the concurrent removal of CO, then again the export of ozone is

underestimated. The relative constancy of the slope found at the three progressively more distant sites suggest that this last effect is not a major one.

On the other hand, if some of the CO emitted in Eastern North America is transported to other regions (e.g., the Arctic or the Gulf of Mexico), then the calculation of ozone transported to the North Atlantic would be an overestimate. Given the prevailing wind regimes, such effects are likely to be small, however. Finally, one uncertainty of unknown effect arises since the relationship of ozone to CO has been measured only at the surface and only to the northeast of the major source regions. At higher altitudes or under meteorological conditions when transport is more easterly or southeasterly, a somewhat different ratio of ozone to CO may hold. Further measurements should elucidate this potential difference.

The ozone export estimate is consistent with other work. The NAPAP inventory [Saeger et al., 1989] estimates that 61 billion moles of nitrogen oxides per summer are emitted over eastern North America. [Liu et al., 1987] conclude that on average 10 ozone molecules are produced for each nitrogen oxide molecule emitted in this same region. The product of these numbers - 610 billion moles - yields a rough estimate of the total ozone produced in this region during the summer. Thus, the amount transported to the North Atlantic corresponds to 16% of the total produced. This is in reasonable accord with the value of 25% found in a model study [McKeen et al., 1991] of one stagnant pollution period over eastern North America. They found that the remainder was lost before transport through chemical reaction and surface deposition.

The estimated amount of ozone transported to the North Atlantic from North America may be roughly compared to that injected from the stratosphere. Estimates of this flux are 5×10^{10} molecules per cm^2 per second [Danielsen and Mohnen, 1977; Mahlman et al., 1980] as an annual average. The entire North Atlantic covers about 40 million km^2, of which about 17 million km^2 lie in the temperate region between Europe and North America. The above flux acting through the summer over this temperate region yields 110 billion moles, a quantity very similar in magnitude to the estimate for continental transport, which is concentrated in this temperate region.

The stratospheric flux enters the upper troposphere, and a large fraction is removed by photochemical processes before it can be transported to the lower troposphere [Liu et al., 1980]. The transport from the continent directly enters the lower troposphere. Therefore, during the summer, the ozone budget in the lower troposphere over the temperate North Atlantic is dominated by ozone that is photochemically produced from anthropogenic emissions. This conclusion is in accord with the large fraction of the variance in the ozone and CO levels measured at the three sites that is captured by the linear relationships.

WINTERTIME CHEMISTRY IN NORTH ATLANTIC AIR MASSES

The relationship of ozone and CO in the wintertime must reflect the chemical reactions in the atmosphere that are responsible for the removal of ozone by the anthropogenic emissions. One reaction sequence that has been postulated to remove ozone is

$$2\,X\,(NO + O_3 \rightarrow NO_2 + O_2)$$
$$NO_2 + O_3 \rightarrow NO_3 + O_2$$
$$NO_2 + NO_3 \rightarrow N_2O_5,$$

which gives the overall result that three ozone molecules are removed for every two molecules of NO that are emitted. The molar emission ratio of NO to CO over North America is approximately 0.21 [Saeger et al., 1989]. Thus, if the above reactions were to proceed to completion, the ozone to CO linear regression in winter should give a slope of -0.31. Ozone also reacts with other anthropogenic species such as aliphatic hydrocarbons. Contributions from such reactions would give even larger negative slopes. However, the observed slope from the overall regression in Figure 2b is only -0.12. A somewhat steeper slope seems to fit the data with CO levels below 160 ppbv, but this slope is still only about -0.17. Other processes such as wintertime photochemical production of ozone may be important in the more polluted air masses that dominate the linear regression. Surface deposition, which affects ozone but not CO, would also decrease the slope if it occurs to an important degree after the injection of the pollutants.

RELATIONSHIPS OF OZONE, PAN AND THE LIGHT ALKANES IN THE NORTH PACIFIC

Roberts et al. [1984] have shown that the measurement of two NMHCs from common sources can provide a useful "clock" for monitoring the photochemical processing that has occurred in an air parcel since the NMHCs were injected. NMHCs are photochemically removed from the atmosphere by reaction with hydroxyl radicals. If two NMHCs react with these radicals at significantly different rates, then the ratio of the concentrations of the more reactive to that of the less reactive will decrease exponentially with a rate constant equal to the product of the average hydroxyl radical concentration times the difference of their respective reaction rate constants. The ratio of the concentrations of two NMHCs, rather than the concentration of either, is selected because it is less sensitive to the degree of pollution of the air mass and dilution or mixing processes than are the concentrations themselves. Roberts et al. [1984] used the ratio of the aromatic NMHCs,

toluene and benzene, whose ratio has an e-folding time of about two days. For a tracer of anthropogenic ozone in marine regions, a longer lifetime is desired, so slower reacting NMHCs, the light alkanes, are used here.

Figure 4 compares the exponential decay of two light alkane concentration ratios. Data from several rural and remote field sites, as well as urban data are included. Of the rural and remote data sets, two are from the Pacific Ocean, one is from the Atlantic Ocean and the other two are from continental rural U.S. sites. The relatively good agreement among the urban data sets from three separate continents indicate that, on average and compared to the range of ratios covered by the photochemical aging process, the emission ratios are not a strong function of the region of origin.

In Figure 4 a clear correlation (the correlation coefficient for all plotted data points = 0.95) exists that continues from the urban data, through the rural continental measurements and the marine data from both the Pacific and the Atlantic Oceans to the free troposphere measurements from Hawaii, the most remote location. The wide variety of air masses and the wide range of ratios included in Figure 4 suggest the following conclusions: the levels of these light alkanes in all regions from urban centers to the remote oceans are dominated by anthropogenic emissions of relatively constant ratios; the measured ratios of butane to ethane and propane to ethane each evolve from their typical urban ratios in the upper right corner of Figure 4 to smaller ratios down and to the left; and each ratio is able to give a relative measure of the photochemical age of the alkanes in an air parcel over about 6 and 4 e-foldings, respectively. Parrish et al. [1992b] have shown that the relative photochemical ages in the Point Arena data set are consistent with trajectory calculations for the sampled air parcels; the least aged samples traveled rapidly across the Pacific from Asia, while the more aged samples had spent extended periods in the marine boundary layer.

The kinetics of the hydroxyl radical reactions with the alkanes suggests that the slope in Figure 4 should be 2.8 for a representative tropospheric temperature of 280 K [Parrish et al., 1992b]. A linear regression including all of the plotted data points gives a slope of 1.47, which is lower by nearly a factor of two. These deviations from the kinetic behavior are expected [McKeen et al., 1990] from the inevitable mixing of air parcels containing alkanes of different photochemical ages. These deviations are discussed in more detail by Parrish et al. [1992b].

Strictly speaking, the photochemical aging treatment outlined above will apply only to species that are removed from the atmosphere solely by reaction with OH. However, the removal rates for other species may well approximately parallel the rates of the OH reactions with the alkanes. For example, in the marine troposphere the removal processes for ozone are primarily photolysis to $O(^1D)$ followed by reaction with H_2O, and secondarily reaction with HO_2. PAN is primarily removed by thermal decomposition, primarily through bond homolysis to $CH_3C(O)O_2 + NO_2$, followed by removal of the peroxy radical by reaction

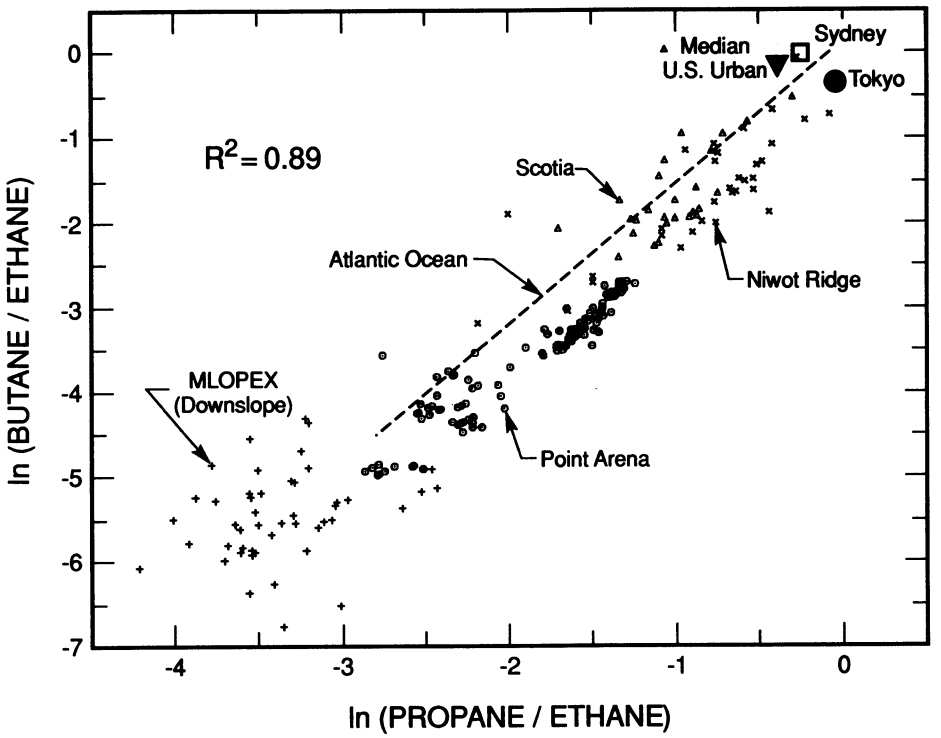

Fig. 4. Correlation of the natural logarithms of two alkane concentration ratios. The open symbols are from the Point Arena measurements. Also included are free troposphere data from the MLOPEX study in Hawaii [Greenberg et al., 1992], Niwot Ridge, Colorado and Scotia, Pennsylvania [H. H. Westberg, unpublished data, 1988]. The dashed line is from the linear least-squares fit given by Rudolph and Johnen [1990], and its extent shows the range of the values they report from their study in the Atlantic Ocean. The three large symbols give ratios for urban data from the U. S. [Seinfeld, 1989], Sydney, Australia [Nelson and Quigley, 1982], and Tokyo, Japan [Uno et al. 1985]. The indicated square of the correlation coefficient corresponds to the linear-least-squares fit to all plotted data points. [Parrish et al., 1992b]

with NO or with another peroxy radical. Thus, the removal of both ozone and PAN from the troposphere will proceed most rapidly under warm, humid and high sunlight conditions, the same conditions that maximize the rate of the OH reaction with the alkanes. Consequently, if the ozone and PAN in an air parcel are produced rapidly from precursors emitted from the same sources (or at least in the same region) as the alkanes, and then are transported to the marine environment where removal processes dominate, then similar photochemical aging behavior may be observed for ozone, PAN and the alkanes.

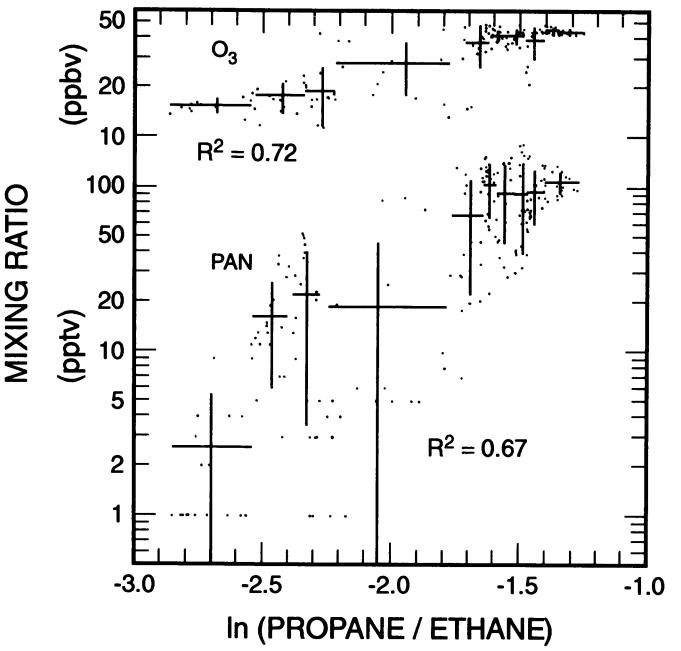

Fig. 5. Correlation of ozone and PAN concentrations at Point Arena with the natural logarithm of the propane to ethane ratio. Each dot gives an independent measurement, and each cross gives the averages of the abscissa and ordinate data for 10% of the respective data set. The horizontal and vertical bars indicate the ranges of the abscissa values and the standard deviations of the ordinate values, respectively. Each R^2 is the square of the correlation coefficient for the respective individual measurements. [Parrish et al., 1992b].

Figure 5 shows that there is a strong correlation of the ozone and PAN concentrations with the photochemical age of the alkanes as indicated by the propane to ethane ratio. Thus, it appears that in these air parcels arriving on the California Coast from the Pacific troposphere, the dominant source of the ozone and PAN are most likely Asian anthropogenic sources, at least in the least aged air parcels.

The slopes from Figure 5 give some information regarding the tropospheric lifetimes of ozone and PAN. If the kinetics were not obscured by the mixing processes discussed earlier, a given slope is equal to the inverse of the ratio of the lifetimes of the two quantities whose logarithms are plotted. Parrish et al. [1992b] show that the mixing effects allow only upper and lower limits of the lifetimes to be derived. It should be emphasized that the derived lifetimes, $\geq$ 19 days for ozone and $\leq$ 2.5 days for PAN, are for the net change in the concentration of ozone and PAN, i.e., the difference between the removal processes and any

in situ production processes. Furthermore, these estimates are averages weighted in an unknown manner over the histories of the air parcels sampled in this study.

CONCLUSIONS

In the lower troposphere over the eastern third of the temperate North Atlantic Ocean, the variance in ozone is primarily due to transport of anthropogenic pollution, both in summer and in winter. Ozone and CO correlate positively in summer and negatively in winter. An approximate budget indicates that transport of ozone photochemically produced from anthropogenic emissions dominates over stratospheric injection during the summer in the lower troposphere over the temperate North Atlantic. Reaction of ozone with anthropogenic emissions evidently dominates the ozone variance in the winter.

In air masses flowing onshore to North America from the Pacific Ocean, the ratios of the light alkanes provide a measure of the degree of photochemical aging that has occurred since the alkanes were emitted. This behavior, along with collaborative trajectory calculations, indicates that the alkane levels are determined by transport to the marine area from continental sources, most likely Asian, followed by photochemical removal over the Pacific Ocean. Since the concentrations of PAN and ozone correlate well with the alkane ratios, it is concluded that the observed PAN and ozone were dominated by continental sources and removal processes in the marine areas as well.

Since it is concluded that a major input of ozone to the temperate North Atlantic is transport of ozone photochemically produced from anthropogenic sources in North America, and since the ozone levels in onshore flow in Europe will strongly affect the ozone levels on that continent, the noted increase of boundary layer ozone levels in Europe [Volz and Kley, 1988] may well be partially attributable to transport from North America. Likewise, transport from Europe likely affects Asia. Finally, the Point Arena measurements provide evidence for the impact of Asian sources on the levels of ozone arriving on west coast of the U.S. The overall result is then be a general increase in the levels of ozone in the temperate latitudes of the Northern Hemisphere. Such hemisphere wide air pollution has been identified in satellite data [Fishman et al., 1991], and is in accord with recent modeling studies [Hough and Derwent, 1990].

REFERENCES

Buhr, M. P., M. Trainer, D. D. Parrish, R. E. Sievers, and F. C. Fehsenfeld, Assessment of pollutant emission inventories by principal component analysis of ambient air measurements, *Geophys. Res. Lett., 19*, 1009-1012, 1992.

Danielsen, E. F. and V. A. Mohnen, Project dust storm report: Ozone transport, in situ measurements, and meteorological analyses of tropopause folding, J. Geophys. Res., 82, 5867-5877, 1977.

Duce, R. A. et al., The atmospheric input of trace species to the world ocean, *Global Biogeochem. Cycles, 5*, 193-259, 1991.

Fehsenfeld, F. C. and S. C. Liu, Tropospheric ozone: The distribution and sources, *in Ozone in the Troposphere*, edited by Sturgiss and Hewitt, Elsevier, 1992.

Fishman, J., K. Fakhruzzaman, B. Cros, and D. Nganga, Identification of widespread pollution in the Southern Hemisphere deduced form satellite analyses, *Science, 252*, 1693-1696, 1991.

Fishman, J. and W. Seiler, Correlative nature of ozone and carbon monoxide in the troposphere: Implications for the tropospheric ozone budget, *J. Geophys. Res., 88*, 3662-3670, 1983.

Greenberg, J.P., P.R. Zimmerman, W.A. Pollock, R.A. Lueb, and L.E. Heidt, Diurnal variability of atmospheric methane, nonmethane hydrocarbons and carbon monoxide at Mauna Loa, *J. Geophys. Res., 97*, 10395-10413, 1992.

Grosvenor, M. B., Ed., *National Geographic Atlas of the World*, National Geographic Society, Washington D. C., 1963.

Hough, A. M. and R. G. Derwent, Changes in the global concentration of tropospheric ozone due to human activities, *Nature, 344*, 645-648, 1990.

Liu, S. C., D. Kley, M. McFarland, J. D. Mahlman, and H. Levy II, On the origin of tropospheric ozone, *J. of Geophys. Res., 85*, 7546-7552, 1980.

Liu, S. C., M. Trainer, F. C. Fehsenfeld, D. D. Parrish, E. J. Williams, D. W. Fahey, G. Hübler, and P. C. Murphy, Ozone production in the rural troposphere and the implications for regional and global ozone distributions, *J. Geophys. Res., 92*, 4191-4207, 1987.

Logan, J. A., M. J. Prather, S. C. Wofsy, and M. B. McElroy, Tropospheric chemistry: A global perspective, *J. Geophys. Res., 86*, 7210-7254, 1981.

Mahlman, J. D., H. Levy II, and W. J. Moxin, Three-dimensional tracer structure and behavior as stimulated in two ozone precursor experiments, *J. Atmos. Sci., 37*, 655-685, 1980.

McKeen, S.A., M. Trainer, E.Y. Hsie, R.K. Tallamraju, and S.C. Liu, On the indirect determination of atmospheric OH radical concentrations from reactive hydrocarbon measurements, *J. Geophys. Res., 95*, 7493-7500, 1990.

McKeen, S. A., E.-Y. Hsie, M. Trainer, R. Tallamraju, and S. C. Liu, A regional model study of the ozone budget in the Eastern United States, *J. Geophys. Res., 96*, 10809-10845, 1991.

Parrish, D. D., J. S. Holloway, M. Trainer, P. C. Murphy, G. L. Forbes, and F. C. Fehsenfeld, Export of North American ozone pollution to the North Atlantic Ocean, *Science*, submitted, 1992a.

Parrish, D. D., C. J. Hahn, E. J. Williams, R. B. Norton, F. C. Fehsenfeld, H. B. Singh, J. D. Shetter, B. W. Gandrud, and B. A. Ridley, Indications of photochemical histories of Pacific air masses from measurements of atmospheric trace species at Pt. Arena, California, *J. Geophys. Res.*, in press, 1992b.

Parrish, D. D., M. Trainer, M. P. Buhr, B. A. Watkins, and F. C. Fehsenfeld, Carbon monoxide concentrations and their relation to concentrations of total reactive oxidized nitrogen at two rural U.S. sites., *J. Geophys. Res., 96*, 9309-9320, 1991.

Pierson, W. R., A. W. Gertler, and R. L. Bradow, Comparison of the SCAQS tunnel study with other on-road vehicle emission data, *J. Air Waste Manage. Assoc.*, *40*, 1495-1504, 1990.

Piotrowicz, S. R., C. J. Fischer, and R. S. Artz, Ozone and carbon monoxide over the North Atlantic during a boreal summer, *Global Biogeochem. Cycles*, *4*, 215-224, 1990.

Pszenny, A. A. P., J. N. Galloway, R. S. Artz, and J. F. Boatman, Overview of the 1988 GCE/CASE/WATOX studies of biogeochemical cycles in the North Atlantic region, Global Biogeochem. *Cycles*, *4*, 121-131, 1990.

Nelson, P.F., and S.M. Quigley, Non-methane hydrocarbons in the atmosphere of Sydney, Australia, *Environ. Sci. Technol.*, *16*, 650-655, 1982.

Roberts, J. M., F. C. Fehsenfeld, S. C. Liu, M. J. Bollinger, C. Hahn, D. L. Albritton, and R. E. Sievers, Measurements of aromatic hydrocarbon ratios and NO_X concentration in the rural troposphere: Observation of air mass photochemical aging and NO_X removal, *Atmos. Environ.*, *18*, 2421-2432, 1984.

Rudolph, J., and F.J. Johnen, Measurements of light atmospheric hydrocarbons over the Atlantic in regions of low biological activity, *J. Geophys. Res.*, *95*, 20583-20591, 1990.

Saeger, M. et al., *The 1985 NAPAP emissions inventory (version 2): Development of the annual data and modelers' tapes*, 1989.

Seinfeld, J. H., Urban air pollution: State of the science, *Science, 243*, 745-752, 1989.

Singh, H. B., W. Viezee, and L. J. Salas, Measurements of selected C_2 - C_5 hydrocarbons in the troposphere: Latitudinal, vertical, and tempora variations, *J. Geophys. Res.*, *93*, 15861-15878, 1988.

Uno, I., S. Wakamatsu, R.A. Wadden, S. Konno, and H. Koshio, Evaluation of hydrocarbon reactivity in urban air, *Atmos. Environ.*, *19*, 1283-1293, 1985.

Volz, A. and D. Kley, Evaluation of the Montsouris series of ozone measurements made in the nineteenth century, *Nature*, *332*, 240-242, 1988.

Watson, R. T., H. Rodhe, H. Oeschger, and U. Siegenthaler, Greenhouse gases and aerosols, *in Climate Change. The IPCC Scientific Assessment*, edited by J. T. Houghton, G. J. Jenkins, and J. J. Ephraums, Cambridge University Press, Cambridge, 1990.

Whepdale, D. M. and J. L. Moody, Large-scale meteorological regimes and transport processes, *in The Long-Range Atmospheric Transport of Natural and Contaminant Substances*, edited by A. H. Knap, pp. 3-36, Kluwer Academic Publishers, Dordrecht, 1990.

THE ATMOSPHERIC DISTRIBUTION OF NO, O_3, CO, AND CH_4 ABOVE THE NORTH ATLANTIC BASED ON THE STRATOZ III FLIGHT

D.H. Ehhalt, F. Rohrer, and A. Wahner
Institut für Atmosphärische Chemie
Forschungszentrum Jülich
Postfach 1913, W-5170 Jülich, Germany

INTRODUCTION

In June 1984 several French and German research groups joined in the STRATOZ III aircraft campaign to measure the global distribution of a number of trace gases. The first part of that campaign led across the Northern Atlantic with stops at Prestwick, Scotland; Keflavik, Iceland; Sondrestrom, Greenland, and Goose Bay, Canada, all falling in the zonal belt between roughly 55° N and 65° N latitude (see Figure 1). During the ascents from and descents to these airports vertical profiles were measured for NO by Drummond et al., [1988] and for O_3, CO, CH_4 by Marenco et al. [1989a,b]. Figure 2 presents the data coverage projected onto the altitude by longitude plane at 60° N latitude. Also measured was PAN but with a much lower sampling density [Rudolph et al., 1987]. The measurements took place between the early morning on June 4, 1984, beginning with the descent to Prestwick, and the late morning of June 6, 1984, ending with the ascent from Goose Bay, and resulted in altogether 8 vertical profiles. As indicated in Figure 2 the aircraft, while gradually climbing or descending, also covered large horizontal distances. Thus, the term "vertical profile" is somewhat of a figure of speech. The flight pattern, however, is useful in more evenly filling the altitude by longitude plane with data points.

Therefore, and because of the short sampling interval of two days only, these data are well suited to construct a snapshot of the 2-D zonal distributions of the mixing ratios in the 55° N to 65° N latitude band across the Atlantic. Emphasis is on the NO as one of the major drivers of atmospheric chemistry; CO and CH_4 serve mainly as tracers.

The measured NO contours are investigated by comparing them against those modelled by a simple channel model. The resulting differences are explained on the basis of the actual wind pattern, and the distribution of the NO sources.

MEASURED 1-D AND 2-D DISTRIBUTIONS

As an example of the original data, Figure 3 shows the set of NO, O_3, CO, and CH_4 profiles measured during the descent to Sondrestrom on the mid morning of June 5, 1984, about halftime through the North Atlantic flight. Also shown is a profile of the NO_x mixing

NATO ASI Series, Vol. I 7
The Tropospheric Chemistry of Ozone in the Polar Regions
Edited by H. Niki and K. H. Becker

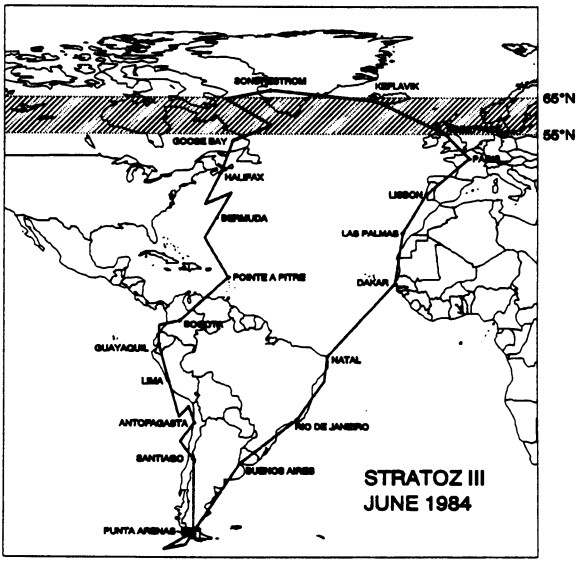

Fig. 1: Flight track of the STRATOZ III mission (4 - 26 June 1984).

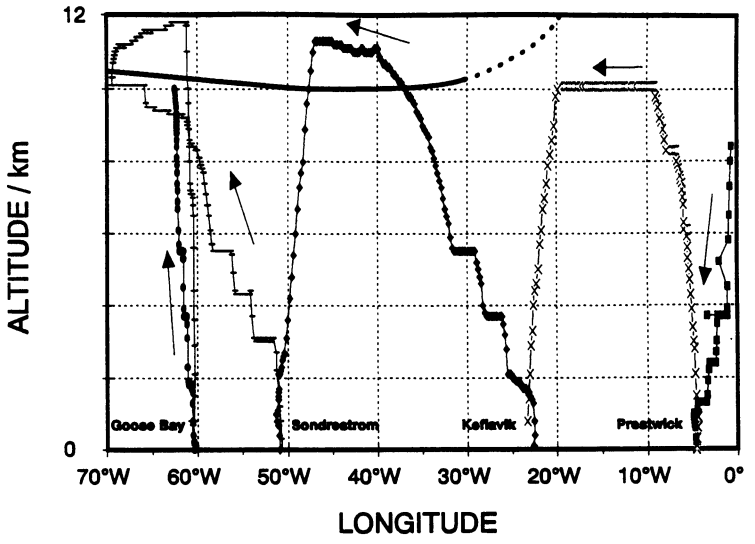

Fig. 2: Data coverage during STRATOZ III at about 60° N latitude projected onto the altitude by longitude plane. The solid line indicates the height of tropopause. The dashed part of the line is uncertain and derived from local radiosonde ascents at Lerwick.

ratio which is derived from the measured NO and O_3 mixing ratios and a calculated seasonal photolysis rate of NO_2. The profile of potential temperature is used as a meteorological indicator for the tropopause height. On that day and location the tropopause was at 10 km altitude. The most obvious feature of these profiles is the transition in mixing ratio going from the troposphere to the stratosphere, (i.e., a strong increase in NO, NO_x and O_3 which have strong stratospheric sources and a decrease in CO and CH_4, for which the stratosphere acts as a sink). The higher values of NO (and NO_x) close to the earth's surface are probably due to pollution encountered when approaching the airport, and are not necessarily representative of the boundary layer over the Atlantic.

The individual profiles in Figure 3 are fairly typical for the mean of all 8 vertical profiles as seen from Figure 4 which shows a superposition of the data points from all profiles together with the resulting mean profiles. Considering the vast stretch of air masses covered the scatter in the data is rather small. Also shown are all the PAN measurements along that flight leg. The data are a bit sparse to call this a typical vertical PAN profile over the North Atlantic, but they are suggestive. They show a clear vertical pattern: an increase with altitude within the free troposphere and a decrease when crossing into the stratosphere. The tropospheric PAN concentrations measured here are low compared to those observed at the same latitudes over North America during the ABLE 3A campaign in July and August 1988 up to 6 km altitude [Singh, private communication, 1990]. They agree well, however, with the vertical PAN profile predicted by a 1D-model for the marine summertime atmosphere [Kasting and Singh, 1986].

Because they are at the center of our interest, the vertical NO profiles at each location are presented in Figure 5. These are average profiles in the sense that the data were averaged over 1 km height intervals to even out the occasional nonuniform data coverage. An occasional gap at a given height was filled by interpolation between the mean mixing ratios at the adjacent heights.

In order to better perceive any gradual longitudinal change in the trace gas mixing ratios, we use these vertical profiles at different longitudes (but within the 55° N to 65° N latitude band) to construct longitude by altitude contours of constant mixing ratio. We do this by superimposing the mixing ratios of the averaged local profiles of Figure 5 on the flight tracks shown in Figure 2, and then connecting the points of constant mixing ratio. In the case of NO only 6 profiles are available for this purpose: The ascent at Sondrestrom and descent at Goose Bay were at sunrise and early morning, respectively, with high zenith angles such that the photolysis rates of NO_2 were not consistent with those for the other NO profiles. This procedure results in a rather clear cut 2-D distribution of NO. Its contours are shown in Figure 6. The corresponding altitude-by-latitude contours for CO, CH_4, and O_3 are shown in Figures 7-9.

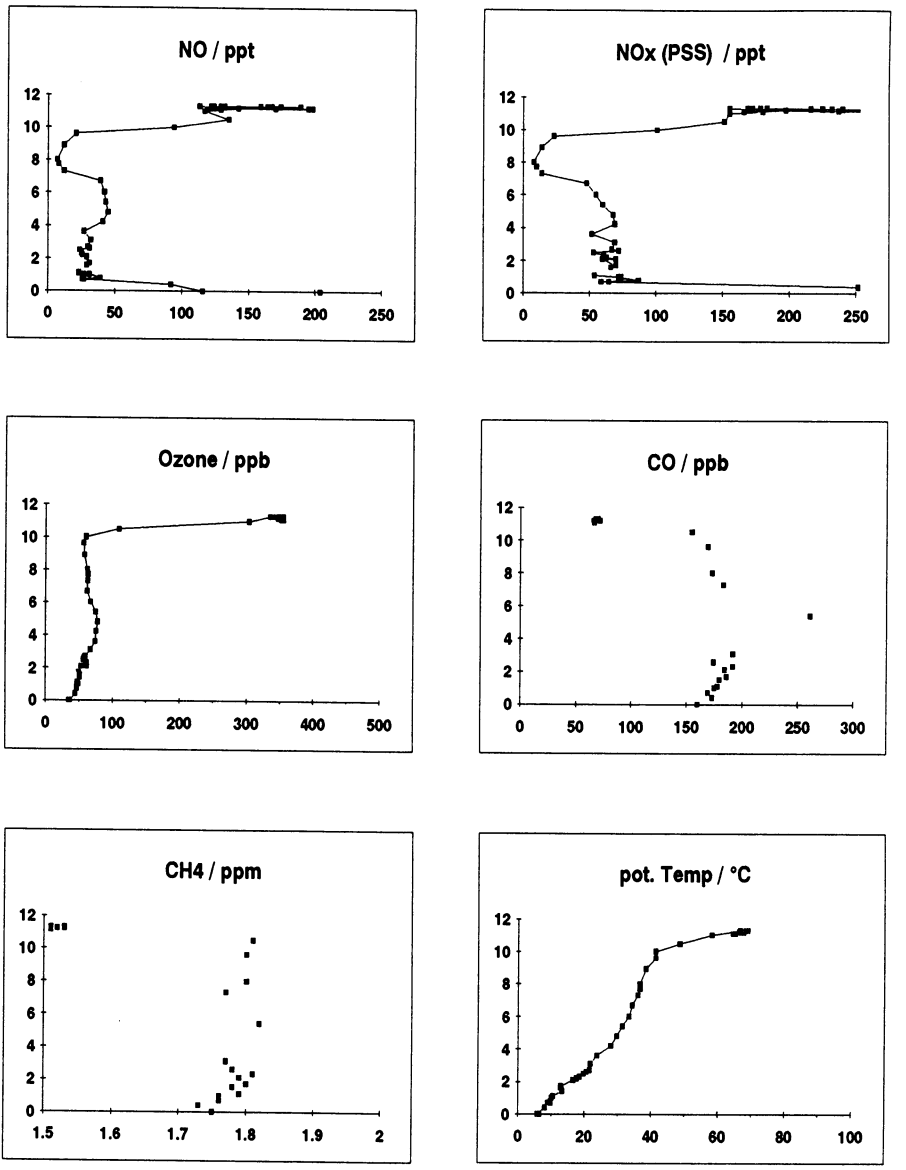

Fig. 3: Measured individual vertical profiles of NO, O_3, CO, CH_4, and potential temperature during the descent to Sondrestrom (morning of June 5, 1984). The vertical profile of NO_x is calculated (see text).

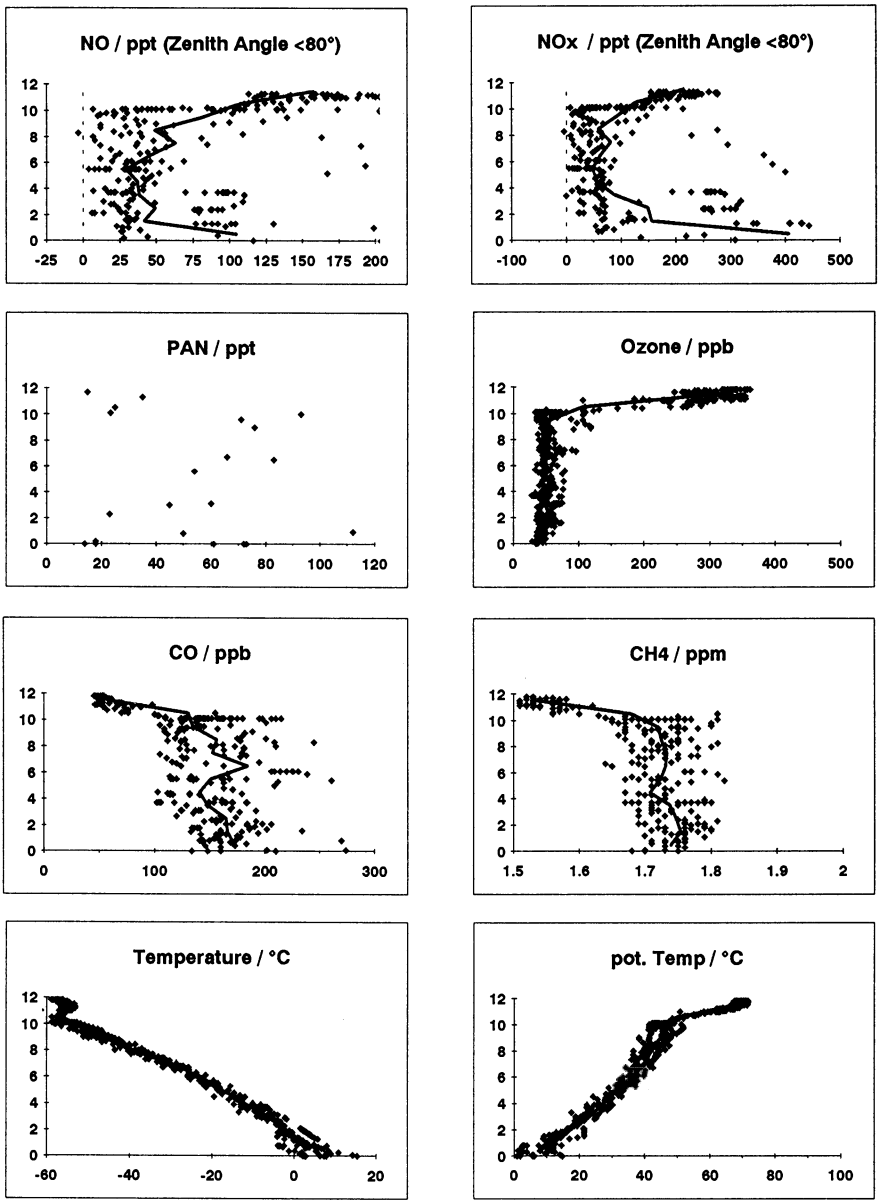

Fig. 4: All measured vertical profiles of NO, NO_x , O_3 , CO, CH_4 , PAN, temperature, and potential temperature during the descents and ascents shown in figure 2. The solid lines show the resulting mean profiles.

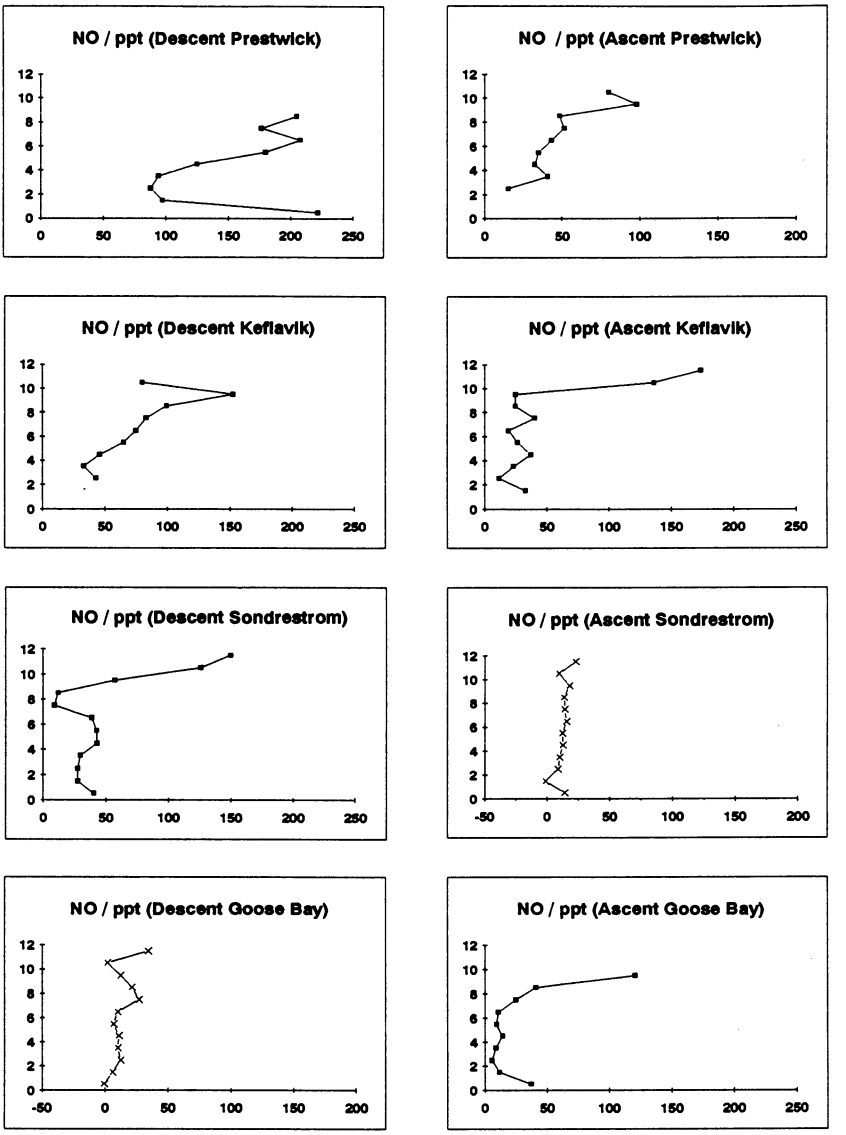

Fig. 5: Measured, mean vertical profiles of NO during the descents and ascents shown in figure 2.
Crosses: Measurements at sun zenith angle > 80°.
Flights: descent Prestwick, early morning 6/4/84; ascent Prestwick, mid morning 6/4/84; descent Keflavik, mid morning 6/4/84; ascent Keflavik, mid morning 6/5/84; descent Sondrestrom, mid morning 6/5/84; ascent Sondrestrom, sunrise 6/6/84; descent Goose Bay, early morning 6/6/84; ascent Goose Bay, late morning 6/6/84.

Before discussing the pattern of the NO contours in any detail, we pause for a moment to estimate what kind of pattern we should expect based on a climatological average. That pattern we will then use as a reference case to compare against the actual contours measured during June 4-6, 1984.

MODELLING OF THE 2-D ZONAL DISTRIBUTION OF NO IN THE 55° N-65° N LATITUDE BAND

For this purpose we adapted the channel model reported by Ehhalt et al., [1992], to the conditions at the 55° N - 65° N latitude band. The transport in that model treats only the vertical transport explicitly. The horizontal transport is introduced by allowing the NO_x source terms, surface boundary conditions and vertical transport to change in time commensurate with a displacement in longitude by a 5 m s^{-1} westerly wind. This is equivalent to moving the whole air column treated in the model zonally around the globe with a vertically uniform wind speed. The wind speed corresponds to the zonally and vertically averaged west wind component in June at 55° - 65° N latitude [Houghton, 1985]. It takes about 46 days to circle the globe or 40, 000 time steps of 100s.

The model covers the altitudes from 0 to 16 km with a 1 km height resolution except for the two lowest levels which are located at 0.1 and 0.5 km altitude. The tropopause is located at 10 km altitude. Temperature and density profiles are those of the U.S. Standard Atmosphere [1976]. The model includes a fast vertical transport which injects air parcels from the planetary boundary layer directly into all tropospheric levels above 1 km altitude. The injection rates for the fast vertical transport for 55° N – 65° N latitude are quite similar to those for the 40° N - 50° N band given by Ehhalt et al. [1992] except for the 8 - 10 km height interval over the continents where the present exchange rates are only 0.06 $(days)^{-1}$, only 60 % of that in the 40° N - 50° N latitude band.

Chemistry is also kept to a minimum in this model. It includes the fast interconversion of NO and NO_2 and the conversion of NO_2 to HNO_3 via the reaction with OH and a small nighttime conversion via NO_3 to nitrate. The vertical OH and O_3 profiles are fixed to literature values. The current vertical OH profile for June at 60° N is taken from Spivakovsky et al. [1990], that of O_3 from Dütsch [1978]. This results in a chemical lifetime for NO_x of about 0.75 days in the boundary layer and 4 days at 10 km altitude. NO_2 is allowed to dry deposit over the continents only, and HNO_3 dry deposits over the whole surface. HNO_3 is also removed by rainout. For details, see Ehhalt et al. [1992].

The NO_x sources contributing to the atmospheric burden are listed in Table 1. Only the stratospheric input is zonally uniform. It is introduced by a downward flux at 16 km altitude of 1.5 x 10^{12} molecules m^2 s^{-1}. The surface sources of NO are represented by an

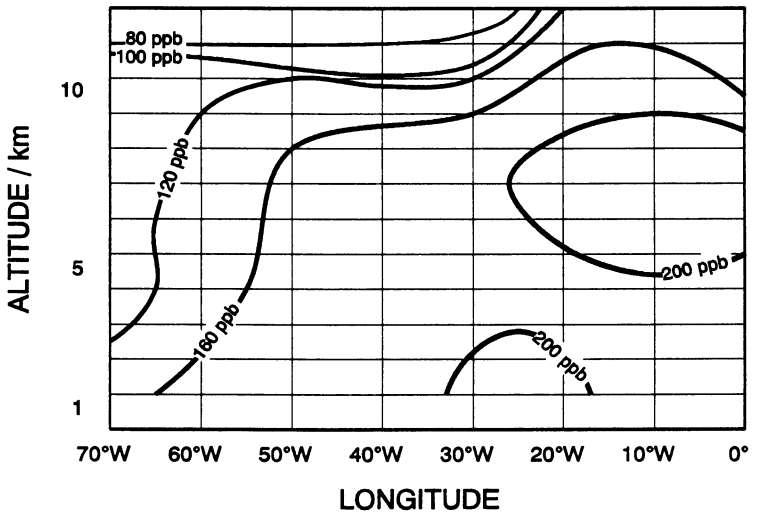

Fig. 6: Contour plot of the measured zonal two-dimensional distribution of NO at 55° - 65° N latitude in the longitudinal interval between 70° W and 0° W. Isolines above 10 km altitude and east of 30° W, where no data are available, are extrapolated.

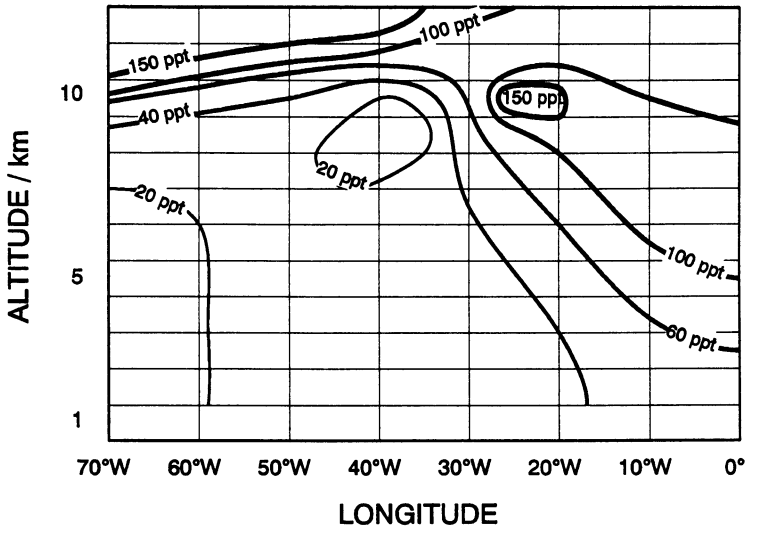

Fig. 7: Contour plot of the measured zonal two-dimensional distribution of CO at 55° - 65° N latitude in the longitudinal interval between 70° W and 0° W. Isolines above 10 km altitude and east of 30° W, where no data are available, are extrapolated.

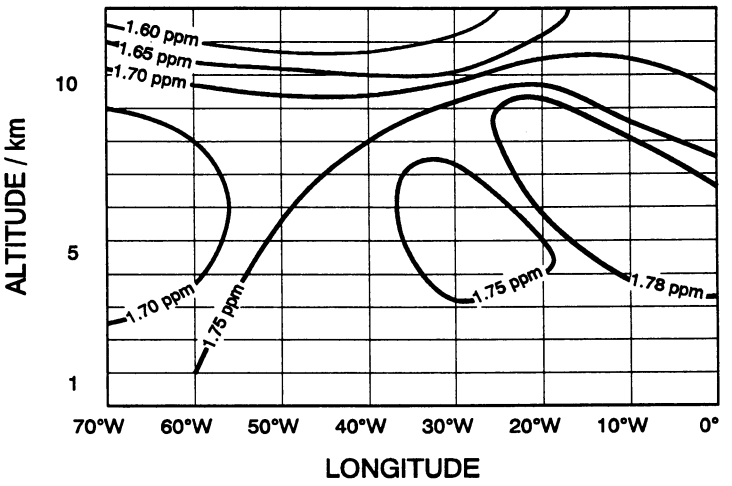

Fig. 8: Contour plot of the measured zonal two-dimensional distribution of CH_4 at 55° - 65° N latitude in the longitudinal interval between 70° W and 0° W. Isolines above 10 km altitude and east of 30° W, where no data are available, are extrapolated.

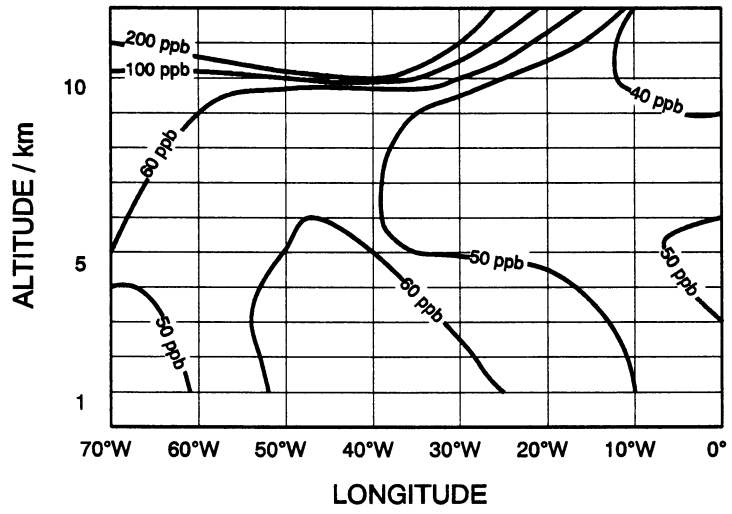

Fig. 9: Contour plot of the measured zonal two-dimensional distribution of O_3 at 55° - 65° N latitude in the longitudinal interval between 70° W and 0° W. Isolines above 10 km altitude and east of 30° W, where no data are available, are extrapolated.

Table 1. NO_x Emissions in the 55° - 65° N Latitude Band for June 1984[a]

Source	Emission Rate in 55° - 65° N, 10^6 t N/yr	Fraction in 55° - 65° N, %
Surface sources		
total	1.65	4.4
fossil fuel	1.6	7.7
burning	0.15	3.1
Lightning	0.043	12.6
Aircraft, civil	0.024[b]	3.9
Stratosphere		

a) Emissions are given in absolute terms and as fraction of the global strengths of the individual sources.
b) Only 1/4 of this stratospheric input is assumed to be in the form of NO_x; the major part is HNO_3.

upward flux boundary condition at 0 km. That flux vanishes over the oceans and varies with longitude over the continents to closely represent the natural and anthropogenic inputs. The surface flux is adopted from Hameed and Dignon [1988] and maximizes over Europe: (i.e., at 0° E - 60° E longitude).

The inputs by lightning and aircraft are volume sources. Their zonally averaged height distributions at 55° N - 65° N latitude are shown in Figure 10. We note that at those latitudes most of the aircraft injection is above 10 km altitude, the model's tropopause height. Naturally, lightning and aircraft input are zonally non-uniform. A fair share of the input by aircraft, about 33%, is emitted over the northern Atlantic region. The lightning input is concentrated over the continents.

The model yields a zonal NO distribution at all longitudes. The section between 70° W and 0° W, which is of interest here, is enlarged and shown in Figure 11. It exhibits a rather regular behavior of the NO isolines. That means, our reference case which assumes only westerly winds and no south to north transport, has more or less horizontal isolines of constant NO mixing ratio across the Atlantic, except in the lower eastern corner of that section where the surface input from the European continent makes itself felt. At the levels above the tropopause the isolines bunch together, indicating the strong vertical gradient caused by the stratospheric downward flux of NO. All other variations are rather *subtle*. Still the contributions of the various sources to the local NO mixing ratio changes quite a bit as the air moves over the Atlantic. This is seen in Figure 12, which describes a sequence of vertical NO and NO_x profiles derived from the model calculations and identifies by the

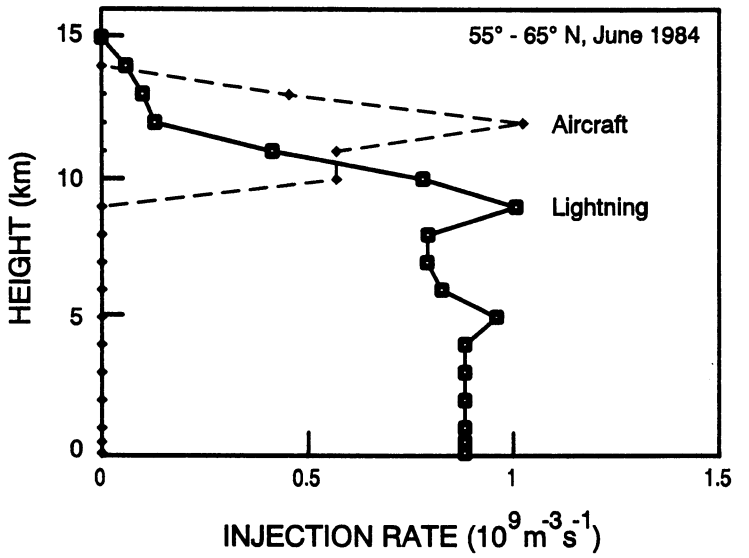

Fig. 10: Vertical profile of the zonally averaged NO_x injection rate by lightning (open squares) and aircraft (solid diamonds) used as input for the model calculations.

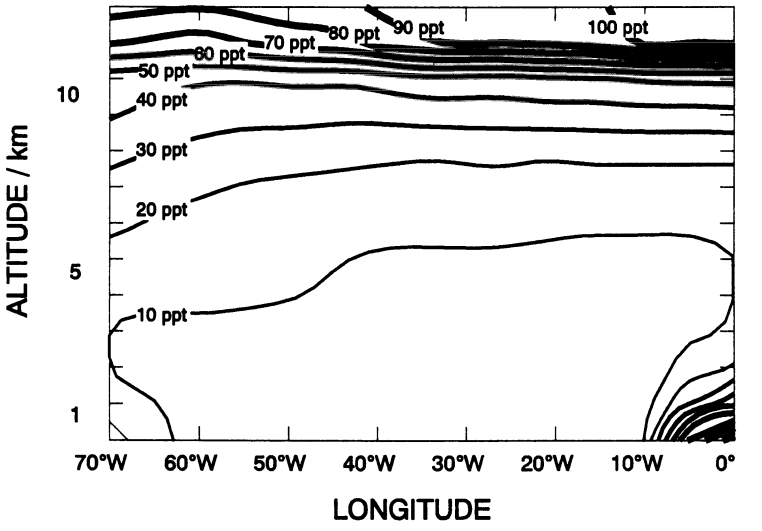

Fig. 11: Contour plot of the calculated zonal two-dimensional distribution of NO at 55° - 65° N latitude in the longitudinal interval between 70° W and 0°.

different shadings the various contributions to the local NO_x mixing ratio. Clearly the contribution from aircraft emissions increase considerably towards the east: at 10 km altitude it rises from 15% at 65° W to 60% of the total mixing ratio at 5° W longitude, while the others, except the uniform stratospheric contribution, decrease correspondingly. This is due to the fact that over the Atlantic the surface sources vanish completely and the lightning input diminishes greatly, whereas the regional input by aircraft becomes quite large. The chemical losses of NO_x in the upper troposphere are compensated, in fact slightly overcompensated, by the increased NO input from aircraft.

DISCUSSION

It is obvious that the actual 2D-distribution of the NO mixing ratio over the northern Atlantic represented in Figure 6 differs significantly from the reference case in Figure 11, which is thought of representing the climatological average. On the whole, the measured NO concentrations are significantly higher than the calculated ones nearly everywhere within the displayed cross section. One of the major differences occurs at the tropopause altitude,

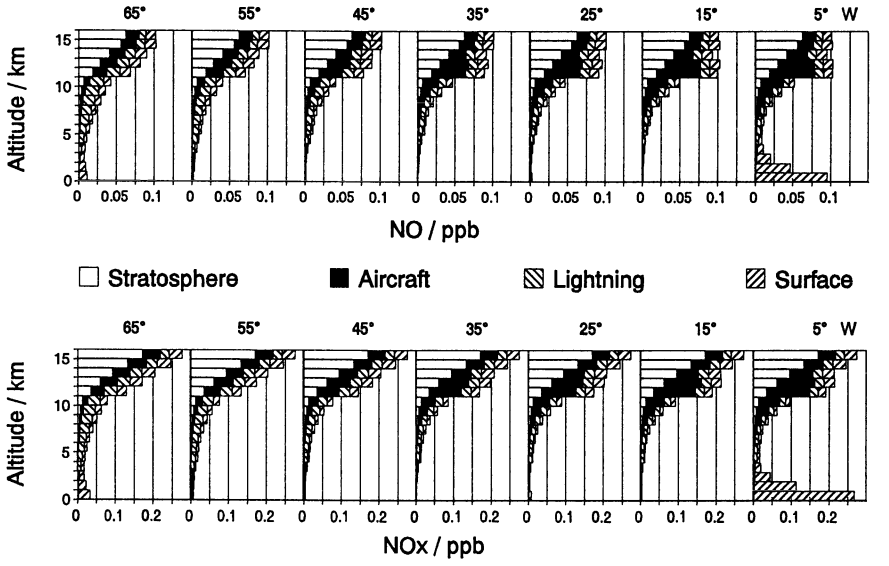

Fig. 12: Calculated vertical mixing ratio profiles of NO (top panel) and NO_x (bottom panel) at 10° longitude intervals between 70° W and 0°. The different shadings indicate the contributions from the individual sources.

where the measured contours in the western half of the cross section exhibit a much steeper increase in concentration when going into the stratosphere than the reference case. The possible reasons for this will be discussed later. At the same time the measurements in the eastern half of the cross section gave relatively small gradients around 10 km altitude. This is due to the fact that the actual tropopause altitude rose from 10 km in the western part to 11 km in the eastern part and was not reached by the aircraft in the first two vertical profiles.

The most conspicuous feature in the actual NO distribution, however, is a pattern of strongly inclined isolines of constant NO mixing ratio between 30° W and 0° longitude, indicating a ridge of high NO concentrations slanted upward in westward direction. Based on the NO isolines alone, it is difficult to unequivocally assign a cause to this finding. It could be both, an intrusion of stratospheric air or upward transport of NO_x-rich boundary layer air from the continents. However, a look at the 2-D fields of CH_4, CO, and O_3, however, which serve as tracers for stratospheric and boundary layer air, tells us that these elevated NO concentrations must be due to upward moving surface air: The mixing ratios of CH_4, CO, which have surface sources only, show similar elevated contours as NO, whereas the contours of O_3 hardly exhibit any increase. If the elevated NO came from the stratosphere, we would expect the 100 ppt NO isoline to be matched by a 100 ppb O_3 isoline (see the stratospheric parts of Figure 6 and 9), whereas the actual O_3 mixing ratio in that region of the troposphere is at most 50 ppb, close to the tropospheric average. This speaks strongly against a stratospheric and for a boundary layer origin of that air mass.

To locate the origin of that air mass more closely we take a look at the 500 hPa pressure map of the area from June 5, 1984, 00 GMT (Figure 13), (i.e., about half time through the flight campaign). Clearly, the geopotential height contours in Figure 13 exhibit a dipole type blocking case described by Iverson [1992], a situation which persisted for about a week. However, the pattern of the zonal NO distribution is mostly influenced by air from the European continent funneled northward and westward between the low pressure region over France and the high pressure region northeast of Iceland, and not so much by the blocking action, which deflects the air coming off the North American continent to the North. An isobaric trajectory indicates that the air encountered during the flight over Prestwick and Keflavik, which showed the highest NO concentrations, had left middle Europe some 30 hours earlier after having described a half circle over Europe for some 20 hours, plenty of time to pick up pollutants, an airflow which resembles one of the schematic representations of air pollution transport to the Arctic given by Raak [1991].

The elevated mixing ratios of CH_4 and CO observed at 60° W on June 6 are probably due to the blocked flow from the North American continent, although, judging from the 500 hPa map, the flow from Europe could have penetrated to that longitude a few days earlier.

The wind pattern indicated in the 500 hPa map of Figure 13 was quite similar at the other tropospheric pressure levels and persisted for several days (June 3 to June 6). One would, therefore, expect the actual vertical NO profiles over the northern Atlantic, at Prestwick for example, to correspond to the NO profile over middle Europe modified by the travel out over the Atlantic. That modification consists of a fast decay in NO_x and therefore, of NO in the lower troposphere and a slow decay in the upper troposphere.

Unfortunately, there is no measured NO profile over middle Europe for that time period. But a comparison with the modelled NO profile for 40° N - 50° N latitude [from Ehhalt et al., 1992] shows that expectation to be a reasonable one (Figure 14). For further comparison the modelled profile over northern Europe at 55° N - 65° N latitude is also shown. It could not account for the NO profile measured over Prestwick.

Only the western most part of the actual 2-D cross sections could have conformed with the reference case. This is shown in Figure 15 by the 500 hPa pressure map from June 7, 1984, 00 GMT. As the trajectory indicates, the air flow was more or less straight from the west. Indeed, the vertical profile of NO measured at Goose Bay, although showing a few layers of slightly elevated mixing ratio, agrees on average well with the calculated NO profile for 65° W longitude for the troposphere (Figure 16). We may take this as an indication that our simple channel model simulates the climatologically averaged distribution of the tropospheric NO mixing ratio reasonably well. This had already been observed for the simulation of the 40° N - 50° N latitude band.

As the 2D distribution of NO (Figure 6) indicates, however, above the tropopause the measurements show a much more rapid increase of the NO mixing ratio than does the modelled distribution. This is most likely due to a general downward motion of air in the lower stratosphere which tends to compress the isolines of mixing ratio at the tropopause. This effect is also visible in the contours of CH_4 and CO which show a steeper decrease above the tropopause than predicted by a model which simulates stratospheric vertical transport by eddy diffusion only and does not include a mean downward motion.

CONCLUSION

Due to a fortunate coincidence the flight of STRATOZ III encountered a dipole type blocking situation over the North Atlantic which caused northwestward transport of polluted air from Europe, all the way to the Arctic Circle. Because of the persistence of that weather situation this transport was mapped into the observed 2D fields of NO, CO, and CH_4, despite limited spatial resolution of the measurements.

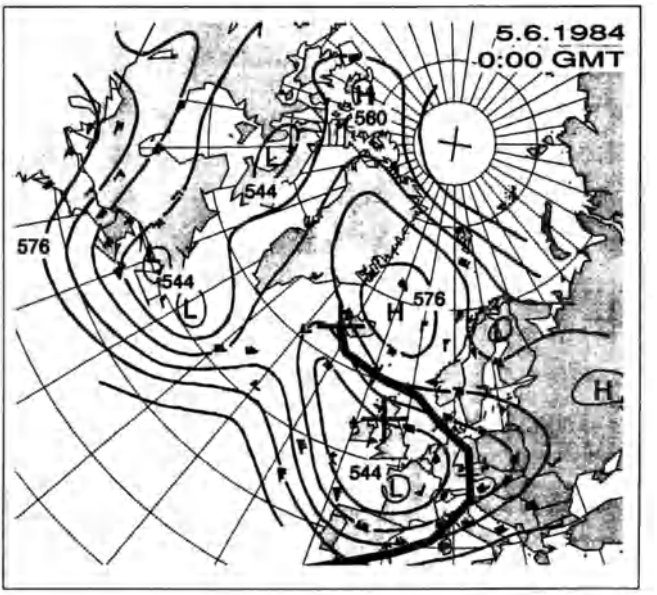

Fig. 13: Weather map at 500 hPA from June 5, 1984, 00 GMT. The bold line indicates the isobaric back trajectory for 72 hours (tick marks every 12 hours). The bold crosses indicate the location of the ascent and descent (Keflavik and Prestwick) on this day.

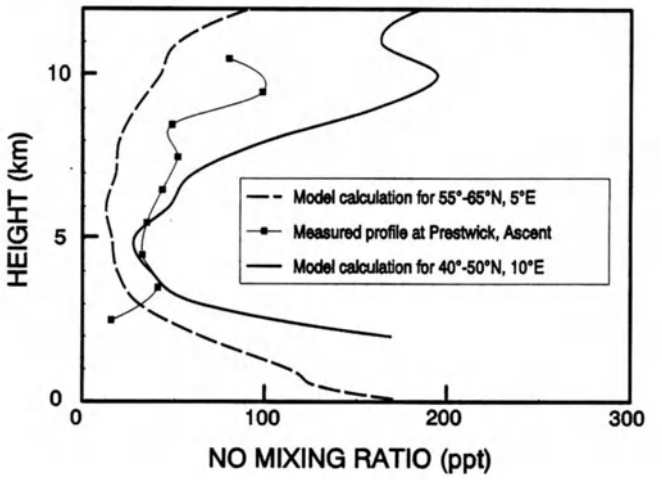

Fig. 14: Vertical profile of the NO mixing ratio. Squares: measured profile at Prestwick, ascent; solid line: model calculation for 40° - 50° N, 10° E; dashed line: model calculation for 55° - 65° N, 5° E.

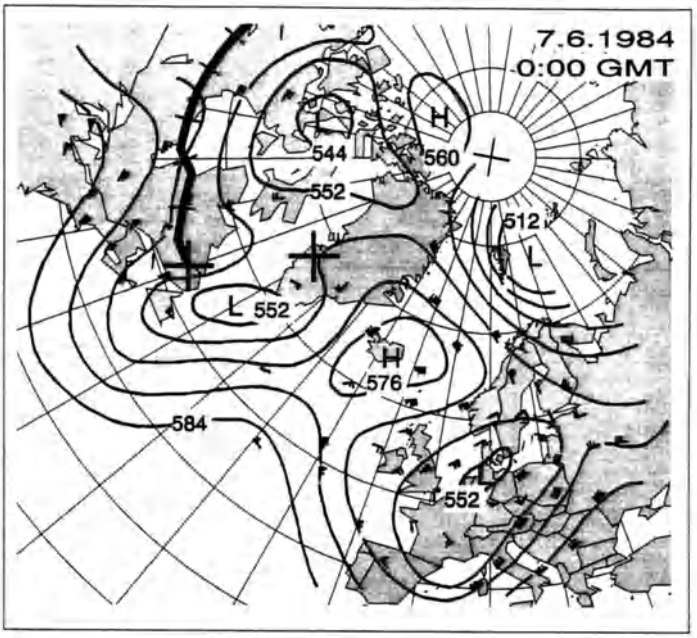

Fig. 15: Weather map at 500 hPA from June 7, 1984, 00 GMT. The bold line indicates the isobaric back trajectory for 72 hours (tick marks every 12 hours). The bold crosses indicate the location of the ascent and descent (Sondrestrom and Goose Bay).

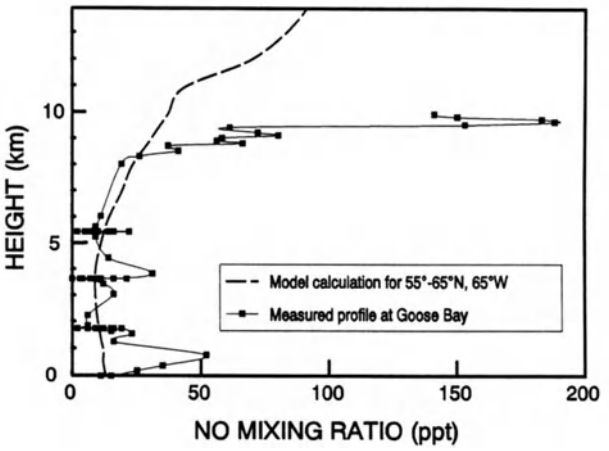

Fig. 16: Vertical profile of the NO mixing ratio. Squares: Measured profile at Goose Bay, ascent; dashed line: model calculation for 55° - 65° N, 65° W.

REFERENCES

Drummond, J. W., D. H. Ehhalt, and A. Volz, Measurements of nitric oxide between 0-12km altitude and 67° N - 60° S latitude obtained during STRATOZ III, *J. Geophys. Res.*, *93*, 15,831-15,849, 1988.

Dütsch, H. U., Vertical Ozone Distribution on a Global Scale, *Pageogh.*, *116*, 511-529, 1978.

Ehhalt, D. H., F. Rohrer, and A. Wahner, Sources and Distribution of NO_X in the Upper Troposphere at Northern Mid-Latitudes, *J. Geophys. Res. 97*, 3725-3738, 1992.

Hameed, S., and J. Dignon, Changes in the geographical distributions of global emissions of NO_X and SO_X from fossil-fuel combustion between 1966 and 1980, *Atmos. Environ.*, *22*, 441-449, 1988.

Houghton, D. D., *Handbook of applied meteorology*, Wiley, N.Y., 1985.

Iversen, T., Meterology and transport of air masses in arctic regions, this issue, 1992.

Kasting, J. F., and H. Singh, Nonmethane hydrocarbons in the troposphere: impact on the odd hydrogen and odd nitrogen chemistry, *J. Geophys. Res. 91*, 13239-13256, 1986.

Marenco, A., and F. Said, Meridional and vertical ozone distribution in the background troposphere (70° N-60° S; 0-12 km altitude) from scientific aircraft measurements during the STRATOZ III experiment (June 1984), *Atmos. Environ.*, *23*, 201-214, 1989a.

Marenco, A., M. Macaigne, and S. Prieur, Meridional and vertical CO and CH_4 distributions in the background troposphere (70° N-60° S; 0-12 km altitude) from scientific aircraft measurements during the STRATOZ III experiment (June 1984), *Atmos. Environ.*, *23*, 185-200, 1989b.

Raatz, W. F., The climatology and meteorology of Arctic air pollution, in *Pollution of the Arctic Atmosphere*, W. T. Sturges, editor, Elsevier Pub., London 1991, p 13-42.

Rudolph, J., B. Vierkorn-Rudolph, and F. X. Meixner, Large-scale distribution of peroxyacetylnitrate results from the STRATOZ III flights, *J. Geophys. Res.*, *92*, 6653-6661, 1987.

Spivakovsky, C. M., R. Yevich, J. A. Logan, S. C. Wofsy, and M. B. McElroy, Tropospheric OH in a three-dimensinal chemical tracer model: an assessmant based on observations of CH_3CCl_3, *J. Geophys. Res.*, *95*, 18441-18471, 1990.

U.S. standard atmosphere, 1976 GPO, Washington, 1976.

SPECTROSCOPIC MEASUREMENT OF BROMINE OXIDE, OZONE, AND NITROUS ACID IN ALERT

M. Hausmann, T. Rudolf, and U. Platt
Institut für Umweltphysik
Universität Heidelberg
INF 366, D-6900 Heidelberg
Germany

INTRODUCTION

Recently, episodic destruction of boundary-layer ozone has been observed in the arctic [Barrie et al., 1989, Barrie et al., 1988, Bottenheim et al., 1990, Mickle et al., 1889, Oltmans et al., 1983]. Those episodes, when ozone levels drop from the normal 30-40 ppb to unmeasurable (<3 ppb) levels, appear to be associated with high concentrations of "filterable bromine" (bromine that can be collected on cellulose filters). While it is not clear what the exact nature of filterable bromine is, it was hypothesized by several authors [Barrie et al., 1988, Bottenheim et al 1990] that the active component of filterable bromine might be BrO radicals.

Several processes have been suggested to produce BrO radicals during arctic springtime conditions:

1. Photolysis of bromoform gas ($CHBr_3$) produced biologically in the ocean [Barrie et al., 1988] form Br-atoms.
2. Formation of BrNO or $BrNO_2$ by reaction of NO_2 or N_2O_5, respectively, with NaBr contained in sea salt aerosol particles [Finlayson-Pitts et al., 1989, Finlayson-Pitts et al., 1988, Finlayson-Pitts and Johnson, 1990, Sturges, 1989]. The species BrNO and $BrNO_2$ are both rapidly photolyzed to yield Br-atoms.
3. Photochemical reaction of sea-salt Br^- on the surface of aerosol particles or snow pack to form Br_2. Br_2 would be rapidly photolyzed to from Br-atoms [McConnell et al., 1992].

Bromine atoms react rapidly with O_3 to form bromine oxide radicals. Ozone destruction would then be catalyzed by one of the following reaction cycles:

I.)

$$BrO + BrO \rightarrow 2\,Br + O_2 \quad (1)$$

$$Br + O_3 \rightarrow BrO + O_2 \quad (2)$$

net reaction: $2\,O_3\text{-}BrO_x \rightarrow 3\,O_2$ ($BrO_x = BrO + Br$)

NATO ASI Series, Vol. I 7
The Tropospheric Chemistry of Ozone in the Polar Regions
Edited by H. Niki and K. H. Becker

II.)

$$BrO + HO_2 \rightarrow BrOH + O_2 \quad (3)$$

$$BrOH + h\nu \rightarrow Br + OH \quad (4)$$

$$Br + O_3 \rightarrow BrO + O_2 \quad (5)$$

$$OH + O_3 \rightarrow HO_2 + O_2 \quad (6)$$

net reaction: $2\,O_3 \rightarrow BrO_X, HO_X \rightarrow 3\,O_2$

Reactions of Br-atoms with HO_2 or HCHO would rapidly convert BrO_X to HBr:

$$Br + HO_2 \rightarrow HBr + O_2 \quad (7)$$

$$Br + HCHO \rightarrow HBr + CHO \quad (8)$$

thus, deactivating the "catalyst" BrO_X. Ultimately, the extent of ozone destruction will not only depend on the magnitude of the BrO_X source, but also on the efficiency of reactions reconverting HBr to BrO_X. The homogeneous reaction:

$$HBr + OH \ -h\nu \rightarrow Br + H_2O$$

would be slow at the low OH concentrations expected for arctic sunrise conditions. Therefore, following Duce et al. [1965], McConnell et al. [1992] suggested a heterogeneous mechanism, that can be summarized as:

$$4\,Br^- + O_2 + 4\,H^+ - h\nu \rightarrow 2\,Br_2 + 2\,H_2O$$

In this way BrO_X levels would be maintained at relatively high levels.

Direct identification of BrO under arctic sunrise conditions are, therefore, a critical test of the theories described above. To date, differential optical absorption spectrometry appears to be the only technique to detect specifically BrO in the free atmosphere.

In this manuscript we describe direct measurements of BrO made during April 1992 in the arctic by long path differential optical absorption spectroscopy (LP-DOAS) during the Polar Sunrise Experiment 1992 [Barrie et al., 1991]. A novel design of a LP-DOAS instrument was used.

EXPERIMENTAL

Measurement site: The measurements were carried out in the north Canadian arctic at the station of Alert (82.3°, 62.2° W). It is sited at the shore of the arctic ocean, 850 km from the north pole (Figure 1a). During the period described here from April 1 to April 22,

1992 the sun was above the horizon all day, but shaded by the mountain range in the west for about 4 hours per day.

To avoid contamination of the measurements by local air pollution, the experiment was installed in a laboratory container located about 7 km to the south of the Alert camp (Figure 1b).

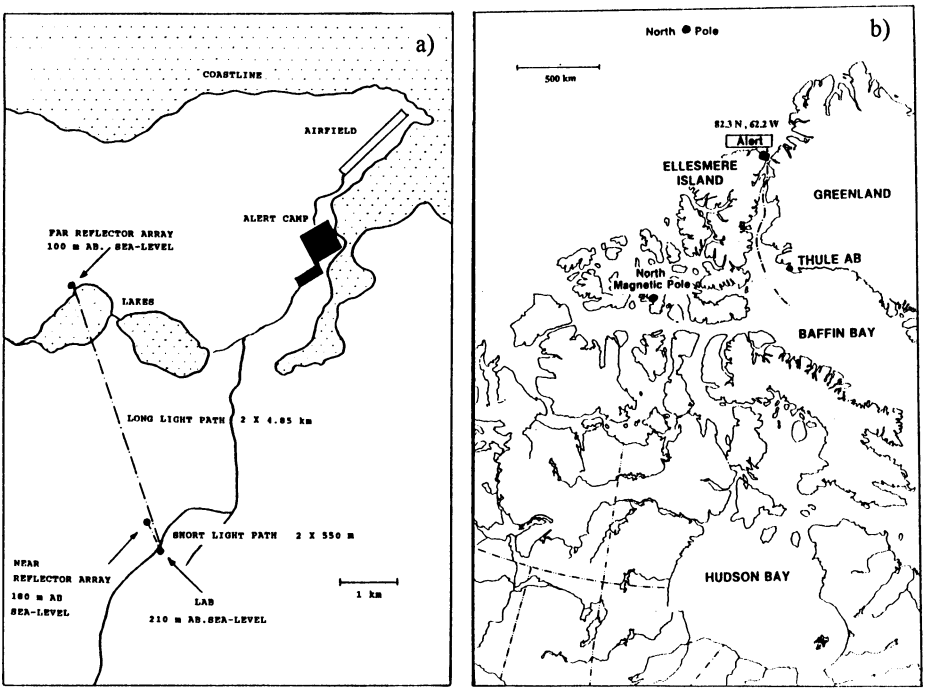

Fig. 1: Panel a: Light path arrangement at the Alert Measurement site. Panel b: Location of the Alert station 82.3° N, 62.2° W

Coaxial long path DOAS system: We used a new design of a DOAS spectrometer, which is based on the principle of Platt and Perner [1983]. In contrast to the classic design, with search light type light source and spectrometer, at either end of the light path, respectively, here a design of two coaxially arranged Newton type telescopes [Axelson et al., 1990] in combination with retroreflector arrays to send and receive the light beam (Figure 2) are used. A Xenon arc lamp (XBO 450) is mounted in the focus of a parabolic mirror (F = 600 mm). The outer ring-shaped part of the parabolic mirror is used to send the light to retroreflector array (Figure 2), and the inner part is used for reception of the reflected beam. The light beam is sent to a retroreflector array. In Alert, two retroreflector arrays were

mounted on small towers (ca. 3 m high) outside the camp. One array with 24 retroreflector prisms, each 60 mm in diameter, was sited at 4.85 km distance, a second array with two retroreflectors of the same diameter was mounted at 550 m distance. Thus, two light paths of 9.7 km and 1.1 km, respectively, were available. The received light is focused into quartz fiber bundle consisting of seven single fibers (135 μm diameter each), with a hexagonal arrangement at the entrance and an arrangement in a vertical row at the exit.

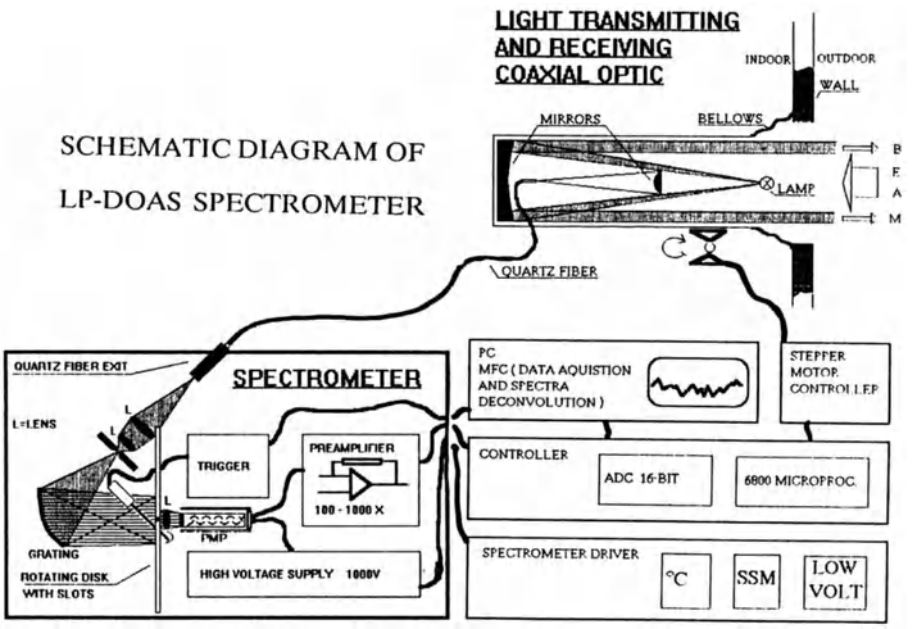

Fig. 2: Schematic diagram of the Long Path Differential Optical Absorption Spectrometer (LP-DOAS).

To optimize the alignment of the beam, the whole telescope arrangement is mounted in a frame which can be moved in horizontal and vertical direction by two stepper motors. The light intensity can be optimized by the measurement program running on a personal computer. It allows to align the light beam (to a maximum intensity of the received light) by an automatic program routine. The reflector arrays need neither precise adjustment nor readjustment. Beside this, they require no power supply, which is important in a remote area. Thus, the coaxial light beam configuration has practical advantages in comparison to the standard LP-DOAS light beam setup, where the sending part (search light) and the receiving part (simple Newton type telescope) are separated [Platt and Perner, 1983].

The spectrometer uses a holographic flat field grating, a slotted disc as scanning device, and a photomultiplier as detector (Figure 2). The spectral resolution applied in Alert was about 1.0 nm and the spectral range from 320 nm to 386 nm was scanned. The light is entered into the spectrometer via the quartz fiber bundle. To adapt the aperture of the fibers (F 7.5) to the spectrometer (F 2.7), the exit of the fiber bundle is imaged on the entrance slit of the spectrometer by a pair of quartz lenses.

The optical system was developed to reduce the most important optical secondary effects affecting the quality of the spectrometer. Those include: the internal stray light of the spectrometer, the so called re-entry spectra of the spectrometer, the other order spectra of the diffraction grating, and the varying illumination of the spectrometer aperture, caused by the turbulence of the atmosphere. The two lenses imaging the exit of the fiber bundle on the entrance slit have the additional function of a pre-dispersive element. Due to the chromatic aberrations of the lenses, there is one wavelength only, which is focussed best on the entrance slit. This causes an attenuation on the light flux entering the spectrometer outside the scanned wavelength range, and thus a reduction of the internal stray light. Re-entry spectra are avoided by arranging the optical components (surfaces) in a way that the other order spectra will not illuminate the grating a second time via reflections on the optical components [Pierson and Goldstein, 1989]. To attenuate diffuse scattering of other order spectra of the grating, the spectrometer is equipped with light absorbing internal surfaces. In particular, the zero order of the grating is attenuated in a Woods horn type arrangement. The variation of the illumination of the aperture of the spectrometer is reduced by the introduction of the quartz fiber.

Measurements: The instrument was operational during April 2 to 21, 1992. However, frequent occurrence of poor visibility due to ice-fog formation, as well as frost deposition on the retroreflector prisms allowed measurements only less than 50% of the time (cf. Figure 5). Even when measurements were possible, sometimes poor visibility and thus low received light levels made extremely long integration times (up to 30 hours) necessary. The measurements were running in the following sequence: first, the signal over the 9.7 Km light path was integrated for 4 minutes, and then a background signal was recorded for 1 min. Next, the signal over the 1.1 km light path was integrated for one minute and a next background signal was recorded for 15 seconds. This sequence was repeated continually during the regular run.

DATA EVALUATION

Within the indicated spectral range there are strong absorption bands of O_3, BrO, HONO, and CH_2O (see Figure 3). The data were evaluated according to the usual DOAS procedures [Platt and Perner, 1983]. Relatively strong instrument-generated fixed structures due to problems (meanwhile solved) with the new optical design appeared in the spectra . In order to remove the instrument structure, ratios of spectra taken in sequence at 9.7 Km and 1.1 km light path were formed. Thus, the yielding spectra, which were essentially (but not completely) free of the above structure, with an effective light path length of 8.6 Km. To record the pure instrument structure a lamp was placed in front of the quartz fiber entrance. Thus, the gained spectrum was later used to be fitted to the air spectra (see below). Furthermore, a high path filtering process was applied. The usually performed method to divide the measured spectra by a fitted polynomial of suitable (usually fifth) order, was replaced by a process based on division by digitally smoothed spectra.

To record the relative reference spectrum of ozone and formaldehyde by the spectrometer a quartz cell, filled with the respective trace gas, was placed in front of the entrance of the quartz fiber bundle. The reference spectra of BrO and HONO were prepared by degrading the cross section spectra by Wahner et al. [1988] and Bongartz et al. [1991], respectively, to the dispersion and the spectral resolution of the spectrometer. The reference spectra and the instrument structure were subjected to the same high pass filtering process as the air spectra. This procedure yielded a differential absorption cross section for 339 nm band of 7.89×10^{-18} cm^{-2} for BrO and 3.62×10^{-19} cm^{-2} for HONO. Due to the variability of the air temperature during the measurements between 235 K and 254 K, an accuracy of BrO cross section of ±5 % had to be taken into account. The HONO cross section was referred to 277 K. The resulting spectra were then evaluated for BrO, O_3, and HONO by fitting the respective reference spectra. The BrO and O_3 reference spectra and the instrument structure were fitted simultaneously.

A sample spectrum for this case is shown in Figure 3, Panel (a),. The upper trace shows an air spectrum (high pass filtered in the way described above) and a superimposed fit of BrO, O_3 and the instrument structure (smooth line) within the wavelength limits of 325 nm to 355 nm. This example demonstrates that the particular absorption spectrum of the individual trace gases can be found: The center trace of Panel (a) shows the air spectrum after dividing it by the simultaneously fitted O_3 spectrum and instrument structure only (noisy line), superimposed by the fitted BrO spectrum (smooth line). The equivalent for O_3, after dividing the air spectrum by the fitted BrO spectrum and instrument structure, is shown in the bottom trace. The corresponding concentrations are 13 ppt for BrO and 22 ppb for O_3, respectively. From this example it can be seen that when absorption structures of both O_3 and BrO were found, it was possible to distinguish very well between O3 and BrO. Six

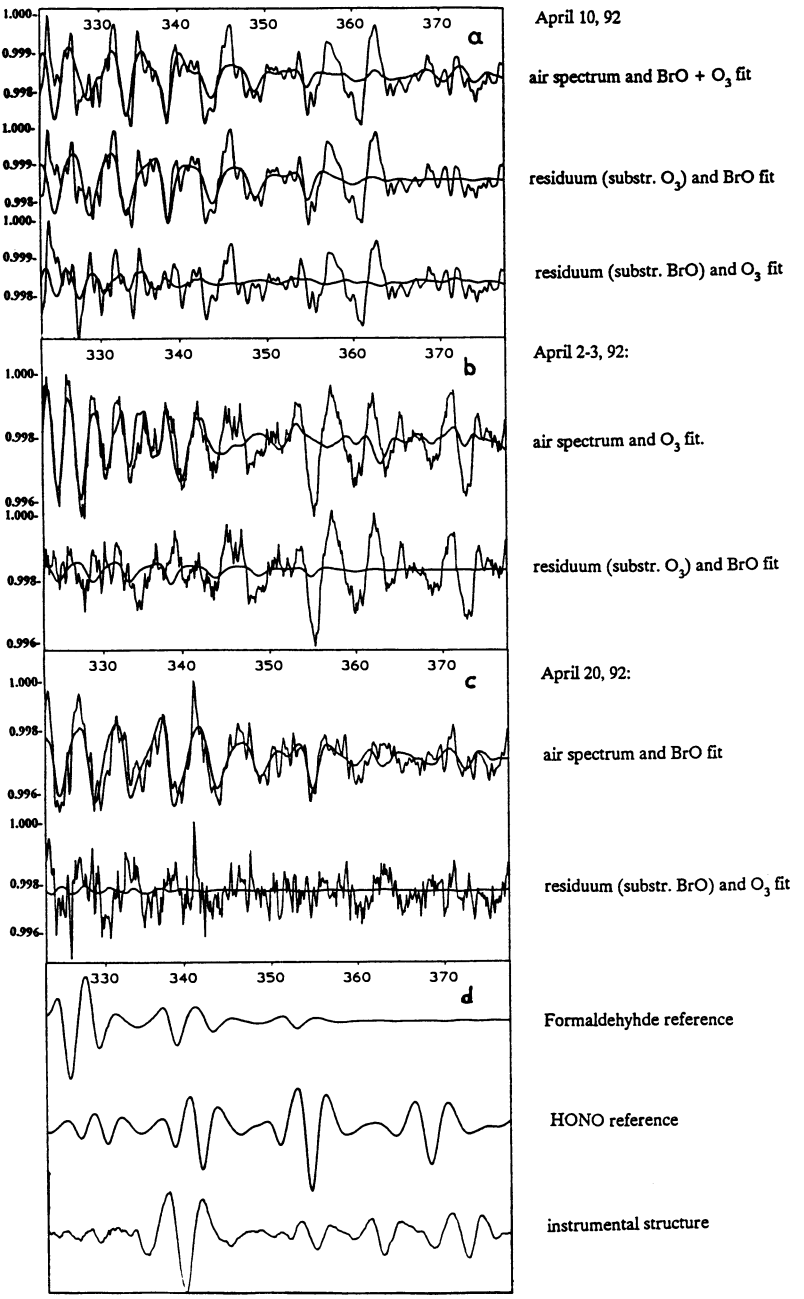

Fig. 3: Examples of measured long path air absorption spectra: (Continued on next page)

Panel (a)

Upper trace: Air absorption spectrum (noisy line) taken on April 10, 1992, overlaid by a spectrum obtained by simultaneous fit of BrO- and O_3- reference spectra and residual instrument spectrum (smooth line).

Center trace: Residuum of the air absorption spectrum after subtracting the fitted ozone spectrum and instrument structure, overlaid by the fitted BrO spectrum. The absorption structures corresponds 13 ppt BrO.

Bottom trace: Residuum of the air absorption spectrum after subtracting the fitted BrO- reference spectrum and the instrument structure, overlaid by the fitted ozone reference spectrum. The absorption structures corresponds 22 ppb O_3.

Panel (b):

Upper trace: Air absorption spectrum taken on April 2-3, 1992, overlaid by the fitted ozone reference- and instrument spectrum (smooth curve). The absorption structures correspond to 39 ppb ozone

Lower Trace: Residuum of air spectrum after subtracting the fitted ozone reference spectrum and the instrument spectrum, overlaid by the fitted BrO reference spectrum (smooth curve). An upper limit for BrO of about 4 ppt is deduced.

Panel (c):

Upper trace: Air absorption spectrum taken on April 20, 1992, overlaid by the fitted BrO reference spectrum and the instrument spectrum. The absorption structure corresponds to about 17 ppt BrO.

Bottom trace: Residuum of air spectrum after subtracting the fitted BrO reference and the instrument spectrum, overlaid by the fitted ozone reference spectrum. No ozone absorption can be found.

Panel (d):

High pass filtered reference spectra of formaldehyde (upper trace), HONO (center trace), and residual instrumental structure (bottom trace).

characteristic absorption bands of BrO between 328 nm and 358 nm were included in the fit, while for O_3 five bands between 323 nm and 338 nm were used.

In Panel (b) an example of an air spectrum with high ozone concentration (39 ppb) and BrO concentration below the detection limits is given. The upper trace represents the air spectrum, superimposed by the simultaneously fitted ozone spectrum and instrument structure (smooth line). The bottom trace shows the residuum of the air spectrum after dividing it by the fitted spectra. A fitted BrO reference spectrum is superimposed, indicating the upper BrO limit of about 4 ppt.

In Panel (c), the example of the strongest BrO absorption found is given. The upper

trace in Panel (c) shows the air spectrum superimposed with a BrO spectrum (smooth line), the clearly visible absorption structure corresponds to about 17 ppt BrO. In the residuum (bottom trace) the fit of an ozone reference spectrum (showing no correlation) corresponds to a limit of about 4 ppb ozone concentration.

After dividing all air spectra by the fitted corresponding reference spectra, the residual spectra thus obtained were used to calculate absorption by HONO. Large residual structures appeared within the wavelength region of the strong HONO absorption bands between 353 nm and 378 nm. They show distinctive bands of varying strength at 355 nm, 360 nm, and 372 nm which are not yet identified. Thus, for the HONO concentration only upper limits can be given.

In Figure 3, Panel (d) the reference spectra of CH_2O (upper trace) HONO (center trace) and instrument structure (bottom trace) are shown.

RESULTS AND DISCUSSION

Figure 4 shows the comparison of ozone concentrations measured in-situ by a short path UV-absorption instrument (TECO 409) [Anlauf,1992] with the DOAS results. The data agree within a few ppb, indicating quite homogeneous air masses over the 4.85 km separation between the spectrometer and the retroreflectors (at least with respect to ozone). In Figure 5, time series of BrO, O_3, and HONO are shown. Bromine oxide levels range from the detection limit of roughly 3 ppt up to a maximum of about 17 ppt. Presently, only upper limits ranging from about 16 ppt to 240 ppt can be given for HONO (see above).

Interestingly, there seems to be no negative correlation between ozone and BrO (see Figure 6), as was found during earlier measurements for filterable bromine [Barrie et al., 1988]. Moreover, preliminary calculations indicate that the observed BrO levels are probably too low to cause rapid ozone loss.

Using the BrO self reaction scheme (cycle I) the ozone lifetime can be calculated as:

$$\tau_{O_3} = [O_3]/2k_1[BrO]^2$$

taking reaction (1) as rate limiting step, where k1 = 3.2 10^{-12} cm^3 s^{-1} [Le Bras, 1992]. Figure 7 shows the ozone lifetime as a function of the BrO concentration (solid line) for $[O_3]$ = 1 10^{12} cm^{-3} (33 ppt at 244 K). According to this reaction scheme, the typical BrO concentration values of 1 10^8 cm^{-3} to 5 10^8 cm^{-3} (roughly 3.5 ppt to 17 ppt) correspond to ozone lifetimes of about 181 days to 7 days. However, as shown in Figure 4, the ozone does disappear within a few hours or less. For the typical observed ozone depletion times of a few hours a BrO concentration of about 4 10^9 cm^{-3} (120 ppt) would be necessary. A model run

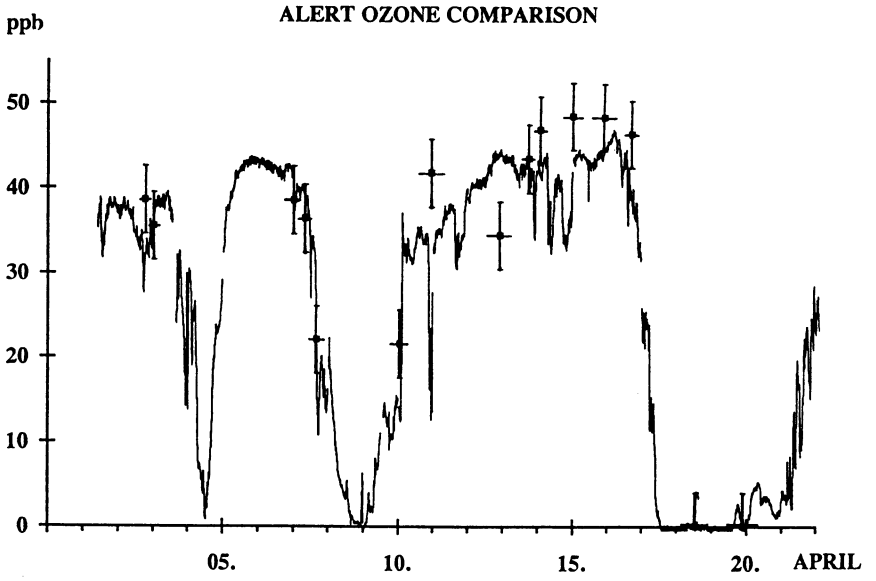

Fig. 4: Comparison of ozone concentrations measured in-situ by a short path UV-absorption instrument [Anlauf, 1992] (drawn line) and LP-DOAS (crosses), respectively. Time scale: tic marks indicate 000 local time (GMT plus 4 hours).

for cycle I, using the starting condition of a high BrO level ($[BrO]_0 = 4.5\ 10^9\ cm^{-3}$), gave the ozone half-life of about 1.5 hours, as shown in Figure 8. It is interesting that BrO should only exist during the time span of $d[O_3]/dt < 0$, because the reaction of ozone with Br atoms (reaction (2)) will produce BrO only as long as sufficient ozone is available. As soon as the BrO destruction by the fast BrO self reaction (1) will dominate the weakened BrO production (reaction (2)), the BrO concentration will sink rapidly to the favour of the formation of Br atoms (converting to Br_2 and further bromine compounds). Of course, before the ozone depletion has started, no Br atoms and thus no BrO are expected to be present. This means that BrO can only be measured during the decreasing period of ozone for about 1 to 3 hours or possibly less, due to the fact that the ozone depletion events occurred in a kind of fast collapsing spikes. However, during the depletion of ozone very high BrO levels of $5\ 10^9\ cm^{-3}$ and more should be found. As mentioned above, high integration times of a few hours were necessary to detect BrO. Thus, short periods of high BrO could have been averaged out. Since all measurements were composed of 20 minutes observations, such

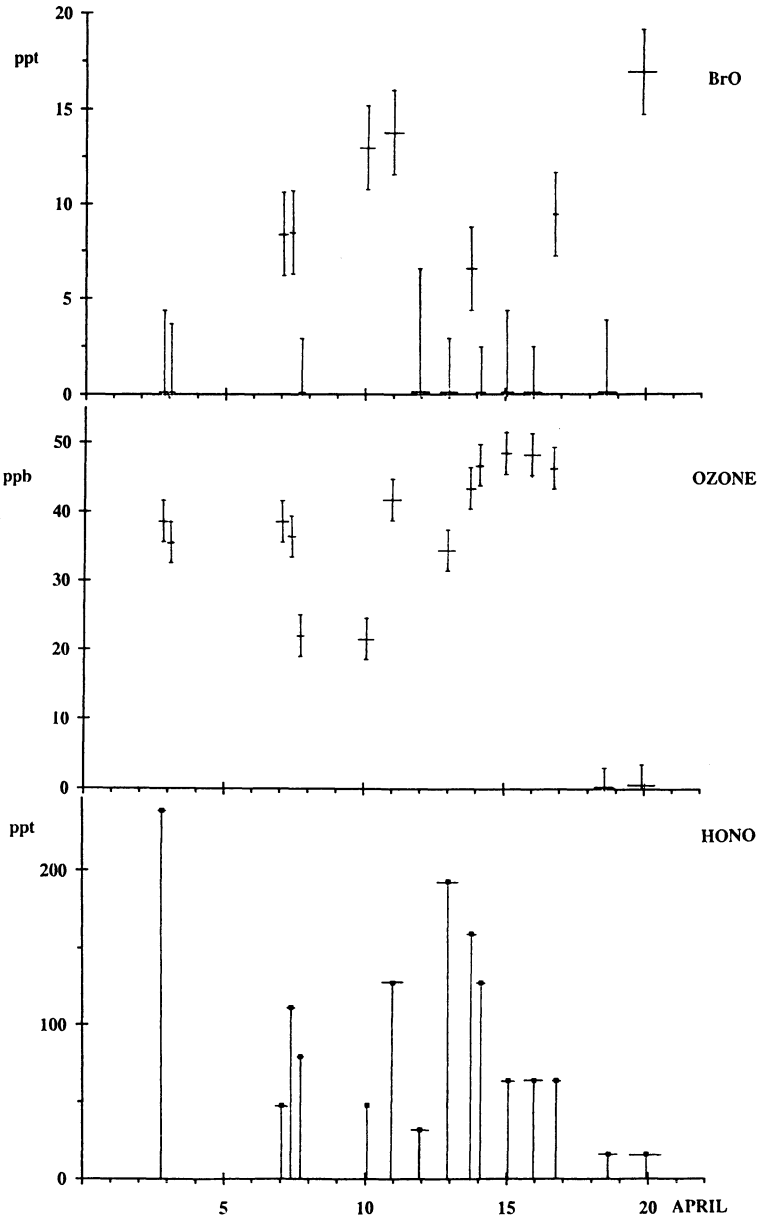

Fig. 5: Long path measurements of BrO (a), O3 (b), and HONO (c) concentrations. HONO data are upper limits only. Time scale: tic marks indicate 000 local time (GMT plus 4 hours).

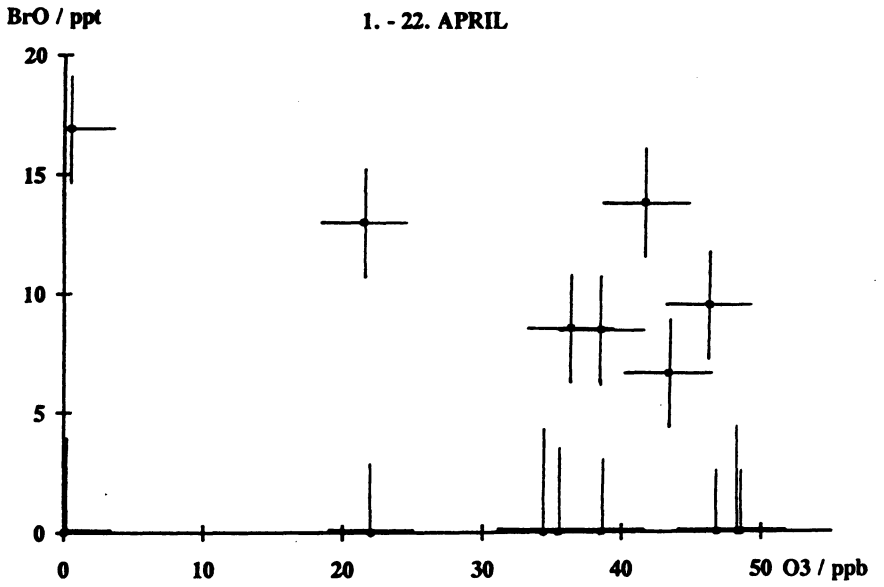

Fig. 6: Plot of BrO versus O_3 concentrations as measured by DOAS

high BrO levels would have been found at least in the individual spectra. Another aspect of this reaction mechanism can be shown for the measurements of April 19 to April 20, where the highest BrO level of 5.1 10^8 cm^{-3} (17 ppt) and the simultaneous ozone concentration limit of 1.1 10^{11} (3.6 ppb) were found. Namely, the ozone was depleted (April 18 to April 19) the BrO was expected to stay low. But, only little ozone is necessary to yield the observed BrO concentration, because of the relationship:

$$[BrO] = (0.5[Br][O_3]k_2/k_1])^{1/2}$$

Thus, we conclude that the observed ozone depletion could only be explained by reaction cycle I if the reported reaction constant k_1 is reported too small by a factor of about 100, which should be considered highly unlikely.

Using the reaction cycle II (BrO + HO_2 - scheme), the ozone lifetime can be calculated as:

$$\tau_{O_3} = [O_3]/k_3[BrO][HO_2]$$

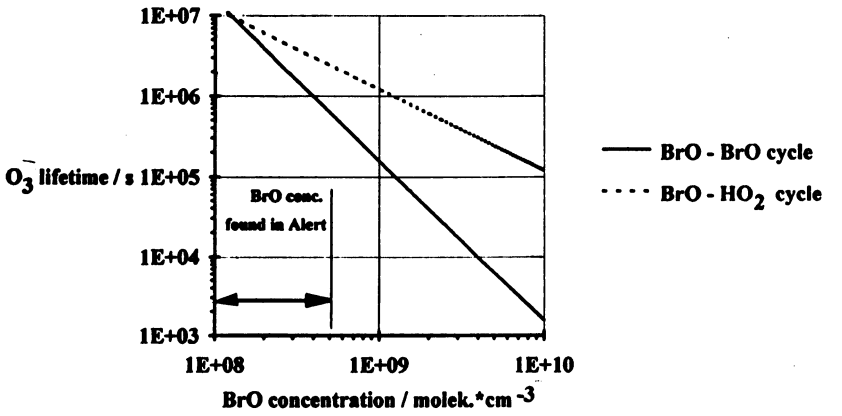

Fig. 7: Ozone lifetime for reaction cycle I (solid line) and cycle II (dotted line). $[O_3]$ = 1 x 10^{12} cm^{-3} (see text).

taking reaction (3) as rate limiting step, where k_3 = 3.3 10^{-11} cm^3 s^{-1} [Le Bras, 1992]. Figure 7 shows the ozone lifetime as a function of the BrO concentration (dotted line) for $[O_3]$ = 1 10^{12} cm^{-3} (33 ppt) and $[HO_2]$ = 2.5 x 10^7 cm^{-3} (0.8 ppt). The ozone lifetime corresponding to this scheme is even longer than the results of cycle I. Furthermore, as mentioned above, additional competitive reactions of Br with HO_2 and HCHO (reaction (7) and (8)) have to be taken into consideration. Thus, cycle II as well does not seem to be able to explain the observed ozone depletion.

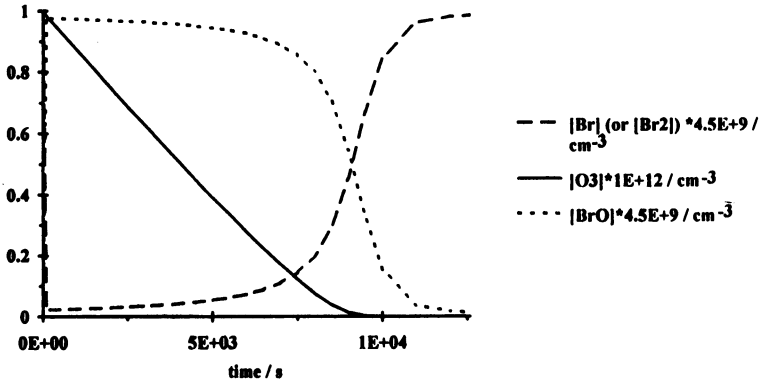

Fig. 8: Model calculation of the development of the O_3, BrO, and Br concentration using reaction scheme I. The initial concentrations were $[O_3]$ = 1 x 10^{12} cm^{-3}, [BrO] = 0, and [Br] = 4.5 x 10^9 cm^{-3}, respectively.

However, it appears that ice-fog formation and thus low visibility coincides with periods of low ozone concentration. Therefore, measurements of BrO during times of low ozone could only rarely be made. More measurements are clearly needed before firm conclusions about the involvement of BrO in ozone destruction can be drawn.

Acknowledgements: The authors thank Barrie and Bottenheim of Atmospheric Environment Service (AES, Downsview, Ontario) for there particular help performing this experiment. A special thank to Anlauf (AES) for making his ozone data at our disposal. The financial support within the framework of the intergovernmental agreement on scientific and technological cooperation between Canada and Germany is also grateful acknowledged.

REFERENCES

Anlauf, K., Atmospheric Environment Service, Downsview Ontario, personal communication, 1992.

Axelson, H., B. Galle, K.Gustavsson, P. Ragnarsson, and M. Rudin, A transmitting / receiving telescope for DOAS-measurements using retroreflector technique, *Techn. Dig. Series* 4, 641 - 644, 1990.

Barrie, L., J. Bottenheim, R. Leaitch, W. Hart, and N. Trivet, Polar sunrise experiment 1992 - a proposal, Atmospheric Environment Service, Ontario Canada, 1991.

Barrie, L.A., G. Den Hartog, J.W. Bottenheim, and S. Landsberger, Anthropogenic aerosols and gases in the lower troposphere at Alert, Canada in April 1986, *J. Atmos. Chem.* 9, 101-127, 1989.

Barrie L.A., J.W. Bottenheim, R.C. Shnell, P.J. Crutzen and R.A. Rasmussen, Ozone destruction and photochemical reactions at polar sunrise in the lower Arctic atmosphere, *Nature* 334, 138-141, 1988.

Bongartz, A., J. Kames, F. Welter, and U. Schuhrath, Near-UV absorption cross section and trans/cis equilibrium of nitrous acid, *J. Phys. Chem* 95, 1076 - 1082, 1991.

Bottenheim, J.W., L. Barrie, E. Atlas, L.E. Heidt, H. Niki, R.A. Rasmussen, and P.B. Shepson, Depletion of lower tropospheric ozone during Arctic spring: The Polar Sunrise Experiment 1988, *J. Geophys. Res.* 95, 18555 - 18568, 1990.

Duce, R. A., J. Winchester, and T.W. Van Nah, Iodine, bromine, and chlorine in the Hawaiian marine atmosphere, *J. Geophys. Res.* 70, 1775 - 1799, 1965.

Finlayson-Pitts, B. J., M.J. Ezell. and J.N Pitts, Formation of chemically active chlorine compounds by reactions of atmospheric NaCl particles with gaseous N_2O_5 and $ClONO_2$, *Nature* 337, 241-244, 1989.

Finlayson-Pitts, B. J. and S.N. Johnson, The reaction of NO_2 with NaBr: Possible source of BrNO in polluted marine atmospheres, *Atmos. Environ.* 22, 1107 - 1112, 1988.

Finlayson-Pitts, B. J., F.E. Livingston, and H.N. Berko, Ozone destruction and bromine photochemistry in the Arctic spring, *Nature.* 343, 622 - 625, 1990.

Le Bras, G., Reaction of BrO radicals relevant to polar chemistry, presented at the *NATO Advanced Research Workshop*: The tropospheric chemistry of ozone in the polar regions, August 1992, Nova Scotia, 1992.

McConnell, J. C., G.S. Henderson, L. Barrie, J. Bottenheim, H. Niki, C.H. Langford and

E.M.J. Templeton, Photochemical bromine production implicated in Arctic boundary-layer ozone depletion, *Nature* 355, 150-152, 1992.

Mickle, R. E., J.W. Bottenheim, R.W. Leaitch and W. Evans, Boundary layer ozone depletion during AGASP-II, *Atmos. Environ.* 23, 2443 - 2449, 1989.

Oltmans, S.J., P.J. Sheridan, R.C. Schnell, R.E. Peterson , J.W. Winchester, L.A. Barrie, J.D. Kahl, and W.D. Komhyr, Springtime Surface Ozone Fluctuations at High Arctic Latitudes and Their Possible Relationship to Atmospheric Bromine. *Ozone in the Atmosphere, Proc. of the Quadrennial Ozone Symposium 1988* (edited by Bojkov R. D. and Fabian P.), pp. 498-501 Deepak Publishing, Hampton, 1989.

Platt, U., and D. Perner, Measurements of atmospheric trace gases by long path differential UV/visible absorption spectroscopy, *Optical and Laser Remote Sensing* (edited by Killinger D. K. and Mooradien A.), pp. 95-105, vol. 39 Springer Ser. Optical Sci., 1983.

Platt, U., Perner D. and H. Paetz, Simultaneous measurement of atmospheric CH_2O, O_3, and NO_2 by differential optical absorption, *J. Geophys. Res.* 84, 6329-6335, 1979.

Pierson, A., and J. Goldstein, Stray light in spectrometers: Causes and Cures, *Lasers & Optics,* Sep. issue, 67 - 74, 1989.

Sturges, W. T., Comment on the paper by Finlayson Pitts and Johnson, *Atmos. Environ.* 23, 1167 - 1168, 1989.

Wahner, A., A.R. Ravishankara, S.P. Sander R.R. Friedl, Absorption cross section of BrO between 312 and 385 nm at 298 and 223 K, *Chem. Phys. Lett.* 152, 6, 507 - 512, 1988.

ICE CORE ANALYSIS IN ARCTIC AND ANTARCTIC REGIONS

M. Legrand
Laboratoire de Glaciologie et Géophysique
de l'Environnement du CNRS
B.P. 96, 38402, St Martin d'Hères
Cédex, France.

INTRODUCTION

The relative remoteness of continental polar regions from natural and anthropogenic sources of various chemicals suggests that their atmosphere represents the best present-day example of the "background atmosphere" for their respective hemispheres and are, therefore, very sensitive to any natural and/or anthropogenic changes. Due to their distinct seasonal cycle with a long polar night and their very cold temperatures, polar regions can be considered as a kind of "giant natural laboratory", in which it is probably much simpler than elsewhere to check the complex chemistry governing major biogenic cycles (S, N and C). Furthermore, a unique specificity of polar regions comes from the desposition of solid particles accumulated on polar ice sheets, which offers the possibility to reconstruct the paleoenvironnement of the Earth back to several hundred thousands years.

Over the last decades, international programs have extracted ice cores from Greenland and Antarctica which contain detailed records concerning past climate, trace gas content of the atmosphere and precipitation chemistry. Studies of the ice chemistry and the interpretation of these records in terms of the composition of the atmosphere have opened up a powerful new scientific field called "glaciochemistry". Such studies started rather slowly due to technical difficulties associated with both the low detection limits and the contamination control required when working at the low levels characteristic of polar precipitation samples. A second problem concerns the lack of physical understanding of how trace airborne chemicals are incorporated into snow, which can limit the interpretation of data in terms of atmospheric chemistry.

In this paper, we present the state-of-the-art glaciochemistry, focusing mainly on the soluble mineral species (Na^+, NH_4^+, K^+, Ca^{++}, Mg^{++}, H^+, F^-, Cl^-, NO_3^- and SO_4^{--}) and some light carboxylates. After a brief overview of contamination control techniques of trace measurements, we discuss the basics of the ionic composition of snow as well as the origins and sources of these chemicals in polar regions. Then, we discuss what we have learned from such glaciochemical studies. First, we discuss the glaciochemistry of primary aerosols (sea salt and terrestrial compounds), in particular their response to large climatic changes which have occurred in the past. Second, we discuss the glaciochemistry of the secondary sulphur

NATO ASI Series, Vol. I 7
The Tropospheric Chemistry of Ozone in the Polar Regions
Edited by H. Niki and K. H. Becker

aerosols (e.g., aerosol produced during gas-to-particle conversion) and the modulation of its budget by both large volcanic eruptions and marine biogenic emissions. Third, we discuss NO_3^- ice core data in terms of the atmospheric N-cycle (i.e., contribution of various sources to its budget, anthropogenic influence via acidification of precipitation or recent "ozone hole"), and we point out that some difficulties exist because HNO_3 is not irreversibly trapped in snow layers. Finally, we show that Greenland precipitation exhibits some large increases in NH_4^+ and organic acid contents in narrow layers, suggesting that the atmosphere in high northern latitudes have been disturbed by strong inputs originating from high latitudes forest fires.

STATE-OF-THE ART IN GLACIOCHEMICAL STUDIES

Dating of snow layers: Various methods which depending on the accuracy required, the time period considered and the location (e.g., high or low accumulation rates), can be used to provide dating of depth profiles. First of all, numerous stratigraphical methods based on the seasonal changes in the isotopic composition of the ice or in the content of various chemical species (e.g., sea salt, H_2O_2, and acidic species) may be used to establish accurate dating of ice cores [Hammer, 1989]. This technique can fail, however, due to either a too small accumulation rate or the smoothing with depth of the initial concentrations, such as the isotopic composition of water [Johnson, 1977) and the H_2O_2 content [Sigg and Neftel, 1991].

Some large and well-documented atmospheric perturbations that have taken place in the past can be used as "reference horizons". For instance, the spread of radioactive debris over the entire world via the stratosphere has served as a reference for dating snow layers deposited in 1955 and 1965 [Piccioto and Wilgain, 1963]. Similarly, large volcanic injections of SO_2 in the atmosphere provide numerous acidic reference layers in Antarctica [Legrand and Delmas, 1987] and Greenland [Lyons et al., 1990; Hammer, 1989] to date ice cores over the last thousands of years. Along deep ice cores, chronological information is obtained by comparing isotopic profile features reflecting great climatic changes both in ice and in sea sediments.

Analytical procedures: Comprehensive studies of the soluble species trapped in snow layers require two analytical techniques. Ion chromatography is used to determine Na^+, NH_4^+, K^+, Ca^{++}, Mg^{++}, F^-, Cl^-, NO_3^-, SO_4^{--} and light carboxylates. This technique is sensitive enough to detect ppb (ng/g) and sometimes sub-ppb level even using a very small sample volume (5 ml). The H^+ content of melted ice is determined by using an acid titration method which prevents samples from contamination by the CO_2 dissolution during the melting step [Legrand et al., 1982].

Referring to the low level samples employed for characterizing polar precipitations, it appears important to discuss briefly the contamination control. First, ice cores have generally been contaminated in their outside surfaces during the drilling procedure. Decontamination of ice core sections were often successfully performed by washing and melting the ice with ultra-pure water [Finkel and Langway, 1985, Legrand et al., 1984] in studying mineral species. However, as recently pointed out by Legrand et al. (1992), such a technique causes problems when measuring the $CH_3SO_3^-$ content of the ice. Subsequently, we designed an ice core lathe to remove mechanically the outer part of ice cores in a cold room and experiments showed this procedure was successful for mineral as well as for organic species determinations.

Since some species of interest are present in the ambient air of our laboratories in the gas phase, special cautions have to be taken when melting the samples. Indeed, the concentration of NH_4^+ [Legrand et al., 1984], $HCOO^-$ and CH_3COO^- [Legrand and Saigne, 1988] of ultra-pure samples exposed to the atmosphere within a clean air bench increased dramatically within few hours relative to the expected levels of polar precipitation. To prevent the samples from such a rapid contamination, we therefore put decontaminated ice samples in air-tight bottles kept closed during the melting step.

Achievement and significance of the ionic balance: Various water-soluble chemical compounds are expected to be trapped in snow layers (Figure 1), including those compounds found in sea salt which are emitted by oceans surrounding the ice sheets. Soil-derived particles emitted from continental areas provide soluble species such as Ca^{++}, CO_3^{--}, SO_4^{--} and Mg^{++}. Aside from these two primary aerosol inputs, the photochemical oxidation of various trace gases emitted by the marine and continental biosphere and more recently by human activities provide numerous secondary aerosol and gaseous species which can be trapped in snow layers. Based on this picture, it appears that although the Al content of snow can be useful to trace back the dust content of the past atmosphere, the problem concerning major ions is more complex. For instance, SO_4^{--} present in polar ice corresponds to inputs of various chemical compounds ($CaSO_4$, Na_2SO_4 or H_2SO_4) from various sources (oceans, continents and biogenic emissions). This example illustrates the need to perform a comprehensive study of soluble species in order to be able to reconstruct the initial association between the ions and subsequently, to discuss these data in terms of origins and sources.

In antarctic ice on which comprehensive studies of ionic species have been conducted [Legrand, 1987; Mulvaney and Peel, 1988], the imbalance ΔC between cations and anions represents less than 5% of the ionic budget (in μEq/l units):

$$\Delta C = [Na^+] + [NH_4^+] + [K^+] + [H^+] + [Ca^{++}] + [Mg^{++}] - [F^-] - [Cl^-] - [NO_3^-] - [SO_4^{--}] - [CH_3SO_3^-] - [HCOO^-] - [CH_3COO^-] \quad (1)$$

$$\Sigma = [Na^+] + [NH_4^+] + [K^+] + [H^+] + [Ca^{++}] + [Mg^{++}] + [F^-] + [Cl^-] + [NO_3^-] + [SO_4^{--}] + [CH_3SO_3^-] + [HCOO^-] + [CH_3COO^-] \quad (2)$$

Na^+, H^+, Ca^{++}, Mg^{++}, Cl^-, NO_3^- and SO_4^{--} represent major ions present in ice deposited in central antarctic regions under present climatic conditions as well as during past colder climate (Figure 2a and 2d). NH_4^+, $CH_3SO_3^-$ and K^+ represent a weak contribution (0.2 μEq/l) as compared with the total ionic budget ($5\Sigma = 30$ μEq/l). F^- and carboxylates provide an insignificant part of the ionic budget [Saigne et al., 1987; Legrand and Saigne, 1988]. The balance $\Delta C=0$ achieved between cations and anions of the antarctic ice can be expressed by the following equation:

$$[Na^+] + [Mg^{++}] + [Ca^{++}] + [H^+] = [Cl^-] + [NO_3^-] + [SO_4^{--}] \quad (3)$$

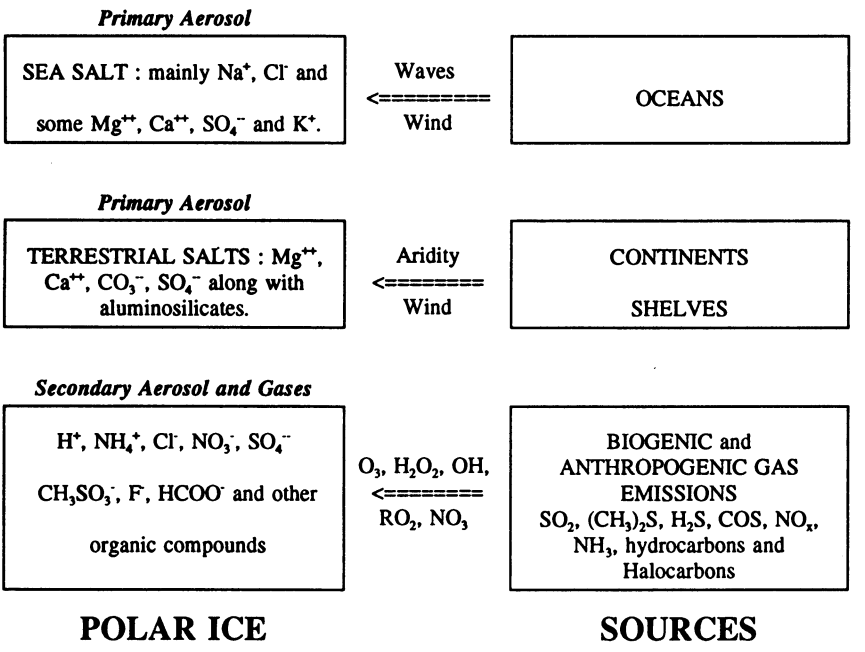

Fig. 1. Schematics showing various soluble impurities expected to be trapped in polar snow layers and their corresponding origins and sources.

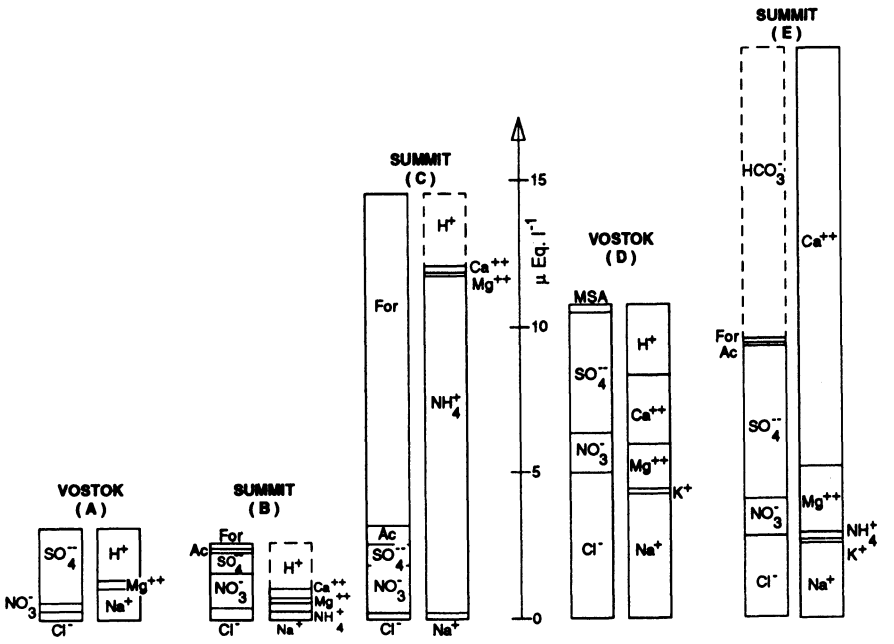

Fig. 2. Mean ionic distribution of soluble species trapped in ice corresponding to present climatic conditions in Antarctica (2a), Greenland (2b) and to glacial stages in Antarctica (2d), in Greenland (2e). Dashed lines are used when the acidity measurements have not been performed. The figure 2c corresponds to large and sporadic perturbation of the mean Greenland ice composition (see section 3-4).

As discussed by Legrand [1987], the Na content measured by chromatography corresponds to the sum of two fractions: the first mainly marine in origin is soluble in water, and the second coming along with dust is not solubilized during the melting step but hereafter during the elution in the ion chromatography. We have, therefore, corrected our Na data from this dust contribution using the Al content of our sample. Subtracting the sea salt contribution from the equation (3) using the Na content (after the above mentioned correction) and the sea salt composition from Holland [1978], we obtain the basic equation which describes terrestrial and gas derived impurities:

$$[H^+] + [Ca^{++}]^* + [Mg^{++}]^* = [Cl^-]^* + [NO_3^-] + [SO_4^{--}]^* \quad (4)$$

where $[X]^*$ = "excess-X" representing the non sea-salt contribution of X.

In snow deposited under present climatic conditions, Ca^{++*} and Mg^{++*} are present at low levels in relation to weak terrestrial inputs [Legrand et al., 1988]. $[Cl^-]^*$ can have positive or negative values, and the equation (4) is here reduced to:

$$[H^+] = [Cl^-]^* + [NO_3^-] + [SO_4^{--}]^* \quad (5)$$

This equation describes the acid components and indicates that besides sea salt, the ice deposited under present climatic conditions contains HNO_3 and H_2SO_4 plus either Na_2SO_4 or HCl corresponding to negative or positive $[Cl^-]^*$ values. During colder climate, $[Ca^{++}]^*$ and $[Mg^{++}]^*$ are significant, $[Cl^-]^*$ is close to zero, and thus, equation 4 becomes:

$$[Ca^{++}]^* + [Mg^{++}]^* + [H^+] = [NO_3^-] + [SO_4^{--}]^* \quad (6)$$

As discussed by Legrand et al. [1988], ice corresponding to such glacial conditions contains HNO_3, H_2SO_4, sea salt and terrestrial salts (Ca^{++*} and Mg^{++*} associated with SO_4^{--*} and NO_3^-) but not carbonates.

The ionic budget of Greenland ice has not yet been fully characterized, and we report here a preliminary picture (Figures 2b, 2c and 2e) based only on ion chromatographic data [Legrand et al., unpublished data] without concurent H^+ measurements. In contrast to antarctic ice, we observe a significant contribution of NH_4^+ and organic acid to the ionic budget (Figure 2b), probably due to a larger impact of continental biospheric emissions.

As suggested by changes in Na^+ and Ca^{++} (Figure 2d and 2e), both Greenland and Antarctic ice cores reveal enhanced input of sea salt and dust during Glacial Age as compared with the present warm stage. However, it appears that during such cold climate the ice was alkaline in Greenland and remained acidic in Antarctica.

ATMOSPHERIC CHEMICAL CHANGES INFERRED FROM ICE CORE DATA

Primary aerosol content of present and past atmospheres: Sea salt content of polar snow is very high in coastal regions of ice sheets, but decreases rapidly inland as a function of elevation [Herron and Langway, 1979; Legrand and Delmas, 1985], reaching low values (10 to 30 ppb of Na) in central ice sheets. In central Greenland [Steffenson, 1988; Mayewski et al., 1987; Whitlow et al., 1992] as well as in Antarctica [Legrand and Delmas, 1988], the sea-salt content of snow layers exhibits large increase in winter as a result of more frequent advections of marine air masses despite a large expansion of sea ice. We here emphasize that at the South Pole the Na^+ content ranges from 3 ng/g in summer to 16 ng/g in winter snow layers [Legrand et al., 1992], reflecting rather well the atmospheric concentration (7 and 34 ng/m^3 in summer and winter, respectively) [Cunningham and Zoller, 1981; Tuncel et al.,

1989]. It was also found that the sea salt aerosol can be altered during its transport from oceans towards the high plateau of ice sheets [Legrand and Delmas, 1988]. Indeed, as previously discussed, we identify HCl and Na_2SO_4 in ice deposited under present climatic conditions according to the sea salt reaction:

$$H_2SO_4 + 2\ NaCl\ (sea\ salt) \rightarrow Na_2SO_4 + 2\ HCl \qquad (7)$$

The sea-salt content of polar ice have been strongly modulated by past climatic conditions. For instance, the Na_m^+ profile along the Vostok core which spans the last climatic cycle (Figure 3b), shows low values during warm stages and a gradual increase over the Last Glacial Age with a particularly large increase (by a factor 4) during the last great climatic transition which occurred at 15,000 yrs B.P. (e.g., at 350 m depth). Because the Na^+_m content of ice exhibits an accumulation rate effect linked with the dry deposition process [Legrand and Delmas, 1988], a part of observed changes along the Vostok core is linked to the reduction of the snow accumulation rate between warm stages and the Last Glacial Age. However, such an effect can only explain 25% of observed variations, and the remaining variations (e.g., a factor 3 change at 15,000 yrs B.P.) are representative of actual atmospheric sea salt concentration changes. Such data, therefore, suggest that during cold climate despite a large sea ice expansion (up to 1000 km) which increased the distance from the open ocean to the high antarctic plateau, the sea salt content of the antarctic atmosphere was enhanced. This reflects a greater production rate of sea salt due to higher wind speed at the sea surface and/or a more efficient meridional transport between mid and high latitudes.

The Cl/Na_m ratio varies widely over the last 160,000 yrs (Figure 3c) on both sides of the bulk sea water reference value (1.8), but remains very close to 1.8 under full glacial conditions. This absence of sea-salt fractionation during very cold stages could be linked with the high turbulence of the atmosphere which probably limited the efficiency of reaction (7).

Several previous studies have pointed out that ice deposited during cold climate conditions in Greenland and Antarctica contains much more dust than ice deposited at the present time [Cragin et al., 1977; Petit et al., 1981; Hammer et al., 1985]. The Ca^{++*} (a good tracer of dust [Legrand et al., 1988]), Vostok profile (Figure 3d) shows that the contrast between warm and cold stages is higher for sea salt. Such a large increase during full glacial stages reflects expansion of arid areas and the emergence of parts of the continental shelves [De angelis et al., 1987].

Sulphur-derived species: Various possible origins of non sea salt SO_4^{--} present in polar precipitation and the corresponding potential sources are summarized in Figure 4. SO_4^{--} profiles (Figure 5) covering the last 200 years obtained in Greenland and Antarctica

ice revealed huge short-time perturbations corresponding to major volcanic events like the Tambora (1815). Moreover, the non-volcanic background SO_4 level of Greenland deposits has revealed the increasing SO_2 fossil fuel burning emissions of the Northern hemisphere.

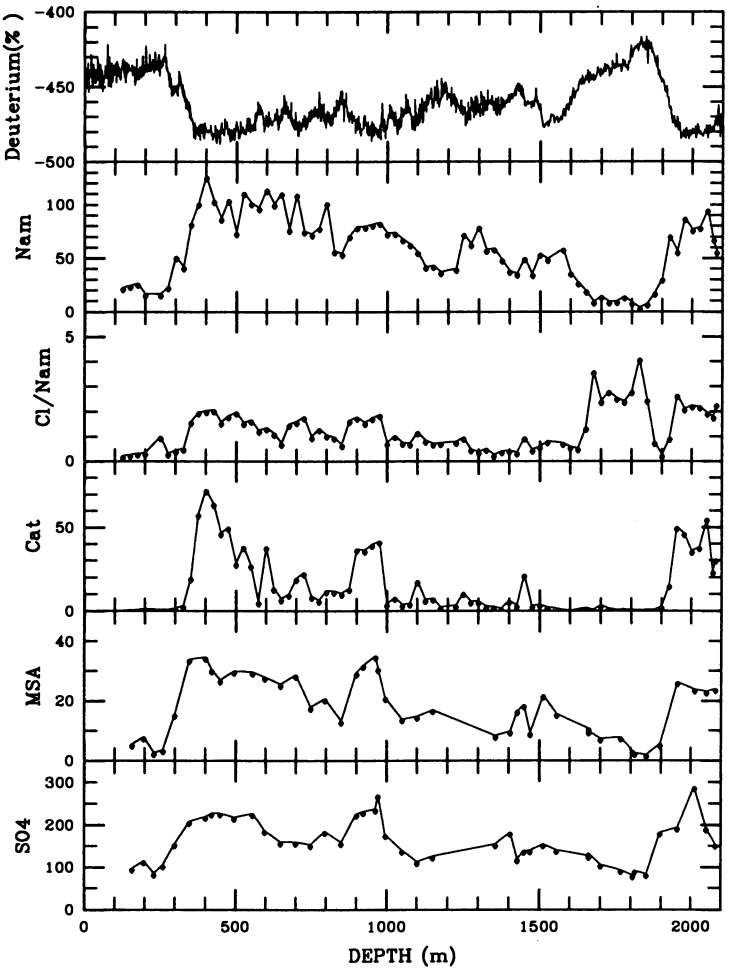

Fig. 3 . Vostok ice core profiles: (from top to bottom): (a) Deuterium isotope profile from Jouzel et al. [1987]. (b) marine sodium, (c) Cl/Na marine weight ratio, (d) non-sea salt calcium, (e) MSA, (f) non-sea salt SO_4^{--} from Legrand et al. [1988] and Legrand et al. [1991]. b, d, e, f are reported in ppb.

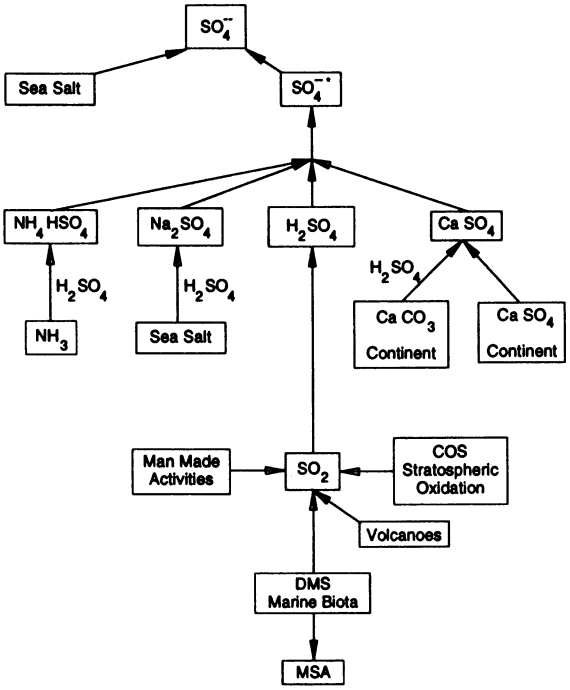

Fig. 4. Possible origins and sources of SO_4^{--} present in polar snow and ice.

Origins and variations of the non-volcanic SO_4 budget of the natural atmosphere have been investigated mainly by Antarctic ice core studies. First, MSA and SO_4^{--*} depth profiles along the Vostok core (Figure 3e and 3f) shows similar trends with a moderate glacial-interglacial increase, suggesting that SO_4^{--*} is mainly derived from DMS marine emissions in Antarctica [Legrand et al., 1991]. Furthermore, a study of MSA content of south polar snow [Legrand and Feniet-Saigne, 1991] suggests a short-term modulation of the sulphur-derived species budget by El Nino events. These two studies point out the important role of DMS marine emissions in controlling the Antarctic non-volcanic SO_4 budget. Similar Greenland ice core studies are currently underway to estimate the contribution of various sources to the non-volcanic SO_4 budget of high latitude northern hemisphere.

Nitrogen oxide-derived species: As discussed above, NO_3^- is mainly present in polar snow as HNO_3. The relative contribution of the various NO_x sources (e.g., soil exhalation, anthropogenic emissions, biomass burning, lightning, galactic cosmic rays, N_2O stratospheric oxidation, N_2 mesospheric and thermospheric dissociation) to its budget remains poorly

established. The 200-year NO_3^- profile obtained in Greenland (Figure 5) demonstrates the recent increase due to long range transport of pollution from middle northern latitudes [Mayewski et al., 1990]. Over the last two centuries, the NO_3^- content at South Pole has remained fairly constant, but an increase of the spring-summer maximum in NO_3^- occurred in very recent years (Figure 5). A possible interpretation of such recent variations in terms of atmospheric changes may invoke the denitrification of the lower stratosphere by sedimentation of polar stratospheric clouds [Mayewski and Legrand, 1990]. However, such conclusion must be treated with caution because of a suspected post-depositional effect (e.g., smoothing of the seasonal signal with depth) for HNO_3 which present in the atmosphere in the gase phase, is not necessarily trapped irreversibly in snow layers (see Neftel, this volume).

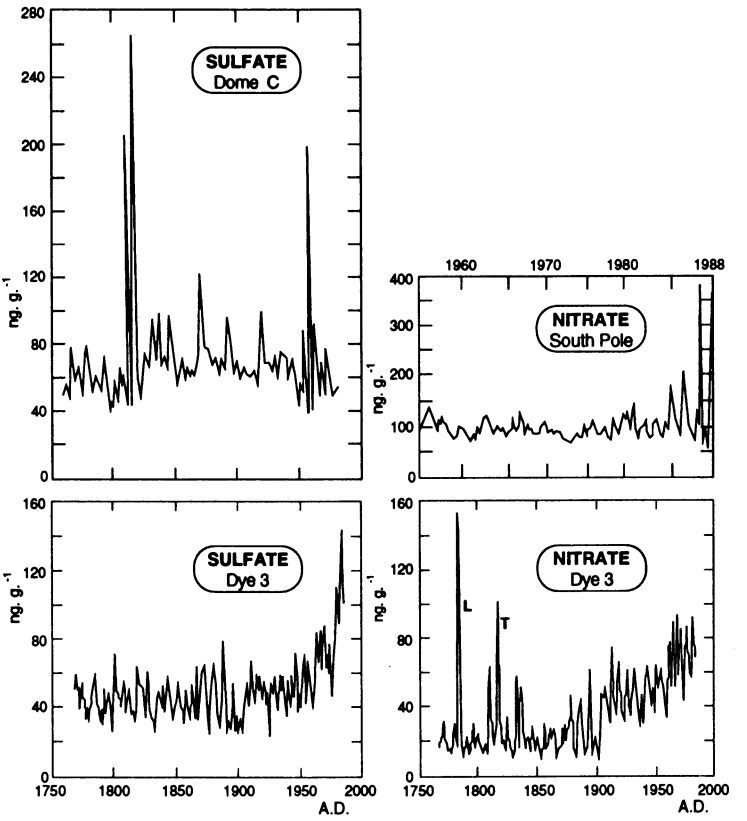

Fig. 5. Recent evolution of the SO_4^{--} and NO_3^- content of Greenland (Dye 3, Mayewski et al., 1990) and of Antarctic snow layers [Dome C., Legrand and Delmas, 1988; South Pole, Mayewski and Legrand, 1990, respectively].

The respective contribution of various NO_x sources to the HNO_3 budget of the pre-industrial high latitude southern atmosphere has recently been investigated [Legrand et al., 1989; Legrand and Kirchner, 1990], suggesting a major contribution by lightning, biomass burning and N_2O stratospheric oxidation and discarding the impact of NO_x production in the high atmosphere.

Organic acids: Very recently, glaciochemical studies started to investigate some organic species including formaldehyde [Staffelbach et al., 1991; Neftel, this volume] and organic acids present in polar ice. These studies of reactive species trapped in snow layers can provide useful information on the oxidative capacity of the past atmosphere.

For example, the large NH_4^+ perturbations, accompanied by a large increase of several organic acids and an absence of NO_3^- changes in Greenland snow layers (see Figure 2c) caused by high latitudes forest fires [Legrand et al., 1992], suggest that the photochemistry of these high latitude regions of the northern hemisphere have been strongly disturbed in the past. Another study of these NH_4^+ sporadic perturbations recorded in Greenland ice [Legrand and De Angelis, to be submitted] shows that the chemical signature of such biomass burning inputs have been modified in the past, in particular with the presence of nitrite (NO_2^-).

CONCLUSION

In this paper we have discussed what we have learned about chemical composition of the past atmosphere by studying the chemistry of Greenland and Antarctic ice cores. Concerning species derived from primary (sea salt and dust) and secondary (MSA and SO_4) aerosols, concentrations measured in ice reflect, to a large extent, atmospheric changes and suggest that the composition of our atmosphere is very sensitive to climatic variations with enhanced inputs of sea salt, dust and to a lesser extent, marine biogenic-derived species during cold climatic conditions. Such studies have also shown the reaction of the atmosphere to other natural (volcanic eruptions, El Nino, forest fires) phenomena.

Concerning the gas-phase species (e.g., HNO_3 and some organic acids) present in the atmosphere, the interpretation of records is less straightforward and we point out here the need for studying the "air-snow" transfer function.

Two international projects (Greenland Ice Core Project and Greenland Ice Sheet Project) are currently underway to recover ice cores in Central Greenland which cover the same time period as that of Vostok in Antarctica. Such ice cores will certainly provide in the future very interesting scientific topics, in particular on the role of biospheric continental emissions on the composition of high northern latitude atmospheres.

Acknowledgements: This work was supported by CNRS (Programme Environnement)

REFERENCES

Cragin, J.H., M.M. Herron, C.C. Langway and G. Klouda, Interhemispheric comparison of changes in the composition of atmospheric precipitation during the late cenozoic area, in *Polar Oceans*, edited by M.J. Dunbar, 617-631, Arctic Institute of North America, Calgary, Can., 1977.

Cunningham, W.C. and W. Zoller, The chemical composition of remote area aerosols, *J. Aerosol Sci.*, 12, 367-384, 1981.

De Angelis, M., N.I. Barkov and V.N. Petrov, Aerosol concentrations over the last climatic cycle (160 kyr) from an Antarctic ice core, *Nature*, 325, 318-321, 1987.

Finkel, R.C. and C.C. Langway, Global and local influences on the chemical composition of snowfall at Dye 3, Greenland: the record between 10 ka B.P. and 40 ka B.P., *Earth and Plan. Sc. Lett.*, 73, 196-206, 1985.

Hammer, C.U., H.B. Clausen, W. Dansgaard, A. Neftel, P. Kristinsdottir and E. Johnson, Continuous impurity analysis along the Dye 3 deep ice core, in *Greenland ice core: Geophysics, Geochemistry and Environment, Geophys. Monogr. Ser.*, vol. 33, edited by C.C. Langway, Jr. et al., 90-94, AGU, Washington, D.C., 1985.

Hammer, C., Dating by physical and chemical seasonal variations and reference horizons, *The Environmental Record in Glaciers and Ice Sheets*, Eds. H. Oeschger and C.C. Jr. Langway, Dahlem Konferenzen, 99-121, 1989.

Herron, M.M. and C.C. Langway Jr., Dating of Ross Ice Shelf cores by chemical analysis, *J. of Glaciol.*, 24, 3052-3060, 1979.

Holland, H., *The Chemistry of the Atmosphere and Oceans*, Chap. 5, Wiley-Interscience, New York, 1978.

Johnson, S.J., Stable isotope homogenization of polar firn and ice, *Isotopes and Impurities in Snow and Ice*, IAHS Publ., 118, 210-219, 1977.

Legrand, M., A. Aristarain and R.J. Delmas, Acid titration of polar snow, *Analyt. Chem.*, 54, 1336-1339, 1982.

Legrand, M., M. De Angelis and R.J. Delmas, Ion chromatographic determination of common ions at ultratrace levels in Antarctic snow and ice, *Anal. Chim. Acta*, 156, 181-192, 1984.

Legrand, M. and R.J. Delmas, Spatial and temporal variations of snow chemistry in Terre Adélie (East Antarctica), *Ann. of Glaciol.*, 7, 20-25, 1985.

Legrand, M. and R.J. Delmas, A 200-year continuous record of volcanic H_2SO_4 in the antarctic ice sheet, *Nature*, 327, 671-676, 1987.

Legrand, M., Chemistry of antarctic snow and ice, *J. de Phys.*, 48, 77-86,1987.

Legrand, M. and C. Saigne, Formate, acetate and methanesulfonate in Antarctic ice: some geochemical implications, *Atmos. Environ.*, 22, 1011-1017, 1988.

Legrand, M., C. Lorius, N.I. Barkov and V.N. Petrov, Vostok (Antarctica) ice core: Atmospheric chemistry changes over the last climatic cycle (160,000 years), *Atmos. Environ.*, 22, 317-331, 1988.

Legrand, M. and R.J. Delmas, Formation of HCl in the Antarctic atmosphere, *J. Geophys. Res.*, 93, 7153-7168, 1988.

Legrand, M., F. Stordal, I.S.A. Isaksen and B. Rognerud, A model study of the stratospheric budget of odd nitrogen including effects of solar cycle variations, *Tellus*, 41, 413-426, 1989.

Legrand, M. and S. Kirchner, Origins and variations of nitrate in south polar precipitation, *J. of Geophys. Res.*, 95, 3493-3507, 1990.

Legrand, M., C. Feniet-Saigne, E.S. Saltzman, C. Germain, N.I. Barkov and V.N. Petrov, Ice-core record of oceanic emissions of dimethylsulphide during the last climate cycle, *Nature*, 350, 144-146, 1991.

Legrand, M. and C. Feniet-Saigne, Methanesulfonic acid in south polar snow layers: a record of strong El Nino, *Geophys. Res. Lett.*, 18, 187-190, 1991.

Legrand, M., C. Feniet-Saigne, E.S. Saltzman and C. Germain, Spatial and temporal variations of methanesulfonic acid and non sea salt sulfate in antarctic ice, *J. Atmos. Chem.*, 14, 245-260, 1992.

Legrand, M., M. De Angelis, T. Staffelbach, A. Neftel and B. Stauffer, Large perturbations of ammonium and organic acids content in the Summit-Greenland ice core: Fingerprint from forest fires, *Geophys. Res. Lett.*, 19, 473-475, 1992.

Lyons, W.B., P.A. Mayewski, M.J. Spencer, M.S. Twickler and T.E. Graedel, A northern hemisphere volcanic chemistry record (1869-1984) and climatic implications using a south Greenland ice core, *Annals of Glaciol.*, 14, 176-182, 1990.

Mayewski, P.A., M.J. Spencer, W.B. Lyons and M.S. Twickler, Seasonal and spatial trends in South Greenland snow chemistry, *Atmos. Environ.*, 21, 863-869, 1987.

Mayewski, P.A., W.B. Lyons, M.J. Spencer, M.S. Twickler, C.F. Buck and S. Whitlow, An ice-core record of atmospheric response to anthropogenic sulphate and nitrate, *Nature*, 346, 554-556, 1990.

Mayewski, P., and M. Legrand, Recent increase in nitrate concentration of antarctic snow, *Nature*, 346, 258-260, 1990.

Mulvaney, R., and D.A. Peel, Anions and cations in ice cores from Dolleman island and the Palmer land plateau, Antarctic Peninsula, *Annals of Glaciol.*, 10, 121-125, 1988.

Piccioto, E.E. and S. Wilgain, Fission product in antarctic snow, a reference level for measuring accumulation, *J. Geophys. Res.*, 68, 5965-5972, 1963.

Saigne, C., S. Kirchner and M. Legrand, Ion-chromatographic measurements of ammonium, fluoride, formate, acetate and methanesulfonate ions at very low levels in Antarctic ice, *Anal. Chim. Acta*, 203, 11-21, 1987.

Sigg, A. and A. Neftel, Evidence for a 50% increase in H_2O_2 over the past 200 years from a Greenland ice core, *Nature*, 351, 557-559, 1991.

Staffelbach, T., A. Neftel, B. Stauffer and D. Jacob, A record of the atmospheric methane sink from formaldehyde in polar ice core, *Nature*, 349, 603-605, 1991.

Steffenson, J.P., Analysis of the seasonal variations of dust, Cl^-, NO_3^- and SO_4^{--} in two central Greenland firn cores, *Ann. of Glaciol.*, 10, 171-177, 1988.

Tuncel, G., N.K. Aras and W.H. Zoller, Temporal variations and sources of elements in the South Pole atmosphere: nonenriched and moderately enriched elements, *J. Geophys. Res.*, 94, 13,025-13,038, 1989.

Whitlow, S., P.A. Mayewski and J.E. Dibb, A comparison of major chemical species input timing and accumulation at South pole and Summit Greenland, *Atmos. Environ.*, in press.

A RECORD OF ATMOSPHERIC OXIDANT FROM POLAR ICE CORES OVER THE PAST 100,000 YEARS: DREAM OR REAL POSSIBILITY?

Albrecht Neftel and Katrin Fuhrer
Klima- und Umweltphysik
Physikalisches Institut, Universität Bern

INTRODUCTION

The principal oxidants of the earth's atmosphere are O_3, OH radical and H_2O_2. The total atmospheric burden of these three species determines the oxidation capacity of the atmosphere [Thompson, 1992]. Each of these species reacts with different atmospheric trace constituents, and determines their atmospheric lifetimes. In particular, the OH radical reacts very fast with almost all naturally and anthropogenically emitted species; therefore, this radical has the nickname "tropospheric vacuum cleaner" [Graedel, 1978].

Ozone acts as a greenhouse gas both in the stratosphere and in the troposphere. While the ozone layer in the stratosphere is crucial for life on the earth, its concentration in the planetary boundary layers reaches toxic levels in many areas of the globe, due to the increased emissions of NO_x and hydrocarbons. High levels of oxidants enhance the formation of the strong acids HNO_3 and H_2SO_4, which are largely responsible for the well-known acid rain phenomena. The spatial distribution of the oxidants, therefore, also determines the spatial distribution and deposition of the strong acids.

Why is a historical record of the oxidation capacity of interest? Why can it be justified to send enthusiastic students during lovely summers to the middle of the cold, white nowhere to collect miles of chemical data from ice cores? Anthropogenic emissions have caused a drastic change in the chemical conditions of the atmosphere since industrialisation. Many fluxes have more than doubled within a very short time. The earth's atmosphere has never experienced this situation in the last 10,000 years of the current interglacial. Obviously, there is a large concern about the future state of our atmosphere and its consequences for the climatic conditions. Model calculations making predictions about these changes will finally be verified at the point in time for which they were made. Variations in the past offer the possibility of verifying such predictions when past climatic fluctuations can be adequately described. A reconstruction of the oxidizing capacity of the atmosphere would be an important piece to assemble the whole puzzle. At best, driving forces can be inferred and the needed intensity of feedback mechanisms can be derived from the observations.

NATO ASI Series, Vol. I 7
The Tropospheric Chemistry of Ozone in the Polar Regions
Edited by H. Niki and K. H. Becker

POSSIBILITIES OF A RECONSTRUCTION OF ATMOSPHERIC OXIDANTS

It is the chemical nature of these oxidants that they are very reactive and therefore, have only a limited lifetime. Ozone and H_2O_2 in the troposphere have a lifetime of at most several weeks; hence, their concentrations vary with latitude, longitude, altitude and season [Logan, 1985]. OH radicals have a lifetime of a few seconds; their concentration can be regarded as a property of the local chemical system in the atmosphere. If the burden of atmospheric oxidants has to be reconstructed, a suitable archive must be found. Well-documented instrumental measurements are preferable, but the time period covered by reliable measurement of the atmospheric concentration of the oxidants is short. Sporadic surface ozone measurements predate 1970 and suggest that surface ozone levels have increased by a factor of 2-3 over the last 100 years in northern continental mid-latitudes [Volz and Kley, 1988]. At other more remote locations, trends are relatively weak and are only based on short time series (compared to time scales covered by the analysis of polar ice cores). For OH and H_2O_2 the few direct measurements do not allow establishing any trends.

Polar ice cores are perhaps the only archive containing more or less direct information on oxidants on a much longer time scale. They are located in high latitudes, and therefore, do provide only direct information about the atmospheric concentration above the ice sheets from where they originated. Other considerations, mainly based on model considerations, have to provide the link from such local parameters to their global significance.

POLAR ICE CORES - THE COLD ARCHIVES

Figure 1 shows a cross-section of an ideal ice sheet. Greenland comes close to this. Snow containing traces of different atmospheric constituents accumulates at higher elevation in the interior and is lost at the edges by calving of icebergs due to melting in the summer periods. By drilling a core in the middle of such an ice sheet, a complete chronology of past snow deposition from the same location is recovered. Due to ice flow, yearly layers become thinner with time. Recovering ice cores all the way through an ice sheet is a difficult task and requires a large and costly operation. In July 1992, the European drill operation in Summit, Central Greenland reached bedrock and provided 3,028 meter new ice core, the longest core drilled to date, covering more than 200,000 years back in time.

Figure 2 shows a scheme of the transformation of snow to ice, which occurs in the uppermost part of the ice sheet. During the early lifetime of the snow, the sharp edges of the flakes are rounded off, because the water vapour pressure is inversely proportional to the radius of curvature (Kelvin effect) leading to a reduction in the specific surface. Additionally, temperature gradients induced by the diurnal as well as the seasonal variations lead to

evaporation and recondensation of water molecules. Any species that are only absorbed on the surface and have vapour pressures similar to or larger than water vapour pressure over ice, will be redistributed in the snow and firn. Deeper down the snow is compressed by rearrangements of the snow grains. Above a density of about 550 kg/m^3, further rearrangement of ice grains no longer leads to an increase in the density. Sintering and plastic deformation become the dominant processed leading to increased density. At a density of about 800 kg/m^3, the pores are gradually pinched off to form individual bubbles [Schwander and Stauffer, 1984]. These bubbles contain atmospheric air of the past.

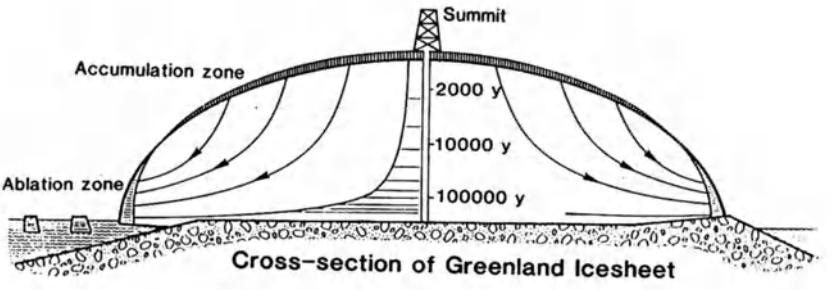

Fig. 1: Cross section through an idealized ice sheet with flow lines is indicated.

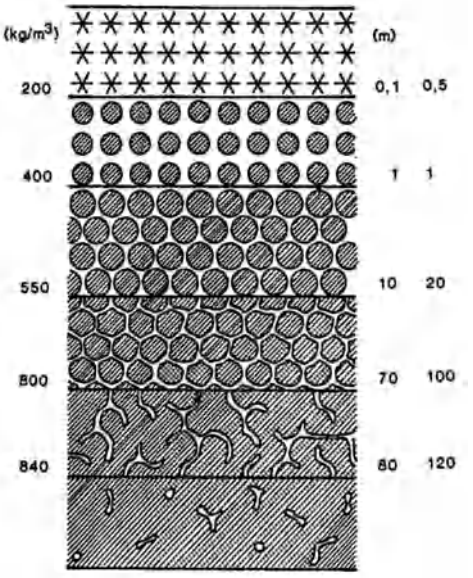

Fig. 2: Schematic transformation from snow to ice. Depth to age relations are arbitrary.

Polar ice cores contain two different categories of atmospheric information: i) the composition of the air in the bubbles; and ii) the concentrations of the different trace species in the snow or ice. Species that are directly related to the oxidation capacity of the atmosphere and that have been measured to date are: CH_4 concentrations in the air extracted from the bubbles; H_2O_2 and HCHO concentrations in the ice. Up to now, experimental difficulties excluded measuring other species that would be closely related to the oxidation capacity: mainly CO and eventually O_3 and OH concentrations in the bubbles. It is very unlikely that the latter two molecules would be preserved in the enclosed bubbles; it seems likely that they reacted at the ice surface of the bubbles with the enclosed gases already in the open pore space of the firn. But a final proof of this hypothesis has not been given to date. Many other chemical species have been investigated [see also the contribution by M. Legrand in this volume]. Fully oxidised species, e.g., sulphate, do not tell us too much about the oxidation rate. Ratios between the different oxidation states would be needed. In most of the analysis of snow and ice samples, neither sulphite nor nitrite concentration has been found. Exceptions are discussed by M. Legrand in this volume.

It should be noted that a concentration measurement of a certain species from polar ice or snow samples is always a mean value over a certain time period. In case of analysis of the air in bubbles, the averaging time corresponds to the time period of the gas enclosure and is at least several years. The time span of the enclosure process depends upon the mean temperature and the accumulation rate. Measurements of trace species in the bulk have a much better time resolution which is limited by microscale redistribution processes in the snow and firn and also by the analytical procedure. Irreversibly deposited species, e.g., sulphate, that have a very low water vapour can, in principle, be traced to individual snowstorm events. The thinning of the annual layer due to the flow of the ice masses deep down in the ice sheet sets another limit to the achievable temporal resolution. This short overview of the functioning of the cold archive should demonstrate an important aspect: taking information out of chemical measurements from polar ice cores about the history of atmospheric oxidants is comparing apples and pears. Information is largely available only as mean values over a longer time period, whereas oxidant concentrations in the atmosphere change over much shorter time scales.

WHAT DO WE KNOW ABOUT THE CONCENTRATION OF HCHO AND H_2O_2 IN ICE CORES?

HCHO: HCHO itself is not an oxidant, but is an oxidation product of hydrocarbons; in the remote polar regions it comes mainly from methane. The atmospheric methane record of the last 160,000 years is known from polar ice cores [Chappellaz, 1990, Etheridge et al.,

1988; Stauffer et al, 1985; Stauffer et al., 1988]. If the atmospheric formaldehyde record is also known, it may be possible to establish a record of the oxidation capacity over the polar ice sheet. With this hypothesis in mind we started to measure HCHO concentrations in polar snow and ice. Upon first analysis we found quite a consistent picture which can be summarised as follows:

- Initial HCHO concentrations in freshly fallen snow are not preserved.
- A new equilibrium is established between 20 to 50 cm below the surface, reflecting most probably a multi-year mean atmospheric concentration.
- In both Greenland and Antarctic ice cores a lower HCHO to CH_4 ratio was found for glacial time as compared to Holocene values.

From these results, Staffelbach et al. [1991] concluded that the OH radical concentration was lower in the polar atmosphere during glacial conditions. Continuous measurements along the new Summit deep core considerably changed our view of the HCHO concentration in ice.

Figure 3 shows the continuous HCHO record of the new Summit core measured directly in the field during the season 1991 together with the Ca^{2+} record. The data cover roughly the time interval 6,000 years B.P. to 40,000 years B.P. The climatic development from 40,000 years B.P. to present day conditions is characterised by the major transition from glacial conditions to the present interglacial stage. The glacial period, with the transition into the interglacial, is characterised by frequent changes from typically cold conditions (characterized by high Ca^{2+} concentrations) to warm conditions (characterized by low Ca^{2+} concentrations). These transitions occur over an extremely short depth interval. There is a high probability that the time interval of the transitions was only a few decades, as it has been already found in the deep core from Dye 3 [Dansgaard et al., 1984; Oeschger and Langway, 1989]. All climatic changes are accompanied by large concentration changes of many species. In part of the cold stages, the HCHO values parallel the Ca^{2+} concentrations and are roughly ten times higher as what are expected based on previous results. Obviously, this behaviour is not consistent with our previous assumption that the HCHO concentration in ice reflects a multi-year mean atmospheric average. In many respect during the cold stages, HCHO concentration behaves like an irreversibly deposited species. This clearly points out that we do not understand the transfer behaviour between the ice and the atmosphere, and that at present we cannot translate ice concentrations and their variations in meaningful atmospheric variations that can be used by atmospheric modellers. The transfer function is the eye of the needle to reconstruct the oxidation capacity from CH_4 and HCHO measurements.

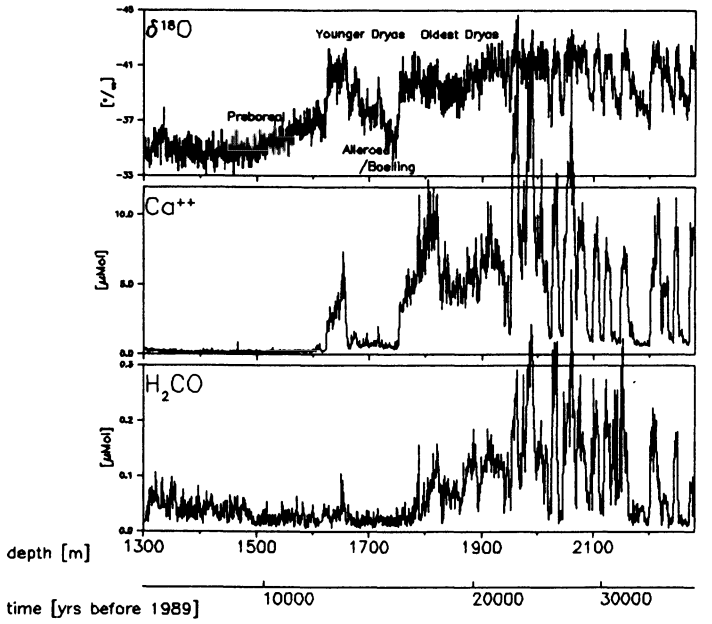

Fig. 3: $d^{18}O$ [Johnson et al., 1992], Ca^{2+} and HCHO results from the Summit 1991 drill season.

H_2O_2: Exactly 10 years ago during another NATO ASI in Corfu, Jacob and Neftel developed the idea to measure H_2O_2 in polar snow and ice. It was quite surprising to find this meta-stable compound in rather high concentrations [Neftel et al., 1984]. Since then, we have systematically investigated the behaviour of this compound in snow, ice and also in the polar atmosphere.

The prominent features of H_2O_2 in polar snow and ice can be summarised as follows:

- H_2O_2 concentration in snow and ice that can be related to atmospheric concentrations are only preserved in locations with low dust concentrations and cold temperature.
- The H_2O_2 signatures of individual snowfalls are lost during the firnification process. The mean displacement length of H_2O_2 molecules in the firm is 12-13 cm ice equivalent, integrated over the whole firnification process.
- Continuous measurements from ice cores from Central Greenland are the most promising data to reconstruct an atmospheric record covering the last 1,000 years. The continuous records from the Dye 3 and Summit cores give evidence of an increase of the mean H_2O_2 concentration of 50% over the last 200 years. Figure 4 shows the continuous series of the yearly mean concentrations from Dye 3 and Summit in Greenland.

- H_2O_2 disintegration occurs most probably on dust particles by a slow process in the dark. This disintegration erases the memory of the ice cores for H_2O_2 over time scales of several thousands of years.
- The sparse published H_2O_2 concentrations from locations in the interior of the Antarctica point to a systematic loss with depth in the upper firn.

As is the case for the HCHO measurements, the hurdle to extract direct atmospheric concentrations from the ice concentrations is the imperfect knowledge about the transfer function. Neftel [1990] wrote in another ARW contribution that the atmosphere-ice transfer function for polar conditions is well described by a co-condensation model. Co-condensation means that the ice has the same H_2O_2 to H_2O ratio as the surrounding gas phase. Two years later we realised that this picture is much too simple.

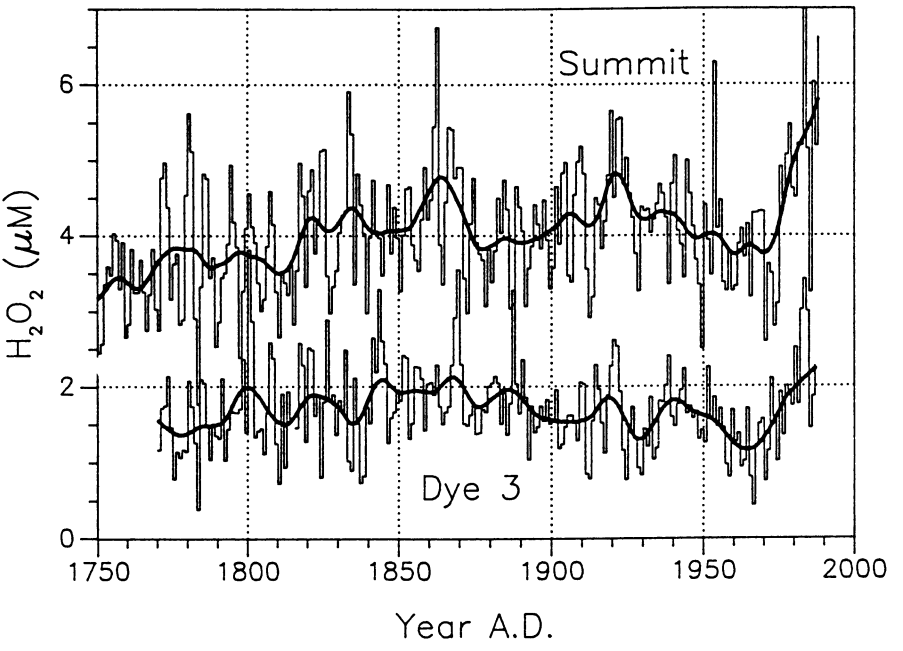

Fig. 4: Comparison of annual mean H_2O_2 concentration from Summit (upper trace) and Dye 3 (lower trace) [from Sigg and Neftel, 1991]

TRANSFER FUNCTION - A CONCEPTUAL PICTURE

The transfer function : $T = \frac{c_{Atmosphere}}{c_{ice}}$ can be divided into four parts:

$$\frac{c_{Atmosphere}}{c_{ice}} = \frac{c_{Atmosphere}}{c_{Atmospherelocal}} \cdot \frac{c_{Atmospherelocal}}{c_{Snow}} \cdot \frac{c_{Snow}}{c_{Firn}} \cdot \frac{c_{Firn}}{c_{Ice}}$$

$c_{Atmosphere}$ means an atmospheric concentration that can be used or is predicted by numerical model. It is, therefore, often a mean concentration over a mixed air volume, the size of which depends on the specific model used. The local atmospheric concentration determines what will be incorporated into the ice. The ratio of the two depends mainly on the source strength and distribution, the synoptic weather conditions, the atmospheric lifetime and vertical exchange in the planetary boundary layer. The second term contains the scavenging behaviour. Both in-cloud and below-cloud scavenging have to be considered, as does dry deposition.

In the early lifetime of the snow, redistribution occurs depending on the vapor pressure and air ventilation of the firn. Also crucial is to what extent the trace species can be incorporated into the ice matrix, i.e., the partitioning between air-ice. During the whole firnification process diffusion occurs over the open pore space, which leads to a smoothing of the seasonal variability. The degree of smoothing depends not only on the vapor pressure, but also on the absorption and adsorption characteristics of the ice surface. Finally, the chemical composition in the ice is changing due to very slow reactions.

We say that H_2O_2 and HCHO are reversibly incorporated into snow, which means that their concentrations change in the days and months after the snow is deposited. The recording quality of a specific site for reversible species depends not only on accumulation and temperature, but also on the seasonal distribution of the accumulation and the intensity of air exchange between the snowpack and the atmosphere. The key to understanding the relation between ice and atmospheric concentrations then becomes a question of relating diurnal and seasonal changes in atmospheric parameters to those in snow and ice. The goal must be to develop a model to predict snow and ice concentrations with depth and time, given concentrations in the air at corresponding times and locations. The inverse function would then relate the measured ice concentration with the atmospheric concentration.

A number of questions have to be answered in order to successfully develop such a model:

- Where are the species located in the ice (partitioning surface/bulk)?
- How large is diffusion in ice and along the surfaces?

- What is the sticking probability of molecules at the ice-air interface?
- What are the seasonal variations of the concentrations in the surface air layer?
- How large is the ventilation rate due to atmospheric pressure changes and wind induced micropressure changes?
- What kind of photochemical reactions occur on the surface of ice grains?

Laboratory and field studies must clarify these urgent questions. Since techniques for the analysis of H_2O_2 are available, it seems reasonable to use this molecule as a surrogate for other reversible deposited species. During the 1990 summer season, Sigg et al. [1992] conducted measurements of gas-phase H_2O_2 at Summit, and found concentrations of 2 - 3 ppb, which are considerably higher than expected from model calculations. The concentrations showed a strong diurnal variation, which has to be explained by a storage of H_2O_2 during the night on the surface.

In the laboratory the uptake and release of H_2O_2 by snow was investigated with a series of column experiments (-3° C and -45° C) in a cooperation between the Physical Institute, University of Bern and the Department of Hydrology, University of Arizona, Tucson. The experiments showed a large uptake of H_2O_2, which was greater at lower temperature: the uptake could be reversed when the column was flushed with pure air. From these experiments a temperature dependent transfer coefficient has been derived (Figure 5). These coefficients are one tenth of the transfer coefficients based on the co-condensation model and less than one percent of the Henry coefficient extrapolated to temperatures below 0° C. A mathematical treatment of these first experiments is presented in Conklin et al. [1992]

Snow and ice will adjust their concentrations according to the surrounding air concentration and the effective transfer function. Going from summer to winter conditions, the snow uptake capacity will increase and the air concentration needed to maintain the ice concentration will drop. H_2O_2 uptake is further complicated by temperature profiles in the uppermost part of the firn, which are positive in summer and negative in winter. During the winter months the cold surface layer, with its high uptake capacity, is capable of depleting the layers underneath. If the atmospheric concentration in wintertime drops below the corresponding equilibrium concentration of the initial snow, a loss has to be expected. This suspected loss will be important at locations with low accumulation rates. In case the accumulation rate is large enough, e.g., at Siple station, the previous summer layers are under a thick enough snow layer, so that H_2O_2 molecules entering the gas phase will be retained rather than flushed out.

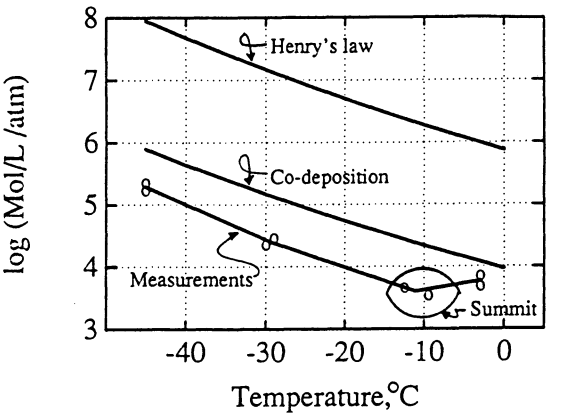

Fig. 5: Comparison of various equilibrium transfer functions with experimental data. Measurements are from the laboratory experiments. The area marked "Summit" reflects conditions in Greenland.

In order to relate a measured snow or ice concentration from a polar sample to an atmospheric concentration, the vertical concentration profile of the H_2O_2 concentration above and in the snowpack as function of time has to be known. Such experiments are planned under the umbrella of the working group on Snow-Atmosphere Chemical Exchange of the International Commission on Snow and Ice [Bales et al., 1992].

HCHO exhibits an additional complexity. Detailed analysis on pit studies showed that HCHO concentrations decrease rapidly with time after snowfall [Staffelbach et al., 1991]. Minimum values are found at 5-15 cm below the surface. Further below the surface (20-50 cm), the concentration increases and reaches a weak maximum that coincides with the last winter snow. The absence of a seasonal structure points to a large displacement length or a low sticking coefficient. Therefore, the hole at a few centimeter below the surface is not rapidly filled up again. The most likely explanation for the minimum just below the surface is a loss of HCHO by photolytic degradation. The light flux is strongly attenuated by the snow, so the photolysis rate of HCHO in the snow pack decreases strongly with depth. Photochemical reactions on snow surfaces have to be taken into account in the concept of transfer functions. At present, we cannot indicate values for transfer coefficients as in the case for H_2O_2. The only thing that we could do is to speculate whether systematic concentration changes reflect, to a large extent, changes in the atmospheric concentration and not changes of the transfer behaviour.

A REVIEW OF SOME PECULIAR FEATURES OF HCHO AND H_2O_2 CONCENTRATIONS IN POLAR ICE CORES

Do HCHO Summit data contradict the previous measurements?

As mentioned above, the new continuous HCHO data measured along the Summit core show at a first glance, a radically different picture than the one we developed based on a few discrete samples from the Dye 3 core from South Greenland and from the Byrd core in West Antarctica. A more detailed inspection shows that HCHO concentrations were lowest during the period of deglaciation (15,000 - 10,000 years B.P.), with the exception of the beginning of the Younger Dryas. Within the Younger Dryas the co-variation of HCHO with Ca^{2+} vanishes, whereas at the beginning increase in the concentrations of both species is parallel. Ca^{2+} concentration can be regarded as a surrogate for the aerosol load of the ice sheet. It is likely that either HCHO is brought into the ice with these aerosols or HCHO is produced in conjunction with these aerosols. The load and the character of the aerosols deposited on the Central plateau of Greenland might differ considerably from those deposited on the Southern part of Greenland. At present, we cannot offer any consistent explanation to what causes the measured HCHO concentrations; it is our hope that more detailed chemical analysis may solve some of the most urgent questions. Discussions with M. Legrand and M. Molina during this workshop brought up the question to what extent ice is alkaline during the cold stages may enhance the uptake of HCHO. Nevertheless, we would like to point out that at the end of the glaciation and before and after the Younger Dryas, similar low HCHO values were found in the Summit core as in the Dye 3 core. Thus, the conclusion drawn in the paper by Staffelbach et al. [1991] are not ruled out. Again, it clear that our present knowledge about the transfer function is far from being perfect; it is even not clear in what form HCHO is deposited to the snow surface. Examination under present day conditions points to a purely reversible species, where only the gas phase is of relevance; whereas the continuous record points out that heterogeneous chemical processes has the same importance.

THE BYRD H_2O_2 RECORD: A REVISED VERSION

In 1986, we published a paper entitled "Long-term record of H_2O_2 in polar ice" [Neftel et al., 1986]. At that time we were puzzled by data from the Byrd core, which showed a large scatter but much higher value in ice from the time period 5,000 - 15,000 years B.P., compared to relatively young samples. We were somewhat unsure about how to interpret the data. We felt it unlikely that the H_2O_2 peak would reflect a corresponding

change in the atmospheric concentration. The conclusion was obvious, and perhaps the most abused statement in science can be expected here: more measurements and more research were needed!

In the meantime, we had a closer look at the H_2O_2 data from West Antarctica to bring some light into the dark. Continuous measurements along a shallow core from Siple station located on the edge of West-Antarctica, (mean air temperature: -24° C; mean yearly accumulation rate: 0.5 meter water equivalent), show the expected behaviour: clear seasonal variations and mean concentrations comparable to Dye 3. These observations are not inconsistent with atmospheric model concentrations [Sigg and Neftel, 1990]. Remeasurement on different core sections from Byrd station (mean air temperature: -28° C, accumulation rate: 0.13-0.18 meter water equivalent per year) from a newly drilled shallow core and from the old deep core essentially confirmed the previous results. Figure 6 shows three sections from the shallow core: H_2O_2 concentrations in the shallow core are only 20 - 50% of the concentration found at Siple. If a transfer function as given in Figure 5 is assumed, this would mean a much lower atmospheric concentration at Byrd station as compared to Siple station (based on yearly mean values), which is unlikely to be real [D. Jacob, personal communication]. There must be another effect that tends to systematically reduce the H_2O_2 concentration initially present in the snow deposited at Byrd.

As discussed above, the atmospheric concentration during the winter could be lower than the "equilibrium" concentration corresponding to the previous summer layers. By ventilation of air through the upper part of the firn, H_2O_2 can be depleted. These hypothetical low winter concentrations could be a consequence of the shielding effect of the circumpolar vortex. Siple lies just on the edge or outside the vortex, whereas Byrd lies inside the vortex.

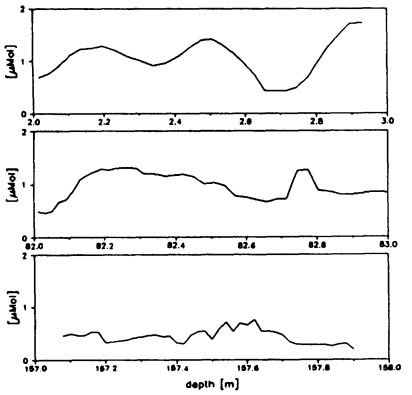

Fig. 6: Continuous H_2O_2 measurements on three core section from a new shallow core from Byrd.

In order to maintain the initial H_2O_2 summer concentration during the wintertime, air masses with some H_2O_2 must be brought to the site. This is very likely to be the case for Greenland: Temperature records from Summit show fast, large and frequent fluctuations which must be associated with transport of air masses from lower latitudes. Systematic analysis of wintertime atmospheric H_2O_2 concentration in polar regions is not available. Investigations on the high alpine research station at Jungfraujoch, Switzerland demonstrate a dependence of the H_2O_2 level on the 4 day back trajectories. It is our hypothesis that mainly the winter concentrations modulate what is retained initially in the ice cores.

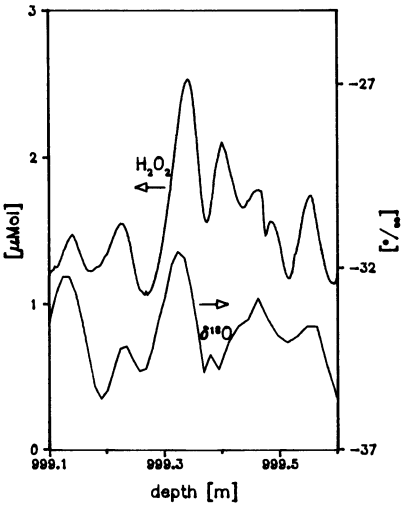

Fig. 7: Detailed analysis of a section (1,000 m.b.s.) from the Byrd core drilled in 1968

Figure 7 shows detailed analysis from sections around 1,000 metres below the surface from the Byrd deep core, thus, within the broad "1986 peak". Again high and varying concentrations are found. This time the samples were continuously analysed and revealed patterns which suggested a seasonal fluctuation. (The present-day accumulation rate at Byrd is too low for seasonal changes of either $d^{18}O$ or H_2O_2 would be preserved.) Detailed measurements of the $d^{18}O$ variations in the core section confirmed the seasonal structure of the fluctuation, a rough calculation of the initial $d^{18}O$ distribution by the procedure by Johnsen [1972] yields summer-to-winter ratios that are similar to present day surface values. The reappearance of seasonal fluctuations in the Byrd core explains the scatter that we found earlier and were unable to explain. In order for seasonal fluctuations to survive, the accumulation rate must have been considerably higher, more than twice the present day value of 13-18 cm. water equivalent per year. Also, the mean H_2O_2 concentration in the ice is

higher than the concentration corresponding to the last 1,000 years. Was the atmospheric concentration also higher at Byrd station 15,000 - 5,000 years B.P.? Not necessarily! The distribution of accumulation over the Antarctic is mainly determined by the circumpolar vortex which shields off the interior of Antarctica. Under present day conditions, Siple station receives three times as much precipitation than Byrd station; 10,000 years ago, the Byrd area must get the same amount in order for the seasonal changes to be preserved. Either the vortex system was spatially shifted, or it was generally weaker. It is beyond the scope of this contribution to discuss possible reasons for such a shift; the important thing here is that the H_2O_2 measurements gives a hint of a changed meteorological pattern and not necessarily changed oxidation capacity.

CONCLUSIONS

There is not an easy determined parameter in polar ice cores which yields a measure for the burden of atmospheric oxidants. O_3 and OH are most likely not recorded at all. Under special circumstances, H_2O_2 shows a concentration pattern that might reflect an atmospheric pattern. The chemical information in the ice core has to be decoded, and a quantitative understanding of the transfer function has to be developed in the near future. At present, the most information regarding reversibly deposited species is available for H_2O_2.

Acknowledgements: We would like to thank Roger Bales for carefully reviewing the manuscript and converting the "Swiss English" to "American English" and Andi Sigg for valuable discussion. We are grateful to Chet Langway Jr. for providing us with the samples from the New Byrd core. Martin Anklin and Markus Möll helped with the measurements in Greenland. This work was supported by a grant from the Swiss Office for Science and Education over a COST 611 project.

REFERENCES

Bales, R. C., J. Dibb and A. Neftel, EOS Article, 1992.

Chappellaz, J., J.M. Barnola, D. Raynaud, Y.S. Korotkevich and C. Lorius, Ice-core record of atmospheric methane over the past 160,000 years, *Nature, 345*, 127-131, 1990.

Conklin, M.H., A. Sigg, A. Neftel and R.C. Bales Atmosphere-Snow transfer function for H_2O_2: microphysical considerations, (submitted to JGR, August 1992).

Dansgaard, W., S.J. Johnsen, H.B. Clausen, D. Dahl-Jensen, N. Gunderstrup, C. Hammer and H. Oeschger, North Atlantic climatic oscillations revealed by deep Greenland ice cores. *In Climate Processes and Climate Sensitivity Geophysical Monograph 29* 288-298, AGU, Washington DC, 1984.

Etheridge, D.M., G.I. Pearman, and F. de Silva, Atmospheric trace gas variations as revealed by air trapped in an ice core from Law Dome, Antarctica, *Annuals of Glaciology, 10*, 28-33, 1988.

Fuhrer, K., A. Neftel, M. Anklin, M. Möll and V. Maggi, Continuous in situ measurements of chemical species along the new GRIP ice core from Summit, Central Greenland, (submitted).

Graedel, T.E., Chemical compounds in the Atmosphere Academic Press, New York, 1978.

Intergovernmental Panel in Climate Change ICPP, *Climate Change - The IPCC Scientific Assessment*, Press syndicate University of Cambridge, 1990.

Johnsen, S.J., Stable Isotope Homogenization of Polar Firn and Ice, *International Association of Hydrological Sciences Publication 118*, Isotopes and Impurities in Snow and Ice, Grenoble, 210, 1977.

Logan, J.A., Tropospheric Ozone: Seasonal behaviour, trends and anthropogenic influence, *J. Geophys. Res., 90*, 10463-10482, 1985.

Neftel, A.; P. Jacob and D. Klockow, Measurements of hydrogen peroxide in polar ice samples, *Nature, 311*, 43-45, 1984.

Neftel, A.; P. Jacob and D. Klockow, Long-term trend of Hydrogen Peroxide in polar ice cores, *Tellus, 38B*, 262-270, 1986.

Neftel, A., and A. Sigg, Hydrogen Peroxide in solid precipitation, Fourth European symposium on physico-chemical behaviour of atmospheric pollutants, D. Reidel Publ. Comp. 500-510, 1987.

Neftel, A., Use of snow and firn analysis to reconstruct past atmospheric composition *in: Seasonal Snowpacks - Processes of compositional changes*. Eds., T.D. Davies, M. Tranter and H.G. Jones. Springer Verlag Series G: Ecological Sciences Vol. 8 385-416, 1990.

Oeschger, H. and C.C. Langway Jr., The Environmental Record in Glaciers and Ice Sheets. *Physical, Chemical and Earth Science Research Report 8*, John Wiley & Son., 1989.

Schwander, J. and B. Stauffer, Age difference between polar ice and the air trapped in its bubbles, *Nature, 311*, 45-47, 1984.

Sigg, A. and A. Neftel, Seasonal variations of hydrogen peroxide in polar ice cores. *Annual Glaciol., 10*, 157-162, 1988.

Sigg, A., T. Staffelbach, and A. Neftel, Gas phase measurements of hydrogen peroxide in Greenland and their meaning for the interpretation of H_2O_2 records in ice cores, *J. of Atmos. Chem., 14*: 223-232, 1992.

Stauffer, B., G. Fischer, A. Neftel and H. Oeschger, Increase of atmospheric methane recorded in Antarctic ice core, *Science, 229*, 1386-1388, 1985.

Stauffer, B., E. Lochbrunner, H. Oeschger and J. Schwander, Methane concentration in the glacial atmosphere was only half that of the preindustrial Holocene, *Nature, 332*, 812-814, 1988.

Stauffer, B. and A. Neftel, What have we learned from the ice cores about atmospheric changes in the concentrations of nitrous oxide, hydrogen peroxide, and other trace species; The changing atmosphere, Eds. F. S. Rowland and I.S.A. Isaksen, John Wiley and Son 63-77 Dahlem Konferenzen, 1988.

Staffelbach, T., A. Neftel, B. Stauffer and D. Jacob, Formaldehyde in polar ice cores; a possibility to characterize the atmospheric sink of methane in the past, *Nature, 349*, 603-605, 1991.

Thompson, A.M., The oxidizing capacity of the earth's atmosphere: Probable past and future changes, *Science, 256*, 1157-1165, 1992.

Volz, A., and D. Kley, Ozone measurements made in the 19th century: An evaluation of the Montsouris series, *Nature, 332*, 240-242, 1988.

SOURCES OF ORGANOBROMINES TO THE ARCTIC ATMOSPHERE

Robert Moore, Ryszard Tokarczyk and Charles Geen
Department of Oceanography
Dalhousie University
Halifax, Nova Scotia
Canada B3H 4J1

INTRODUCTION

Atmospheric measurements of bromine compounds were stimulated by the recognition that bromine was a potential catalyst in the destruction of ozone. In the course of these studies, it became apparent that bromoform ($CHBr_3$) concentrations in the arctic atmosphere can be strongly seasonal; Cicerone et al. [1988] reported maxima at Point Barrow between December and February, and minima between June and August. Sturges and Barrie (1988) reported that atmospheric particulate Br peaked each year just after the Arctic dawn, with levels two orders of magnitude higher than could be explained by marine, automotive or crustal sources. Barrie et al. [1988] subsequently found that ozone depletion occurs in the arctic troposphere in springtime, and that ozone and filterable bromine concentrations were inversely correlated. These observations, together with the recent work of McConnell et al. [1992], have raised the question of the origin of arctic atmospheric bromine.

The ocean, as the main exchangeable reservoir of bromine, is the most obvious potential source of bromine to the atmosphere, but attention must be given to processes which produce specific compounds such as $CHBr_3$, and more generally to the processes that produce the separation of bromine from seasalt sodium reported by Sturges and Barrie (1988) in arctic aerosols.

A good deal of research has been done into aspects of $CHBr_3$ production by marine seaweeds, and a reasonable understanding of some biochemical aspects is now available. In general, why these compounds should be synthesised has not been clearly established, though the reason most commonly given is that the presence of toxic halocarbons in the algae provides some defence against predation [McConnell and Fenical, 1979].

It is clear that the ability to produce halocarbons is widespread amongst the macrophytes. McConnell and Fenical [1979] have provided an extensive list of halogenated metabolites in red algae of the family *Bonnemaisoniaceae*. Among the compounds listed are $CHBr_3$, $CHBr_2Cl$, and $CHBrCl_2$. Gschwend et al. [1985] identified these compounds among the products of several species of macrophyte (brown algae, *Ascophyllum nodosum* and *Fucus vesiculosis*, green algae, *Enteromorpha linza* and *Ulva lacta*, and the red alga, *Gigartina stellata*).

NATO ASI Series, Vol. I 7
The Tropospheric Chemistry of Ozone in the Polar Regions
Edited by H. Niki and K. H. Becker

De Boer et al. [1986] reported the presence of vanadium-containing bromoperoxidase enzymes in the marine brown alga, *Ascophyllum nodosum*. De Boer and Wever (1988) subsequently proposed a mechanism for bromination of organic compounds by this enzyme, in which production of oxidized bromine species such as HOBr was the key step. Wever et al. [1991] have suggested that macrophytes might release HOBr to the water column, and that this brominates dissolved organics yielding amongst other compounds, $CHBr_3$. A possible explanation for the common occurrence of chlorobromomethanes in seawater is via bromoiodomethane production. A bromoperoxidase is capable of oxidizing iodide, and therefore mixed bromoiodomethanes can be produced; it has been suggested that these react with chloride in seawater yielding bromochloro-derivatives [Theiler et al. 1978]. Evidence has recently been found for chloroperoxidase activity in a vanadium-containing bromoperoxidase from *Ascophyllum nodosum* [Soedjak and Butler, 1990].

On account of the strong seasonality of bromine in the arctic atmosphere, it is worth looking at what is known about temporal variation in the strength of biological sources. The work of Gschwend et al. [1986] did not show clear evidence for seasonality in the release of polybromomethanes by seaweeds, for while a laboratory study initially showed a strong temporal signal in release, it did not recur a year later. Field studies indicated only weak seasonality, which the authors suggested might be indicative of the involvement of epiphytic fungi in the production of the organobromine compounds.

In spite of the widespread occurrence of haloperoxidases in nature, there are no reports of their occurrence in phytoplankton. To some extent, this may be due to the greater difficulty of obtaining the necessary quantities of material for study. However, a number of studies of laboratory cultures of phytoplankton have not shown production of trihalomethanes. A major problem here is that non-production of the compounds in the laboratory does not demonstrate that they cannot be produced under certain conditions, for example at a particular stage in the growth or demise of an organism. Nonetheless, as increasing numbers of such experiments fail to yield compounds like $CHBr_3$, it becomes increasingly unlikely that they have a major source in common oceanic phytoplankton species. (These comments should not be taken to apply also to methyl halides - CH_3Cl, CH_3Br, and CH_3I, which very likely have a different production mechanism than the trihalomethanes.)

Questions that need to be addressed include: Does the ocean provide a significant source of organic bromine to the arctic atmosphere? What is the relative importance of the Arctic Ocean and more temperate seas as sources of organic bromine to the arctic atmosphere? Within the oceans what are the sources of volatile organobromine compounds? This last question is related to the relative importance of coastal and pelagic zones as sources.

This paper provides some information on the strengths of $CHBr_3$ sources from temperate and arctic, coastal and pelagic marine environments. It considers some evidence for the possible involvement of arctic ice algae as a $CHBr_3$ source. Measurements are reported of high concentrations of $CHBr_3$ in arctic snow samples.

METHODS

Halocarbons were measured after purging from a 5 mL water sample and transfer to a Varian 3400 gas chromatograph fitted with an electron capture detector. Compounds routinely measured are: $CHBr_3$, $CHBr_2Cl$, $CHBrCl_2$, CH_2Br_2, CH_2ClI and CH_3I; details are given in Moore and Tokarczyk [1992a]. Snow samples were collected in glass bottles fitted with a screw cap. The containers were cleaned by baking in a vacuum oven before use. The snow sample was gently compacted into the bottle using a glass plunger, and an aluminium foil was placed over the top of the bottle before capping. The samples were left frozen until analysis when they were allowed to warm in the laboratory, and when completely melted the bottle was opened and the liquid contents drawn into a clean glass syringe. The analysis was then as for seawater samples, except that snow samples containing especially high levels of halocarbons were measured on 2 mL aliquots. No correction has been made for distribution of the gases between the liquid and gas phase, but efforts were made to minimise errors from this source by filling the vessel as full as possible with snow, and by making the measurements as soon as possible after the snow had melted. Ice cores were collected using a Sipre corer, and subsections were taken from the centre of the core to minimise contamination. These were crushed and stored in the same way as snow samples.

Water samples were also obtained from an *in situ* incubator. This is a device which seals a cylindrical cup into the bottom surface of the ice, thereby isolating a sample of the ice algae which can then be studied for release or uptake of components. It was designed for C-14 productivity measurements [Herman et al. 1992], but in the current work was used to estimate fluxes of halocarbons from the ice-algal community into the water column.

RESULTS AND DISCUSSION

Bromoform in the N.W. Atlantic and Baffin Bay

Measurements have been made of the suite of halocarbons as vertical water column profiles in the North West Atlantic and in Baffin Bay. The surface data which are most relevant to air-sea exchange of the compounds are illustrated for $CHBr_3$ in Figure 1. A detailed description of the vertical profiles is given in Moore and Tokarczyk [1992a] and, for chloroiodomethane (CH_2ClI), in Moore and Tokarczyk [1992b]. Clearly apparent from the figure are the higher concentrations of $CHBr_3$ in coastal waters compared with the open ocean, consistent with the known source from seaweeds. Only in the case of CH_2ClI did the

distribution show the highest concentrations in surface waters at some pelagic stations, which we argue provides evidence for a source other than macrophytes, coming perhaps from pelagic plankton or bacteria.

In the case of the samples having $CHBr_3$ concentrations higher than 2 ng/L, we can be reasonably confident that they are supersaturated relative to the atmosphere. This is based on a set of atmospheric data from P.B. Shepson (personal communication) which indicate that atmospheric concentrations were in the range 0.34 to 1.44 pptv, with a mean value of 1.03 pptv. For water at 0 °C, and using Fogelqvist's [1985] calculated non-dimensional Henry's Law constant of 0.009, these would correspond to equilibrium water concentrations ranging between 0.43-1.8 ng/L (mean 1.3 ng/L). Where the water temperatures are higher than 0 ^{o}C the equilibrium water concentrations will be lower.

From the oceanic data that we present, we are able to show that the $CHBr_3$ flux to the atmosphere calculated by Liss [1986] on the basis of very limited surface ocean measurements is most probably a large overestimate. He used a surface ocean value of 10 ng/L [from Fogelqvist, 1985, and Dyrssen and Fogelqvist, 1981], and an atmospheric level of 0.7 pptv [from Penkett et al. 1985]. With these values the concentration at equilibrium with the atmosphere is around 0.2 ng/L at 20 °C, which is much smaller than the surface concentration used. Consequently, the flux is largely insensitive to the value selected for the Henry's Law constant. The resulting flux was $2x10^{12}$ g/yr, which he pointed out would be only halved if the much higher atmospheric concentration (15±13 pptv) measured by Berg et al. [1984] in the Arctic were used. Our data suggest that for the open ocean a concentration of *ca.* 1.2 ng/L would be more realistic. At such low values it becomes necessary to take into account the water temperature of each sample when calculating the flux. With the present uncertainties in the Henry's Law constants, and in the water and air measurements, it will be difficult to establish whether the pelagic surface waters are a source or sink for the compound.

Coastal waters can have widely varying concentrations of $CHBr_3$ depending on the proximity of macro-algal sources. We have measured concentrations in waters sampled directly from beds of macro-algae with concentrations in excess of 400 ng/L. Dyrssen and Fogelqvist [1981] reported values of around 70 ng/L for $CHBr_3$ at two coastal sites in Svalbard. Tokarczyk [unpublished data] found an average value of 99 ng/L for surface water in a 5 month period (January - June) in the Bedford Basin, Nova Scotia. From our N.W. Atlantic and Baffin Bay datasets we find concentrations in the range 4-30 ng/L at near-shore locations. An average concentration of 20 ng in coastal waters would yield an estimated global source of *ca.* $8x10^{10}$ g/yr, based on 2% of the ocean being categorised as coastal. This may be compared with the rough estimate of *ca.* 10^{10} g/yr made by Gschwend et al. [1985] for the atmospheric source of organobromines from macrophytes.

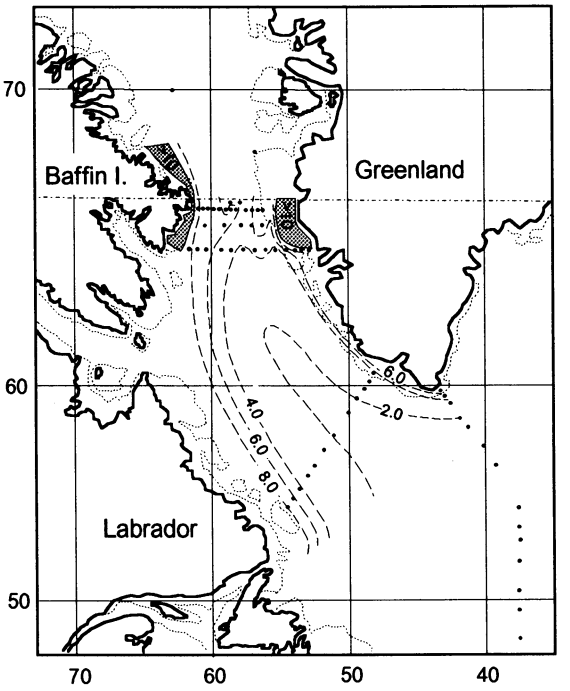

Fig. 1. Surface distribution of bromoform in the N.W. Atlantic Ocean and Davis Strait. Concentrations in ng/L.

We have measured the same halocarbons in ice-covered waters of the Beaufort Sea in the period March 17-21, 1991. The results showed that the surface waters exhibit little variation in $CHBr_3$ concentrations (range 1.6 to 2.9 ng/L; Figure 2) and have even more uniform concentrations of CH_2Br_2 (1 to 1.3 ng/L). In this case, the measurements included waters 250 km from the shore, so that the results should not be complicated by the presence of macrophytes. Again, using a Henry's Law constant of 0.009 for $CHBr_3$, the waters would have an equilibrium atmospheric concentration of 1.3-2.3 pptv. Three air samples measured for $CHBr_3$ at Tuktoyaktuk contained levels between 0.95 and 3.34 pptv (mean 1.85 pptv). Therefore, at this location the waters are probably not appreciably supersaturated, and furthermore cannot act as a significant source to the atmosphere on account of the almost complete ice-cover. As reported below, snow samples which were collected at some of the stations showed $CHBr_3$ concentrations two orders of magnitude greater than those in the seawater. Unfortunately this work did not include either measurements in the ice itself, or measurements of the chlorophyll concentration at the ice-water interface. Consequently, we have no information on possible production of $CHBr_3$ by ice algae in this region.

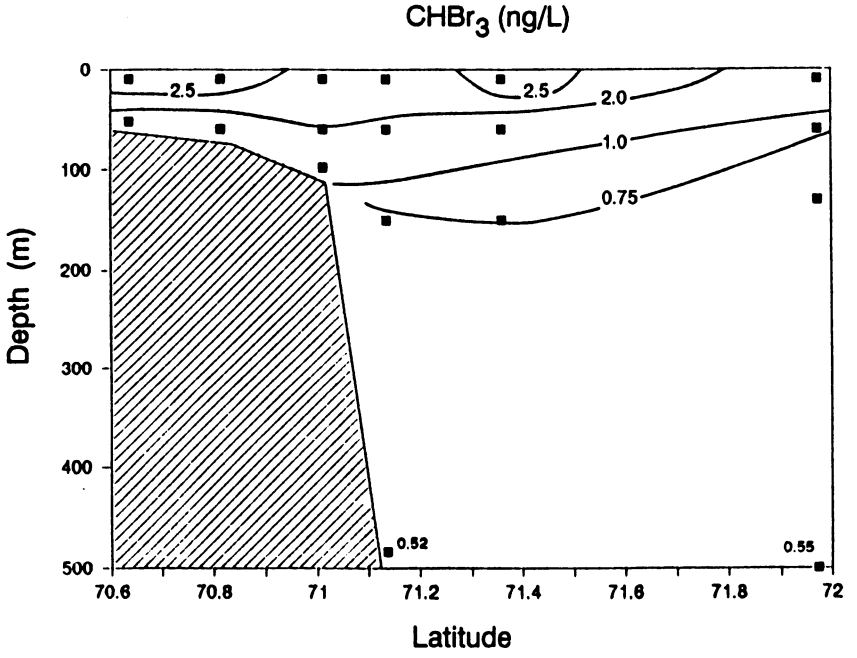

Fig. 2. Vertical section of dissolved bromoform in the Beaufort Sea.

Water column profiles were measured in a coastal location off Resolute Bay, NWT in mid-April and mid-May 1992. The sampling dates were chosen to fall near the beginning of the spring bloom of ice algae, and during a second period when the growth rate and biomass would be high (Figure 3). In each profile (Figure 4a) $CHBr_3$ concentrations decrease with depth indicative of a source, local or advective, at shallow depth. Between the two dates it appears that there has been some enhancement in the concentrations of $CHBr_3$ in the water column (by *ca.* 4 ng/L near the surface). However, in the case of the measurements made on May 10, several water samples from just below the ice collected on the next day as part of the *in situ* incubation experiment showed $CHBr_3$ concentrations that were substantially lower at around 8 ng/L. This might be due to lateral inhomogeneity in the water column, which would also be consistent with differences between measurements made on April 12 and 13, (illustrated for $CHBr_3$ in Figure 4a but found for all the compounds measured). In view of the presence of macrophyte growths near the shore, such inhomogeneity is to be expected, and it prevents us from confirming that there was any general increase in concentrations of $CHBr_3$ in the water column over the period of this experiment.

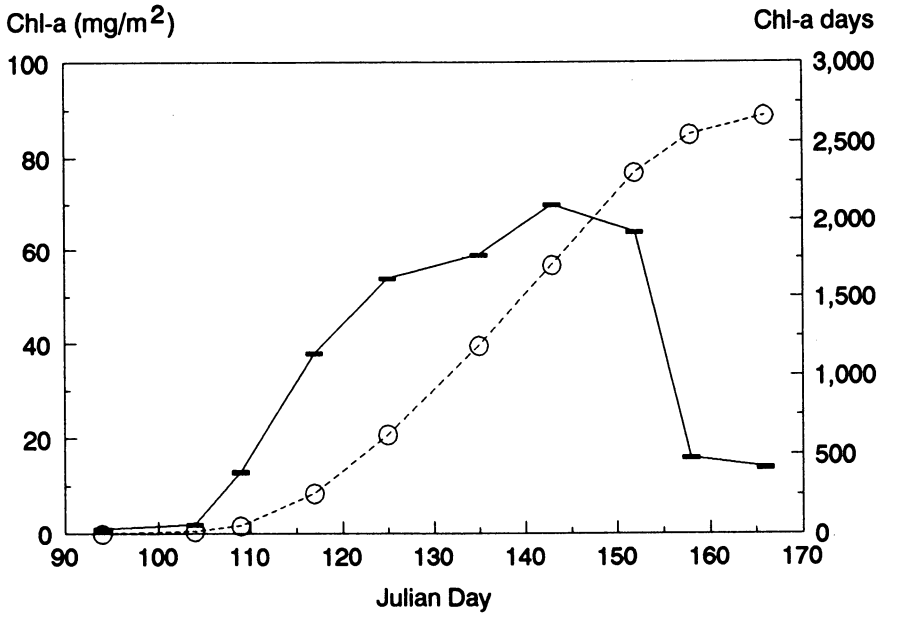

Fig. 3. Chlorophyll-a (mg/m^2) in ice cores *vs.* time at Resolute Bay, 1989 (courtesy R. Smith). Chlorophyll integrated over time also shown.

At the same site, halocarbons were measured in two sea-ice Sipre cores also collected in mid-April and mid-May (Figure 4b). The highest concentration of chlorophyll was present in the sample closest to the water interface. Several significant observations can be made: first that there are higher concentrations of $CHBr_3$ in the ice that contained the bulk of the ice algae; second, higher concentrations of $CHBr_3$ were measured in the ice-bottom sample in May when the algal biomass was higher; and third, in each core $CHBr_3$ was higher near the upper surface of the ice than within. Dealing first with the ice-water interface, the results are consistent with production of $CHBr_3$ by a component of the ice algae - in accord with reports by Sturges et al. [1992a]. While $CHBr_2Cl$, like $CHBr_3$, had a higher concentration in the deepest section of the ice-core, its concentration in this sample was no higher than the upper water column. Dibromomethane, which frequently shows a distribution like that of $CHBr_3$ in seawater, also showed only a small increase in concentration at the bottom of the ice-core, with its levels not reaching those of the underlying water. This suggests that while $CHBr_3$ might have a source in the ice-algal community, CH_2Br_2 and probably $CHBr_2Cl$ did not. This is supported by data from the *in situ* incubation experiments.

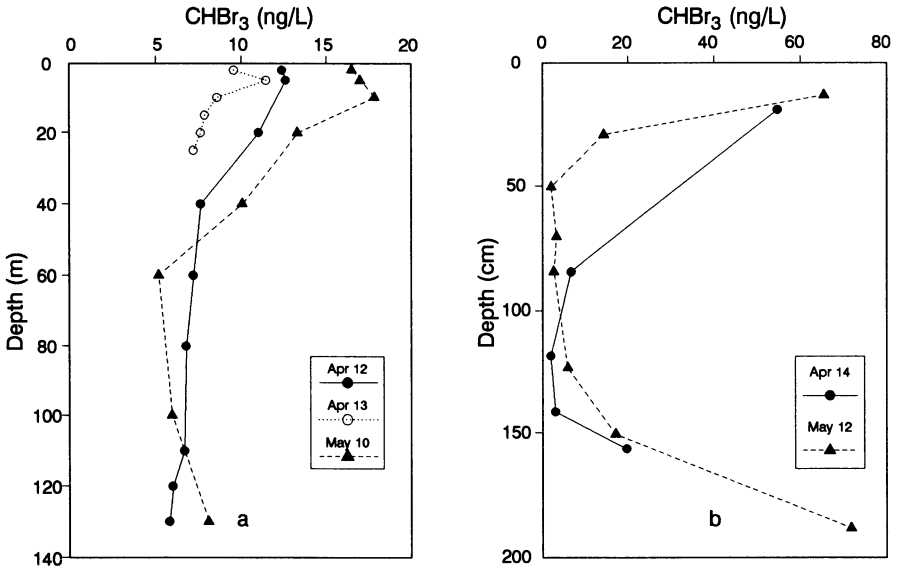

Fig. 4. a) Water column profiles of dissolved bromoform at Resolute Bay, N.W.T. (April and May 1992); b) bromoform in two sea-ice cores from the same site.

The *in situ* incubator was used in mid-April and again in mid-May in an attempt to estimate the flux of halocarbons into the water column from the bottom of the ice. On each occasion a water sample was collected from just below the ice for measurement of ambient halocarbon concentrations. At the end of the incubation period the concentration of halocarbons was measured in the trapped water sample, and also in a sample of the ice that was recovered at the same time. The results (Table 1) show that only in the case of $CHBr_3$ was there a significantly higher concentration in the ice than in the water column. In both of the incubation experiments the difference in concentration between beginning and end of the experiment was small (*ca.* 1.8 ng/L) and subject to relatively high uncertainty as the difference in two larger numbers. This number would be equivalent to a flux of *ca.* 2 μg $CHBr_3$ m^{-2} day^{-1}.

However, interpretation of the results is made more difficult by the proximity of these samples to a shore where macrophytes grow. There is the possibility, mentioned above, that release of HOBr by seaweed might result in bromination of organics from other sources - in this case it could be organics released by the ice algae. An alternative possibility is that the macrophytes release bromoperoxidase enzymes which, in the presence of hydrogen peroxide, bromide ion, and a suitable organic substrate, could yield organobromine compounds. All of

these conditions could be provided by the ice-algal community [Palenik and Morel, 1987; Cooper et al. 1988].

Table 1. Results of *in situ* incubation experiments at Resolute Bay 1992; *A* April 15 (duration 2.1 hr), *B* May 11 (duration 2.2 hr).

A	$CHBr_3$ (ng/L)	$CHBr_2Cl$ (ng/L)	CH_2Br_2 (ng/L)
Ambient seawater concentration	8.2	0.7	1.7
Concentration after incubation	10.0	0.7	1.9
Change in concentration	1.8	0.0	0.2
Concentration in ice sample	68.5	1.0	1.0

B	$CHBr_3$ (ng/L)	$CHBr_2Cl$ (ng/L)	CH_2Br_2 (ng/L)
Ambient seawater concentration	8.2	0.5	1.4
Concentration after incubation	10.1	0.6	1.6
Change in concentration	1.9	0.1	0.2
Concentration in ice sample	55.2	0.4	0.9

The only phytoplanktons that have been reported to be producers of $CHBr_3$ are certain species of ice algae from both polar regions [Sturges et al., 1992a & b]. Our laboratory experiments with cultured phytoplankton, including a number of ice-algal species, have not so far shown production of $CHBr_3$, and additionally our Atlantic field measurements have not yielded evidence for $CHBr_3$ production by phytoplankton. Thus, it does not appear that the ability to synthesise and release bromoform is a common facility of phytoplankton.

Interpretation of the high concentrations of $CHBr_3$ in the ice-bottom samples from Resolute is made difficult by the complexity of the biological community occurring there. Throughout the observation period pennate diatoms were dominant (> 90%) both in terms of cell numbers and bio-volume. Centric diatoms such as *Thallasiosira hyperborea* and *Chaetoceros sp.* existed but with relatively low biomass. Other flagellates, which were mainly *Peridinium sp.* (Dinoflagellates) and *Cryptomonas sp.*, were observed in every sample but were not significant. This pennate diatom dominated community was typical of the high arctic. During the sampling time, species succession can be observed. In April the dominant

species was *Nitzschia arctica*, forming ribbon shaped colonies (39% in biomass), and second in abundance was arborescent colony forming *Nitzschia frigida* (33% in biomass). After one month both species increased in cell numbers. However, the increase of *N. frigida* was greater than that of *N. arctica* accounting for 40-50% of the total algal biomass. It should be noted that this does not form an exhaustive description of the biological community at the ice-water interface which also included zooplankton and bacteria. The possibility exists that production of $CHBr_3$ is not due simply to one or more of the predominant phytoplankton species identified in these samples. Minor components could be responsible, including bacteria or interactions between species.

There are several potential explanations for the higher concentration of $CHBr_3$ in the upper part of the ice cores. It could reflect higher concentrations in surface sea water early in the winter, decreasing with time. Alternatively, it is conceivable that the compounds have migrated into the core from the upper surface. As described below, we have measured very much higher concentrations of $CHBr_3$ in snow collected from the sea-ice than in the ice or underlying water. If any snow melts early in the freeze-up, percolation of the meltwater could result in high concentrations in the upper part of the ice. A third possibility is that the compounds are generated within the ice by an oxidation process involving bromide ion and organic compounds in the ice that had their origins in seawater. With only two sets of measurements available from a single site, we are not able to determine which mechanism is most likely.

Effect of ice-cover on release of halocarbons in the Arctic Ocean

The exchange of gaseous halocarbons between ocean surface and atmosphere must be inhibited by the presence of ice cover, so it follows that for a given level of supersaturation of surface waters, the Arctic Ocean and northern seas will be a less effective source of halocarbons to the atmosphere. As a first approximation we will assume that exchange occurs only through an ice-free surface. Estimates of the annual variation of ice cover have been adapted from Mysak and Manak [1989] who presented data from a 32-year survey of Arctic sea-ice concentrations on a 1-latitude grid. Their results were grouped into 7 geographic sub-regions which excluded the central Arctic Ocean. We have included this region which, they point out, has permanently greater than 9/10 ice-coverage, giving an Arctic Ocean fractional ice-coverage on a monthly basis as shown in Figure 5. We suggest that the coverage is accurate to about 10%.

To obtain a clearer idea of the temporal source function of any phytoplankton-produced halocarbons in arctic regions, the potential for loss to the atmosphere has to be combined with an index of the surface water concentration. This quantity is not known. If chlorophyll concentration is taken to be an approximate index of production rate, the total

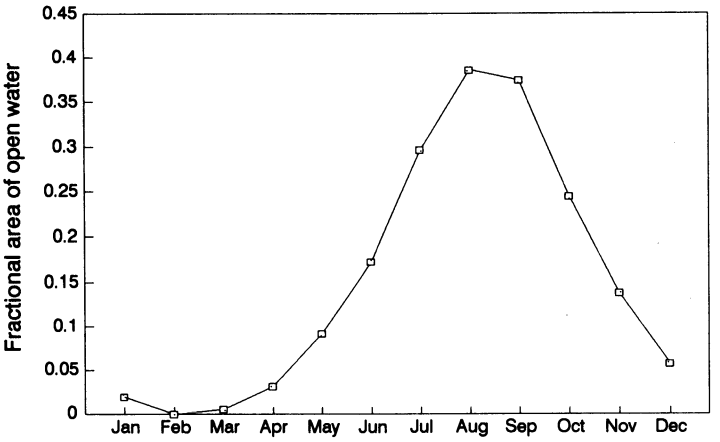

Fig. 5. Fraction of open water in the arctic region: points represent fractions at the end of each month [adapted from Mysak and Manak, 1989].

production of halocarbon may be approximated by the time integral of chlorophyll. (A more rigorous calculation might include the product of irradiance and chlorophyll concentration). In Figure 3 are plotted chlorophyll-a concentrations per m^2 at Resolute Bay in spring, the integrated chlorophyll (chlorophyll-days) and, in Figure 6, the product of integrated chlorophyll and fractional open water. This final quantity is intended to represent the form of the $CHBr_3$ flux to the atmosphere which we can estimate until mid-June. The source strength is normalized to the maximum value which is at the end of the time period. This indicates that any flux of $CHBr_3$ from the Arctic Ocean due to ice-algal production is likely to be low until about June, the increase at that time being due to a combination of plankton release and increasing open water.

On account of the fact that leads can occur locally at virtually any time of the year, there will always be the possibility of a local, short term source of $CHBr_3$ to the atmosphere provided that the surface waters are supersaturated. Amongst the assumptions made here is that halocarbon production occurs uniformly during the growth cycle, as opposed to enhanced production during stationary phase or senescence. The latter would delay halocarbon production.

These estimates indicate that neither the relatively high concentrations of $CHBr_3$ in the Arctic atmosphere in the period December-February [Cicerone et al., 1988], nor the springtime peak in particulate, non-seasalt bromine [Sturges and Barrie, 1988] are likely to be explained primarily in terms of their production by epontic ice algae in the Arctic Ocean.

At present there are almost no measurements to show whether arctic surface waters away from the coast do contain significantly elevated bromoform levels due to ice-algal

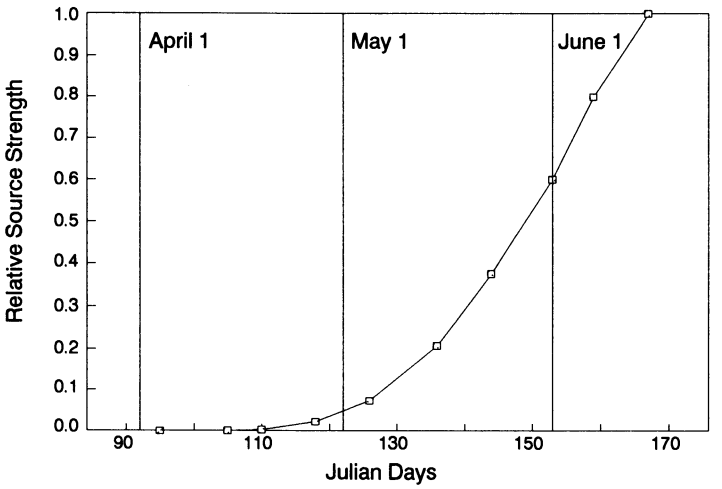

Fig. 6. Product of integrated chlorophyll and fractional open water area. Values are normalised to the value at the end of the chlorophyll-a time series in mid-June.

production. Our measurements from the Beaufort Sea may be too early in the spring to reveal ice-algal influence, and the only other report we have is that of Krysell [1991] who recorded a maximum $CHBr_3$ concentration of 4 ng/L at a depth of a few meters below the ice at 85, north of Svalbard in July, just 1.1-2.4 ng/L higher than the springtime Beaufort Sea levels.

An influence of the extensive ice-cover of the Arctic Ocean must be to increase the residence time of marine-derived halocarbons in the upper waters with respect to loss to the atmosphere. Concentrations will tend to grow to a higher average value than in ice-free seas, and other loss processes, such as hydrolysis, halogen exchange, and advection from arctic regions, will assume increased importance.

Bromoform in Arctic snow

We have made some measurements of halocarbons in snow collected from the sea-ice, and have found high concentrations of a number of organobromines, especially less volatile compounds such as $CHBr_3$ (Table 2). The highest concentrations of $CHBr_3$ were found in samples from the Beaufort Sea collected in late March. Samples collected further north at Resolute Bay in April and May, contained on average, lower concentrations, and much lower levels were found in snow samples collected in Alert on northern Ellesmere Island. All of these samples were taken at or near sea level; and samples collected at 1550 m elevation on the Agassiz icecap showed very low concentrations of $CHBr_3$. We suggest that he presence

Table 2. Concentrations of bromoform and chlorodibromomethane in arctic snow samples. Numbers in brackets are the number of measurements that have been averaged; *a* denotes Alert samples collected from the ground rather than from a snow collector.

Sample Location	Temp C	$CHBr_3$ (ng/L)	$CHBr_2Cl$ (ng/L)
Beaufort Sea			
Latitude Longitude			
71 58.4 134 49.4	-31	509	51
71 21.6 134 1.3	-28	417	36
71 8.2 133 40.4	-23	237	9
70 48.9 133 17.0	-25	538	16
70 38.1 133 0.5	-23	118	8
Tuktoyaktuk		201	14
Tuktoyaktuk		82	4
Tuktoyaktuk		48	5
Tuktoyaktuk		128	24
Alert (Oct 90)		0 (1)	0
Alert (Nov 90)		2 (1)	0
Alert (Dec 90)		6 (4)	0.4
Alert (Jan 91)		5 (3)	0.1
Alert (Feb 91)		2 (2)	0
Alert (Mar 91)		8 (2)	0.7
Alert (Apr 91)		8 (1)	1.2
Alert (Apr 91)*a*		20 (4)	2.2
Agassiz Icecap (fresh snow at 1550 m)	-14	0.6	0
Resolute (Apr 92)		177	10
Resolute (Apr 92)		193	12
Resolute (May 92)		56	5
Resolute (May 92)		120	16

of $CHBr_3$ and other halocarbons of similar volatility in snow might be due to freezing of these compounds onto the snow from the atmosphere, and that the source of the compounds to the atmosphere in winter lies beyond the periphery of the Arctic Ocean. Under these circumstances it would be expected that concentrations in snow would decrease along the trajectory of the air mass entering the arctic region, perhaps explaining why concentrations of

$CHBr_3$ tend to decrease as we sample further north. Outside the ice-covered arctic seas release of these compounds from the ocean, and particularly its margin, can occur earlier in the year. It is also interesting to note that Nightingale [1991] found that the highest concentrations of $CHBr_3$ in the North Sea occurred in February (his data include measurements from February to October). However, measurements made by Tokarczyk in the Bedford Basin, Nova Scotia, did not show any clear seasonal cycle.

McConnell et al. [1992] have suggested that brominated organic compounds may be produced by reaction of Br atoms which are themselves formed by photolysis of Br_2. Also, they suggest that aerosols and ice crystals in the arctic atmosphere are likely to be efficient scavengers of brominated organics from the atmosphere. These ideas could provide the basis of an alternative explanation for enhanced levels of brominated organics in arctic snow.

SUMMARY

From measurements in the N.W. Atlantic we suggest that the flux of $CHBr_3$ from the ocean to the atmosphere needs to be separately estimated for coastal and pelagic zones. The first has relatively high concentrations of dissolved $CHBr_3$ due to the presence of growths of macrophytes, and open ocean waters are closer to equilibrium with the atmosphere such that flux estimates depend more critically on the value selected for the Henry's Law constant and the atmospheric concentrations.

In the Arctic Ocean low concentrations, *ca.* 2 ng/L, were measured in Beaufort Sea surface waters in late March. At the same time concentrations as high as 500 ng/L were measured in snow samples collected from above the sea ice far off shore. Higher water column concentrations were measured in a coastal site off Resolute Bay in both April and May. At that site $CHBr_3$ was found to be enriched in ice-bottom samples containing ice algae. Measurements of fluxes into the water column from the ice yielded values near our detection limits.

We suggest that if ice algae are producers of $CHBr_3$, their contribution to the flux into the atmosphere would probably be maximal in mid-summer, and would not therefore be related to the $CHBr_3$ maximum reported for November to January, or to the peak in particulate bromine seen in at the beginning of April.

Limited measurements of $CHBr_3$ in arctic snow suggest that concentrations decrease with increasing latitude. This might be the result of the compound being precipitated from air masses entering the arctic region. The $CHBr_3$ could have its origin in more southerly marine areas of open water.

Acknowledgements: We wish to thank H. Melling for assistance with work in the Beaufort Sea, the officers and crew of CSS Hudson for work in the N.W. Atlantic. Ice algae identifi-

cation and counting was done by Dr. Sakae Kudoh, National Institute of Polar Research, Tokyo. A time series of chlorophyll-a in ice cores at Resolute Bay was kindly provided by Dr. Ralph Smith. We thank J. Spry for assistance with in situ incubations, and L. Barrie, R. Koerner and R. Chaumont for snow samples from Ellesmere Island. The authors gratefully acknowledge helpful comments from E. Fogelqvist. The work was supported by the Natural Sciences and Engineering Research Council of Canada, and by the Polar Continental Shelf Project.

REFERENCES

Barrie, L.A., J.W. Bottenheim, R.C. Schnell, P.J. Crutzen and R.A. Rasmussen, Ozone destruction and photochemical reactions at polar sunrise in the lower Arctic atmosphere, *Nature*, **334**, 138-141, 1988.

Berg, W.W., L. E. Heidt, W. Pollack, P.D. Sperry, and R.J. Cicerone, Brominated organic species in the Arctic atmosphere, *Geophys. Res. Lett.*, **11**, 429-432, 1984.

Cicerone, R.J., L.E. Heidt and W.H. Pollock, Measurement of atmospheric methyl bromide and bromoform, *J. Geophys. Res.*, **93**, 3745-3749, 1988.

Cooper, W.J., R.G. Zika, R.G. Petasne and J.M.C. Plane, Photochemical formation of H_2O_2 in natural waters exposed to sunlight, *Environ. Sci. Technol.*, **22**, 1156-1160, 1988.

de Boer, E., and R. Wever, The reaction mechanism of the novel vanadium- bromoperoxidase. A steady-state kinteic analysis, *J. Biol. Chem.*, **263**, 12326-12332, 1988.

de Boer, E., Y. van Kooyk, M.G.M. Tromp, H.Plat, and R. Wever, Bromoperoxidase from *Ascophyllum nodosum*: a novel class of enzymes containing vanadium as a prosthetic group? *Biochimica et Biophysica Acta*, **869**, 48-53, 1986.

Dyrssen, D., and E. Fogelqvist, Bromoform concentrations of the Arctic Ocean in the Svalbard area, *Oceanologica Acta*, *4*, 313-317, 1981.

Fogelqvist, E., Carbon tetrachloride, tetrachloroethylene, 1,1,1-trichlorethane and bromoform in Arctic seawater, *J. Geophys. Res.*, **90**, 9181-9193, 1985.

Gschwend, P.M., J.K. MacFarlane and K.A. Newman, Volatile halogenated organic compounds released to seawater from temperate marine macroalgae, *Science*, *227*, 1033-1036, 1985.

Gschwend, P.M., and J.K. MacFarlane, Polybromomethanes. A year-round study of their release to seawater from *Ascophyllum nodosum* and *Fucus vesiculosis*, Organic Marine Geochemistry, ACS Symposium Series **305**, 314-322, 1986.

Herman, A.W., D.F. Knox, J. Conrad and M.R. Mitchel. Instrument for measuring sub-ice algal profiles and productivity *in situ*, *Can. J. Fish. Aq. Sci.* In Press, 1992.

Krysell, M., Bromoform in the Nansen Basin in the Arctic Ocean, *Mar. Chem.*, **33**, 187-197, 1991.

Liss, P.S., The air-sea exchange of low molecular weight halocarbon gases, In, *The role of air-sea exchange in geochemical cycling*, Ed. P. Buat-Menard, D. Reidel Publishing Company, 1986.

McConnell, J.C., G.S. Henderson, L. Barrie, J. Bottenheim, H. Niki, C.H. Langford and E.M.J. Templeton, Photochemical bromine production implicated in Arctic boundary-layer ozone depletion, *Nature*, **355**, 150-152, 1992

McConnell, O.J., and W. Fenical, Antimicrobial agents from marine red algae of the family

Bonnemaisoniaceae. In *Marine algae in pharmaceutical science*, Eds. A.H. Hoppe, T. Levring and Y. Tanaka; Walter de Gruyter, Berlin, N.Y., 1979.

Moore, R. M., and R. Tokarczyk, Volatile biogenic halocarbons in the Northwest Atlantic, Submitted to *Global Biogeochemical Cycles*, 1992a.

Moore, R. M., and R. Tokarczyk, Chloroiodomethane in N. Atlantic waters: a potentially significant source of atmospheric iodine, *Geophys. Res. Letts.* **19**, 1779-1782, 1992b.

Mysak, L., and D.K. Manak, Arctic sea-ice extent and anomalies, 1953-1984, *Atmosphere-Ocean* **27**, 376-405, 1989.

Nightingale, P.D., Low molecular weight halocarbons in seawater. Ph.D. Thesis, University of East Anglia, 1991.

Palenik, B., and F.M.M. Morel, Hydrogen peroxide production by a marine phytoplankter, *Limnol. Oceanogr.*, **32**, 1365-1369, 1987.

Penkett, S.A., M.R. Jones, M.J. Rycroft, and D.A. Simmons, An interhemispheric comparison of the concentrations of bromine compounds in the atmosphere, *Nature*, **318**, 550-553, 1985.

Soedjak, H.S., and Butler, A. Chlorination catalyzed by vanadium bromoperoxidase, *Inorg. Chem.*, **29**, 1990.

Sturges, W.T., and L.A. Barrie, Chlorine, bromine and iodine in Arctic aerosols, *Atmospheric Environ.* **22**, 1179-1184, 1988.

Sturges, W.T., G. Cota and P.T. Buckley, Bromoform emission from Arctic ice algae, *Nature*, **358**, 660-662, 1992a.

Sturges, W.T., C.W. Sullivan, R.C. Schnell, L.E. Heidt and W.H. Pollock, Bromoalkane production by antarctic ice algae, *Tellus*, **45B**, 1992b. In press.

Theiler, R., J.C. Cook, L.P. Hager and J.F. Siuda, Halohydrocarbon synthesis by bromo-peroxidase, *Science*, **202**, 1094-1096, 1978.

Wever, R., M.G.M. Tromp, B.E. Krenn, A. Marjani and M. Van Tol, Brominating activity of the seaweed *A. nodosum*: Impact on the biosphere, *Envir. Sci. Technol.*, **25**, 446-449, 1991.

HYDROCARBONS EMISSION FROM THE OCEAN

B. Bonsang
Centre des Faibles Radioactivités
Laboratoire mixte CNRS/CEA
91198 Gif-sur-Yvette FRANCE

INTRODUCTION

Non-methane hydrocarbons (NMHCs), particularly alkenes oxidized either by ozone, OH and NO_3 radicals can have a significant impact on the photochemistry of the remote background atmosphere [Donahue and Prinn, 1990], and are able, in turn, to influence the budget of these oxidants. Strong evidences for a residual tropospheric background hydrocarbons have been reported by several authors working in remote areas [Rudolph and Ehhalt, 1981; Bonsang and Lambert, 1985; Greenberg and Zimmerman, 1984]. Particularly, alkenes despite their high reactivity are found at significant levels from 10 pptv to 100 pptv in the southern hemisphere and even in the antarctic continent far from usual anthropogenic sources [Rudolph et al., 1989]. The existence of a marine production by outgassing of superficial seawater was first reported by Lamontagne et al. [1974] working in the Pacific Ocean, and the origin of light hydrocarbons was ascribed to local emissions from the ocean surface by photochemical degradation of dissolved organic carbon [Wilson et al., 1970]. Beside the chemical aspect linked to the photochemistry of the remote marine atmosphere, non-methane hydrocarbons are useful indicators of air/sea exchange kinetics due to their very different atmospheric lifetimes. Bonsang et al. [1991] have shown recently that it is possible to ascertain from the vertical distribution of NMHC in the atmosphere the existence of fast and non-steady state processes of exchanges between the ocean and the atmospheric boundary layer.

In order to understand the role of the ocean in the budget of NMHCs and eventually in the tropospheric photochemistry, the fluxes of NMHCs from superficial seawater have been evaluated by different authors, [Rudolph and Ehhalt, 1981; Bonsang et al., 1988] and discussed by Donahue and Prinn [1990]. A large discrepancy, mainly due to the different method of estimation used was pointed out with significant consequence of the uncertainty on the impact of oceanic NMHC emissions on the tropospheric background chemistry. A major aspect is the variability of this oceanic source, which appears to be an important factor and must be parametrized by knowing the production mechanisms of NMHC in seawater. Investigations on the vertical profiles in seawater in connection with classical physical and biological parameters are in progress in order to understand the production in the seawater column. Global budgets in the water column and the atmosphere must be also compared in order to validate the different methods of flux determination at the air-sea interface.

NATO ASI Series, Vol. I 7
The Tropospheric Chemistry of Ozone in the Polar Regions
Edited by H. Niki and K. H. Becker

CONCENTRATIONS OF NMHCs IN SURFACE SEAWATER AND GEOGRAPHICAL VARIABILITY

Concentrations of dissolved NMHC in superficial seawater are usually determined from stripping with ultrapure gases, according to the technique first described by Swinnerton and Linnenbom [1967]. Seawater samples are collected by means of oceanographic bottles or stainless steel devices checked for contamination, or continuously pumped through stainless steel lines extending beyond the hull of the ship. Seawater samples are transferred into a chamber where volatile NMHCs are stripped from the water and collected in stainless steel canisters or immediately analysed. Theoretical calculations or experimental determinations of the efficiency of this procedure usually agree for a quantitative extraction of the light NMHCs. Concentrations in seawater are expressed usually in pico moles/litre or nl of gas per litre of water in standard conditions.

During the past years, measurements of dissolved NMHCs in superficial seawater were performed by different authors: in the Pacific ocean by Lamontagne et al. [1974] and Donahue and Prinn [1992]; in the Indian Ocean and in the Pacific near Hawaii and Polynesia by Bonsang et al. [1988, 1990]; in the Atlantic Ocean by Plass et al. [1991]. All these authors agree that there is a dominant contribution of dissolved alkenes (mainly ethene and propene) in superficial seawater, and that there is a significant contribution of C_2-C_3 alkanes. For comparison, averaged concentrations obtained from different oceanic areas are presented in Table 1. Figure 1 shows the geographical variability for typical species. A variability of about one order of magnitude is observed for the hydrocarbons, depending on the investigated area. It can be observed that ethene concentration range from 2 - 5.3 nl/l in the Pacific Ocean to 36 nl/l in the South Indian ocean, propene varies from 0.6-1 nl/l. for the Pacific Ocean to 15 nl/l. in the South Indian ocean. Very high values are usually obtained in the continental shelf as observed by Bonsang et al. [1991] close to the Atoll of Polynesia. In the Atlantic Ocean an extended set of values reported by Plass et al. [1991] ranges from 1.5 to 3.5 nl/ litre and 0.74 to 1.75 nl/ litre, respectively, for ethene and propene. Significant latitudinal gradients are also observed. A difference by a factor 4 to 5 was observed for the seawater content in hydrocarbons between the North and South Indian Ocean [Bonsang et al., 1988]. Similarly, Plass et al. [1991] have shown the occurrence of very clear and regular north to south gradient of dissolved NMHC for the Atlantic Ocean (Table 1).

Besides light C_2-C_3 hydrocarbons, other species have been detected in surface seawater, including alkanes and alkenes up to C_6 [Bonsang et al., 1988]. Acetylene was also recently detected in superficial seawater at concentrations of the order of 0.5-1 nl/litre [Kanakidou et al., 1988] and also observed by Plass et al. [1991] in the Atlantic Ocean at concentrations ranging from 0.08 to 0.1 nl/l. More recently, Bonsang et al. [1992] have shown the existence of diene and particularly isoprene (2 methyl 1,3 butadiene) in superficial seawater of the Mediterranean and the Pacific Ocean at concentrations of the order of 0.2 nl/litre.

TABLE 1: Average concentrations of hydrocarbons in superficial seawater (10^{-9} L of gas/litre of water)

Specie	Indian Ocean (a)		Pacific Ocean (b)	Atlantic Ocean (c)	Atlantic Ocean (d)	Atlantic Ocean (d)	Mediterranean (e)
	5°S-25°S	15°N-5°S	20°N-15°S	35°N-25°S	35°N-8°N	3°S-30°S	42°N
C_2H_4	23.3	6.97	1.79	6.52	3.52	1.51	8.58
C_3H_6	11.6	2.96	0.81	3.10	1.75	0.74	2.74
$1\text{-}C_4H_8$	3.39	0.79	0.25	1.94	1.01	0.43	1.21
C_2H_6	7.66	0.91	0.17	2.62	2.30	0.31	2.11
C_3H_8	4.72	0.71	0.09	1.43	0.7	0.14	1.13
nC_4H_{10}	2.00	0.33	0.02	1.06	0.15	0.03	0.72
iC_4H_{10}	1.21	0.20	-	0.63	0.06	0.03	0.30
C_2H_2	nd	<0.1	<0.1	0.93	0.10	0.08	1.27

(a) Bonsang et al. [1988]; (b) Donahue and Prinn [1992]; (c) this work, results from ASTEX cruise; (d) Plass et al. [1991]; (e) this work, including the seasonal variability (see text).

SUPERSATURATION OF SURFACE SEAWATER AND COMPOSITION DISSOLVED HYDROCARBONS IN THE SEAWATER

Typical concentrations of non-methane hydrocarbons on remote marine atmosphere are of the order of 1 ppbv (ethane), 0.5-1 ppbv (propane), and sub-ppb levels for other NMHCs [Rudolph et al. 1981; Bonsang and Lambert 1985; Greenberg and Zimmerman, 1984]. Despite the fact that a controversy exists regarding the alkenes mixing ratios in remote background atmosphere [Donahue and Prinn, 1990], it can be ascertained that the typical reactive NMHC level ranges between 10 to 100 pptv. Using the Henry's Law constant of non-methane hydrocarbons deduced from solubility data of McAuliffe [1966], the supersaturation in the light non-methane hydrocarbons appears to be of the order of two to three orders of magnitude. As a consequence, the ocean acts as a net source of light hydrocarbons for the atmosphere. Taking into account its Henry Law constant of the order of 1 (dimensionless), it appears also that acetylene is weakly supersaturated. Vertical gradients of acetylene performed in the Pacific Ocean over the Hao Atoll [Kanakidou et al., 1988] show a clear decrease as a function of the altitude in the boundary layer, which suggests the existence of a local marine source. However, the supersaturation of other open oceanic areas is not clearly established (Table 1), and the existence of the marine source of acetylene is still subject of controversy [Plass et al., 1991].

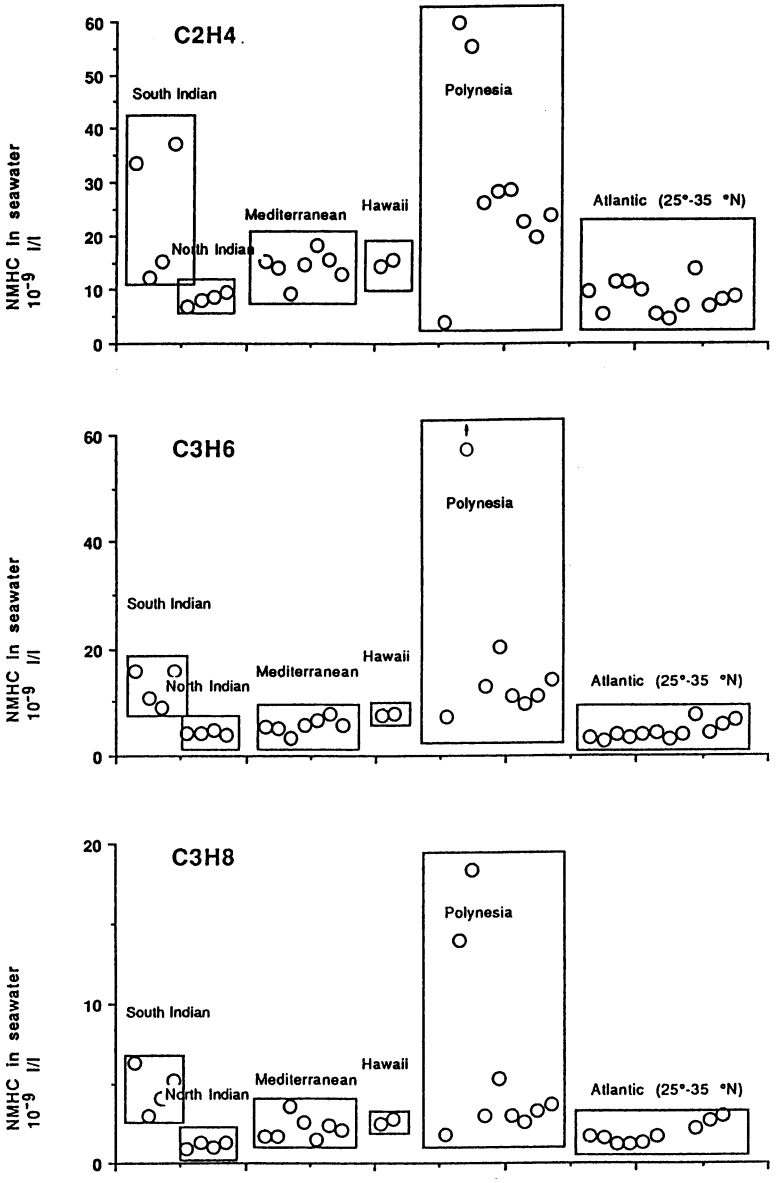

Fig. 1. Vertical profiles of temperature, fluorescence, ethene, propene and acetylene in the Mediterranean. Results of the DYFAMED cruise [Bonsang et al., 1990].

The existence of a typical composition of dissolved NMHCs in seawater was first pointed out by Bonsang et al. [1988, 1991]. Figure 2 represents the comparison of averaged compositions normalised to propane for the Pacific and Indian Ocean; its shows a dominant contribution of alkenes whose concentrations exceed those of their saturated homologs. In each group of alkenes or alkanes, the concentrations decreases with increasing carbon number. One significant fact is a very good agreement between several authors for surface seawater composition in C_2-C_3 alkenes. For the different areas investigated and presented in Figure 1, the ethene/propene ratio appears to be constant with an average value of 2.2 ± 0.6 (Figure 3). Plass et al. [1991] reported an ethene/propene ratio of 2.1 ± 0.4 for the Atlantic Ocean waters, Lamontagne et al. [1974] a value of 3.6 ± 1.5, and Donahue and Prinn [1992] an identical ratio of 2.2 ± 0.5. A relatively good agreement is also obtained for the ethane/propane ratio which, however, seems to be more variable. For the Atlantic Ocean, Plass et al. [1991] established the existence of a quasi-constant value of 3.2 greater than the average of 2.1 deduced from our data including different oceanic areas.

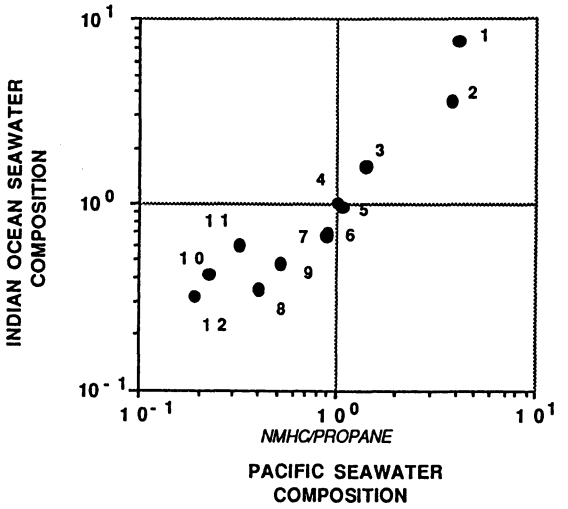

Fig. 2. Vertical profiles of C_2-C_3 hydrocarbons in the Pacific Ocean. Results of the HYDROLOC cruise [Bonsang et al., 1990]. 1: Ethene, 2: Propene, 3: Ethane, 4: Propane, 5: 1-Butene, 6: 1 Pentene, 7: n-Pentane, 8: iso-Pentane, 9: n-Butane, 10: 1-Hexene, 11: n-Hexane, 12: iso-Butane

VERTICAL DISTRIBUTIONS AND ORIGIN OF HYDROCARBONS IN SEAWATER

There are still only a few measurements of the vertical distribution of hydrocarbons in seawater which can help to establish direct relationship with dissolved organic carbon or biomass

content in the water column. Preliminary measurements by Swinnerton and Linnenbom [1967] have shown that concentrations of the C_1 to C_4 hydrocarbons generally decrease with increasing depth, with a maximum located in the surface waters in the Atlantic or between 30 and 50 m depth in the Gulf of Mexico. A series of vertical profiles have been undertaken in the Mediterranean from October 1989 to April 1992, and was correlated with the vertical profiles of classical parameters such as fluorescence and temperature. From this series of measurements we can demonstrate that the vertical distribution of NMHC in depth shows a maximum of concentration in the euphotic zone near the surface (Figure 4). For most of the light hydrocarbons measured, particularly for C_2-C_3 alkanes and alkenes, this maximum is located near the thermocline, but is not directly linked to the fluorescence maximum located at 60-70 m depth. The origin of the hydrocarbons is probably connected with photochemical degradation of organic carbon in seawater, as previously shown by Wilson et al. [1970] in laboratory experiments.

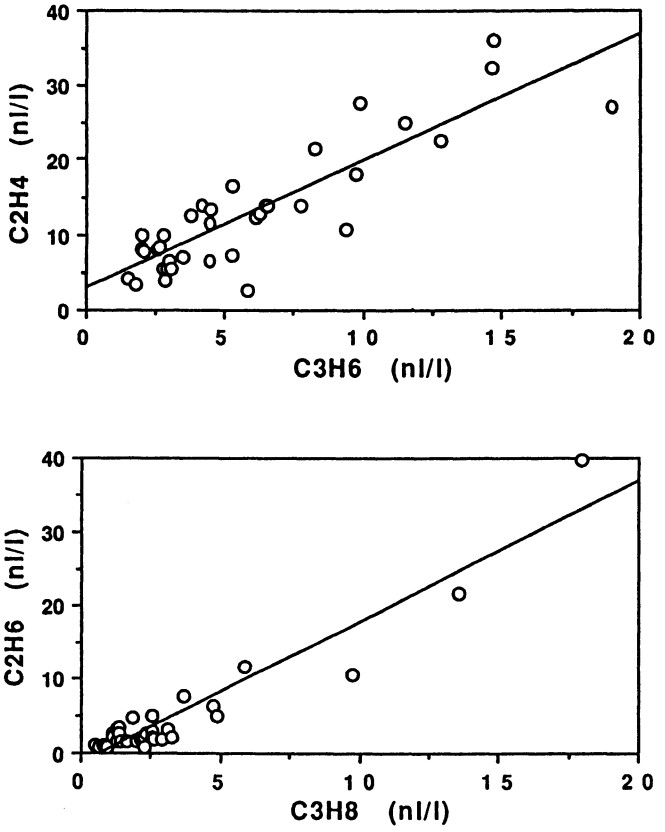

Fig. 3. Ethene-propene, and ethane-propane relationship for superficial seawater concentrations

The vertical distribution of NMHC with depth shows that their relative abundance, particularly the ethene/propene ratio, are constant in the euphotic layer. Below this layer, a slight change of composition can be observed. However, light alkenes remain the dominant species. The vertical distribution of acetylene in the water column differs from that of the other NMHCs. The concentration is constant and close to 1 ppbv in the whole water column from the surface to 1500 m, particularly in the Mediterranean (Figure 4).

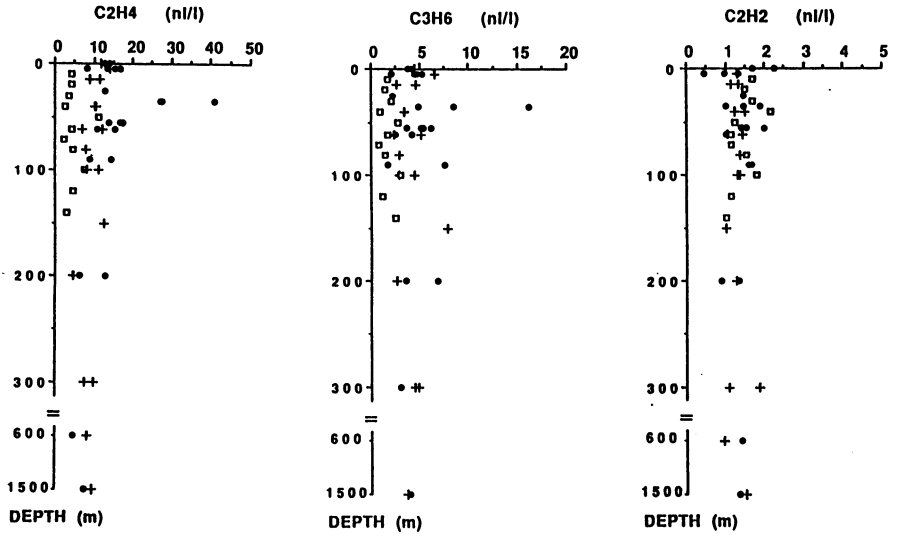

Fig. 4. Seasonal variability of hydrocarbons in the seawater column (Mediterranean: 43°24'N. 7° 52'E). squares: January, crosses: May, circles: October

The seasonal variability of hydrocarbons in seawater was investigated through systematic measurements in the Mediterranean in the euphotic zone and even down to 1500 m depth. The variability reveals the existence of relatively low concentrations in winter (January, February) increasing until May and October, which suggests a strong influence of a biologically derived production. This variability is observed for most of the hydrocarbons measured, i.e., alkanes and alkenes from C_2 to C_5, except for acetylene which appears constant with season (Figure 4). The biological origin of acetylene has not be established. Clearly, further investigation on the lifetime of this species in seawater is needed to completely understand its budget in the water column.

GLOBAL BUDGET FOR NMHC MARINE PRODUCTION

Global budget of the oceanic NMHC sources can be estimated by various techniques. Rudolph and Ehhalt [1981] have estimated from the oceanic hydrocarbon measurements of Swinnerton and Lamontagne and the formulation of Liss and Slater [1974] for transport across the air-sea interface, the flux F is given by: F = Kw (Cw - Ca/H), where Kw is the piston velocity, Cw the hydrocarbon concentration in seawater, Ca the hydrocarbon concentration in the atmosphere, and H the Henry's constant (dimensionless). These calculations were compared to the destruction rate in an atmospheric column. A reasonable agreement was found by the two estimation methods for C_2-C_3 alkanes and alkenes. An estimation by Plass et al. [1991], with the same approach based on their extensive set of data in the Atlantic Ocean, is presented in Table 2.

TABLE 2. Global emission rates of non-methane hydrocarbons from the oceans given in 10^8 molecules cm^{-2} s^{-1} and 10^{12} g Carbon/Year (Italic)

	Plass et al. [1991]	Donahue and Prinn [1990]	This work [1992]
C_2H_4	3.6 (*1.7*)	54 (*117*)	18 (*8.3*)
C_3H_6	1.8 (*1.35*)	88 (*66*)	10 (*7.5*)
1-C_4H_8	1.0 (*0.9*)	43 (*38*)	2.9 (*2.6*)
C_2H_6	2.2 (*1.0*)	2.7 (*1.2*)	4.4 (*2.0*)
C_3H_8	0.7 (*0.46*)	5.6 (*3.7*)	2.9 (*1.9*)
iC_4H_{10}	0.07 (*0.07*)	14 (*14*)	0.7 (*0.7*)
n-C_4H_{10}	0.14 (*0.14*)	25 (*25*)	1.4 (*1.4*)
C_2H_2	0	nd	1.3 (*0.6*)

Taking into account the large supersaturation of the different NMHCs with respect to the atmosphere, it is reasonable to assume that the flux from the ocean to the atmosphere is given by the product of the piston velocity times the seawater concentration. From the estimation of the flux of a single species, a global estimation for the other hydrocarbons can be made because the fluxes are in the ratio of the abundance of hydrocarbons in seawater. This piston velocity is a function of the Schmidt number, and a small correction depending on the diffusivity of the considered species in water must be applied. The oceanic flux of propane was estimated from comparison of the global distribution of atmospheric propane and Radon-222 mainly emitted from the continents and partly from the ocean [Bonsang and Lambert, 1985; Bonsang et al., 1991]. Using an experimental linear Log-Log relationship between propane and Radon-222, and

knowing the global continental flux of Radon-222, the global continental flux of propane is estimated at TgC/Yr. From this figure a global oceanic flux of propane of 1.9 TgC/Yr is obtained. Global fluxes are derived for other species and presented in Table 2. A different approach based on the computation of the atmospheric removal in an atmospheric column by Donahue and Prinn [1990] is also indicated in this table. As pointed out by these authors, this determination leads to high values, which can be due either to an overestimation of column removal rates, or advection from continental or remote sources. However, a reasonable agreement for ethane and propane fluxes can be observed in this Table.

CONCLUSIONS

Light non-methane hydrocarbons supersaturated in surface seawater are outgassed to the atmosphere where they can significantly contribute to the atmospheric background in remote areas. The main species observed are ethene and propene with a concentration ratio of approximately 2.2. The great variability of the concentrations appears to be dependent on the season and the area investigated, with large supersaturations in the coastal areas and upwelling zones. Besides ethene and propene, other saturated and unsaturated hydrocarbons are also supersaturated with a larger contribution of alkenes and a decreasing contribution with increasing carbon number. Except for acetylene, the existence of a typical composition in surface seawater and in the euphotic zone suggests one single mechanism of production of light NMHCs connected with photochemical processes. Geographical variations shows that larger supersaturations are obtained in high productive zones, the relation with biological activity is also confirmed by the seasonal variability observed in the euphotic layer. On the whole, the contribution of the ocean in the non-methane hydrocarbon production can reach a figure of 10 Tg of carbon per year within a factor two uncertainty. Considering the upper limit of this estimation, the marine flux of non-methane hydrocarbons can contribute significantly to their budget in remote areas.

REFERENCES

Bonsang, B., and G. Lambert, Nonmethane hydrocarbons in an oceanic atmosphere, *J. Atmos.Chem. 2*, 257-271. 1985.

Bonsang, B., M. Kanakidou, G. Lambert and P. Monfray, The marine source of C_2-C_6 aliphatic hydrocarbons, *J. Atmos.Chem., 6*, 3-20, 1988.

Bonsang, B., M. Kanakidou and G. Lambert, Sur la faible variabilité de composition relative des hydrocarbures légers non méthaniques dissous dans l'eau de mer superficielle, *C.R. Acad. Sci. Série II*, 495-500, 1989.

Bonsang, B., M. Kanakidou and G. Lambert, NMHC in marine atmosphere: preliminary results of monitoring at Amsterdam Island, *J. Atmos. Chem. 11*, 169-178, 1990.

Bonsang, B., D. Martin, G. Lambert, M. Kanakidou, J.C. Le Roulley and G. Sennequier, Vertical distribution of non-methane hydrocarbons in the remote marine boundary layer, *J. Geophys. Res.*, 1991.

Bonsang, B., C. Polle and G. Lambert, Evidence for marine production of isoprene, *Geophys. Res. Lett. 11*, 1129-1132, 1992.

Donahue, N.M., and R.G. Prinn, Non-methane hydrocarbons chemistry in the remote marine boundary layer, *J. Geophys. Res., 95*, 18387-18411, 1990.

Donahue, N.M., and R.G. Prinn, In-situ nonmethane hydrocarbon measurements on SAGA 3, *J. Geophys. Res.* submitted, 1992.

Greenberg, J.P. and P.R. Zimmerman, Non methane hydrocarbons in remote troposphere, *J. Geophys. Res., 89*, 4767-4778, 1984.

Kanakidou, M., B. Bonsang, J.C. Le Roulley, G. Lambert, D. Martin, and G. Sennequier, marine source of atmospheric acetylene, *Nature, 333*, 51-52, 1988.

Lamontagne, R.A., J.W. Swinnerton, and W.J. Linnenbom, Hydrocarbons in the North and South pacific, *Tellus, 26*, 71-77 1973.

Mc Auliffe, Solubility in water of paraffin, cycloparaffin, olefin, acetylene, cycloolefin and aromatic hydrocarbons, *J. Phys. Chem., 70*, 1267-1275, 1966.

Plass C., R. Koppmann, and J. Rudolph, Light hydrocarbons in the surface water of the Mid-Atlantic, Submitted to *J. Atmos. Chem*, 1991.

Rudolph, J., and D.H. Ehhalt, Measurements of C_2-C_5 hydrocarbons over the North Atlantic, *J. Geophys. Res., 86*, 11959-11964, 1981.

Rudolph, J., A. Khedim, and D. Wegenbach, The seasonal variations of light nonmethane hydrocarbons in the antarctic troposphere, *J. Geophys. Res., 94*, 13039-13044, 1989

Swinnerton, J.W and V.J. Linnenbom, Gaseous hydrocarbons in seawater: determination, *Science, 56*, 1119, 1120, 1967.

Swinnerton, J.W., and V.J. Linnenbom, Determination of the C_1 to C_4 hydrocarbons in seawater by gas chromatography, *J. of Gas Chromatogr., 5*, 570-573, 1967.

Wilson, D.F., J.W. Swinnerton, and R.A. Lamontagne, Production of carbon monoxide and gaseous hydrocarbons in seawater: relation to dissolved organic carbon, *Science, 168*, 1577-1579, 1970.

THE CYCLE OF TROPOSPHERIC PHOSGENE

T.P. Kindler, W.L. Chameides, P.H. Wine, D. Cunnold, F. Alyea
School of Earth and Atmospheric Sciences
Georgia Institute of Technology
Atlanta, GA 30332, USA

I. Introduction

Phosgene ($COCl_2$) is produced in the earth's atmosphere from the degradation of a variety of chlorinated compounds including tetrachloroethylene (C_2Cl_4), trichloroethylene (C_2HCl_3), chloroform ($CHCl_3$), methylchloroform (CH_3CCl_3), and carbon tetrachloride (CCl_4). These chlorinated compounds fall into two generic reactivity classes: 1. Tetrachloroethylene, trichloroethylene, chloroform., methylchloroform, the four reactive phosgene parent compounds (referred to here as the RPP compounds) that are primarily destroyed in the troposphere by reaction with OH; and 2. Carbon tetrachloride which is unreactive in the troposphere and is destroyed primarily by photolysis in the stratosphere. Thus the degradation of the RPP compounds lead to the production of tropospheric phosgene, while CCl_4 and to some extent also the RPP compounds leads to the production of stratospheric phosgene. Tropospheric phosgene is in turn believed to be removed from the atmosphere by rainout and ocean deposition (Singh, 1976), while stratospheric phosgene is thought to be destroyed by photolysis (Crutzen et al., 1978).

In determining the Chlorine Loading Potentials (CLPs) of phosgene's parent compounds, it has been implicitly assumed that all the phosgene produced in the troposphere is removed in the troposphere. However if, instead of being removed in the troposphere, a small fraction of the tropospheric phosgene is transported into the stratosphere and photochemically degraded there, the chlorine released in this degradation could contribute to the destruction of stratospheric ozone and thus necessitate an upward correction in the CLPs of the RPP compounds. To address this issue, we have developed a model to simulate the tropospheric cycle of phosgene and thereby determine the fraction of phosgene produced in the troposphere that is destroyed in the stratosphere.

II. Model Formulation

The basic framework for our model calculations is the 2-dimensional model of Cunnold et al. (1983) and Prinn et al. (1988). The model, which was developed and validated using the ALE/GAGE datasets, distributes and transports atmospheric tracers in the vertical

NATO ASI Series, Vol. I 7
The Tropospheric Chemistry of Ozone in the Polar Regions
Edited by H. Niki and K. H. Becker

and latitudinal directions. This is accomplished by apportioning the atmosphere into 12 hydrostatic boxes. Boxes n = 1 through 4 are located in the lower troposphere (i.e., 0 - 500 mb), boxes n = 5 through 8 in the upper troposphere (i.e., 500 - 200 mb), and boxes n = 9 through 12 in the stratosphere (i.e., above 200 mb). Each set of 4 boxes at a given height are in turn distributed latitudinally between 90° S and 30° S, 30° S and the equator, the equator and 30° N, and 30° N and 90° N.

The concentration, $C^n(J)$, of species J in the n^{th} box is determined in the model by integrating the time-dependent mass continuity equation

$$\frac{\partial C^n(J)}{\partial t} = -\frac{C^n(J)}{\tau^n(J)} + S^n(J) + T^n(J) \qquad (1)$$

where $\tau^n(J)$ is the lifetime of J against photochemical loss and/or wet removal in box n, $S^n(J)$ represents the production of J from photochemical processes (and emissions for the surface boxes) within box n, and $T^n(J)$ represents the net transport of J into box n from neighboring boxes. In the model, transport between boxes is simulated using zonally averaged meridional and vertical velocities and eddy diffusion coefficients; these parameters were taken from Newell et al. (1969) and appropriately modified to optimize the model's ability to reproduce the observed distribution of $CFCl_3$ as described by Cunnold et al. (1983) and Prinn et al. (1989).

Three loss processes are considered in the determination of $\tau^n(J)$: loss via reaction with tropospheric OH, loss in the troposphere by wet removal, and photochemical destruction in the stratosphere. Thus

$$\tau^n(J) = \tau^n_{OH}(J) + \tau^n_{wet\text{-}tot}(J) \qquad \text{for n = 1, 8} \qquad (2)$$

and

$$\tau^n(J) = \tau^n_{pchem\text{-}strat}(J) \qquad \text{for n = 9, 12} \qquad (3)$$

The lifetime, $\tau^n_{OH}(J)$, against loss via reaction with tropospheric OH is calculated using the seasonally varying OH distribution derived to reproduce the methylchloroform distribution and trend observed from the ALE/GAGE network (Cunnold et al., 1983; Prinn et al., 1989). Thus,

$$\tau^n_{OH}(J) = \frac{1}{C^n(OH)\, k_{OH}(J)} \qquad (4)$$

where $k_{OH}(J)$ is the rate constant for reaction of J with OH. The lifetime, $\tau^n_{wet\text{-}tot}$, against loss due to wet removal is treated in the model using the parameterization described in the next section. The effective lifetime, $\tau^n_{pchem\text{-}strat}(J)$, against loss in the stratosphere is determined using a one-dimensional eddy diffusion model with absorption cross sections taken from Heydtmann (1991).

III. Tropospheric Wet Removal

Kinetic and photochemical data suggest that phosgene is essentially unreactive in the troposphere; its rate constant with OH is likely to be quite small as is its absorption cross section in the near UV and visible (Singh, 1976, Heydtmann, 1991). On the other hand, phosgene is known to dissolve in water and hydrolyze (Manogue and Pickford, 1960) and as a result is most likely removed from the troposphere by rainout, washout, and dry deposition onto the ocean and other wet surfaces (Singh, 1976; Wine and Chameides, 1989). Thus a simulation of the phosgene atmospheric cycle requires a quantitative treatment of its wet removal in rain and to the ocean. To properly simulate these loss processes, we adopted a wet removal parameterization based on the formulations of Johnson (1981), Wine and Chameides (1989), and Butler et al. (1991). This parameterization is described below.

A schematic illustration of our wet removal parameterization is presented in Figure 1. We consider two removal pathways - one pathway involving removal by clouds and the other removal by deposition to the ocean. For each pathway, we adopt the stagnant-film model (Dankwerts, 1970) to represent the rate at which a species is lost from the atmosphere. In this model, the flux, $\Phi_i(J)$, of species J through pathway i is represented by the ratio of the species' atmospheric concentration, C(J), and a parameter referred to as the pathway "resistance", R, which has units of s/cm. Thus,

$$\Phi_i(J) = \frac{C(J)}{R_i} \qquad (5)$$

The total flux, $\Phi_{wet\text{-}tot}(J)$, through both pathways is then determined by adding the two resistances as if they formed a parallel circuit, so that

$$\Phi_{wet\text{-}tot}(J) = \frac{C(J)}{R_{tot}} = C(J)\left[\left[\frac{1}{R_{ocean\text{-}tot}}\right]+\left[\frac{1}{R_{cloud\text{-}tot}}\right]\right] \qquad (6)$$

where $R_{ocean\text{-}tot}$ and $R_{cloud\text{-}tot}$ represent the resistances for loss to the ocean and to clouds and rain, respectively.

As illustrated in Figure 1, deposition to the ocean is assumed to be controlled by four processes; these are transport from the free troposphere to the marine boundary layer, transport through a thin "film" or stagnant layer between the atmosphere and the ocean surface, transport through a thin film on the ocean surface, and transport into and loss via hydrolysis in the ocean. In the case of the last process, we consider downward transport and hydrolysis in two ocean layers - the mixed layer and the so-called deep ocean below the thermocline.

Similar to the formulation in Equation (5) for the total pathway resistance, the flux or loss due to each of the four processes used to simulate ocean deposition can be represented by the ratio between a concentration and a resistance specific to at process. Because these process-specific resistances act in series it can be easily shown that

$$R_{ocean\text{-}tot} = \left[\frac{r_{atm} + r_{air\text{-}film} + r_{ocean\text{-}film} + r_{ocean}}{f_{ocean}}\right] \qquad (7)$$

where f_{ocean} is the fraction of the surface covered by ocean and the r's are used to represent the resistances for each of the processes listed above. For our simple o^{th} order calculations, f_{ocean} is assumed to be 0.7, while for our 2-dimensional model calculations it is allowed to appropriately vary with latitude. The process-specific resistances, r, like the total pathway resistance, R, have units of s/cm. In general it can be shown by solving the one-dimensional diffusion equation (or Fick's Law), that r is given by the thickness of the layer of transport (often referred to as the film thickness) divided by the appropriate diffusion coefficient (Dankwerts, 1970).

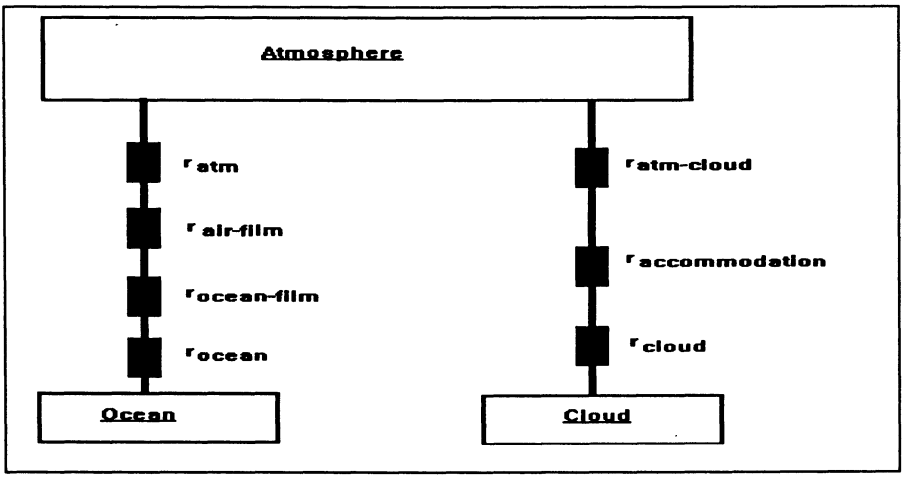

Fig. 1: Schematic illustration of the processes included in the wet removal parameterization.

Loss in clouds is assumed to be controlled by three processes; these are transport from the ambient atmosphere to the interstitial air of a cloud, transport to and accomodation on the droplet surface, transport into and hydrolysis within the droplet interior. As in the case of ocean deposition, the total resistance due to rainout can be represented as a sum of the regime-specific resistances so that

$$R_{cloud\text{-}tot} = (r_{atm\text{-}cloud} + r_{accommodation} + r_{droplet}) \qquad (8)$$

where the r's are again used to represent the resistances through each of the transport regimes.

While the r-values can in general vary considerably depending on the specific species' thermodynamic properties and the assumed state of the atmosphere and ocean, a few generalizations can be made for the range of species considered here and for the conditions

assumed for the atmosphere and ocean. We find, for instance, that loss to the ocean in our calculations is always limited by the ocean film resistance ($r_{ocean\text{-}film}$) and/or the ocean resistance (r_{ocean}). For all cases considered here, the resistances due to transport from the free troposphere to boundary layer (r_{atm}) and to the ocean surface ($r_{air\text{-}film}$) have a negligible impact; these resistances are only important for species with extremely high solubilities and/or hydrolysis rates and such species are not considered in this work.

For removal by clouds we find that $r_{droplet}$, the resistance to transport into and hydrolysis in the droplet, is generally the dominant term, with $r_{atm\text{-}cloud}$, the resistance due to transport from the atmosphere to the interstitial air of the cloud, making a non-negligible contribution in the case of species with relatively large solubilities and/or hydrolysis rates. Note that for our determination of $r_{accomodation}$, we have assumed that the accomodation coefficient, α, is always greater than 10^{-6}; this assumption seems reasonable in light of several different laboratory experiments which all yield accomodation coefficients significantly larger than 10^{-6} for a variety of species of varying solubilities (see for example De Bruyn et al.,1992). Given this assumption for α, we find that $r_{accomodation}$ has a negligible impact on the overall rate of rainout for all species considered here. This later result, which is equivalent to having thermodynamic equilibration of the species between the gas and aqueous phases of the cloud, is consistent with more detailed cloud chemistry calculations which yield gas/aqueous phase equilibration times for soluble species in clouds of only several seconds or less (Chameides, 1984; Schwartz, 1986).

IV. 0'th Order Evaluation of Wet Removal Lifetimes

Before describing the application of the wet removal parameterization to our 2-dimensional model, it is useful to use the parameterization in a 0-dimensional mode to roughly estimate the range of wet removal lifetimes that we might expect to find for species as a function of their solubility and hydrolysis rate. To carry out this "0^{th} order evaluation" we assume that all species are distributed in the atmosphere with constant mixing ratios. The globally-averaged, wet removal lifetime, $\tau^{avg}_{wet\text{-}tot}(J)$, for J can then be estimated by

$$\tau^{avg}_{wet\text{-}tot}(J) \approx \frac{H_A * C(J)}{\Phi_{tot}} = H_A * \left[\frac{1}{\frac{1}{R_{ocean\text{-}tot}} + \frac{1}{R_{cloud\text{-}tot}}} \right] \qquad (9)$$

where H_A is the atmospheric scale height (taken here to be 8.4 km).

Wet removal lifetimes calculated from Equation (8) using ocean and rainout resistances appropriate for globally averaged atmospheric and oceanic conditions are plotted as a function of the species' solubility and hydrolysis rate constants in Figure 2. The total wet removal lifetime increases dramatically with decreasing solubility and decreasing hydrolysis

rates with lifetimes of the order days for species with solubilities and hydrolysis rates greater than 1 (in units M/atm and 1/s, respectively) and thousands of years for species with solubilities less than 10^{-4} M/atm and hydrolysis rate constants less than 10^{-2} 1/s. Although not illustrated in a figure it is interesting to note that when $k < 10^{-2}$ 1/s, ocean deposition is the dominant removal pathway, while when $k > 10^{-2}$ 1/s cloud removal is the dominant pathway. Interestingly, the relative importance of the two pathways is largely independent of H. This occurs because for the range of H's and k's considered here, both $R_{ocean\text{-}tot}$ and $R_{cloud\text{-}tot}$ vary as 1/H and thus their ratio is independent of H.

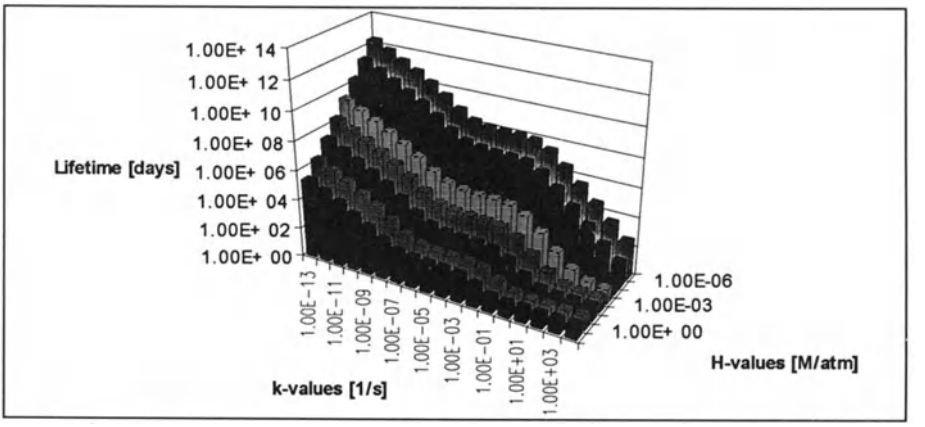

Fig. 2. 0^{th} order estimate of species' atmospheric lifetime against wet removal as a function of the species' solubility, H, and hydrolysis rate constant, k.

The general findings presented in Figure 2 are illustrated in greater detail in Table 1, where we list the parameters used and the resulting lifetimes for phosgene, methylchloroform, and carbon tetrachloride. The wet removal lifetimes are found to vary from only about 50 days for phosgene (with cloud removal dominating), to about 100 years for methyl chloroform and to 1,500 years for carbon tetrachloride (with ocean deposition dominating).

Table 1. 0^{th} order estimation of $\tau_{wet\text{-}tot}$, the wet removal lifetime of phosgene ($COCl_2$), methyl chloroform (CH_3CCl_3), and carbon tetrachloride (CCl_4) using Equation (9)*.

	$COCl_2$	CH_3CCl_3	CCl_4
A. Ocean deposition			
H, solubility constant (M/atm)	0.1	0.08	0.00554
k_1, hydrolysis rate constant in mixed layer (1/s)	1	1.25×10^{-8}	1.57×10^{-8}
k_2, hydrolysis rate constant at thermocline (1/s)	0.33	2.3×10^{-9}	3.02×10^{-9}
r_{atm} (s/cm)	3.5	3.5	3.5
$r_{air\text{-}film}$ (s/cm)	1.25	1.25	1.25
$r_{ocean\text{-}film}$ (s/cm)	70.75	88.44	$1.28*10^3$
r_{ocean} (s/cm)	6.58×10^{-2}	3.37×10^3	4.03×10^4
$R_{ocean\text{-}tot}$ (s/cm)	75.57	3.47×10^3	4.16×10^4
$\tau_{ocean\text{-}tot}$ (years)	2.88	131.9	1.58×10^3
B. Cloud deposition			
H, solubility constant (M/atm)	0.1	0.08	0.00554
Rate Constant Hydrolysis (1/s)	1	7.61×10^{-9}	9.66×10^{-9}
α, accommodation coefficient	$> 10^{-6}$	$> 10^{-6}$	$> 10^{-6}$
$r_{atm\text{-}cloud}$ (s/cm)	1.0	1.0	1.0
$r_{accommodation}$ (s/cm)	< 0.54	< 0.62	< 0.67
$r_{hydrolysis}$ (s/cm)	4.20	6.91×10^8	7.85×10^9
$r_{rainout}$ (s/cm)	1.29×10^5	1.62×10^5	2.32×10^6
$R_{cloud\text{-}tot}$ (s/cm)	5.74	1.61×10^5	2.32×10^6
$\tau_{cloud\text{-}tot}$ (years)	0.15	4.28×10^3	6.18×10^4
C. Total wet removal			
$\tau_{wet\text{-}tot}$ (years)	0.15	127.91	1.54×10^3

* Calculations ssumed: a global mean T for the mixed layer of 293 K, and 283 K for thermocline (REF), a mixed layer depth of 75 m (Lin et al. 198x), and T for clouds of 290 K. Solubility and hydrolysis rate constants for COCl2, CH3CCl3, and CCl4 taken from Manogue and Pickford (1960), Gerkens and Franklin (1989), and Jeffers et al. (1989), respectively. Data for phosgene is uncertain (Worsnop et al., 1992); in order to obtain an upper limit to the amount of tropospheric phosgene that might be injected into the stratosphere we adopted conservative H- and k-values for phosgene.

V. 2-Dimensional Simulation of Tropospheric Phosgene

Tropospheric phosgene is defined as that phosgene produced from the OH-initiated oxidation of the four RPP compounds, as indicated in Table 2. The strength and distribution of each of these sources is determined by first simulating the cycle of each of the four RPP compounds in the 2-dimensional model with the appropriate OH rate constants taken from DeMore et al. (1992) and the appropriate anthropogenic emission rates taken from the literature. In each case, the emission rate is assumed to be constant in time and to vary latitudinally in the manner described by Midgley (1989). In the case of methylchloroform, we included loss via wet deposition as described in Section III as well as loss via OH oxidation.

The results of these simulations are summarized in Table 2. We estimate a total tropospheric production rate of about 110 pptv/yr with almost half coming from tetrachloroethylene and the remainder apportioned fairly evenly among the other three compounds. Although not illustrated here, we find that the majority of the phosgene is produced in the lower troposphere and in the Northern Hemisphere; this is to be expected given the distribution of the RPP compounds and their emissions. Figure 3 illustrates the model-calculated distribution of tropospheric phosgene as a function of altitude and latitude. In Figure 4, a comparison is presented between the model-calculated annual cycle of tropospheric phosgene mid-latitude northern-hemispheric boxes (i.e., n = 1 and 5) and that implied by the airborne measurements of Wilson et al. (1988). The agreement in general is quite good, with the model producing an annually averaged concentration of about 21 pptv and observations indicating an average of roughly 17 pptv.

Table 2. Summary of simulations of the RPP compounds and their phosgene production rates.

RPP compound	Phosgene yield per RPP oxidized by OH	Release rate (kt/yr)	Average concentration (pptv)	Average residence time (yr)	Phosgene production rate (ppt/yr)	Percentage of total (%)
C_2Cl_4	2	580	8.81	0.36	48.70	44.3
CH_3CCl_3	1	614	154.03	5.65	27.62	25.1
C_2HCl_3	1	300	1.78	0.026	16.08	16.0
$CHCl_3$	1	300	12.45	0.7	17.55	14.6

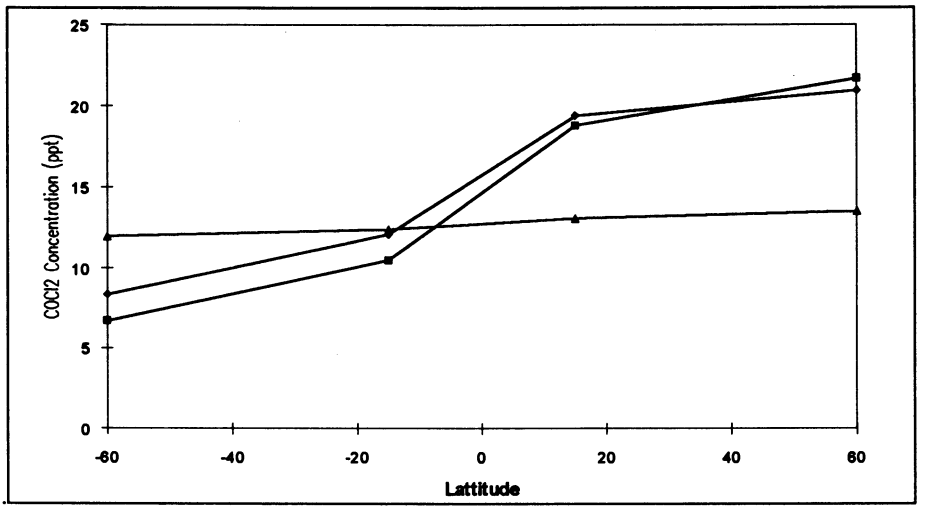

Fig. 3. The latitudinal and vertical distribution calculated for tropospheric phosgene (i.e, phosgene produced from the tropospheric oxidation of the four RPP compounds). The solid squares represent the lower troposphere, the solid diamonds represent the upper troposphere and the solid triangle represent the stratosphere.

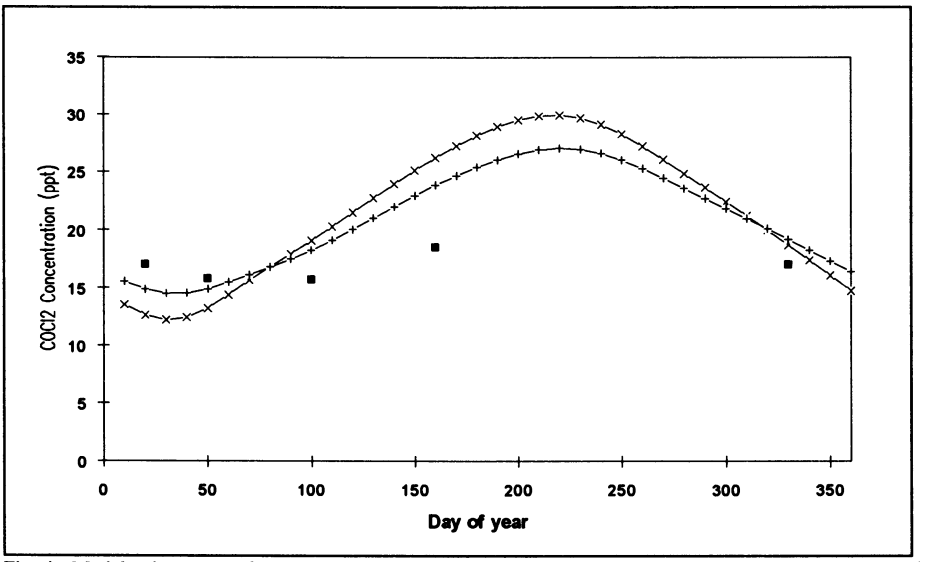

Fig. 4. Model-calculated and observed tropospheric phosgene concentrations as a function of time of year in the northern hemisphere above 30 ^{o}N. The model-calculated concentrations are for boxes n = 1 (represented by +-+-+) and n = 5 (represented x-x-x). The observed concentrations are from the mid-tropospheric measurements over Europe of Wilson et al. (1988) and are represented by solid squares.

Table 3 summarizes the budget of tropospheric phosgene inferred by the 2-dimensional model. Of the total 110 pptv of tropospheric phosgene produced annually by the oxidation of the RPP compounds, we find that 99.8% is directly removed from the atmosphere via wet deposition and only 0.2% is transported to the stratosphere and photochemically destroyed there. The very small fraction of phosgene lost to the stratosphere is caused by two effects: 1. The rapid removal of phosgene by clouds; and 2. The slow rate of loss of phosgene in the stratosphere which allows the vast majority of the phosgene that is transported into the lower stratosphere to be returned to the troposphere before it is photolyzed. Note also that in agreement with our earlier 0^{th} order calculations, we find that removal by clouds dominates over that of ocean deposition.

Table 3. Model-calculated budget for tropospheric phosgene (i.e., phosgene produced from the oxidation of the four RPP compounds).

PROCESS	RATE (pptv/yr)	% OF TOTAL
Total source (see Table 4)	110.0	100
Loss via cloud removal in lower troposphere	86.8	78.9
Loss via cloud removal in upper troposphere	19.1	17.4
Loss via ocean deposition	3.8	3.5
Total wet deposition	109.7	99.8
Transport to and loss in stratosphere	0.2	0.2
Total loss	110.0	100

VI. Conclusions

The tropospheric cycle of phosgene is driven by production from the OH-initiated oxidation of four reactive halocarbons, namely methylchloroform, tetrachloroethylene, chloroform and trichloroethylene. Our calculations indicate that the phosgene produced from these compounds is rapidly removed from the atmosphere by hydrolysis in cloudwater with an average atmospheric lifetime of about 50 days. Simulations of this cycle with a two-dimensional model yield reasonably good agreement with observations of tropospheric phosgene and its parent compounds, with a slight overestimate in the average phosgene concentration. These results suggest that the quantum yields of phosgene from its parent compounds may be somewhat smaller than assumed here and/or that the H- or k-values for phosgene adopted here from Manogue and Pigford (1960) are too small. In any case, our calculations suggest that it is unlikely that a significant fraction of the phosgene produced in the troposphere is transported and decomposed in the stratosphere and thus that tropospheric phosgene has no role in the depletion of stratospheric ozone.

Acknowledgement: The research for this work was supported in part by funds from the European Chlorinated Solvent Association/Halogenated Solvents Industry Alliance as part of their participation in the Alternate Fluorocarbon Environmental Acceptability Study and by the National Science Foundation under Grant ATM-8905901.

X. References

Bandy, A.R., D.L. Scott, B.W. Blomquist, S.M. Chen, and D.C. Thornton (1992) Low yields of SO_2 from dimethylsulfide oxidation in the marine boundary layer. Geophys. Res. Lett 19: 1125-1127

Butler, J.H., J.W. Elkins, T.M. Thompson, and B.D. Hall (1991) Oceanic consumption of CH3CCl3: implications for tropospheric OH. J. Geophys. Res 96: 22347-22355

Chameides,W.L. (1984) The photochemistry of a remote marine stratoform cloud. J. Geophys. Res 89: 4739-4755

Cunnold, D.M., R. G. Prinn, R.A. Rasmussen, P.G. Simmonds, F.N. Alyea, C.A. Cardelino, A.J. Crawford, P.J. Fraser, and R.D. Rosen (1983) The atmospheric lifetime experiment 3: Lifetime methodology and application to three years of $CFCl_3$ data. *J. Geophys. Res* 88: 8379-8400

Crutzen, J.P., I.S. Isaaksen and J.R. McAfee (1978) The impact of the chlorocarbon industry on the ozone layer. J. Geophys. Res 83: 345-363

Danckwerts, P.V. (1970) Gas-Liquid Reactions. McGraw-Hill New York

De Bruyn, W.J., S.X. Duan, X.Q. Shi and P. Davidovits (1992) Tropospheric heterogeneous chemistry of haloacetyl and carbonyl halides. Geophys. Res. Lett. 19: 1939-1942

DeMore, W.B., S.P. Sander, D.M. Golden, R.F. Hampson, M.J. Kurylo, C.J. Howard, A.R. Ravishankara, C.E. Kolb, M.J. Molina (1992) Chemical Kinetics and Photochemical Data for Use in Stratospheric Modeling, Evaluation No. 10, Jet Propulsion Laboratory Publication 92-20

Gerkens, R.R., and J.A. Franklin (1989) The rate of degradation of 1,1,1-trichloroethane in water, Chemosphere19: 1929-1937.

Heydtmann, H. (1991) Physics and Chemistry of the atmosphere, poster, *Bunsen Discussion Meeting*, Schliersee, RFG, 1991.

Jeffers, M.P., L.M. Ward, L.M. Woytowitch, and N.L. Wolfe (1989) Homogenous hydrolysis rate constants for selected chlorinated methanes, ethenes, and propanes. (1989) Environ. Sci. Technol. 23: 965-969.

Johnson, J.E. (1981) The lifetime of carbonyl sulfide in the troposphere. Geophys. Res. Lett. 8: 938-940

Manogue, W.H. and R.L. Pigford (1960) The kinetics of the absorption of phosgene into water and aqueous solutions. A.I.Ch.E. Journal 6(3): 494-500

Midgley, P. (1989) The production and release to the atmosphere of 1,1,1-trichloroethane (methyl chloroform) Amos. Env. 23: 2663-2664.

Newell, R.E., D.G. Vincent, and J. W. Kidson (196) Interhemispheric mass exchange from meteorological and trace surface observations. Tellus 21: 641-647

Prinn R., D. Cunnold, P. Simmonds, F. Alyea, R. Boldi, A. Crawford, P. Fraser, D. Gutzler, D. Hartley, R. Rosen, and R. Rasmussen (1992) Global average concentration and trend for hydroxyl radicals deduced from ALE/GAGE trichloroethane data for 1978-1990. J. Geophys. Res. 97: 2445-2461

Schwartz, S.E. (1986) Mass-transport considerations pertinent to aqueous-phase reactions of gases in liquid-water clouds, in Chemistry of Mulitphase Atmospheric Systems, NATO ASI Series, Springer-Verlag, Berlin

Singh, H.B. (1976) Phosgene in the ambient air. Nature 264: 428-429.

Wilson, S.R., P.J. Crutzen, G. Schuster, D.W.T. Griffith and G. Helas (1988) Phosgene measurments in the upper troposphere and lower stratosphere. Nature 334: 689-691

Wine, P., and W.L. Chameides (1989) Possible atmospheric lifetimes and chemical reaction mechanisms for selected HCFCs, HFCs, CH3CCl3 and their degradation products against dissolution and/or degradation in seawater and cloudwater, in Scientific Assessment of Stratospheric Ozone, Vol 2, Appendix: AFEAS Report, World Meteorological Organization

CHEMICAL INTERACTIONS OF TROPOSPHERIC HALOGENS ON SNOW/ICE

Mario J. Molina
Department of Earth, Atmospheric and Planetary Sciences
and Department of Chemistry
Massachusetts Institute of Technology
Cambridge, MA 02139
U.S.A.

INTRODUCTION

It has become clear in recent years that ice surfaces can efficiently promote chemical reactions between neutral gas phase species. The best known example involves the activation of chlorine in the presence of polar stratospheric clouds through the reaction of HCl with chlorine nitrate ($ClONO_2$) [e.g., Molina et al., 1987; Tolbert et al., 1987; Hanson and Ravishankara, 1991] or with HOCl [Hanson and Ravishankara, 1992; Abbatt and Molina, 1992]:

$$HCl + ClONO_2 \rightarrow Cl_2 + HNO_3 \quad (1)$$

$$HCl + HOCl \rightarrow Cl_2 + H_2O \quad (2)$$

Both reactions generate Cl_2, a species that rapidly photolyzes in the atmosphere. The mechanism of these unusual heterogeneous processes is beginning to be elucidated, and it is expected that important chemical processes also occur on ice/snow surfaces in the troposphere.

HCl vapor is not abundant enough in the atmosphere to co-condense with water to form solid hydrates, even under polar stratospheric conditions. This can be seen in Figure **1**, which represents an HCl/H_2O phase diagram. In contrast, HNO_3 forms a trihydrate, leading to the most common type of polar stratospheric clouds, the so-called type I PSCs. On the other hand, recent laboratory studies have shown that HCl vapor interacts strongly with ice surfaces [Abbatt et al., 1992; Hanson and Ravishankara, 1992a], while earlier work indicated a very low solubility for HCl in bulk ice [e.g., Elliot et al., 1991]. Our work indicates that at a given temperature the ice surface melts if it is exposed to HCl partial pressures above those characteristic of the ice-liquid equilibrium system, i.e., above the vapor pressure of an aqueous hydrochloric acid solution in equilibrium with ice at that temperature (e.g., 10^{-6} torr at 200 K, as shown in Figure 1). At smaller HCl partial pressures HCl vapor is also rapidly taken up by the ice surface, but only in monolayer amounts; this is shown in Figure 2, which presents our laboratory results.

NATO ASI Series, Vol. I 7
The Tropospheric Chemistry of Ozone in the Polar Regions
Edited by H. Niki and K. H. Becker

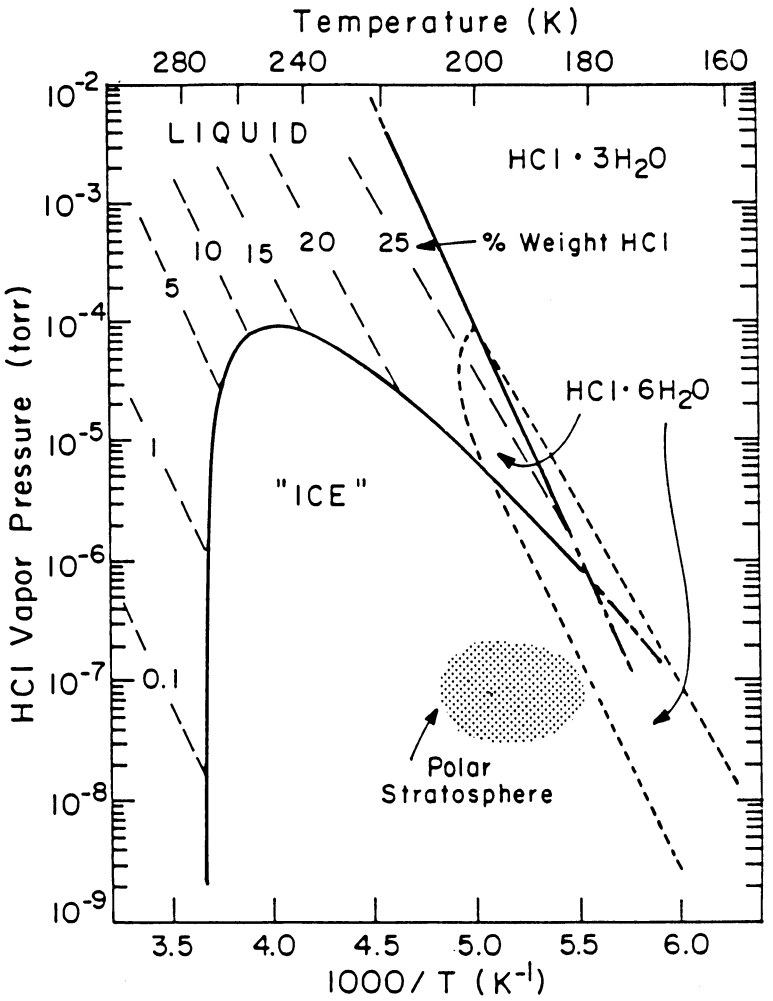

Fig. 1. Phase diagram for the HCl/H_2O system. The dashed lines represent HCl vapor pressures for liquids whose composition is given in % wt. HCl; the lines are straight, as expected from the Clausius-Clapeyron equation. The solid lines represent coexistence conditions for two phases. The dotted lines are phase stability boundaries for HCl hexahydrate, which only forms upon warming supercooled liquid solutions.

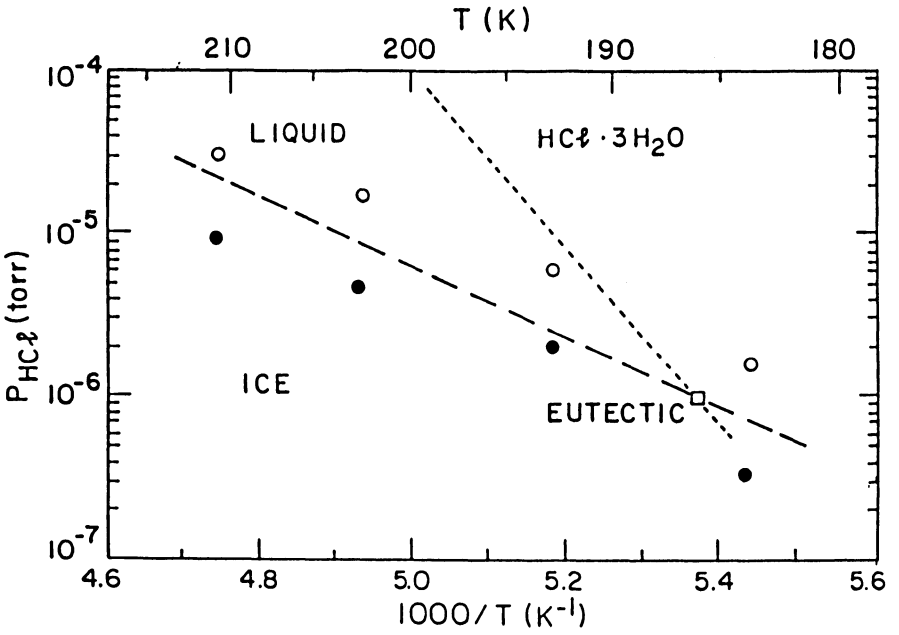

Fig. 2. Experimental temperature and HCl partial pressure conditions for the laboratory measurements of HCl vapor uptake by ice films. The open and solid circles represent uptake amounts of greater than 0.5% wt. and less than 0.005% wt. respectively.

Laboratory investigations of the reactions of HCl with $ClONO_2$ or with HOCl indicate that the reaction probabilities are equally large — above 0.1— at the lower and at the higher HCl partial pressures; there appears to be no change in the reaction mechanism as the system moves away from the liquid-solid equilibrium coexistence conditions into the solid (ice) stability regime. We measured reaction probabilities on ice surfaces using a fast-flow technique; a schematic of the apparatus is shown in Figure 3. Our results are in good agreement with those measured by other investigators, as summarized by Hanson and Ravishankara [1992b].

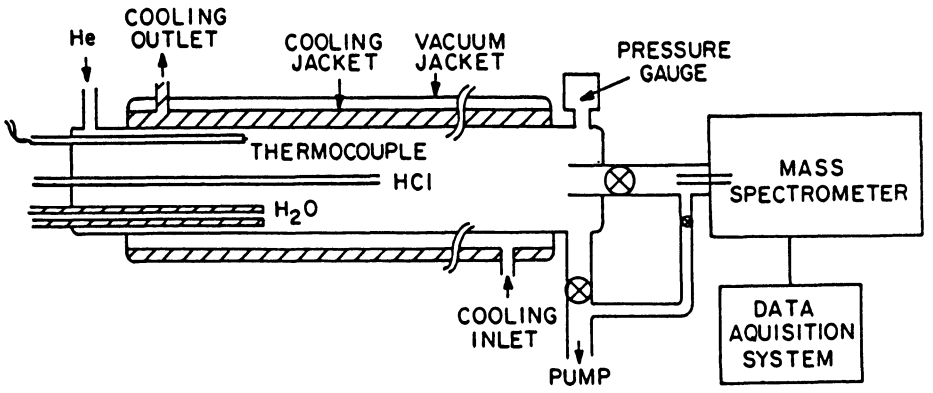

Fig. 3. Schematic representation of the fast-flow apparatus employed for the reaction probability measurements. The ice substrate was deposited on the walls of the cylindrical tube.

We have interpreted these results by assuming the formation of a liquid-like layer of hydrochloric acid solution at the ice surface [Molina, 1992], analogous to the well-documented liquid-like layer present at the surface of pure ice at temperatures down to about -20° C. The presence of HCl lowers the freezing point of water very significantly, down to -87° C for a 1:6 HCl/H_2O solution. The formation of the liquid-like layer can be rationalized with thermodynamic arguments involving surface free energies: in the case of ice these energies are higher for a solid-gas surface than for a liquid-gas plus a solid-liquid surface:

$$G_{sg} > G_{gl} + G_{ls}$$

where G_{sg} is the surface free energy of the solid-gas interface, G_{gl} that of the gas-liquid interface, and G_{ls} that of the liquid solid interface.

Physical adsorption alone cannot explain the experimental results on the uptake of HCl by ice. Kroes and Clary [1992] estimate that only a very small fraction of a monolayer (about 10^{-5} or less) of HCl should be formed for typical stratospheric conditions, because the energy associated with hydrogen bonding of undissociated HCl to the ice surface is very weak, namely of the order of 5 kcal/mole. Our view is that the HCl solvates as it interacts

with the ice surface, a process which involves instead 18 kcal/mole. Recent experiments in our laboratory are consistent with this liquid-like surface mechanism, and not with physical adsorption: we have shown that in terms of HCl uptake ice single crystals show practically the same behavior as the thin ice films we had worked with earlier, thus, ruling our artifacts related to grain boundaries or triple points, as suggested by Kroes and Clary [1992].

The implications of our proposed mechanism for atmospheric chemistry are significant: the ice surface promotes ionic-type reactions analogous to those occurring on bulk liquid water. Hence, information on the thermodynamics and kinetics of aqueous reactions can be used to predict ice chemistry. Consider, for example, reaction (2); its equilibrium constant in aqueous solution is given as follows [Pankow, 1991]:

$$K_{eq} = \frac{[Cl_2]}{[HOCl][H^+][Cl^-]} = 2 \times 10^3$$

The Cl_2 product rapidly evaporates from the ice surface as a result of its low solubility in liquid water, compared to that of HCl and of HOCl, driving the reaction far to the right. Furthermore, the rate constant for the aqueous reaction has been determined by Eigen and Kustin [1962]: it is a very fast reaction, so that in the atmosphere the rate-determining step should be gas phase diffusion of the reactants; the reaction in solution occurs on a much faster time scale.

Using these type of arguments one concludes that reactions analogous to (1) and (2), but involving bromine and/or chlorine should also proceed efficiently under atmospheric conditions, as has been shown experimentally by Hanson and Ravishankara [1992]. These reactions can be represented as follows:

$$HX + YONO_2 \rightarrow XY + HNO_3 \qquad (3)$$

$$HX + HOY \rightarrow XY + H_2O \qquad (4)$$

$$XY + h\nu \rightarrow X + Y \qquad (5)$$

where X and Y are either Cl or Br. Reactions (3) and (4) are oxidation-reduction reactions: the oxidation state of the halogen in the species HOY and $YONO_2$ is +1; it is 0 in XY, and -1 in HX.

Other oxidation-reduction reactions involving ice surfaces and halogens, which are potentially important in the atmosphere, include the following:

$$H_2O_2 + HX \rightarrow HOX + H_2O \qquad (6)$$

$$HY + HOX \rightarrow H_2O + XY \qquad (7)$$

Net reaction: $H_2O_2 + HX + HY \rightarrow 2H_2O + XY$ (8)

where, as before, X and Y are Cl or Br. As is the case with reactions (3) and (4), the halogen molecules XY rapidly evaporate from the ice surface because of their relatively low solubility in liquid water, driving the reaction towards the product side.

The Cl and Br reactions discussed above could play an important role in the rapid disappearance of ozone in the Arctic troposphere at sunrise. The rapid photolysis of Cl_2, Br_2 or BrCl in the gas phase (reaction 5) would provide an important source of free radicals, which might efficiently destroy ozone by the following sequence of reactions:

$$BrO + ClO \rightarrow Br + Cl + O_2 \quad (9)$$

$$Br + O_3 \rightarrow BrO + O_2 \quad (10)$$

$$Cl + O_3 \rightarrow ClO + O_2 \quad (11)$$

Net reaction: $2O_3 \rightarrow 3O_2$

Reaction (11) would occur in competition with hydrogen abstraction from hydrocarbons:

$$Cl + RH \rightarrow HCl + R \quad (12)$$

where R is a hydrocarbon radical. Also, reaction (9) occurs in competition with halogen nitrate formation:

$$XO + NO_2 + M \rightarrow XONO_2 + M \quad (13)$$

This reaction, followed by (3), (5), and (10) or (11) should lead to the removal of NO_2 from the gas phase, transforming this species to HNO_3; ozone depletion would not occur efficiently until this NO_2 removal proceeds to a significant extent, as is the case in the polar stratosphere [e.g., Molina, 1991]. Similarly, reaction (12), coupled to reactions (3) or (4), (5), and (10) or (11) should lead to the depletion of hydrocarbons in the gas phase. That is, if ozone depletion takes place in the Arctic troposphere by reaction of ozone with Br or Cl atoms, one predicts that the parcels of air with very low ozone levels should initially contain low levels of NO_2 and hydrocarbons. It is possible that by the time these low-ozone air parcels are sampled the levels of NO_2 and hydrocarbon have increased, if there are local sources for these species; however, simple mixing with other air parcels is not a satisfactory explanation, because the ozone levels themselves would not remain low. Field experiments and modeling calculations such as those presented in this workshop are beginning to elucidate the actual mechanism which takes place in the Arctic troposphere. Additional experiments

and calculations incorporating the above reactions will be needed to provide more definitive tests for these predictions.

References

Abbatt, J.P.D., and M.J. Molina, The heterogeneous reaction of HOCl + HCl Æ Cl_2 + H_2O on ice and nitric acid trihydrate: reaction probabilities and stratospheric implications, *Geophys. Res. Lett.*, *19*: 461-464, 1992

Abbatt, J.P.D., K.D. Beyer, A.F. Fucaloro, J.R. McMahon, P.J. Wooldridge, R. Zhang, and M.J. Molina, Interactions of HCl vapor with water-ice: implications for the stratosphere, *J. Geophys. Res.*, 1992, in press.

Eigen, M., and K. Kustin, The kinetics of halogen hydrolysis, *J. Amer. Chem. Soc.*, *84*: 1355-1360, 1962.

Elliot, S., R.P. Turco, O.B. Toon, and P. Hamill, Incorporation of stratospheric acids into water ice, *Geophys. Res. Lett.*, *4*: 425-428, 1990.

Hanson, D.R., and A.R. Ravishankara, The reaction probabilities of $ClONO_2$ and N_2O_5 on polar stratospheric cloud materials, *J. Geophys. Res.*, *96*: 5081-5090, 1991.

Hanson, D.R., and A.R. Ravishankara, Investigation of the reactive and nonreactive processes involving $ClONO_2$ and HCl on water and nitric acid doped ice, *J. Phys. Chem.*, *96*: 2682-2691, 1992a.

Hanson, D.R., and A.R. Ravishankara, Reactions of halogen species on ice surfaces, 1992b (this workshop).

Kroes, G.J., and D.C. Clary, Adsorption of HCl on ice under stratospheric conditions: a computational study, *Geophys. Res. Lett.*, *19*: 1355-1358, 1992.

Molina, M.J., Heterogeneous chemistry on polar stratosphere clouds, *Atm. Environ.*, *25A*: 2535-2537, 1991.

Molina, M.J., The probable role of stratospheric 'ice' clouds: heterogeneous chemistry of the 'ozone hole', in *CHEMRAWN VII, The chemistry of the atmosphere: its impact on global change*, J.G. Calvert (ed), Blackwell, Oxford, U.K., 1992, in press.

Molina, M.J., T.L. Tso, L.T. Molina, and F.C.Y. Wang, Antarctic stratospheric chemistry of chlorine nitrate, hydrogen chloride and ice: release of active chlorine, *Science*, *238*: 1253-1257, 1987

Pankow, J.F., *Aquatic chemistry concepts*, Lewis Publishers, Chelsea, Michigan, 1991.

Tolbert, M.A., M.J. Rossi, R. Malhotra, and D.M. Golden, Reaction of chlorine nitrate with hydrogen chloride and water at Antarctic stratospheric temperatures, *Science*, *238*: 1258-1260, 1987.

REACTIONS OF HALOGEN SPECIES ON ICE SURFACES

David R. Hanson[1] and A.R. Ravishankara[1,2]
Aeronomy Laboratory
National Oceanic and Atmospheric Administration
325 Broadway
Boulder CO 80303

INTRODUCTION

Halogen species play critical roles in the chemistry of ozone in the stratosphere. The roles played by bromine and chlorine in stratospheric ozone destruction via catalytic cycles have been studied extensively. These halogen species may also be important in the ozone chemistry of the Arctic troposphere [Barrie et al. 1988]. In particular, bromine chemistry has been implicated in the observed episodic destruction of tropospheric O_3 in the Arctic spring. Such an O_3 loss could be due to the liberation of bromine from inactive to active forms [Barrie et al., 1988; McConnell et al., 1992]. Conversion of inactive halogen species such as the hydrogen halides, chlorine nitrate, and bromine nitrate to forms that are capable of affecting the concentrations of tropospheric O_3 are likely to take place over the ice surfaces which are present during polar winter and early spring. Yet, the heterogeneous processing of bromine compounds on ice surfaces has not been studied. Therefore, we have carried out a series of laboratory measurements to investigate the reactive and non-reactive uptake of atmospherically important halogenated species such as $ClONO_2$, $BrONO_2$, HCl, and HBr onto ice layers located on the inner wall of a cylindrical flow tube at 200(±10) K.

High concentrations of $CHBr_3$ have been observed in the Arctic regions and $CHBr_3$ has been suggested to be a precursor for the active bromine which can destroy O_3. The observed episodic ozone losses in the Arctic troposphere are very rapid. The gas-phase photochemical liberation of Br from $CHBr_3$ is too slow to explain the observed rapid variations. Therefore, we investigated if hydrolysis of $CHBr_3$ could take place on ice and in a 58% (w/w) sulfuric acid solution and subsequently lead to very rapid Br release.

[1] Also affiliated with the Cooperative Institute for Research in Environmental Sciences, University of Colorado, Boulder, CO 80309

[2] Also affiliated with the Department of Chemistry and Biochemisty, University of Colorado, Boulder, CO 80309

NATO ASI Series, Vol. I 7
The Tropospheric Chemistry of Ozone in the Polar Regions
Edited by H. Niki and K. H. Becker

EXPERIMENTS

The apparatus used for these studies have been described in detail previously by Hanson and Ravishankara [1991, 1992a] and hence will not be described here. We will only note here the features that are necessary to understand the current work. The gas-phase concentrations of the reactants of interest were monitored with a chemical-ionization mass spectrometer (CIMS). By choosing an appropriate reactant ion for the CIMS, sensitive (detection sensitivity of $\sim 10^7$-10^9 cm^{-3}) and selective (discrimination against similar compounds) detection of many species is possible. Also, the reactants and products can often be detected simultaneously. The high sensitivity of the CIMS allows for the use of reactant concentrations that are typically found in the atmosphere. The signal due to the product ion of an ion-neutral reaction is proportional to the concentration of the neutral and, hence, the absolute concentrations of the neutrals can be obtained via calibration. Moreover, because the signals are proportional to the concentrations of the detected neutral species, the determination of pseudo-first order rate constants and, hence, uptake coefficients are straight forward. For example, our 'workhorse' reactant ion during the course of this work, SF_6^- (made by thermal electron attachment to SF_6), reacts with HBr, HCl, HNO_3, $ClONO_2$, and $BrONO_2$ via F^- transfer producing $F^-{\cdot}X$ and it also charge transfers with Cl_2, BrCl, and Br_2 producing X^-, where X is the reactant [Ikezoe et al., 1987]. The first-order rate coefficient for the loss of the reactant gas phase species or the formation of the gas-phase product were measured by monitoring the relative concentrations as functions of the exposure time. Reaction probabilities were determined from these first-order loss rate coefficients using the standard analysis for flow tubes [Howard, 1979; Brown, 1978; Hanson et al., 1992a]. Physical uptake was quantified by measuring the amount of a species that was lost to a known amount of surface area, thus yielding an estimate for its surface coverage [Hanson and Ravishankara, 1991].

Bromine nitrate was prepared by the method described by Spencer and Rowland [1977]. The N_2O_5 and $ClONO_2$ were produced using the procedures described by Davidson et al. [1978, 1987]. The HCl (Scientific Gas Products, 99.5% pure) and HBr (Matheson Gas products, >99.8% pure) were used as supplied. Tribromomethane, $CHBr_3$, from Aldrich (>99% pure) was purified by storing on copper turnings followed by distillation. Helium (Bureau of Mines) was used as supplied. Knowledge of impurities in the samples used is not critical to the measurements reported here; however, there were no major interfering impurities in these samples as indicated by the CIMS instruments.

RESULTS AND DISCUSSION

For better presentation, this section is divided into sub-sections dealing with (a) the uptake of hydrogen halides, (b) the reactions of inorganic halogen compounds on an ice surface, and (c) the uptake of $CHBr_3$ onto ice.

(a) **Uptake of hydrogen halides:** Physical and/or chemical adsorption of HF, HCl and HBr on ice were studied by exposing these molecules to ice surfaces and monitoring their gas-phase concentrations. Our observations on the behavior of HCl has been previously described in detail [Hanson and Ravishankara, 1992a]. To summarize, at low concentrations of HCl (~ 10^{10} cm^{-3}), the surface of ice saturated and lead to a monolayer coverage of HCl, i.e., ~5 x 10^{14} cm^{-2}. Before saturation, the uptake coefficient was ≥ 0.3. At much higher concentrations of HCl, the uptake was unlimited and the uptake coefficient was ≥ 0.3. The behavior at high [HCl] was attributed to the formation of a layer which was a mixture of HCl and H_2O, i.e., a liquid solution or an HCl-hydrate. The variation of HBr concentration with exposure to ice is shown in Figure 1.

As seen in the figure, the uptake was found to be very efficient ($\gamma > 0.2$). We attribute this unlimited, efficient uptake to the formation of an HBr-H_2O solution rather than the formation of an HBr multi-layer [Hanson and Ravishankara, 1992b]. In contrast to HCl and HBr, the direct physical uptake of HF on ice was virtually unobservable. To test if a small fraction of the HF was adsorbed on ice and if it could possibly react with $ClONO_2$, we exposed $ClONO_2$ and HF simultaneously to the ice surface. Only the formation of HOCl, the known product of the $ClONO_2$ reaction with $H_2O_{(s)}$, was observed. Therefore, we conclude that the uptake of HF on ice is very small and, if any HF did adsorb, it was not reactive towards $ClONO_2$ or HOCl.

It is interesting to compare the behavior of the three hydrogen halides. The uptake of HF is much less than that of HCl, which in turn is less than that of HBr. Since the uptake of HCl and HBr, which are stronger acids than HF, are so much more efficient, we postulate that the uptake of HCl and HBr is due to dissociation of these molecules on the surface. The HF bond is too strong to allow efficient dissociation on the ice surface. In other words, HCl and HBr are taken up very efficiently because they can dissociate. Based on this hypothesis, we predict that the uptake of HI should also be very efficient.

The implication of these findings and conclusions to atmospheric chemistry is clear: Ice particles in the atmosphere will efficiently scavenge HCl and HBr (and also HI) where they can undergo heterogeneous reactions with other reactants.

(b) **Reactions of inorganic halogen compounds on an ice surface:** We have previously shown that $ClONO_2$ uptake on ice is reactive and leads to the formation of HOCl

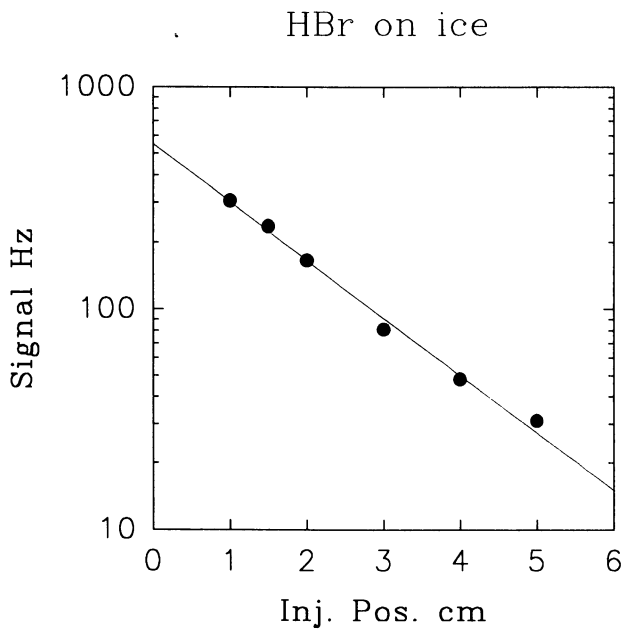

Fig. 1. The loss of HBr as a function of exposure to an ice surface. The average carrier gas flow velocity was 2000 cm s^{-1}. The uptake did not decrease with exposure time. The initial concentration of HBr was ~2 x 10^{10} cm^{-3}.

[Hanson and Ravishankara, 1992a]. We have also shown that the reactions of surface adsorbed HCl with $ClONO_2$ is very efficient and leads to the formation of $HNO_{3(s)}$ and Cl_2 (which is released into the gas phase). We postulated that this reaction on ice can proceed in a step-wise manner: $ClONO_2$ reacts with $H_2O_{(s)}$ to give HOCl and the product HOCl reacts withHCl to give the observed products. This hypothesis, along with the observations made under different ratios of HCl to $ClONO_2$, simplifies the scheme for reactions on atmospheric ice surfaces.

The uptake of $BrONO_2$ on ice is shown in Figure 2. The uptake coefficient was > 0.3. The uptake was reactive because HOBr, one of the products of hydrolysis of $BrONO_2$, was clearly seen in the gas phase. It also means that HOBr readily comes off the ice surface.

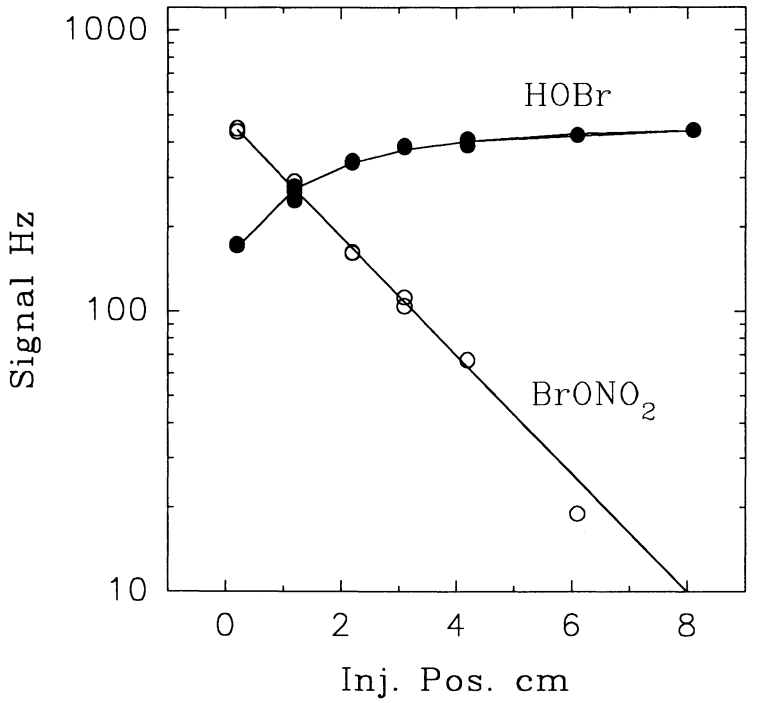

Fig. 2. The loss of $BrONO_2$ as it was exposed to an ice surface. The loss rate constant for $BrONO_2$ yields an uptake coefficient > 0.3. The simultaneous production of HOBr is evident. The growth rate coefficient for HOBr leads to the same uptake coefficient as was calculated from the loss of $BrONO_2$.

The results of simultaneous exposure to ice of $BrONO_2$ and HCl and of $ClONO_2$ and HBr are shown in Figures 3 and 4, respectively. The products of the reaction of $BrONO_2$ with adsorbed HCl are BrCl and $HNO_{3(s)}$. Similarly, the products of the reaction of $ClONO_2$ with HBr are BrCl and $HNO_{3(s)}$. We did notice, however, that BrCl reacted further with HBr, if it were available, to make Br_2 and HCl.

The above observations are consistent with $XONO_2$ reacting directly with H*Y* to produce the observed products (where *X* and *Y* are Cl or Br). These observations do suggest, however, an alternative simple mechanism for the reaction of $XONO_2$ with H*Y* on a pure ice surface. In the first step, $XONO_2$ is hydrolized on ice to make $HNO_{3(s)}$ and $HOX_{(s)}$, and the H*Y* molecule is (dissociatively) adsorbed on ice. The adsorption of HOCl has been observed and an adsorption energy of -14 (±2) kcal mol^{-1} was measured at 200K [Hanson and Ravishankara, 1992a]. Subsequently, the $HY_{(s)}$ and adsorbed HO*X* react to give $H_2O_{(s)}$ and *XY*. Since *XY* is not adsorbed efficiently on ice, it desorbs and prevents any

back reaction of *XY* with H_2O to make *HY* and HO*X*. In the above scheme, the chronology of the uptake of H*Y* and *X*ONO_2 does not matter, since both HO*X* and HO*Y* remain on the surface long enough to react there. Therefore, we believe that the reaction of any HO*X*

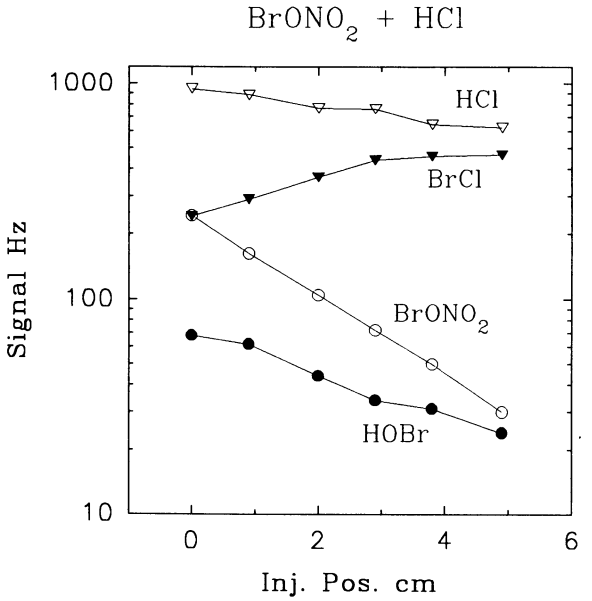

Fig. 3. Plots for the loss of $BrONO_2$ (open circles) and HCl (open triangles) as they were simultaneously exposed to an ice surface. The signal due to HOBr, (filled circles) which is a product of the hydrolysis of $BrONO_2$, also decreases. The product of the reaction of HCl with either HOBr or $BrONO_2$, BrCl, (filled triangles) is seen to rise. The mechanistic implications of these observations are given in the text.

(made on the surface or taken up from the gas phase) with the hydrogen halides is efficient on the ice surface for *X* and *Y* = Cl, Br, or I. This has been expressly shown to be true for the case of HOCl + HCl reaction [Hanson and Ravishankara, 1992a]. The above observations also lead us to conclude that these types of reactions are confined to the surface layer.

The atmospheric implications of these findings is clear. In the presence of ice, $ClONO_2$, $BrONO_2$, HBr, and HCl (and by extrapolation HI and $IONO_2$) are heterogeneously processed to liberate active forms of halogens. In the absence of the hydrogen halides, the nitrates ($ClONO_2$ and $BrONO_2$) would still react with water to produce HOCl or HOBr, which can go back to the gas phase.

We also studied the reaction between HBr and N_2O_5 on ice by monitoring the gas-

phase concentrations of HBr and N_2O_5 [Hanson and Ravishankara, 1992b]. We found it to proceed quite efficiently on this surface. We did not identify the products of this reaction. However, based on thermochemical considerations, we postulated the products to be either BrONO + HNO_3 or $BrONO_2$ + HONO.

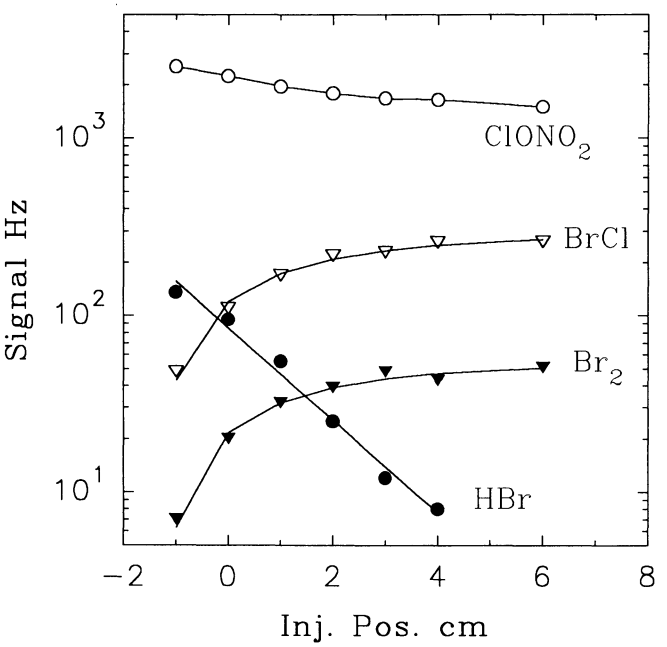

Fig. 4. Plots for the loss of $ClONO_2$ and HBr as they were simultaneously exposed to an ice surface. The product of the reaction of HBr with either HOCl or $ClONO_2$, BrCl, was seen to rise. The production of Br_2 was attributed to the reaction of BrCl with HBr. The mechanistic implications of these observations are given in the text.

(c) **Uptake of $CHBr_3$ onto ice:** Since high concentrations of $CHBr_3$ have been observed in the Arctic regions, we investigated whether hydrolysis of $CHBr_3$ could take place on ice and in a 58% (w/w) sulfuric acid solution. The loss of $CHBr_3$ was monitored when exposed to an ice or sulfuric acid surface. $CHBr_3$ was detected as Br^- formed by its reaction with O^- in the CIMS. The loss process on ice at 220K was found to be immeasurably slow, $\gamma < 6 \times 10^{-5}$ at the 95% confidence level, as shown in Figure 5.

The uptake of $CHBr_3$ onto 58% w/w acid at 220K is depicted in Figure 6 and shows a reversible Henry's Law-type physical absorption. The initial uptake coefficient was observed to be 3×10^{-3} for an exposure time of ~ 0.5 s. The uptake decreased rapidly to a value of 2×10^{-4} after the sulfuric acid was exposed to $CHBr_3$ for a time period of ~20 s.

The exposure was ceased and the $CHBr_3$ taken up by the acid was observed to come back into the gas phase, as shown in the figure. The uptake coefficient measured for a 20 s exposure time, 2×10^{-4}, is likely to be an upper limit to the uptake coefficient due to hydrolysis on 58% w/w acid.

Based on these observations, we believe that $CHBr_3$ has to be degraded to liberate bromine by processes other than direct uptake by ice particles. Our measurements also suggest that significant concentrations of $CHBr_3$ cannot be stored on the ice surface for subsequent release.

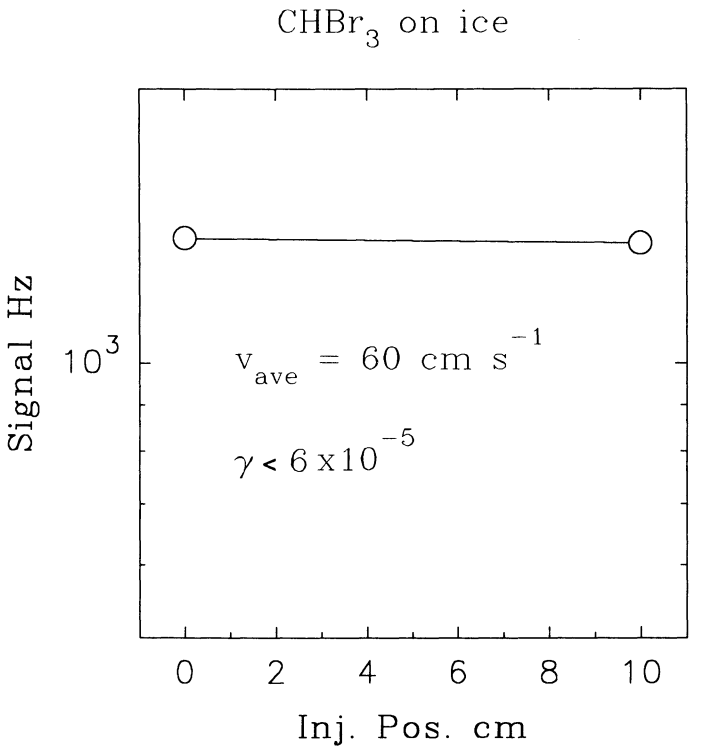

Fig. 5. A plot of the signal due to $CHBr_3$ as a function of exposure to an ice surface. No measurable loss in $CHBr_3$ signal was seen and no products were detectable. It is concluded that $CHBr_3$ is not lost efficiently on ice surfaces.

ATMOSPHERIC IMPLICATIONS

We have shown that HCl, HBr, and (by extrapolation) HI are rapidly taken up by ice and that $ClONO_2$ and $BrONO_2$ are hydrolyzed on the ice surface to give HOCl and HOBr,

respectively. When H*Y* and *X*ONO2 are simultaneously exposed to ice, the product of *X*ONO2's surface hydrolysis, HO*X*, reacts efficiently with H*Y* to give XY. The halogen molecule produced desorbs very efficiently into the gas phase. Lastly, the surface uptake (either physical or reactive) of CHBr3 is very inefficient on ice.

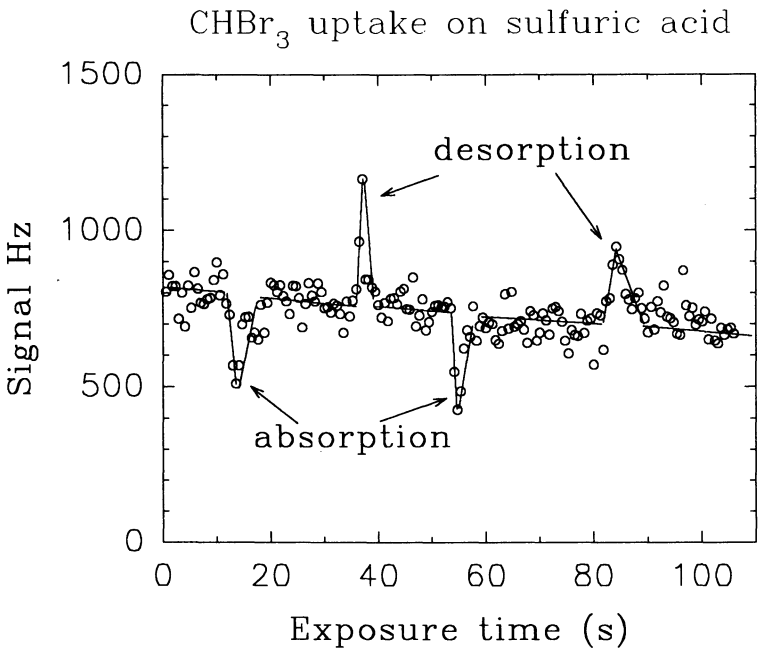

Fig. 6. Two cycles of CHBr3 absorption and desorption are shown as it was exposed and not exposed, respectively, to a 58% w/w H2SO4 solution at 220 K. The average carrier velocity was 70 cm s^{-1} and the acid covered 25% of the glass flow tube wall.

Based on these results, along with the slowness of the gas phase processes to release Br from the organic molecule (in particular CHBr3), we suggest another sequence of processes for the release of Br. A species such as BrONO2 is made by the "normal" gas phase reactions and sequesters active bromine. The release of active Br from this compound is due to its reactions on ice which could lead to very prompt release of active bromine that could destroy O3. If this is true, then the observed correlation of increases in particulate bromide with decreases in O3 abundances may be more a symptom of the atmospheric phenomenon than the cause!

REFERENCES

Barrie, L. A., J. W. Bottenheim, R. C. Schnell, P. J. Crutzen, and R. A. Rasmussen, *Nature, 334*, 138, 1988.

Brown, R. L., *J. Res. Natl. Bur. Stand. U. S., 83*, 1, 1978.

Davidson, J. A., A. A. Viggiano, C. J. Howard, I. Dotan, F. C. Fehsenfeld, D. L. Albritton, and E. E. Ferguson, *J. Chem.. Phys., 68*, 2085, 1978.

Davidson, J. A., C. A. Cantrell, R. E. Shetter, A. H. McDaniel, and J. G. Calvert, *J. Geophys. Res., 92*, 10921, 1987.

Hanson, D. R., and A. R. Ravishankara, *J. Geophys. Res., 95*, 5801, 1991.

Hanson, D. R. and A. R. Ravishankara, *J. Phys. Chem., 96*, 2682, 1992a.

Hanson, D. R. and A. R. Ravishankara, *J. Phys. Chem.*, in press, 1992b.

Howard, C. J., *J. Phys. Chem., 83*, 3, 1979.

Ikezoe, Y., S. Matsuoaka, M. Takebe, and A. Viggiano, *Gas Phase Ion-Molecule Reaction Rate Constants through 1986*, Ion Reaction Research Group of the Mass Spectroscopy Society of Japan, Tokyo, 1987.

McConnell, J. C., G. S. Henderson, L. Barrie, J. Bottenheim, H. Niki, C. H. Langford, and E. M. Templeton, *Nature, 355*, 150, 1992.

Spencer, J. E. and F. S. Rowland, *J. Phys. Chem., 82*, 7, 1978.

HETEROGENEOUS REACTIONS OF CHLORINE COMPOUNDS

Cornelius Zetzsch and Wolfgang Behnke
Fraunhofer-Institut für Toxikologie und Aerosolforschung
Nikolai-Fuchs-Straße 1, W-3000 Hannover 61, Germany

INTRODUCTION

Major tropospheric sources of HCl are the intrusion of acids [HNO_3, Martens et al., 1973, and H_2SO_4, Hitchcock et al., 1980] into sea spray aerosol [Cadle and Robbins, 1960], the direct release of HCl from coal power plants [Lightowlers and Cape, 1988], the release of Cl_2 [Hov, 1985], a photolytic source of Cl atoms which react with hydrocarbons to form again HCl, and a minor source is the photodegradation of chlorinated hydrocarbons [Behnke and Zetzsch, 1988, 1989a, and Becker and Zetzsch, 1989]. Subsequently, the slow gas-phase reaction of OH radicals with HCl is expected to form atomic Cl. These processes have been reviewed by Cicerone [1981], Warneck [1988], Friend [1990] and Keene et al. [1990] and are leading to global levels of atomic Cl around $10^3 cm^{-3}$ [Singh and Kasting, 1988], provided that the level of HCl is around 1 ppb [Vierkorn-Rudolph et al., 1984, Bächmann and Fuchs, 1987, Keene et al., 1991, although an upper limit of 0.25 ppb has been observed by Harris et al., 1990 in the marine boundary layer].

Determinations of the source strength of Cl in smog chamber experiments [Behnke et al., 1984, Zetzsch, 1987, Zetzsch et al., 1988, Behnke and Zetzsch, 1989b-d] revealed that further sources of atomic Cl exist in the presence of O_3, HCl and humidity, and that Cl_2 (formed by heterogeneous reactions) is observed as a precursor of the atomic Cl. Cl atoms observed in the absence of NO_x [Behnke and Zetzsch, 1989b-d], hence the formation of NOCl and other inorganic nitrogen-containing halides [postulated by Finlayson-Pitts, 1983] cannot account for this source of atomic Cl, that was identified to be Cl_2. The efficiency of different aerosol materials (SiO_2, Fe_2O_3 and TiO_2) for the heterogeneous production of Cl atoms in the presence of O_3, HCl and humidity was investigated in the aerosol smog chamber in an inserted teflon bag [Behnke and Zetzsch, 1989c-d, 1990a].

No formation of atomic Cl was detected with NaCl aerosol in the absence of NO_x [Behnke and Zetzsch, 1990] with the exception of an artifact [Behnke and Zetzsch, 1989d] caused by contamination of the aerosol in a Sinclair-LaMer generator (evaporating NaCl in a hot ceramic tube at 800 °C).

On the other hand, NaCl turned out to be a strong photochemical source of atomic Cl in the presence of NO_x via a reaction of N_2O_5 [Behnke and Zetzsch, 1990, Zetzsch et al.,

NATO ASI Series, Vol. I 7
The Tropospheric Chemistry of Ozone in the Polar Regions
Edited by H. Niki and K. H. Becker

1991, Zetzsch and Behnke, 1992a,b] with deliquescent aerosol (leading to $ClNO_2$), confirming the earlier observations on dry NaCl powder by Finlayson-Pitts et al. [1989]. The sticking coefficient of N_2O_5 on NaCl solution droplets was determined to be 0.032±0.003, independent of relative humidity (determined at up to 92% r.h. and 292K), and the yield of $ClNO_2$ was observed to be higher than the yield of NO_3^- [Behnke et al., 1992]. By model calculations, the global source strength of atomic Cl from this process was estimated to be significant in the lower troposphere at higher latitudes of the northern hemisphere ([Cl] up to $4 \cdot 10^3$ cm^{-3} at 60° latitude, Zetzsch and Behnke, [1992a]). A preliminary study with simulated sea-salt (containing the most relevant trace ions) indicated an even higher efficiency than pure NaCl [Zetzsch et al., 1991].

A contribution of atomic Cl to tropospheric chemistry might form chlorinated compounds, such as phosgene and chloroacetone, which are observed in smog chamber runs [Zetzsch and Behnke, 1992a]. If HCl can be oxidized by O_3 in the presence of aerosols under stratospheric conditions to form Cl_2, such a process would contribute to the chemistry of the antarctic ozone depletion by photolytic formation of atomic Cl. Although in the troposphere the production of atomic Cl is expected to enhance O_3 levels significantly because of the higher reactivity of Cl (as compared to OH) against hydrocarbons, a corresponding production of atomic Br by analogous processes would decrease O_3 in the arctic troposphere because of the much lower reactivity of Br against hydrocarbons.

EXPERIMENTAL

The aerosol smog chamber facility has been described in previous work in detail [Behnke et al., 1987, 1988], and an outline is shown in Figure 1. The chamber is irradiated by medium pressure metal vapour lamps (HMI, Osram), simulating tropospheric sunlight with a cut-off at 300 nm [for some experiments filtered to a cut-off at 360 nm, Behnke et al., 1987], and it consists of a 2.3 m^3 borosilicate glass cylinder, where residence times of the aerosol up to 2 days can be obtained. The glass walls are rinsed with 0.1 n NaOH solution prior to each experiment. Teflon bags (FEP 200A, DuPont) with 0.8 m^3 volume are inserted into the smog chamber for the later experiments to overcome adsorption problems. The aerosol is produced by atomizing aqueous solutions (NaCl) or suspensions of the highly disperse (> 100 m^2g^{-1}) aerosol materials SiO_2 (Aerosil 200, Degussa), Fe_2O_3 (Sicotram orange, BASF) and TiO_2 (PKP anatase, Bayer). In addition, extremely high concentrations of NaCl aerosol were attained by a Sinclair-LaMer generator (Palas LMG-HT), that evaporates NaCl in an air flow at 800 °C and yields a fairly monodisperse aerosol by nucleation with subsequent growth by condensation. Initial concentrations of the NaCl aerosol range from 3 to 8 mg m^{-3} in the glass chamber and are about 1 mg m^{-3} in the teflon

LaMer generator) in earlier experiments and are about 0.1 mg m^{-3} in the later experiments, where the aerosol is pre-aged in a supply bag and then released into the final bag for the determination of sticking coefficients. The size distributions of the aerosol are determined by a differential mobility particle sizer by a rapid scan method in 50 size classes [Behnke et al., 1991]. The concentrations of HCl and HNO_3 in the gas phase are sampled by NaF-coated denuders and are analyzed (as well as aerosol filter samples) for Cl^- and NO_3^- using ion chromatography. Cl_2 is determined by the methyl-orange technique of Kettner and Forwerg [1969], and measurements are corrected for the minor interference of O_3. An automatic cryogenic sample preconcentrator, combined with capillary gas chromatography and FID [Nolting et al., 1988] is used to monitor organic indicator compounds for OH and Cl. Reaction products are monitored and identified by either GC with FID/ECD or by on-line GC/MS.

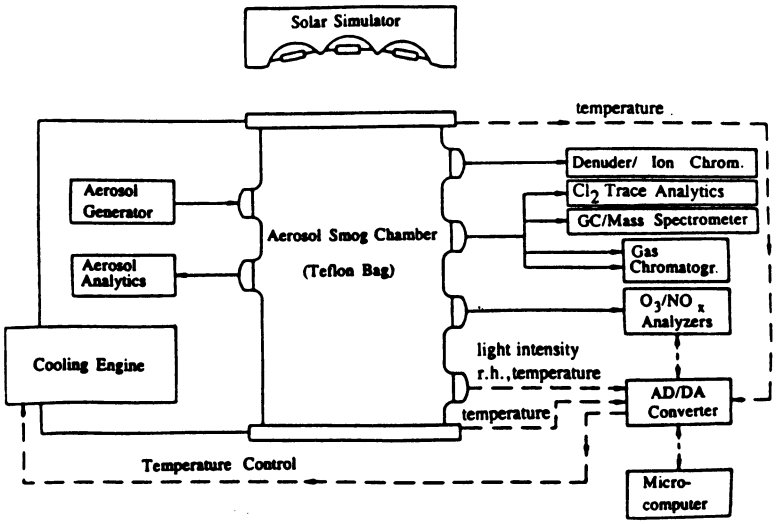

Fig. 1. Block diagram of the aerosol smog chamber facility

DETERMINATION OF THE CONCENTRATION TIME PROFILES AND SOURCE STRENGTHS OF RADICALS

The concentration time profiles of Cl atoms and OH radicals are computed from the degradation of various hydrocarbons, chosen to cover a wide range of the ratio k_{Cl}/k_{OH} [Behnke and Zetzsch, 1987a], by determining the slope and intercept of simple linear regressions of the dilution-corrected data of the indicator hydrocarbons, HC, according to the

integrated rate equation (divided by k_{OH}):

$$-\ln ([HC(t)]/[HC]_o) /k_{OH} = \int[OH]dt + (k_{Cl}/k_{OH})\int[Cl]dt \quad (1)$$

and differentiating the resulting curves, fitted by polynomials.

Since the steady state approximation is well fulfilled for the active species OH and Cl in smog chamber experiments, the source and sink terms for Cl atoms must be equal. A minimum source term for Cl follows from the presence of OH by its reaction with HCl:

$$d[Cl]/dt = k_{OH} [OH] [HCl] \quad (2)$$

The total production of atomic Cl must be equal to the total consumption of Cl atoms, Cl-c, that can be computed with reasonable precision from the time profiles of the injected hydrocarbons, HC, and their known rate constants, k_i, for the reactions with Cl (until the hydrocarbons are degraded to a level of about 50%, where the additional consumption by the reaction products begins to interfere, [Behnke and Zetzsch, 1988 and 1989a], - a method hardly applicable to OH because of the higher reactivities of degradation products against OH):

$$Cl\text{-}c\ (t) = \sum_i k_i[HC_i(t)]\ [Cl(t)] \quad (3)$$

In the presence of Cl_2, the photolysis of Cl_2 yields a further production term for atomic Cl:

$$d[Cl]/dt = 2\ k_{ph}\ [Cl_2(t)] \quad (4)$$

The ratio of the sink term (Cl-c) to the source term (d[Cl]/dt) should be unity in the steady state, hence further sources of Cl not yet considered can be detected from increased values for this ratio (Cl-c/d[Cl]/dt).

RESULTS

Early experiences with NaCl aerosol and NO_x in a glass chamber and a teflon bag

A much stronger source of atomic Cl than the well-known conversion of HCl to Cl by OH was be observed when NaCl aerosol was exposed to a photochemical smog at high concentrations of O_3 in our glass chamber. An example for the consumption of the indicator

compounds for OH and Cl and the corresponding time profiles of OH and Cl, observed in the presence of NaCl aerosol and NO_2, has been shown previously [e.g., Zetzsch, 1991].

Atomic Cl concentrations as high as 10 % of the OH radicals were observed, but the time profile of OH did not coincide well with the time profile of Cl. The source strength of atomic Cl did neither correlate well with the loss of NO_2 nor with the corresponding depletion of Cl^- by the intrusion of HNO_3 into NaCl aerosol [Behnke and Zetzsch, 1987b, 1989c]. It was found that the source strength of Cl correlates with the concentration of O_3 (with a maximum source strength for Cl of $3 \cdot 10^8$ cm^{-3} s^{-1} at the O_3 maximum of 100 ppb after 25 h of irradiation, [Behnke et al., 1987b, Behnke and Zetzsch, 1989c]. Upon addition of O_3 at 1 ppm, the maximum concentration of atomic Cl increased from $2 \cdot 10^5$ to 10^6 cm^{-3}.

Heterogeneous production of Cl_2 from HCl and O_3 in the empty glass chamber

On the other hand, similar production rates of atomic Cl were observed in the glass chamber when the NaCl aerosol was replaced by HCl gas [Behnke and Zetzsch, 1989b] or by chlorinated hydrocarbons as a source of HCl [Behnke and Zetzsch, 1989a], and molecular chlorine was identified as the photolytic precursor of this atomic Cl [Behnke and Zetzsch, 1989b].

Figure 2 shows time profiles of O_3 and Cl_2 in the absence of simulated sunlight in the upper part (i.e., dim daylight conditions of the laboratory), and it shows time profiles of O_3 and the Cl-production in the presence of simulated sunlight (with a cut-off at 360 nm). For this dark experiment, the chamber was filled with purified air at 50% r.h., and HCl was injected at an amount that would correspond to a gas-phase mixing ratio of 600 ppb. This amount is adsorbed completely on the glass walls of the chamber (with a detection limit of 1 ppb of HCl in the gas phase, the total surface area being 11 m^2). When O_3 was admitted to the chamber (to reach a mixing ratio of 350 ppb), the decay of O_3 was observed to be enhanced, and Cl_2 was formed, reaching a final level of $\approx$ 30 ppb. This source strength of active Cl (2 Cl would be formed by photolysis) is observed to correspond to an initial value of $4 \cdot 10^7$ cm^{-3} s^{-1}. A comparison with the decay of O_3 shows that $\approx$ 0.63 precursors of atomic Cl are formed per O_3 consumed.

A stronger source strength of atomic Cl, increased to $\approx 2 \cdot 10^8$ cm^{-3} s^{-1}, is observed in the presence of simulated sunlight at wavelengths > 360 nm (starting with 300 ppb of HCl injected and admitting 350 ppb of O_3), as shown in Figure 3a.

The initial source strength of atomic Cl observed under such irradiation conditions is proportional to the observed consumption rate of O_3, as shown in Figure 3b (summarized from several experiments in the glass chamber). The slope yields a stoichiometry of 0.29 Cl atoms formed per O_3 consumed. A correction for the blank loss of O_3 in the clean chamber

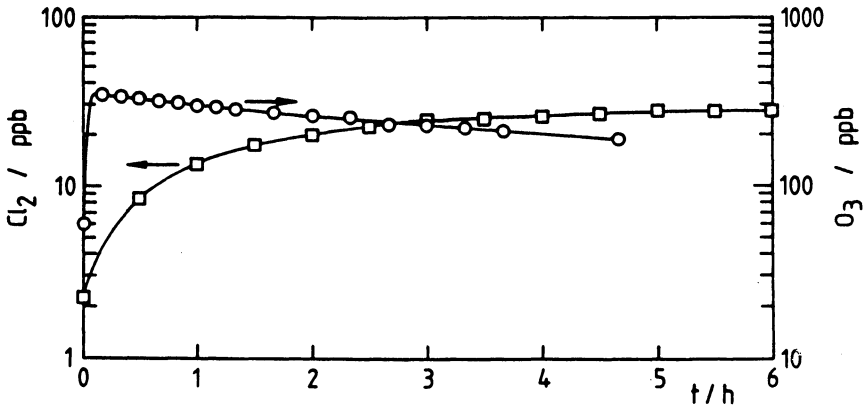

Fig. 2. Formation of Cl_2 in the dark, when admitting O_3 to the glass chamber (where 600 ppb of HCl has been injected beforehand)

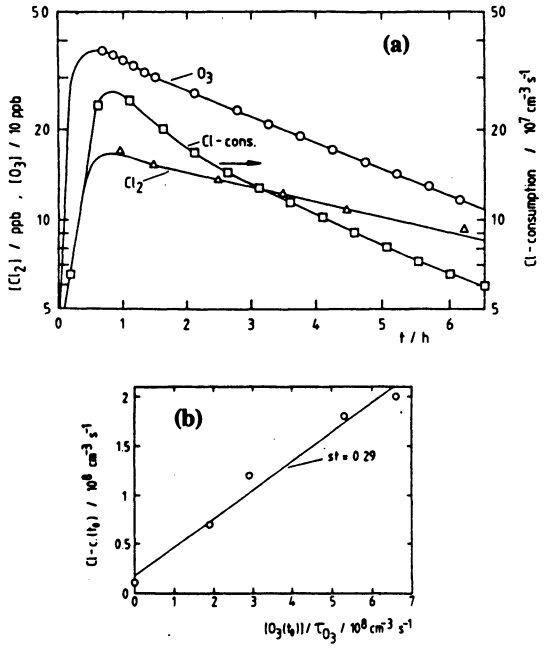

Fig. 3. Source strength of atomic Cl from a mixture containing 300 ppb HCl and 350 ppb O_3 under irradiation by the solar simulator (> 360 nm) **(a)** and stoichiometry of different experiments under similar conditions **(b)**

Table 1: Initial conditions and observed source strength maxima of atomic Cl observed in the glass chamber under irradiation above 360 nm

$[O_3]_o$/ppb	$[HCl]_{inj}$/ppb	Cl-$c_{max}/10^8$ cm^{-3} s^{-1}
365	300	2.0
182	300	1.2
456	300	1.8
0	300	0.1
395	600	0.7

and the loss of O_3 by its reaction with atomic Cl has an only minor influence, increasing the stoichiometry to 0.32. On the other hand, no systematic dependence of the initial source strength of atomic Cl on the experimental conditions, such as the HCl injected and the O_3 admitted (cf. table 1) is found.

Figure 4 shows that, by irradiation of such systems with the full spectrum of the solar simulator (> 300 nm), the source strength of atomic Cl increases to $8 \cdot 10^8$ cm^{-3} s^{-1} with 0.66 Cl atoms formed per O_3 consumed.

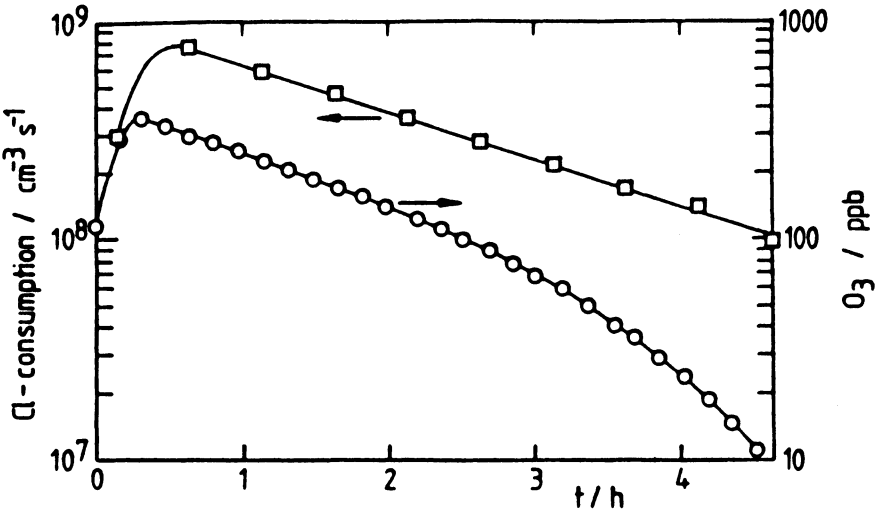

Fig. 4. Source strength of atomic Cl from 600 ppb HCl and 365 ppb O_3 under irradiation by the full spectrum of the solar simulator (> 300 nm).

Heterogeneous production of Cl_2 (and possibly HOCl) from HCl and O_3 in a teflon bag in the presence of aerosols

Similar photochemical experiments, performed in an empty teflon bag, failed to form this additional atomic Cl (besides that produced by OH + HCl). This observation indicates a heterogeneous reaction on the glass surface, that is responsible for the production of the additional atomic Cl. It should be noted again that HCl gas is adsorbed on the glass walls after injection (immediately and almost completely), whereas recoveries better than 50% can be obtained in the teflon bag.

Further experiments were performed in a teflon bag in the presence of aerosols (SiO_2, TiO_2 and Fe_2O_3) to clarify the nature of the heterogeneous source of atomic Cl. Two of these experiments are shown in Figure 5, where the source strength of atomic Cl has been determined in a teflon bag with an amount of HCl injected corresponding to 300 ppb in the presence of SiO_2 aerosol at 1 mg/m^3 and 1 ppm initial concentration of O_3. One experiment of Figure 5 (a) is performed in the presence of humidity (50% r.h.), the other one (b) in the absence of humidity (< 5% r.h.). It can be seen in Figure 4 that the source strength of Cl correlates well with the concentration of O_3 at 50% r.h., and that the source is by one order of magnitude stronger in the presence of humidity. In the dry experiment the source strength increases with time: this may be caused by a slow increase of humidity by permeation from outside into the teflon bag.

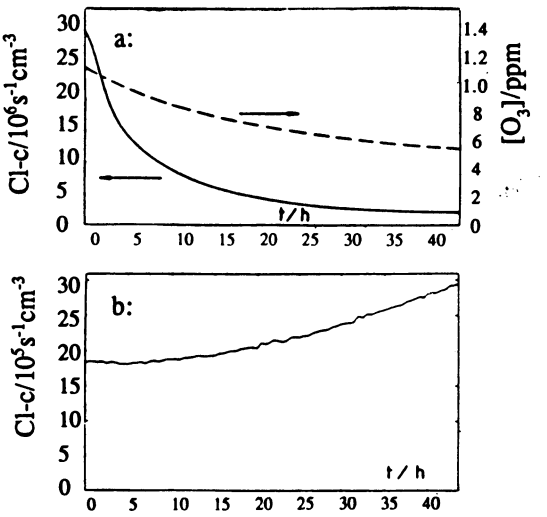

Fig. 5. Production of atomic Cl in a teflon bag in the absence of NaCl and NO_x but instead, in the presence of O_3, HCl and SiO_2 aerosol at 1 mg/m^3. One experiment is in the presence of humidity (a: 50% r. h.), and the other one in the absence of humidity (b: < 5% r.h.)

Further experiments on the formation of Cl were performed in the presence of O_3, HCl, humidity and Fe_2O_3 aerosol and with TiO_2 aerosol even in the absence of O_3 using a cut-off of the UV at 360 nm. The observed rate of formation of Cl was compared with the expected rate of the well-known [Paraskevopoulos and Singleton, 1988] gas-phase reaction:

$$OH + HCl \rightarrow H_2O + Cl$$

revealing that the maximum formation of Cl was higher by factors of 8 (SiO_2), 5 (Fe_2O_3) and 1000 (TiO_2). Figure 6 shows a comparison of the source strength of atomic Cl (determined from the consumption of the indicator compounds) with the production of Cl_2 (determined by the methyl orange method), observed in an experiment in the presence of TiO_2 aerosol. Only the first two measurements of Cl_2 agree with the observed source strengths of atomic Cl. The later measurements indicated an interference of another oxidizing compound in the methyl orange method, e.g., of HOCl or Cl_2O [Pourbaix diagram of the contribution by Langford and Lavigne, this volume).

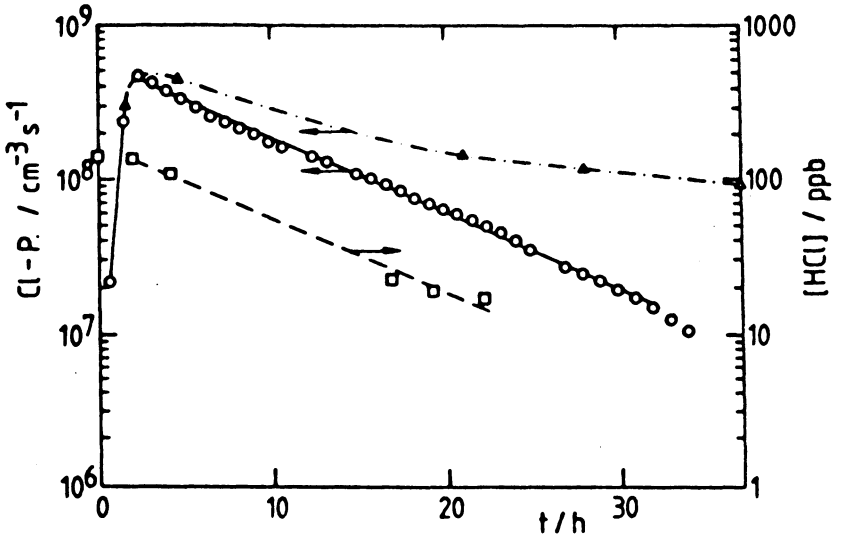

Fig. 6. A comparison of the production rates of atomic Cl, determined from the observed consumption of the indicator compounds by Cl, with the photolytic production from Cl_2 determined by the methyl orange technique). Also included is the concentration of gaseous HCl (determined by a denuder technique).

Production of atomic Cl in the presence of contaminated NaCl aerosol and simulated sea spray

The NaCl aerosol of the Sinclair-LaMer generator turned out to be a strong photochemical producer of atomic Cl under irradiation in teflon bag experiments with O_3 in the absence of NO_x [Behnke and Zetzsch, 1989d]. On the other hand, no atomic Cl was observed in similar experiments with aerosol, produced by atomizing aqueous solutions at room temperature. It was found by denuder measurements, that the Sinclair-LaMer aerosol was contaminated by HCl gas and that either its special, non-crystalline structure or a contamination by NaOH or constituents of the ceramic tube released by the high-temperature production process must be responsible for this artifact [Behnke and Zetzsch, 1990b].

Another typically contaminated type of NaCl aerosol is natural sea-spray. We, therefore, produced an aqueous solution of the major soluble elements and ions of seawater in adjusted amounts (in decreasing abundance): Na, Mg, Ca, K, Sr, Fe, Mo, Zn, Ni, Cu, Sn, Mn, V, Ti, Ce, Ag, Y, Co, Cl^-, SO_4^{2-}, Br^-, CO_3^{2-}, BO_3^{3-}, SiO_3^{2-}, F^-, NO_3^-, PO_4^{3-}, and I^- to produce a fairly natural sea-spray aerosol by atomizing this solution. This aerosol was exposed to a mixture of O_3 and NO_2 for a dark period of 100 min and then irradiated. The data in Figure 7 show that the seasalt is able to produce significantly higher concentrations of atomic Cl than pure NaCl [Zetzsch et al., 1991].

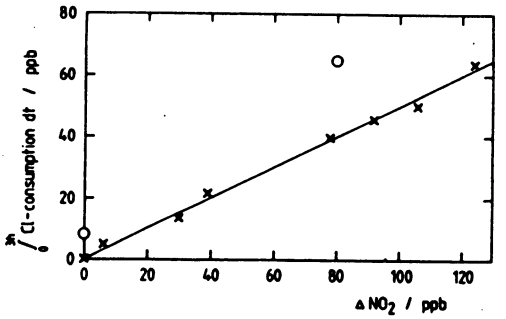

Fig. 7. Production of atomic Cl from simulated sea spray (o) and pure NaCl (x)

Occurrence of chlorinated reaction products

The degradation of the hydrocarbons (used as indicators for OH and Cl in the runs) by Cl in the glass chamber leads to a production of chlorinated compounds, which are identified by GC/ECD and GC/MS. These are summarized in table 2 (other compounds observed were 1,1-dichloro-3-butanone, another, yet unidentified ketone and CCl_4).

Table 2: Yields of chlorinated compounds (order of magnitude, given in % of the hydrocarbon consumed) observed in the glass chamber in the presence of HCl, NO_x and O_3 under irradiation above 300 nm

Precursor	Phosgene	Chloroacetone	1,1-Dichloroacetone	1,1-Dichloro-2-butanone
Toluene	0.1		1	0.01
n-Hexane	0.1		1	1
2,2,4-Trimethyl pentane		0.01		
Tetramethyl pentane	0.01	1	0.1	

Similar products were found in teflon bag experiments with aerosols. An example of such a formation with NaCl aerosol from a Sinclair-LaMer generator has been published [Zetzsch and Behnke, 1992], where phosgene reached a level of almost 10 ppb and the sum of the organic chlorine finally exceeded the gaseous HCl. With SiO_2 or Fe_2O_3 aerosol in the teflon bag, only phosgene was found as photochemical degradation product. An extremely strong formation of chloroacetone, phosgene and 1,1-dichloroacetone was observed with TiO_2 and is displayed in figure 8.

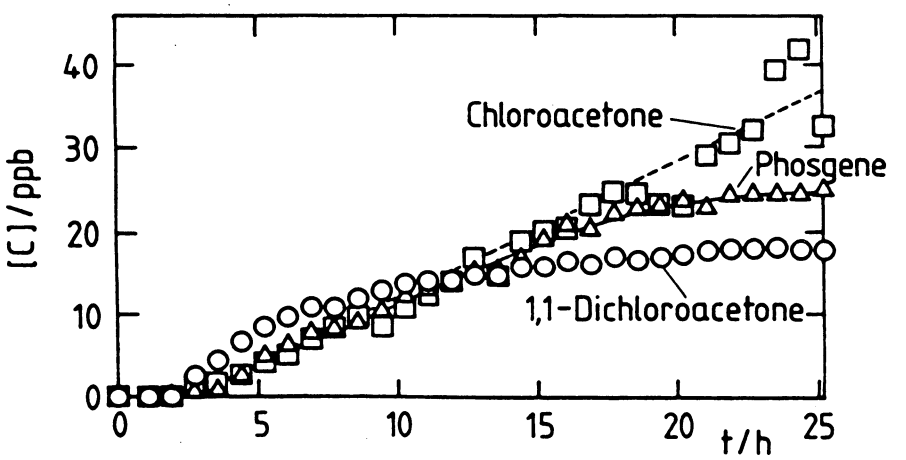

Fig. 8. Heterogeneous formation of chlorinated degradation products observed by irradiation of TiO_2 aerosol (above 360 nm) and the hydrocarbons of table 2 in the presence of 300 ppb HCl in a teflon bag

DISCUSSION

A summary of the approximate source strength maxima, Cl-c_{max}, of the experiments is given in table 3.

Table 3. Approximate heterogeneous source strengths of Cl observed in various experiments at 50% relative humidity in the absence and presence of aerosols

Type of Surface	Conditions	Surface/Volume ($m^2\ m^{-3}$)	Cl-c_{max} ($cm^{-3}s^{-1}$)
Glass chamber	darkness	5	$4 \cdot 10^7$
"	$h\nu > 360$ nm	1	$2 \cdot 10^8$
"	$h\nu > 300$ nm	1	$1 \cdot 10^9$
SiO_2 aerosol	darkness	0.2	$< 2 \cdot 10^6$
"	$h\nu > 300$ nm, dry	"	$< 2 \cdot 10^6$
"	$h\nu > 300$ nm, 50% r.h.	"	$1 \cdot 10^8$
Fe_2O_3 aerosol	$h\nu > 300$ nm	0.15	$1\text{-}3 \cdot 10^8$
TiO_2 aerosol	$h\nu > 360$ nm	0.15	$6 \cdot 10^8$
"	$h\nu > 360$ nm	"	$1 \cdot 10^{10}$
NaCl aerosol, pure	$h\nu > 300$ nm	0.01	$< 2 \cdot 10^6$
NaCl aer., contam.	$h\nu > 300$ nm	0.1	$1 \cdot 10^9$

Cl_2 has been observed to be a main precursor of the observed Cl. Only at the beginning of the irradiation, there is good agreement of both determinations of the source strength of Cl in Figure 6. The discrepancy at longer irradiation times may be due to an interference of other compounds in the methyl orange method which are less efficient in producing Cl than Cl_2 does. This might hold for HOCl and probably for some oxides of chlorine. The photolysis of aqueous chlorine (that may be taken as a model of the adsorption layer on the aerosol) has been investigated very recently in detail by Nowell and Hoigné [1992a]. It is dominated by the photolysis of ClO^- (that is more efficient than HOCl in most natural waters), and the half-life of Cl_2 varies between 60 min at pH 5 and 10 min at pH 8. The yield of OH is observed to increase accordingly at decreasing pH [Nowell and Hoigné, 1992b]. Some mechanisms can be suggested for the production of Cl_2 and HOCl which are available from liquid phase studies. OH can oxidize Cl^- to Cl_2, according to Jayson et al. [1973] and McElroy [1988]:

$$OH + Cl^- \rightarrow OH^- + Cl$$
$$Cl + Cl^- \rightarrow Cl_2^-$$
$$2\,Cl_2^- \rightarrow Cl_2 + 2\,Cl^-$$

Furthermore, O_3 can oxidize Cl^- to form ClO^- [Hoigné et al., 1985] that releases Cl_2 in acidic solution [Eigen and Kustin, 1962]:

$$O_3 + Cl^- \rightarrow ClO^- + O_2$$
$$HCl + H^+ + ClO^- \rightarrow Cl_2 + H_2O$$

In the heterogeneous phase the oxidation of HCl by O_3 may be enhanced by similar processes as the formation of H_2O_2 in the presence of O_3 and humid surfaces observed by Heikes [1984], (possibly catalyzed by Lewis acid centres) according to:

$$O_3\,(ads) + H_2O \rightarrow H_2O_2 + O_2$$
$$O_3\,(ads) + HCl \rightarrow HOCl + O_2$$

since the electrophilic properties of O_3 are known to be enhanced in the adsorbed state [Bailey, 1982]. In the presence of semiconductors, photocatalysis is expected to oxidize Cl^- and OH^- by the sequence:

$$TiO_2 + h\nu \rightarrow TiO_2\,(h^+ + e^-)$$
$$e^- + O_2 \rightarrow O_2^-$$
$$H^+ + O_2^- \rightarrow HO_2$$

and:

$$h^+ + OH^- \rightarrow OH$$
$$h^+ + Cl^- \rightarrow Cl$$

as has been concluded in previous aerosol smog chamber experiments from increased concentrations of OH in the presence of TiO_2 aerosol [Behnke et al., 1987a, 1988]. Such processes occurring on fly ash particles may be responsible for an obvious discrepancy in the determination of OH from degradation rates of hydrocarbons in the Ruhr-area [Neuber et al., 1982], which suggests a contribution of atomic Cl [Zetzsch, 1987, Zetzsch and Becker, 1989]. Coal fired power plant plumes quite often contain HCl gas at the ppm level [Lightowlers and Cape, 1988], and fly ash contains Ti at a level of $\approx 1\%$ on average and higher portions of Fe (forming semiconducting oxides as well). Furthermore, most fly ashes are coated by water soluble salt layers, and are therefore potential candidates for a photocatalytic production of atomic Cl.

The observation of chlorinated organic compounds cannot be explained by homogeneous gas-phase reactions of atomic Cl which would lead to HCl via an abstraction mechanism. Heterogeneous reactions (of ClO^-) are thought to be responsible for these products, in accord with the observation of CCl_4 from a heterogeneous photochlorination of trichloroacetic acid in the presence of NaCl aerosol [Behnke and Zetzsch, 1991].

In the arctic troposphere, ozone destruction was interpreted to be caused by a formation of BrO_x in the arctic spring [Barrie et al., 1988]. It should be noted, that Br^- (in contrast to Cl^-) is known to destroy ozone in a catalytic chain in the aqueous phase [Haag and Hoigné, 1988]. Finlayson-Pitts et al. [1989] observed the formation of $BrNO_2$ in the presence of N_2O_5 (g) and NaBr (s), and McConnell et al. [1992] discussed the possibility of Br_2 formation from the reaction of Br^- and H_2O_2. Both species may be formed in a similar way as $ClNO_2$ and Cl_2 in our experiment.

CONCLUSIONS

Although the present experiments have not been performed under stratospheric conditions, the results imply that HCl can be oxidized by O_3 in the dark to photochemically active Cl_2 in the presence of aerosol surfaces, e.g., PSC's. The activity of various types of aerosol (ice crystals, nitric acid, sulfuric acid, inorganic minerals from meteorite debris and volcanoes) must be checked, before an estimate of the stratospheric relevance can be given.

A strong influence of aerosols is expected for tropospheric chemistry with a source of atomic Cl exceeding the well-known source of the gas-phase reaction of OH with HCl by far. Molecular chlorine is identified as the main photolytic precursor of atomic Cl in the absence of NO_x. It appears that O_3 can oxidize surface-adsorbed HCl or Cl^- more rapidly than known from the aqueous phase. Furthermore, HCl is oxidized extremely rapidly in the presence of semiconducting mineral (metal oxide) aerosols by photocatalytic action to form Cl_2 and other photolytic precursors of atomic Cl. These Cl atoms add on to the chemistry of OH and contribute thereby to the photochemical smog, thus, enhancing the levels of tropospheric ozone. An analogous production of atomic Br would consume O_3 because of the much lower reactivity of atomic Br against hydrocarbons.

Fairly long-lived chlorinated products, such as phosgene, chlorinated ketones and CCl_4 (observed in aerosol smog chamber experiments), are expected to be formed from heterogeneous reactions in the troposphere.

Acknowledgements: This work was supported by the Bundesminister für Forschung und Technologie. The experimental contributions of M. Elend, H.U. Krüger, Petra Kühn, Gisela Pfahler, V. Scheer and J. Zorn are gratefully acknowledged.

REFERENCES

Bailey, P.S., *Ozonation in Organic Chemistry, Vol II: Non-Olefinic Compounds*, Wiley, New York, 1982

Bächmann, K., G. Fuchs, In: Formation, Distribution and Chemical Transformation of Air Pollutants (Ed. R Zellner), *DECHEMA Monogr. 104*: 79-89, VCH-Verlagsgesellschaft, Weinheim, 1987.

Barrie, L.A., J.W. Bottenheim, R.C. Schnell, P.J. Crutzen, R.A. Rasmussen, *Nature 334:* 138-141, 1988.

Behnke, W., C. Zetzsch, Proceedings of the 3rd French German Workshop on Tropospheric Chemistry by Laboratory Studies, 6-8. October 1987, Leinsweiler Hof, *Rep. No. 15* (FB 8, Physikalische Chemie): 59-60, Universität Gesamthochschule Wuppertal, 1987

Behnke, W., C. Zetzsch, Final Report *BMFT-PTU 325-4007-0744158* to the Bundesminister für Forschung und Technologie, 1988.

Behnke, W., C. Zetzsch, In: *Halogenierte organische Verbindungen in der Umwelt, VDI-Berichte 745*: 153-162, VDI-Verlag, Düsseldorf, 1989a.

Behnke, W., C. Zetzsch, In: *Ozone in the Atmosphere. Proc. Quadr. Ozone Sympos. 1988* (Eds. R Bojkov and P Fabian), pp. 519-523, Deepak, Hampton, VA, 1989b.

Behnke, W., C. Zetzsch, In: *Our Changing Atmosphere. Proc. 28th Liège Int. Astrophys. Colloqium* (Eds. P J Crutzen, J-C Gérard and R Zander), pp. 493-498, Inst. d'Astrophysique, Université de Liège, 1989c.

Behnke, W., C. Zetzsch, *J. Aerosol Sci. 20*: 1167-1170, 1989d.

Behnke, W., C. Zetzsch, In: Physico-Chemical Behaviour of atmospheric pollutants. *Proc. 5th European Sympos., Varese 1989* (eds. G Restelli, G Angeletti), pp 277-282, Kluwer, Dordrecht, 1990a.

Behnke, W., C. Zetzsch, *J. Aerosol Sci. S21*: S229-S232, 1990b.

Behnke, W., C. Zetzsch, *Proc. STEP-HALOCSIDE/AFEAS workshop: Kinetics and Mechanism for the Reactions of Halogenated Organic Compounds in the Troposphere* (ed. M McFarland, H Sidebottom), pp. 144-149, University College, Dublin, 1991.

Behnke, W., F. Nolting, C. Zetzsch, *Abstr. 16th Inf. Conf. on Photochemistry*, Harvard, MA, 1984.

Behnke, W., F. Nolting, C. Zetzsch, *J. Aerosol Sci. 18*: 65-71, 1987a.

Behnke, W., G. Pfahler, C. Zetzsch, In: *Abstr. XIIIth Internat. Conf. Photochem.*, pp. 90-91, Budapest, 1987b.

Behnke, W., W. Holländer, W. Koch, F. Nolting, C. Zetzsch, *Atmos. Environ., 22*: 1113-1120, 1988.

Behnke, W., H-U. Krüger, V. Scheer, C. Zetzsch, *J. Aerosol Sci., S22*: S609-S612, 1991.

Behnke, W., H-U. Krüger, V. Scheer , C. Zetzsch,. *J. Aerosol Sci.* (in press), 1992.

Cadle, R.D., R.C. Robbins, *Disc. Faraday Soc. 30*: 155-161, 1960.

Cicerone, R.J., *Rev. Geophys. Space Phys., 19*: 123-129, 1981.

Eigen, M., K. Kustin, *J. Amer. Chem. Soc., 84*: 1355-1360, 1962.

Finlayson-Pitts, B.J., *Nature, 306*: 676-677, 1983.

Finlayson-Pitts, B.J., M.J. Ezell, J.N. Pitts Jr, *Nature, 337*: 241-244, 1989a.

Finlayson-Pitts, B.J., Livingston, H.N. Berko, *J. Phys. Chem., 93:* 4397-4400, 1989b.

Friend, J.P., In: Scientific Assessment of Stratospheric Ozone: 1989, *WMO 20*, Vol. II (AFEAS Report), pp.427-447, WMO, Geneva, 1989.

Haag, W.R., J. Hoigné, In: *Ozone, Science and Engineering (Internat. Ozone Association) Vol 6,* pp 103-114, Pergamon, Oxford, 1984.

Harris, G.W., D. Klemp, T. Zenker, J.P. Burrows, 1990) In: Physico-Chemical Behaviour of Atmospheric Pollutants. *Proc. 5th European Sympos., Varese 1989* (Eds. G. Restelli, G. Angeletti), pp. 644-650, Kluwer, Dordrecht, 1990.

Heikes, B.G., *Atmos. Environ., 18*: 1433-1445, 1984.

Hitchcock, D.R., L.L. Spiller, W.E. Wilson, *Atmos. Environ., 14*: 165-182, 1980.

Hoigné, J., H. Bader, W.R. Haag, J. Staehelin. *Water Res., 19*: 983-1004, 1985.

Hov, O., Norway. *Atmos. Environ., 19*: 471-485, 1985.

Jayson, C.G., B.J. Parsons, A.J. Swallow, *J. Chem. Soc. Faraday Trans., I, 69*: 1597-1607, 1973.

Keene, W.C., A.A.P. Pszenny , D.J. Jacob, R.A. Duce, J.N. Galloway, J.J. Schultz-Tokos, H. Sievering, J.F. Boatman, *Biogeochemical Cycles, 4*: 407-430, 1990.

Kettner, K., W. Forwerg, *Atmos. Environ., 3*: 215-220, 1969.

Lightowlers, P.J., N.J. Cape, *Atmos. Environ. 22*: 7-15, 1988

Martens, C.S., J.J. Wesolowski, R.C. Harris, R. Kaifer, *J. Geophys. Res. 78*: 8788-8792, 1973.

McConnell, J.C., G.S. Henderson, L. Barrie, J. Bottenheim, H. Niki, C.H. Langford, E.M.H. Templeton, *Nature, 355:* 150-152, 1992.

Neuber, E., H.W. Georgii, J. Müller, *Physico-Chemical Behaviour of Atmospheric Pollutants, Proc. 2nd Europ. Symposium held in Varese, Italy* (Eds. B Versino, H Ott), pp. 469-481, Reidel, Dordrecht, 1982.

Nolting, F., W. Behnke, C. Zetzsch, *J. Atmos. Chem., 6*: 47-59, 1988.

Nowell, L.H., J. Hoigné, *Water Res., 26:* 593-598, 1992a.

Nowell, L.H., J. Hoigné, *Water Res., 26:* 599-605, 1992b.

McElroy, W.J., *J. Phys. Chem., 94*: 2435-2441, 1990.

Paraskevopoulos, G., D.L. Singleton, *Rev. Chem. Intermediates, 10*: 139-218, 1988.

Singh, H B, J.F. Kasting, *J. Atmos. Chem., 7*: 262-285, 1988.

Vierkorn-Rudolph, B., K. Bächmann, B. Schwarz, F.X. Meixner, *J. Atmos. Chem., 2*: 47-63, 1984b.

Wagner, I., J. Karthäuser, H. Strehlow, *Ber. Bunsenges. Phys. Chem., 90*: 861-867, 1986.

Warneck, P., *Chemistry of the Natural Atmosphere* (Internat. Geophys. Ser. Vol. 41), Academic Press, San Diego, CA, 1988.

Zetzsch, C., In: Formation, Distribution and Chemical Transformation of Air Pollutants (ed. R Zellner), *Dechema Monograph, 104*: 187-212, VCH-Verlagsgesellschaft, Weinheim, 1987.

Zetzsch, C., *Pollution Atmosphérique, S33*: 89-103, 1991.

Zetzsch, C., K.H. Becker, In: Halogenierte organische Verbindungen in der Umwelt, *VDI-Berichte, 745*: 97-127, VDI-Verlag, Düsseldorf, 1989.

Zetzsch, C., W. Behnke, *Ber. Bunsenges. Phys. Chem., 96*: 488-493, 1992a.

Zetzsch, C., W. Behnke, In: *EUROTRAC annual report 1991, part 6 HALIPP*: 89-94, EUROTRAC ISS, Garmisch-Partenkirchen, 1992b.

Zetzsch, C., G. Pfahler, W. Behnke, *J. Aerosol Sci., 19*: 1203-1206, 1988.

Zetzsch, C., M. Elend, H-U. Krüger, P. Kühn, V. Scheer, W. Behnke, In: Atmospheric oxidation processes, *COST 611/EUROTRAC Joint Workshop, Madrid 1990*: 167-170, CEC Brussels, 1991.

LIQUID PHASE PHOTOCHEMISTRY IN RELATION TO TROPOSPHERIC CHEMISTRY OF HALOGENS

J. Allen Lavigne and Cooper H. Langford
Department of Chemistry, The University of Calgary
2500 University Drive, N.W.
Calgary, Alberta T2N 1N4

INTRODUCTION

This paper reviews some of the aqueous photochemistry studied in our laboratories and elsewhere which could be extrapolated, albeit with due caution, to photochemical processes in a tropospheric situation. Attention has been limited to cases of chromophores that could possibly be found in an aerosol phase and which would have been in contact with halogens in the liquid-phase so as to have formed or be able to form halogen-chromophore combinations. Foremost amongst the chromophores having potential to be of significance in the liquid phase photochemistry of tropospheric components, we consider three: simple Iron(III) species; the iron (hydrous) oxides such as Fe_2O_3; and organic materials such as dissolved organic material (DOM), all of which are known to play a major role in the photochemical processes in natural waters.

IRON(III) SPECIES

Iron is a major component of many particles suspended at various altitudes in the atmosphere. Shaw [1991] reports 102 ng/m^3 for aerosol (dust) collected in Alaskan tropospheric air. It constitutes one of the major contributors in his analysis of 16 common elements. A part of Shaw's results are presented in Table 1, where it can be seen that only Al is more abundant.

Faust and Hoigne [1990] report iron concentrations of 10^{-7} to 10^{-4} M in air-saturated rain droplets. The dominant monomeric Fe(III) species present, under laboratory conditions at pH 2 to 5, is $Fe(OH)^{2+}$. Iron content is 5.5 ppb to 5.5 ppm monomeric Fe(III). (It should be mentioned that $Fe(OH)^{2+}$ is more precisely $Fe(H_2O)_5(OH)^{2+}$ but the former will be used throughout this paper.) Sources for iron vary, but are most often of wind blown dust and fly ash origin. It seems evident that, considering atmospheric "cleansing" mechanisms, the iron eventually finds its way out by either wet or dry deposition. Typical sea water concentrations for Iron are 0.002 mg/L, and for Cl, Br, F and I are 19800 mg/L, 68.9 mg/L, 1.4 mg/L and 0.064 mg/L respectively [Waite, 1989]. Shaw reports values for Cl and Br in particulate matter of 82.6 ng/m^3 and 2.76 ng/m^3, respectively. The dominant halogen species in sea spray and particulates is obviously Cl^-, and overwhelmingly so. Polyatomic anions of

NATO ASI Series, Vol. I 7
The Tropospheric Chemistry of Ozone in the Polar Regions
Edited by H. Niki and K. H. Becker

multiple charge such as sulphate (SO_4^{2-}) are larger and have lower charge densities and will thus compete less favourably for the metal cation than will monatomic anions. Thus, halo-compounds are expected to be important. Organic ligands play an important role in the chelation of metal ions. Equilibrium and chemical speciation are treated extensively in standard references such as Stumm and Morgan [1981].

Table 1: Elemental mass concentrations by neutron activation of Alaskan tropospheric aerosol samples. (Reduced results obtained from Shaw [1991])

element	At. No.	mean	element	At. No.	mean
Na	11	95.7	Fe	26	102.0
Al	13	167.0	Co	27	0.112
Cl	17	82.6	As	33	0.210
K	19	55.8	Se	34	0.053
Ti	22	22.3	Br	35	2.76
V	23	0.181	Sb	51	0.071
Cr	24	0.885	Cs	55	0.015
Mn	25	0.255	La	57	0.074

Mass concentrations are in ng/m^3

There is scant information regarding the true speciation in both atmospheric droplets and aerosols. Recently, however, Dedik et al. [1992] have characterized samples of aerosols filtered in Mainz (F.R.G.). Their results show that the predominant oxidation state of iron, as analyzed by Mossbauer spectroscopy, is Fe(III) (about 75%) with lesser amounts of Fe(II) (10%) and with some mineral forms identifiable (magnetite, hamatite, and goethite, 8, 6, and 2% respectively). The form considered here is Fe(III). We also consider the photochemical behaviour of hematite. Fe may be present as monomeric complexes, dimers, polymers, or colloidal hydrous oxide. Nevertheless, Faust and Hoigne [1990] consider the following simple equilibrium between the amorphous hydrous oxide, $Fe(OH)_3(s)$, and monomeric Fe(III) species in cloud and rain as;

$$Fe(OH)_3(s) + H^+ \rightleftarrows Fe(OH)_2^+ + H_2O \quad (1)$$

$$Fe(OH)_3(s) + 2H^+ \rightleftarrows Fe(OH)^{2+} + 2H_2O \quad (2)$$

The photoinduced reduction of monomeric Iron(III) produces Iron(II) and can be represented as;

$$Fe(OH)^{2+} \xrightarrow{h\nu} Fe(II) + OH \qquad (3)$$

where OH is the hydroxyl radical, and the primary excitation is in a ligand to metal charge transfer (LMCT) band. Fe(II) can then be re-oxidized to Fe(III) by oxidants. We see below that OH can lead to oxidation of halides. Although other Fe(III) complexes are also reactive, only chloro and bromo complexes will be discussed here as they are found in sea water and biological degradation products.

The absorption spectrum for Fe(III) showing the charge transfer band for $Fe(OH)^{2+}$ is reproduced in Figure 1.

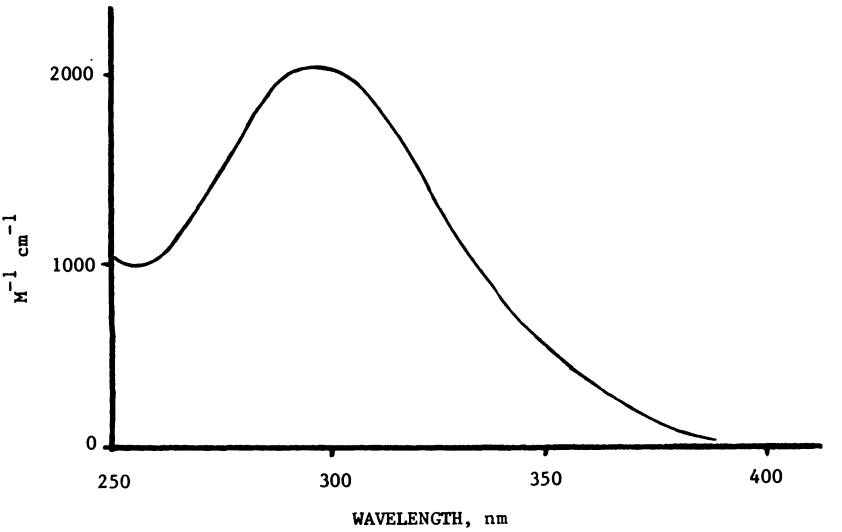

Fig. 1: Molar absorptivities for Fe(III) at pH = 4. (Reduced reproduction from Faust and Hoigne [1990])

Langford and Carey [1975] have studied the charge-transfer photochemistry of aqueous Fe^{3+}. Using tert-butyl alcohol as a scavenger, they were able to propose the following reactions for halogen to metal charge-transfer photochemistry of chloropenta-aquairon (III);

$$Fe^{III}Cl^{2+} \xrightarrow{h\nu} {}^{*}Fe^{III}Cl^{2+} \xrightarrow{k_1} Fe^{2+} + Cl \qquad (4)$$

Scavenging of the primary Cl radical by t-butyl alcohol established that the primary yield of this process is 0.186 under 350 nm excitation. In a medium of moderate chloride

concentration, a main reaction of Cl is a recombination of the radical with a chloride ion giving the chloride radical ion;

$$Cl\cdot + Cl^- \xrightarrow{k_4} Cl_2^- \qquad (5)$$

which can effect the re-oxidation of Fe(II);

$$Cl_2^- + Fe^{2+} \xrightarrow{k_5} Fe^{III}Cl^{2+} + Cl^- \qquad (6)$$

In summary, upon excitation of the chloride to metal charge transfer band at 350 nm, the $Fe^{III}Cl^{2+}$ reacts photochemically with primary yield for Cl of 0.093, (one-half the 0.186 yield for Fe(II) in the presence of a scavenger). Overall reaction products are, however, Fe^{3+} and the chloride ion Cl^- unless some scavenger can intervene. It is important to realize that scavengers will not usually be present in concentrations high enough to produce overall Cl^- oxidation yields near the limit of 0.093.

Parallel chemistry, of course, arises for bromide complexes of iron. The charge transfer spectra of $Fe^{III}Cl^{2+}$ and $Fe^{III}Br^{2+}$ are presented in figure 2 [Fox, 1975]. In the case of $Fe^{III}Br^{2+}$, charge transfer absorption extends well into the visible region of the spectrum.

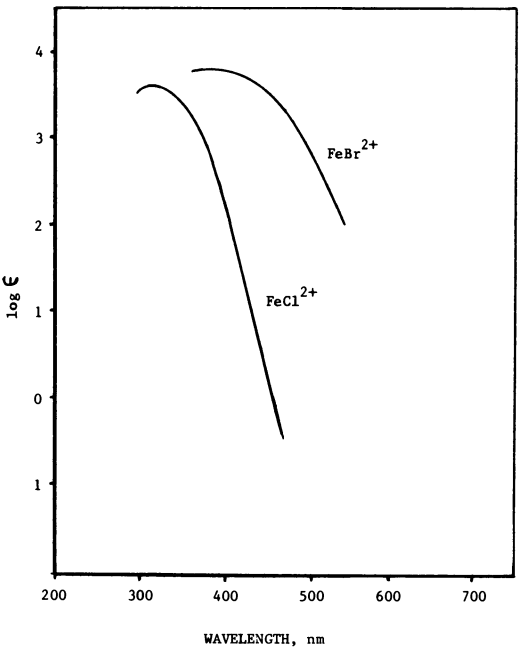

Fig. 2: Absorption spectra of $Fe^{III}X^{2+}$ complexes in aqueous solutions [Fox, 1975]

In the same work [Langford and Carey, 1975] a mechanism for the photoreaction of hydoxypentaaquairon(III) is summarized as;

$$Fe^{III}OH^{2+}_{aq} \xrightarrow{h\nu} {}^{*}Fe^{III}OH^{2+}_{aq} \xrightarrow{H_2O,k_1} Fe^{2+} + OH + H^{+} \qquad (7)$$

The primary products here are the reduced Fe(II) species and a hydroxyl radical. As in the case of Cl^-, OH re-oxidization of Fe^{2+} yields a hydroxyde ion, and Fe^{3+}. Net oxidation by OH will be much less efficient than the limiting yield of 0.63 at 350 nm.

OXIDES OF IRON

One iron oxide of particular interest is hematite (α-Fe_2O_3). Faust and Hoffmann [1986] studied the photoassisted charge transfer reactions of Fe(III)-S(IV) surface complexes using this oxide. They had previously shown [Hoffmann and Jacob, 1984] that most iron present at high concentrations (even $> 10^{-3}$ M) in urban fogs and clouds was "operationally" classifiable as "soluble" or micro-colloidal, despite its thermodynamic insolubility at intermediate pH.

Irradiation of α-Fe_2O_3 at 375 nm creates "holes" trappable mainly on oxygen ions, and electrons trappable mainly on iron. The net effect is more or less the equivalent of oxide ligand to Fe(III) charge transfer excitation. The oxidation of S(IV) can be represented: adsorption;

$$\alpha\text{-}Fe_2O_3 + S(IV) \rightarrow \alpha\text{-}Fe_2O_3\text{-}S(IV)\ (surface) \qquad (8)$$

band gap excitation to give a hole in the valence band and an electron in the conduction band;

$$\alpha\text{-}Fe_2O_3\ (solid) + h\nu\ (375\ nm) \rightarrow \alpha\text{-}Fe_2O_3(e^-_{cb}, h^+_{vb}) \qquad (9)$$

the "hole" may oxidize surface-S(IV) to surface S(V);

$$h^+_{vb}(Fe_2O_3) + S(IV) \xrightarrow{surface} S(V)\ (surface) \qquad (10)$$

and reduction of the lattice oxide by the "electron";

$$Fe^{3+}(lattice/surf.) + (Fe_2O_3)e^-_{cb} \rightarrow Fe^{2+}(lattice/surf.) \qquad (11)$$

which is followed by solvation of Fe^{2+} from the lattice surface;

$$Fe^{2+} \xrightarrow{lattice/surface} Fe^{2+}_{aq} \qquad (12)$$

which gives oxidized sulphur and reduced iron. In contrast, OH may also be the product of

e^- trapping if O_2 is adsorbed on the surface. This could arise if conduction band electrons scavenged by O_2 gives rise to superoxide radical anions, O_2^- which can disproportionate to give H_2O and the hydroxyl radical, OH . This is, however, likely to be a minor pathway.

In summary, these reactions have the effect to increase the concentrations of dissolved Fe(II) (and, in oxygenated water, Fe(III)) above what would otherwise be expected from equilibrium with the waters and atmosphere. Faust and Hoffmann [1989] suggest that this would increase the rate of iron cycling in both surface and atmospheric waters, and also increase the rate of reactions involving dissolved iron species to an amount greater than that predictable by the equilibrium proposed in reactions (1) and (2) earlier.

More importantly for our purposes, this "band-gap" photo-chemistry has been shown to be capable of the oxidation of water. Near-UV photolysis of aqueous suspensions of the Fe(III) oxide minerals lepidocrocite, γ-FeOOH, [Waite and Morel, 1984] and hematite, α-Fe_2O_3 [Haupt and Peretti, 1984] in water with no organic substrates present yielded Fe^{2+}_{aq} and molecular oxygen, respectively, as the observed products. Electrons and holes photogenerated within the iron oxide semiconductor lattice are scavenged by surface sites to produce ions;

$$(\text{surface})\text{-}Fe^{III}(:OH^-) \xrightarrow{e-(cb)} Fe(II) + OH^- \qquad (13)$$

or radicals, respectively;

$$(\text{surface})\text{-}Fe^{III}(:OH^-) \xrightarrow{h+(vb)} Fe(III) + OH \qquad (14)$$

Yields are limited by the short diffusion length of electrons and holes in the iron oxide semiconductors [Kiwi and Grätzel, 1987]. Existing evidence implies that the quantum yield of reaction varies over orders of magnitude, depending on the particular crystalline iron oxide [Waite, 1985]. Amorphous and crystalline (hydrous) iron oxides are present in airborne particles.

The most reactive species obtained is from reactions (3), (7) and (14), namely the OH radical. Once hydroxyl radicals are generated, they provide access to the oxidized species of Cl^- and Br^-. Some important reactions of these are summarized here: first, oxidation of a halide;

$$OH + X^- \rightarrow X + OH^- \qquad (15)$$

$$X + X^- \rightarrow X_2^- \qquad (16)$$

where rate constants with both Br^- and Cl^- are in the order of 10^{10} [Dorfman and Adams, [1973].

One other important OH reaction is hydrogen abstraction from organic compounds, where the hydrogenated HCFC's and HFC's are of particular interest, for example [Cooper et al., 1990];

$$CH_3F + OH \rightarrow H_2O + CH_2F \quad (17)$$

The reaction of reaction (17) may be significant in reducing the lifetimes for HCFC's [Burkholder et al., 1991].

Burkholder et al. [1991] also discuss the significance of the hydroxyl radical on the fate of various small brominated species. We see from reactions (17) that they can be made into halocarbon radicals which are further reacted according to the other species available in their particular environment. Bromoalkanes are usually found in sea water and in organisms in sea water [Berg and Sperry, 1983] and as such are present in the environments we have been discussing.

In the field of soil and water chemistry, it has been known for some years that chloroform species can originate from the chlorination procedures used in waste water treatment and pretreatments [Rook, 1976]. Dissolved organic materials (DOM) such as the fulvic and humic substances are suspected to be a major source of these hydrochlorocarbons in drinking water. Analogous reactions can easily arise in natural water. Indeed, hydrobromocarbons could also arise from the photochemical Br production and reaction with DOM. Such products would be susceptible as well to hydrogen abstraction and further radical generation reaction (17).

Another reaction of the hydroxyl radical of particular interest is that with ozone [Crutzen, 1974];

$$O_3 + OH \rightarrow HO_2 + O_2 \quad (18)$$
$$HO_2 + O_3 \rightarrow OH + 2O_2 \quad (19)$$

These reactions are but representative of some of the many possibilities that may arise with the hydroxyl radical, and other papers in this Proceeding cover a number of these other reactions.

PHOTOCHEMISTRY OF DISSOLVED ORGANIC MATERIALS

There has been considerable work performed lately dealing with the photochemistry of both well characterized fulvic acids such as the Armadale [Power et al., 1987], and various natural humic mixtures [Cooper, 1989]. Fulvic acid absorbs strongly in the near-ultraviolet, with primary photochemistry being photoionization with formation of a solvated electron and its associated cation radical [Power et al., 1987]. The major photophysical pathway is triplet

formation [Bruccoleri et al., 1990; Langford et al., 1992], with an apparent quantum yield for the Armadale sample of 0.65 at pH 5. Of possible significance to atmospheric aerosol chemistry is that it is suspected that the triplets are associated with the lower molecular weight components, more likely to be accommodated in particles. The quantum yields for solvated electrons and associated radicals are lower, about 0.09 at pH 2 [Power et al., 1987].

Subsequent photochemical pathways depend on the fate of the three primary photoproducts; the triplets, the solvated electrons, and their associated cation radicals. The most abundant reactive species available in illuminated aerated waters are molecular oxygen (average $[O_2] = 2.5 \times 10^{-4}$ M), and the fulvic acid itself. At low pH (<4), H^+ becomes an effective scavenger of the solvated electron. Singlet oxygen can be formed by scavenging the triplets [(reaction 20)]. Three reactions most likely to represent the overall photochemical processes involving oxygen are;

$$^3FA + {}^3O_2\,(aq) \rightarrow {}^1FA + {}^1O_2\,(aq) \qquad (20)$$

$$e^- + {}^3O_2\,(aq) \rightarrow O_2^-\,(aq) \qquad (21)$$

$$R^+\,(aq) + O_2\,(aq) \rightarrow RO_2^+ \qquad (22)$$

In the second reaction, (21), the superoxide ion disproportionates rapidly to hydrogen peroxide (approximately 24-40% does not) [Cooper et al., 1989]. The organic peroxy radical is quite reactive, also it is the least characterized. The solvated electron could, under favourable conditions, be captured by the fulvic acid. The peroxy radicals, likewise, can react with the fulvic acid itself, producing a variety of phenoxyl radicals [Power et al., 1986], the lifetimes of which are short (microseconds) and are suspected of being further quenched by molecular oxygen. Overall, competition provided by the components of the fulvics for the primary photoproducts could be quite significant in aerated natural waters. Nevertheless, small concentrations of the oxidizing OH radical are the results of light absorption by DOM allowing another entry to halogen oxidation.

ACCESSIBLE OXIDATION STATES OF THE HALOGENS

Oxidation of the chloride ion to chlorine is limited to the molecular species Cl_2 only in strongly acid media. In neutral or alkaline solutions, oxidation of chloride ions leads to the formation of oxygen derivatives including hypochlorites (HClO, ClO^-), chlorites ($HClO_2$, ClO_2^-), chlorates (ClO_2, ClO_3^-) and perchlorates (ClO_4^-). Figure 3 shows the Pourbaix diagram (also known as pH-E_H diagrams) for chlorine oxidation states -1, 0, an +1. Access to the positive oxidation states of the bromine arises similarly.

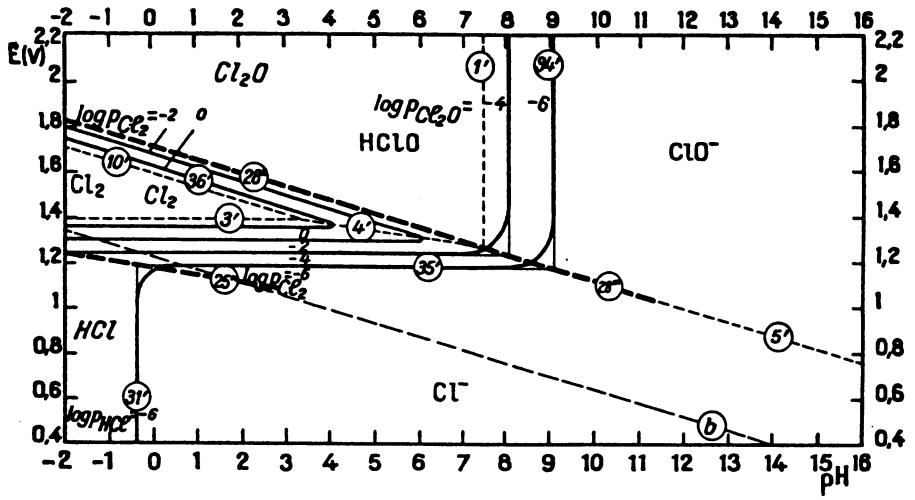

Fig. 3: Equilibria between dissolved Cl^-, Cl_2, HClO, ClO^- and gaseous HCl, Cl_2, Cl_2O. (Pourbaix [1974])

CONCLUSIONS

In the confines of this short paper we have focused on photo-chemical processes which initiate halide oxidation in the liquid-phase. The overall halogen chemistry is very rich. The work by Pourbaix is an atlas containing many more pH-pE diagrams and the reader is referred to his volume for further thermodynamics of halogens. The subsequent chemistry of oxidized halogens is much too rich to be included in this paper, but is presented in other papers in this workshop.

REFERENCES

Bruccoleri, A., C.H. Langford, C. Arbour, Pulsed photoacoustic evaluation of intersystem crossing quantum yields in fulvic acid, *Environ. Technol., 11*, 169-172, 1990.

Burkholder, J.B., et al., Atmospheric fate of CF_3Br, CF_2Br_2, CF_2ClBr, and CF_2BrCF_2Br,. *J. Geophys. Res., 96* (D3), 5025-5043, 1991.

Cooper, D.L., N.L. Allan, A. McCulloch, Reactions of hydro- fluorocarbons and hydrochlorofluorocarbons with the hydroxyl radical, *Atmos. Environ., 24A* (9), 2417-2419, 1990.

Cooper, W.J., R.G. Zika, R.G. Petasne, and A.M. Fischer, Sunlight-induced photochemistry of humic substances in natural waters: Major reactive species, Chapter 22 in "*Aquatic Humic Substances*", American Chemical Society, pp. 334-362, 1989.

Crutzen, P.J., Photochemical reactions by and influencing ozone in the troposphere, *Tellus, 26,* 47-57, 1974.

Dedik, A.N., P. Hoffman, and J. Ensling, Chemical characterizationof iron in atmospheric aerosols, *Atmos. Environ., 26A (14)*, 2545-2548, 1992.

Dorfman, L.M., G.E. Adams, Inorganic electron transfer reactions, In "Reactivity of the Hydroxyl Radical in Aqueous Solutions, NSDRS-NBS, 46: U.S. Department of Commerce, Washington, DC., pp 32-37, 1973.

Faust, B.C., and M.J. Hoffmann, Photoinduced reductive dissolution of α-Fe_2O_3 by bisulfite, *Environ. Sci. Technol., 20*, 943-948, 1986.

Faust, B.C., and J. Hoigne, Photolysis of Fe(III)-hydroxy complexes as sources of OH radicals in clouds, fog, and rain, *Atmos. Environ., 24A* (1), 79-89, 1990.

Fox, M., The Photolysis of Simple Inorganic Ions in Solution, chpt. 8 in "*Concepts of Inorganic Chemistry*", Adamson, A.W., and Fleischauer, P.D., Eds., Wiley-Science Publ., John Wiley & Sons, Toronto; p. 343, 1975.

Haupt, J., and J. Peretti, J., *R. Nouv. J. Chim., 8*, 633, 1984.

Hoffmann, M.R., D.J. Jacob, In "*Acid Precipitation: SO_2, NO, and NO_2 Oxidation Mechanisms: Atmospheric Considerations*"; Calvert, J.G., Ed.; Butterwork: Stoneham, MA; pp 101-172, 1984.

Kiwi, J., and M. Grätzel, Light-induced Hydrogen formation and photo-uptake of Oxygen in colloidal suspensions of α-Fe_2O_3, *J. Chem. Soc., Faraday Trans. 1*, 83, 1101-1108, 1987.

Langford, C.H., and J.H. Carey, The charge transfer photochemistry of the hexaaquoiron(III) ion, the chloropentaaquairon(III) ion, and the u-dihydroxo dimer explored with tert-butyl alcohol scavenging, *Can. J. Chem., 53* (16), 2430-2435, 1975.

Langford, C.H., A. Bruccoleri, D.K. Sharma, Evaluation of Photoproduct Quantum Yields in Fulvic Acid. ACS Division of Environmental Chem., Pre-prints of papers presented at the *203rd ACS National Meeting, vol. 32* (1), 216-220, 1992.

Pourbaix, M., Atlas of Electrochemical Equilibria in Aqueous Solutions,. National Assoc. of Corrosion Engg.: Cebelcor, Brussels. p. 598, 1974.

Power, J.F., Ph.D. Thesis, Laser Studies of the Photophysics of Humic Substances. Concordia University, Montreal, 1986.

Power, J.F., D.K. Sharma, C.H. Langford, R. Bonneau, J. Joussot-Dubien, J., Laser flash photolytic studies of a humic substance, in *ACS Symp. Ser., no. 327*, pp. 157-173, 1987.

Rook, J.J., Haloforms in Drinking Water, *J. Am. Water Works Assoc., 58* (3), 168-172, 1976.

Shaw, G.E., Aerosol chemical components in Alaska Air Masses. 1. Aged Pollution. J. Geophys. Res., 96(D12), 22357-22368, 1991.

Stumm, W., and J.J. Morgan, *Aquatic Chemistry*, John Wiley and Sons, Toronto, 551 pp., 1981.

Waite, T.D., and Morel, F.M., Photoreductive dissolution of colloidal iron oxides in natural waters, *Environ. Sci. Technol.*, 18, 860, 1984.

Waite, T.D., In; *Abstract of papers, 1909-th National Meeting of the American Chemical Society*, Chicago, ILL.; American Chemical Society: Washington, D.C.; GEOC0067, 1985.

Waite, T.D., Mathematical modelling of trace element speciation, Chapter 5 in, *Trace Element Speciation: Analytical Methods and Problems*, G.E. Batley, ed.: CRC Press, Baco Raton, Florida, p.151, 1989.

OZONE-HO_X PHOTOCHEMISTRY IN THE TROPOSPHERE - LATITUDINAL DEPENDENCE OF REACTION RATES

R. A. Cox
Marine and Atmospheric Sciences Directorate
Natural Environment Research Council
Polaris House
North Star Avenue
Swindon, Wiltshire
SN2 1EU, UK

BACKGROUND

An important role of photochemical reactions in controlling ozone concentrations in the background 'unpolluted' troposphere was first suggested nearly 2 decades ago [Crutzen, 1973; Chameides and Walker, 1973]. This followed the important paper by Levy [1972] where the existence of relatively large concentrations of hydrogen containing free radicals (OH and HO_2) and associated organic species derived from the breakdown of atmospheric methane, would be present in the sunlit atmosphere. The early suggestions have lead to the development of a comprehensive theory of tropospheric photochemistry which underlies our current understanding of the budget of tropospheric ozone and the oxidising properties of the atmosphere [Logan et al., 1981, Isaksen, 1988]. The central feature of this theory is the generation of a steady state concentration of OH radicals primarily through ultra violet photolysis of ozone and subsequent reaction with water of the excited O (^1D) oxygen atoms produced. The OH radicals react with many atmospheric trace gases, leading to their oxidation by a mechanism in which the OH radical can be regenerated. This oxidation process serves to control the concentration of many volatile organic compounds, including those containing sulphur, nitrogen and halogens, as well as the organic constituents such as NO, NO_2 and SO_2. The oxidation processes can lead either to ozone loss or additional ozone production, depending on the local availability of nitrogen oxides. The mechanism of these processes is now quite well known as a result of intensive studies over the last 20 years, stimulated by the problem of photochemical oxidant production in air polluted by combustion - derived NO_x and non-methane hydrocarbons. This has led to the development of sophisticated photochemical models of the production and loss of ozone in the boundary layer and in the free troposphere [Derwent and Jenkin, 1982; Crutzen and Gidel, 1983; Isaksen and Hov, 1987; Hough, 1991].

Most models have described the O_3-HO_x photochemistry primarily in terms of a homogeneous gas phase chemical mechanism, with photochemical reaction rates calculated for clear sky solar radiation. More recently the role of clouds, both in their effects on solar

NATO ASI Series, Vol. I 7
The Tropospheric Chemistry of Ozone in the Polar Regions
Edited by H. Niki and K. H. Becker

radiation and hence the rate of photochemically driven processes, and in their effects through chemical removal and reaction in the liquid phase, has been considered [Logan et al., 1981; Hough, 1988; Lelieveld and Crutzen, 1990]. The influence of clouds, which occupy only about 15% of the volume of the lower troposphere, could have a significant effect on the global budgets of ozone and other trace gases, influenced by photochemical oxidation as well as their more obvious local effects.

Because the O_3-HO_2 system is driven by photochemistry, large seasonal and latitudinal variations in the rates of reaction and the overall chemical fluxes are expected. Further variations in chemical activity will result from the local atmospheric trace gas composition which can be influenced by pollution. Thus, there is a strong contrast between the northern and southern hemispheres and between mid-latitude source regions and remote regions such as the Arctic and Antarctic. The interplay of transport, airmass origin, local atmospheric physics and chemistry, therefore influences the atmospheric chemical behaviour at a given place.

The O_3-HO_x system is essentially 'fast photochemistry' reflecting local conditions. The relaxation time of the chemical system is short enough (a few minutes), so that the key reactive species are not influenced by transport. This offers, in principle, the possibility of testing the photochemical theory by local in-situ atmospheric measurements. Several factors have made such tests difficult. Firstly, fast response measurement of the very low concentrations of reactive species such as OH, HO_2 and organic radicals has presented a considerable technical challenge, as yet not fully overcome. Secondly, measurements that have been made reveal that, in the surface atmosphere the chemistry is exceedingly complex and sensitive to local sources and to the advection of pollutants from elsewhere [Ehhalt et al., 1991]. The best location for such tests should have relatively invariant concentrations of the longer lived gases such as O_3, H_2O_2, CH_4, CO and no local sources of reactive species such as NO_x and volatile organics. Polar and maritime regions, high mountain sites, or airborne measurements, offer the best prospects for testing the local O_3-HO_x fast photochemistry. Experimental evidence will always require a comprehensive suite of measurements covering as far as possible all the physical and chemical factors influencing the chemical system.

An alternative method of testing the validity of the tropospheric O_3-HO_x photochemistry on a global scale is through the evaluation of the budgets of longer lived constituents which are removed by OH radicals and which have known sources. Examples are the use of ^{14}CO [Volz et al., 1981; Derwent and Volz-Thomas, 1989] and methyl chloroform [Singh, 1977; Prinn et al., 1987]. These methods give global mean tropospheric OH contribution of (6-8) x 10^5 molecule cm^{-3}. More sophisticated analysis using 3-D concentration fields shows that most of the photochemical activity is in the tropical middle troposphere [WMO, 1989].

Recently, it has been suggested that significant non-photochemical O_3-HO_x (free radical) chemistry may occur at night-time. This could be of potential significance in polar regions, for the ozone budget during winter-time. The non-photochemical free radical chemistry requires: 1) the presence of reactive volatile organic substances which are capable of supplying free radicals by reaction with NO_3, ozone or other night-time oxidising agents; 2) the presence of significant concentrations of NO_x together with O_3, favouring the production of NO_3 radicals, through the reaction of NO_2 with ozone. Thus, advection of polluted air into the Arctic would tend to favour this process.

MECHANISMS OF OZONE PRODUCTION AND LOSS

The mechanisms of ozone production and loss involving HO_x photochemistry have been discussed in detail in a number of reviews [Logan et al., 1981; Cox, 1988]. Here we summarise the main processes involved in production of 'odd hydrogen' radicals, OH and HO_2, photochemical ozone formation and loss, and the influence of cloud photochemical processes.

Photochemical production of radicals: The primary source of radicals in the troposphere is the photodissociation of ozone to produce $O(^1D)$ atoms followed by their reaction with water vapour:

$$O_3 + h\nu \ (\lambda > 310 \text{ nm}) \rightarrow O(^1D) + O_2 \quad (1)$$
$$O(^1D) + H_2O \rightarrow 2\ OH \quad (2)$$

In the background atmosphere the most important interconversion reactions are those of OH with CO and CH_4 leading to the production of hydroperoxy (HO_2) and methyl peroxy radicals (CH_3O_2) respectively:

$$OH + CO \rightarrow H + CO_2 \quad (3)$$
$$H + O_2 + M \rightarrow HO_2 + M \quad (4)$$
$$OH + CH_4 \rightarrow CH_3 + H_2O \quad (5)$$
$$CH_3 + O_2 + M \rightarrow CH_3O_2 + M \quad (6)$$

About 70% of the OH radicals react with CO and 30% with CH_4, to initiate a series of reactions which lead to oxidation of organics and production and/or loss of ozone, with some regeneration of OH radicals, constituting a short chain reaction.

HO_2 is converted back to OH via reaction with NO or O_3; CH_3O_2 is converted first to CH_3O (via reaction with NO) which is then converted to HO_2 by reaction with O_2.

$$HO_2 + NO \rightarrow NO_2 + OH \quad (7)$$
$$HO_2 + O_3 \rightarrow 2O_2 + OH \quad (8)$$
$$CH_3O_2 + NO \rightarrow CH_3O + NO_2 \quad (9)$$
$$CH_3O + O_2 \rightarrow HO_2 + HCHO \quad (10)$$

When stable products are formed the process leads to loss of radicals, thereby influencing the overall steady state, e.g.,

$$HO_2 + HO_2 \rightarrow H_2O_2 + O_2 \quad (11)$$
$$CH_3O_2 + HO_2 \rightarrow CH_3OOH + O_2 \quad (12)$$

Additional photochemical sources of organic radicals (and hence RO2) come from photolysis of carbonyl compounds, e.g.

$$HCHO + h\nu\,(<320\text{ nm}) \rightarrow H + HCO \quad (13)$$
$$CHCH_3CHO + h\nu\,(<320\text{ nm}) \rightarrow CH_3 + CH_3 \quad (14)$$

Similar photolysis reactions occur for longer chain aldehydes and ketones and their derivatives (including dicarbonyls), produced in the oxidation of more complex organic molecules. These can lead to production of more complex RO_2 radicals by reaction of the photofragments with O_2.

The presence of additional volatile organic molecules which react with OH will tend to increase this complexity of the peroxy radical 'pool'. More complex peroxy radicals will lead to a greater variety of product molecules [Atkinson R., 1990].

Photochemical Ozone Formation: Peroxy radicals cause production of ozone in the lower atmosphere by perturbation of the photostationary state of the $NO\text{-}NO_2\text{-}O_3$ system. The photostationary state for the reactions:

$$NO_2 + h\nu\,(< 400\text{ nm}) \rightarrow NO + O \quad (15)$$
$$O + O_2 + M \rightarrow O_3 + M \quad (16)$$
$$NO + O_3 \rightarrow NO_2 + O_2 \quad (17)$$

yields the following relationship for the ozone concentration:

$$[O_3] = \frac{J_{NO_2}[NO_2]}{k_{17}[NO]} \quad (i)$$

where J_{NO_2} is the rate of photodissociation of NO_2 via reaction 15. Additional conversion of NO to NO_2 via reaction with RO_2 (or HO_2), i.e.,

$$RO_2 + NO \rightarrow NO_2 + RO \qquad (18)$$

leads to an increase in the ratio of $[NO_2]$ to [NO] and hence an increase in the local ozone concentration. The relaxation time for the photochemical steady state is approximately 100 seconds under typical daytime conditions in the lower atmosphere, and therefore as the ratio of $[NO_2]$ to [NO] changes due to the flux through reaction 18 over a typical time scale of a few hours, the ozone concentration changes according to equation (i).

The net ozone production will be maximum if all the RO_2 radicals react with NO to form NO_2 in reaction (18). Any reaction which competes against this will reduce local ozone production and moreover, if non-radical products are formed, the reaction will serve to reduce overall radical concentration.

Reactions leading to photochemical ozone loss: When the concentrations of nitrogen oxides are low, peroxy radicals undergo mutual and self-reactions and, since theory indicates HO_2 is the most abundant peroxy radical, the reaction of RO_2 with HO_2 is most important.

$$RO_2 + HO_2 \rightarrow ROOH + O_2 \qquad (19)$$

The main product of these reactions is the corresponding hydroperoxide, which is a closed shell molecule and therefore the overall process leads to radical loss. Stable products other than ROOH can be formed (e.g., $RCHO + H_2O + O_2$) but evidence for these channels is indirect and not compelling, except for the acylperoxy reaction with HO2 which forms O_3 and carboxylic acid as well. Hydroperoxides formed in this way can be removed from the atmosphere in one of several ways:

a) Photolysis in which the O-O bond is broken to form OH plus an alkoxy radical:

$$ROOH + h\nu \rightarrow RO + OH \qquad (20)$$

b) Attack by hydroxyl radicals, which can occur at either end of the molecule. For example, for CH_3OOH, Vaghianni and Ravishankara [1990] showed that the following channels were competitive:

$$OH + ROOH \rightarrow H_2O + RO_2 \qquad (21)$$

$$OH + ROOH \rightarrow H_2O + R'CHOOH \qquad (22)$$

The first pathway simply regenerates the original peroxy radical, whereas attack on the reactive C atom in the organic part leads to the formation of an unstable hydroperoxyalkyl radical which decomposes very rapidly to form hydroxyl plus a carbonyl compound.

$$R'CHOOH \rightarrow R'CHO + OH \qquad (23)$$

c) The third removal path is by physical removal in rain, snow or dry deposition.

The homogeneous processes a) and b) are competitive in the sunlit boundary layer, but photolysis will dominate in the upper troposphere; heterogeneous physical removal is probably on average about an order of magnitude slower.

The net effect of the $RO_2 + HO_2$ reaction on atmospheric chemistry depends on the fate of the hydroperoxide product: photolysis leads to regeneration of OH and HO_2 radicals which then promote further oxidation:

$$OH + h\nu \rightarrow RO + OH \qquad (20)$$
$$O + O_2 \rightarrow R'CHO + HO_2 \qquad (24)$$
$$H + CO \ (+O_2) \rightarrow CO_2 + HO_2 \qquad (1)$$

In this case the effective role of the reaction of RO_2 with HO_2 is to reduce the concentration of odd hydrogen radicals by 'storage' as ROOH.

If the hydroperoxide is removed by hydroxyl radical attack on the -OOH group (e.g., by reaction 21), the overall effect with reaction 19 is:

$$O_2 + HO_2 \rightarrow ROOH + O_2 \qquad (19)$$
$$H + ROOH \rightarrow H_2O + RO_2 \qquad (21)$$
$$\overline{O_2 + OH \rightarrow H_2O + O_2}$$

Thus, the net effect is simply removal of odd-hydrogen radicals from the atmosphere, thereby slowing down all photochemically driven oxidation processes. Physical removal of ROOH will have a similar effect but with removal of carbon as well.

Finally, if ROOH is removed by reactions 22 and 23, the overall effect is the same as the occurrence of an alternative channel for reaction 18 to give a carbonyl product.

$$RO_2 + HO_2 \rightarrow ROOH + O_2 \qquad (19)$$
$$OH + ROOH \rightarrow H_2O + R'CHO + OH \qquad (22 \ \& \ 23$$
$$\overline{RO_2 + HO_2 \rightarrow R'CHO + H_2O + O_2}$$

Thus all the pathways following the $RO_2 + HO_2$ reaction tend to lead to a reduction on the rate of reactions initiated by ozone photolysis. A similar situation exists for the self-reactions of RO_2 radicals;

$$RO_2 + RO_2 \rightarrow \text{Products} \qquad (25)$$

The most important reaction in this category is the self reaction of HO_2 to form hydrogen peroxide:

$$HO_2 + HO_2 \rightarrow H_2O_2 + O_2 \qquad (11)$$

The kinetics of this reaction, its pressure, temperature and water vapour dependencies are now well established. As with the organic hydroperoxides, H_2O_2 can be removed from the atmosphere by photolysis, hydroxyl radical attack and by physical removal. In this case the removal in rain and cloud is relatively more important, and hydrogen peroxide plays an important role as an oxidising agent in the precipitation elements. Self reactions of organic peroxy radicals appear to be less important in the atmosphere, except under some circumstances.

The dominance of chemical production or loss processes for ozone in the background troposphere is expected to be highly sensitive to competition between HO_2 and RO_2 reaction with NO and with other species and hence to the local NO_x and peroxy radical abundance. This is illustrated in Figure 1 which shows the reactions involved in the oxidation of CH_4 to formaldehyde and CO. The competition between the two reactions of CH_3O_2 with NO and HO_2 determines whether CH_4 oxidation leads to O_3 production or loss. When reaction with NO is dominant, the net overall process is:

$$CH_4 + 4O_2 + h\nu \rightarrow HCHO + H_2O + 2O_3 \qquad (26)$$

When reaction with HO_2 is dominant and CH_3OOH is photolysed, the overall process leads to no net change in ozone.

$$CH_4 + O_2 + h\nu \rightarrow HCHO + H_2O \qquad (27)$$

If CH_3OOH reacts with OH or is physically removed, ozone loss will occur due to that lost in creating the radicals.

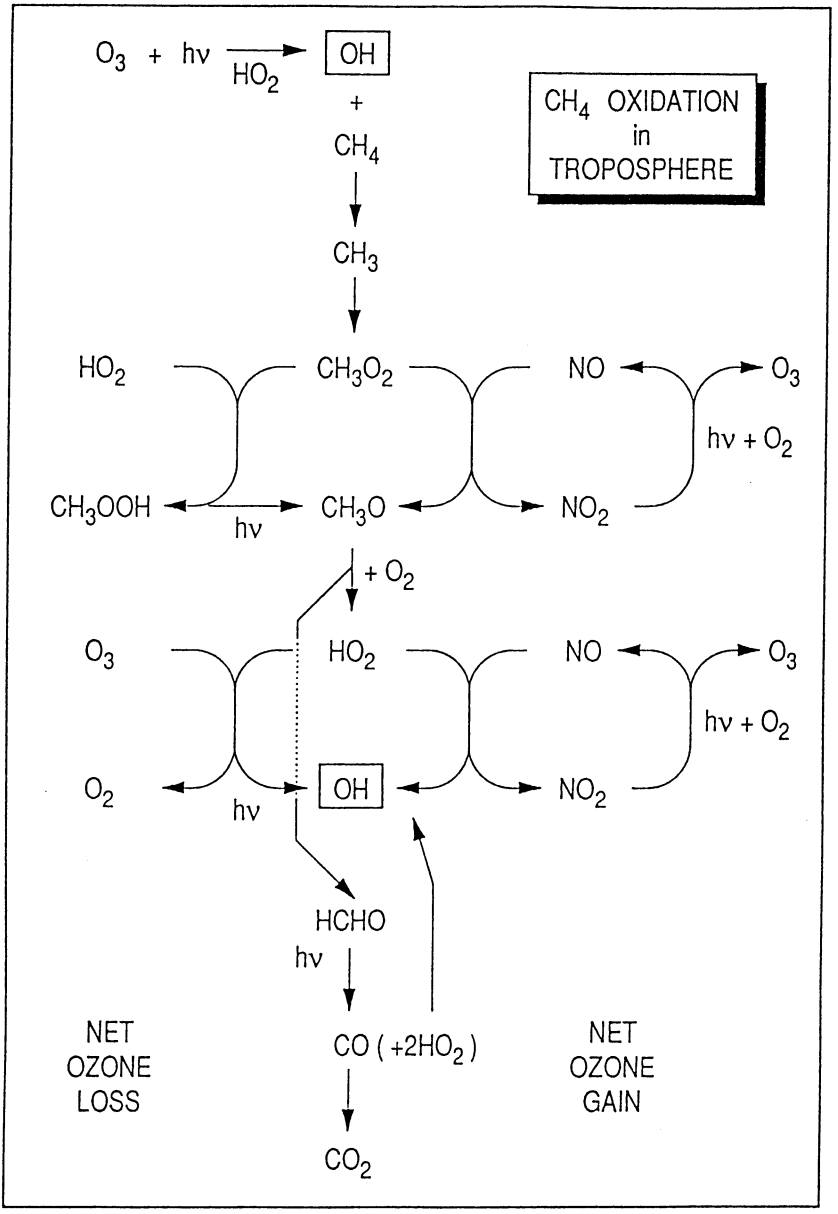

Fig. 1. Simplified mechanism NO_x for oxidation of methane in the troposphere.

The sensitivity of the chemistry increases further when the subsequent oxidation of HCHO is considered. Following the photolysis of formaldehyde in the absence of NO, up to 2 molecules of ozone are removed overall:

$$\begin{aligned} HCHO + h\nu &\rightarrow H + HCO && (28)\\ H + O_2 + M &\rightarrow HO_2 + M && (2)\\ HCO + O_2 &\rightarrow CO + HO_2 && (29)\\ 2HO_2 + 2O_3 &\rightarrow 4O_2 + 2OH && (8)\\ \hline HCHO + 2O_3 &\rightarrow H_2O + CO_2 + 2O_2 \end{aligned}$$

In the presence of NO, two molecules of ozone are produced since reaction 8 is replaced by 7:

$$\begin{aligned} HO_2 + NO &\rightarrow NO_2 + OH && (7)\\ \hline HCHO + 4O_2 &\rightarrow H_2O + CO + 2O_3 \end{aligned}$$

In these cycles it is the competition between HO_2 reaction with O_3 and NO which determines the balance between production and loss of ozone. The critical concentration of NO where the ozone removal mechanism starts to compete is determined by the magnitudes of the rate constants for the reactions 7 and 8, and the local steady state concentrations of HO_2, which is controlled by the rates of the principal radical production and loss processes, in particular the self reaction of HO_2, (reaction 11), and reaction with RO_2, (reaction 19). Estimates based on simple box model calculations show that the critical concentration of NO is approximately 10 ppt (3×10^8 molecule/cm^3 at 1 atm. pressure and 298 K) for predicted ambient HO_2 concentrations in the unpolluted troposphere. This corresponds to NO_x = 40 ppt. Such low daytime concentrations of NO are only achieved in very clean tropospheric air.

Chemistry in Clouds: Chameides and Davis [1981] and Lelieveld and Crutzen [1990] have discussed the mechanism of O_3-HO_x chemistry in clouds. Scavenging of HO_2 radicals by cloud droplets is extremely efficient at pH prevalent in cloud water. Dissolved HO_2 dissociates into H^+ and the superoxide ion, O_2^-

$$HO_2 \rightleftarrows H^+ + O_2^- \qquad (AQ.1)$$

The O_2 reacts rapidly with dissolved ozone

$$O_3 + O_2 + H_2O \rightarrow OH + 2O_2 + OH^- \qquad (AQ.2)$$

This provides an aqueous phase chemical recycling of NO_2 to the more reactive OH radical, which can react with dissolved HCHO (in the hydrated form: $CH_2(OH)_2$), H_2O_2, and $HCOO^-$) to give HO_2 again. This sequence leads to direct ozone loss in clouds.

In addition, the scavenging of HCHO as a result of the following reactions in solution:

$$HCHO + H_2O \rightarrow CH_2(OH)_2 \qquad (AQ.3)$$

$$CH_2(OH)_2 + O_2 \rightarrow HCOOH + 2HO_2 \qquad (AQ.5)$$

leads to lower gas-phase HCHO concentrations and less production of HO_x by gas-phase photolysis, (reaction 5). Moreover, the scavenging of HO_2 by clouds will reduce the gas-phase concentration of HO_2, whilst NO, which is only sparingly soluble in water, remains in the gas phase. Thus, 'separation' of NO from HO_2 leads to reduction in ozone production through the NO_2-NO-HO_x photochemical system, in the presence of clouds.

In cold environments (268 K for example), a larger fraction of the gases such as H_2O_2, CHO and HCOOH are dissolved and the aqueous phase generation and recycling of HO_2 from OH can be up 5 times larger than direct scavenging of HO_2 from the gas phase. At higher temperatures the recycling is less efficient (i.e., the chain length of reactions AQ.1 to AQ.5 is less), but O_3 destruction rate through reaction AQ.2 occurs at an appreciable rate for the entire residence time of air in clouds [Lelieveld and Crutzen, 1990]. Overall, therefore, clouds should provide net overall destruction of ozone in day-light, although there is little observational evidence to support this. Moreover, when the clouds are composed of ice, as is predominant in polar regions in most seasons, these reactions will be modified and may not occur at all.

DISCUSSION OF FACTORS INFLUENCING O_3-HO_x PHOTOCHEMISTRY IN POLAR REGIONS

The structure and physical behaviour of the troposphere in polar regions is conditioned by two major factors: the large seasonal variation in solar insolation and the predominantly ice covered surface. The main physical factors that affect atmospheric chemistry are:

1) Low air temperatures which prevail through most of the year.
2) Solar intensity is weak and subject to strong attenuation at short wave lengths due to long atmospheric path lengths.
3) Air is relatively dry due to low temperatures and restricted advection from low latitudes.

4) Stable boundary layer with restricted vertical mixing and venting of surface air.

We now consider the influence of these factors on the key processes involved in O_3-HO_x photochemistry.

In this analysis the recommended kinetic data from the most recent IUPAC evaluation [Atkinson et al., 1992] has been used. The photolysis rates are taken from the work of Hough [1988], who used a 2-stream (upward and downward) isotopic scattering model which included the effects of surface albedo, Raleigh and aerosol scattering and three layers of cloud. A simple box model for the marine boundary layer which is assumed to have a depth of 1 km., has been used for calculations to contrast the surface O_3 - HO_x chemistry in mid-latitude regions and in polar regions. The model contains simple O_x - HO_x - NO_x chemistry for the surface atmosphere, with modules for CH_4 oxidation and BrO_x chemistry to simulate HO_x and bromine mediated ozone depletion in the boundary layer. The model is set up so that O_3 is maintained in a steady state of 20 ppb by balance between downward transport and surface deposition, in the absence of chemical loss. Reactive species such as H_2O_2, and HNO_3 are deposited at the ground (vg = 1 cm/s), and all species are exchanged with the free troposphere with a time constant of 1 day.

Temperature effects on reaction rate: Most of the free radical reactions involved in atmospheric photochemistry have relatively small temperature coefficients. However, temperature effects are significant because, in general, the reactions leading to removal of free radicals have negative temperature coefficients whilst the propagation reactions, which enhance oxidation of trace gases and ozone production/loss, have positive temperature coefficients. Thus there will be a tendency for radical concentrations to decrease at low temperatures and a slowing down of the reactions leading to ozone production through NO_x mediated chain reactions. This effect is clear in the model calculations of local radical steady state concentrations shown in Figure 2.

The magnitude of the temperature effect on the rate coefficients is illustrated in Figure 3 which shows data for the important RO_2 + HO_2 termination reactions and for propagation reactions involving HO_2 and OH. The temperature dependencies are from the recommended Arrhenius expressions from the most recent IUPAC evaluation [Atkinson et al., 1992]. It will be seen that the RO_2 + HO_2 rate coefficient increases by about a factor of 2 as the temperature drops from 298 K to 238 K.

The OH + CH_4 reaction shows a very strong positive temperature dependence; other hydrocarbons which are more reactive show a lower activation energy and the relative importance of reaction of OH with non-methane hydrocarbons, especially alkenes (which have zero or negative temperature dependence), will increase in polar regions.

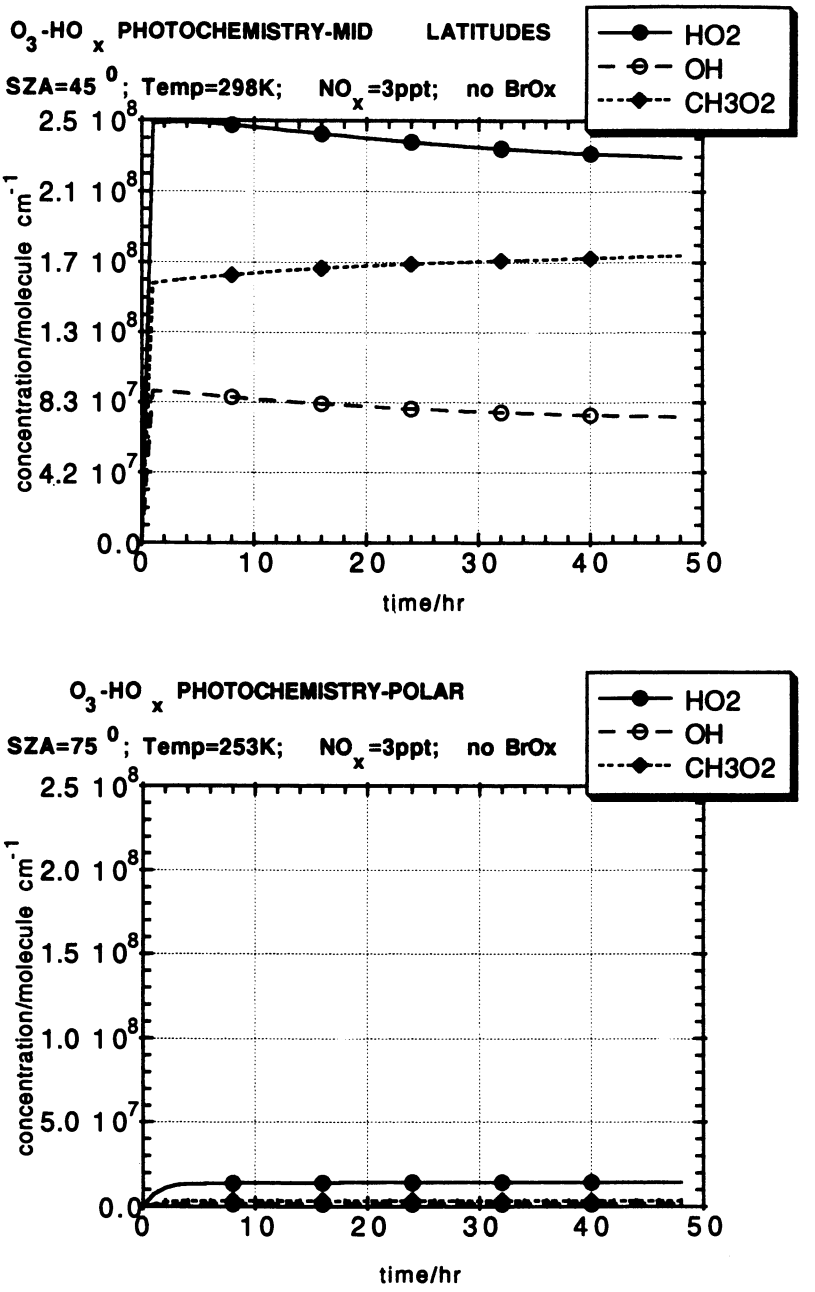

Fig. 2. Comparison of free radical concentrations in mid-latitude and polar troposphere; [OH] x100.

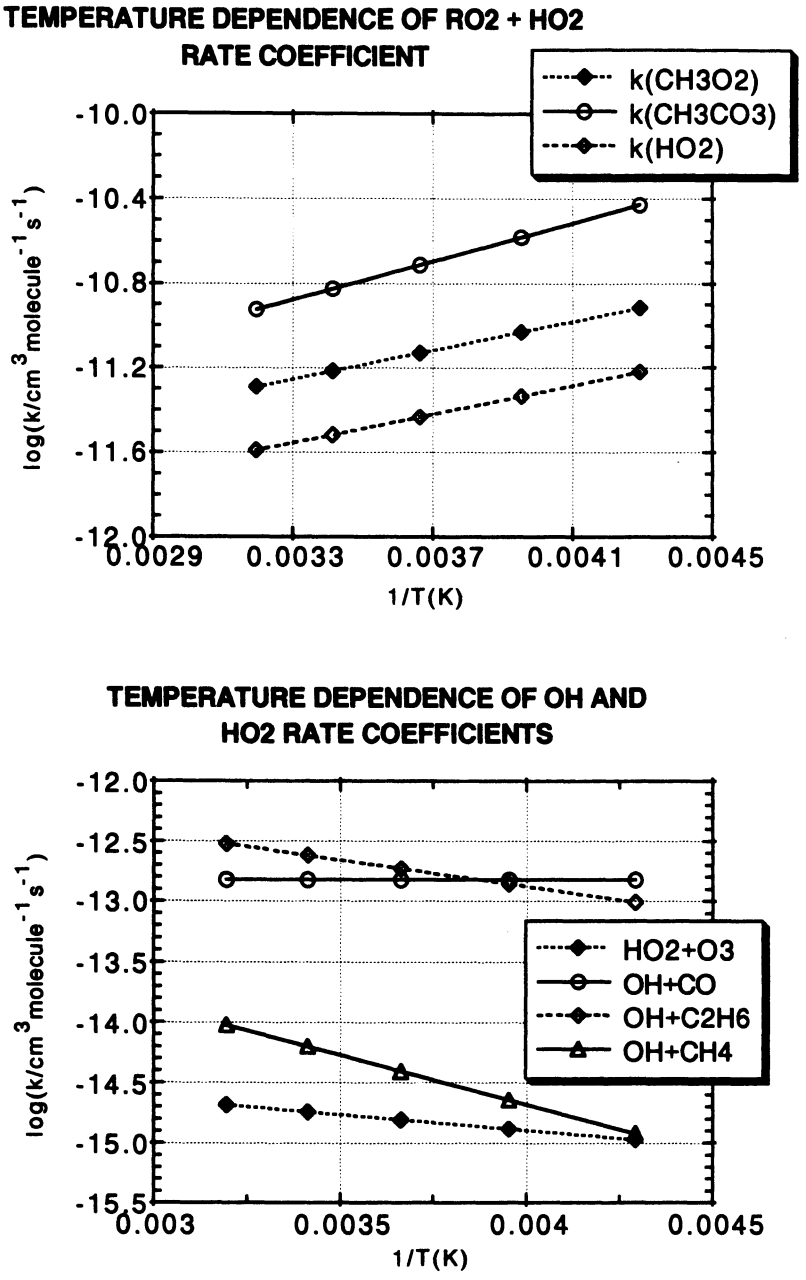

Fig. 3. Temperature dependence of rate coefficient for reactions involved in tropospheric HO_x Chemistry.

Latitude effects on Photolysis Rates: Figure 4 illustrates the effect of solar angle on the photolysis rates of selected photochemically active molecules. For molecules which absorb in the near UV at $\lambda > 350$ nm (e.g., NO_2, and HONO) the J-value falls by a factor of 10 between 0° and 80° SZA. For molecules absorbing at shorter wavelengths, which are attenuated more effectively at high SZA, the fall off is greater. In the case of O_3 photolysis to produce O (^1D), the fall-off is more than 3 orders of magnitude. In polar regions the effect is offset slightly by the effect of the abedo of the underlying ice surface, which increases the J-value by approximately factor of 2, with no large wavelength discrimination (see Figure 4).

Effect of Latitude on Photochemical Reactivity: Figures 5 and 6 show a comparison of the photochemistry occurring in the boundary layer at SZA of 45° and 75°, temperatures of 298 K and 253 K, and H_2O = 8 torr and 0.8 torr corresponding to mid-latitude and 'polar sunrise' conditions, respectively. The box model was run with initial NO_x concentrations of 3 ppt and 300 ppt, representing clean maritime and 'polluted remote' situations.

At mid-latitudes, there is significant O_3 loss accompanying the formation of peroxide products in the 'low NO_x' case but in the 'high NO_x' O_3 production occurs initially, until NO_x concentrations have declined due to conversion to HNO_3. HCHO formation is greatly enhanced at high NO_x due to the higher rate of CH_4 oxidation and conversion of the CH_3O_2 radical to HCHO, as opposed to CH_3OOH.

Under polar conditions there is no significant loss of ozone with either levels of NO_x, the small drop in O_3 being due to relaxation to the 20 ppb balance in [O_3], between input from aloft and deposition. The very low level of products formed reflect the low photochemical activity; HCHO is again enhanced relatively in the presence of NO_x.

A further experiment was performed under low NO_x, polar conditions, in which 20 ppt of BrO radical was introduced initially and the effect on O_3 examined. The results are shown in Figure 7. Initially, the BrO titrated all the NO_x to $BrONO_2$, and thereafter the BrO declined as it was converted to HOBr (by reaction with HO_2) and subsequently to absorbed bromine (BRADS) by absorption on particles (= 1 day). Ozone was significantly depleted in the early stages but recovered towards the 'no chemistry' steady state as BrO_x declined. Ozone loss is substantially greater if the exchange with the free troposphere is restricted.

CONCLUSIONS

These calculations show that the level of photochemical reaction in the simple O_3-HO_x photochemistry is almost exclusively controlled by the rate of production of HO_x radicals from the UV photolysis of ozone. Since J (O^1D) and H_2O mixing ratio are a strong

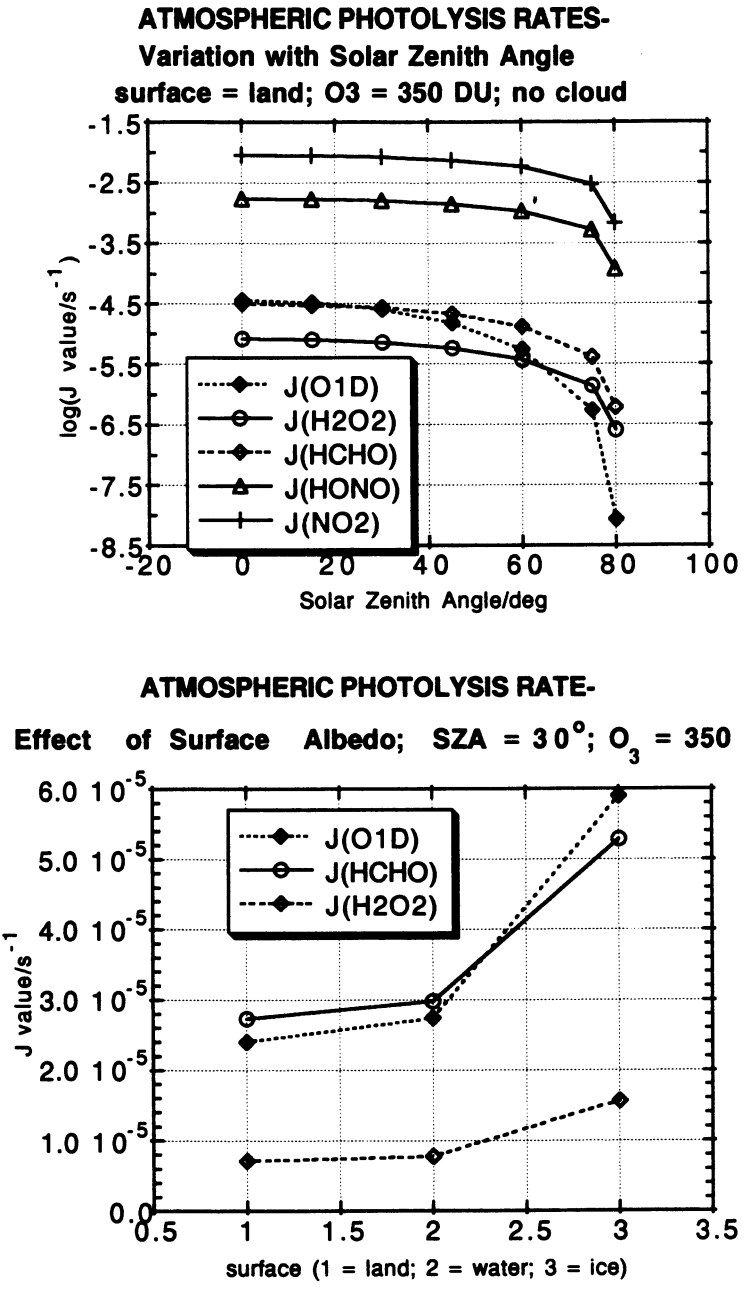

Fig. 4. Atmospheric photolysis rates calculated using a 2-stream isotropic scattering model for different solar zenith angles and surface albedos. All calculations with no clouds.

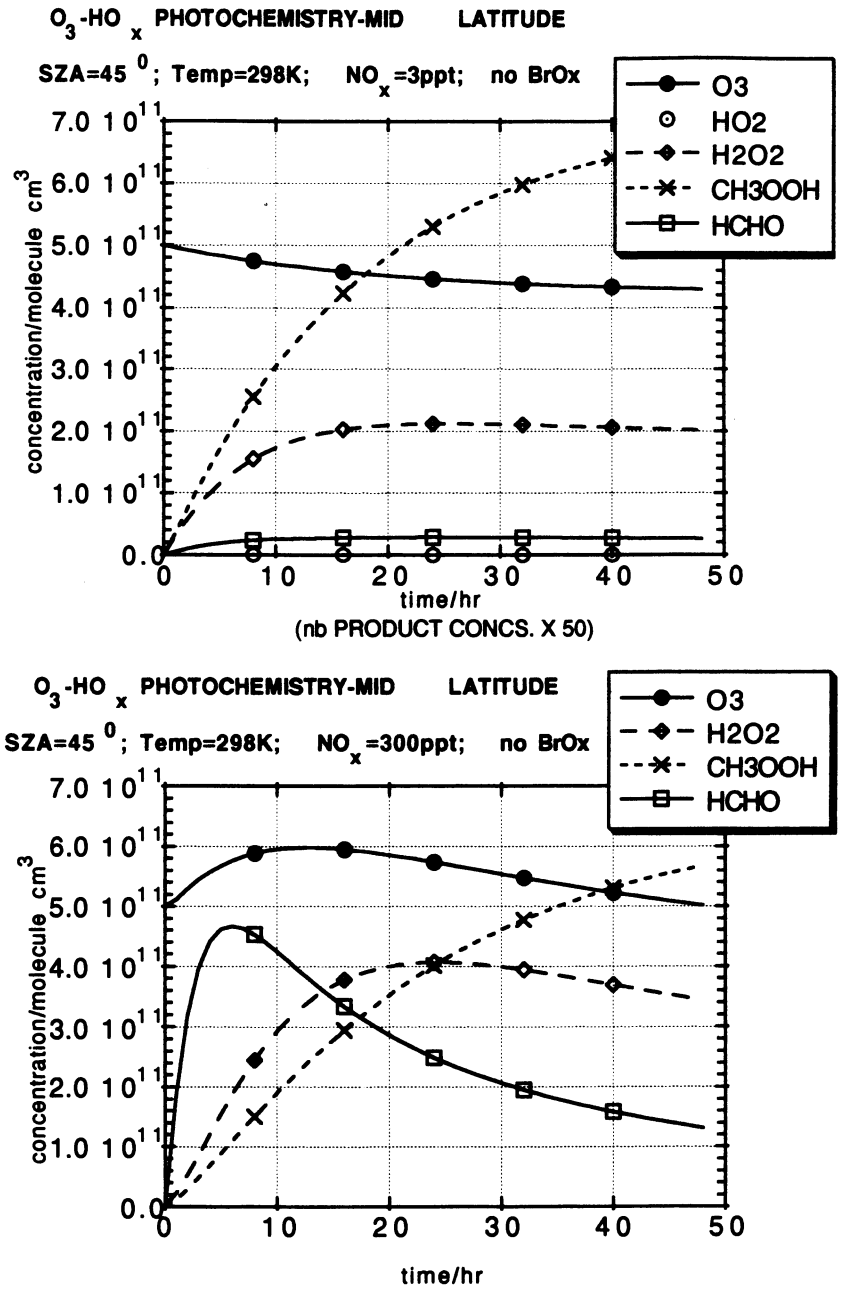

Fig. 5. Comparison of ozone and related HO_x species in mid latitude tropospheric with low and high NO_x.

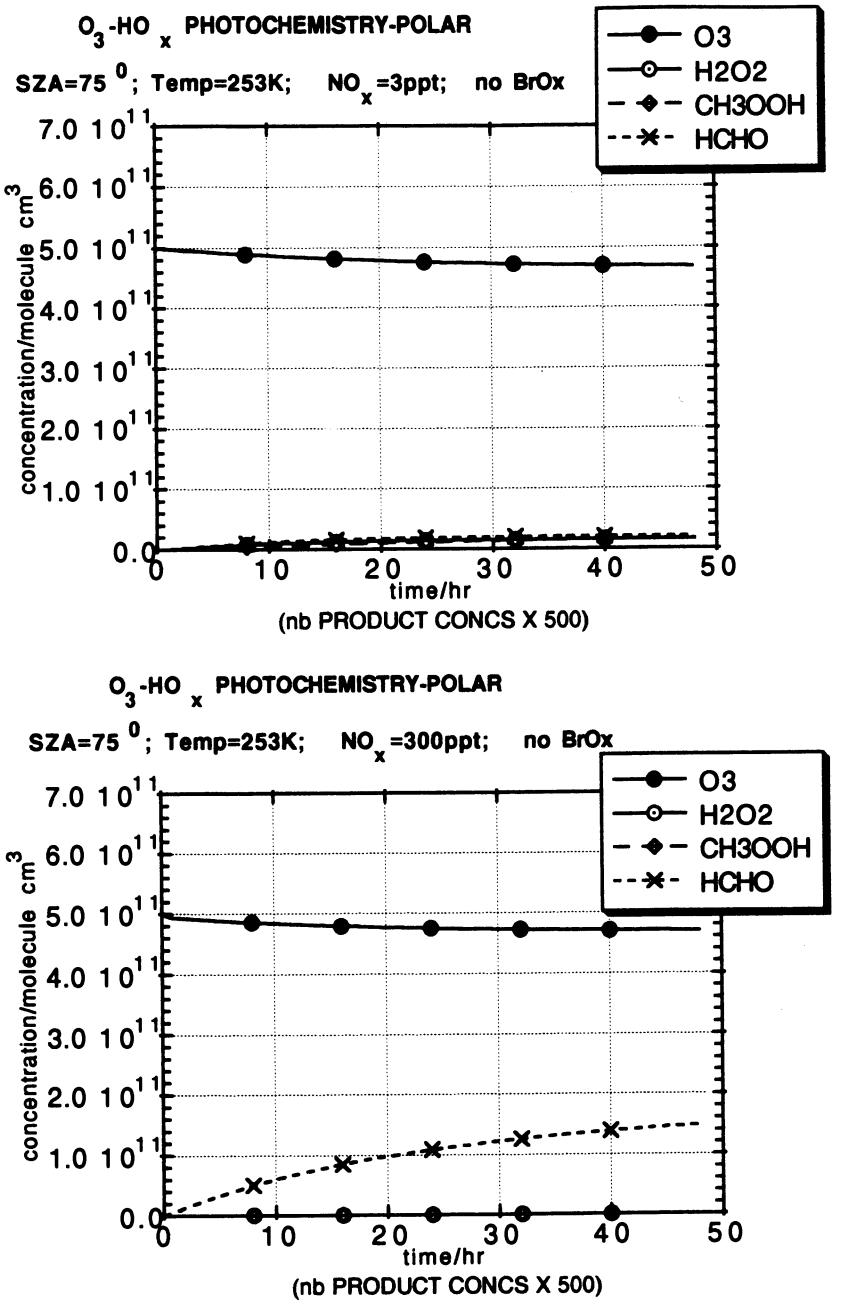

Fig. 6. Comparison of ozone and related HO_x species in polar troposphere with low and high NO_x.

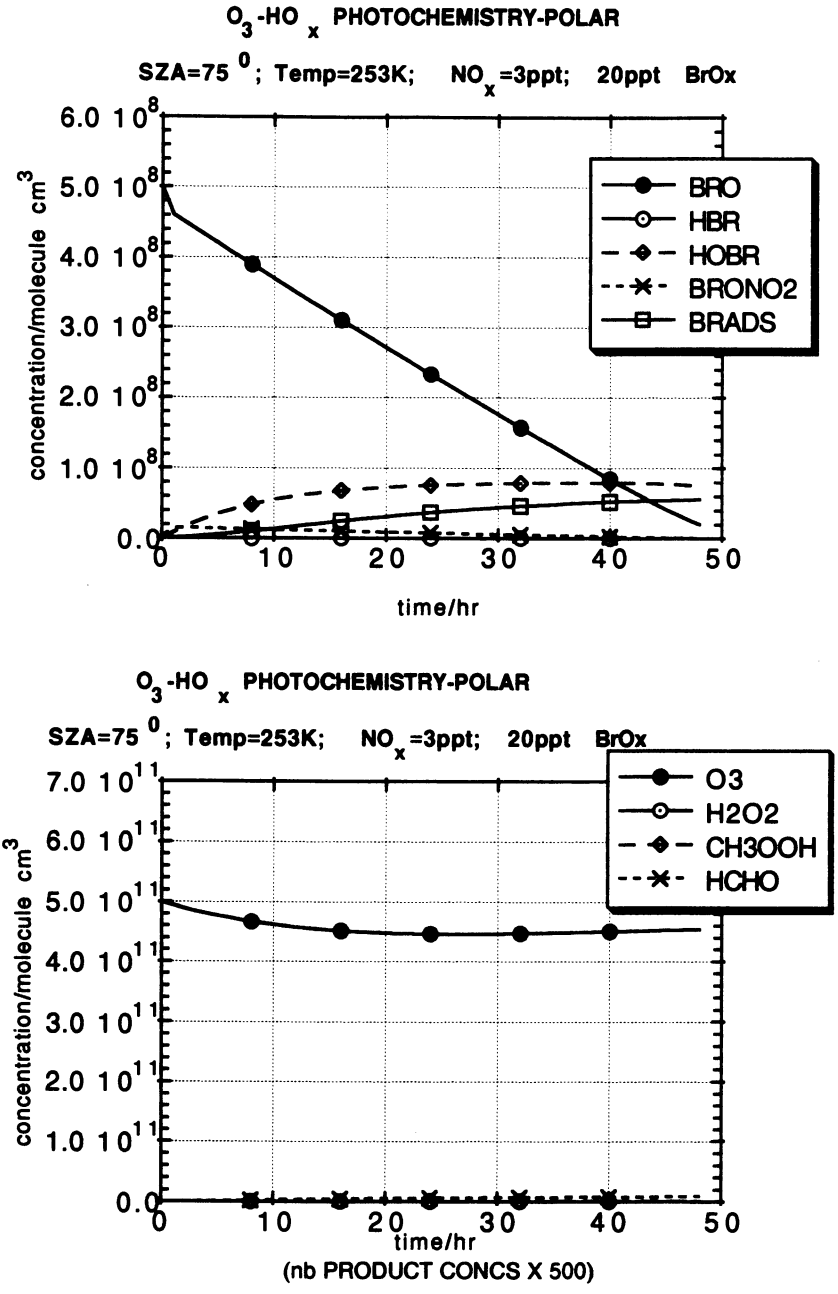

Fig. 7. Ozone and BrO_x species in the polar troposphere with low and high NO_x.

function of solar illumination and temperature respectively, HO_x radical production in polar regions is extremely weak. Thus, the main agent for trace gas oxidation and ozone production and loss mechanisms, the OH radical, is diminished in concentration, and other mechanisms must be involved to explain any observed local atmospheric reactivity in the Arctic and Antarctic boundary layer.

REFERENCES

Atkinson, R., Gas phase tropospheric chemistry of organic compounds - a review. *Atm. Environ., 24A* 1-42, 1990.

Atkinson, R., D. L., Baulch, R.A. Cox, R.F. Jr. Hampson, J.A. Kerr and J. Troe, Evaluated Kinetic and Photochemical Data for Atmospheric Chemistry: Supplement IV Summary Sheet, *Atm. Environ., 26A*, 1187-1230, 1992.

Chameides, W., and J.C.G. Walker, A photochemical theory of tropospheric ozone. *J. Geophys. Res., 78*, 8751-8760, 1973.

Cox, R.A., Atmospheric Chemistry of NO_x and hydrocarbons influencing tropospheric ozone in 'Tropospheric ozone; regional and global scale interactions', Isaksen I.S.A. (Ed) *NATO ASI Ser. C, Vol. 227*, D.R. Reidel , Dordrecht, 1988.

Crutzen, P.J., A discussion of the chemistry of some minor constituents in the stratosphere and troposphere. *Pure and Applied Geophys.*, 106-108, 1973.

Crutzen, P.J. and L.T. Gidel, A two-dimensional photochemical model of the atmosphere, 2. The tropospheric budgets of the anthropogenic chlorocarbons, CO, CH_4, CH_3Cl and the effect of various NO_x sources on tropospheric ozone. *J. Geophys. Res., 88*, 6641-6661, 1973.

Derwent, R.G. and M.E. Jenkin, Hydrocarbons and the long range transport of ozone and PAN across Europe. *Atm. Environ., 25A*, 1661-167, 1991.

Ehhalt, D.H., H.-P. Dorn and D. Poppe, The chemistry of the hydroxyl radical in the troposphere, Proc. Roy. Soc. Edinburgh, 97B, 17-34, 1991.

Hough, A., Development of a two-dimensional global tropospheric model: Model Chemistry. *J. Geophys. Res., 96 D4*, 7325-7362, 1991.

Isaksen, I.S.A., (Ed) Tropospheric ozone, regional and global scale interactions. *NATO ASI Ser. C. Vol. 227*, D.R. Reidel, Dordrecht, 1988.

Lelieveld, J. and P.J. Crutzen, Influences of cloud photochemical processes on tropospheric ozone, *Nature, 343*, 227-233, 1990.

Levy, H., II, Normal atmosphere: Large radical and formaldehyde concentrations predicted, *Science, 173*, 141-143, 1972.

Logan, J.A., M.J. Prather, S.C. Wofsy, M.B. McElroy, Tropospheric Chemistry: A global perspective. *J. Geophys. Res., 86* 7210-7254, 1981.

Platt, U., G. Le Bras, G. Poulet, J.P. Burrows, G.K. Moortgat, Peroxy radicals from night-time reaction of NO_3 with organic compounds, *Nature, 348*, 147-149, 1990.

Vaghjiani, G.L. and A.R. Ravishankara, Kinetics and Mechanism of OH reaction with CH_3OOH, *J. Phys. Chem., 93*, 1948- , 1989.

WMO, Scientific assessment of stratospheric ozone: 1989 Volume II, Appendix: AFEAS Report. World Meteorological Organisation Global Ozone Research and Monitoring Project - Report No. 20, 1989.

Volz-Thomas, A., D.H. Ehhalt and R.G. Derwent, Seasonal and latitudinal variation in ^{14}CO and the tropospheric concentration of hydroxyl radicals, *J. Geophys. Res., 86*, 5763-5171, 1981.

Derwent, R.G. and A. Voltz-Thomas., The tropospheric lifetime of halocarbons and their reaction with OH radicals; an assessment based on the concentration of ^{14}CO, in WMO, 1989 (See this ref. list).

Singh, H.B., Preliminary estimates of average tropospheric OH concentrations in the northern and southern hemispheres, *Geophys. Res. Letters, 4*, 453-456, 1977.

Prinn, R.G., D. Arnold, R.A. Rasmussen, P. Simmonds, F.N. Alyea, A.J. Crawford, P. Fraser, and R. Rosen, Atmospheric trends in methyl chloroform and the global average for the hydroxyl radical, *Science, 238*, 945-950, 1978.

ClO + ClO → PRODUCTS: A CASE STUDY IN HALOGEN MONOXIDE DISPROPORTIONATION AND RECOMBINATION REACTIONS

Stanley P. Sander, Scott L. Nickolaisen and Randall R. Friedl
Jet Propulsion Laboratory
California Institute of Technology
Pasadena, California 91109

INTRODUCTION

The phenomenon of ozone depletion in the springtime Arctic boundary layer is similar in several respects to the ozone hole in the Antarctic stratosphere. In both cases, heterogeneous chemistry on ice and acid-ice surfaces may be responsible for altering the partitioning of halogen-containing species between long-lived and photochemically labile forms. As a result of this repartitioning, the mixing ratios of ClO and BrO radicals become sufficiently high that self-reactions of these species can become the dominant rate-limiting steps in catalytic ozone destruction cycles. It is important, therefore, to understand the rates and mechanisms of these reactions under ambient atmospheric conditions.

Of the ten reactions of the type

$$XO + XO \rightarrow \text{products}$$
$$XO + YO \rightarrow \text{products}$$

where X, Y = F, Cl, Br, I, there are experimental data on five (FO + FO, ClO + ClO, ClO + BrO, BrO + BrO and IO + IO). For these reactions a picture is emerging which relates their potential energy surfaces to their pressure and temperature dependence behavior, branching ratios and other characteristics. In many ways, the ClO + ClO reaction is the best model to examine because of its complex behavior and extensive characterization in the literature. In this paper, we will discuss previous work on ClO + ClO and present the results of recent flash photolysis studies which illuminate the mechanism of this reaction.

PREVIOUS WORK ON THE ClO + ClO REACTION

Background: The reaction ClO + ClO → Products (1) has been studied extensively by direct and indirect methods for several decades. Early work on the photolysis of Cl_2-O_3 mixtures [Finkelnburg et al., 1932; Norrish and Neville, 1934] suggested the importance of the ClO +

NATO ASI Series, Vol. I 7
The Tropospheric Chemistry of Ozone in the Polar Regions
Edited by H. Niki and K. H. Becker

ClO reaction in propagating the chain destruction of O_3. The first direct studies of reaction (1) did not come about until the development of the flash photolysis technique and the subsequent identification of the ultraviolet absorption spectrum of ClO [Porter and Wright, 1953; Edgecombe et al., 1958]. Since these early studies, rate constants for reaction (1) have been measured using several kinetic techniques including flash photolysis-ultraviolet absorption [Basco and Dogra, 1971; Basco and Hunt, 1979; Sander et al., 1989; Trolier et al., 1990], discharge flow-ultraviolet absorption [Clyne and Coxon, 1966; Clyne and Coxon, 1968; Clyne and White, 1971], discharge flow-mass spectrometry [Clyne et al., 1975] and molecular modulation-ultraviolet absorption [Johnston et al., 1969; Cox et al., 1979; Cox and Derwent, 1979; Burrows and Cox, 1981; Hayman et al., 1986; Simon et al., 1990].

Potential Energy Surface and ClO Dimer Isomers: The essential features of this reaction may be summarized by reference to the potential energy diagram shown in Figure 1. While this diagram is not intended to be a complete representation of all possible reaction pathways and intermediates for the reaction, several important features have now been confirmed. The diagram shows that there are a number of important features of the potential energy surface that strongly influence the kinetics of the ClO + ClO reaction. These include: 1) the presence of one or more stable $(ClO)_2$ isomers that provide pathways for termolecular reactions and 2) the presence of a number of adiabatic and non-adiabatic product channels that provide pathways for bimolecular reactions. Many of these processes are experimentally well-established and will be discussed in more detail below.

Considerable progress has been recently made in the experimental and theoretical characterization of the $(ClO)_2$ isomers. The ClO + ClO reaction surface is characterized by a fairly deep potential well ($\approx$ 17 kcal mole^{-1}) corresponding to the most stable form of $(ClO)_2$ which has been determined to have the structure of chlorine peroxide, ClOOCl, by submillimeter spectroscopic studies [Birk et al., 1989]. Another isomer of $(ClO)_2$, chloryl chloride ($ClClO_2$) has recently been identified by matrix and gas-phase infrared and ultraviolet absorption spectroscopy [Muller and Willner, 1992a;b], but its thermal stability and barriers toward isomerization are not well established. Because of the extensive rearrangement required in the direct formation of chloryl chloride from the ClO self-reaction, the A-factor for this process is expected to be small. The isomer ClOClO has not yet been identified spectroscopically but would be expected to play a role in the reaction channel leading to Cl + OClO. Computational studies of the relative energies of the ClO dimer isomers have suggested that chloryl chloride lies between 0.9 and 7.7 kcal mole^{-1} in energy above chlorine peroxide [McGrath et al., 1990; Rendell and Lee, 1991; Stanton et al., 1991; Lee et al., private comm.].

Termolecular Component: The existence of one or more strongly bound $(ClO)_2$ intermediates is also suggested by kinetics studies which have examined the termolecular pathways of the ClO + ClO reaction. While $(ClO)_2$ has been a postulated intermediate in the self-reaction of ClO radicals since the first study of this reaction by a direct technique [Porter and Wright, 1953], Porter and co-workers did not observe a dependence of the observed bimolecular rate constant on the total pressure of inert gas, which would have provided strong support for this mechanism. This observation was first made by Johnston et al. [1969] using the new technique of molecular modulation with detection by infrared and ultraviolet absorption. The dependence on inert gas pressure at 298 K was subsequently observed by several other workers [Basco and Hunt, 1979; Cox et al., 1979]. The temperature dependence of the termolecular component was first studied by Hayman et al. [1986] between 268 and 328 K and subsequently between 195 and 250 K by Sander et al. [1989] and Trolier et al. [1990].

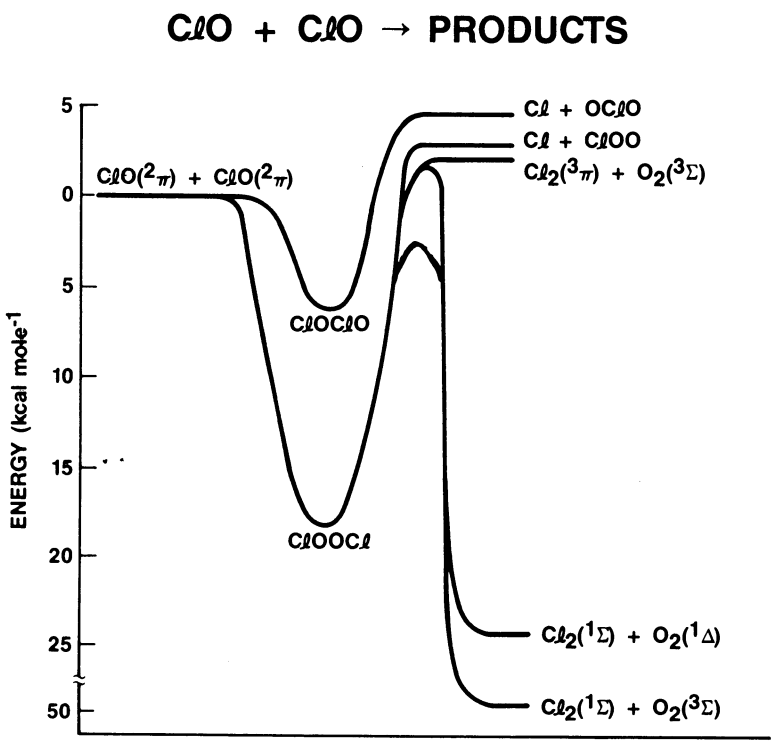

Fig. 1. Potential energy diagram for the ClO + ClO reaction. Neither the indicated potential barriers for the bimolecular product channels nor the zero-point energies of the isomers of $(ClO)_2$ are well known.

Bimolecular Components: In addition to the reaction pathways leading to formation of $(ClO)_2$ isomers, there are also a number of bimolecular channels:

$$ClO + ClO \rightarrow Cl_2 (^1\Sigma, ^3\Pi) + O_2 \quad (1a)$$
$$\rightarrow Cl + OClO \quad (1b)$$
$$\rightarrow Cl + ClOO \quad (1c)$$

Reactions (1b) and (1c) are endothermic by (3.1 $\pm$ 2.0) and (3.1 $\pm$ 1.0) kcal^{-1} mole^{-1} at 298 K, respectively. Reaction (1a) is endothermic by 2.4 kcal^{-1} mole^{-1} for production of Cl_2 in the $^3\Pi$ state and exothermic by 48.8 kcal^{-1} mole^{-1} for production of Cl_2 in the ground electronic state, however, the latter is a non-adiabatic channel and consequently may have a significant activation barrier [Toohey, 1988].

Past experimental studies of the overall rate constant for the bimolecular channels and the branching ratios have suffered from a number of complications including secondary reactions which regenerate ClO via channels 1b and 1c, and formation and decomposition of ClOOCl on the time scale of the experiment. In addition, most experimental systems have relied upon ultraviolet absorption for the detection and measurement of ClO, OClO, ClOO and Cl_2 in these experiments. Because the time dependence of [ClO] is governed by a second-order rate law, the absolute concentration of ClO radicals must be determined. Problems associated with the measurement of ClO cross sections, as well as the presence of interfering absorbers have therefore provided additional complications. As a result, the overall rate constant and branching ratios for the bimolecular channels remain poorly established.

The results of previous studies of the bimolecular channels of reaction (1) have been summarized by Simon et al. [1990]. Measured values for the overall rate constant, k_1 (298 K), range between 0.57 and 11.3 x 10^{-14} cm^3 molecule^{-1} s^{-1} with values of 1.2 and 1.0 x 10^{-14} cm^3 molecule^{-1} s^{-1} being recommended by the NASA and IUPAC data evaluation panels, respectively [DeMore et al., 1992; Atkinson et al., 1992]. The temperature dependence of reaction (1) was measured by Porter and Wright [1953] who found that k_1 was independent of temperature over the range 293-433 K, and Clyne and Coxon [1968] who obtained the expression, $k_1 = (5.8 \pm 1.7) \times 10^{-13} \exp(-1250/T)$ cm^3 molecule^{-1} s^{-1} over the temperature range 300-450 K.

Branching Ratio Measurements: Branching ratios for the bimolecular components of the ClO + ClO reactions come from two types of experiments: measurements of quantum yields in the chlorine-photosensitized decomposition of a source gas such as O_3, Cl_2O or OClO, and time-resolved experiments using flash photolysis, discharge-flow or molecular modulation which measure the concentrations of reactive intermediates such as ClO and

ClOO as well as stable products. The results of both types of experiments will be discussed below.

Early flash photolysis studies of reaction (1) [Porter and Wright; 1953; Edgecombe et al., 1957] concluded that reaction (1) had only one product channel which formed $Cl_2 + O_2$ via the decomposition of a stabilized Cl_2O_2 intermediate, i.e.,

$$ClO + ClO \rightleftarrows Cl_2O_2 \rightarrow Cl_2 + O_2$$

Radical channels were not considered. While Edgecombe et al. [1957] observed the formation of OClO in the photolysis of systems containing Cl_2O, this was ascribed to the reaction

$$ClO + Cl_2O \rightarrow OClO + Cl_2$$

rather than to a channel of the ClO + ClO reaction. Benson and Buss [1957] argued that in order to account for the long chain lengths observed in photolytic decompositions of Cl_2O and OClO, the self-reaction of ClO must involve a step which produced atomic chlorine and a new species, ClOO:

$$ClO + ClO \rightarrow Cl + ClOO$$

They also suggested that the termination of ClO in the flash photolysis experiments was due to the exothermic back-reaction of these species,

$$Cl + ClOO \rightarrow Cl_2 + O_2.$$

In their molecular modulation study, Johnston and co-workers confirmed the involvement of the ClOO radical in this mechanism and concluded that both the Porter et al. [1953] and Benson and Buss [1957] mechanisms were important. Clyne and Coxon [1968] observed emission from Cl_2 ($^3\Pi$)($v \leq 9$) in their discharge-flow experiments and assumed that the Cl + ClOO reaction was the source, although later work showing that ClOO is less stable than previously thought casts doubt on this interpretation. In similar discharge-flow experiments using mass spectroscopic detection at low pressure, Clyne, McKenney and Watson [1974] identified a reaction channel producing OClO, obtaining a branching ratio of about 0.05 at 298 K. Several groups have subsequently studied reaction (1) using molecular modulation and have measured branching ratios [1a:1b:1c] for all three channels including Cox and Derwent [1979] [0.50:016:0.34], Burrows and Cox [1981] [0.35:0.34:0.31], and Simon et al. [1990] [0.34:0.34:0.32]. Temperature dependences for the branching ratios have not yet been reported using a direct method.

Information on the bimolecular branching ratios has also been obtained from quantum yield studies. Both Lin et al. [1975] and Wongdontri-Stuper et al. [1979] measured quantum yields for O_3 destruction in the photolysis of Cl_2. At 298 K, both groups obtained quantum yields around 6 in the presence of N_2 buffer gas, implying that $k_{1c}/k_{1a} \approx 2$. From simultaneous measurements of O_3 and OClO, Wongdontri-Stuper et al. [1979] obtained branching ratios of 0.34,0.032 and 0.63 for reactions (1a), (1b) and (1c), respectively. These values are consistent with the results of Lin et al. [1975].

The quantum yield can be related to the rate constants for reactions (1a), (1b) and (1c) by the expression,

$$\phi = 2\,(1 + (k_{1c} + 0.5k_{1b})/(k_{1a} + 0.5k_{1b}))$$

The quantum yields inferred from the branching ratios measured in the time-resolved work of Cox and Derwent [1979], Burrows and Cox [1981] and Simon et al. [1990] vary between 3.4 and 3.9, and therefore disagree significantly with the values derived from the static studies.

Both Lin et al. [1975] and Wongdontri-Stuper et al. [1979] observed that the quantum yield decreased rapidly with temperature, reaching the limiting value of 2 at temperatures between -20 °C. and 0 °C. As discussed by Watson [1980], this dependence on temperature is too large to be explained by the temperature dependences of the elementary reaction channels. With recent improvements in the understanding of the stability of chlorine peroxide [Cox and Hayman, 1988], it now seems likely that the observed temperature dependence of the quantum yield is influenced by secondary reactions involving ClOOCl, i.e.,

$$\begin{aligned} ClO + ClO + M &\rightarrow ClOOCl + M \\ Cl + ClOOCl &\rightarrow Cl_2 + ClOO \\ ClOO + M &\rightarrow Cl + O_2 + M \\ \hline \text{Net:}\quad ClO + ClO &\rightarrow Cl_2 + O_2 \end{aligned}$$

This mechanism is equivalent to the ClOOCl-catalyzed termination of ClO, a process which effectively increases k_{1a} and therefore reduces the quantum yield at temperatures below 25 °C, where ClOOCl becomes increasingly stable.

In summary, previous work on the ClO + ClO reaction has established with reasonable certainty the pressure and temperature dependences of the termolecular rate constant with several inert gases under conditions important for atmospheric modelling. The bimolecular component remains poorly understood by comparison. At room temperature, the sum of the rate constants for the bimolecular channels lies in the range (1-2) x 10^{-14} cm^3 $molecule^{-1}$ s^{-1}, and information on the temperature dependence of the overall reaction has

been obtained only at low pressures. Significant disagreements exist between branching ratios inferred from time-resolved and static studies although both types of experiments have shown that the OClO channel is relatively minor. There are no published data on the temperature dependences of the branching ratios.

FLASH PHOTOLYSIS STUDIES OF THE MECHANISM OF THE ClO + ClO REACTION

In order to elucidate the mechanism of the ClO + ClO reaction, we have studied the reaction using the flash photolysis-ultraviolet absorption technique. The experimental apparatus has been described in detail previously [Watson et al., 1979; Sander et al., 1989]. ClO radicals were produced by flash photolysis of Cl_2-Cl_2O mixtures,

$$Cl_2 + h\nu \rightarrow 2\ Cl \qquad (\lambda > 300\ nm)$$
$$Cl + Cl_2O \rightarrow ClO + Cl_2$$

Time dependences of the concentrations of ClO, OClO, Cl_2 and Cl_2O were monitored by long-path absorption spectroscopy using both monochromator/photomultiplier and spectrograph/optical multichannel analyzer detectors over a 7.2 m path length. ClO and OClO concentrations were quantified using the differential absorption method to eliminate possible artifacts associated with variations in the concentrations of background absorbers (Cl_2O, Cl_2 and ClOOCl).

In order to simplify the measurement of the branching ratios for channels 1a, 1b and 1c, the reaction was studied under conditions in which contributions from selected reaction channels could be neglected. This was accomplished by carrying out some experiments in which Cl was the excess reagent and other experiments in which Cl_2O was the excess reagent. This approach is analogous to that used by Sander and Watson [1981] to study the branching ratios of the BrO + BrO reaction. The details of these experimental conditions and the results will be discussed below.

Excess Cl_2O: Using excess Cl_2O over Cl, chlorine atoms produced in reactions (1b) and (1c) were rapidly and stoichiometrically converted to ClO. The rate equation for ClO is then given by,

$$-d[ClO]/dt = (2k_f[M] + k_T)[ClO]^2 - k_r[M][ClOOCl]$$

where $k_T = k_{1a} + 0.5\ k_{1b}$ and k_f and k_r are the rate constants for the termolecular component of the ClO + ClO reaction,

$$ClO + ClO + M \rightleftarrows ClOOCl + M \qquad (k_f, k_r)$$

The rate equation for ClO under these conditions has no analytical solution. The approach is to monitor the observed ClO time dependence and to solve the kinetic mechanism iteratively to obtain values of k_T, k_f and k_r, which give the best least-squares fit to the data. For this procedure to accurately retrieve the three rate coefficients, the time scale for the ClOOCl equilibrium reactions (k_f, k_r) must be considerably shorter than the time scale for ClO termination (k_T). This is illustrated in Figure 2, which shows a plot of ClO optical density at 300 K and 350 torr of N_2. The decay is clearly divided into a regime at short reaction times where ClO rapidly establishes an equilibrium with ClOOCl, and a much slower decay at longer times which reflects the formation of Cl_2 and OClO. At pressures greater than about 200 torr of N_2 at 300 K, the time scales are sufficiently different to permit unambiguous determination of k_f, k_r and k_T. While the experiment which monitors ClO gives only the effective termination rate constant, $k_T = k_{1a} + 0.5\ k_{1b}$, the two termination rate constants can be determined separately by monitoring the time dependence of OClO. This is because the OClO yield is determined primarily by k_{1b} while the rate of OClO formation is determined by both k_{1a} and k_{1b}. It is important to note that because Cl_2O is in large excess over Cl, the reactions

$$Cl + ClOOCl \rightarrow ClOO + Cl$$
$$Cl + ClOO \rightarrow \text{products}$$
$$Cl + OClO \rightarrow 2ClO$$

cannot compete with the $Cl + Cl_2O$ reaction and may be neglected.

Excess Cl: If conditions are employed such that Cl is in excess over Cl_2O, then the reaction conditions assume a simple, analytic form. Under these conditions, the ClO + ClO reaction channel which produces ClOOCl is a termination reaction because the ClOOCl reacts rapidly with Cl to produce more atomic chlorine, the excess reagent. Reactions (1a) and (1c) are also termination channels. However, the channel producing OClO (reaction 1b) is not a termination reaction because the Cl + OClO reaction rapidly regenerates ClO. The decay of ClO is governed by second-order kinetics and the apparent rate constant is given by,

$$k_{obs} = (k_{1a} + k_{1c}) + k_f[M]$$

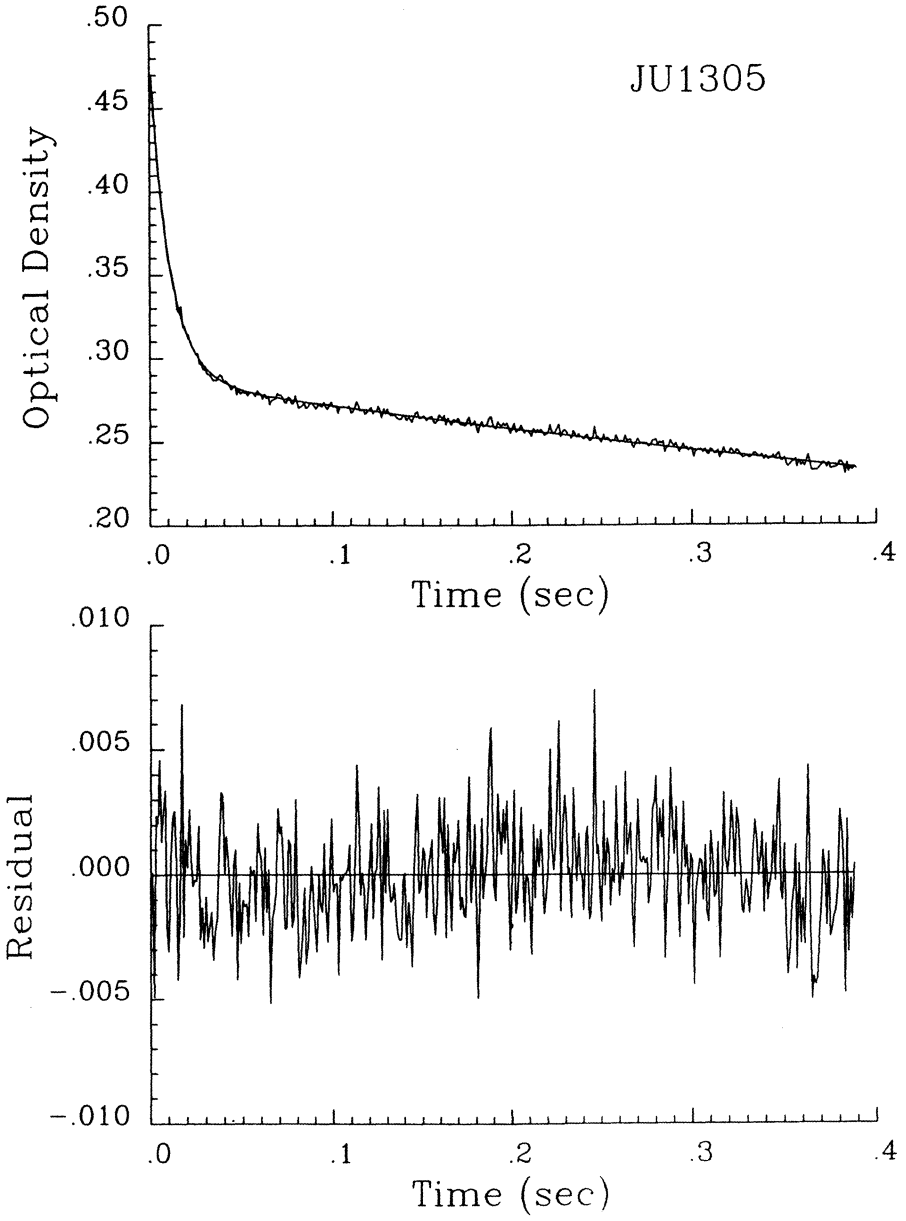

Fig. 2. Decay of ClO at 300 K in the photolysis of Cl_2O-Cl_2 mixtures. The initial rapid decay is due to the formation and equilibration of ClOOCl. The subsequent slower decay is due to the bimolecular termination reactions which form Cl_2 and OClO. The initial ClO concentration is about 1 x 10^{14} molecules cm^{-3}.

Plots of k_{obs} vs. [M] will, therefore, have slopes equal to k_f and intercepts equal to (k_{1a} + k_{1c}).

Results: Many kinetic runs were carried out using both excess Cl and excess Cl_2O stoichiometric conditions. From experiments carried out under both sets of conditions, the rate constants and branching ratios for the bimolecular components are given by,

$k_{1a} = (5.4 \pm 1.5) \times 10^{-15}$ cm^3 molecule^{-1} s^{-1} $\quad R_{1a} = 0.31$

$k_{1b} = (3.1 \pm 1.0) \times 10^{-15}$ cm^3 molecule^{-1} s^{-1} $\quad R_{1b} = 0.18$

$k_{1c} = (9.1 \pm 1.8) \times 10^{-15}$ cm^3 molecule^{-1} s^{-1} $\quad R_{1c} = 0.52$

at 298 K. The overall rate constant for the bimolecular components is, therefore, given by:

$$k_1 (298 \text{ K}) = (1.8 \pm 0.2) \times 10^{-15} \text{ cm}^3 \text{ molecule}^{-1} \text{ s}^{-1}$$

This lies in the range of recent previous determinations of k_1 (see above). For the excess Cl experiments, measurements were obtained over the temperature range 260-390 K with the results being given by

$$k_{1a} + k_{1c} = (6.2 \pm 1.0) \times 10^{-14} \exp(-(1780 \pm 150)/T) \text{ cm}^3 \text{ molecule}^{-1} \text{ s}^{-1}$$

These branching ratios correspond to a quantum yield of 5.1 $\pm$ 0.5 at 298 K, which is in reasonable agreement with the results of Wongdontri-Stuper et al. [1979] and Lin et al. [1975].

As indicated above, rate constants for the termolecular component can be determined using conditions of excess Cl. When combined with low-temperature data from Sander et al. [1989], the recombination rate constant in the limiting low pressure regime was determined to be:

$$k_f = (2.1 \pm 0.5) (T/300)^{-(2.9 \pm 0.5)} \text{ cm}^6 \text{ molecule}^{-2} \text{ s}^{-1}$$

for M = N_2 over the temperature range 195-400 K (Figure 3). Relative collision efficiencies for He, O_2, Ar, N_2, CF_4, SF_6 and Cl_2 were determined to be 0.55, 0.67, 0.85, 1.00, 1.36, 1.79 and 5.0, respectively. The very high apparent collision efficiency for Cl_2 is strongly suggestive of a chaperone mechanism involving a bound $ClO \cdot Cl_2$ complex. The rate constant for the unimolecular decomposition of ClOOCl, k_f, was also derived from the excess Cl experiments and found to be $(3.9 \pm 1.5) \times 10^{-18}$ cm^3 molecule^{-1} s^{-1} at 298 K in the limiting low pressure regime. The equilibrium constant determined from the ratio k_f / k_r at 298 K is 5.4×10^{-15} s^{-1}, which is very similar to the value determined by Cox and Hayman [1988] using molecular modulation.

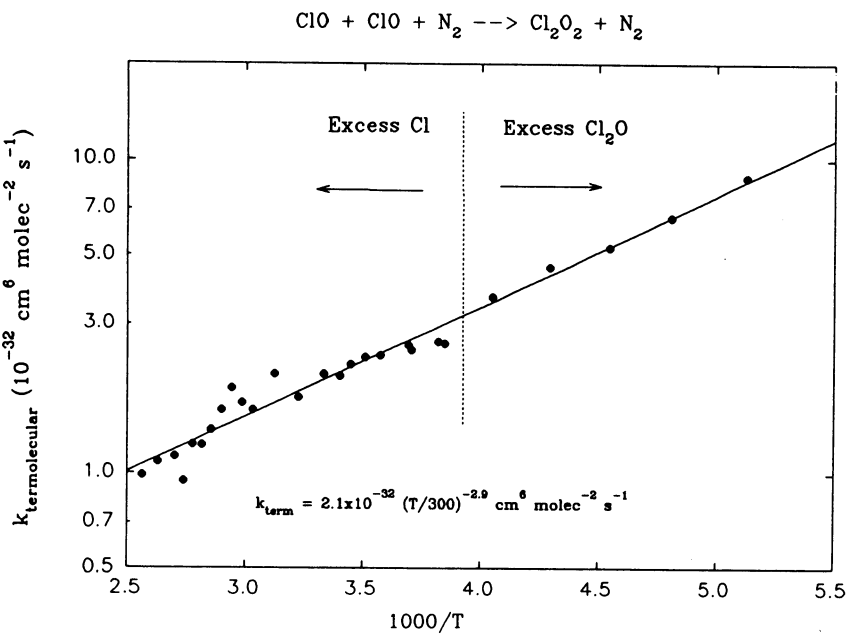

Fig. 3. Temperature dependence of the termolecular component of the ClO + ClO reaction.

CONCLUSION

The ClO + ClO reaction plays an important role both in stratospheric ozone chemistry, and as a model for radical-radical reactions that proceed via complex potential energy surfaces. Considerable progress has been made in characterizing the reaction surface, through kinetics studies of the bimolecular and termolecular components, and using theoretical and spectroscopic methods to characterize the ClO dimer isomers. Recent studies have raised several interesting questions which require further study, including the structure and stability of the $ClO \cdot Cl_2$ complex and its apparently large reactivity toward ClO, and the yield of $Cl_2(^3\Pi)$ from the bimolecular component. These and other issues will pose difficult experimental challenges in the future.

Acknowledgements: We acknowledge many stimulating discussions with W. B. DeMore. The research described in this work was performed at the Jet Propulsion Laboratory, California Institute of Technology, under contract with the National Aeronautics and Space Administration.

REFERENCES

Atkinson, R., D. L. Baulch, R. A. Cox, R. F. Hampson, Jr., J. A. Kerr and J. Troe, Evaluated kinetic and photochemical data for atmospheric chemistry: supplement IV, *Atmos. Environ., 26A,* 1187-1230, 1992.

Basco, N. and S. K. Dogra, Reactions of halogen oxides studied by flash photolysis. I. The flash photolysis of chlorine dioxide, *Proc. Roy. Soc. Lond. A., 323,* 29-68, 1971.

Basco, N. and J. E. Hunt, Mutual Combination of ClO radicals, *Int. J. Chem. Kinet., 11,* 649-664, 1979.

Benson, S. W. and J. H. Buss, *J. Chem. Phys., 27,* 1382, 1957.

Birk, M., R. R. Friedl, E. A. Cohen, H. M. Pickett, and S. P. Sander, The rotational spectrum and structure of chlorine peroxide", *J. Chem. Phys., 91,* 6588, 1989.

Burrows, J. P. and R. A. Cox, Kinetics of chlorine oxide radical reactions using modulated photolysis. Part 4. The reactions Cl + Cl_2O → Cl_2 + ClO and ClO + HO_2 → products studied at 1 atm and 300 K, *J. Chem. Soc., Faraday Trans. 1,* 2465-2479, 1981.

Clyne, M. A. A. and J. A. Coxon, Reactions of chlorine oxide radicals. Part 1. Reaction kinetics of the ClO radical, *Trans. Faraday Soc., 62,* 1175-1189, 1966.

Clyne, M. A. A. and J. A. Coxon, Kinetic studies of oxy-halogen radical systems, *Proc. Roy. Soc. A, 303,* 207-231, 1968.

Clyne, M. A. A., D. J. McKenney and R. T. Watson, Reactions of chlorine oxide radicals. Part 5. The reaction 2 ClO($X^2\Pi$) → products, *J. Chem. Soc., Faraday Trans. I, 71,*322-335, 1975.

Clyne, M. A. A. and I. F. White, Reactions of chlorine oxide radicals. Part 3. Kinetics of the decay reaction of the ClO($X^2\Pi$) radical, *Trans. Faraday Soc., 67,* 2068-2076, 1971.

Cox, R. A., R. G. Derwent, A. E. Eggleton and H. J. Reid, Kinetics of chlorine oxide radicals using modulated photolysis. Part 2. ClO and ClOO radical kinetics in the photolysis of Cl_2 + O_2 + N_2 mixtures, *J. Chem. Soc. Faraday Trans. I, 75,* 1648-1666, 1979.

Cox, R. A. and R. G. Derwent, Kinetics of chlorine oxide radical reactions using modulated photolysis. Part 1. Disproportionation of ClO in the Cl_2 photosensitized decomposition of ozone, *J. Chem. Soc. Faraday Trans. I, 75,* 1635-1647, 1979.

Cox, R. A., R. G. Derwent, A. E. J. Eggleton and H. J. Reid, Kinetics of chlorine oxide radicals using modulated photolysis. Part 2. ClO and ClOO radical kinetics in the photolysis of Cl_2 + O_2 + N_2 mixtures, *J. Chem. Soc. Faraday Trans. I., 75,* 1648-1666, 1979.

Cox, R. A. and G. D. Hayman, The stability and photochemistry of dimers of the ClO radical and implications for Antarctic ozone depletion, *Nature, 332,* 796-800, 1988.

DeMore, W. B., S. P. Sander, D. M. Golden, R. F. Hampson, M. J. Kurylo, C. J. Howard, A. R. Ravishankara, C. E. Kolb and M. J. Molina, Chemical kinetics and photochemical data for use in stratospheric modeling, evaluation number 10, JPL Publication 92-20, NASA, Pasadena, California, 1992.

Edgecombe, F. H. C., R. G. W. Norrish and B. A. Thrush, The flash photolysis of chlorine monoxide, *Proc. Roy. Soc. A, 243,* 24-32, 1957.

Finkelnburg, W.,H. J. Schumacher and G. Steiger, Das spektrum und der photochemische zerfall des chlormonoxyds, *Z. phys. Chem. B 15,* 127-156, 1932.

Hayman, G. D., J. M. Davies and R. A. Cox, Kinetics of the reaction ClO + ClO → products and its potential relevance to antarctic ozone, *Geophys. Res. Lett., 13,* 1347-1350, 1986.

Johnston, H. S., E. D. Morris, Jr., and J. Van den Bogaerde, Molecular modulation kinetic spectrometry. ClOO and ClO radicals in the photolysis of chlorine in oxygen, *J. Am. Chem. Soc., 91,* 7712-7727, 1969.

Lee, T. J., C. M. Rohlfing and J. E. Rice, An extensive ab initio study of the structures, vibrational spectra, quadratic force fields and relative energetics of three isomers of Cl_2O_2, submitted to the Journal of Chemical Physics.

Lin, C. L., S. Jaffe and W. B. DeMore, Photochemistry of chlorine-ozone mixtures, paper presented at the American Chemical 169th national meeting, Philadelphia, April, 1975.

McGrath, M. P., K. C. Clemitshaw, F. S. Rowland and W. J. Hehre, Structures, relative stabilities, and vibrational spectra of isomers of Cl_2O_2: the role of the chlorine oxide dimer in Antarctic ozone depleting mechanisms, *J. Phys. Chem., 94,* 6126-6132, 1990.

Muller, H. S. P. and H. Willner, Gas phase studies on chloryl chloride, $ClClO_2$, *Ber. Bunsenges. Phys. Chem., 96,* 427-431, 1992a.

Muller, H. S. P. and H. Willner, Synthesis and properties of chloryl chloride, $ClClO_2$, *Inorg. Chem., 31,* 2527-2534, 1992b.

Norrish, R. G. W. and G. H. J. Neville, The decomposition of ozone photosensitized by chlorine, *J. Chem. Soc., 1864-1872,* 1934.

Porter, G. and F. J. Wright, Studies of free radical reactivity by the methods of flash photolysis: The photochemical reaction between chlorine and oxygen, *Discuss. Faraday Soc., 14,* 23-34, 1953.

Rendell, A. P. and T. J. Lee, An efficient formulation and implementation of the analytic energy gradient method to the single and double excitation coupled-cluster wave function: Application to Cl_2O_2, *J. Chem. Phys, 94,*6219-6228, 1991.

Sander, S. P., R. R. Friedl and Y. L. Yung, Rate of formation of the ClO dimer in the polar stratosphere: Implications for ozone loss, *Science, 245,* 1095-1098, 1989.

Sander, S. P. and R. T. Watson, Kinetics and mechanism of the disproportionation of BrO radicals, *J. Phys. Chem., 85,* 4000, 1981.

Simon, F. G., W. Schneider, G. K. Moortgat and J. P. Burrows, A study of the ClO absorption cross-section between 240 and 310 nm and the kinetics of the self-reaction at 300 K, *J. Photochem. Photobiol. A: Chem., 55,* 1-23, 1990.

Stanton, J. F., C. M. L. Rittby, R. J. Bartlett and D. W. Toohey, Low-lying isomers of the chlorine oxide dimer: a theoretical study, *J. Phys. Chem., 95,* 2107-2110, 1991.

Toohey, D., Kinetic and mechanistic studies of reactions of bromine and chlorine species important in the Earth's stratosphere, Ph.D. thesis.

Trolier, M., Mauldin III, R. L. and A. R. Ravishankara, Rate coefficient for the termolecular channel of the self-reaction of ClO, *J. Phys. Chem., 94,* 4896-4907, 1990.

Watson, R. T., Laboratory studies of halogen compounds of atmospheric interest, in *Proceedings of the NATO Advanced Study Institute on Atmospheric Ozone: Its Variation and Human Influences,* A. Aiken, ed., Federal Aviation Administration Report FAA-EE-80-20, 429-466, 1980.

Watson, R. T., S. P. Sander, S. P. and Y. L. Yung, A pressure and temperature dependence kinetics study of the NO + BrO → NO2 + Br reaction: Implications for stratospheric bromine photochemistry", *J. Phys. Chem., 83,* 2936, 1979.

Wongdontri-Stuper, W., R. K. M. Jayanty, R. Simonaitis and J. Heicklen, The Cl_2 photosensitized decomposition of O_3: the reactions of ClO and OClO with O_3, *J. Photochem., 10,*163-186, 1979.

THERMAL STABILITY OF PEROXYNITRATES

K.H. Becker, F. Kirchner and F. Zabel
Bergische Universität - GH Wuppertal
Gaußstraße 20
5600 Wuppertal 1
FRG

INTRODUCTION

PAN [$CH_3C(O)O_2NO_2$] has been measured ubiquitously in the troposphere, and in the stratosphere HO_2NO_2 has also been analysed. The thermal lives of both compounds as a function of pressure and temperature have been established reasonably well by laboratory studies, in particular for PAN. Other peroxynitrates including the halogenated derivatives are less important as NO_x carriers or temporary RO_2 reservoirs in the atmosphere at least at ambient temperature. Other loss processes of peroxynitrates, besides thermal decomposition, are the reaction with OH radicals and photolysis. A few experimental results also seem to support heterogeneous decomposition of RO_2NO_2 on surfaces. The relative importance of thermal decomposition rate, photolysis rate and rate of the OH reaction depends on temperature, pressure, spectral distribution of solar light intensity and the OH concentration. In principle, lower temperature and lower pressure at higher altitudes increase the importance of photolysis and OH reactions as sinks of RO_2NO_2, because thermal decomposition rates become much slower. The RO_2NO_2 are produced by the addition of NO_2 to RO_2 radicals. The RO_2-NO_2 bond energy is relatively weak and lies in the range of 85 - 120 kJ/mol according to recent measurements. Because these bond energies determine the thermal life-times, it can be estimated that at 1 bar total pressure and room temperature, the lifetime ranges from 10^{-1} to 10^4 s. In the present work, the thermal lifetimes of a variety of RO_2NO_2 species were studied as a function of temperature and pressure. The observed pressure dependencies of the thermal decomposition rates were fitted by calculations based on the Troe-treatment of unimolecular reactions. The data obtained within the present work allow predictions about the thermal decomposition rates of RO_2NO_2 species not yet studied.

EXPERIMENTAL

The experiments were performed in a 420 l photoreactor thermostatable between -30 and +50 °C. Generally, the peroxynitrates RO_2NO_2 were produced by photolytically generating the radicals R from appropriate precursor compounds in the presence of O_2 and NO_2. In most cases, R radicals were formed from RH via H abstraction by Cl atoms. HO_2NO_2 was prepared in a dark reaction by exposing liquid H_2O_2/water mixtures to

NATO ASI Series, Vol. I 7
The Tropospheric Chemistry of Ozone in the Polar Regions
Edited by H. Niki and K. H. Becker

gaseous NO_2 and vaporizing HO_2NO_2 from the resulting mixture into the reaction chamber [Barnes et al., 1982]. At the appropriate temperatures, the equilibrium

$$RO_2 + NO_2 (+M) \rightleftarrows RO_2NO_2 (+M) \qquad (2,-2)$$

is established. Upon addition of NO this equilibrium is disturbed by scavenging the RO_2 radicals according to:

$$\begin{aligned} RO_2 + NO &\rightarrow RO + NO_2 \qquad (1) \\ &\rightarrow RONO_2 \end{aligned}$$

In a large excess of NO, reaction (2) cannot compete with reaction (1) and, after correction for wall loss, the first order decay rate constant of RO_2NO_2 is equal to k_{-2}.

k_{-2} was experimentally determined as a function of temperature and pressure for a variety of different RO_2NO_2. The concentrations of RO_2NO_2, NO_2 and NO were measured by long-path IR absorption (typically 50.4 m) using a built-in White mirror system and a Fourier-transform spectrometer. Several interferograms were averaged to improve the signal-to-noise ratio. Total reaction times were between 2 and 20 min.

RESULTS

The temperature dependence of k_{-2} as obtained in the present work at total pressures close to 1 bar in N_2 is shown in figure 1. The corresponding Arrhenius parameters are summarized in table 1. The results in parenthesis have to be considered as preliminary, and others marked by < > had to be estimated by comparison with analogous compounds where E_a and A values have been measured. For the measured activation energies the error limits given denote precision only and are 2 σ. In those cases where an A value had to be assumed, the stated error limits of the activation energies correspond to the large uncertainty of the preexponential factor. Results for different R are presented in the order of their rate constant at 298 K, as calculated from the Arrhenius parameters. This order is essentially the same as for the RO_2-NO_2 bond energies (see discussion section) except for R = H, CH_3 and $ClCH_2$ where k_{-2} is subject to considerable fall-off at atmospheric pressure.

Typically, the pressure dependence of k_{-2} was derived from measurements at several total pressures between 10 and 1000 mbar for a selected temperature. The fall-off was analyzed according to the method of Troe [1979], by which unimolecular rate constants can be calculated from an analytical expression and the parameters A_0, A_∞, $E_{a,0}$, $E_{a,\infty}$ and Fc. The parameter values determined in this work for the thermal decomposition of a variety of peroxynitrates are collected in table 2. They allow to calculate k_{-2} for all temperatures and pressures which are relevant for the atmosphere.

The pressure dependence of k_{-2} is most easily demonstrated in terms of the reverse reaction which has the identical fall-off but only a slight temperature dependence. In those

cases where k_2 has been measured by other research groups, the equilibrium constants $K_{eq}(T) = k_{-2}/k_2$ were derived using second law and third law methods. The pressure dependence of k_2 as calculated from these equilibrium constants and the k_{-2} data from the present work are shown in figure 2. The high and low pressure limiting rate constants, k_∞ and k_0, are included in figure 2, so that the degree of fall-off can be easily estimated at a given gas density [M].

DISCUSSION

In table 3 the present data on k_{-2} are compared with literature values where available. The agreement is generally good, in particular for the thermal decomposition of PAN. The data in tables 1 and 2 and figures 1 and 2 show the following:

1. At atmospheric pressure and 298 K, there are three groups of peroxynitrates with respect to their thermal lifetimes (τ): (a) RO_2NO_2 with R = R'CH_2 and R' = H or organic group where τ is in the order of 0.3 s; (b) RO_2NO_2 with R = H, R'O or halogenated methyl where τ is in the order of 10 s; (c) RO_2NO_2 with R = R" C(O) where τ is in the order of 2000 s.
2. Although the high pressure preexponential factors, A_∞, of k_{-2} seem to increase with increasing activation energy, the differences in thermal lifetimes are mainly due to different activation energies (i.e., bond energies).
3. Except for HO_2NO_2 and $CH_3O_2NO_2$, the pressure effects on k_{-2} are of minor importance for tropospheric conditions, the average fall-off changing by a factor of 2 to 3 between the ground and the tropopause.

Tables 1 and 2 suggest the following rules which allow an estimation of the thermal lifetimes of peroxynitrates when no experimental data are available:

1. Increasing electron drawing effects of the R group leads to increasing thermal lifetimes of RO_2NO_2;
2. A carbonyl group next to the peroxy group such as in all PAN-type peroxynitrates [R"$C(O)O_2NO_2$] results in a strong increase in the thermal lifetime by several orders of magnitude, with the k_{-2} values lying within a range of a factor 10 depending on the nature of R".
3. In peroxynitrates of the type R'$CH_2O_2NO_2$, the CH_2 group strongly reduces the effect of R' on the thermal lifetime of RO_2NO_2 [e.g., $CFCl_2CH_2O_2NO_2$ and $CH_3C(O)CH_2O_2NO_2$ as compared to $CFCl_2O_2NO_2$ and $CH_3C(O)O_2NO_2$].
   According to these rules, the thermal lifetime of $CH_3C(CH_2)C(O)O_2NO_2$ which can be formed in the atmospheric degradation of isoprene, is expected to be close to that of $C_6H_5C(O)O_2NO_2$. The decomposition rate constant of the former ($k_{298} = 3.5 \times 10^{-4}$

s^{-1}) has recently been measureed by Roberts and Bertman [1992]. Within error limits, this value in fact agrees with the corresponding rate constant for $C_6H_5C(O)O_2NO_2$ ($3.1x10^{-4}$ s^{-1}, see table 1).

Combining the rate data from the present work with literature data, a box model was used to calculate the abundance of RO_2NO_2 and other related species in the tropopause at 220 K and 50 mbar. These calculations indicate that $CH_3C(O)O_2NO_2$ is the most abundant peroxynitrate followed by $CH_3O_2NO_2$ and HO_2NO_2. Longer chain alkylperoxynitrates are unimportant due to their short thermal lifetimes. No calculations were carried out with respect to halogenated species.

At lower latitudes, thermal decomposition will be the most efficient loss process of PAN and PAN-type peroxynitrates. In polar regions, however, thermal lifetimes are longer by several orders of magnitude, and PAN can accumulate to higher stationary mixing ratios.

REFERENCES

Barnes, I., V. Bastian, K.H. Becker, E.H. Fink and F. Zabel, Reactivity studies of organic substances towards hydroxyl radicals under atmospheric conditions, *Atmos. Environ., 16*, 545-550, 1982.

Barnes, I., K.H. Becker, E.H. Fink, A. Reimer, F. Zabel, and H. Niki, FTIR Spectroscopic study of the gas phase reaction of HO_2 with H_2CO, *Chem. Phys. Lett., 115*, 1-8, 1985.

Bridier, I., F. Caralp, H. Loirat, R. Lesclaux, B. Veyret, K.H. Becker, A. Reimer, and F. Zabel, Kinetic and theoretical studies of the reactions $CH_3C(O)O_2 + NO_2 + M \rightleftarrows CH_3C(O)O_2NO_2 + M$ between 248 and 393 K and between 30 and 760 torr, *J. Phys. Chem., 95*, 3594-3600, 1991.

Kirchner, F., F. Zabel and K.H. Becker, Kinetic behaviour of benzoylperoxy radicals in the presence of NO and NO_2, *Ber. Bunsenges. Phys. Chem., 95*, 893-900, 1991.

Köppenkastrop, D. and F. Zabel, Thermal Decomposition of Chlorofluoromethyl Peroxynitrates, *Int. J. Chem. Kinet., 23*, 1-15, 1991.

Roberts, J.M. and S.B. Bertman, Thermal decomposition of peroxyAcetic nitric anhydride (PAN) and peroxymethacrylic nitric anhydride (MPAN), *Int. J. Chem. Kinet.*, 297-307, 1992.

Troe, J., Predictive possibilities of unimolecular rate theory, *J. Phys. Chem., 83*, 114-126, 1979.

Zabel, F., "Thermische stabilität von peroxynitraten", Habilitationsschrift, Wuppertal, 1992.

Zabel, F., A. Reimer, K.H. Becker, and E. H. Fink, Thermal decomposition of alkyl peroxynitrates, *J. Phys. Chem., 93*, 5500-5507, 1989.

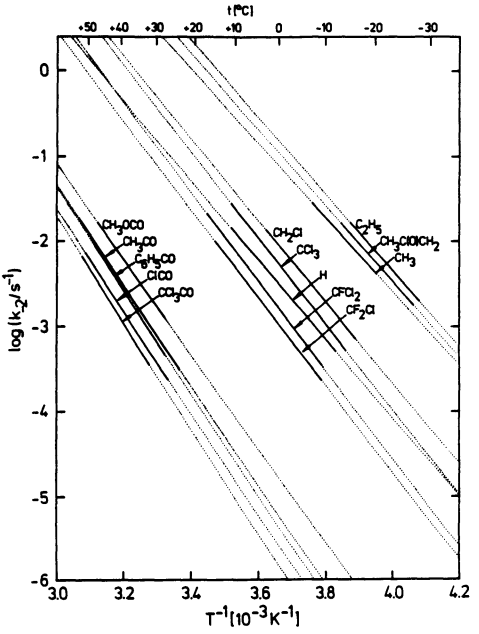

Fig. 1. Arrhenius plots for the rate constants reactions RO_2 NO_2 (+M) → RO_2 + NO_2 (+M) at total pressures between 800 and 1000 mbar (see table 1); the chemical formulae represent the R groups

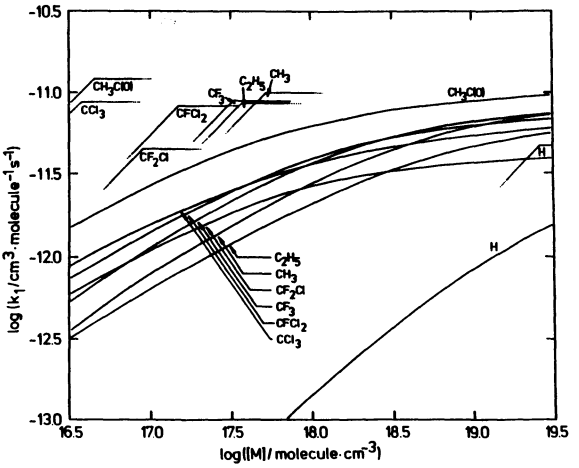

Fig. 2. Fall-off curves for the rate constants of reactions RO_2 + NO_2 (+M) → RO_2 + NO_2 (+M); rate constants are calculated from equilibrium constants and the pressure dependent data on k_{-2} from the present work; arrows designate the respective group R; straight lines are limiting low and high pressure rate constants, k_0 and k_∞ (Zabel, 1992).

Table 1. Experimental Arrhenius parameters (E_a, A) for reactions $RO_2NO_2 + (M) \rightarrow RO_2 + NO_2$ (+M) at atmospheric pressure (M = N_2)

R	p [mbar]	$k_{(298K)}$ [s^{-1}] [a]	E_a [kJ/mol]	A [$10^{16} s^{-1}$]
C_4H_9 [b]	800	(6.5)	<86.2>	(0.83)
C_6H_{13} [b]	800	(5.8)	<86.2>	(0.75)
C_8H_{17} [b]	800	(3.7)	<86.2>	(0.48)
C_2H_5 [b]	800	3.7	86.2±4.0	0.47
$CH_3C(O)CH_2$	800	2.6	85.6±15	0.26
CF_2ClCH_2	1000	2.5	90.7±3.6	< 2 >
$CFCl_2CH_2$	1000	2.1	91.2±3.6	< 2 >
CH_3 [b]	1000	1.65	83.8 [c]	0.080 [c]
$C_6H_5CH_2$	1000	(1.5)	90.3±6.3	< 1 >
$HOCH_2$ [b]	600 [d]	(1.0)	<85.3>	(0.09)
CH_3OCH_2	1000	0.44	92.2±5.4	0.64
$ClCH_2$	800	0.26	91.7±2.9	0.31
$CH_3C(O)OCH(CH_3)$	1000	(0.24)	(94.9)	< 1 >
$C_6H_5OCH_2$	1000	0.23	95.0±6.8	< 1 >
CCl_3 [b]	800	0.19	96.8±1.4	1.8
H	1000	0.08	89.2±2.2	0.036
CCl_2F [b]	800	0.066	100.3±1.8	2.5
$CClF_2$ [b]	800	0.040	98.7±1.8	0.8
$CH_3OC(O)$	1000	0.00084	107.0±2.2	0.48
$C_6H_5OC(O)$	1000	(0.00056)		
$CH_3C(O)$ [b]	1000	0.00040	112.9±1.9	2.5
$C_6H_5C(O)$ [b]	1000	0.00031	116.4±3.8	7.9
ClC(O)	800	0.00017	115.1±3.2	2.6
$CCl_3C(O)$	800 [d]	0.00012	119.3±4.0	9.6
$CFCl_2C(O)$	1000 [d]	0.00011	118.2	< 6 >
$CF_2ClC(O)$	1000	0.00009	118.9	< 6 >
$CF_3C(O)$	1000	0.00008	119.2	< 6 >

a) calculated from the Arrhenius parameters E_a and A;
b) data already published by Barnes et al. [1985], Zabel et al. [1989], Köppenkastrop and Zabel [1991], Bridier et al. [1991], and Kirchner et al. [1992];
c) calculated for 1 bar N_2 with the parameters in table 2;
d) M = synth. air

Table 2. Kinetic parameters for the unimolecular decomposition rate constants of reactions RO_2NO_2 (+M) → RO_2 + NO_2 (+M)[a]

R	$E_{a,\infty}$ [b] [kJ/mol]	A_∞ [10^{16} s^{-1}]	F_c	A_0 / [N_2] [cm^3/s]	$E_{a,0}$ [kJ/mol]
C_2H_5	86.7 ± 4.0	0.76	0.4	3.5 x 10^{-4}	77.7
CH_3	87.8 ± 5.9	1.1	0.4	9.0 x 10^{-5}	80.6
$ClCH_2$	93.5 ± 2.9	1.05	0.4	6.6 x 10^{-4}	85.9
CCl_3	98.3 ± 1.4	4.8	0.22	6.3 x 10^{-3}	85.1
H	92.9 ± 7.2	0.57	0.5	4.1 x 10^{-5}	88.5 [c]
CCl_2F	101.8 ± 1.8	6.6	0.28	1.01 x 10^{-2}	90.3
$CClF_2$	99.7 ± 1.7	1.6	0.30	1.8 x 10^{-3}	87.3
$CH_3OC(O)$	108.1 ± 4.0	0.88	0.3	4.7 x 10^{-3}	94.6
$CH_3C(O)$	113.3 ± 2.5	3.9	0.3	5.5 x 10^{-3}	100.3
$C_6H_5C(O)$	117.0 ± 3.8	11.3	0.25	3.4 x 10^{-2}	92.6
$ClC(O)$	116.7 ± 3.2	7.1	0.3	6.9 x 10^{-3}	105.6
$CCl_3C(O)$	120.1 ± 5.0	16	0.12	5.4 x 10^{-1}	98.5

a) Data taken from Zabel [1992], unimolecular rate constants k are calculated by the equations [Troe, 1979] $\log(k/k_\infty) = \log\{(k_0/k_\infty)/(1+k_0/k_\infty)\} + \log F_c \times \{1+[\log(k_0/\infty)/N_c]^2\}^{-1}$, $N_c = 0.75 - 1.27 \log F_c$, $k_0 = A_0 \exp(-E_{a,0}/RT)$, $k_\infty = A_\infty \exp(-E_{a,\infty}/RT)$;

b) Errors are essentially based on the 2σ errors of Arrhenius plots determined close to either the high or low pressure limit;

c) ± 2.2 kJ/mol (2σ)

Table 3. Comparison of thermal decomposition rate constants at atmospheric pressure from the present work with literature data

R	p [mbar]	A [10^{16} s^{-1}]	E_a [kJ/mol]	k_{298K}	ref.
CH_3	470	0.6	89.1 ± 1.3	1.4	[1]
	1000	0.08	83.8	1.65	this work
H	1000	0.014	86.6 ± 2.1	0.09	[2]
	1000	0.036	89.2 ± 2.2	0.08	this work
CCl_3	1000	1.42	95.6	0.25	[3]
	800	1.8	96.8 ± 1.4	0.19	this work
CCl_2F	1000	4.0	102.3 ± 5.0	0.047	[4]
	800	2.5	100.3 ± 1.8	0.066	this work
$CH_3C(O)$	1000	0.079	104.0 ± 3.2	0.00046	[5]
	1000	2.0	112.6 ± 3.8	0.00037	[6]
	1000	3.2	113.0	0.00049	[7]
	1000	25	119.2 ± 2.1	0.00031	[8]
	1000	2.5	112.8 ± 2.4	0.00042	[9]
	1000			0.00033 [297 K]	[10]
	1000			0.00028 [296 K]	[11]
	800	2.3	112.9 ± 1.9	0.00040	this work
$C_6H_5C(O)$	1000	0.085	105.4 ±12.6	0.00028	[12]
	1000	0.16	108.4 ± 3.8	0.00016	[13]
	1000	7.9	116.4 ± 3.8	0.00031	this work
ClC(O)	1000	6.3	115.9 ± 9.6	0.00030	[14]
	800	9.6	115.1 ± 3.2	0.00018	this work

[1] A. Bahta, R. Simonaitis, J. Heicklen, J. Phys. Chem. 86 [1982] 1849.
[2] R.A. Graham, A.M. Winer, J.N. Pitts, Chem. Phys. Lett. 51 [1977] 215.
[3] R. Simonaitis, J. Heicklen, Chem. Phys. Lett. 68 [1979] 245.
[4] R. Simonaitis, S. Glavas, J. Heicklen, Geophys. Res. Lett. 6 (1979) 385.
[5] R.A. Cox, M.J. Roffey, Environ. Sci. Technol. 11 (1977) 900.
[6] D.G. Hendry, R.A. Kenley, J. Am. Chem. Soc. 99 (1977) 3198.
[7] U. Schurath, V. Wipprecht, First European Symposium on Photochemical Behaviour of Atmospheric Pollutants, Ispra, Italy, 1979, Book of Abstracts.
[8] J. M. Roberts, S.B. Bertman, Int. J. Chem. Kinet. 24 (1992) 297.
[9] E.C. Tuazon, W.P.L. Carter, R. Atkinson, J. Phys. Chem. 95 (1991) 2434.
[10] H. Niki, P.D. Maker, C.M. Savage, L.P. Breitenbach, Int. J. Chem. Kinet. 17 (1985) 525.
[11] C.T. Pate, R. Atkinson, J.N. Pitts Jr., J. Environ. Sci. Health, A11 (1976) 19.
[12] T. Ohta, I. Mizoguchi, Environ. Sci. Techol. 15 (1981) 1229.
[13] R.A. Kenley, D.G. Hendry, J. Am. Chem. Soc. 104 (1982) 220.
[14] J.W. Spence, E.O. Edney, P.L. Hanst, Chem. Phys. Lett. 56 (1978) 478.

TEMPERATURE DEPENDENCE (256-296K) OF THE ABSORPTION CROSS-SECTIONS OF BROMOFORM IN THE WAVELENGTH RANGE 285-360 NM

Geert K. Moortgat, Richard Meller and Wolfgang Schneider*
Max-Planck-Institut für Chemie
Air Chemistry Department
Saarstrasse 23
D 6500 Mainz
Germany

INTRODUCTION

It has recently been recognized that brominated methanes could play an important role in the chemical processes occurring in the atmosphere, since they may provide a source of Br atoms. Indeed, Br species are known to participate in the ozone catalytic destruction cycle initiated through the formation of BrO radicals:

$$Br + O_3 \rightarrow BrO + O_2$$
$$BrO + BrO \rightarrow 2\,Br + O_2$$

BrO radicals have been detected during Antarctic and Arctic springtime ozone depletion events in the stratosphere [Brune and Anderson, 1989; Carroll et al., 1989], and in the troposphere [Hausmann et al., 1992].

It is believed that natural and/or anthropogenic brominated hydrocarbons are the precursor of the Br species. A series of specific organic bromine gases, such as bromomethanes, bromoethanes and some mixed bromochlorofluorocarbons, have been detected in stratospheric [Lal et al., 1985] and tropospheric samples [Singh et al., 1983; Berg et al., 1984; Rasmussen and Khalil, 1984; Penkett et al., 1985; Cicerone et al., 1988]. Those observations led to the conclusion that the oceans are the major global natural source of bromine, mainly for CH_3Br and CH_2Br_2 [Sturges and Harrison, 1986]. Moreover, field measurements in the Arctic areas in the lower troposphere have indicated that there exist a large source of bromoform ($CHBr_3$) during the spring warming-up period, which has been attributed to biological activities in the Arctic ocean [Barrie et al., 1989; Bottenheim et al., 1990]. This sudden bromine release was manifested with an ozone depletion in the local boundary layer. It was proposed by Barrie et al. [1988] that the ozone destruction mechanism is initiated by the photolysis of bromoform gas, although other bromine sources were also explored [Bottenheim et al., 1990; Finlayson-Pitts et al., 1990; McConnell et al., 1992].

---

* Present address: Deutsche Forschungsanstalt für Luft- und Raumfahrt, D-8031 Oberpfaffenhofen, Germany.

NATO ASI Series, Vol. I 7
The Tropospheric Chemistry of Ozone in the Polar Regions
Edited by H. Niki and K. H. Becker

The fate of $CHBr_3$ in the lower troposphere is not well established. Removal may occur through reaction with OH radicals and/or by photolysis. Recently, Gillotay et al. [1989] have measured the temperature dependence of the absorption cross-sections of bromoform in the range 170-290 nm. Non-published results by Cox and Penkett [1987] and Schneider and Moortgat [1988] have indicated that its UV spectrum extends even further to longer wavelengths, but that the shape of the spectrum exhibits a strong upwards curvature, not observed in other brominated methanes and ethanes [Molina et al., 1982; Gillotay and Simon, 1990]. This effect was tentatively attributed to the presence of absorbing species present to stabilize $CHBr_3$.

In order to assess the photodissociation rate constant of $CHBr_3$ in the troposphere, it is important to know its absorption spectrum and temperature dependence thereof in the critical wavelength range 285-360 nm. This paper deals with the measurement of the temperature dependence in the range 256-296 K of its UV absorption spectrum in the cited wavelength range. This study extends the previous investigation by Gillotay et al. [1989] in the same temperature range. The combined data of both studies are used to calculate the photodissociation rate constants of bromoform in the atmosphere.

EXPERIMENTAL

The absorption cross-sections have been measured in two different apparati, both equipped with monochromator, photomultiplier and diode-array detectors, as described in two recent publications [Meller et al., 1992; Bauer et al., 1992]. One system (A) implemented a cell of 63 cm optical pathlength, whereas the other system (B) was equipped with multipass optics, with a base path length of 120 cm. A total absorption pathlength of 980 cm was used in the latter configuration. Both cells are temperature regulated in the range 220-320 K. Both systems used stabilized deuterium lamps ((A) Hereaus 200 W and (B) Hamamatsu 30 W) and Tungsten Filament/Halogen (HR4, 40 W) light sources. For system (A), a 0.5 m Jobin-Yvon monochromator was used with a grating having 600 groves/mm; system (B) implemented a 0.5 m B&M monochromator with a similar grating.

Measurements between 245 and 340 nm were carried out at 296 K in apparatus (A) at pressures ranging from 0.2-4.0 torr. Cell (B) was used for the long wavelength section of the spectrum at pressures varying between 0.075 and 3.5 torr, depending on the working temperature (296 K: 2.0-3.5 torr; 286 K: 0.75-1.8 torr; 276 K: 0.4-0.8 torr; at 266 K: 0.25-0.5; at 256 K: 0.075-0.15 torr). Absolute capacitance pressure gauges (MKS, 10 torr range, 0.15% maximum deviation) were used in both setups.

The spectrum was calculated from Beer-Lambert's law, $\sigma(\lambda,T) = \ln [I_0 (\lambda)/I(\lambda,T)] / l N$ where σ represents the absorption cross-section (cm^2 $molecule^{-1}$) at wavelength λ and temperature T, l the length (cm) of the optical path in the cell, and N the number density

(molecule cm^{-3}) of $CHBr_3$; I_0 and I refer to the transmitted light intensity obtained at each diode in the array detector with the evacuated (or nitrogen gas, see later) and the filled cell, respectively. Typically, a spectrum was obtained by summing 100 scans, each scan consisting of a 2 s exposure of the total array. Recorded spectra were transferred via a detector interface to a computer for analysis. The reported absorption cross-sections of $CHBr_3$ at each temperature were obtained by averaging a minimum of seven independent measurements each at a different pressure.

RESULTS AND DISCUSSION

First attempts to measure the bromoform UV absorption spectrum were performed in the single path cell (A) in the range 245-340 nm and resulted in the occurrence of a tail at k > 320 nm, as was previously observed by Cox and Penkett [1987]. Although several sources of $CHBr_3$ were purchased from various manufacturers (Merck and Aldrich) and all samples were further purified by double vacuum distillation, the tailing absorption seemed to be persistent during all trial measurements.

Finally, $CHBr_3$ was purified in a special procedure. The bromoform used was purchased from Merck and contained 1-2% ethanol and traces of bromine, which resulted in the light-brown color of the solution. Prepurification was performed by pumping off the ethanol at 10 °C, and storing over Cu-turnings over a few days to remove the bromine. This solution was then distilled twice, and stored over Cu-turnings in the dark until being used for final measurement. The purified sample of $CHBr_3$ was checked by infrared absorption spectroscopy and contained no absorption features due to ethanol.

Even with the precautions taken, the tail-effect was not completely suppressed even when freshly purified $CHBr_3$ was used. However, performing the measurements in the long path cell (B), the tail was lowered by one order of magnitude, indicating that the tail-effect is caused by an optical artifact. Moreover, it was observed that the use of an equivalent pressure N_2 gas (several torr) as reference gas (for the measurements of I_0) removed completely the tail-effect. As a consequence, all temperature dependent measurements of the absorption cross-sections were obtained with N_2 gas as reference gas.

The long tail absorption feature appearing in the spectrum is shown in Figure 1 in the range 290-360 nm, where the spectrum of Cox and Penkett [1987] (single path) is compared with our measurements (multiple path) using highly purified $CHBr_3$ and the evacuated cell as reference signal. The long wavelength absorption spectrum of $CHBr_3$ obtained at 296 K using 5 torr N_2 as reference gas is also displayed. At wavelengths shorter than 300 nm the absorption cross-sections were found to be in excellent agreement with the measurements made by Gillotay et al. [1989] obtained at 295 K; these data are also displayed in Figure 1.

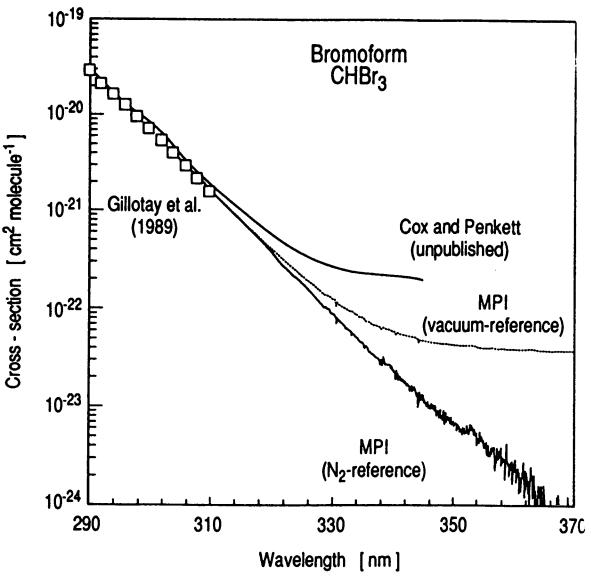

Fig. 1. Measured UV absorption cross-sections of $CHBr_3$ compared with spectra obtained by Gillotay et al. [1989] and Cox and Penkett [1987] (see text).

Uncertainties in the measured optical pathlength, temperature, pressure and absorbance contribute to the overall uncertainty in the measured absorption cross-sections. The pressure, temperature and pathlength each are uncertain by about 1%. The accuracy of the absorption measurement was primarily determined by the stability of the baseline (I_O) during the measurement. The overall uncertainty was within ± 3% in the wavelength range 285-320 nm, increasing to larger values at longer wavelengths.

The absorption spectra of $CHBr_3$ were measured in apparatus (B) at various temperatures T = 296, 286, 276, 266 and 256 K in the wavelength range 285-360 nm, and are displayed in Figures 2 and 3. Measurements at lower temperatures were not possible due to the very low vapor pressure of bromoform.

As shown in Figures 2 and 3, an exponential dependence of the absorption cross-sections is observed. The observed temperature dependence of σ is qualitatively consistent with the expected spectral changes due to the variation with temperature of the vibrational and rotational level population distribution in the ground electronic state.

The published cross-sections of $CHBr_3$ obtained by Gillotay et al. [1989] in the range 200-300 nm at 250 and 295 K are shown in Figure 2, together with our spectrum (245-290 nm) obtained at 296 K in apparatus (A), which is in excellent agreement with those

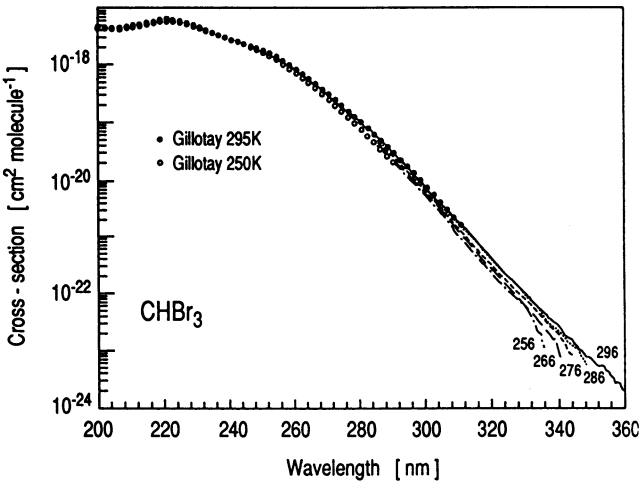

Fig. 2. UV absorption cross-sections for $CHBr_3$ in the range 200-360 nm over the temperature range 250-296 K. The data obtained in this study are combined with previous measurements of Gillotay et al. [1989].

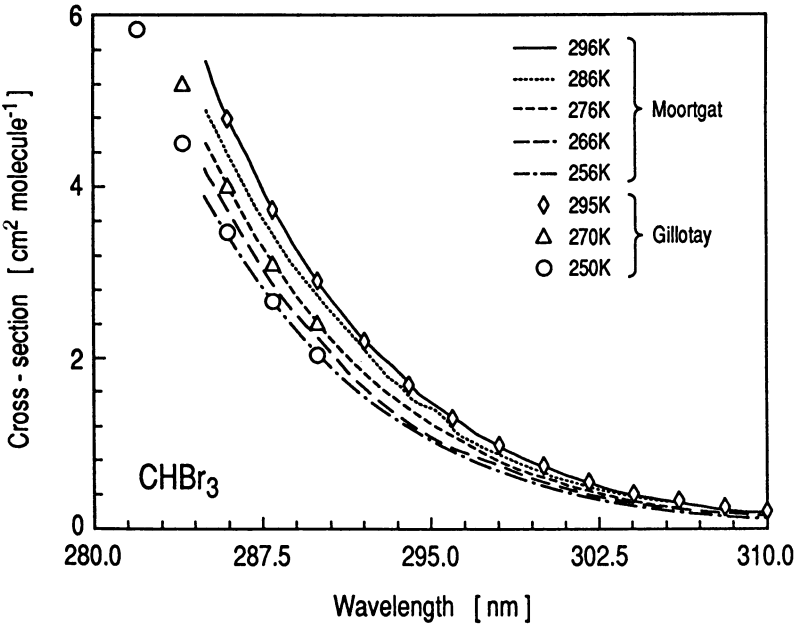

Fig. 3. UV absorption cross-sections for $CHBr_3$ in the range 285-310 nm over the temperature range 250-296 K. The data obtained in this study are combined with previous measurements of Gillotay et al. [1989].

Table 1: Absorption cross-sections of $CHBr_3$ at different temperatures averaged over 2 nm intervals (10^{-23} cm^2 $molecule^{-1}$).

Wavelength	Temperature, K				
[nm]	296	286	276	266	256
286	4810	4340	3990	3710	3420
288	3750	3440	3110	2850	2650
290	2880	2710	2400	2200	2040
292	2220	2090	1840	1660	1570
294	1700	1570	1400	1240	1190
296	1280	1170	1060	946	897
298	951	854	795	739	676
300	719	644	594	555	502
302	530	482	442	410	368
304	394	361	328	302	268
306	298	271	242	222	194
308	226	203	178	162	137
310	171	151	132	118	95.6
312	127	114	97.1	86.6	71.8
314	95.2	85.2	71.5	63.4	53.6
316	71.2	63.7	52.8	46.2	39.9
318	52.9	48.0	39.3	34.3	29.5
320	39.0	36.6	29.6	25.1	21.4
322	28.9	27.7	22.1	18.4	15.6
324	21.5	20.7	16.5	13.7	11.8
326	16.2	15.8	12.7	10.3	9.21
328	12.1	12.2	9.81	7.75	7.12
330	9.16	9.36	7.49	5.65	5.16
332	6.90	6.73	5.67	4.27	3.32
334	5.25	4.70	4.27	3.05	1.77
336	3.96	3.25	3.22	2.23	
338	3.07	2.51	2.36	1.59	
340	2.40	2.05	1.76		
342	1.76	1.51	1.13		
344	1.35	1.15			
346	1.02	0.84			
348	0.80				
350	0.64				
352	0.54				
354	0.46				
356	0.32				
358	0.24				
360	0.17				
362	0.13				

measurements. Figure 3 contains also the data of Gillotay et al. [1989] obtained at 250, 270 and 295 K. Numerical values are listed in Table 1 at 2 nm interval in the wavelength range 286-340 nm for the selected temperatures.

At every temperature T, the measured UV absorption cross-sections at $\lambda > 290$ nm were found to obey the linear function:

$$\ln \sigma(\lambda) = Y(\lambda) = A + A' \lambda \tag{1}$$

At every wavelength T the cross-sections varied linearly with temperature:

$$\ln \sigma(T) = Y_0(\lambda) + X(\lambda) (T - T_0) \tag{2}$$

where Y_0 represents the absorption cross-sections at $T_0 = 273$ K and $X(\lambda)$ the temperature gradient. $X(\lambda)$ is wavelength dependent and could be expressed by:

$$X(\lambda) = B + B' \lambda \tag{3}$$

The cited functions could be combined in the following equation:

$$\ln \sigma(\lambda,T) = (A_0 + A_0' \lambda) + (B + B' \lambda) (T - T_0) \tag{4}$$

Linear regression of the data resulted in the following constants:

$A_0 = -2.37616$ $\quad B = -0.0618350$

$A_0' = -0.1475688$ $\quad B' = 0.000241014.$

Equation (4) is valid in the wavelength range 290-340 nm.

This equation was used to calculate the bromoform absorption cross-sections as a function of temperature over the spectral intervals used in atmospheric modeling calculations. The computed data are displayed in Table 2 for the range 290-342.5 nm for five selected temperatures used by Gillotay et al. [1989]. Table 2 must thus be considered as an extension of the absorption cross-section data base for $CHBr_3$ published by these authors.

The temperature dependent absorption cross-sections presented in Table 2 for the range 290-342.5 nm, combined with the data set obtained by Gillotay et al. [1989] for the wavelength range 170-290 nm, were used for the calculation of the photodissociation rate constants of $CHBr_3$ using a radiative transfer model [Meller, 1991]. The photodissociation rate constants are given in Figure 4 as a function of altitude for three zenith angles 0, 50 and 70 degrees. Photodissociation rate constants obtained at ground level are also presented as a

Table 2: Absorption cross-sections of bromoform at different temperatures averaged over spectral intervals used in atmospheric modeling calculations (10^{-23} cm^2 $molecule^{-1}$).

Wavelength	Temperature, K				
[nm]	290	270	250	230	210
289.85 - 294.12	2200	1780	1500	1270	1070
294.12 - 298.51	1190	934	722	638	527
298.51 - 303.03	627	481	389	315	254
303.03 - 307.69	327	244	193	153	121
307.69 - 312.50	168	122	94.1	72.8	56.3
312.50 - 317.50	84.0	59.2	44.7	33.8	25.5
317.50 - 322.50	41.2	28.2	20.8	15.3	11.3
322.50 - 327.50	20.2	13.4	9.67	6.96	5.01
327.50 - 332.50	9.99	6.40	4.50	3.16	2.22
332.50 - 337.50	4.88	3.05	2.09	1.44	0.99
337.50 -342.50	2.40	1.45	0.97	0.65	0.44

function of zenith angle in Figure 5 for $CHBr_3$ and are compared with calculated values for HCHO [Meller, 1991]. For typical conditions in early spring (270 K) at 65° N, a photolysis rate constant $J_{CHBr_3} = 2.8 \times 10^{-7}\ s^{-1}$ was calculated for a zenith angle of 65°, using a quantum yield of unity. In order to compare these re-sults with the cited photodissociation rate constants used by Barrie et al. [1989], $J_{CHBr_3} = 6 \times 10^{-7}\ s^{-1}$, we also calculated $J_{HCHO} = 4.2 \times 10^{-4}\ s^{-1}$ (see Figure 5) [Meller, 1991], which can be used as a 'reference molecule' to compensate for the difference in the employed models.

From the ratio of both photodissociation rate constants, $J_{HCHO}/J_{CHBr_3} = 150$, the effective photolysis rate constants of bromoform can be estimated for the conditions used by Barrie et al. [1988]. A value of $J_{HCHO} = 2.15 \times 10^{-5}\ s^{-1}$ would therefore result in $J_{CHBr_3} = 1.4 \times 10^{-7}\ s^{-1}$, which is a factor 4 lower than the value cited by these authors. This lower photolysis rate constant would result in a tropospheric lifetime of three months, making the photolysis of bromoform a less favourable candidate for an active bromine source.

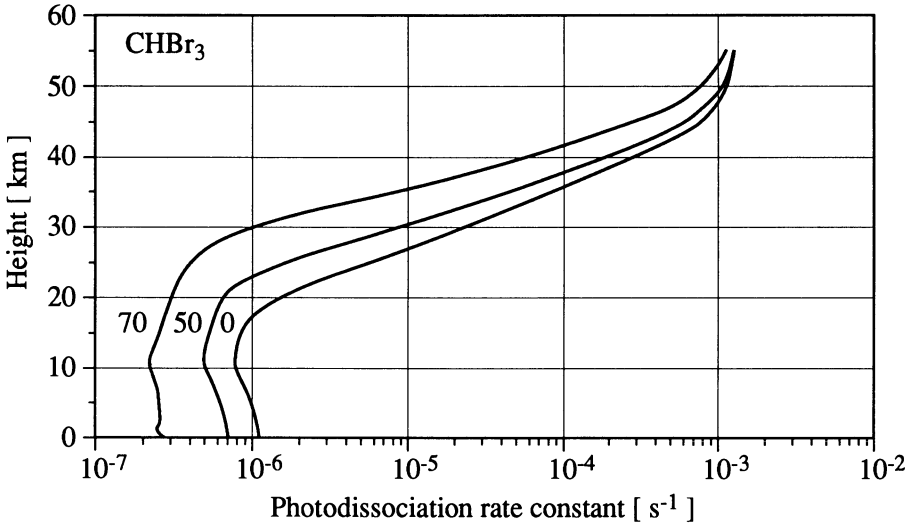

Fig. 4. Photodissociation rate constants of $CHBr_3$ as a function of altitude and zenith angle.

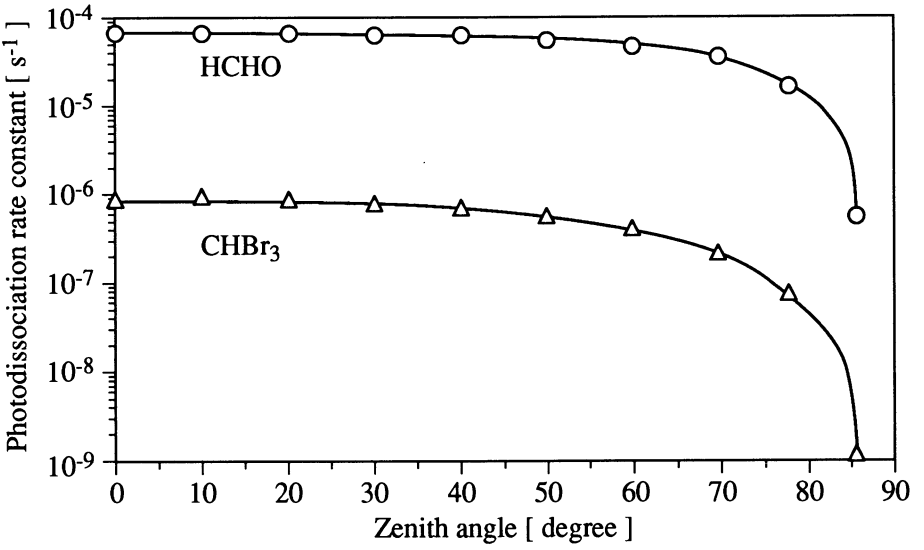

Fig. 5. Comparison of photodissociation rate constants of $CHBr_3$ and HCHO as a function of zenith angle at ground level.

REFERENCES

Barrie, L.A., J.W. Bottenheim, R.C. Schnell, P.J. Crutzen and R.A. Rasmussen, Ozone destruction and photochemical reactions at polar sunrise in the lower Arctic atmosphere, *Nature, 334*, 138-141, 1988.

Barrie, L.A., G. den Hartog, J.W. Bottenheim and S. Landsberger, Anthropogenic aerosols and gases in the lower troposphere at Alert, Canada in April 1986, *J. Atmos. Chem., 9*, 101-127, 1989.

Bauer, D., J.N. Crowley and G.K. Moortgat, The UV absorption spectrum of the ethylperoxy radical and its self-reaction kinetics between 218 and 333 K, *J. Photochem. Photobiol. A: Chem., 65*, 329-344, 1992.

Berg, W.W., L.E. Heidt, W. Pollock, P.D. Sperry, R.J. Cicerone and E.S. Gladney, Brominated organic species in the arctic atmosphere, *Geophys. Res. Lett., 11*, 429-432, 1984.

Brune, W.H. and J.G. Anderson, In situ observations of BrO over Antarctica: ER-2 aircraft results from 54° S to 72° S latitude, *J. Geophys. Res., 94*, 16639-16647, 1989.

Bottenheim, J.W., L.A. Barrie , E. Atlas, L.E. Heidt, H. Niki, R.A. Rasmussen and P.B. Shepson, Depletion of lower tropospheric ozone during Arctic spring: the polar sunrise experiment 1988, *J. Geophys. Res., 95*, 18555-18568, 1990.

Carroll, M.A., R.W. Sanders, S. Solomon and A.L. Schmeltekopf, Visible and near-ultraviolet spectroscopy at McMurdo Station, Antarctica 6. Observations of BrO, *J. Geophys. Res. 94*, 16633-16638, 1989.

Cicerone, R.J., L.E. Heidt and W.H. Pollock, Measurements of atmospheric methylbromide and bromoform, *J. Geophys. Res. 93*, 3745-3749, 1988.

Cox R.A. and S.A. Penkett, Absorption spectrum of bromoform, Private communication, 1987.

Finlayson-Pitts, B.J., F.E. Livingston and H.N. Berko, Ozone destruction and bromine photochemistry in the Arctic spring, *Nature, 334*, 622-625, 1990.

Gillotay D, A. Jenouvrier, B. Coquart, M.F. Merienne and P.C. Simon, Ultaviolet absorption cross-sections of bromoform in the temperature range 295-240 K, *Planet. Space Science, 37*, 1127-1140, 1989.

Gillotay, D. and P.C. Simon, Ultraviolet absorption cross-sections of photoactive species of stratospheric interest, *Aeronomica Acta*, A - N° 356, 1990.

Hausmann, M., T. Rudolph and U. Platt, Spectroscopic measurements of bromine oxide, ozone and nitrous oxide in Alert, Tropospheric chemistry of ozone in polar regions, NATO ARW, Ang 23-28, Wolfville, Nova Scotia, Canada, 1992.

Lal, S., R. Borchers, P. Fabian and B.C. Krüger, Increasing abundance of $CBrClF_2$ in the atmosphere, *Nature, 316*, 135-136, 1985.

Meller, R., Absolute Absorptionsquerschnitte von Formaldehyd in der Gasphase, Diplom Thesis, University of Mainz, 1990.

Meller R., W. Raber, J.N. Crowley, M.E. Jenkin and G.K. Moortgat, The UV-visible absorption spectrum of methylglyoxal, *J. Photochem. Photobiol. A: Chem., 62*, 163-171, 1991.

McConnell, J.C., G.S. Henderson, L.A. Barrie, J.W. Bottenheim, H. Niki, C.H. Langford and E.M.J. Templeton, Photochemical bromine production implicated in Arctic boundary-layer ozone depletion, *Nature, 355*, 150-152, 1992.

Molina, L.T., M.J. Molina and F.S. Rowland, Ultraviolet absorption cross sections of several brominated methanes and ethanes of atmospheric interest, *J. Phys. Chem.*, *86*, 2672-2676, 1982.

Penkett S.A., B.M.R. Jones, M.J. Rycroft and D.A. Simmons, An interhemispheric comparison of the concentrations of bromine compounds in the atmosphere, *Nature*, *318*, 550-553, 1985.

Rasmussen R.A. and M.A.K. Khalil, Gaseous bromine in the arctic and arctic haze, *Geophys. Res. Lett.*, *11*, 433-436, 1984

Schneider,, W. and G.K. Moortgat, Absorption spectrum of bromoform at 298 K, unpublished results, MPI, Mainz, 1988.

Singh, H.B., L.J. Salas and R.E. Stiles, Methylhalides in and over the eastern Pacific (40° N-32° S), *J. Geophys. Res. 88*, 3684-3690, 1983.

Sturges, W.T. and R.M. Harrison, Bromine in marine aerosols and the origin, nature and quantity of natural atmospheric bromine, *Atmospheric Environment*, *20*, 1485-1496, 1986.

OXIDATION OF ORGANIC SULFUR COMPOUNDS

I. Barnes, K.H. Becker and R.D. Overath
Physikalische Chemie, FB 9
Bergische Universität - Gesamthochschule Wuppertal
5600 Wuppertal 1, FRG

INTRODUCTION

Dimethylsulfide (CH_3SCH_3, DMS) is one of the major natural organic sulfur compounds emitted to the atmosphere [Aneja and Cooper, 1989], and consequently much effort has been directed towards understanding its oxidation mechanisms particularly with the OH radical [Yin et al., 1990; Tyndall and Ravishankara, 1991]. All of the product studies on the reaction of OH with DMS have been carried out at room temperature and no information is currently available on the effects that temperatures such as those prevalent in the Arctic or Antarctic may have on the product distributions. For example, results from field measurements in the remote Southern Hemisphere show a higher yield of methanesulfonic acid (CH_3SO_3H, MSA) and a lower yield of SO_2 from DMS oxidation compared to other world areas [Berresheim et al., 1989, 1990], suggesting a change in the product distribution at low temperatures. The various mechanistic and product studies indicate that the products of the oxidation of DMS will be very much dependent on the atmospheric fate of the initially formed OH-DMS adduct and also the intermediate CH_3S radical whose loss will be controlled by reactions with either O_2 or trace species such as O_3 and NO_x. The kinetics and mechanisms of the reactions of CH_3S and O_2, O_3 and NO_x are still speculative.

The recent implication of the involvement of halogens in the observed Arctic boundary-layer ozone depletion [Barrie et al., 1988; McConnell et al., 1992] suggests that the reactions of halogen atoms and halogen oxides, in particular Br and BrO, with DMS may play an important role in coupling the halogen and sulfur cycles. The reactions of halogens with DMS are expected to proceed via either direct abstraction or complex addition pathways, while those of the halogen oxides are expected to proceed via addition pathways [Barnes et al., 1987; Martin et al., 1987; Barnes et al., 1989a,b; Daykin and Wine, 1990; Barnes et al., 1991a,b; Maguin et al., 1991; Overath, 1991].

Presented here are results from studies on the reactions of chlorine and bromine atoms with DMS at room temperature and also the halogen oxides XO (X = Cl, Br and I) with DMS [Barnes et al., 1991b; Overath, 1991] as a function of temperature. Further, an ongoing product study of the 254 nm photolysis of dimethyldisulfide (CH_3SSCH_3, DMDS)

NATO ASI Series, Vol. I 7
The Tropospheric Chemistry of Ozone in the Polar Regions
Edited by H. Niki and K. H. Becker

designed at understanding the reactions of the CH_3S radical leading to SO_2 and MSA formation in the atmosphere will be briefly discussed.

EXPERIMENTAL

Rate constants for the reactions of Cl and Br atoms with DMS were carried out in a 420 l Duran glass reactor using the relative kinetic technique. Details of the experimental set-up and kinetic method can be found in Barnes et al. [1984, 1989c]. The Cl atoms were generated using the 254 nm photolysis of phosgene (Cl_2CO) and the bromine atoms by the photolysis of molecular bromine with fluorescent lamps (Philips TL05/40W, λ_{max} = 360 nm). The concentration-time behavior of reactants and products were monitored in situ by long path FTIR spectroscopy.

The reactions of IO, BrO and ClO with DMS were studied under pseudo-first-order conditions at temperatures between 265-338 K and total pressures of 0.5-6.8 mbar He using the discharge flow - mass spectrometry technique. Details can be found in Barnes et al. [1991b] and Overath [1991].

FTIR product studies of ppm levels of DMDS were carried out as a function of O_2 partial pressure at a total pressure of 1000 mbar (O_2 + N_2) in a 1,080 l quartz glass reaction chamber by 298 K. Further details can be found in Barnes et al. [1992].

RESULTS AND DISCUSSION

Reactions of Cl and Br with DMS: From the 254 nm photolysis of Cl_2CO (20-30 ppm), DMS (10-35 ppm) and a reference hydrocarbon, mainly propane (10-20 ppm), at 760 torr total pressure of N_2 and 298 $\pm$ 2 K the following rate coefficient has been obtained from 6 experiments for the reaction of Cl atoms with DMS:

$$k\,(Cl + DMS) = 2.6 \pm 0.2 \times 10^{-10}\ cm^3\ molecules^{-1}\ s^{-1}$$

A value of $k = 1.6 \times 10^{-10}$ cm^3 $molecule^{-1}$ s^{-1} has been used for the reference reaction of Cl with propane [DeMore et al., 1992]. Substituting N_2 for synthetic air had no effect on the measured rate coefficient. The value supersedes the preliminary value of $(2.0 \pm 0.3) \times 10^{-10}$ cm^3 $molecule^{-1}$ s^{-1} previously reported from this laboratory in Barnes et al. [1989b] which was based on only one experiment. The new value is a little lower but in reasonable agreement with the value of Nielsen et al. [1990] of $(3.2 \pm 0.3) \times 10^{-10}$ cm^3 $molecule^{-1}$ s^{-1} obtained at 295 K and 740 torr N_2 using a competitive technique and also the value of $(3.3 \pm 0.5) \times 10^{-10}$ cm^3 $molecule^{-1}$ s^{-1} for 297 K and P = 700 torr N_2 obtained using the LP-RF technique and reported by Wine [this volume].

Preliminary FTIR studies have been carried out on the products formed in the Cl initiated oxidation of DMS using Cl_2CO/DMS mixtures in 760 torr of synthetic air and 298 K. The observed products include CO, HCl, HCHO, SO_2 and DMSO. Figure 1 shows the typical concentration-time behavior of reactants and products. The sulfur balance was typically between 70 and 80%. An analysis of the product spectrum indicates that at least one major compound, probably sulfur containing, still remains to be identified. The formation of products such as HCHO and SO_2 clearly shows that an overall abstraction pathway is operative. However, the formation of DMSO implies that there may be some complex interaction between Cl, DMS and O_2 involving a Cl addition adduct. The investigations are still at a very early stage; it is not yet possible to make firm conclusions concerning the reaction mechanism. Such chamber systems are also susceptible to secondary chemistry [Yin et al., 1990; Barnes et al., 1991a] which still needs to be checked.

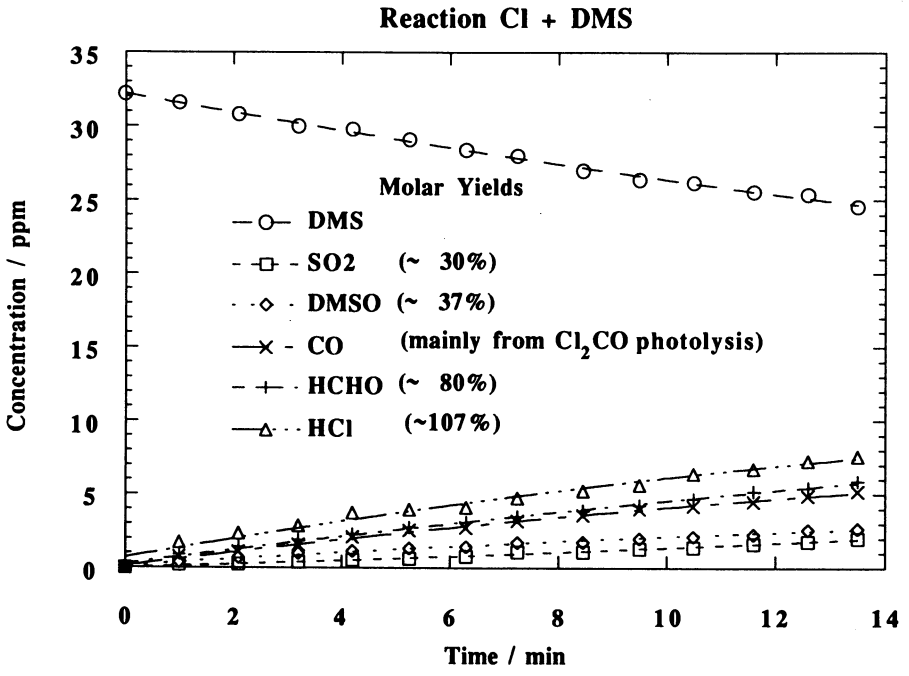

Fig. 1. Typical concentration-time behavior of reactants and products in a Cl_2CO/DMS/air photolysis mixture

The rate coefficients obtained using the relative kinetic technique for the reaction of Br and DMS as a function of O_2 partial pressure at a total pressure 750 torr (N_2 + O_2) and 298 K are listed in Table 1. The rate coefficients for the reactions of Br with the reference hydrocarbons are strongly dependent on O_2 partial pressure, total pressure and temperature and were calculated according to the expression [Barnes et al., 1989c]:

$$k_{Br + isooctane} = (4.16 \pm 0.33) \times 10^{-12} \exp(-(1820 \pm 26)/T) \text{ cm}^3 \text{ molecule}^{-1} \text{ s}^{-1}$$

$$k_{Br + acetylene} = \frac{1.15 \times 10^{-34} \exp(987/T) [O_2]}{58.3 \exp(-1979/T) + [O_2]/[M]} \text{ cm}^3 \text{ molecule}^{-1} \text{ s}^{-1}$$

$$k_{Br + ethene} = \frac{4.49 \times 10^{-34} \exp(1155/T) [O_2]}{2370 \exp(-2675/T) + [O_2]/[M]} \text{ cm}^3 \text{ molecule}^{-1} \text{ s}^{-1}$$

Table 1. Results for the reaction Br + DMS as a function of the O_2 partial pressure at a total pressure of 750 torr (N_2 + O_2) and 298 ± K

$[O_2]$ (torr)	Reference	k(Br + DMS) / k(Br + Reference)	$k_{Br+DMS} \times 10^{-14}$ (cm^3 $molecule^{-1}$ s^{-1})
<0.1	isooctane	6.9 ± 0.6	6.5 ± 0.5
10	ethene	3.0 ± 0.2	6.9 ± 0.4
25	ethene	1.5 ± 0.1	7.3 ± 0.5
50	acetylene	2.5 ± 0.3	7.3 ± 0.9
100	acetylene	2.1 ± 0.2	8.9 ± 0.8
150	acetylene	2.0 ± 0.5	9.6 ± 1.0
300	acetylene	2.1 ± 0.3	11.4 ± 1.7
500	acetylene	1.6 ± 0.4	9.5 ± 2.4

The rate coefficient for the reaction of Br with DMS was found to increase with increasing partial pressure of O_2. This O_2 dependence has been observed for the reaction of Br with other unsaturated hydrocarbons [Barnes et al., 1989c]. This behavior can be interpreted by the addition of Br to DMS forming an adduct which can either decompose or react with O_2 forming products: $Br + (CH_3)_2S + M \rightleftarrows (CH_3)_2SBr + M$; $(CH_3)_2SBr + O_2$

→ products. As mentioned above for Cl with DMS the reactions of organic sulfur compounds in chambers can be effected by secondary chemistry such as reactions with OH, CH_3S or CH_3SO_x radicals, so that the present results must be treated with some caution until a more thorough investigation is performed. Possible influences such as reaction with OH, CH_3S or CH_3SO_x radicals have not yet been exhaustively investigated, however, the high Br concentration of $\sim 10^{12}$ atoms cm^{-3} produced in the reaction system would suggest that contributions from any OH radicals formed will be negligible. Furthermore, experiments in which DMDS was photolyzed in the presence of DMS in either pure N_2 or air did not result in the loss of DMS [Barnes et al., 1988; Nielsen et al., 1990]. This supports that CH_3S or CH_3SO_x radicals will also not affect the results.

The kinetics of the reaction of Br with DMS has been studied using time-resolved resonance fluorescence spectroscopy to monitor the temporal behavior of $Br(^2P_{3/2})$ and the results are reported by Wine in this NATO-ARW report. He finds evidence for both reversible adduct formation and hydrogen abstraction pathways. At low temperate and atmospheric pressure, the rate coefficients for the addition of Br to DMS exceed 10^{-10} cm^3 $molecule^{-1}$ s^{-1}, while the adduct lifetime toward unimolecular decomposition varies from about 0.05 s at 220 K to 0.0007 s at 260 K. At temperatures above 375 K they found that decomposition of the $(CH_3)_2Br$ adduct was rapid and that hydrogen abstraction dominated. They also concluded that the reaction of the $(CH_3)_2SBr$ adduct with O_2 is slow.

A qualitative FTIR product analysis has been carried out for $Br_2/DMS/N_2/O_2$ photolysis mixtures. The upper trace of Figure 2 shows a difference spectrum obtained after 20 min irradiation in 760 torr synthetic air and the lower trace after the same irradiation time in 760 torr of N_2. In nitrogen the main products were HBr and CH_3SCH_2Br, suggesting that under these conditions the reaction proceeds mainly by hydrogen abstraction forming CH_3SCH_2 radicals which then react with the molecular bromine: $CH_3SCH_3 + Br \rightarrow CH_3SCH_2 + HBr$; $CH_3SCH_2 + Br_2 \rightarrow CH_3SCH_2Br + Br$. Small concentrations of SO_2 and CO are also formed probably due to reactions of CH_3SCH_2 with the ppm levels of O_2 which are always present in the chamber even when it is filled with N_2. In air the observed products include CO, HBr, CH_3SCH_2Br, HCHO, CH_3OH, SO_2 and DMSO. From the products it is obvious that the abstraction channel is still a major pathway, however, the formation of DMSO suggests also that some complex interaction of O_2 with a $(CH_3)_2SBr$ adduct is also occurring. The yield of DMSO has been estimated to be approximately 30%.

Reactions of IO, BrO and ClO with DMS: Table 2 compares the rate coefficients measured for the reaction of IO, BrO and ClO with DMS in this work with other values reported in the literature for 298 K. The following Arrhenius expressions were obtained for the reactions of IO and BrO with DMS:

$$k(IO+DMS) = (1.77^{+0.28}_{-0.22}) \times 10^{-13} \exp[-(775 \pm 532)/T] \text{ cm}^3 \text{ molecule}^{-1} \text{ s}^{-1}$$

$$k(BrO+DMS) = (9.17^{+2.54}_{-2.24}) \times 10^{-14} \exp[(343 \pm 78)/T] \text{ cm}^3 \text{ molecule}^{-1} \text{ s}^{-1}$$

Table 2. Experimental and literature rate coefficients for the reactions of IO, BrO and ClO radicals with DMS at 298 K

Reaction	k [cm^3 $molecule^{-1}$ s^{-1}]	Method	Reference
IO + DMS	$(3.0 \pm 1.5) \times 10^{-11}$	FT-IR	Barnes et al. [1987]
	$(1.5 \pm 0.5) \times 10^{-11}$	DF-MS	Martin et al. [1987]
	$\leq 3.5 \times 10^{-14}$	LFP-LPA	Daykin and Wine [1990]
	$(1.15 \pm 0.2) \times 10^{-14}$	DF-MS	Maguin et al [1991]
	$(8.8 \pm 2.1) \times 10^{-15}$ 0	DF-MS	this work / Barnes et al., [1991a, b]
BrO + DMS	$(2.65 \pm 0.65) \times 10^{-13}$	DF-MS	Barnes et al. [1989]
	$(2.40 \pm 0.6) \times 10^{-13}$	DF-EPR	Le Bras et al. [1991]
	$(2.7 \pm 0.5) \times 10^{-13}$	DF-MS	this work / Barnes et al. [1991a, b]
ClO + DMS	$(3.9 \pm 0.5) \times 10^{-14}$	DF-MS	Barnes et al. [1989]
	$(9.5 \pm 2.0) \times 10^{-15}$	DF-MS	this work / Barnes et al. [1991a, b]

DF - MS: discharge flow - mass spectrometry
FT-IR: Fourier transform infrared spectrometry
LFP-LPA: Laser flash photolysis - long pathlength absorption

The rate coefficient for the reaction of IO with DMS obtained in this study is in good agreement with the recent values of Daykin and Wine [1990] and Maguin et al. [1991]. The earlier study by Martin et al. [1987] is now known to have been influenced by wall reactions. However, the reason for the high value obtained in the FTIR steady state photolysis study of $NO_2/I_2/DMS/N_2$ in this laboratory [Barnes et al., 1987] is still not clear. Similar experiments have subsequently been performed in this laboratory using the photolysis of methylene iodine in the presence of O_3 as a NO_x free source for IO radicals [Barnes et al., 1991a]: $CH_2I_2 + h\upsilon \rightarrow CH_2I + I$; $CH_2I + O_2 \rightarrow HCHO + I$; and $I + O_3 \rightarrow IO + O_2$. Two molecules of O_3 were consumed for each molecule of CH_2I_2 photolyzed. Computer simulations of the decay of DMS using this IO source lead to a value of $k = (1.2 \pm 0.3) \times$

10^{-14} cm^3 $molecule^{-1}$ s^{-1} as rate coefficient for the reaction of IO with DMS in good agreement with the recent values in Table 2. Examples of the data are shown in Figure 3. The studies also show that the reaction results in quantitative conversion of DMS in dimethylsulfone (CH_3SOCH_3, DMSO): IO + DMS → DMSO + I.

The recent values of the rate coefficients for the reaction of BrO with DMS from this laboratory [Barnes et al., 1991a,b] and Le Bras et al. [1991] are in good agreement with a previous determination from this laboratory [Barnes et al., 1989a] and the value for ClO with DMS represents an improvement on the previous value from this laboratory [Barnes et al., 1991a]. Both reactions lead to the formation of DMSO, in the case of BrO FTIR studies give yields of 90±20% (Figure 4), however, in the case of ClO quantification is difficult.

All of the rate coefficients were found to be independent of pressure in the range studied. The small temperature dependence measured for the reactions of IO and BrO with DMS should be considered as preliminary and need confirmation by other work using an independent method. The reactivity of XO towards DMS takes the order BrO > ClO ≈ IO. From a consideration of the exothermicities the order IO>BrO>ClO would be expected. The reason for the observed trend is not clear.

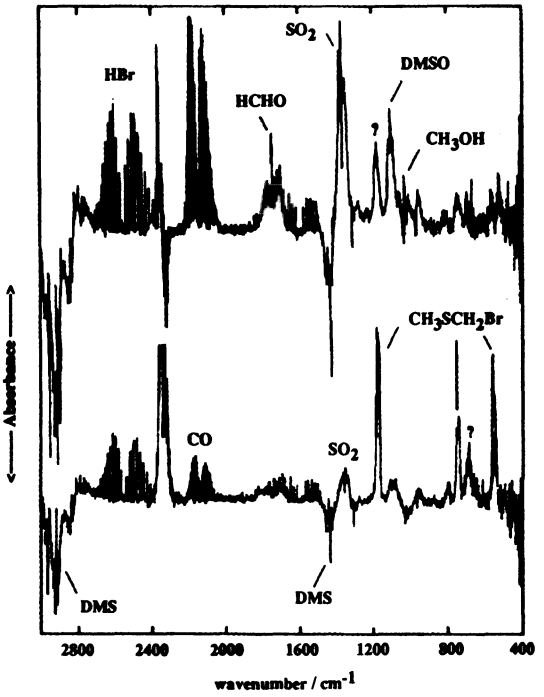

Fig. 2. Difference FTIR-spectra obtained after 20 min irradiation of 20 ppm Br_2 and 20 ppm DMS in 760 torr of synthetic air (above) and 760 torr of N_2 (below)

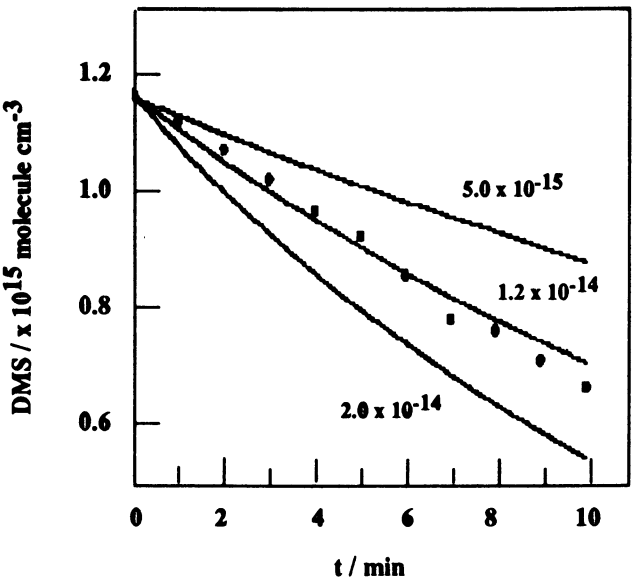

Fig. 3. Decay of DMS in a CH_2I_2/O_3/DMS/air photolysis system. The filled circles are the experimental points and the solid lines are computer simulations of the reaction system for different values of the rate coefficient for the reaction IO + DMS → DMSO + I.

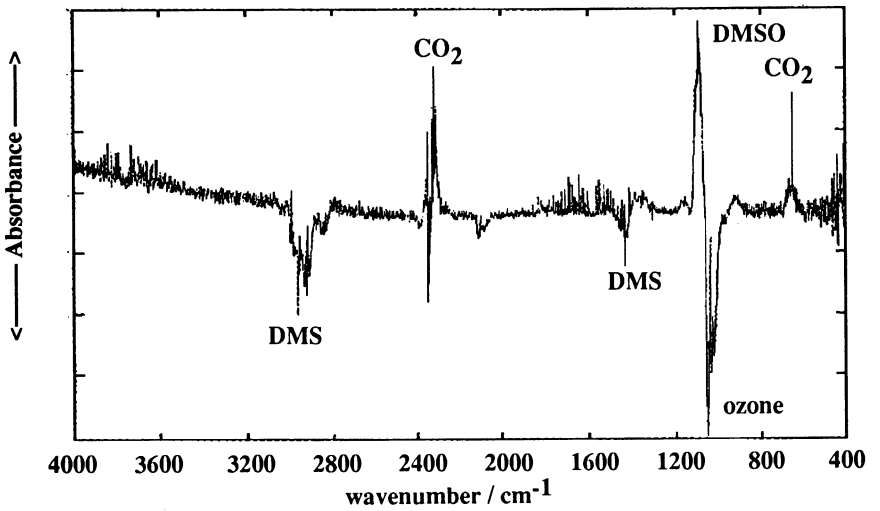

Fig. 4. Products of the BrO + DMS reaction: FTIR difference spectrum after 10 min irradiation of a Br_2/O_3/DMS reaction mixture at 760 torr total pressure of synthetic air and 298 ± 2K

The low atmospheric concentrations of IO and ClO in combination with their low rate coefficients with DMS make these reactions negligible as sinks for DMS in the atmosphere [Barnes et al., 1991a]. However, Barrie et al. [1988] have calculated that the BrO concentration could be as high as 10 ppt in the lower Arctic atmosphere which when taken in conjunction with the rate coefficient for its reaction with DMS at 298 K would give a residence time of $\tau \approx 4.2$ h for DMS. Since the residence time of DMS due to reaction with OH is of the order of 46 h, reaction of BrO might be a significant sink for DMS if the predictions of its atmospheric concentration prove to be valid.

An upper limit of $< 5.6 \times 10^{-14}$ cm^3 $molecule^{-1}$ s^{-1} has been determined for the reaction of BrO with CH_3SH and formation of HOBr has been observed. Maguin et al. [1991] have reported a value of $(1.0 \pm 0.5) \times 10^{-15}$ cm^3 $molecule^{-1}$ s^{-1} for the reaction of IO with CH_3SH and also observed HOI as product.

Products of the 254 nm photolysis of DMDS: The products of the 254 nm photolysis of DMDS as a function of the O_2 partial pressure at a total pressure of 1000 mbar ($N_2 + O_2$) as measured at 298 K after 10 min irradiation in a 1,080 l reaction chamber by FTIR are listed in Table 3. The major sulfur-containing compounds are SO_2 and CH_3SO_3H and the major carbon-containing products CO, HCHO, CH_3OH and CH_3OOH. The SO_2 yield falls from 90% to 65% on reducing the O_2 partial pressure from 200 to 13 mbar, however, for MSA the same variation increased the yield from 7 to 23%. Addition of excess O_3 to the reaction system had no effect on the product distribution with 200 mbar O_2, while with 13 mbar the SO_2 yield increases at the expense of the MSA yield (Table 4). This represents the first study in which MSA has been quantitatively detected in situ in laboratory experiments. The observation of CH_3OOH and CH_3OH provides strong evidence for the formation of CH_3OO radicals in the system.

Experiments in which hydrocarbons were added to the reaction system showed that OH radicals are being formed, and that the oxidation of CH_3S represents one of the OH sources. Other experiments, in which H_2O_2 was added as an additional OH source, showed that the MSA formation was correlated to the OH radical concentration. All the information supports that the further reactions of methyl sulfenic acid (CH_3SOH) formed in the reaction of OH with DMDS are the main source of DMDS in the present work, one possible mechanism is: $OH + CH_3SSCH_3 \rightarrow CH_3SOH + CH_3S$ followed by $CH_3SOH + CH_3SO_3 \rightarrow CH_3SO + CH_3SO_3H$. The results also support that the oxidation of CH_3S by O_2 or O_3 leads primarily to SO_2 formation and not MSA. The results have a number of implications for the oxidation of DMS:

Table 3. Products observed in DMDS/O_2/N_2 photolysis systems after 10 min irradiation as a function of the O_2 partial pressure at 760 torr total pressure and 298 K

O_2 (Torr)	N_2	DMDS Δppm	SO_2 ppm	%	MSA[a] ppm	%	HCHO[a] ppm	%	CH_3OOH ppm	%	CH_3OH ppm	%
150	610	1.52	2.69	**88**	0.21	**7**	2.26	**90**	0.30	**10**	0.07	**2**
100	660	1.21	2.19	**90**	0.21	**9**	1.99	**82**	0.22	**9**	0.05	**2**
50	710	1.08	1.75	**81**	0.35	**16**	1.70	**79**	0.14	**6**	0.05	**2**
25	735	0.76	1.15	**76**	0.27	**18**	1.17	**77**	0.06	**4**	0.05	**3**
10	750	0.26	0.26	**65**	0.09	**23**	0.28	**70**	0.02	**5**	0.01	**3**

a) Corrected for wall loss

Table 4. Molar percentage yields of products from DMDS/O_2/N_2 photolysis mixtures with and without the addition of 4 ppm O_3 for O_2 partial pressures of 150 and 10 torr O_2 and a total pressure of 760 torr

O_2 (torr)	O_3 ppm	DMDS Δppm	SO_2 ppm	%	MSA ppm	%	HCHO ppm	%	CH_3OOH ppm	%	CH_3OH ppm	%
150	0	152	2.69	**88**	0.21	**7**	2.26	**74**	0.20	**10**	0.07	**2**
150	4	0.90	1.65	**92**	0.10	**6**	1.06	**59**	0.40	**22**	0.20	**11**
10	0	0.20	0.26	**65**	0.09	**23**	0.28	**70**	0.02	**5**	0.01	**3**
10	4	1.70	2.80	**82**	0.50	**15**	2.20	**65**	0.60	**18**	0.20	**6**

- CH_3SOH has been postulated as one of the intermediates in the OH initiated oxidation of DMS.

$$OH + CH_3SCH_3 \rightarrow CH_3SCH_2 + H_2O$$
$$\rightarrow CH_3S(OH)CH_3 \rightarrow CH_3SOH + CH_3$$
$$\rightarrow CH_3OH + CH_3S$$

If CH_3SOH is being formed in the reaction of OH with DMS, the results from the present work suggest that high yields of MSA should be observed. However, the available product data from chamber studies [Yin et al., 1990 and references therein] show that high yields of MSA are only obtained in the presence of NO_x. In NO_x free systems the detected yields of MSA are $\leq$ 4% [Barnes et al., 1988; Martinet, 1989; Barnes et al.,

1991b]. This would suggest that CH_3SOH is probably not, therefore, a major intermediate in the OH initiated oxidation of DMS. Otherwise high yields of MSA would have been detected.

- The high yields of MSA generally observed in smog chamber studies of the OH initiated oxidation of DMS in the presence of NO_x are probably due to effective oxidation of CH_3S by NO_2 to CH_3SO_2 or CH_3SO_3. Preliminary experiments in this laboratory suggest the further oxidation of CH_3SO_2 results in high yields of MSA even in the absence of NO_x.

- The addition of O_3 to the reaction system has very little influence on the product distribution. Since the addition of O_3 effectively scavenges the CH_3S radicals, one might expect high yields of MSA if CH_3S is oxidized to CH_3SO_3. However, the yield of MSA remains low, which suggests that the C-S bond is being cleaved early in the oxidation chain. This observation is in agreement with the recent results of Dominé et al. [1992].

CONCLUSIONS

The reactions of chlorine and bromine atoms with DMS may be of importance in the Arctic marine boundary layer. With the rate coefficients presented here atmospheric concentrations of Cl and Br of approximately 10^4 and 10^8 atoms cm^{-3}, respectively, would put these reactions on equal par with reaction with OH radicals as loss processes for DMS. The product analyses at room temperature show that in air both direct abstraction and complex pathways are operative. At the temperatures occurring in the Arctic it is to be expected that the addition pathway, resulting apparently in DMSO formation, will increasingly dominate. Apart from detailed product studies on the reactions of Cl and Br with DMS as a function of temperature, further studies are needed on the effect of O_2 on the Br + DMS reaction, and also as a function of temperature.

With the exception of the reaction of BrO with DMS the reactions of other halogen halides with DMS are probably of negligible importance for the atmospheric oxidation of DMS. If the atmospheric BrO concentrations is as large as recent calculations suggest, then the BrO initiated oxidation of DMS could catalyze the O_3 depletion:

$$\begin{array}{lll} Br + O_3 & \rightarrow & BrO + O_2 \\ BrO + DMS & \rightarrow & Br + DMSO \\ \hline \text{net reaction} \quad DMS + O_3 & \rightarrow & DMSO + O_2 \end{array}$$

The results from the studies on the photolysis products of DMDS suggest that CH_3SOH is not a major intermediate in the OH initiated oxidation of DMS at least not at room temperature. Further, the oxidation of CH_3S with O_2 and O_3 probably results in cleavage of the C-S bond early in the oxidation chain, which precludes the formation of MSA. High yields of MSA are only to be expected when CH_3S is oxidized to either CH_3SO_2 of CH_3SO_3 such as appears to be the case with NO_2 as the oxidant. Therefore, in the atmosphere high yields of MSA are to be expected in areas with high NO_x. This hypothesis is supported by recent field measurements [Barnes et al., 1991a; Mihalopoulos et al., 1992].

REFERENCES

Aneja, V.P., W.P. Cooper, Biogenic sulfur emissions: A review, in biogenic sulfur in the environment, E.S. Saltzman., W.-J. Cooper (Eds), *ACS Symposium Series, American Chemical Society*, Washington ,DC, No. 393, pp. 2-13, 1989.

Barrie, L.A., J.W. Bottenheim, R.C. Schnell, P.J. Crutzen, R.A. Rasmussen, Ozone destruction and photochemical reactions at polar sunrise in the lower Arctic atmosphere, *Nature, 334*: 138-141, 1988.

Barnes, I., K.H. Becker, N. Mihalopoulos, An FTIR study of the photooxidation of dimethyl disulfide, *J. Atmos. Chem.*, to be submitted, 1992.

Barnes, I., B. Bonsang, T. Brauers, P. Carlier, R.A. Cox, H.P. Dorn, M.E. Jenkin, G. Le Bras, U. Platt, Laboratory and field studies of oxidation processes occurring in the atmospheric marine boundary layer, *Air Pollution Research Report 35, Commission of the European Communities*, ISBN 2-87263-064-3, 1991a.

Barnes, I., V. Bastian, K.H. Becker, R.D. Overath, Kinetic study of the reactions of IO, BrO and ClO with dimethylsulfide, *Int. J. Chem. Kinetics, 23*, 579-591, 1991b.

Barnes, I., K.H. Becker, P. Carlier, G. Mouvier, J.L. Jourdain, G. Laverdet, G. Le Bras, Impact of halogen oxides on dimethyl sulfide oxidation in the marine atmosphere, in biogenic sulfur in the environment, E.S. Saltzman, W.J. Cooper, (Eds), *ACS Symposium Series No. 393*, pp 464-475, 1989a.

Barnes, I., V. Bastian, K.H. Becker, and D. Martin, Fourier Transform IR studies of the reactions of dimethyl sulfoxide with OH, NO_3 and Cl atoms, in biogenic sulfur in the environment, E.S. Saltzman, W.J. Cooper, (Eds), *ACS Symposium Series No. 393*, pp 476-488, 1989b.

Barnes, I., V. Bastian, K.H. Becker, R.D. Overath, Z. Tong, Rate constants for the reactions of Br atoms with a series of alkanes, alkenes, and alkynes in the presence of O_2, *Int. J. Chem. Kinetics, 21*, 499-517, 1989c.

Barnes, I., V. Bastian, K.H. Becker, Kinetics and mechanisms of the reaction of OH radicals with dimethyl sulfide, *Int. J. Chem. Kinetics, 20*, 415-431, 1988.

Barnes, I., K.H. Becker, P. Carlier, G. Mouvier, FTIR study of the DMS/NO_2/I_2N_2 photolysis system: The reaction of IO radicals with DMS, *Int. J. Chem. Kinetics, 19*, 489-501, 1987.

Barnes, I., V. Bastian, K.H. Becker, E.H. Fink, Th. Klein, V. Kriesche, W. Nelsen, A. Reimer, and F. Zabel, Untersuchung der reaktionssysteme $NO_X/ClO_X/HO_X$ unter troposphärischen und stratosphärischen Bedingungen, *GSF München*, BPT-Bericht 11/84, ISSN 0176/077, 1984.

Berresheim H., M.O. Andreae, G.P. Ayers, R.W. Gillett, Distributions of biogenic sulfur compounds in the remote southern hemisphere, in E.S. Saltzman, W.J. Cooper (Eds), *Biogenic Sulfur in the Environment, ACS Symposium Series, American Chemical Society*, Washington, DC, No. 393, pp 352-366, 1989.

Berresheim H., M.O. Andreae, G.P. Ayers, R.W. Gillett, J.T. Merrill, V.J. Davis, W.L. Chameides, Airborne measurements of dimethylsulfide, sulfur dioxide, and aerosol ions over the southern ocean south of Australia, *J. Atmos. Chem., 10*, 341-370, 1990.

Daykin, E.P., P.H. Wine, Rate of reaction of IO radicals with dimethylsulfide, *J. Geophys. Res., 95, D11*, 18.547-18.553, 1990.

DeMore, W.B., S.P. Sander, D.M. Golden, R.F. Hampson, M.J. Kurylo, C.J. Howard, A.R. Ravishankara, C.E. Kolb, M.J. Molina, Chemical kinetics and photochemical data for use in stratospheric modeling, *JPL Publication 92-20*, 1992.

Dominé, F., A.R. Ravishankara, C.J. Howard, Kinetics and mechanisms of the reactions of CH_3S, CH_3SO, CH_3SS with O_3 at 300 K and low pressure, *J. Phys. Chem., 96*, 2171-2178, 1992.

Le Bras, G., F. Maguin, A. Mellouki, I.T. Lancar, C. Balestra, in *Laboratory and Field Studies of Oxidation Processes Occurring in the Atmospheric Marine Boundary Layer*, I. Barnes, B. Bonsang, T. Brauers, P. Carlier, R.A. Cox, H.P. Dorn, M.E. Jenkin, G. Le Bras, U. Platt, (Eds.) Air Pollution Research Report 35, Commission of the European Communities, ISBN 2-87263-064-3, pp 106-116, 1991.

Maguin, F., A. Mellouki, G. Laverdet, G. Poulet, and G. Le Bras, Kinetics of the reactions of the IO radical with dimethyl sulfide, methanethiol, ethylene and propylene, *Int. J. Chem. Kinetics, 23*, 237-245, 1991.

Martin, D., J.L. Jourdain, G. Laverdet and G. Le Bras, Kinetic study of the reaction of IO with CH_3SCH_3, *Int. J. Chem. Kinetics, 19*, 503-512, 1987.

Martinet, A., Etudes cinetiques, sous conditions atmospheriques simulees, de reactions elementaires intervenant dans la photooxydation de precurseurs d'acidite en Milieu marin, *Ph.D. Thesis*, l'Université Paris VII, 1989.

McConnell, J.C., G.S. Henderson, L. Barrie, J. Bottenheim, H. Niki, C.H. Langford, and E.M.J. Templeton, Photochemical bromine production implicated in Arctic boundary-layer ozone production, *Nature, 355*, 150-152, 1992.

Mihalopoulos, N., B.C., Nguyen, C. Boissard, J.M. Campin, J.P. Putaud, S. Belviso, I. Barnes, K.H. Becker, Field study of dimethylsulfide oxidation in the boundary layer: Variations of dimethylsulfide, methanesulfonic acid, sulfur dioxide, non-sea-salt sulfate and aitken nuclei at a coastal site, *J. Atmos. Chem., 14*, 459-477, 1992.

Nielsen, O.J., H.W. Sidebottom, L. Nelson, O. Rattigan, J.J. Treacy, and D.J. O'Farrell, Rate constants for the reactions of OH radicals and Cl atoms with diethyl sulfide, di-n-propyl sulfide, and di-n-butyl sulfide, *Int. J. Chem. Kinetics, 22*, 603-612, 1990.

Overath, R., *Ph.D. Thesis*, Physikalische Chemie / FB 9, Bergische Universität - Gesamthochschule Wuppertal, FRG, 1991.

Tyndall, G.S., A.R. Ravishankara, Atmospheric oxidation of reduced sulfur species, *Int. J. Chem. Kinetics, 23*, 483-527, 1991.

Yin, F., D. Grosjean, J.H. Seinfeld, Photooxidation of dimethyl sulfide and dimethyl disulfide, I: Mechanism development, *J. Atmos. Environ., 11*, 309-364.

HALOGEN AND SULFUR REACTIONS RELEVANT TO POLAR CHEMISTRY

P. H. Wine,[1,2,3] J. M. Nicovich,[3] R. E. Stickel,[3] Z. Zhao,[2]
C. J. Shackelford,[4] K. D. Kreutter,[1,3,5] E. P. Daykin,[3,6] and S. Wang[3,7]
Georgia Institute of Technology
Atlanta, GA 30332, U.S.A.

INTRODUCTION

It is widely hypothesized that catalytic cycles involving BrO_X species play an important role in the episodic destruction of ground-level ozone which is observed in the springtime Arctic boundary layer, although the exact mechanism for production of BrO_X radicals remains an open question [Barrie et al., 1988; Bottenheim et al., 1990; Finlayson-Pitts et al., 1990; McConnell et al., 1992]. The critical evidence linking ozone depletion with BrO_X chemistry is an observed negative correlation between ozone and filterable bromine [Bottenheim et al., 1990; Kieser et al., 1992]. In a recent field study of springtime Arctic boundary layer chemistry [Kieser et al., 1992], ozone concentrations and ethane concentrations were found to be correlated; this observation suggests that chlorine atoms (which react rapidly with ethane) may also be an important catalyst for ozone destruction under springtime Arctic conditions.

The possibility that reactions occurring on surfaces of sea-salt aerosol particles can lead to significant production of halogen atoms in the marine boundary layer has received considerable attention in recent years. Production of photochemically labile $X_2(g)$ (X = Cl,Br) via heterogeneous degradation of ozone (possibly involving free radical intermediates) is one suggested pathway for generation of gas phase bromine atoms [McConnell et al., 1992] and chlorine atoms [Zetzsch et al., 1988; Behnke and Zetzsch, 1989; Keene et al., 1990]; however, recent laboratory and modeling studies [Behnke and Zetzsch, 1990; Chameides and Stelson, 1992a, 1992b] suggest that, at least in the case of chlorine, this pathway is not important in the atmosphere. On the other hand, it appears that $ClNO_2$, generated via heterogeneous reaction of N_2O_5 vapor with moist NaCl(s), may represent a

1 School of Chemistry and Biochemistry
2 School of Earth and Atmospheric Sciences
3 Electro-optics and Physical Sciences Laboratory, GTRI
4 School of Physics
5 Now at Dept. of Biochemistry, Brandeis Univ., Waltham, MA 02254
6 Now at EG&G, P. O. Box 1912, MS A1-24, Las Vegas, NV 89125
7 Now at Dalian Institute of Chemical Physics, Chinese Academy of Sciences, P.O. Box 110, Dalian, Peoples Republic of China

NATO ASI Series, Vol. I 7
The Tropospheric Chemistry of Ozone in the Polar Regions
Edited by H. Niki and K. H. Becker

photolytic precursor for atmospherically significant levels of atomic chlorine, even in the remote marine boundary layer where NO_x levels are typically quite low [Behnke and Zetzsch, 1990; Zetzsch and Behnke, 1992; Ganske et al., 1992]. The analogous reaction of N_2O_5(g) with NaBr(s) is one proposed source of springtime Arctic BrO_x radicals [Finlayson-Pitts et al., 1990], although it has been pointed out that generation of sufficient levels of the photolytic precursor $BrNO_2$ would require a longer residence time for Arctic air than is actually observed [McConnell et al., 1992; Patterson and Husar, 1981]. The frequency of ice fogs in the springtime Arctic boundary layer suggests that heterogeneous chemistry similar to that which occurs in polar stratospheric clouds [Poole et al., 1992] may result in partitioning of XO_x (X = Cl,Br) species largely into the reactive forms X and XO.

Dimethylsulfide (CH_3SCH_3, DMS) is a key atmospheric sulfur species. Roughly half the global flux of sulfur into the atmosphere is thought to be natural in origin [Cullis and Hirschler, 1980; Schwartz, 1988] and a significant fraction of all natural sulfur enters the atmosphere as DMS volatilized from the oceans [Andreae, 1986; Bates et al., 1987]. Levels of DMS in polar regions typically peak during springtime when microorganisms which produce DMS are exposed to light after a long dark period [H. Berresheim, private communication]. Hence, under conditions which exist in the springtime Arctic marine boundary layer, reactions of chlorine and bromine atoms with DMS may play an important role in coupling the halogen and sulfur cycles.

Discussed below are the results of recent laboratory studies we have carried out to investigate the kinetics and mechanisms of the X + DMS reactions (X = Cl,Br) [Stickel et al., 1992; Nicovich et al., 1992a]. We also present estimates of sea level (i.e., 760 torr) unimolecular decomposition rates for $BrNO_2$ which are based on kinetic and thermochemical information obtained in our recent study of the Br + NO_2 association reaction [Kreutter et al., 1990].

THE CL + DMS REACTION

Time-resolved resonance fluorescence detection of chlorine atoms following 266 nm laser flash photolysis of $Cl_2CO/DMS/N_2$ mixtures has been employed to study the kinetics of R1 over the temperature and pressure ranges 240-421K and 3-700 torr.

$$Cl + CH_3SCH_3 \rightarrow \text{products} \qquad (1)$$

A complete description of the experimental approach can be found in a recent publication describing our study of the Cl + CS_2 reaction [Nicovich et al., 1990]. In agreement with a recent competitive kinetics study [Nielsen et al., 1990], we find that R1 is very fast, i.e., reaction occurs on essentially every Cl + DMS encounter. Measured rate coefficients at

240K, 297K, and 421K are plotted as a function of pressure in Figure 1. The reaction rate is found to increase with decreasing temperature as would be expected for a very fast reaction whose rate is determined by the magnitude of long range attractive forces between the reactants. The somewhat surprising aspect of the data in Figure 1 is our observation of a clear pressure dependence for k_1. It appears that reaction 1 occurs via both pressure-independent and pressure-dependent pathways; the pressure-dependent pathway must involve collisional stabilization of a $(CH_3)_2S$-Cl adduct.

To gain further insight into the mechanism for reaction 1, we carried out a separate set of experiments where laser flash photolytic (LFP) production of Cl (via 248 nm photolysis of phosgene) was coupled with tunable diode laser absorption spectroscopy (TDLAS) to

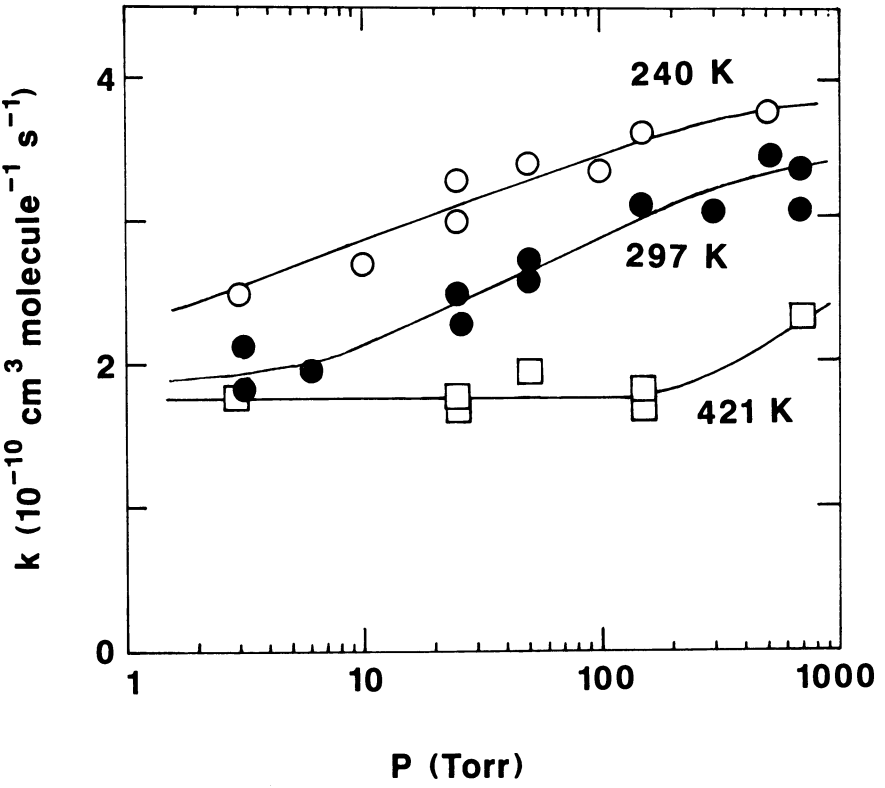

Fig. 1. Rate constants for the Cl + $(CH_3)_2S$ reaction at three temperatures plotted as a function of pressure. The solid lines are "eyeball" fits to the data; their significance is simply as an aid in visualizing the observed pressure dependencies.

Table 1. Yield of HCl from the Cl + DMS reaction as a function of pressure at T = 297 K

Buffer Gas	P(torr)	N[(a)]	HCl Yield
CO_2	0.6	2	0.98
	2.0	19	0.89
	5.0	4	0.79
	10.1	4	0.74
	26	2	0.62
N_2[(b)]	5.0	2	0.85
	10.0	2	0.80
	25	2	0.68
	50	2	0.59
	100	2	0.54
	203	2	0.51

(a) N ≡ number of experiments.
(b) includes one torr of CO_2

measure the HCl product yield at 297K as a function of pressure. A detailed description of the LFP-TDLAS apparatus is given elsewhere [Stickel et al., 1992]. To obtain the HCl yield we carried out back-to-back experiments where the photolytically produced Cl reacted with DMS, then with ethane (C_2H_6); the yield of HCl from the Cl + C_2H_6 reaction is known to be unity. In all experiments, at least 0.6 torr CO_2 was present in the reaction mixture to (a) f acilitate rapid equilibration of the atomic chlorine spin-orbit states and (b) facilitate rapid relaxation of any HCl formed in the v = 1 level. Typical experimental HCl appearance temporal profiles are presented elsewhere [Stickel et al., 1992]. The results of the yield experiments are summarized in Table 1.

The HCl yield approaches unity as P → 0 but decreases with increasing pressure. Although extrapolation of kinetic and yield data to zero pressure is non-trivial, examination of the results in Figure 1 and Table 1 strongly suggests that the following relationship is obeyed:

$$\Phi(P) = k_1(P \rightarrow 0) / k_1 P = 1$$

where $\Phi(P)$ is the HCl yield at pressure P.

The experiments described above demonstrate that hydrogen abstraction is the dominant pathway for reaction 1 in the low pressure limit. With increasing pressure, stabilization of a $(CH_3)_2SCl$ adduct apparently becomes competitive with the hydrogen

abstraction pathway. Under the pressure and temperature conditions of the springtime Arctic boundary layer, it appears that $k_1 \sim 4 \times 10^{-10}$ cm^3 $molecule^{-1}$ s^{-1} and that 60-80% of the overall reaction proceeds via the adduct-forming pathway. The fate of the stabilized adduct remains uncertain, although it clearly does not dissociate to Cl or HCl on the time scale of our experiments (several milliseconds). One interesting possibility is reaction with O_2 to form $(CH_3)_2SO + ClO$; this reaction could represent an unrecognized source of atmospheric $(CH_3)_2SO$. Another energetically feasible pathway for degradation of $(CH_3)_2SCl$ is unimolecular decomposition to $CH_3S + CH_3Cl$, a process which could possibly represent an important source of atmospheric methyl chloride. Clearly, the atmospheric fate of $(CH_3)_2SCl$ warrants further investigation.

THE BR + DMS REACTION

Time-resolved resonance fluorescence detection of bromine atoms following 266 nm laser flash photolysis of $CF_2Br_2/DMS/H_2/N_2$ mixtures has been employed to study the kinetics of reaction 2 as a function of temperature and pressure.

$$Br + CH_3SCH_3 \rightarrow \text{products} \qquad (2)$$

A complete description of the experimental approach can be found in a recent publication describing our studies of the reactions $Br + H_2S \rightleftarrows SH + HBr$ and $Br + CH_3SH \rightleftarrows CH_3S + HBr$ [Nicovich et al., 1992b]. Distinctly different kinetic behavior is observed in the two temperature regimes 260-310K and 375-425K.

In the low temperature regime, i.e., 260-310K, the dominant reaction pathway is found to be reversible adduct formation:

$$Br + (CH_3)_2S + M \rightarrow (CH_3)_2SBr + M \qquad (2a)$$
$$(CH_3)_2SBr + M \rightarrow Br + (CH_3)_2S + M \qquad (-2a)$$

Observation of the kinetics of the approach to equilibrium allows evaluation of $k_{2a}(P,T)$, $k_{-2a}(P,T)$ and, therefore, $K_{eq}(T)$ ($K_{eq} = k_{2a}/k_{-2a}$). Measured rate coefficients are summarized in Table 2. A van't Hoff plot of $\ln K_p$ versus T^{-1} is shown in Figure 2. From the slope of the van't Hoff plot (and a small heat capacity correction) we obtain a value for the enthalpy change associated with reaction 2a, i.e., the $(CH_3)_2S$-Br bond strength; the result is $\Delta H_{298} = -14.5 \pm 1.2$ kcal $mole^{-1}$. We have recently carried out similar measurements of the $(CH_3)_2S$-OH bond strength [Hynes et al., 1992] and find it to be approximately equal to the

Table 2. Rate constants for the reactions Br + $(CH_3)_2S$ + M $\rightleftarrows$ $(CH_3)_2SBr$ + M as a function of temperature[a]

T	P	k_{2a}	k_{-2a}	notes
263	50	4.49	410	
265	50	3.90	380	
267	200	8.25	1,350	
268	50	6.07	730	(b)
269	200	10.1	2,050	(b)
272	25	2.63	500	
274	50	4.16	920	
274	100	5.70	1,380	
274	200	7.49	2,400	
274	400	10.2	3,150	
274	600	11.9	3,600	
285	50	3.18	2,360	
285	200	6.70	5,900	
291	50	2.96	3,210	
291	200	6.69	7,730	
298	50	2.74	5,150	(c)
299	50	3.44	7,430	(b)
300	25	1.77	3,750	
300	50	2.62	5,920	
310	25	1.43	6,810	
310	50	2.11	10,500	

(a) Units are T(K), P(torr), $k_{2a}(10^{-11}$ cm^3 molecule^{-1}s^{-1}), $k_{-2a}(s^{-1})$.
(b) Reactant was DMS-d_6.
(c) Photolyte was Br_2 (it was CF_2Br_2 in all other experiments); Br_2 was photolyzed at 355 nm.

$(CH_3)_2S$-Br bond strength. Hence, a reasonable "guesstimate" for the $(CH_3)_2S$-Cl bond strength is 14-15 kcal mole^{-1}.

At temperatures above 375K, $(CH_3)_2SBr$ decomposition is so rapid that the addition reaction effectively does not occur. In this temperature regime sulfide reactivity toward atomic bromine follows the trend $(C_2H_5)_2S > (CH_3)_2S > (CD_3)_2S$, strongly suggesting that the dominant reaction pathway is hydrogen abstraction:

$$Br + CH_3SCH_3 \rightarrow HBr + CH_3SCH_2 \qquad (R2b)$$

Interestingly, we measure an activation energy for reaction 2b of 5.0 kcal mole^{-1}, while the literature value for CH_3SCH_2 heat of formation [Shum and Benson, 1985] suggests that

reaction 2b is endothermic by 9.0 kcal mole^{-1}; hence, our kinetic results strongly suggest that the C-H bond strength in DMS is 2-4 kcal mole^{-1} weaker than currently thought.

Extrapolation of our kinetic data to conditions typical of the springtime Arctic boundary layer (760 torr, 230-270K) suggests that under the conditions of interest (a) addition of Br to DMS is four to five orders of magnitude faster than hydrogen abstraction; (b) the rate coefficient for the addition reaction is (1.3 ± 0.2) x 10^{-10} cm^3 molecule^{-1} s^{-1};

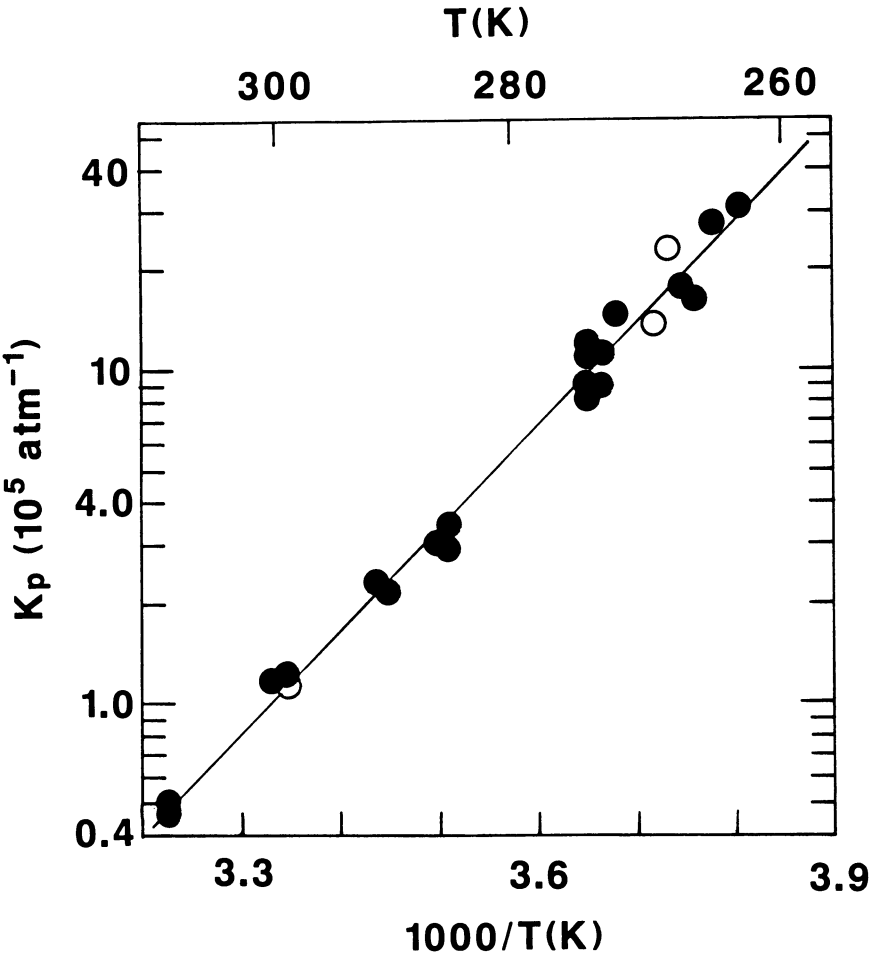

Fig. 2. van't Hoff plot for the equilibrium Br + $(CH_3)_2S \rightleftarrows (CH_3)_2SBr$. Open circles are data obtained using $(CD_3)_2S$ as the sulfide reactant. Solid line is obtained from a least squares analysis; the slope gives ΔH(334K) = -14.6 ± 1.1 kcal mole^{-1} while the intercept gives ΔS(334K) = -22.9 ±3.9 cal mole^{-1} deg^{-1} (errors are 2σ and represent precision only).

and (c) the lifetime of the $(CH_3)_2SBr$ adduct toward unimolecular decomposition is 0.01-0.0001 seconds. The short lifetime of $(CH_3)_2SBr$ toward unimolecular decomposition suggests that the only atmospheric species capable of scavenging $(CH_3)_2SBr$ is O_2.

$$(CH_3)_2SBr + O_2 \rightarrow (CH_3)_2SO + BrO \qquad (3)$$

To search for BrO production from reaction 3, a separate set of experiments was carried out (at 297K) where time-resolved longpath absorption detection in the near ultraviolet was coupled with 248 nm laser flash photolysis of $CF_3Br/DMS/H_2/N_2/O_2$ mixtures; a description of the apparatus is given elsewhere [Daykin and Wine, 1990]. Production of BrO was not observed, but a strong, broad, unstructured absorption feature with $\lambda_{max} \sim 370$ nm was observed. Studies of the appearance kinetics of the absorption feature demonstrate rather conclusively that it is due to $(CH_3)_2SBr$, i.e., a plot of pseudo-first order appearance rate versus [DMS] is linear with slope equal to the (previously measured) k_2 and intercept equal to the (previously measured) k_{-2a}. At 50 torr total pressure the strength and temporal behavior of the transient absorption signal was independent of whether N_2 or O_2 was employed as the buffer gas; this observation suggests that $k_3 < 3 \times 10^{-16}$ cm^3 $molecule^{-1}$ s^{-1}. For assessing the potential role of reaction 3 in atmospheric chemistry under springtime Arctic boundary layer conditions, it will be necessary to extend the time-resolved absorption studies to higher O_2 partial pressures and lower temperatures.

UNIMOLECULAR DECOMPOSITION OF $BrNO_2$

As mentioned in the introduction, Finlayson-Pitts et al. [1990] have proposed that $BrNO_2$ (nitryl bromide), formed via the heterogeneous reaction of N_2O_5 with NaBr on the surface of sea salt aerosol particles, may be an important photolytic precursor to BrO_x radicals in the springtime Arctic boundary layer. However, McConnell et al. [1992] have pointed out a potential problem with the Finlayson-Pitts et al. proposal -- the residence time for an air mass in the Arctic may not be long enough for sufficient buildup of $BrNO_2$ to occur prior to polar sunrise.

Recently, we reported a detailed study of the kinetics and thermochemistry of $Br + NO_2$ association reaction [Kreutter et al., 1990]. Given in Table 3 are upper and lower limit lifetimes toward $BrNO_2$ unimolecular decomposition (i.e., k_4^{-1}) under springtime Arctic boundary layer conditions; the lifetimes are obtained by extrapolation of our data [Kreutter et al., 1990] to 760 torr and low temperature.

$$BrNO_2 + N_2 \rightarrow Br + NO_2 + N_2 \qquad (4)$$

The range of values for k_4^{-1} which are consistent with our data is rather large because the possible roles of the (short lived) isomer BrONO and/or excited electronic state potential energy surfaces could not be quantified due to lack of information. Nonetheless, the data in Table 3 lead to an important conclusion. At temperatures typical of the wintertime and springtime Arctic, i.e., 220 - 260 K, the lifetime of $BrNO_2$ toward unimolecular decomposition is rather short, i.e., usually less than one day. Hence, bromine atoms would be released from the $BrNO_2$ reservoir not only when the sun comes up, but continuously during the dark $BrNO_2$ production period.

Table 3. Lifetime of $BrNO_2$ toward unimolecular decomposition at atmospheric pressure

		k_4^{-1} (days)
T(K)	lower limit	upper limit
200	2.1	840
220	0.054	5.8
240	0.0021	0.14
260	0.00013	0.0057
280	0.000014	0.00029
300	0.0000024	0.000027

Acknowledgments: The research described in this paper was supported by the NSF Atmospheric Chemistry Program (grant ATM-9104807), the NASA Upper Atmosphere Research Program (grant NAGW-1001), and the Georgia Tech Research Institute (internal grant E-8904-038).

REFERENCES

Andreae, M. O., The ocean as a source of atmospheric sulfur compounds, in *The Role of Air-Sea Exchange in Geochemical Cycling*, edited by P. Buat-Menard, pp. 331-362, D. Reidel, Hingham, MA, 1986.

Barrie, L. A., J. W. Bottenheim, R. C. Schnell, P. J. Crutzen, and R. A. Rasmussen, Ozone destruction and photochemical reactions at polar sunrise in the lower Arctic atmosphere, *Nature*, *334*, 138-141, 1988.

Bates, T. S., J. D. Cline, R. H. Gammon, and S. R. Kelly-Hansen, Regional and seasonal variations in the flux of oceanic dimethylsulfide to the atmosphere, *J. Geophys. Res.*, *92*, 2930-2938, 1987.

Behnke, W. and C. Zetzsch, Heterogeneous formation of chlorine atoms from various aerosol in the presence of O_3 and HCl, *J. Aerosol Sci.*, *20*, 1167-1170, 1989.

Behnke, W. and C. Zetzsch, Heterogeneous photochemical formation of Cl atoms from NaCl aerosol, NO_x, and ozone, *J. Aerosol Sci.*, *21*, *Suppl. 1*, s229-s232, 1990.

Bottenheim, J. W., L. A. Barrie, E. Atlas, L. E. Heidt, H. Niki, R. A. Rasmussen, and P. B. Shepson, Depletion of lower tropospheric ozone during Arctic spring: The polar sunrise experiment 1988, *J. Geophys. Res.*, *95*, 18,555-18,568, 1990.

Chameides, W. L. and A. W. Stelson, Aqueous-phase chemical processes in deliquescent seasalt aerosols, *Ber. Bunsenges. Phys. Chem.*, *96*, 461-470, 1992a.

Chameides, W. L. and A. W. Stelson, Aqueous-phase chemical processes in deliquescent seasalt aerosols: A mechanism that couples the atmospheric cycles of S and seasalt alkalinity, *J. Geophys. Res.*, in press, 1992b.

Cullis, C. F., and M. M. Hirschler, Atmospheric sulfur: Natural and man-made sources, *Atmos. Environ.*, *14*, 1263-1278, 1980.

Daykin, E. P., and P. H. Wine, Kinetics of the reactions of IO radicals with NO and NO_2, *J. Phys. Chem.*, *94*, 4528-4535, 1990.

Finlayson-Pitts, B. J., F. E. Livingston, and H. N. Berko, Ozone destruction and bromine photochemistry at ground level in the Arctic spring, *Nature*, *343*, 622-625, 1990.

Ganske, J. A., H. N. Berko, and B. J. Finlayson-Pitts, Absorption cross sections for gaseous $ClNO_2$ and Cl_2 at 298K: Potential organic oxidant source in the marine troposphere, *J. Geophys. Res.*, *97*, 7651-7656, 1992.

Hynes, A. J., A. J. Pounds, T. McKay, J. D. Bradshaw, and P. H. Wine, Detailed mechanistic studies of the OH initiated oxidation of biogenic sulfur compounds under atmospheric conditions, *Twelfth International Symposium on Gas Kinetics*, paper no. G6, Reading, United Kingdom, 1992.

Keene, W. C., A. A. P. Pszenny, D. J. Jacob, R. A. Duce, J. N. Galloway, J. J. Schultz-Tokos, H. Sievering, and J. F. Boatman, The geochemical cycling of reactive chlorine through the marine troposphere, *Global Biogeochem. Cycles*, *4*, 407-430, 1990.

Kieser, B. N., T. Sideris, H. Niki, J. W. Bottenheim, and W. R. Leaitch, Spring 1989 observations of tropospheric chemistry in the Canadian high Arctic, *Atmos. Environ.*, in press, 1992.

Kreutter, K. D., J. M. Nicovich, and P. H. Wine, Kinetics and thermochemistry of the $Br(^2P_{3/2})$ + NO_2 association reaction, *J. Phys. Chem.*, *95*, 4020-4028, 1991. Correction, *J. Phys. Chem.*, *96*, 7146, 1992.

McConnell, J. C., G. S. Henderson, L. Barrie, J. Bottenheim, H. Niki, C. H. Langford, and E. M. J. Templeton, Photochemical bromine production implicated in Arctic boundary-layer ozone depletion, *Nature*, *355*, 150-152, 1992.

Nicovich, J. M., C. J. Shackelford, and P. H. Wine, Kinetics and thermochemistry of reversible adduct formation in the reaction of $Cl(^2P_J)$ with CS_2, *J. Phys. Chem.*, *94*, 2896-2903, 1990.

Nicovich, J. M., C. J. Shackelford, K. D. Kreutter, E. P. Daykin, S. Wang, A. Jefferson, and P. H. Wine, Kinetic and mechanistic studies of the reactions of atomic bromine with dimethylsulfide, to be published, 1992a.

Nicovich, J. M., K. D. Kreutter, C. A. van Dijk, and P. H. Wine, Temperature-dependent kinetics studies of the reactions $Br(^2P_{3/2})$ + $H_2S \rightleftarrows$ SH + HBr and $Br(^2P_{3/2})$ +

$CH_3SH \rightleftarrows CH_3S + HBr$. Heats of formation of SH and CH_3S radicals, *J. Phys. Chem.*, *96*, 2518-2528, 1992b.

Nielsen, O. J., H. W. Sidebottom, L. Nelson, O. Rattigan, J. J. Treacy, and D. J. O'Farrell, Rate constants for the reactions of OH radicals and Cl atoms with diethyl sulfide, di-n-propyl sulfide, and di-n-butyl sulfide, *Int. J. Chem. Kinet.*, *22*, 603-612, 1990.

Patterson, D. E. and R. B. Husar, A direct simulation of hemispherical transport of pollutants, *Atmos. Environ.*, *15*, 1479-1482, 1981.

Poole, L. R., R. L. Jones, M. J. Kurylo, and A. Wahner, Heterogeneous processes: Laboratory, field, and modeling studies, in *Scientific Assessment of Ozone Depletion: 1991*, edited by D. L. Albritton, R. T. Watson, S. Solomon, R. F. Hampson, and F. Ormond, chapter 3, World Meteorological Organization, Global Ozone Research and Monitoring Project - Report No. 25, 1992.

Schwartz, S. E., Are global cloud albedo and climate controlled by marine phytoplankton?, *Nature*, *336*, 441-445, 1988.

Shum, L. G. S., and S. W. Benson, Iodine catalyzed pyrolysis of dimethyl sulfide. Heats of formation of CH_3SCH_2I, the CH_3SCH_2 radical, and the pibond energy in CH_3S, *Int. J. Chem. Kinet.*, *17*, 277-292, 1985.

Stickel, R. E., J. M. Nicovich, S. Wang, Z. Zhao, and P. H. Wine, Kinetic and mechanistic study of the reaction of atomic chlorine with dimethyl sulfide, *J. Phys. Chem.*, in press, 1992.

Zetzsch, C., G. Pfahler, and W. Behnke, Heterogeneous formation of chlorine atoms from NaCl in a photosmog system, *J. Aerosol. Sci.*, *19*, 1203-1206, 1988.

Zetzsch, C. and W. Behnke, Heterogeneous photochemical sources of atomic Cl in the troposphere, *Ber. Bunsenges. Phys. Chem.*, *96*, 488-493, 1992.

REACTIONS OF BrO RADICALS RELEVANT TO POLAR CHEMISTRY

G. Le Bras
Laboratoire de Combustion et Systèmés Rèactifis
CNRS - 45071 - Orléans - Cedex 2
France

INTRODUCTION

The ozone destruction observed at polar sunrise in the lower Arctic atmosphere has been suggested to be linked to catalytic reactions of BrO_x (Br, BrO) radicals [Barrie et al., 1988]. The main catalytical cycle was considered to be the following:

$$\begin{array}{lll} BrO + BrO & \rightarrow & 2Br + O_2 \\ 2(Br + O_3 & \rightarrow & BrO + O_2) \\ \hline \text{net} \quad 2O_3 & \rightarrow & 3O_2 \end{array} \qquad \text{(I)}$$

The potentially important role of BrO_x radicals in the Arctic ozone chemistry was recently confirmed from direct field observations of BrO radicals (Platt et al. 1992).

In relation to these atmospheric observations, laboratory kinetic studies of BrO reactions are reported in this paper. They include the self-combination reaction of BrO occurring in the above cycle, and also the $BrO + HO_2$ reaction which is involved in the following cycle:

$$\begin{array}{lll} BrO + HO_2 & \rightarrow & HOBr + O_2 \\ HOBr + h\nu & \rightarrow & OH + Br \\ OH + O_3 & \rightarrow & HO_2 + O_2 \\ Br + O_3 & \rightarrow & BrO + O_2 \\ \hline \text{net} \quad 2O_3 & \rightarrow & 3O_2 \end{array} \qquad \text{(II)}$$

Kinetic data concerning the reaction of BrO with CH_3SCH_3 (DMS) are also reported, since this reaction might be involved in catalytical depletion of ozone by DMS.

$$\begin{array}{lll} BrO + DMS & \rightarrow & DMSO + Br \\ Br + O_3 & \rightarrow & BrO + O_2 \\ \hline DMS + O_3 & \rightarrow & DMSO + O_2 \end{array} \qquad \text{(III)}$$

In addition to the description of laboratory reaction kinetics studies, some aspects of their possible impact on the Arctic ozone chemistry are discussed.

NATO ASI Series, Vol. I 7
The Tropospheric Chemistry of Ozone in the Polar Regions
Edited by H. Niki and K. H. Becker

In addition to the description of laboratory reaction kinetics studies, some aspects of their possible impact on the Arctic ozone chemistry are discussed.

EXPERIMENTAL KINETIC STUDIES OF BrO REACTIONS USING THE DISCHARGE-FLOW METHOD

The discharge-flow method has been found to be suitable for studying kinetics of BrO reactions. BrO radicals are produced in a flow of helium at low pressure (around 1 torr) from one of the following reactions:

$$Br + O_3 \rightarrow BrO + O_2 \qquad k(298\ K) = 1.2 \times 10^{-12}$$
$$O + Br_2 \rightarrow BrO + Br \qquad 1.4 \times 10^{-11}$$

The rate constants are given in units of cm^3 $molecule^{-1}$ s^{-1}.

Br or O atoms are produced by microwave discharge dissociation of Br_2 or O_2, respectively. The BrO kinetics are monitored in our laboratory by mass spectrometry or EPR spectroscopy. These analytical techniques are coupled to discharge-flow reactors. In the discharge-flow mass spectrometric equipment, the gases are sampled from the reactor by a modulated molecular beam and the BrO radicals are analyzed at their parent peaks (m/e = 95 or 97). In the discharge-flow EPR experiment, BrO is analyzed in the gas phase using a large access cavity (1 in. diameter) crossed by the reactor. In both experiments the absolute concentrations of BrO are determined by the titration reaction:

$$NO + BrO \rightarrow NO_2 + Br \qquad k(298\ K) = 2.1 \times 10^{-11}$$

BrO is calibrated against NO_2 and Br in the mass spectrometric and EPR experiments, respectively, Br atoms being calibrated against O_2. The detection limits for BrO are, respectively, 10^{10} and 10^{11} cm^{-3} by mass spectrometry and EPR (S/N = 1).

In kinetic studies of bimolecular reactions of BrO, pseudo-first order conditions can be achieved only with excess of the other reactant, since the fast self-combination of BrO prevents its use as the excess reactant.

KINETIC RESULTS OF BrO REACTIONS

Reaction BrO + BrO → products

The BrO self combination reaction has been studied at 298 K using the DF-MS technique [Lancar et al.,1991]. This reaction is known to have two bimolecular channels:

$$BrO + BrO \rightarrow 2\,Br + O_2 \quad (1a)$$

$$BrO + BrO \rightarrow Br_2 + O_2 \quad (1b)$$

The total rate constant, $k_1 = k_{1a} + k_{1b}$, expressed from the equation $-d[BrO]/dt = 2\,k[BrO]^2$, was measured using the reaction $O + Br_2 \rightarrow BrO + Br$ as the BrO source. The rate constant obtained at 298 K was: $k_{1a+1b} = (3.2 \pm 0.5) \times 10^{-12}$ cm^3 molecule^{-1} s^{-1}

The branching ratio of channel (1b) was measured using a BrO source free of Br_2. BrO was produced by the reaction $Br + O_3 \rightarrow BrO + O_2$, where Br was generated by the reaction $Cl + C_2H_3Br \rightarrow C_2H_3Cl + Br$. The rate constant k_{1b} of $(4.7 \pm 1.5) \times 10^{-13}$ cm^3 molecule^{-1} s^{-1} was obtained by curve-fitting the experimental kinetic data of BrO and Br_2 (Figure 1).

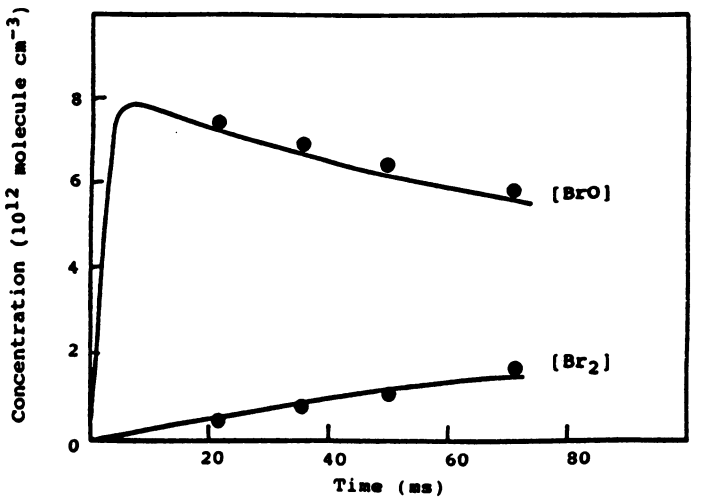

Fig. 1. Reaction BrO + BrO → products. Typical plots of BrO and Br_2 concentrations vs. reaction time $[Br]_0 = 8.8 \times 10^{12}$ cm^{-3}, $[O_3]_0 = 5.83 \times 10^{14}$ cm^{-3}.

The present value of k_1 is about 20% higher that the recommended value of 2.7×10^{-12} [De More et al., 1990] and 30% higher than a recent determination [Turnipseed et al., 1990]. These authors also observed a slight negative temperature dependence of k_1 (i.e., $k_1 = (1.06 \pm 0.20) \times 10^{-12} \exp(251 \pm 56)/T$).

Concerning the k_{1b} determination, the literature values range from 2.8 to 6.6×10^{-13} (Table I).

Table I: Values of k_{1b} at 298 K

k_{1b} (298 K) (10^{-13} cm^3 $molecule^{-1}$ s^{-1})	Technique	Reference
4.1 ± 2.0	FP-UV	Sander and Watson, [1981]
6.6 ± 2.0	M.M.-UV	Cox et al., [1982]
2.8 ± 1.8	DF-MS	Turnipseed et al., [1990]
4.7 ± 1.5	DF-MS	This work

Reaction BrO + HO_2 → products

The BrO + HO_2 reaction has been studied using a double discharge-flow reactor and mass spectrometric analysis [Poulet et al., 1992]. The BrO radicals were produced from the O + Br_2 reaction and HO_2 radicals from Cl/CH_3OH/O_2 mixtures. The rate constant for the BrO + HO_2 reaction was measured from the BrO kinetics monitored under pseudo-first order conditions using an excess of HO_2 over BrO. The absolute HO_2 concentration was determined by chemical titration via the reaction NO + HO_2 → NO_2 + OH. The initial HO_2 concentration ranged from 1 to 5 x 10^{12} cm^{-3}. The rate constant derived at 298 K was k_2 = (3.3 ± 0.5) x 10^{-11} cm^3 $molecule^{-1}$ s^{-1}. Detection of reaction products was also attempted by mass spectrometry. The only product observed was HOBr, suggesting that at 298 K the unique reaction channel is:

$$BrO + HO_2 \rightarrow HOBr + O_2 \qquad \Delta H = -52 \text{ kcal mol}^{-1} \qquad (2)$$

The alternative exothermic channel yielding HBr:

$$BrO + HO_2 \rightarrow HBr + O_3 \qquad \Delta H = -7.6 \text{ kcal mol}^{-1} \qquad (3)$$

would therefore be negligible at 298 K, which does not, however, preclude its occurrence at lower temperatures.

The present determination of k_2 is approximately 6 times higher that the only other published determination [Cox and Sheppard, 1982] by the molecular modulation-UV absorption technique, and the photolysis of O_3 in the presence of Br_2, H_2 and O_2. In this study k_2 was obtained in an indirect way. Another recent indirect determination of k_2 has been obtained from flash photolysis-UV absorption experiments, in which mixtures of Br_2, O_3, Cl_2, CH_3OH and O_2 were photolysed [Bridier et al., 1990]. The value derived,

$k_2 = (3 \pm 2) \times 10^{-11}$, is consistent with our determination. Another value also consistent with these values has been obtained recently by the Harwell group [M. Jenkin, this volume].

An increase of the rate constant k_2 is observed for the XO = HO_2 reaction along the series X = Cl, Br and I. This increase is correlated with the increase of the exothermicity of the channel XO + HO_2 → HOX + O_2, which is not inconsistent with a direct H-atom transfer mechanism.

Table II: Reactions XO + HO_2 → HOX + O_2

X	ΔH Kcal mol^{-1}	$K_{298\ K}$	Reference
Cl	-46.0	5×10^{-12}	De More et al., [1990]
Br	-52.0	3.3×10^{-11}	this work
I	-65.5	1×10^{-10}(a)	Maguin et al., [1992]

(a) value in agreement with that of Jenkin et al. [1991].

Reaction BrO + DMS → products

The reaction BrO + DMS → products (4) has been studied using the discharge flow-EPR method, and monitoring the BrO kinetics by gas phase EPR in the presence of excess DMS. The rate constant k_4 was measured at 298 K: $k_4 = (2.4 \pm 0.6) \times 10^{-13}$ cm^3 $molecule^{-1}$ s^{-1}. The mechanism is supposed to be BrO = DMS → Br + DMSO. However, it was not possible to verify this mechanism, since Br atom could not be detected due to the occurrence of a fast reaction between Br and DMS, as also observed by Wine et al. [1990]. The present value of k_4 is in good agreement with that of Barnes et al. [1991] who obtained $k_4 = (2.7 \pm 0.5) \times 10^{-13}$ cm^3 $molecule^{-1}$ s^{-1} at 298 K using the DF-MS technique. The authors reported DMSO as a product, but a quantitative determination was not possible.

As for XO + HO_2 reactions, a comparison of reactivity can be made for the XO + DMS reactions along the series X = Cl, Br and I. There is no correlation between reactivity and exothermicity for the XO + DMS reaction, and there is no obvious explanation for the higher reactivity of BrO with DMS, as compared to the corresponding reaction ofClO and IO.

Table III: Reactions XO + DMS → X + DMSO

X	ΔH kcal mol^{-1}	k (298 K)	References
Cl	-22.5	$(9.5 \pm 2.0) \times 10^{-15}$	Barnes et al., [1991]
Br	-30.3	$(2.7 \pm 0.5) \times 10^{-13}$	Barnes et al., [1991]
		$(2.4 \pm 0.6) \times 10^{-13}$	this work
I	-43.7	3.5×10^{-14}	Daykin and Wine, [1990]
		$(8.8 \pm 2.1) \times 10^{-15}$	Barnes et al., [1991]
		$(1.5 \pm 0.2) \times 10^{-14}$	Maguin et al., [1991]

POSSIBLE IMPACT OF THE BrO REACTIONS IN THE ARCTIC TROPOSPHERIC CHEMISTRY

As already been assessed by Barrie et al. [1988], cycle I involving the self-combination of BrO radicals can significantly deplete ozone in the Arctic troposphere in spring. The ozone depletion rate is:

$$-d[O_3]/dt = 2k_1[BrO]^2$$

Br_2 produced in channel (1b) is assumed to photolyze rapidly. Taking $k_1 = 3.7 \times 10^{-12}$ and T = 250 K, the ozone depletion rate would be 7.5 ppb/day and 0.19 ppb/day for mean daytime BrO levels of 20 ppt and 10 ppt, respectively, which are not unrealistic [Platt et al., 1992]. Similarly, cycle II involving the BrO + HO_2 reaction can deplete ozone. The ozone depletion rate can be expressed as:

$$-d[O_3]/dt = k_2[BrO][HO_2]$$

if reaction (2) is considered to be the limiting step of cycle II. This assumes that HOBr rapidly photodissociates into OH and Br. HO_2 concentrations have been calculated [Pirre, 1992] under the Arctic tropospheric conditions in early spring considering the photolysis of ozone in the presence of H_2O to be the only source of HO_x. Maximum daytime levels around 1 ppt were obtained for O_3 = 40 ppb, CH_4 = 1.7 ppm, CO = 150 ppb, NO_x = 10 ppt and $H_2O = 10^3$ ppm. Taking HO_2 levels of 1 ppt, ozone depletion rates of 3.3 ppb/day and 1.7 ppb/day are obtained for BrO levels of 20 ppt and 10 ppt, respectively. Therefore, the

ozone depletion rates by cycles I and II may be significant and comparable, with increasing importance of cycle II with decrease of BrO levels. Higher levels of HO_2, resulting from higher H_2O concentrations or additional sources of HO_x, would indeed increase the importance of cycle II. In contrast, a longer lifetime assumed for HOBr, and a non-negligible rate of the HBr forming channel of the BrO + HO_2 reaction would decrease the importance of this cycle. In this respect, further studies are needed on the BrO + HO_2 reaction and HOBr photodissociation to assess the role of cycle II.

Considering finally the BrO + DMS reaction, the potential role of cycle III in depleting ozone is highly dependent on the DMS levels present in the atmosphere of interest. A 5 ppb/day decrease of ozone would require 0.8 ppb and 1.6 ppb of DMS at BrO levels of 20 ppt and 10 ppt, respectively.

REFERENCES

Barnes, I., B. Bastian, K.H. Becker, R.D. Overath, Kinetic studies of the reactions of IO, BrO and ClO with dimethylsulfide, *Int. J. Chem. Kinet., 23*, 579 - 591, 1991.

Barrie, L.A., J.W. Bottenheim, R.C. Schnell, P.J. Crutzen, R.A. Rasmussen, Ozone destruction and photochemical reactions at polar sunrise in the lower Arctic atmosphere, *Nature, 334*, 138 - 141, 1988.

Bridier, I, B. Veyret, R. Lesclaux, CEC discussion meeting, Madrid, 1990.

Cox, R.A., D.W. Sheppard, Rate coefficient for the reaction of BrO with HO_2 at 303 K, *J. Chem. Soc. Faraday Trans, 2*, 78, 1383 - 1389, 1982.

Cox, R.A., D.W. Sheppard, M.P. Stevens, Absorption coefficients and kinetics of the BrO radical using molecular modulation, *J. Photochem. 19*, 189, 1982.

Daykin, E.P., P.H. Wine, Rate of reaction of IO radicals with dimethylsulfide, *J. Geophys. Res. 95*, 18547 - 18553, 1990.

De More, W.B., S.P. Sander, D.M. Golden, M.J. Molina, R.F. Hampson, M.J. Kurylo, C.J. Howard, A.R. Ravishankara, Chemical kinetics and photochemical data for use in stratospheric modeling, *JPL publication 90-1*, 1990.

Jenkin, M.E., R.A. Cox, G.D. Hayman, Kinetics of the reaction of IO radicals with HO_2 radicals at 298 K, *Chem. Phys. Lett. 177*, 272 - 278, 1991.

Lancar, I.T., G. Laverdet, G. Le Bras, G. Poulet, Rate constant and products of the BrO + BrO reaction at 298 K, *Int. J. Chem. Kinet. 23*, 37 - 45, 1991.

Maguin, F., G. Laverdet, G. Le Bras, G. Poulet, Reactions IO + HO_2 and BrO + HO_2: kinetic results and atmospheric impact, XXth Inf. Conf. Photochemistry Atlanta, Ga.

Maguin, F., G. Laverdet, G. Le Bras, G. Poulet, Kinetic study of the reactions IO + HO_2 and IO + NO_2 at 298 K, *J. Phys. Chem., 96*, 1775 - 1780, 1992.

Maguin, F., A. Mellouki, G. Laverdet, G. Poulet, G. Le Bras, Kinetics of the reactions of the IO radical with dimethylsulfide, methanethiol, ethylene and propylene, *Int. J. Chem. Kinetics, 23*, 237 - 245, 1992.

Pirre, M., Private communication, 1992.

Platt, U., et al., presented at the *Symposium on Optical Methods in Atmospheric Chemistry*, Berlin 22 - 24 June, 1992.

Poulet G., M. Pirre, F. Maguin, R. Ramaroson, G. Le Bras, Role of the BrO + HO_2 reaction in the stratospheric chemistry of bromine, *J. Geophys. Res.* in press, 1992.

Sander, S.P., R.T. Watson, Kinetics and mechanism of the disproportionation of BrO radicals, *J. Phys. Chem.*, *85*, 4000, 1991.

Turnipseed, A.A., J.W. Birk, J.G. Calvert, Kinetics of the BrO + BrO reaction, *J. Phys. Chem.*, *94*, 7477 - 7482, 1990.

Wine, P., Private communication, 1990.

A COMPARATIVE ASSESSMENT OF THE ROLE OF IODINE PHOTOCHEMISTRY IN TROPOSPHERIC OZONE DEPLETION

M.E. Jenkin
AEA Environment and Energy
Harwell Laboratory
Oxfordshire OX11 0RA
United Kingdom

INTRODUCTION

Over the past two decades, numerous field measurements have established that methyl iodide (CH_3I) is commonly present as a significant trace constituent of the planetary boundary layer, at concentrations in excess of 1 pptv [Lovelock et al., 1973; Rasmussen et al., 1982; Singh et al., 1983; Barnes et al., 1991; Oram and Penkett, 1991]. These field measurements have shown that the marine regions display systematically higher levels of CH_3I than the remote "clean" continental boundary layer, indicating that the oceans provide a source of CH_3I which is emitted directly into the troposphere. CH_3I has also been detected in polar air masses [Rasmussen and Khalil, 1983], in addition to the observation of springtime maxima in the level of particulate iodine in the Arctic [Sturges and Barrie, 1988; Barrie and Barrie, 1990]. The origin of these emissions is believed to be various types of macroalgae and phytoplankton, which may be found in both coastal waters and the open ocean [Lovelock, 1979; Chameides and Davis, 1980; Manley and Dastoor, 1987; Nightingale, 1991]. Although the precise mechanism is uncertain, it seems clear that these organisms produce CH_3I as part of their normal metabolic processes by "methylating" the iodide present in sea-water and, as a result, the water becomes locally super-saturated with CH_3I causing a flux from the aqueous to the gaseous phase [Singh et al., 1982; Nightingale, 1991]. Consequently, in marine locations of high biomass activity, elevated levels of CH_3I (10 - 40 pptv) have been observed [Rasmussen et al., 1982; Barnes et al., 1991; Oram and Penkett, 1991]. The formation of CH_3I represents, therefore, an important link in the transportation of the life-essential element iodine in the biosphere, providing a means of sea-to-land transport to balance the flux of dissolved I^- entering the sea from the land [Lovelock, 1979].

Although CH_3I is currently the only iodine-containing compound unambiguously identified in the atmosphere, its photo-oxidation occurs moderately rapidly at low altitudes, and potentially produces a range of inorganic iodine "reservoir" compounds, which may be interconverted by reactions involving the short-lived intermediates, I atoms and IO radicals [Chameides and Davis, 1980; Jenkin et al., 1985; Chatfield and Crutzen, 1990]. In some

NATO ASI Series, Vol. I 7
The Tropospheric Chemistry of Ozone in the Polar Regions
Edited by H. Niki and K. H. Becker

respects, the chemistry is analogous to the well-established chemical cycles involving chlorine and bromine which are known to deplete O_3 in the stratosphere [WMO, 1992 and references therein], and to the bromine photochemistry implicated in ground level Arctic O_3 depletion [Barrie et al., 1988; Finlayson-Pitts et al., 1990]. Since iodine-containing species are photodissociated more rapidly than their chlorine and bromine-containing counterparts (for example, see spectra of CH_3X species in Figure1), there is the potential for high I atom production rates at low altitudes, and a possible resultant impact on O_3 levels. This possible role for iodine was first considered by Chameides and Davis [1980]. Using the limited information available in the literature for kinetics and absorption cross sections of iodine-containing species, together with parameters for a series of potentially important reactions estimated by analogy with corresponding reactions of chlorine and bromine species, they were able to demonstrate that iodine photochemistry might lead to O_3 depletions comparable with those resulting from the background HO_x chemistry. In recent years, available information on the kinetics and spectroscopy of iodine-containing species has increased

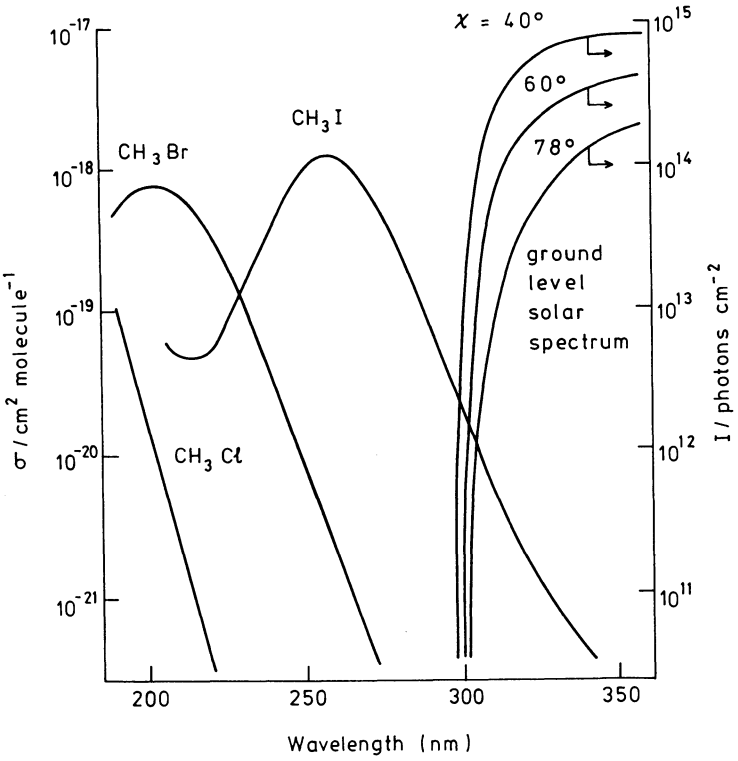

Fig. 1: UV absorption spectra of the CH_3X species and the calculated ground level solar fluxes as a function of solar zenith angle as reported by Peterson [1976].

dramatically [Atkinson et al., 1992]. Although the values of many of the key parameters have bee found to be extremely close to the estimates of Chameides and Davis [1980], there are inevitabl some notable exceptions which will modify the conclusions. In the sections that follow, curren understanding of the formation, interconversion and removal of inorganic iodine compound following the photodissociation of CH_3I is reviewed, with emphasis placed on the potential for O destruction in comparison with BrO_x chemistry and HO_x chemistry.

THE CHEMISTRY OF IODINE IN THE PLANETARY BOUNDARY LAYER

Our current knowledge of the gas-phase chemistry of iodine is summarised in Fig.2. The major sink for CH_3I in the troposphere is photodissociation to produce I atoms, which occurs on a timescale of ca. 5 days for $\chi = 40°$, and about 2 months for $\chi = 78°$:

$$CH_3I + \xrightarrow{h\nu} CH_3 + I \qquad (1)$$

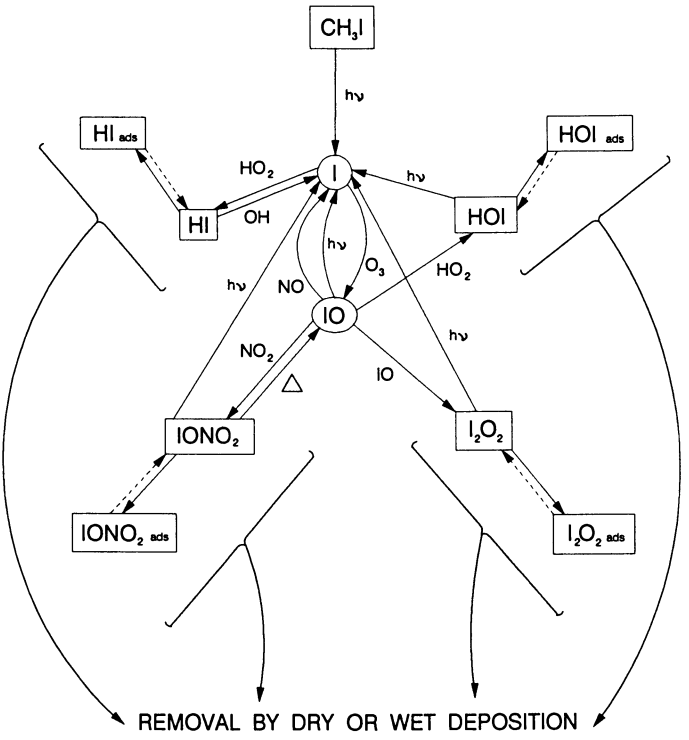

Fig. 2: Gas phase interconversions of iodine compounds in the troposphere

Unlike Cl or Br atoms, which may be scavenged by reaction with various organic species, I atoms are unable to abstract H atoms from saturated organic molecules, and do not add to unsaturated organic molecules. The predominant reaction for I atoms is with O_3, which typically occurs on the timescale of ca. 2s ($[O_3]$ = 20 ppbv), and leads to the production of IO radicals. At the low levels of NO_x observed in the remote boundary layer (typically less than 50 pptv), the major fate of IO is photodissociation to regenerate I atoms again. This cyclic interchange of I and IO has no net chemistry, since O_3 is also regenerated:

$$I + O_3 \rightarrow IO + O_2 \quad (2)$$

$$IO + \xrightarrow{h\nu} I + O \quad (3)$$

$$O + O_2 (+ M) \rightarrow O_3 (+ M) \quad (4)$$

The average lifetime of IO with respect to photodissociation is ca. 30s for $\chi = 40°$, and a few minutes for $\chi = 78°$. At higher NO_x levels, I atoms are also regenerated by the reaction of IO with NO which is able to compete with reaction (2):

$$IO + NO \rightarrow I + NO_2 \quad (5)$$

$$NO_2 + \xrightarrow{h\nu} NO + O \quad (6)$$

However, the subsequent photolysis of NO_2 leads to regeneration of both NO and O_3 (via reaction (4)), and a cycle with no net chemistry is once again completed. These two "null cycles" play a dominant role in the chemistry of iodine in the troposphere.

Since the interconversion of I and IO occurs comparatively rapidly, their behaviour is coupled and they may be collectively referred to as IO_x. As shown in Fig.2, IO_x is believed to be sequestered in the troposphere in the form of the reservoir species HI, HOI, $IONO_2$ or I_2O_2, formed by the following radical termination reactions:

$$I + HO_2 \rightarrow HI + O_2 \quad (7)$$

$$IO + HO_2 \rightarrow HOI + O_2 \quad (8)$$

$$IO + NO_2 (+M) \rightarrow IONO_2 (+M) \quad (9)$$

$$IO + IO (+M) \rightarrow I_2O_2 (+M) \quad (10)$$

The relative abundance of these gas-phase reservoir species depends on both their rates of formation by reactions (7)-(10), and their lifetimes before regeneration of IO_x by the following reactions:

$$OH + HI \rightarrow H_2O + I \quad (11)$$

$$HOI + \xrightarrow{h\nu} OH + I \quad (12)$$

$$IONO_2 + \xrightarrow{h\nu} NO_3 + I \quad (13)$$

$$IONO_2 (+M) \rightarrow IO + NO_2 (+M) \quad (14)$$

$$I_2O_2 + \xrightarrow{h\nu} O_2 + 2I \quad (15)$$

The absolute gas-phase concentrations of the inorganic iodine species is influenced strongly by their rate of physical removal which occurs by both direct deposition to ground or sea, and by attachment to the atmospheric aerosol. The lack of available information on the rates of these physical removal processes, and their dependence on speciation, represents a major uncertainty in the description of the behaviour of iodine in the atmosphere. The aqueous phase chemistry of inorganic iodine species is also complex. Although volatile species such as I_2 and HOI may be formed in solution, available information suggests that oxidation to iodate dominates, thereby precluding revolatilisation. Thus, removal of inorganic iodine in cloud water is probably irreversible. It is possible, however, that attachment to solid aerosol components is reversible, with the associated possibility of key chemical processes occurring in the adsorbed phase.

THE POTENTIAL INFLUENCE OF IODINE CHEMISTRY ON O_3

The repeated formation of the reservoir molecules (HI, HOI, $IONO_2$ and I_2O_2), followed by regeneration of IO_x by the reactions described in the last section, potentially has an influence on the chemistry of the boundary layer, which may effect O_3 levels either directly or indirectly.

i) The formation and removal of HI by reactions (7) and (11) leads to net HO_x removal (cycle 1):

$$I + HO_2 \rightarrow HI + O_2 \quad (7)$$

$$OH + HI \rightarrow H_2O + I \quad (11)$$

$$HO_2 + OH \rightarrow H_2O + O_2 \quad (net)$$

The importance of this cycle, however, is very minor indeed, owing to the slow rate of reaction (7) [$k_7 = 3.8 \times 10^{-13}$ cm^3 $molecule^{-1}s^{-1}$ at 298 K: Atkinson et al.,1992]. The lifetime of HI with respect to regeneration of I atoms by reaction (11) is ca. 9 hours for [OH] = 10^6 molecule cm^{-3}.

ii) The chemistry of formation and removal of $IONO_2$ by reactions (9) and (13) is dominated by a null cycle, since the NO_3 produced photolyses rapidly, leading mainly to the regeneration of NO_2, with no net effect on O_3:

$$IO + NO_2 (+M) \rightarrow IONO_2 (+M) \quad (9)$$

$$IONO_2 + \xrightarrow{h\nu} NO_3 + I \quad (13)$$

$$I + O_3 \rightarrow IO + O_2 \quad (2)$$

$$NO_3 + \xrightarrow{h\nu} NO_2 + O \quad (16)$$

$$O + O_2 (+ M) \rightarrow O_3 (+ M) \quad (4)$$

iii) Studies of the self reaction of IO have shown the reaction to be dominated by a rapid association channel at atmospheric pressure, believed to lead to the production of the dimeric species, I_2O_2 [$k_{10} = 5.2 \times 10^{-11}$ cm^3 $molecule^{-1}s^{-1}$: Atkinson et al., 1992]. The subsequent chemistry of I_2O_2 potentially leads to O_3 loss by a cycle analogous to that involving Cl_2O_2 which destroys O_3 in the polar stratosphere (cycle 2):

$$IO + IO (+M) \rightarrow I_2O_2 (+M) \quad (10)$$

$$I_2O_2 + \xrightarrow{h\nu} O_2 + 2I \quad (15)$$

$$2x(I + O_3 \rightarrow IO + O_2) \quad (2)$$

$$2O_3 \rightarrow 3O_2 \quad (net)$$

I_2O_2 has never been positively identified in laboratory studies, and evidence for its existence comes primarily from kinetics observations. Although Sander [1986] observed product absorptions in the near uv during flash photolysis investigation of reaction (10), which may be due partially to I_2O_2, no residual absorptions have been observed at the IO monitoring wavelength (427 nm) by any workers studying this reaction. By analogy with red shifts commonly observed for Cl-, Br- and I-containing homologues, I_2O_2 would be expected to have an absorption spectrum extending well into the visible region, and a corresponding short lifetime before photolysis and regeneration of I atoms. Apparently this is not the case, and consequently the potential of cycle 2 for O_3 depletion is probably severely limited, since physical removal of I_2O_2 is estimated to compete effectively with its photolysis.

The behaviour of IO should be contrasted with that of BrO, for which the direct Br atom forming channel of the self reaction dominates, providing a comparatively efficient cycle for O_3 destruction:

$$XO + XO \rightarrow O_2 + 2X \quad (17)$$
$$2x(X + O_3 \rightarrow XO + O_2) \quad (18)$$
$$2O_3 \rightarrow 3O_2 \quad (net)$$

On the basis of currently available data [Atkinson et al., 1992], the direct I atom forming channel of the IO self-reaction represents $\leq$ 20% of the overall reaction at atmospheric pressure and 298 K. It is highly likely, however, that IO and BrO will react rapidly, leading to the probable production of Br and I:

$$IO + BrO \rightarrow I + Br + O_2 \quad (19a)$$
$$\rightarrow IBr + O_2 \quad (19b)$$
$$\rightarrow IOOBr \quad (19c)$$

There have currently been no studies of this reaction.

iv) Perhaps the greatest potential for O_3 removal as a result of iodine photochemistry occurs as a result of the formation and removal of HOI by reactions (8) and (12) (cycle 3):

$$IO + HO_2 \rightarrow HOI + O_2 \quad (8)$$
$$HOI + \xrightarrow{h\nu} OH + I \quad (12)$$
$$I + O_3 \rightarrow IO + O_2 \quad (2)$$
$$HO_2 + O_3 \rightarrow OH + 2O_2 \quad (net)$$

The reaction of IO with HO_2 has recently been found to be rapid ($k_8 = 6.4 \times 10^{-11}$ $cm^3molecule^{-1}s^{-1}$: Jenkin et al., 1991; $k_8 = 1.03 \times 10^{-10}$ $cm^3molecule^{-1}s^{-1}$: Maguin et al., 1992], with the product HOI detected by mass spectrometry [Maguin et al., 1992]. The values of k_8 obtained in the two studies differ by about a factor of 1.5. This may be due to the existence of a second significant channel of the reaction, forming OH, I and O_2, which would not be measurable in the chemical system employed by Jenkin et al. 1991], since OH and I would rapidly regenerate HO_2 and IO:

$$IO + HO_2 \rightarrow OH + I + O_2 \quad (8a)$$

Clearly, this reaction would enhance the efficiency of cycle 3. Analogous channels for reactions involving ClO and BrO are endothermic by 21 and 12 kJ mol^{-1}, respectively. On the basis of the commonly accepted heat of formation of IO of 176 kJ mol^{-1} [Atkinson et al., 1989; DeMore et al., 1990], channel (8a) is exothermic by some 45 kJ mol^{-1}, and the trend is

continued. However, a significantly reduced heat of formation of 107 kJ mol^{-1} may be calculated from a recent determination of the bond dissociation energy of IO [Reddy et al., 1989], which would suggest channel (8a) is about 25 kJ mol^{-1} endothermic.

In the absence of a significant contribution of channel (8a) to the reaction, the efficiency of cycle 3 is governed by the stability of HOI, and in particular whether photodissociation can compete with physical removal. Jenkin [1991] has recently observed uv/visible product absorptions during the 254 nm photolysis of H_2O_2 in the presence of I_2. HOI is expected to be produced in this system from the reaction of OH with I_2:

$$H_2O_2 + \xrightarrow{h\nu} OH + OH \quad (20)$$

$$OH + I_2 \rightarrow HOI + I \quad (21)$$

The observed product spectrum, calibrated relative to I_2 removed, is shown in Fig.3 along with the uv spectrum of HOCl. Preliminary measurements by Schindler [1991] have established that gas-phase HOBr has a uv absorption spectrum which lies between that of HOCl, and the product absorptions measured by Jenkin [1991], which are believed to be due to HOI. With this assumption, a lifetime of 3 minutes for HOI with respect to photodissociation ($\chi = 40°$) may be calculated.

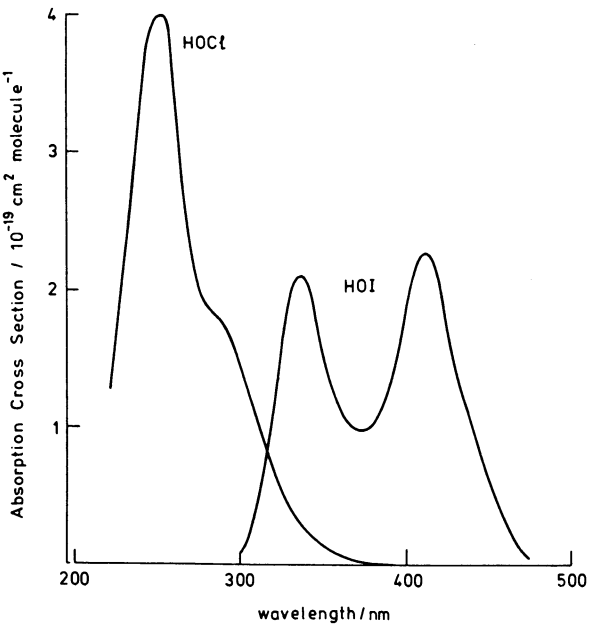

Fig. 3: Gas phase absorption spectra of HOCl and HOI

Recent calculations incorporating the most up to date kinetic and spectroscopic data for relevant reactions of iodine species [Jenkin, 1991; Barnes et al., 1991] have established that the iodine chemistry outlined above can result in O_3 depletion, but that the effect is minor. Almost all the calculated O_3 depletion occurs as a result of cycle 3 involving HOI formation, but this only amounts to about 10% of the O_3 depletion occurring at mid latitudes as a result of the well-known HO_x chemistry (CH_3I concentration = 20 pptv).

These calculations also predicted HOI to be the major gas-phase reservoir owing to its rapid production by reaction (8) being the predominant loss process for the active IO_x species. In the absence of sunlight, the only loss process included for HOI was irreversible physical removal by deposition or attachment to aerosol, which was assumed to occur on the timescale of ca. 1 day. At present, it is not clear if this is realistic. It should be noted that unambiguous detection of gaseous HOI in laboratory systems has proved notoriously difficult, apparently owing to a combination of gas phase and heterogeneous processes, and judgement has to be reserved on whether the current description of HOI behaviour in the atmosphere is adequate, particularly for the polar troposphere. The recent measurement of the uv/visible spectrum [Jenkin, 1991] was apparently complicated by heterogeneous interferences, as was measurement of k_8 in the same apparatus [Jenkin et al., 1991], where slow regeneration of IO_x occurred, presumably due to decomposition of HOI at the vessel wall. Earlier studies in which both HOI and HOBr were generated in a 200 l teflon bag [Jenkin et al., 1984] from the rapid reactions of OH with I_2 or Br_2 under steady state photolysis conditions, demonstrated that the X_2 species were rapidly regenerated. Evidence was presented to support a mechanism in which the HOX species reacted directly with the OH precursor, nitrous acid (HONO), which was present at ppmv levels, presumably by a gas phase mechanism :

$$HOX + HONO \rightarrow XNO_2 + H_2O \quad (22)$$

$$XNO_2 + XNO_2 \rightarrow X_2 + 2NO_2 \quad (23)$$

$$X + XNO_2 \rightarrow X_2 + NO_2 \quad (24)$$

Recent field measurements discussed at this workshop support the presence of non-negligible concentrations of HONO in the polar troposphere. Clearly the reactions of HOI or HOBr with HONO (or similar reactions with other atmospheric trace constituents) might occur, possibly facilitated by the atmospheric aerosol, allowing release of catalytic IO_x or BrO_x from the reservoir species. In the absorbed phase, reaction (22) may be considered to be an "ionic" reaction between X^+OH^- and $H^+NO_2^-$.

The reaction of BrO with HO_2 has recently been found to have a rate coefficient of ca. 3×10^{-11} cm^3 $molecule^{-1}$ s^{-1} at 298 K [Poulet et al., 1992; Veyret, 1991; Hayman, 1992]. The rapid rates of this reaction, and of the reaction of IO with HO_2 raise some

interesting questions concerning the possible abstraction of labile aldehydic H atoms by IO or BrO, or the reaction of these species with other peroxy radicals such as CH_3O_2, which may be abundant in the remote troposphere. The mechanisms for the reactions of IO and BrO with HO_2 are not defined at present but, as discussed previously for ClO [Mozurkewich, 1986; Toohey and Anderson, 1989], the product HOX species may be formed either by direct H-atom abstraction via an XO-HOO intermediate, or by initial formation of an OX-OOH adduct, with subsequent elimination of HOX and O_2 from a cyclic intermediate (or indeed formation of OH, I and O_2 from cyclic OI-OOH). If the former dominates, then IO and BrO may also be expected to abstract labile, aldehydic H atoms:

$$XO + HCHO \rightarrow HOX + HCO \qquad (25)$$

If the latter mechanism operates, the reactions of XO with other peroxy radicals may be important, e.g. :

$$XO + CH_3O_2 \rightarrow X + CH_3O + O_2 \qquad (26)$$

It is interesting to note that there is a reported kinetic measurement of reaction (26) for X = Cl [Simon et al., 1989], even though the reaction is calculated to be slightly endothermic [on the basis of heats of formation given in Atkinson et al, 1989]. For X = Br and I, the reactions are exothermic.

REFERENCES

Atkinson, R., D.L. Baulch, R.A. Cox, R.F. Hampson, J.A. Kerr, J. Troe, Evaluated kinetic and photochemical data for atmospheric chemistry: Supplement III, *J. Phys. Chem. Ref. Data, 18*, 881-1097, 1989.

Atkinson, R., D.L. Baulch, R.A. Cox, R.F. Hampson, J.A. Kerr, J. Troe, Evaluated kinetic and photochemical data for atmospheric chemistry: Supplement IV, *J. Phys .Chem. Ref. Data, 21*, 1992.

Barnes, I., B. Bonsang, T. Brauers, P. Carlier, R.A. Cox, H.P. Dorn, M.E. Jenkin, G. Le Bras, U. Platt, Laboratory studies of oxidation processes occurring in the atmospheric marine boundary layer, *CEC Air Pollution Research Report 35*, CEC B-1040, Brussels, Belgium, 1991.

Barrie, L.A., M. J. Barrie, Chemical composition of lower tropospheric aerosols in the high Arctic: six years of observations, *J. Atm. Chem., 11*, 211-226, 1990.

Barrie, L.A., J.W. Bottenheim, R.C. Schell, P.J. Crutzen, R.A. Rasmussen, Ozone destruction and photochemical reactions at polar sunrise in the lower Arctic atmosphere, *Nature, 334*, 138-141, 1988.

Chameides, W.L., D.D. Davis, Iodine: its possible role in tropospheric photochemistry, *J.*

Geophys. Res., 85, 7383-7398, 1980.

Chatfield, R.B., P.J. Crutzen, Are there interactions of iodine and sulphur species in marine air photochemistry? *J. Geophys. Res. 95*, 22319-22341, 1990.

DeMore, W.B., S.P. Sander, D.M. Golden, M.J. Molina, R.F. Hampson, M.J. Kurylo, C.J. Howard, A.R. Ravishankara, Chemical kinetics and photochemical data for use in stratospheric modelling, *JPL Publication 90-1*, 1990.

Finlayson-Pitts, B.J., F.E. Livingston, H.N. Berko, Ozone destruction and bromine photochemistry at ground level in the Arctic spring, *Nature, 343*, 622-625, 1990.

Hayman, G.D., AEA Environment and Energy, Harwell Laboratory, UK, Private communication, 1992.

Jenkin, M.E., Kinetic and spectroscopic studies of peroxy radical reactions related to tropospheric photo-oxidation chemistry, *PhD Thesis, University of East Anglia*, UK, 1991.

Jenkin, M.E., K.E. Clemitshaw, R.A. Cox, Kinetics of the reaction of OH with I_2,. *J. Chem. Soc. Faraday Trans, 2, 80*, 1633-1641, 1984.

Jenkin, M.E., R.A. Cox, D.E. Candeland, Photochemical aspects of tropospheric iodine behaviour, *J. Atm. Chem., 2*, 359-375, 1985.

Jenkin, M.E., R.A. Cox, G.D. Hayman, Kinetics of the reaction of IO radicals with HO_2 radicals at 298 K, *Chem. Phys. Lett., 177*, 272-278, 1991.

Lovelock, J.E., Gaia - A new look at life on Earth. Chapter 6, Oxford University Press, Oxford, UK, 1979.

Lovelock, J.E., K.J. Maggs, R.J. Wade, Halogenated hydrocarbons in and over the Atlantic, *Nature, 241*, 194-196, 1973.

Maguin, F., G. Laverdet, G. Le Bras, G. Poulet, Kinetic study of the reactions IO + HO_2 and IO + NO_2 at 298 K, *J. Phys. Chem.*, in press, 1992.

Manley, S.L, M.N. Dastoor, Methyl halide production from the giant kelp macrocystis, and estimates of global CH_3X production by kelp, *Limnol. Oceanogr., 32*, 707-715, 1987.

Mozurkewich, M., Reactions of HO_2 with free radicals, *J. Phys. Chem., 90* 2216-2221, 1986.

Nightingale, P.D., *PhD Thesis University of East Anglia*, UK.

Oram, D., S.A. Penkett, University of East Anglia, UK, Private communication, 1991.

Peterson J.T., Calculated actinic fluxes for air pollution photochemistry applications. *EPA Report 600/4-76-0025*, U.S. EPA, Research Triangle Park, NC, USA 1976.

Poulet G., M. Pirre, F. Maguin, R. Ramaroson, G. LeBras, Role of the BrO + HO_2 reaction in the stratospheric chemistry of bromine, *J. Geophys. Res.*, in press, 1992.

Rasmussen, R.A, M.A.K Khalil, Rare trace gases at the south pole, *Antarctic Journal of the US.*, 250-251, 1983.

Rasmussen, R.A, M.A.K. Khalil, R. Gunawardena, S.D. Hoyt, Atmospheric Methyl Iodide, *J. Geophys. Res., 87*, 3086-3090, 1982.

Reddy, R.R., T.V.R. Rao, A.S.R. Reddy, Curve fitting approach: On the dissociation energies of ClO and IO, *Indian J. Pure and Applied Phys. 27*, 243-245, 1989.

Sander, S.P., Kinetics and mechanism of the IO + IO reaction, *J. Phys. Chem., 90*, 2194-2199, 1986.

Schindler, R.N., University of Kiel, FRG, Private communication, 1991.

Simon, F.G., J.P. Burrows, W. Schneider, G.K. Moortgat, P.J. Crutzen, Study of the Reaction ClO + CH_3O_2 at 300 K. *J. Phys. Chem., 93*, 7807-7813, 1989.

Sturges, W.T, L.A. Barrie, Chlorine, bromine and iodine in Arctic aerosols, *Atmos. Environ., 22*, 1179-1194, 1988.

Toohey, D.W., J.G. Anderson, Theoretical investigations of reactions of some radicals with HO_2. 1. Hydrogen abstractions by direct mechanisms, *J. Phys. Chem., 93* 1049-1058, 1989.

Veyret, B., University of Bordeaux, France, Private communication, 1991.

WMO, Scientific assessment of ozone depletion: 1991, *World Meteorological Organisation Global Ozone Research and Monitoring Project - Report No. 25,* WMO, Geneva, Switzerland, 1992.